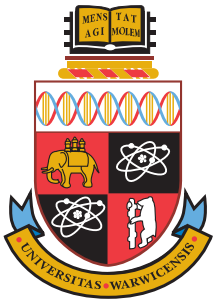


# A Systems and Molecular Analysis of G Protein-mediated Signalling

by

Wayne Daniel Croft

A thesis submitted to the University of Warwick
in partial fulfilment of the requirements for the
degree of Doctor of Philosophy

Systems Biology Doctoral Training Centre

May 2012

Supervisors: Dr Graham Ladds and Professor David Rand

# Declaration of Authorship

I, WAYNE DANIEL CROFT, declare that this thesis titled, 'A SYSTEMS AND MOLECULAR ANALYSIS OF G PROTEIN-MEDIATED SIGNALLING' and the work presented in it are my own. I confirm that:

- This work was done wholly or mainly while in candidature for a research degree at this University.
- Where any part of this thesis has previously been submitted for a degree or any other qualification at this University or any other institution, this has been clearly stated.
- Where I have consulted the published work of others, this is always clearly attributed.
- Where I have quoted from the work of others, the source is always given. With the exception of such quotations, this thesis is entirely my own work.
- I have acknowledged all main sources of help.
- Where the thesis is based on work done by myself jointly with others, I have made clear exactly what was done by others and what I have contributed myself.

Signed: _____

Date: _____

UNIVERSITY OF WARWICK

# *Abstract*

Systems Biology Doctoral Training Centre

Doctor of Philosophy

by

Wayne Daniel Croft

The ability of cells to respond correctly to signals from their microenvironment is an essential prerequisite of life. Many external signals are detected through G protein-coupled receptor (GPCR) signalling pathways, which control all aspects of eukaryotic physiology. Ligand-bound GPCRs initiate signalling by promoting exchange of GDP for GTP on the G$\alpha$ subunit of heterotrimeric G proteins, thereby facilitating activation of downstream effectors. Signalling is terminated by the hydrolysis of GTP to GDP through intrinsic GTPase activity of the G$\alpha$ subunit, in a reaction catalysed by the regulator of G protein signalling (RGS) proteins.

Due to the problem of complexity in higher eukaryotic GPCR signalling, the mating-response in *Schizosaccharomyces pombe* has been used to study GPCR signalling in isolation. *In vivo* data from quantitative assays of reporter strains and live-cell fluorescence microscopy informs the development of an ordinary differential equation model of the signalling pathway, first described by Smith et al., 2009.

The rate of nucleotide exchange on the G$\alpha$ (Gpa1) is a key molecular mechanism controlling duration and amplitude of signalling response. The influence of this is investigated through characterisation of Gpa1 nucleotide exchange mutants and perturbation of reaction rate parameters in the computational model. Further, this thesis also presents data relating to the temporal and spatial regulation of Rgs1 (the sole RGS protein for Gpa1). Using an inter-disciplinary approach, evidence is provided to suggest that an interaction between Rgs1 and the C-terminal tail of the GPCR (Mam2) tethers Rgs1 to the plasma membrane to facilitate its function.

Finally, quantification of signalling at the single cell level is described. Time-lapse live-cell imaging of fluorescent reporter cells is optimised and single cell signalling response quantified using image analysis software. Single cell quantification provides greater insight into temporal dynamics, cell-to-cell variability, and highlights the existence of mechanisms for cellular decision-making.

# *Acknowledgements*

There are many people, without whom this thesis would not be possible and I would like to express my gratitude to them all.

First and foremost, I would like to thank my supervisor Dr Graham Ladds for his support, commitment and hard work throughout the project. As a result of his efforts he has developed me into a better scientist, I honestly could not have wished for a better supervisor.

Many thanks to my second supervisor Professor David Rand, who contributed with insightful ideas and with the mathematical model development.

Thank you to all of the members of the lab group who have helped make my time as a PhD student both memorable and enjoyable. Thanks to Professor John Davey for useful input in lab meetings. In the projects infancy, Dr Benjamin Smith for his excellent guidance on the modelling and for giving me the opportunity to extend his initial work. Dr Emma Godfrey, Dr Eilish McCann and Antonia Nilsson for their help and guidance on various lab techniques. Thank you to Dr Michael Bond, Dr Magdelena Mos, Cate Weston, Kate Richardson, Ingrid Tigges and Jeanette Bennett for making the lab such a great place to work.

I would like to thank Dr Till Bretschneider and Richard Tyson for support with technical issues using their single cell tracking software QuimP, providing us with an excellent tool to advance the project.

My thanks go to the Systems Biology DTC director Vicky Buchanan-Wollaston and all of the Systems Biology staff for giving me the opportunity to do this project and through the doctoral training centre program, aiding my academic development.

Thank you to my advisory panel Dr Alex Conner, Dr Keith Vance and Dr Barbel Finkenstadt for helpful advice and feedback in regular meetings throughout the project.

Special thanks goes to all my family and friends for their love and support, and for being there when needed. A final thank you goes to my wife Deborah Croft who has put up with me during the stresses and strains of a PhD project, often having to play second fiddle to work commitments. To Debby: Thank you for your love and patience.

# Contents

# List of Figures

# List of Tables

# Abbreviations

| | |
|---|---|
| **7TM** | 7 **T**rans-**M**embrane |
| **AA** | **A**mino **A**cid |
| **AC** | **A**denylyl **C**yclase |
| **AGS** | **A**ctivator of **G** Protein **S**ignalling |
| **AMPA** | $\alpha$-**A**mino-3-hydroxy-5-**M**ethyl-4-isoxazole**P**ropionic |
| **ARF** | **A**DP-**R**ibosylation **F**actors |
| **ATP** | **A**denosine **T**ri**P**hosphate |
| bp | base pair |
| **cAMP** | **c**yclic **A**denosine **M**ono**P**hosphate |
| **CFU** | **C**olony **F**orming **U**nit |
| **CNS** | **C**entral **N**ervous **S**ystem |
| **DAG** | **D**i**A**cyl**G**lycerol |
| **DEP** | **D**ishevelled, **E**GL-10, **P**leckstrin |
| **DMM** | **D**efined **M**inimal **M**edia |
| **DNA** | **D**eoxy**Ribose** **N**ucleic **A**cid |
| *E. coli* | *Escherichia coli* |
| $\mathbf{EC_{50}}$ | p**E**ffective **C**oncentration$_{50}$ |
| $\mathbf{EDT_2}$ | **E**thane**D**i**T**hiol$_2$ |
| **EGF** | **E**pidermal **G**rowth **F**actor |
| **FlAsH** | **F**luorescein **A**rsenical **H**airpin |
| **FOA** | 5-**F**luoro-**O**rotic **A**cid |
| **FRET** | **F**luorescent **R**esonance **E**nergy **T**ransfer |
| **GAP** | **G**TPase **A**ccelerating **P**rotein |
| **GDI** | **G** Protein **D**issociation **I**nhibitor |
| **GDP** | **G**uanosine **D**i**P**hosphate |
| **GEF** | **G**uanosine Nucleotide **E**xchange **F**actor |

| | |
|---|---|
| **GFP** | **G**reen **F**luorescent **P**rotein |
| **GIRK** | **G** protein-gated **I**nwardly **R**ectifying potassium ($\mathbf{K}^+$) |
| **GPCR** | **G** **P**rotein-**C**oupled **R**eceptor |
| **GRK** | **G** protein **R**eceptor **K**inase |
| **GTP** | **G**uanosine **T**ri**P**hosphate |
| **IFN** | **I**nter**F**ero**N** |
| **IGF-I** | **I**nsulin-like **G**rowth **F**actor-I |
| **$IP_3$** | **I**nositol tri**p**hosphate |
| **JAK** | **JA**nus **K**inase |
| **MAPK** | **M**itogen **A**ctivated **P**rotein **K**inase |
| **MAPKK** | **M**itogen **A**ctivated **P**rotein **K**inase **K**inase |
| **MAPKKK** | **M**itogen **A**ctivated **P**rotein **K**inase **K**inase **K**inase |
| mCherry | monomeric Cherry |
| **OD** | **O**ptical **D**ensity |
| **ODE** | **O**rdinary **D**ifferential **E**quation |
| **ONPG** | **O**-**N**itro**P**henyl-D-**G**alactoside |
| **ORF** | **O**pen **R**eading **F**rame |
| **PCR** | **P**olymerase **C**hain **R**eaction |
| **PDE** | **P**artial **D**ifferential **E**quation |
| **PDGF** | **P**latelet **D**erived **G**rowth **F**actor |
| **PDZ** | **P**SD95 **D**lg1 **Z**o1 |
| **$pEC_{50}$** | Negative Natural Logarithm of Median **E**ffective **C**oncentration |
| **$PI_3K$** | **P**hospho**I**nositide **3**-**K**inase |
| **$PIP_2$** | **P**hosphatidyl**I**nositol 4,5-bis**p**hosphate |
| **PKC** | **P**rotein **K**inase **C** |
| **PLC** | **P**hospho**L**ipase **C** |
| **PM** | **P**lasma **M**embrane |
| **RGS** | **R**egulator of **G** Protein **S**ignalling |
| **RTK** | **R**eceptor **T**yrosine **K**inase |
| *S. cerevisiae* | *Saccharomyces cerevisiae* |
| **S.E.M** | **S**tandard **E**rror of the **M**ean |
| **STAT** | **S**ignal **T**ransduction and **A**ctivators of **T**ranscription |
| *S. pombe* | *Schizosaccharomyces pombe* |

| | |
|---|---|
| **TGF$\beta$** | **T**ransforming **G**rowth **F**actor $\beta$ |
| **TM#** | **T**rans-**M**embrane Domain # |
| **UTR** | **U**n**T**ranslated **R**egion |
| **VEGF** | **V**ascular **E**ndothelial **G**rowth **F**actor |
| **YE** | **Y**east **E**xtract |
| **YFP** | **Y**ellow **F**luorescent **P**rotein |

# Chapter 1

# General Introduction

## 1.1 Cellular Signalling

One of the essential prerequisites of life is the ability of cells to perceive and respond correctly to signals from their microenvironment. Cells require inputs from both their environment and from neighbouring cells to advise their development, differentiation and eventual death. Eukaryotic cells have evolved a variety of intricate and efficient signalling mechanisms to enable them to detect external signals and to respond to them appropriately.

The concept of a single external signal activating a single internal signalling pathway to produce a single cellular response is an over-simplification. In reality, the process is further complicated by the integration and processing of multiple signals with a large amount of cross-talk and various feedback processes that combine, to form what are better described as, signalling networks. Despite the complexity of such signalling networks and such a noisy environment, a single cell is able to perceive, integrate and process many different signals through the interactions of a wide variety of peptides, proteins and small molecules to produce an appropriate cellular response.

Common to many signalling pathways is the presence of receptors that can 'detect' the extracellular signal. These receptors are primarily proteins that span the outer cell membrane at least once and transmit the signal from the external environment to the inside of the cell. This transmission is often in the form of the modified receptor triggering the subsequent binding and modification of intracellular components. Once the signal is inside the cell, a diverse sequence of reactions is initiated that interpret the signal into the required response.

Many disease states can arise if the normal behaviour of such signalling networks are disrupted. One example is autoimmune disease, which can result from disruption of signalling networks that govern the correct recognition of pathogens within the body (Clarke and Sperandio, 2005). Another well studied example is Cancer, which can result when the signalling networks controlling cell division and cell death become disrupted, leading to

uncontrolled cell proliferation (Jones and Thompson, 2009). To improve our understanding of how to detect and treat such signalling related diseases, we must understand more about the mechanisms utilised for signal processing.

Due to the complex nature of signalling networks and the often large number of diverse signalling molecules involved, it is difficult and time-consuming to interpret the role of each individual molecule in the network. As a result of this, many researchers are now taking systems biology approaches to study cell signalling. This often involves an iterative cycle of gathering 'wet-laboratory' data along with mathematical modelling of the signalling networks to try to understand the mechanisms for how a large number of signalling components can combine to give particular systems level responses.

### 1.1.1 Common Signalling Examples

Stripped down to its simplest form, signalling consists of a signal, a translator and a response. The translator detects the signal and translates it into the response (effector). The response or effector can utilise three possible mechanisms to alter the cell's behaviour in response to the signal; alter gene expression, alter ion balance and alter enzyme activity.

A well studied signalling example is the receptor tyrosine kinase (RTK) protein family (Robinson et al., 2000). At least 50 different ligands have been identified for RTKs, many of which are growth factors including epidermal growth factor (EGF), vascular endothelial growth factor (VEGF), platelet-derived growth factor (PDGF), insulin-like growth factor-I (IGF-I) and insulin. Predominantly, signalling via RTKs controls mitogenesis and cell differentiation (Schlessinger et al., 1992). As a result, overactivity through excessive growth factor binding or overexpression of RTKs is often oncogenic (Rodrigues and Park, 1994). One of the most highly studied examples of signalling through RTKs is insulin signalling. Insulin, the major hormone controlling energy storage, controls a number of cellular processes required to optimise uptake and storage of circulating fuels through binding and activating its specific RTK (Avruch, 1998). The binding of ligands to these receptors induces receptor dimerisation and auto-phosphorylation of the kinase domain. This promotes the binding and subsequent phosphorylation and activation of secondary proteins. One example of an important protein that binds to phosphorylated RTKs is Ras. Ras is implicated in human cancers, with about 20 % of human cancers being due to mutations in this protein (Bos, 1989). Other well studied examples of signalling molecules regulated by RTKs include phospholipase C (PLC), phosphoinositide 3-kinase (PI3K) and mitogen-activated protein kinase (MAPK) cascades (Robinson et al., 2000).

A similar type of receptor having intrinsic enzyme activity and activation through receptor dimerisation are the receptor serine/threonine kinases. These receptors have a limited number of target proteins, the most studied of these being the SMADS. The SMAD proteins are homologs of both the *Drosophila melanogaster* protein, mothers against decapentaplegic

(MAD) and the *Caenorhabditis elegans* protein SMA. The name is a combination of the two. SMADS are transcription factors, which form complexes and migrate to the nucleus following phosphorylation by the activated receptor (Massagué and Wotton, 2000). The prototype superfamily of growth factors that activate serine/threonine kinase receptors are the transforming growth factor-$\beta$ (TGF-$\beta$) family, which exert a wide range of effects on a variety of cell types, for example they regulate cell growth, differentiation, matrix production and apoptosis. Many also have important functions during the development of embryos by influencing pattern formation and tissue specification (Heldin et al., 1997). The SMADs can act in a positive manner, transferring the signal from the receptor to the nucleus or in an inhibitory manner, by preventing this signal transfer. Some SMADS have been identified as being tumour suppressor genes and mutant SMADS have been identified in a significant proportion of both pancreatic and colorectal cancers (Padgett et al., 1998).

Other well known signalling pathways involve receptors that are linked to soluble protein kinases such as receptors linked to the Janus Kinases (JAKs). JAKs are tyrosine kinases that utilise the Signal Transduction and Activators of Transcription (STAT) pathways. The receptors activating JAK-STAT pathways are often activated by cytokines, predominantly to co-ordinate immune responses (O'Shea et al., 2002). Examples of such receptors include the interferon (IFN) family, the interleukin receptors and some RTKs.

Some ligand induced signalling does not require any additional activation of internal signalling cascades. For example some receptors also behave as ligand-gated ion channels, which open and close to allow the transport of ions across the plasma membrane. The prototypic ligand-gated ion channel is the nicotinic acetylcholine receptor (Dajas-Bailador and Wonnacott, 2004), which consists of a pentamer of protein subunits, with binding sites for acetylcholine. When bound, acetylcholine alters the receptor's configuration and causes an internal pore to open allowing $Na^+$ ions to flow down their electrochemical gradient into the cell. When the intracellular $Na^+$ concentration rises to the point at which the positive charge within the cell is enough to depolarise the membrane, an action potential is initiated. The main function of the acetylcholine receptor family is to transmit signals for the neurotransmitter acetylcholine at neuromuscular junctions and in the central and peripheral nervous systems, therefore this type of signalling is vital for neurological processes (Leonard and Bertrand, 2001). Ligand-gated ion channels are neurotransmitter receptors and are therefore important in the transmission of electric signals across junctions between nerve cells.

Calcium signalling represents yet another common signalling mechanism. Cytoplasmic calcium exerts many regulatory effects on enzymes and proteins within the cell (reviewed by Berridge, 1993). The most common signalling pathway that increases cytoplasmic calcium concentration is the PLC pathway. Many cell surface receptors, including G protein-coupled receptors (GPCRs) and RTKs activate the enzyme PLC. PLC hydrolyses the membrane

phospholipid phosphatidylinositol 4,5-bisphosphate ($PIP_2$) to form inositol triphosphate ($IP_3$) and diacylglycerol (DAG), two classical second messengers. DAG activates the protein kinase C (PKC) enzyme, while $IP_3$ diffuses to the sarcoplasmic/endoplasmic reticulum, binds to its receptor ($IP_3$ receptor), which is a $Ca^{2+}$ channel, and thus releases $Ca^{2+}$ from the endoplasmic reticulum. Ion channel receptors are also very important in calcium signalling. $Ca^{2+}$ ions are second messengers that can affect the activity of a number of target proteins and ligand-gated ion channels can function to regulate the intracellular $Ca^{2+}$ concentration.

In some instances, the receptor receiving the signal is not required to be on the plasma membrane. These intracellular receptors are transcription factors or enzymes, which become activated by binding to small, lipophilic ligands that can cross the plasma membrane and get inside the cell. Steroid hormones such as testosterone and cortisol are examples of such ligands, which activate intracellular receptors to induce a cellular response through altered gene expression (Evans, 1988). This type of signalling is common in cell development and differentiation.

## 1.2 G Proteins

Another very important type of signalling mechanism that is probably the most widely studied is whereby receptors are coupled to their intracellular target proteins via what is known as a guanine-nucleotide-binding protein (G protein). G proteins are very highly conserved components of signalling pathways, which behave as molecular switches to directly regulate a large number of cellular processes such as transplasma membrane signal transduction, cytoskeleton assembly, vesicle/protein transport and cell growth.

G proteins can be broadly characterised into two main groups; the monomeric G proteins and the heterotrimeric G proteins (Figure 1.1). The monomeric G proteins form part of the Ras superfamily, whilst the heterotrimeric G proteins are dissociable heterotrimer complexes comprising of G$\alpha$, G$\beta$ and G$\gamma$ subunits, of which the G$\alpha$ is the nucleotide-binding component (Oldham and Hamm, 2008). Heterotrimeric G proteins couple to membrane spanning receptors to transmit extracellular signals to the inside of the cell.

Both classes of G proteins bind the guanine nucleotides GDP and GTP and share common mechanisms of activation and de-activation. In an inactive state they are covalently bound to a single molecule of GDP. Activation is via the exchange of GDP for GTP and de-activation occurs via the hydrolysis of GTP, returning the protein back to the inactive GDP-bound state. Activation is a result of changing conformation of two switch regions in the G protein, dependent on its nucleotide-bound state. Exchange of GDP for GTP results in a stabilisation of the G protein-effector binding site as a result of interactions of the $\gamma$-phosphate of GTP and the conserved switch I and switch II regions of the protein (Sprang,

1997). This functionality is conferred by a ∼20 kDa G domain that is conserved across all G proteins (Lambright et al., 1994). In the case of the heterotrimeric G proteins this occurs on the G$\alpha$ subunit and activation of G$\alpha$ results in dissociation of the heterotrimeric complex.

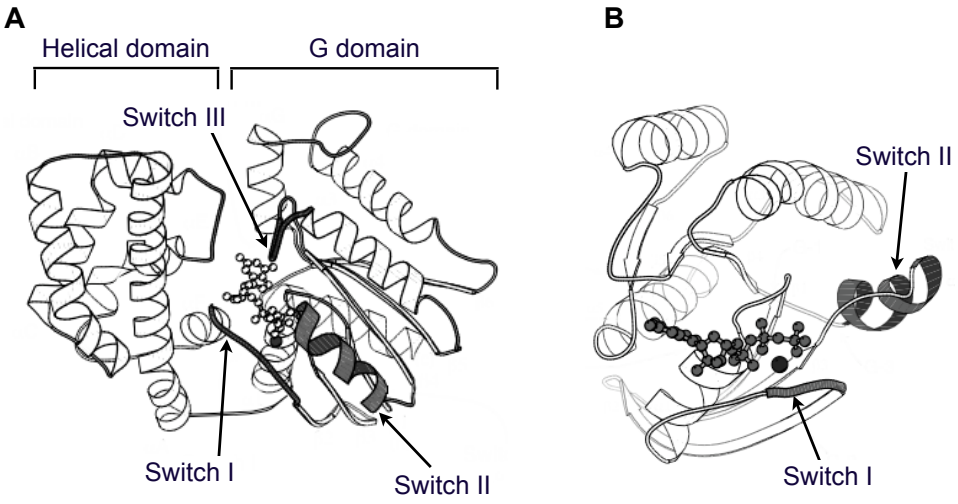


FIGURE 1.1: **Structural similarities between G$\alpha$ proteins and monomeric G proteins.** The ribbon diagrams represent the structure of a G$\alpha$ protein (G$\alpha_i$) (A) and a small monomeric G protein (Ras) (B). Both proteins are depicted in complex with a non-hydrolysable GTP analog, indicated in the form of a ball and stick model. The solid sphere represents the $Mg^{2+}$ cofactor of the two proteins. The switch regions are indicated in grey, and the G domain and Helical domain of the larger G$\alpha_i$ protein are highlighted. The G domain of G$\alpha$ proteins displays strong structural similarity to the monomeric G proteins, particularly with regard to the highly conserved switch regions. Figure adapted from Sprang, 1997.

### 1.2.1 Monomeric G Proteins

Some of the earliest monomeric G proteins to be identified were the p21 Ras oncogenes, a 21 kDa family of proteins that were found because of their activation in many human cancers (Gibbs and Marshall, 1989; Stites et al., 2007). The Ras superfamily is divided into five subfamilies (Ras, Rab, Rho, Ran and Arf) based on similarity in sequence and function (Wennerberg et al., 2005). All operate as GTPase switches in signal transduction pathways (Figure 1.2). Activation through the binding of GTP is facilitated through upstream guanine-nucleotide-exchange factors (GEFs). The downstream effectors have higher affinity for the GTP-bound configuration than for the GDP-bound form, therefore are activated when the G protein becomes GTP-bound. The signal is terminated when the $\gamma$ phosphate of the bound molecule of GTP is hydrolysed returning the G protein to its GDP-bound form. The majority of monomeric G proteins have intrinsic GTPase capability with the only exception to this being the Arf family (Randazzo and Kahn, 1994). Typically the

rate of this intrinsic hydrolysis reaction is slower than physiological responses would require, therefore rapid hydrolysis has to be achieved through GTPase-accelerating proteins (GAPs). Such proteins bind to monomeric G proteins through a highly conserved 'arginine finger', which inserts a catalytic arginine residue into the active-site causing the rapid hydrolysis of GTP (Scheffzek et al., 1997).

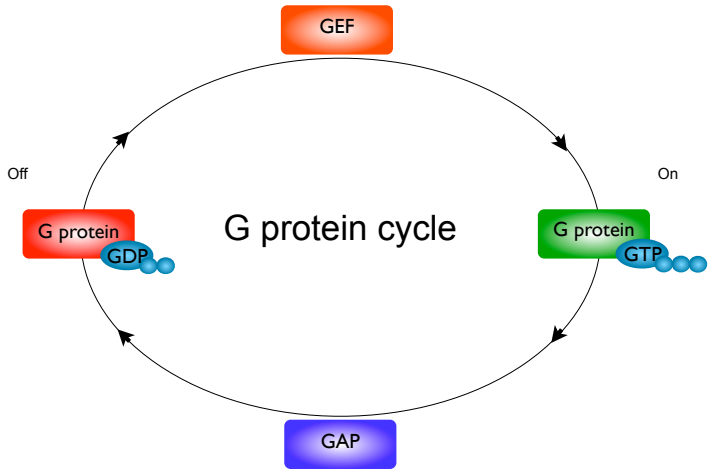


FIGURE 1.2: **Schematic of the G protein cycle.** The inactive GDP-bound 'off' state G protein undergoes guanine nucleotide exchange to become active and enter the GTP-bound 'on' state. This reaction can be accelerated through the interaction with a GEF. The GTP-bound protein can hydrolyse the $\gamma$ phosphate to return it to the GDP-bound 'off' state. This hydrolysis can be accelerated by interaction with a GAP.

### 1.2.2 Heterotrimeric G Proteins

When a heterotrimeric G protein has not been activated by a GPCR, the G$\alpha$ subunit is bound to a molecule of GDP. Upon agonist stimulation of the receptor, nucleotide exchange occurs on the G$\alpha$ subunit and GDP is replaced by the ~1,000 fold more abundant GTP. Switch regions I, II and III on the G$\alpha$ subunit undergo conformational change as a result of the nucleotide exchange event and this reduces the affinity of the G$\alpha$ for the G$\beta$ and G$\gamma$-subunits, causing dissociation of the G$\alpha$ from the G$\beta\gamma$-complex (Johnston and Siderovski, 2007; Sprang, 1997). These two subunits can then regulate the activity of effector proteins, thereby bringing about changes in cellular behaviour (Figure 1.3). Other studies have suggested an alternative mechanism in which dissociation of the G$\alpha$ and G$\beta\gamma$ subunits may not actually be required for downstream signalling (Bunemann et al., 2003; Wang et al., 2009). Instead, the receptor induces changes in the conformation of the G protein that exposes previously buried sites on the G$\alpha$ and G$\beta\gamma$ for interaction with respective effectors. A large number of different heterotrimeric G protein signalling molecules can be expressed within a cell at any given time, with human cells containing genes for at least 18 G$\alpha$ subunits, 5 G$\beta$ subunits and 12 G$\gamma$ subunits (Gilman, 1987).

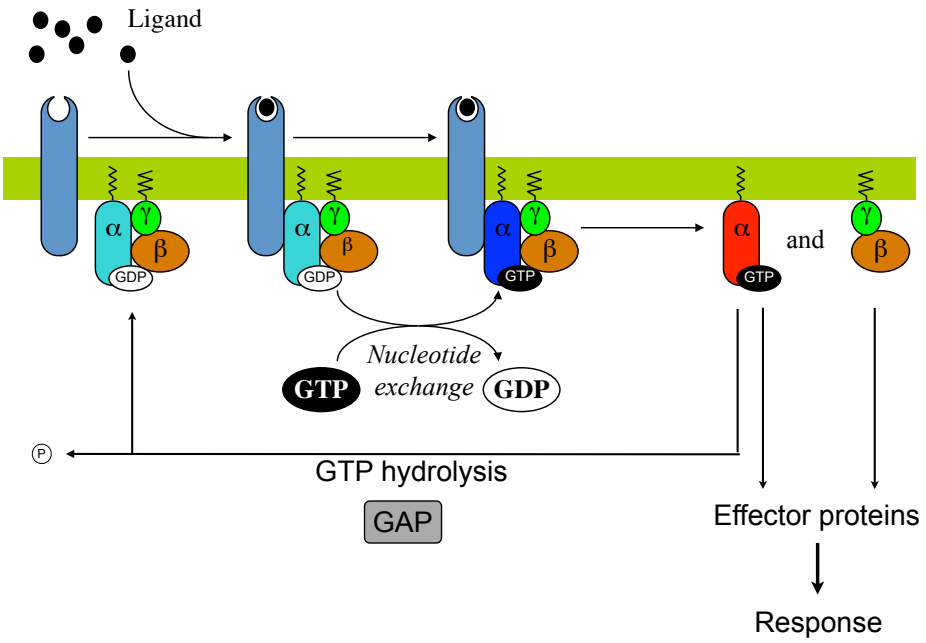


FIGURE 1.3: **Heterotrimeric G protein signalling.** Upon ligand binding to the receptor, nucleotide exchange occurs on the G$\alpha$ and GDP is replaced by GTP. This causes dissociation of the heterotrimer and activated G$\alpha_{\text{GTP}}$ and G$\beta\gamma$ are freed to activate downstream signalling pathways. The G$\alpha$ is switched off through the catalysis of GTP hydrolysis by a GTPase activating protein (GAP). GTP is hydrolysed back to GDP and the heterotrimer re-forms.

#### 1.2.2.1 Signal Transduction via G$\alpha$ Subunits

The type of G$\alpha$ subunit is generally what is used to classify the G protein heterotrimer (Neves et al., 2002), as the G$\alpha$ subunit is more commonly the signal propagator. The G$\alpha$ family of proteins share 45-80 % amino acid identity (Rens-Domiano and Hamm, 1995) and classification is based largely upon the effector molecules that it interacts with (Table 1.1).

| Family | Family Members | Common Role |
|---|---|---|
| G$\alpha_s$ | G$\alpha_s$ and G$\alpha_{olf}$ | Stimulate adenylate cyclase activity |
| G$\alpha_i$ | G$\alpha_i$, G$\alpha_o$, G$\alpha_t$ and G$\alpha_{gust}$ | Inhibit adenylate cyclase activity, phototransduction (G$\alpha_t$) |
| G$\alpha_q$ | G$\alpha_q$, G$\alpha_{11}$, G$\alpha_{14}$, G$\alpha_{15}$ and G$\alpha_{16}$ | Stimulate PLC-$\beta$ activity |
| G$\alpha_{12}$ | G$\alpha_{12}$ and G$\alpha_{13}$ | Rho family GTPase signalling |

TABLE 1.1: **G$\alpha$ protein family.** The four main classes of G$\alpha$ proteins, including family members and the main associated signalling role of each family.

The G$\alpha_s$ and G$\alpha_i$ families are responsible for regulating intracellular levels of cyclic adenosine monophosphate (cAMP) via the stimulation or inhibition of adenylate cyclase respectively (Taussig and Zimmermann, 1998). The G$\alpha_i$ family represent the most widely

expressed type of G$\alpha$ and have additional roles in the PLC pathway and in the opening of $K^+$ channels (Peleg et al., 2002). The G$\alpha_q$ family have important roles in the mobilisation of intracellular calcium via the production of $IP_3$ and DAG, which trigger the release of calcium from intracellular stores and the activation of PKC (reviewed by Neves et al., 2002). Finally, members of the G$\alpha_{12}$ family activate a variety of effectors, including phospholipase D, a $Na^+/H^+$ exchanger and nitric oxide synthase (reviewed by Wettschureck and Offermanns, 2005).

#### 1.2.2.2 Signal Transduction via G$\beta\gamma$ Subunits

The G$\beta\gamma$ subunits are also capable of activating a host of downstream effectors. The G$\beta$ subunit comprises of two domains, an N-terminal $\alpha$ helix and a $\beta$-propeller structure consisting of seven tryptophan-aspartate repeats (Lambright et al., 1996). The G$\gamma$ subunit interacts with G$\beta$ via an N-terminal helical domain to form the dimer. The G$\beta\gamma$ dimer has roles in localising the G$\alpha$ at the plasma membrane (Evanko et al., 2000) and also as signal transducers in a variety of signalling cascades (reviewed by Clapham and Neer, 1997). Downstream effectors for G$\beta\gamma$ include $Ca^{2+}$ channels, MAPKs, phospholipases, PI3 kinases and G protein-coupled receptor kinases (GRKs). The G$\beta\gamma$ dimer also has important roles in mediating the opening of inwardly rectifying $K^+$ (GIRK) channels primarily in neurons of the central nervous system (CNS) (He et al., 2002). In some cases both the G$\beta\gamma$ and the G$\alpha$ bind to the same effector molecule, thus generating competing or collaborative effects (Sunahara et al., 1996).

### 1.2.3 Post Translational Modifications and Localisation

Both monomeric and heterotrimeric G proteins can be post translationally modified, primarily to influence their localisation. The majority of monomeric G proteins are modified at their C-terminus by the addition of a hydrophobic prenyl group to promote membrane attachment. Prenylation occurs at a consensus CAAX (with A being any aliphatic residue) motif. In many cases the monomeric G proteins are also modified with a palmitoyl moiety upstream of the prenyl group (Wennerberg et al., 2005). The exceptions to this are the Ran and Arf family. Arf proteins are membrane associated, but do this through myristoylation (Donaldson, 2008). Ran proteins shuttle between the cytoplasm and the nucleus, regulating nuclear transport and are therefore not prenylated, but instead contain a DEDDDL motif promoting nuclear localisation to mediate interaction with nuclear proteins (Lui and Huang, 2009).

Heterotrimeric G proteins, being coupled to transmembrane receptors, must be targeted to the plasma membrane to allow receptor mediated signal transduction. Interaction with transmembrane receptors aids plasma membrane localisation, but G protein heterotrimers are also capable of membrane localisation in the absence of a receptor binding partner. Most

G$\alpha$ subunits are modified at their N-terminus by the covalent attachment of myristoyl and palmitoyl groups at consensus sequences in the protein. These modifications target the G$\alpha$ to the membrane. In addition, all G$\beta\gamma$ dimers are modified through the attachment of a prenyl group to the C-terminus of the G$\gamma$ subunit, promoting their membrane association (Evanko et al., 2000). The heterotrimer can then be assembled on the cytosolic face of the endoplasmic reticulum before it is transported to the plasma membrane (Marrari et al., 2007).

### 1.2.4 G Protein Mutations

Some common activating mutations in the amino acid residue sequence of both monomeric G proteins and G$\alpha$ subunits have been identified that can alter the protein's activity in terms of the protein's GTP binding/GTP hydrolytic cycle. As this GTPase cycle determines the on/off state, such mutations can have large impacts on cellular processes that are controlled by G protein signalling events. Two essential residues have been identified that are necessary for GTPase activity; an arginine ('arginine finger') found in either the Switch I domains of G$\alpha$ subunits or in the region contributed to by GAP binding of monomeric G proteins and a highly conserved glutamine residue in the Switch II region of both G$\alpha$ subunits and monomeric G proteins (Majumdar et al., 2006). Mutations in the arginine residue have been found to inhibit GTPase activity in G$\alpha_s$, resulting in constitutive activation of adenylate cyclase in human pituitary tumours (Landis et al., 1989). The glutamine residue has been found to be mutated in the small monomeric G protein Ras in many human tumours and the mutations are carried by some animal retroviruses (Landis et al., 1989; Der et al., 1986). Indeed, a variety of human tumours and diseases have been associated with mutations in either of these two residues in the G$\alpha_i$ and G$\alpha_s$ proteins (Landis et al., 1989; Weinstein et al., 1991). Post translational modifications by the bacterial exotoxin cholera toxin, catalyses the ADP ribosylation of residue $Arg^{201}$ of G$\alpha_s$, resulting in constitutive activation due to reduction of the intrinsic GTPase activity. Pertussis toxin ADP ribosylates a cysteine residue close to the carboxy-terminus of members of the G$\alpha_{i/o}$ family, resulting in uncoupling of these G proteins from their receptors (Birnbaumer et al., 1990). These actions are responsible for some of the clinical manifestations of *Vibrio cholerae* and *Bordetella pertussis* infection, respectively. A number of other human disease causing mutations have been identified in G proteins that effect the protein's activation/deactivation by interfering with the nucleotide exchange or by influencing heterotrimer formation, receptor binding or effector binding events (reviewed by Weinstein and Shenker, 1993).

## 1.3 GPCR Signalling

A wide variety of external signals are detected through the use of GPCR signalling pathways. GPCRs are a class of cell surface receptors, which are characterised by containing 7 trans-membrane (7TM) domains (Figure 1.4). The TM $\alpha$-helices are joined by intra- and extra-cellular loops of differing lengths. The N-terminal region is extracellular and a C-terminal tail extends into the cytoplasm. The GPCR superfamily of proteins is highly diverse and very large (Venter et al., 2001), with greater than 800 coding sequences found in the human genome alone (Fredriksson et al., 2003). They are extremely important and highly studied due to their implications in many human diseases and are estimated as being the target of ∼50-60 % of all modern drugs (Flower, 1999). GPCRs have a wide variety of ligands, including peptides, ions, amines, organic odorants, lipids, proteins, nucleotides, pheromones and photons. Ligand binding to an active extracellular site on the receptor is thought to allow interactions between TM3 and TM6 helices. Resulting conformational changes in TM6, expose interaction sites on the second (IC2) and third (IC3) intracellular loops, and allow the binding of a G protein via contacts with the C-terminus of $G\alpha_{GDP}$ (Ballesteros et al., 2001). Despite this large range of ligands, most GPCRs share a common signalling mechanism of coupling to, and activating G proteins, which propagate the signalling reaction (Pierce et al., 2002). Commonly, each GPCR couples to a heterotrimeric G protein complex consisting of a G$\alpha$ subunit and a G$\beta\gamma$ dimer (Figure 1.3).

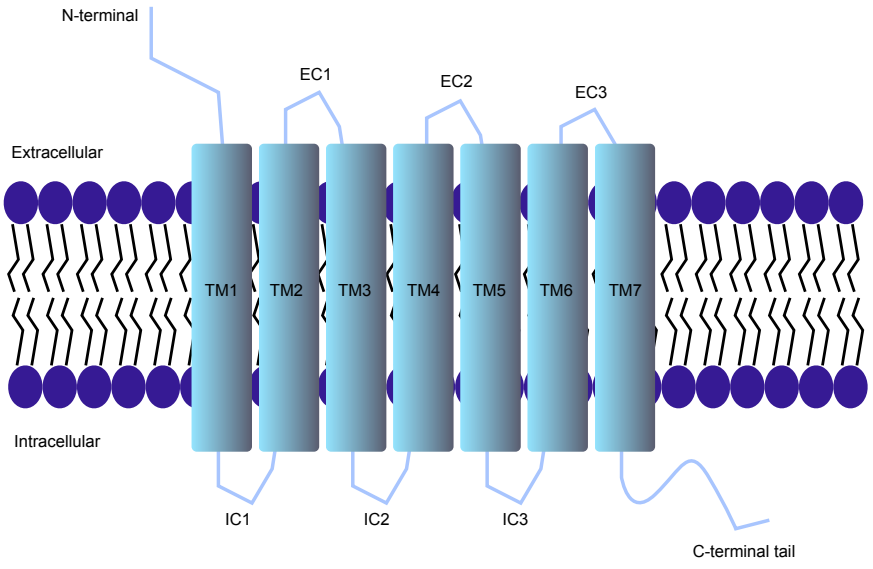


FIGURE 1.4: **Schematic of a GPCR structure.** G protein coupled receptors (GPCRs) are composed of seven transmembrane-spanning $\alpha$-helical regions (denoted TM1-7). Each transmembrane domain is connected by alternating intracellular or extracellular loop regions (denoted IC1-3 and EC1-3). GPCRs also contain an extracellular N-terminal region and an intracellular C-terminal region, which is thought to form an eighth helical region oriented along the plasma membrane.

GPCRs are classified based on residues and motifs contained within the N-terminal extracellular region (see Bockaert and Pin, 1999 for full classification). GPCRs are characterised into six groups. The Group I GPCRs contain receptors related to the prototypical GPCR rhodopsin and are the largest and most studied of the GPCR family. Such receptors are characterised by containing a highly conserved region of ~20 residues and predominantly bind to small ligands (van Rhee and Jacobson, 1996). The Group II family members are part of the secretin receptor family and are characterised by having large N-terminal domains, which bind large peptide ligands (Laburthe et al., 1996). Group III members have a large extracellular domain that is hinged to allow ligand binding (O'Hara et al., 1993). Group III receptors are related to the metabotropic glutamate receptor family. Group IV members are fungal mating pheromone receptors, group V members are cAMP receptors that control development in the slime mould *Dictyostelium discoideum* and group VI members are known as Frizzled/Smoothened receptors.

## 1.4 Regulation of G Protein Signalling

G protein-mediated signalling has to be tightly regulated in order to produce controlled cellular responses. The most crucial point of regulation is considered to be the nucleotide-bound state of the G proteins. The two crucial processes which control this are guanine nucleotide exchange by GEFs and intrinsic GTP hydrolysis catalysed by proteins with GAP activity, such as the regulators of G protein signalling (RGS) proteins. Whether the G protein is in the GTP or GDP-bound state, and for how long, is thought to determine the amount of signal that will be transmitted through the pathway (Ross, 2008). Additionally there are other regulatory mechanisms, many of which are common to most cellular signalling pathways. Additional levels of regulation can be applied by controlling the subcellular localisation of important signalling molecules such as the GPCR, the G proteins and associated regulatory proteins. Organisation of multi-protein complexes through scaffold proteins is also sometimes a requirement for GPCR signal transduction (Hall and Lefkowitz, 2002). Another example is receptor trafficking to the plasma membrane, which is important in controlling sensitisation and desensitisation to the ligand stimulus (Moore et al., 2007; Jean-Alphonse and Hanyaloglu, 2010).

### 1.4.1 RGS Proteins

An observation that the physiological rates of GTP hydrolysis observed *in vivo* were much faster than the rates observed *in vitro* indicated a probable involvement of accessory proteins (Vuong and Chabre, 1990). These proteins were later discovered to be the RGS family of proteins (Koelle and Horvitz, 1996). RGS proteins are capable of increasing the rates of intrinsic GTP hydrolysis on G$\alpha$ subunits by up to 2,000-fold (Hepler, 1999). RGS proteins

therefore, play a pivotal role in determining the strength and duration of a G protein signalling response.

The prototype RGS family protein, SST2 was identified in a screen on the budding yeast *Saccharomyces cerevisiae* searching for mutants that demonstrated supersensitivity to pheromone induced growth arrest, which is a GPCR mediated signalling response (Chan and Otte, 1982a,b). Since this finding, other RGS proteins were identified in a number of higher eukaryotes (reviewed by De Vries et al., 2000) with human cells containing genes for in excess of 30 different RGS proteins (Hill et al., 2006).

RGS proteins are defined by a highly conserved 120 amino acid domain known as the RGS-fold. This RGS-fold can accelerate GTP hydrolysis in two ways, either by stabilising the intermediate transition state of GTP hydrolysis (Berman et al., 1996) or by destabilising the active state. Hydrolysis is promoted by the RGS-fold contacting the three switch regions of the G$\alpha$ subunit, but no direct contacts are formed with the GTP molecule itself (Tesmer et al., 1997). Additionally to the RGS-fold, many RGS proteins contain other domains and motifs conferring functionalities additional to their well-characterised GAP activity.

#### 1.4.1.1 RGS Proteins as GAPs

The activity of RGS proteins as GAPs has been widely demonstrated through *in vitro* assays using recombinant proteins (De Vries et al., 2000), *in vivo* assays and using receptor/G protein/effector complexes reconstituted in vesicles (Hepler, 1999). RGS proteins can stabilise the transition state of GTP hydrolysis. Studies using the rat RGS4 in complex with G$\alpha_i$ demonstrated that this RGS protein stabilises the flexible regions of G$\alpha_i$ into a conformation resembling the transition state. This stabilisation is thought to lower the activation energy that is required for GTP hydrolysis (Tesmer et al., 1997).

#### 1.4.1.2 GAP-independent Activity

In addition to GAP activity, RGS proteins are known to be capable of G protein signalling regulation via other GAP-independent mechanisms. These mechanisms fall under the general term of effector antagonism. RGS proteins behaving as effector antagonists will compete with effector molecules for the binding to G$\alpha_{\mathrm{GTP}}$, therefore having a negative influence on signal transduction by limiting free G$\alpha_{\mathrm{GTP}}$ available for signal propagation. A number of RGS proteins have now been reported to act via effector antagonism. For example, RGS2, RGS3 and to a lesser extent RGS10 inhibited signalling by a constitutively active (GTPase-deficient) G$\alpha_q$ (Scheschonka et al., 2000). Some GRKs are known to contain RGS-fold domains (e.g. GRK2), but have little or no associated GAP activity, therefore effector antagonism could be the only and most important inhibitory mechanism (Carman et al., 1999). However, it is often unclear in any given circumstance whether RGS-mediated inhibition of signalling is through GAP activity and/or effector antagonism.

The physical interactions of RGS proteins with the G$\alpha$ subunits occurs via the switch regions in G$\alpha$. These regions are also involved in the binding of downstream effectors and G$\beta\gamma$ dimers. Given this, it is also possible that some RGS proteins can interact directly with the effectors themselves, possibly forming a G$\alpha$-RGS-effector complex. As an example, it has been shown that the GAP activity of RGS9 on G$\alpha_t$ is enhanced by potential binding to the phosphodiesterase-$\gamma$ (PDE$\gamma$) subunit and that is is possible for a complex of G$\alpha_t$-RGS9-PDE$\gamma$ to be formed (McEntaffer et al., 1999).

#### 1.4.1.3 RGS Proteins as GDIs

Some RGS proteins are also capable of signalling regulation by behaving as guanine nucleotide dissociation inhibitors (GDIs). This activity is conferred by the presence of a C-terminal GoLoco motif, which can bind selectively to inactive G$\alpha$ subunits to impede the release of GDP and therefore limit G protein activation. RGS12 and RGS14 are examples of such proteins found to act as GDIs in addition to having GAP activity for G$\alpha_i$ and G$\alpha_o$ respectively (Kimple et al., 2001). The presence of both an RGS domain and a GoLoco domain could enable the interaction with two G$\alpha$ subunits in a cooperative manner to more efficiently inhibit signal propagation.

#### 1.4.1.4 RGS Proteins as Positive Regulators

G proteins are active in their GTP-bound state and typically will only activate downstream effectors when in this G$\alpha_{\text{GTP}}$ conformation. Since RGS proteins enhance the return to the inactive G$\alpha_{\text{GDP}}$ conformation, they are commonly regarded as being negative regulators of signalling. However, in some cases the presence of RGS proteins in a signalling pathway has been suggested to have a positive effect on G protein signalling potentiation (Milligan, 1998). For example RGS4 accelerates the opening of G protein gated $K^+$ channels upon the addition of an agonist. This channel is regulated by a G$\beta\gamma$ effector and the argument is that the receptor and RGS cooperate to prime the G protein or the G$\beta\gamma$ subunits for rapid activation (Doupnik et al., 1997). One suggestion for how this is possible is that the GPCR-RGS interaction blocks the GAP activity (Wang et al., 2007). A more sophisticated explanation is that of kinetic scaffolding (Zhong et al., 2003), which describes that the rapid kinetics associated with GPCR-mediated GTP binding and GAP-accelerated hydrolysis allows greater interaction time between the G protein and the receptor than would be possible through normal diffusion (Ross, 2008). A convincing example of an RGS protein being capable of behaving as a positive regulator is proposed in the mating-response of fission yeast (Smith et al., 2009). Here GTP hydrolysis on the G$\alpha$ catalysed by Rgs1 is demonstrated to be required to achieve maximal signalling response.

#### 1.4.1.5 Mammalian RGS Proteins

Being key regulators of a variety of signalling cascades governing important cellular processes, RGS proteins have been implicated in a number of disease states, including congestive heart failure and cardiac hypertrophy (Zhang et al., 1998), morphine addiction (reviewed by Garzón et al., 2005) and multiple different cancers (reviewed by Hurst and Hooks, 2009).

Mammalian RGS proteins are classified based on amino acid sequence identity within the RGS-fold and the additional domains and motifs that they contain. Common additional motifs identified that contribute to interactions forming signalling complexes include the G protein gamma subunit-like (GGL) domain and the PDZ domain (an acronym combining the first letters of three proteins that share the domain; post synaptic density protein (PSD95), Drosophila disc large tumor suppressor (Dlg1), and zonula occludens-1 protein (zo-1)). Another common domain is the DEP domain (named because of their original identification in the three proteins Dishevelled, EGL-10 and Pleckstrin) (Ponting and Bork, 1996). The GGL domain has roles in complex formation by binding to G$\beta$5 subunits (Snow et al., 1998), whilst PDZ and DEP domains confer specific functions and contribute to interactions forming signalling complexes. The PDZ domain plays a role in the organisation of protein complexes on the membrane through binding to consensus C-terminal motifs in target proteins (reviewed by Craven and Bredt, 1998). DEP domains consist of ∼90 conserved amino acid residues and are implicated in membrane localisation (Wong et al., 2000) and GPCR-RGS interactions (Kovoor et al., 2005) (reviewed by Chen and Hamm, 2006). The RGS superfamily of proteins is divided into five subfamilies; RZ, B/R4, R7, R12 and RA (Figure 1.5).

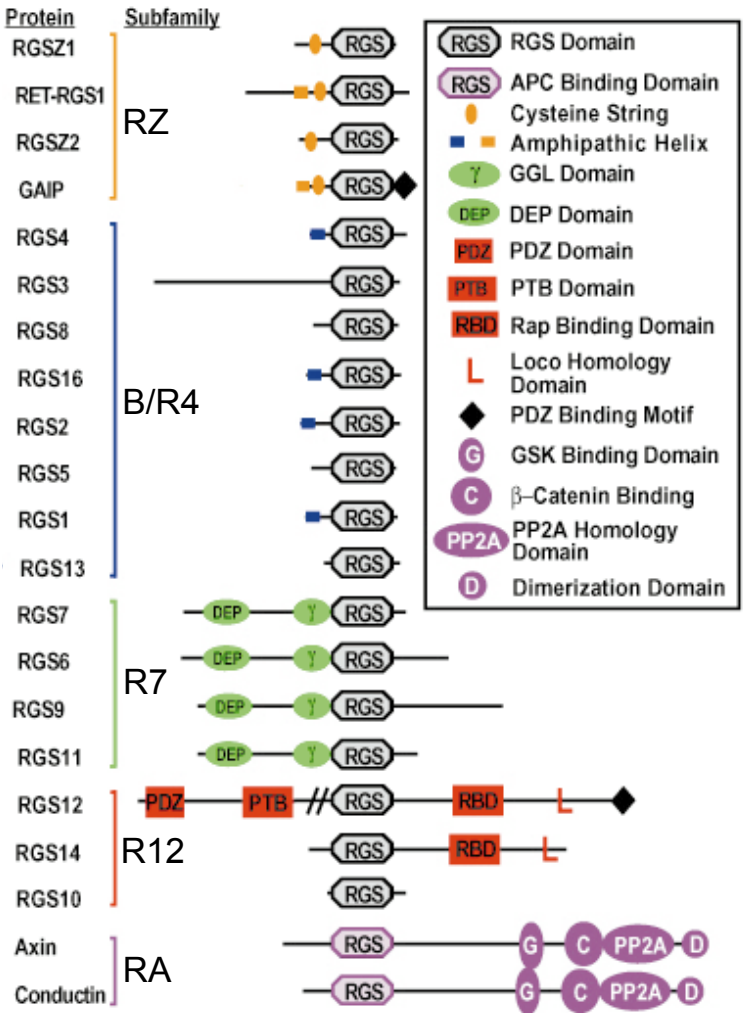


FIGURE 1.5: **RGS protein families.** The five RGS subfamilies are characterised by amino acid sequence similarity of the RGS-fold and the presence of additional domains and motifs. The families are named RZ, B/R4, R7, R12 and RA, although alternative nomenclatures are sometimes used. Figure adapted from (Ross and Wilkie, 2000)

The most studied of the mammalian RGS subfamilies is the B/R4 family, which is the simplest of all the RGS subfamilies. The B/R4 subfamily are ideal candidates for the study of action of the conserved RGS-fold as they consist of little more than this domain, with the only exception being RGS3, which has extended length compared to the other B/R4 members (reviewed by Bansal et al., 2007). The short amphipathic helix regions found in some of these subfamily members has been implicated as having roles in interaction with the plasma membrane and numerous other signalling components to give these simple RGS proteins some added selectivity for interaction with receptors and G proteins (reviewed by Neitzel and Hepler, 2006).

### 1.4.2 AGS Proteins

Additional regulatory proteins have been identified by functional yeast-based screens for receptor-independent activation of G protein signalling (Blumer et al., 2007). Such regulators were named activators of G protein signalling (AGS) proteins due to their ability to activate heterotrimeric G proteins independently of any receptor activity. Studies on this unexpected mode of regulation are of particular interest for possible therapeutic intervention to target heterotrimeric G proteins directly, bypassing the cell surface receptors in a similar manner to therapeutic interventions proposed for RGS proteins (Cho et al., 2004). AGS proteins have been grouped based on function, rather than sequence similarities and there are three distinct groups determined by their mechanism of G protein activation. Group I AGS proteins function as GEFs in a similar manner to GPCRs, promoting exchange of GDP for GTP on the G$\alpha$ subunit and can therefore be antagonised by GTP hydrolysis promoting RGS proteins. Group II and III AGS proteins activate by influencing G protein subunit interactions rather than nucleotide exchange. Group II contain G protein regulatory (GPR) motifs and bind preferentially to G$\alpha_{GDP}$, whilst group III AGS proteins bind to the G$\beta\gamma$ dimer. Both of these mechanisms promote the dissociation of the heterotrimer and hence activation of downstream effectors (Blumer et al., 2005).

### 1.4.3 G Protein Coupled Receptor Kinases

GRKs can regulate signalling by specifically phosphorylating agonist occupied or activated GPCRs (reviewed by Pitcher et al., 1998). Phosphorylation of the receptor by GRKs has roles in the impairment of receptor signalling and in desensitisation to ligand. Phosphorylation results in the receptor being specifically targeted to bind to cytoplasmic inhibitory proteins known as arrestins. Arrestins block GPCR binding to G proteins via two mechanisms. Firstly, arrestin binding to the cytoplasmic tip of the GPCR obstructs the binding site for the heterotrimeric G-protein, preventing its activation (desensitisation). Secondly, arrestins provide a link between the receptor and elements of the internalisation machinery, clathrin and clathrin adaptor, which promotes receptor internalisation via coated pits and subsequent transport to internal compartments, called endosomes (Von Zastrow and Kobilka, 1992). There are seven mammalian GRKs, which all contain an N-terminal domain that is homologous to the RGS-fold domain of the RGS protein family. Despite the presence of RGS domains, GAP activity of GRKs has not been demonstrated and the role of this domain in GRKs is poorly understood. Despite the lack of GAP activity, the RGS domains may be required for selectivity of interaction with certain G$\alpha$ subunits (Hepler, 1999).

### 1.4.4 Spatial Regulation

Additional levels of regulation can be imposed by the subcellular distribution of signalling components within the cell. Protein-protein interaction specificity requires that the interacting partners be localised in close proximity to each other within the cell, therefore altering spatial distributions of such proteins can influence signalling activity. Indeed, previous studies have shown that heterotrimeric G proteins can localise to internal membranes in addition to plasma membranes and are thought to play a role in vesicular transport along the exocytic pathway. G$\alpha$ subunits have been shown to localise to the Golgi in exocrine rat pancreas, independently of their G$\beta\gamma$ binding partners, suggesting that in some cases G$\alpha$ subunits reside in internal membrane structures in their active GTP-bound form (Denker et al., 1996).

Altered subcellular localisation of regulatory proteins such as proteins with GAP activity to attenuate the signal following activation, can provide another level of regulation. Many RGS proteins show subcellular distribution patterns that are likely to affect specificity. Sometimes the distribution is constant, whereas other times it is dynamic to regulate interactions with the G protein and also other signalling components. Despite being regulators of G protein signalling, and therefore interacting with signalling molecules that commonly reside in a plasma membrane localisation, many RGS proteins have been found to be localised to the cytosol and the nucleus (Willars, 2006). Controlling membrane localisation of RGS proteins is therefore another mechanism for signalling regulation and many cellular mechanisms contributing to RGS membrane targeting have been identified. Plasma membrane recruitment of RGS can in some cases occur as a result of G protein activation, as has been shown to be the case for RGS4 (Druey et al., 1998; Dulin et al., 1999). In other cases, for example with RGS2, purely the enhanced expression of specific un-activated G$\alpha$ subunits or GPCRs is sufficient to promote plasma membrane localisation (Roy et al., 2003). Other cellular mechanisms for placing RGS proteins near their target G proteins include putative intrinsic transmembrane spans (RET-RGS1) (Faurobert and Hurley, 1997), post-translational lipid modifications such as palmitoylation to assist subcellular targeting (RGS-GAIP and RGS4) (De Vries et al., 1996) and domains essential for electrostatic interactions with membrane lipids (such as in RGS4) (Srinivasa et al., 1998). Additionally, scaffolding proteins that assemble RGS proteins in complexes with receptors and target G proteins have also been proposed (Hepler, 1999).

Novel mechanisms have also been suggested for regulation of G$\alpha$ signalling by the segregation of GAPs from G$\alpha$ in clathrin-coated pits or membrane microdomains. For example, following agonist activation of the $\delta$-opiod receptor (DOR), it and its associated G$\alpha_i$ move together into clathrin-coated pits where they encounter the GAP for G$\alpha_i$ to attenuate signalling (Elenko et al., 2003). Additional mechanisms controlling subcellular localisation of G protein signalling regulatory proteins such as RGS and AGS proteins may involve

protein-protein or protein lipid interactions that are themselves regulated by a variety of mechanisms, possibly including post-translational modifications. Some RGS proteins are capable of direct interactions with specific GPCRs, which could provide additional control over plasma membrane targeting of the RGS to facilitate interaction of RGS with its target G protein.

### 1.4.5 GPCR-RGS Interaction

Studies have shown that RGS proteins are capable of selectively inhibiting signalling of the same G$\alpha$ subunit depending on the GPCR that they are coupled to. This implies mechanisms for RGS to selectively bind to specific GPCRs (extensively reviewed in Abramow-Newerly et al., 2006). Specific GPCR-RGS interaction is also supported by evidence for some RGS proteins showing selective association with the plasma membrane when co-expressed with different GPCRs (Roy et al., 2003).

An example is RGS12, which contains an N-terminal PDZ domain, a domain found in a growing list of diverse signalling proteins that enables recognition of specific binding motifs found at the C-terminus of target proteins (Ponting et al., 1997). Many GPCRs contain such PDZ binding motifs within their C-terminus (Snow et al., 1998). Screening receptor C-termini revealed that RGS12 binds via its PDZ domain to a specific binding motif only on the interleukin 8B receptor. This observation suggests that cells could determine specific RGS-G$\alpha$ interactions through RGS association with specific receptors, rather than specific G proteins.

Specific domains, namely the DEP domain within RGS proteins have been shown to interact directly with internal loop regions (Sandiford and Slepak, 2009) and the intracellular C-terminal tail of GPCRs to promote selectivity of RGS activity (Ballon et al., 2006). For example the RGS9-2 DEP domain directs this protein towards the D2 dopamine receptor but not the M2 muscarinic receptor (Kovoor et al., 2005). The *S. cerevisiae* RGS protein SST2, interacts with the C-terminal tail of its cognate receptor STE2 via DEP domains present in its N-terminus (Ballon et al., 2006) and RGS2 shows selectivity by binding directly to the IC3 loop of the M1 muscarinic acetylcholine receptor (Bernstein et al., 2004). The association between GPCR and RGS protein enables RGS to be in close proximity to its substrate the $G\alpha_{GTP}$ that is coupled to the receptor at the plasma membrane. This may therefore be important for ensuring limited spontaneous G protein signalling and rapidly attenuating ligand induced signalling response. Additionally, phosphorylation events on some GPCRs such as the *S. cerevisiae* STE2, have been implicated as influencing the interaction by the blocking of RGS binding (Ballon et al., 2006). The molecular mechanisms for DEP domain mediated specificity remain poorly understood. SST2 for example has two DEP like domains, which poses the questions of whether just one is sufficient for GPCR interaction or possibly a single RGS is capable of interaction with a GPCR dimer.

## 1.5 GPCR Signalling in Yeast

The investigations into G protein-mediated signalling are often hampered within mammalian systems by the large number of components and crosstalk between different pathways. As a result of this, the combinatorial complexity makes it very difficult to interpret experimental data from mammalian GPCR signalling systems. Yeast present an attractive alternative in which to analyse individual G protein signalling pathways (Ladds and Davey, 2004). Mechanisms in yeast are similar to those in higher eukaryotes, but there are much fewer components and they can be easily manipulated.

The experimentally tractable budding yeast *S. cerevisiae* has been extensively used as a model organism to investigate GPCR signalling. *S. cerevisiae* has two GPCR signalling pathways; one for glucose-sensing and one for mediating a pheromone response during the mating process (Versele et al., 2001). Investigations have primarily focused on the pheromone induced GPCR signalling pathway and have made a number of significant contributions to our overall understanding of GPCR signalling. The G$\beta\gamma$ subunits were proven to be capable of activating signalling cascades in addition to the G$\alpha$ subunit (Whiteway et al., 1989). The first RGS proteins were identified and subsequently analysed (Dohlman and Thorner, 1997). AGS proteins were also shown to be capable of ligand-independent activation of signalling (Cismowski et al., 1999). It was also shown that many of the *S. cerevisiae* components could be functionally replaced with the mammalian counterparts, allowing analysis of the mammalian proteins in a much simpler, less crowded background. Mammalian GPCRs (Dowell et al., 2002), G$\alpha$ subunits (Minic et al., 2005), G$\beta$ subunits (Ajit and Young, 2005), RGS proteins (Li et al., 2004) and AGS proteins (Cismowski et al., 1999) have all been functionally expressed in the budding yeast pheromone-response pathway. This replacement approach has also been successfully used to couple non-yeast GPCRs to the pheromone response pathway in reporter strains, therefore providing a system for high-throughput screens of ligands (Ladds et al., 2005b). One issue with using *S. cerevisiae* to investigate GPCR signalling is that the G$\alpha$ subunit, which is commonly the signal propagator in mammalian systems, behaves as a negative regulator through binding the signal propagator G$\beta\gamma$. As a result of this, the regulatory effects on the pathway output by components altering the GTPase activity of the G$\alpha$ will qualitatively differ from those in a system where G$\alpha$ is the signal propagator. GPCR signalling in *S. cerevisiae* is therefore more suited to investigations into G$\beta\gamma$ signalling rather than G$\alpha$ signalling.

An alternative yeast GPCR signalling system is the pheromone-response pathway within the distantly related fission yeast *Schizosaccharomyces pombe*. In this GPCR signalling pathway it is the G$\alpha$ subunit which propagates the signal in response to pheromone induced GPCR activation. *S. pombe* exist as haploid cells of two separate mating types (M-type and P-type), but under conditions of nutrient limitation, they undergo a process of conjugation

that is initiated by the reciprocal exchange of pheromones (Davey, 1998). Pheromone (P-factor) secreted by the P-type cells is detected by mating type specific GPCRs on cells of the opposite mating type, which leads to the activation of a G$\alpha$ subunit (Gpa1), which then propagates the mating-response (Ladds and Davey, 2004). Mating-response is generated in the same manner in P-type cells, through the recognition of M-factor secreted by the M-type cells. With the exception of the ligand and GPCR, the signalling components are identical in each mating type cell.

The signalling response to pheromone stimulus can be quantified in *S. pombe* with the use of reporter strains that have been engineered such that the pheromone inducible serine carboxypeptidase gene (*sxa2*) open reading frame (ORF) is replaced with a quantifiable reporter gene. Sxa2 is a serine carboxypeptidase, expression of which is increased in response to P-factor stimulation. It is secreted from the cell to degrade extracellular P-factor by digestion at its C-terminal leucine residue as one of the cells mechanisms of recovery from stimulation (Ladds et al., 1996a; Ladds and Davey, 2000). As a result, it is a suitable candidate for replacement in creation of reporter strains, as such reporters will have markedly increased transcription in response to P-factor and will allow for a prolonged signalling response. Previously, reporter strains have been created through replacement of *sxa2* with either *lacZ*, encoding $\beta$-galactosidase (Didmon et al., 2002) or a fluorescent reporter gene (Smith *et al.*, in preparation). This results in the reporter being under the control of the pheromone inducible promoter for *sxa2*. A quantitative readout of signalling can then be obtained in terms of either $\beta$-galactosidase activity or fluorescence intensity. The resulting pattern of reporter gene expression is very similar to that of *sxa2* (Didmon et al., 2002).

## 1.6 Fission Yeast as a Model Organism

Fission yeast provides an ideal model eukaryotic cell system for the study of cellular processes. Signalling components are utilised that show a high degree of conservation to those in higher eukaryotic systems, therefore information obtained from such a model organism is often transferrable. Yeast cells have relatively simple signalling cascades that are utilised to sense environmental changes and facilitate appropriate cellular responses. Their genetic tractability allows manipulation of selected genes that encode components of signalling systems and the introduction of reporter constructs to obtain quantifiable readouts of signalling response. Reporters can include auxotrophic markers to allow growth-based assays, enzymes such as $\beta$-galactosidase to allow enzymatic activity assays and more recently Green Fluorescent Protein (GFP) (Smith *et al.,* in preparation) and luciferase (Nilsson, unpublished data) to allow fluorescence and bioluminescence assays. Fission yeast *S. pombe* has been extensively utilised to study cell signalling events. Applications have included the

study of GPCRs, heterotrimeric G proteins, MAP kinase cascades, cellular variation and ligand screens for novel therapeutic compounds (reviewed by Ladds et al., 2005b).

### 1.6.1 Nutrient Sensing

Being capable of sensing environmental nutrients is key to the survival of a unicellular organism such as *S. pombe*. Additionally, for *S. pombe* cells, nutrient sensing plays an important role in the regulation of mating. Glucose-sensing is via the binding of extracellular glucose molecules to the GPCR Git3. This binding event results in signal propagation through the activation of the G$\alpha$ subunit Gpa2 of the associated heterotrimeric G protein (Welton and Hoffman, 2000). $Gpa2_{GTP}$ stimulates activation of the adenylate cyclase Cyr1, which catalyses the conversion of ATP -> cAMP, thus increasing the concentration of cAMP within the cell (Ivey and Hoffman, 2005). The increase in cAMP levels stimulate cAMP-dependent protein kinase (PKA), which results in the inhibition of the production of Ste11, a multiply phosphorylated transcription factor involved in regulating many genes (reviewed by Davey, 1998), including the genes required for sexual development (Maeda et al., 1990). As a result, when glucose concentration is sufficient, cells will continue to grow and divide by mitotic fission.

Under conditions of nutrient limitation, the stimulation of Cyr1 activity is lost, hence the cellular concentration of cAMP falls through its conversion into AMP by the phosphodiesterase Cgs2 (Hoffman et al., 2005). As a result the inhibition of sexual development through PKA activity is also lost resulting in the expression of the transcription factor Ste11. Ste11 initiates the transcription of a number of genes required for the mating-response, therefore when nutrients are low, cells will arrest and initiate a mating-response.

In the *sxa2* replacement transcriptional reporter strains, the *cyr1* gene is removed, thus preventing these cells from expressing adenylate cyclase. This modification renders the cells perpetually susceptible to stimulation by pheromone (Kawamukai et al., 1992; Maeda et al., 1990). The advantage of this modification is that nutritional deprivation is not required to induce a measurable response through the mating-response pathway.

### 1.6.2 The Mating-response

In nutrient rich conditions during mitotic growth, *S. pombe* divide by binary fission when the cell has reached a critical length. When cells are starved of nutrients, both M and P cells produce diffusible pheromones; M cells expressing M-factor and P cells producing P-factor. The M cells also express the GPCR Mam2, for detection of P-factor (Kitamura and Shimoda, 1991), whilst the P cells express the GPCR Map3, for detection of M-factor (Tanaka et al., 1993). Both of these pheromone receptors couple to the same G$\alpha$ subunit Gpa1 (Obara et al., 1991). The receptors are activated by the binding of pheromone from

the opposite mating partner, resulting in arrest of the cell cycle, polar growth towards the source of the pheromone, subsequent fusion of the opposite mating types followed by meiosis and sporulation (reviewed by Davey, 1998) (Figure 1.6).

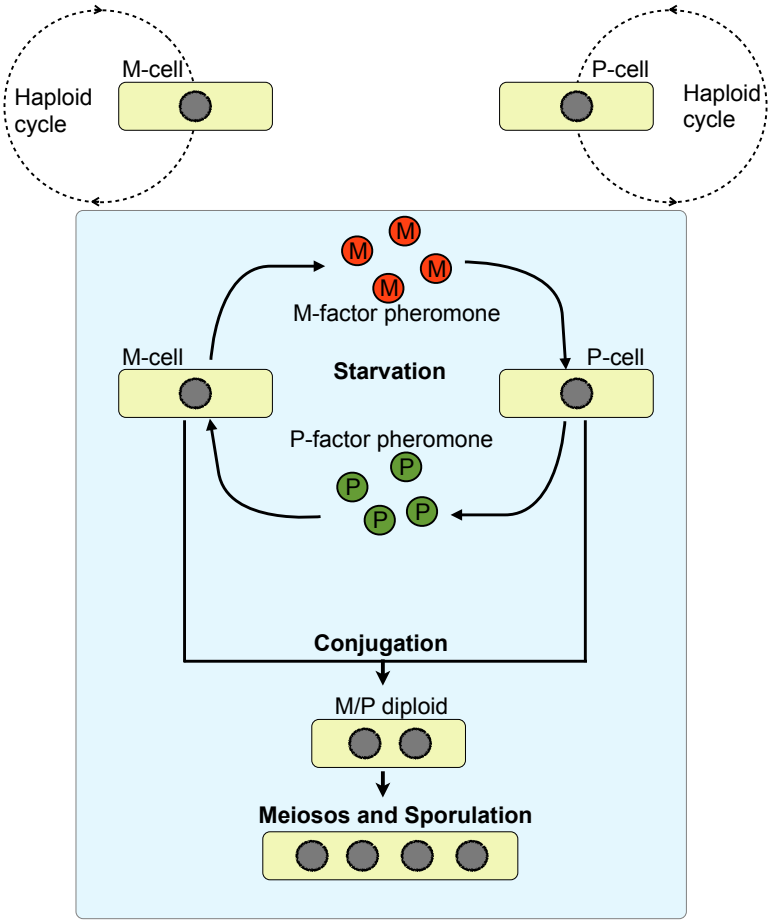


FIGURE 1.6: **Mating in *S. pombe*.** Under non-nutrient limiting conditions, *S. pombe* exists as haploid cells of two mating types; M-cells and P-cells and undergoes replication by mitotic fission. When starved of nutrients, cells of the opposite mating type secrete mating-type specific pheromones. Pheromone is detected by cell surface receptors and triggers cellular responses resulting in chemotropic growth towards the opposite mating partner, conjugation to fuse cells and subsequent meiosis and sporulation.

A requirement for mating to occur is that cells are maintained in a haploid state such that they can fuse to form the diploid zygote. As a consequence, the detection of pheromone by the opposite mating type promotes arrest of cells in $G_1$ phase of the cell cycle, when they contain a single copy of the genetic material. This process is complex, as the initial condition (starvation of nutrients), which is required for the pheromone induced mating-response, is also able to arrest cells in $G_1$ phase. A solely pheromone-dependent cell cycle arrest can, however, be observed through perturbing the nutritional sensing through deletion of the *cyr1* gene (Davey and Nielsen, 1994).

Initiation of the mating-response signalling pathway is via the binding of pheromone to the cell surface GPCRs (Mam2 or Map3). This binding event triggers the activation of Gpa1 through guanine nucleotide exchange, converting $Gpa1_{GDP}$ to $Gpa1_{GTP}$. The GTP-bound Gpa1 activates the downstream small monomeric G protein Ras1 via an as yet undetermined mechanism, although it is likely to involve Ste6, as this protein has been shown to be required for Ras1 activation in response to pheromone (Hughes et al., 1990). Being a small monomeric G protein, Ras1 is activated and deactivated in a similar manner to Gpa1. Activation of Ras1 is via a GEF (Ste6 the likely candidate) and is deactivated through GTP hydrolysis, catalysed by a protein with GAP activity, Gap1 (Imai et al., 1991). Ras1 provides a branching point in the pathway, with activated Ras1 being able to activate two different downstream response pathways.

One pathway involves activation of a MAP kinase cascade via the promotion of the MAPKKK Byr2 to the plasma membrane (Bauman et al., 1998) where it becomes activated. Precise details of this activation are unclear, but it is likely to involve two other proteins; the p21-activated kinase (PAK) Shk1 and Ste4 (Marcus et al., 1995; Barr et al., 1996). Previous studies have shown that interaction between Shk1 and Byr2 are effective at promoting the formation of the active Byr2 conformation (Tu et al., 1997). It is thought that Ste4 is required for stabilisation, or further activation of Byr2, as it acts upstream of Byr2 and interacts at a different site to Ras1, suggesting that both Ras1 and Ste4 can interact with Byr2 independently (Barr et al., 1996). Two other proteins; rad24/25, which are homologous to mammalian 14-3-3 proteins, have been shown to have a negative impact by restricting plasma membrane translocation of Byr2 and are therefore in competition with Ras1 in terms of controlling Byr2 localisation and subsequent activation (Ozoe et al., 2002). Once activated at the plasma membrane, Byr2 phosphorylates the MAPKK Byr1, which then phosphorylates the MAPK Spk1 (Toda et al., 1991). Spk1 has been shown to localise to the nucleus and activates the transcription factor Ste11 via phosphorylation (Kjaerulff et al., 2005). Ste11 is part of a group of chromosomal proteins known as high mobility group (HMG) transcription factors. Such proteins are thought to play a role in human disorders such as benign tumor formation (Rajeswari and Jain, 2002). Ste11 binds to a 10bp T-rich (TR) consensus sequence (TTCTTTGTTY) present in the promotors of the genes required for sexual differentiation, therefore initiating expression of genes required for mating (Sugimoto et al., 1991) (Figure 1.7).

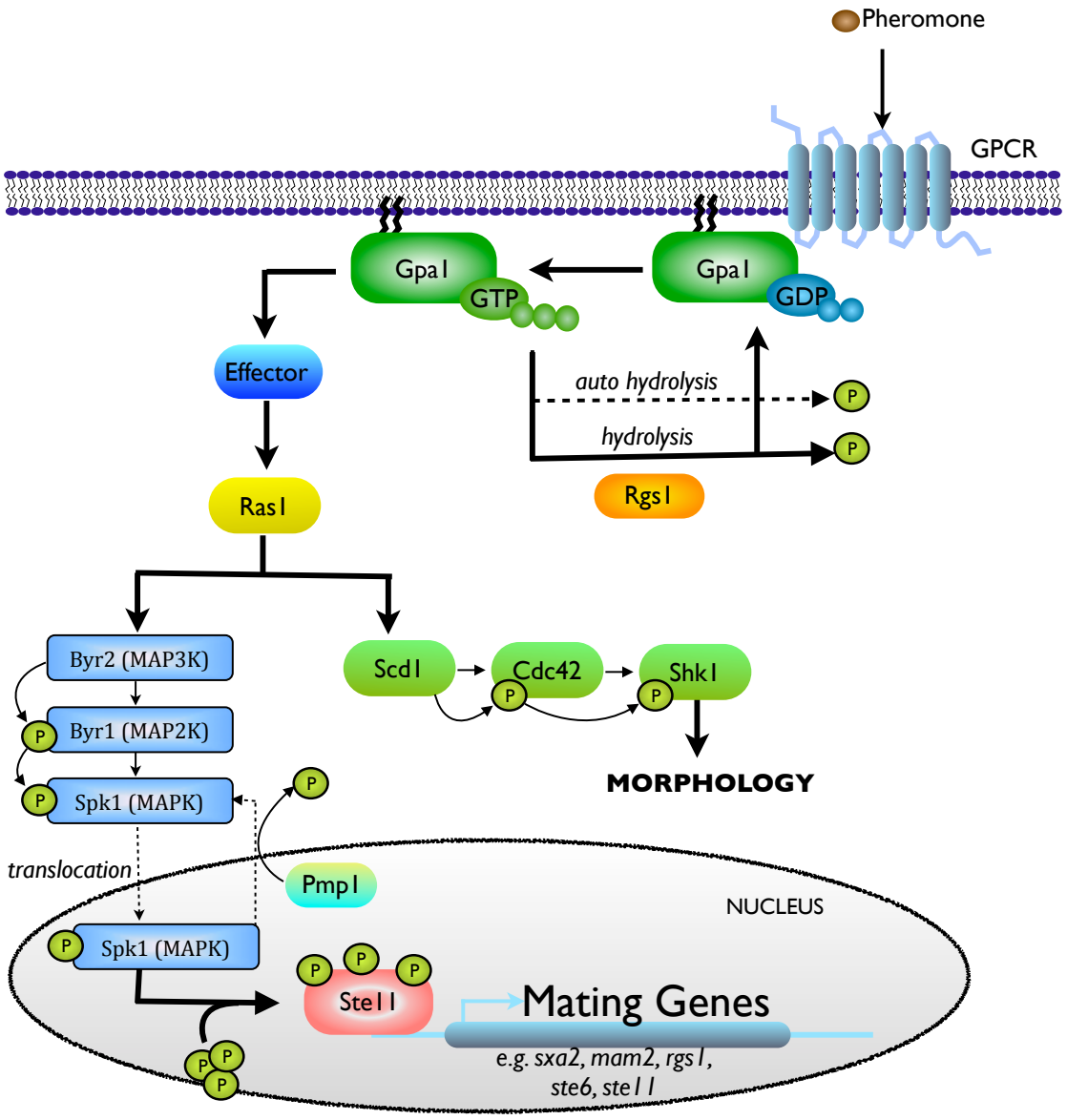


FIGURE 1.7: **Pheromone-response pathway.** Mating responses are initiated by the binding of the mating pheromones to receptors on the surface of target cells; P-factor pheromone binds to a 7-span receptor; Mam2 on the cell surface that is coupled to the G$\alpha$ subunit; Gpa1. Pheromone stimulation leads to the formation of $Gpa1_{GTP}$. The effector(s) that link active $Gpa1_{GTP}$ to activating Ras1 are still to be determined. One target downstream of the effector(s) is the mitogen-activated protein (MAP) kinase cascade comprised of Byr2 (a MAP kinase kinase kinase (MAP3K)), Byr1 (a MAP2K), and Spk1 (a MAPK). Substrates of Spk1 include the Ste11 transcription factor that regulates the expression of proteins required for mating. Pmp1 is a phosphatase that negatively regulates Spk1 by dephosphorylation. $Gpa1_{GTP}$also activates a second signalling pathway, by activation of Scd1, a protein which is involved in controlling cell morphology. Both the transcription and morphology pathways are mediated by Ras1. Signalling is terminated within these cells by the action of a number of proteins including Rgs1, a GTPase-activating protein (GAP) for Gpa1. Pheromone inducible *sxa2* can be replaced with either *lacZ* or a gene encoding a fluorescent protein to generate yeast strains for quantitative measuring of the pheromone response.

The second pathway downstream of active Ras1 controls a morphology response to the pheromone stimulation that is essential for the fusion of mating partners. This occurs via the activation of another effector for Ras1; Scd1, which is a GEF for the Rho-like monomeric G protein Cdc42 (Rincon et al., 2007; Onken et al., 2006). Activated Cdc42 can then activate the downstream Shk1 protein (Marcus et al., 1995). The target for Shk1 is Tea1, which acts at the cell tip to regulate microtubule dynamics and recruit tip proteins to the poles forming a complex known as a polarisome, which is required for recruitment of actin to the cell ends and therefore controls cell elongation. The pheromone induced activation of this pathway results in a morphology response in the form of elongation of the cell towards its mating partner, forming what is referred to as a shmoo (Davey et al., 1995) (Figure 1.7).

### 1.6.3 Regulation of The Mating-response

As is the case with many signalling mechanisms, the extent of the signalling response is regulated at various points in the signalling pathway through the action of proteins that regulate the amplitude, timing and recovery from the response. Cells must be capable of adapting to high levels of stimulation for subsequent cellular processes to continue. In the case of *S. pombe* M cells, one such mechanism of adaptation to high levels of P-factor pheromone is to express Sxa2 in order to remove the extracellular P-factor by degradation. Sxa2 is important for the recovery of the mating-response, allowing cells that do not mate to return to vegetative cell growth (Davey and Nielsen, 1994; Imai and Yamamoto, 1992).

Another mechanism of adaptation to extracellular stimuli is through the removal of cell surface receptors, therefore preventing further stimulation. Receptor internalisation in *S. pombe* has not been previously described, but GPCRs in general are known to be internalised via receptor phosphorylation events (Ferguson, 2001). A number of possible sites for phosphorylation have been identified on the C-terminal tail of the M-type cell GPCR Mam2, which appear to be required for pheromone-dependent internalisation (McCann, unpublished data).

There are two known proteins with GAP activity regulating the pheromone response; Rgs1, being the only RGS protein family member present in *S. pombe* and Gap1. Rgs1 displays GAP activity on the G$\alpha$ subunit Gpa1 and itself is upregulated in response to pheromone (Pereira and Jones, 2001), therefore providing a feedback loop acting at the level of the G$\alpha$. Cells lacking Rgs1 can initiate the mating-response but display hypersensitivity to pheromone and are unable to conjugate with cells of the opposite mating type (Watson et al., 1999). Rgs1 localisation has been shown to be predominantly nuclear and does not appear to translocate in response to pheromone stimulation (Pereira and Jones, 2001). There are four conserved domains in Rgs1, the RGS-fold, a fungal-DR domain (fungal differentiation regulator) and two DEP domains. Removal of any one of these domains

results in cells that are deficient in mating (Pereira and Jones, 2001). Counter intuitively, Rgs1 has been shown to confer both negative and positive regulation on pheromone signalling, dependent on the concentration of pheromone stimulation of the signalling pathway. Rgs1-catalysed GTP hydrolysis of $Gpa1_{GTP}$ has been shown to be of significant importance, both in controlling sensitivity of response and to achieve maximal signalling through the recycling of the G$\alpha$ subunit (Smith et al., 2009).

Gap1 is the other protein with GAP activity regulating pheromone induced signalling. Gap1 is the only GAP for Ras1 in *S. pombe*, and again a loss in this GAP results in cells having a hypersensitivity to pheromone, implicating it as having a negative role in signalling through Ras1 (Imai et al., 1991).

An additional means of rapidly attenuating signalling is through dephosphorylation of components of the MAP kinase cascade. The final MAP kinase in the cascade Spk1, is considered to be a primary site for this inactivation and it has been suggested that Spk1 is dephosphorylated by the phosphatase Pmp1 (Didmon et al., 2002). A consequence of this event is that further phosphorylation of Ste11 is prevented, therefore leading to a reduction in expression of pheromone induced genes. Negative regulation of the signalling pathway is key to a functional signalling response. Each of Pmp1, Rgs1, Gap1 and Sxa2 are required for cells to be capable of efficient mating (Imai et al., 1991; Imai and Yamamoto, 1992; Watson et al., 1999; Didmon et al., 2002). This highlights the importance of mechanisms to attenuate the response and to prevent against overstimulation in the physiological signalling response.

## 1.7 Reporters of Signalling

To be able to probe a signalling network to investigate signal transduction and the role of signalling components in signal regulation requires some quantifiable readouts of the response. Ideally, especially when attempting to model signalling networks, it is advantageous to have as many different quantifiable readouts, at as many different points in the network as possible to give a range of information on signal amplitude and temporal dynamics. These multiple readouts would then have to be integrated to aid modelling efforts and to interpret the signalling behaviour. The luxury of multiple quantifiable readouts is not very often afforded, hence quantification of signalling response will commonly only involve one or two measures of activity. In model signalling systems such as the mating-response in yeast, the most commonly used measure is through ligand stimulated expression of a transcriptional reporter gene. The most widely used method of quantification of signalling in yeast is through enzymatic assay of $\beta$-galactosidase reporter strains (Didmon et al., 2002), but increasingly other reporter systems are being explored.

### 1.7.1 Fluorescent Proteins as Reporters

The first fluorescent protein to be identified was the green fluorescent protein (GFP) isolated from the jellyfish *Aequorea Victoria*, which fluoresces green when exposed to blue or ultraviolet light. Since the discovery of GFP, there has been an explosion of new fluorescent protein variants, having a wide range of different properties and now there are in excess of 18 different fluorescent proteins available with emission colours from cyan to far-red for use in biological applications (reviewed by Shaner et al., 2005). Fluorescent proteins have been utilised in studies of gene expression, protein and nuclear acid localisation, protein-protein interactions, protein-DNA interactions and cell tracking. Fluorescent proteins provide a highly attractive alternative to use as transcriptional reporters of signalling instead of having to perform enzymatic assays. Advantages over other reporters include ease of quantification, reduced cytotoxicity, no requirement for additional substrates to obtain a readout and no requirement for the disruption of cellular integrity. Additionally, the wide choice of fluorescent reporters aids their utility and allows for the use of multiple different fluorescent reporters in the same cell population.

One of the biggest advantages of using fluorescence as a reporter of signalling is that it can be combined with time-lapse microscopy to perform live-cell imaging experiments. This can be a very powerful tool, as it allows the monitoring of signalling activity in terms of fluorescence in real-time in single cells within a population or within whole living organisms. As this approach is not limited by single-time point measurements, information can be obtained on the spatial and temporal dynamics of the process being monitored. In addition, unlike assays using reporter cell populations, single cell data will not be influenced by heterogeneity in the cell population that can often mask the underlying process dynamics (Shav-Tal et al., 2004; Nowotschin and Hadjantonakis, 2009).

#### 1.7.1.1 Quantitative Image Analysis

Live-cell imaging experiments of fluorescent transcriptional reporter cells will elicit data in the form of time-series images of cells displaying changes in cellular fluorescence levels, indicating the level of signalling activity in the cell. This qualitative data can then be subjected to quantitative image analysis software for more in-depth analysis. Often this will require the use of software that is capable of processing the images as input and outputting quantifiable measures in terms of fluorescence intensity values. To obtain single cell measurements over time, this software will also be required to segment single cells within the image and track these cells through space and time, thus giving information on the temporal dynamics of a single cell signalling response.

A number of software packages have been and continue to be developed for the automated tracking and quantification of single cell fluorescence in recent years. Examples of

software include the commercially available 2D and 3D tracking software ImarisTrack and the open source packages CellTrack (Sacan et al., 2008), CellTracker (Shen et al., 2006) and QuimP (Dormann et al., 2002). Such image analysis software has been used in a number of investigations, ranging from cell motility studies looking at cell migration of leokocytes (Lämmermann et al., 2008) to analysis of *Dictyostelium* cell motility (Zanchi et al., 2010) and actin-myosin cytoskeleton reorganisation (Dalous et al., 2008). Single cell tracking and quantification can give a range of single cell measurements, not only for fluorescence intensities, but also cellular morphology (Bosgraaf et al., 2009; Tyson et al., 2010).

## 1.8 Stochasticity

Life at the cellular level is stochastic. The extracellular environment can be highly dynamic and frequently changing. In addition to the variable environment outside the cell, stochasticity is rife inside, with diffusion, gene expression, signal transduction and the cell cycle all being stochastic processes that vary in time and in ways that can be hard to predict (Raj and van Oudenaarden, 2008; Shahrezaei and Swain, 2008). Cells have been able to adapt to the randomness of their environment and are able to respond to different, fluctuating and sometimes contradictory signals. Impressively, they are able to process this noisy information using biochemical networks inside the cell, whose components themselves are variable in state, concentration and localisation. Stochastic effects in a cell's immediate environment can be reduced by cells coming together to form multicellular organisms, yet this reduction is minimal and even in humans, the signals and responses to signals remain highly stochastic (Feinerman et al., 2008; Sigal et al., 2006).

Given a genetically identical population of cells, phenotypic differences can be observed from cell-to-cell. The most striking source of this variability is a randomness in the expression of individual genes. The cause of this fluctuation in gene expression is because of the fact that it requires the discrete and random bio-chemical reactions that are involved in mRNA and protein production. The fact that DNA molecules (and hence the genes encoded therein) are present in relatively low numbers inside a single cell, means that these fluctuations can instead lead to easily detectable differences between otherwise identical cells. Gene expression therefore, must be considered as a stochastic process. The observation that genetically identical cells differ in their gene expression from cell-to-cell is not a new one. Novick and Weiner were amongst the first to show it experimentally by demonstrating that the production of $\beta$-galactosidase in individual cells was highly variable, with induction increasing the proportion of cells expressing the enzyme rather than increasing every cells expression level equally (Novick and Weiner, 1957). Many further attempts have been made since then to characterise the stochastic nature of gene expression. Landmark studies by Elowitz, 2002 investigated the causes of stochastic gene expression by

introducing two copies of the same promotor sequence into the genome of *Escherichia coli*. One promoter driving the expression of cyan fluorescent protein and the other driving the expression of yellow fluorescent protein. They introduced the terms extrinsic and intrinsic noise to explain their findings. Extrinsic fluctuations being those that affect the expression of both copies of the gene equally in a given cell, for example as a result of cell-to-cell variations in RNA polymerases or ribosome numbers. Intrinsic fluctuations should affect each copy of the gene independently and are due to the stochastic nature of transcription and translation.

## 1.9 Cell Fate Decision Systems

It is fundamental, especially in developmental cell biology that living cells have the capability to differentiate into subtypes with specialised attributes. How cells adopt a particular cell fate is often thought to be deterministic, for example a cell will adopt a given fate dependent on proximity to an inductive signal. However, in some cases and in organisms ranging from bacteria to humans, cells will 'choose' fate in a stochastic manner. This stochasticity is speculated as being advantageous to the individual, colony or species (Losick and Desplan, 2008). The mating-response in *S. pombe* is considered to be an example of such a eukaryotic cell fate decision system.

### 1.9.1 Variation in Yeast Mating-response

Clonal populations of cells can exhibit substantial variation in phenotype and this heterogeneity can be essential for many biological processes. In a population of genetically identical *S. pombe* cells, substantial cell-to-cell variation has been observed in the extent of response to mating inducing pheromone, both in terms of expression of pheromone inducible genes and in morphology (Croft and Ladds, unpublished). A number of previous studies have used fluorescent reporter proteins to study cell-to-cell variation in gene expression. Findings from a study on yeast indicate that intrinsic noise contributes very little to the cell-to-cell variation (Raser and O'Shea, 2004). A study in *S. cerevisiae* investigated the cell-to-cell variation, not in gene expression, but in a cell fate decision system: the mating pheromone-response system (Colman-Lerner et al., 2005). In this study, pheromone inducible fluorescent reporter genes are used as the readout for the signalling pathway, thus any differences observed in gene expression would represent differences in operation of the signal transduction pathway. Double fluorescent reporter strains were generated that had integrated in their genomes either two pheromone inducible fluorescent reporters or one pheromone inducible and one constitutively expressed fluorescent reporter. By correlating fluorescence intensities of multiple single cells from these double reporter strains, they were able to separate and quantify the sources of cell-to-cell variation. Variation was found to be

dominated not by random fluctuations in transcription and translation during the response, but by the capacity of a cell to transmit a signal through the pathway ('pathway capacity') and the capacity of a cell to express proteins from genes ('expression capacity'). Active mechanisms, namely the MAP kinases Fus3 and Kss1 have been shown to regulate the extent of variability from cell-to-cell in signalling pathway capacity (Colman-Lerner et al., 2005).

## 1.10 A Systems Biology Approach

Due to the complex nature of biological systems and the often large and interconnected web of components, it is often difficult to obtain a good understanding of system behaviour. The ultimate proof of understanding is to be able to quantitatively and accurately predict all aspects of a system's behaviour. Through measurements and observations, we are provided with the means with which to test such predictions. A systems biology approach seeks to elucidate a better understanding of biological system's behaviour by understanding how the components of the biological system interact to produce a system level response. The approach seeks to fully describe, not only the complexities of a biological system, but also the simplicity in high level system behaviour emerging from the underlying complexity. A systems biology approach will often involve an iterative cycle of building predictive mathematical models based on known biological data, using these models to predict behaviours, testing these predictions through 'wet-laboratory' experiments and subsequent model refinement.

### 1.10.1 Mathematical Modelling of Biochemical Signalling Networks

Cellullar signalling lends itself to systems biology approaches due to the often complex nature and large number of interconnected signalling components involved in a given signalling response. Mathematics is increasingly used to capture such complex signalling systems in the form of equations defining the signalling components, concentrations and reaction rates for all of the signalling processes of the signalling event (reviewed by Klipp and Liebermeister, 2006). By combining the mathematical modelling of the signalling network with technology in the form of computer programming languages and modelling software, a powerful tool is created that can be utilised to simulate '*in silico*' the dynamic responses from the network under known perturbed conditions.

Constructing a model of a particular signalling network is greatly aided by the level of prior knowledge in terms of the chemical reactions that occur, the initial concentrations of species, the kinetic parameters and cellular localisation of signalling components. It is very rare that all parameters will be known prior to constructing a model of a cell signalling network, therefore most models will be incomplete and unknown parameters are

estimated by a processes of model fitting to quantitative experimental data. Such data is often obtained via assays, returning a quantifiable measure of signalling output in response to some stimulus.

#### 1.10.1.1 Mathematical Structure of Biochemical Signalling Network Models

Biochemical signalling network models will often describe the molecules present, their interactions and molecular concentrations. If the dynamics are to be considered, then these concentrations will change with time. To describe such changes, mathematical modellers have a choice of the type of model to use. The models used for signalling networks can be (a) deterministic (defined future states) or probabilistic (incorporating stochasticity), (b) discrete or continuous in respect to time and component concentrations and (c) describe or not describe the processes in space. The choices of a particular model will most likely be dependent on what information is already available and the questions the model will be used to attempt to answer.

In the majority of models, the biochemical reactions are described in a deterministic, continuous manner using rate equations for concentrations of substances and complexes. The mathematical representation for this type of model is in the form of a set of ordinary differential equations (ODEs):

$$\frac{dc_i}{dt} = \sum_{j=1}^{r} n_{ij} v_j (i = 1, .., m), \tag{1.1}$$

where m is the number of biochemical species with the concentrations $c_i$, r is the number of reactions with the rates $v_j$ and the quantities $n_{ij}$ denote the change in stoichiometric coefficients of species i in reaction j. Depending on experimental information, the individual reaction rates can be described using kinetic laws, most commonly used is the law of mass action kinetics, which states that the rate of an elementary reaction (a reaction that proceeds through only one mechanistic step) is proportional to the product of the concentrations of the participating molecules. For example the reaction

$$\mathrm{A} + \mathrm{B} \quad \underset{k_\mathrm{b}}{\overset{k_\mathrm{f}}{\rightleftharpoons}} \quad \mathrm{C} \tag{1.2}$$

gives the reaction rate

$$v = A \cdot B \cdot k_f - C \cdot k_b. \tag{1.3}$$

Parameters $k_f$ and $k_b$ are the forward and backward reaction rate constants.

Within a deterministic model, the spatial distribution of molecules can be incorporated simply by defining species in different compartments or alternatively by describing the dynamics in a continuous space using partial differential equations (PDEs). Alternative examples of different types of model systems used to model signalling networks that are not continuous, but discrete with respect to time and variable values include Petri nets (Takai-Igarashi, 2005), Boolean networks (Kaufman et al., 1999) and cellular automata (Wurthner et al., 2000).

## 1.11 Modelling GPCR and G protein-mediated Signalling

Mathematical modelling has quite a substantial history in modern biology and pharmacology (Fall et al., 2002), and it offers a powerful tool for examining G protein-mediated signalling pathways. Having a good representative model of the system allows one to probe the system with relative ease to investigate which pathways play the largest role, the mechanisms that allow modulation of signalling, desensitisation, or receptor crosstalk and the factors influencing ligand efficacy. Models can also be used to help to identify the points in the network where interruptions would be most effective (i.e. identifying the best drug targets). Such models can be used to run virtual experiments in a mater of seconds that would take weeks in the laboratory, as well as being useful to interpret data and for the motivation of further experiments.

GPCR signalling forms a complicated picture. At the sub-second to sub-minute timescale, ligand binding, interactions of receptors with G proteins, G protein activation/deactivation, and the action of RGS proteins in GAP or non-GAP roles occur. Many downstream signalling molecules can be transiently modulated locally, or over the entire cell. On a slightly longer time scale, receptor phosphorylation, arrestin binding and activation of non-G protein-dependent signalling pathways occur (DeWire et al., 2007; Moore et al., 2007). The trafficking of receptors by internalisation, recycling, routing to lysosomes and upregulation as well as the synthesis of new receptors and regulation of gene expression also occur on a minutes to hours time scale. It can be extremely difficult to intuitively predict the net result of so many simultaneous kinetic processes that contain non-linearities such as feedback, time-varying sequestration of molecules via scaffolds and spatial variations. Modelling - defining reaction schemes and putting in the numbers (reaction rates and concentrations) can help the cause by allowing both qualitative and quantitative insights. Models of GPCR signalling most commonly fall in the category of either equilibrium or kinetic models.

### 1.11.1 Equilibrium Models

In pharmacology, equilibrium models are commonplace (Kenakin, 2004). They describe the transitions between different receptor states and produce steady-state equations for a response in terms of quantities of receptor, G protein and agonist, and equilibrium dissociation constants. Two highly important quantities in drug studies are often also included; the rate constants describing how tightly a ligand binds (affinity) and the maximum response achievable (efficacy). An example of such a model is the cubic ternary complex model (Weiss et al., 1996) (Figure 1.8). Thermodynamic equilibrium models are also used (Onaran et al., 1993; Sayar et al., 2008), which assume that receptors will reside within a range of states with certain probabilities. Ligand and G protein action alters the probabilities, therefore yielding different occupancy distributions.

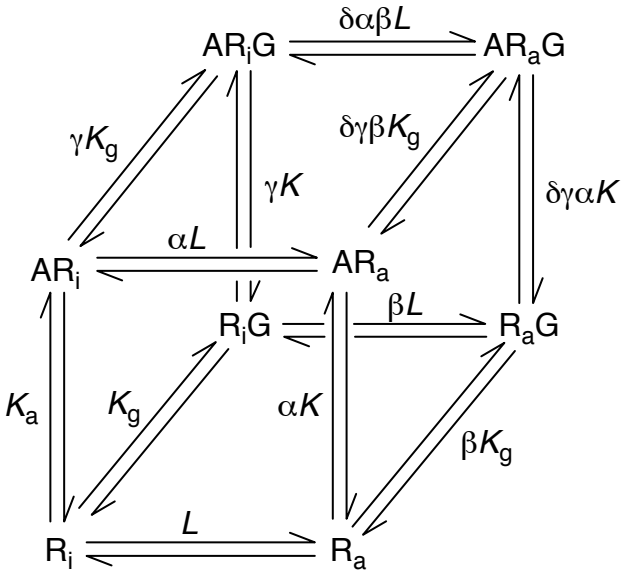


FIGURE 1.8: **Cubic ternary complex model of GPCR signalling.** The receptor can exist in two states; inactive ($R_i$) or active ($R_a$). G protein (G) binds to the activated receptor state $R_a$ to produce the physiological response. The ligand (A) binds to either receptor state and also to the G protein-bound activated receptor giving $AR_aG$. The propensity of the system to produce constitutive activity (spontaneous formation of the active state $R_aG$) is defined by the allosteric constant L (L=[Ra]/[Ri]). Affinity of ligands for the receptors is defined as $K_a$, whereas the efficacy is described by two terms, $\alpha$ and $\gamma$. The $\alpha$ term is the differential affinity of the ligand for $R_a$ and the term $\gamma$ is the differential affinity of the ligand-bound receptor $AR_a$ for G proteins. The inactive receptor species $R_i$ and $AR_i$ are also capable of interaction with G proteins without signalling. The term $\delta$ refers to the differential affinity of the receptor active state (over the inactive state) for the G protein. Figure adapted from Weiss et al., 1996.

### 1.11.2 Kinetic Models

The most widely used type of GPCR signalling network model is a kinetic model, which aims to link the time course of GPCR ligand binding and other receptor level events with the kinetics of early (e.g. G protein activation) and later (e.g. effector activation, MAPK

activation, desensitisation) events further downstream. Models are generally formulated as ODEs, which describe how the concentration of each species varies over time. More detailed examples of how to write such equations can be found in (Lauffenburger and Linderman, 1996). Signalling propagates from GPCRs at the cell membrane to the inside of the cell and many molecules within the cell are likely to be released from discrete sources in response, therefore there are likely to be spatial gradients of the signalling molecules inside the cell. To be able to follow both spatial and temporal information during signalling, PDEs can be used. Stochastic models introduce randomness into a model by using probabilities for events to occur. Unlike a deterministic model, given the same input or starting point, a stochastic model will give a different output each time and simulations must be run multiple times to gather statistics on the range of possible outcomes.

Many ODE modelling efforts have been made to look at the extent that G protein activation/deactivation dynamics modulate downstream responses in the mating-response pathway in *S. cerevisiae* (Hao et al., 2003; Yi et al., 2003; Yu et al., 2008). This is probably the most well studied and biochemically well characterised of all eukaryotic signalling pathways. Much has been learnt and many new hypothesis drawn as a result of modelling efforts on this pathway. The mating-response pathway in the fission yeast *S. pombe* has not been so well studied, and because of some differences in the way the signal is propagated, mathematical modelling of the *S. pombe* mating-response system could offer further insight into the mechanisms of eukaryotic G protein-mediated signalling.

### 1.11.3 Modelling of the *S. pombe* Mating-response

Due to some unexpected biological phenomena within the *S. pombe* mating-response signalling cascade, work has begun to mathematically model this pathway. Transcriptional reporter strains have been utilised to monitor signalling response upon receptor stimulation and a computational kinetic model is under development that can closely predict the signalling response (Smith et al., 2009). These modelling efforts have been based on experimental data, assaying signalling activity from populations of $\sim 10^6$ *S. pombe* reporter cells. Simulations from the kinetic model of signalling based on the mating-response system, closely fit to the signalling response data observed *in vivo*. This model, along with *in vivo* data has demonstrated that RGS-promoted GTP hydrolysis is required for desensitisation at low ligand stimulus but paradoxically, can function to increase the maximal response at high levels of stimulation. Furthermore, this relationship is explicitly dependent on the concentration of RGS (Figure 1.9). To enable an accurate model of the GTPase cycle to be produced that qualitatively models the *in vivo* data, a novel inactive $\hat{G}\alpha_{\mathrm{GTP}}$ bound state has been predicted that occurs following effector activation and requires RGS-catalysed hydrolysis for its release from this inactive state (Figure 1.10; simulations in Figure 1.9).

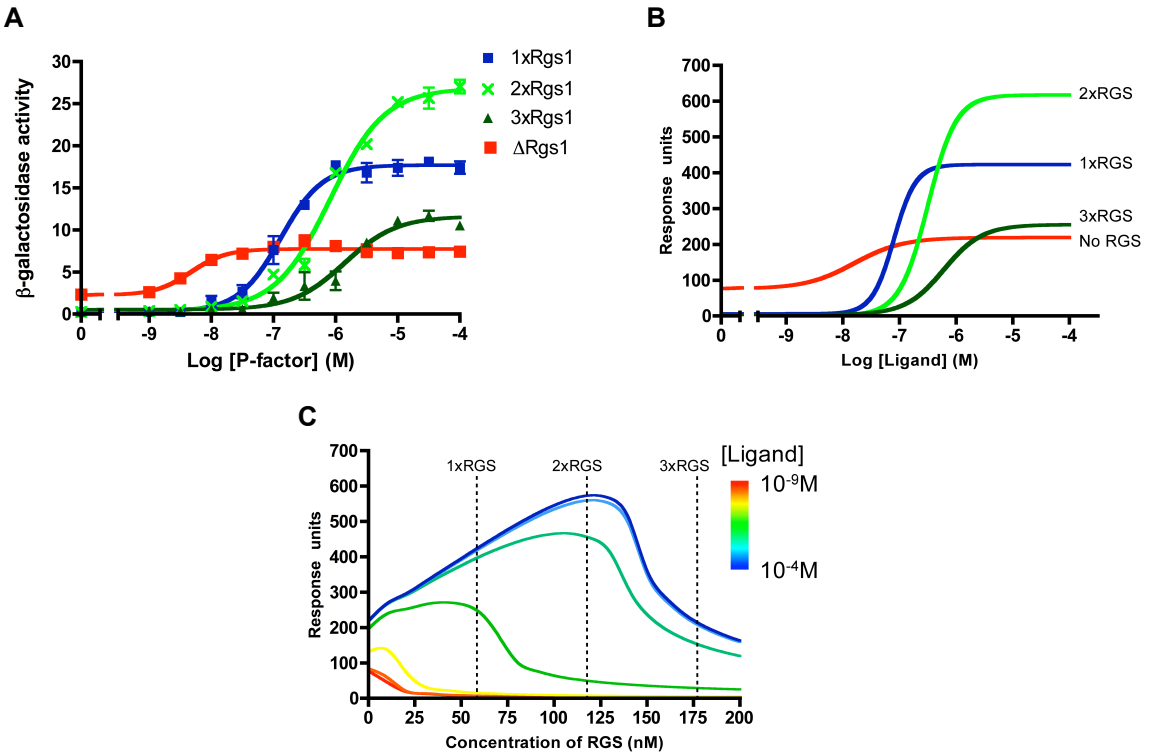


FIGURE 1.9: ***In vivo* and computational simulation of the dependence of GPCR signalling upon RGS concentration.** *In vivo* ligand-dependent transcription for *S. pombe wild-type* (1xRgs1), 2xRgs1, 3xRgs1 and $\Delta$*rgs1* strains as determined using $\beta$-galactosidase activity (A). Computational predictions for the four strains (B). The model captures the feature of the biological system. Computational predictions of the effects upon signal output when RGS concentration is varied (C). Data from Smith et al., 2009.

The reaction scheme for the ODE model includes simple reactions governing the cycling of G protein activation and de-activation (Figure 1.10). Activation reactions are defined, either through spontaneous activation or ligand-activated-receptor (LR) driven exchange of GDP for GTP on the G$\alpha$ species. G protein de-activation is defined by GTP hydrolysis reactions, either through intrinsic or RGS-catalysed hydrolysis of G$\alpha_{\mathrm{GTP}}$. Activation downstream of the G$\alpha$ is modelled simplistically through the activation of a downstream effector by G$\alpha_{\mathrm{GTP}}$. Following effector activation, the G$\alpha$ enters a GTP-bound inert state ($\hat{G}\alpha_{\mathrm{GTP}}$), which cannot activate any more downstream effectors. Recycling of $\hat{G}\alpha_{\mathrm{GTP}}$ returning it to G$\alpha_{\mathrm{GDP}}$ requires the intrinsic or RGS-catalysed hydrolysis of GTP. RGS-catalysed hydrolysis reactions in the model can both negatively (hydrolysis prior to effector activation) and positively (hydrolysis post effector activation to recycle $\hat{G}\alpha_{\mathrm{GTP}}$) influence the signalling response. The model therefore is able to simulate the dual negative and positive roles observed for Rgs1 in regulating the *S. pombe* mating-response (Figure 1.9).

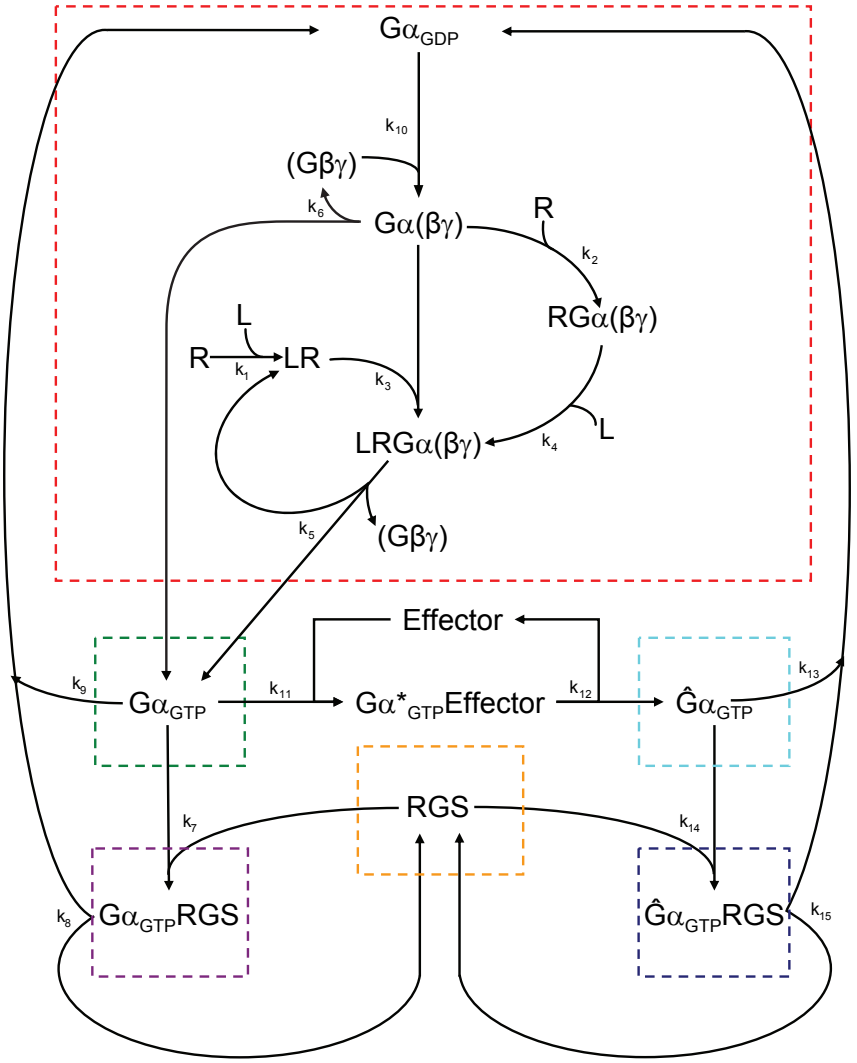


FIGURE 1.10: **Reaction scheme describing the regulation of a G protein within a GPCR signalling cascade.** The reaction scheme includes terms for an RGS accelerating GTP hydrolysis at two separate stages within the sequence ($G\alpha_{GTP}$ and $\hat{G}\alpha_{GTP}$). Binding of a ligand (L) to a receptor (R) is followed by association with a heterotrimeric G protein ($LRG\alpha(\beta\gamma)$). Dissociation of the complex generates GTP-bound G$\alpha$-subunit ($G\alpha_{GTP}$), free $\beta\gamma$-subunits ($G\beta\gamma$) and ligand bound receptor (LR). $G\alpha_{GTP}$ can either hydrolyse the GTP to form GDP-bound G$\alpha$ subunit plus inorganic phosphate ($G\alpha_{GDP}$ + P), which can be accelerated by interaction with an RGS (via formation of a $RGSG\alpha_{GTP}$) or encounter an effector to form the active $G\alpha^*_{GTP}$Effector complex (Ross and Wilkie, 2000). Following effector activation, $G\alpha^*_{GTP}$ enters an inert state ($\hat{G}\alpha_{GTP}$), unable to activate further effectors prior to conversion to $G\alpha_{GDP}$ + P, in a reaction that can be accelerated by RGS activity ($RGS\hat{G}\alpha_{GTP}$). $G\alpha_{GDP}$ + P reverts to $G\alpha_{GDP}$ (P tends to $\emptyset$) and can then re-associate with $G\beta\gamma$ prior to reactivation by a ligand bound receptor. The coloured boxes enclose the key conceptual sections of the model. The red box indicates the states in which the G protein is inactive, the green box indicates the activated (pre-signalling) state and the cyan box holds the inert (post signalling) state. The orange box contains the pathway regulator; in the purple box, the regulator bound to the pre-signalling state and in the dark blue box, the regulator bound to the post-signalling state. Figure from Smith et al., 2009.

Although the Smith *et al.* ODE model can accurately reproduce experimental data (qualitatively), many of the parameters (e.g. reaction rates and concentrations) have been hand tuned and the model does not contain any experimentally determined kinetic data for any of the reactions in the signalling pathway. In addition to this, yeast two-hybrid data that enables investigation of protein-protein interactions has suggested that there is an interaction between the GPCR and the RGS protein in this system, and that this interaction is possibly required for RGS to regulate the signalling response (McCann, unpublished data). The model does not include any GPCR-RGS interaction, therefore it requires further expansion to include this important information.

## 1.12 Outstanding Questions Related to *S. pombe* Mating Response

G protein-mediated signalling is a prime example of how a widely conserved module of few proteins can operate over a wide range of timescales and extents of amplification in a highly controlled and regulated manner. The sophisticated behaviour depends on intrinsic kinetics of the proteins involved; GPCR, G$\alpha$, G$\beta\gamma$, RGS and effector, and the multiple interactions between them. One of the pressing questions yet to be answered is how a GAP protein like Rgs1 that speeds up GTP hydrolysis can be a negative regulator of signalling at low ligand concentrations, yet is required for maximal response at higher ligand concentration (Figure 1.9). The current mathematical model has predicted an inactive $\hat{G}\alpha_{\mathrm{GTP}}$ to account for this phenomena (Smith et al., 2009). Nucleotide exchange, and hence the switching on and off of the G$\alpha$ subunit is central to signal transduction, but as yet there has been little investigation into what effects of altering the nucleotide exchange rate would have on the signalling response. Also at present, many of the parameters of the mathematical model are hand tuned, as kinetic parameters for important interactions in the system are unknown. The model is incomplete in the sense that the effector directly downstream of the G$\alpha$ subunit has not been identified, it does not include the experimentally suggested interactions between the RGS and the GPCR, nor does it include mechanisms other than GTP hydrolysis for terminating the signalling response. The model is a deterministic model, essentially of a single cell response, yet it has been developed based on average experimental dose-response data obtained in population based signalling assays. Because of this, very little information is known on the timing, amplitude and cell-to-cell variability of a pheromone-dependent signalling response at the level of a single cell. In this study, some of these problems are addressed.

## 1.13 Aims

The project is split into two main aims, both consisting of related sub-aims:

- **Biological/Mathematical model development:**

- To investigate affects of altering G$\alpha$ nucleotide exchange rate on signalling response.

- To investigate a probable GPCR-RGS interaction and model its role in the regulation of signalling.

- **Investigate single cell signalling and variation in the signalling response:**

  - To develop time-series live-cell imaging and quantification of transcriptional and morphological single cell signalling response.

# Chapter 2

# Materials and Methods

## 2.1 Materials

### 2.1.1 General Laboratory Reagents

Sigma-Aldrich Co. Ltd. (Poole, Dorset, UK) and Merck BDH Laboratory Supplies (Poole, Dorset, UK) were suppliers of general laboratory reagents. All were of analytical grade unless specifically stated otherwise.

### 2.1.2 Molecular Biology Reagents

Restriction enzymes, T4 DNA ligase and Taq DNA polymerase (from *Thermus aquaticus*) were supplied by Invitrogen Ltd (Paisley, Scotland, UK). Bacterial alkaline phosphatase was supplied by Fermentas (York, UK). FastStart high fidelity enzyme blend was purchased from Roche Diagnostics Ltd (Lewes, East Sussex, UK). All oligonucleotides were synthesised by Invitrogen Ltd.

### 2.1.3 Electrophoresis Reagents

Ultrapure type-I agarose was purchased from Helena Biosciences (Gateshead, Tyne and Wear, UK).

### 2.1.4 Photographic Supplies

DNA gels were visualised using a G:Box iChemi gel documentation system with GeneTool analysis software (Syngene, Cambridge, UK).

### 2.1.5 P-factor

The *Sz. pombe* P-factor pheromone was synthesised by standard solid-phase methodology using a Biotech Instruments BT7300 Peptide Synthesiser by AltaBioscience.

### 2.1.6 Growth Media

Luria broth, yeast extract and select agar were supplied by Invitrogen Ltd. All components of Amino Acid selective medium (AA) and Defined Minimal Medium (DMM; Davey et al., 1995) were purchased from Sigma-Aldrich Co. Ltd. Plates and liquid media for the selective growth of yeast were made using AA media. Rich (Yeast Extract) medium was used with appropriate amino acid supplements (250 $\mu$g/ml) as required. For example, YEALU was YE medium supplemented with adenine, leucine and uracil. Plates were made with 1.5 % select agar. The following media are made by dissolving the reagents in reverse osmotically filtered (RO) water.

Table 2.1: DMM (Per litre)

| | |
|---|---|
| $NH_4CL$ | 5 g |
| $Na_2HPO_4$ | 2.2 g |
| Phthalic acid | 3 g |
| Glucose | 20 g |
| L-adenine (add as required for selective media) | 0.5 g |
| L-leucine (add as required for selective media) | 0.5 g |
| L-uracil (add as required for selective media) | 0.5 g |
| Salts (50x Stock) | 10 ml |
| Vitamins (1,000x Stock) | 1 ml |
| Minerals (10,000x Stock) | 100 $\mu$l |

Table 2.2: Stock solution of salts (50x) (Per litre)

| | |
|---|---|
| $MgCl_2.6H_2O$ | 52.5 g |
| $CaCl_2.2H_2O$ | 735 mg |
| KCl | 50 g |
| $Na_2SO_4$ | 2 g |

Table 2.3: Stock solution of vitamins (1,000x) (Per 100 ml)

| | |
|---|---|
| Nicotinic acid | 1 g |
| Inositol | 1 g |
| Pantothenic acid | 500mg |
| Biotin | 400 mg |

Table 2.4: Stock solution of minerals (10,000x) (Per litre)

| | |
|---|---|
| Citric acid | 1 g |
| Boric acid | 500 mg |
| $MnSO_4.H_2O$ | 500 mg |
| $ZnSO_4.7H_2O$ | 400 mg |
| Molybdic acid | 305 mg |
| $FeCl_3.6H_2O$ | 200 mg |
| KI | 100 mg |
| $CuSO_4.5H_2O$ | 40 mg |

Table 2.5: Yeast extract medium (YE) (Per litre)

| | |
|---|---|
| Yeast extract | 5 g |
| Glucose | 30 g |

Table 2.6: Selective medium (AA) (Per litre)

| | |
|---|---|
| Yeast nitrogen base (without amino acids) | 6.7 g |
| Glucose | 20 g |
| Amino acid mix | 1.5 g |
| Selection amino acid mix | 0.5 g |

Table 2.7: Amino acid mix

| | |
|---|---|
| L-alanine | 2 g |
| L-arginine | 2 g |
| L-asparagine | 2 g |
| L-cysteine | 2 g |
| L-glutamine | 2 g |
| L-glutamate | 2 g |
| L-glycine | 2 g |
| L-isoleucine | 2 g |
| L-lysine | 2 g |
| L-phenylalanine | 2 g |
| L-proline | 2 g |
| L-serine | 2 g |
| L-threonine | 2 g |
| L-tryptophan | 2 g |
| L-tyrosine | 2 g |
| L-valine | 2 g |
| myo-inositol | 2 g |
| para-amino benzoic acid | 0.4 g |

TABLE 2.8: Select amino acid mix (components as required)

| | |
|---|---|
| Adenine | 2 g |
| L-histidine | 2 g |
| L-leucine | 4 g |
| Uracil | 2 g |
| L-methionine | 2 g |

### 2.1.7 Bacterial Strain

Plasmid amplification was performed using *Escherichia coli (E. coli)* strain DH5$\alpha$ supplied by Stratagene (Cambridge, UK). *E. coli* DH5$\alpha$ genotype: *supE44 hsdR17 endA96 thi-1 relA1 recA1 gyrA96.*

### 2.1.8 *S. pombe* Strains

Standard nomenclature has been used to describe the *Sz. pombe* strains used in this thesis (Table 2.9). Deletions of genes are referred to as *yfg1-D10* in which 1,000 base pairs (bp) of the *yfg1* locus have been deleted. Replacement of genes using the selectable *ura4* cassette are referred to as *yfg1::ura4*$^+$. Creation of reporter strains in which expression of a reporter gene is linked to the promoter of an endogenous gene at the original locus are referred to as *pro1>rep1.*

*mat1-M,* $\Delta$*mat2/3* encodes for an M-cell incapable of switching mating type. Deletion of the *mat2* and *mat3* loci prevents mating type switch (Klar and Miglio, 1986).

The majority of strains used in this study contain mutations of the *ade6* gene and deletions of the *leu1* and *ura4* genes, which encode enzymes involved in the biosynthesis of adenine, leucine and uracil respectively.

The product of the *cyr1* gene is adenylate cyclase and disruption of this ORF allows *Sz. pombe* to undergo sexual differentiation during mitotic growth (Maeda et al., 1990).

The *sxa2* gene encodes an extracellular serine carboxypeptidase, which degrades P-factor (Ladds et al., 1996b). Disruption of this ORF prolongs the response to P-factor stimulation and increases the functionality of reporter strains (Didmon et al., 2002).

JY522 is a strain in which *sxa2* has been disrupted by the *ura4*$^+$ cassette. This strain was used in the creation of strains which are reporters of *sxa2* activity, by replacement of the *ura4*$^+$ cassette.

JY544 is the *sxa2>lacZ* reporter strain, in which stimulation of the mating-response pathway with P-factor results in the production of $\beta$-galactosidase.

JY1325 is the *sxa2>GFP* reporter strain in which stimulation of the mating-response pathway with P-factor results in the production of GFP.

JY1337 is a *sxa2>Venus* reporter strain in which stimulation of the mating-response pathway with P-factor results in the production of Venus (a yellow fluorescent GFP derivative, Nagai, 2002).

| **Strain** | **Genotype** |
|---|---|
| JY444 | *mat1-M, Δmat2/3::LEU2-, leu1-32, ura4-D18* |
| JY478 | *mat1-M, Δmat2/3::LEU2-, leu1-32, ura4-D18, rgs1::ura4*$^+$ |
| JY522 | *mat1-M, Δmat2/3::LEU2-, leu1-, ade6-M216, ura4-D18, cyr1-D51, sxa2::ura4*$^+$ |
| JY544 | *mat1-M, Δmat2/3::LEU2-, leu1-, ade6-M216, ura4-D18, cyr1-D51, sxa2>lacZ* (Called JY546 in Didmon et al. (2002)) |
| JY630 | *mat1-M, Δmat2/3::LEU2-, leu1-, ade6-M216, ura4-D18, cyr1-D51, rgs1::ura4*$^+$*, sxa2>lacZ* (Smith et al. (2009)) |
| JY1025 | *mat1-P, Δmat2/3::LEU2-, leu1-, ura4-D18* |
| JY1168 | *mat1-M, Δmat2/3::LEU2-, leu1-, ura4-D18, cyr1-D51, mam2::ura4*$^+$*, sxa2>lacZ* (Ladds and Davey, 2004) |
| JY1169 | *mat1-M, Δmat2/3::LEU2-, leu1-, ura4-D18, cyr1-D51, mam2-D10, sxa2>lacZ* (Ladds and Davey, 2004) |
| JY1285 | *mat1-M, Δmat2/3::LEU2-, leu1-, ura4-D18, cyr1-D51, gpa1-D12, sxa2>lacZ* (Ladds et al., 2007) |
| JY1286 | *mat1-M, Δmat2/3::LEU2-, leu1-, ura4-D18, cyr1-D51, gpa1-D12, rgs1-D14, mam2-D10, sxa2>lacZ* (Ladds et al., 2007) |
| JY1287 | *mat1-M, Δmat2/3::LEU2-, leu1-, ura4-D18, cyr1-D51, gpa1-D12, rgs1-D14, sxa2>lacZ* (Ladds et al., 2007) |
| JY1291 | *mat1-M, Δmat2/3::LEU2-, leu1-, ura4-D18, cyr1-D51, mam2-D10, rgs1-D14 sxa2>lacZ* (Didmon et al., 2002) |
| JY1325 | *mat1-M, Δmat2/3::LEU2-, leu1-, ade6-M216, ura4-D18, cyr1-D51, sxa2>GFP* (Smith, PhD Thesis, 2010) |
| JY1331 | *mat1-M, Δmat2/3::LEU2-, leu1-, ura4-D18, cyr1-D51, rgs1-D14, sxa2>lacZ* (Didmon et al., 2002) |
| JY1333 | *mat1-M, Δmat2/3::LEU2-, leu1-, ade6-M216, ura4-D18, cyr1-D51, sxa2>GFP, rgs1::ura4*$^-$ (Smith, PhD Thesis, 2010) |
| JY1337 | *mat1-M, Δmat2/3::LEU2-, leu1-, ade6-M216, ura4-D18, cyr1-D51, sxa2>Venus* (Ladds, unpublished) |
| JY1341 | *mat1-M, Δmat2/3::LEU2-, leu1-, ura4-D18, cyr1-D51, gpa1::ura4*$^+$*, sxa2>GFP* (Croft, this study) |
| JY1353 | *mat1-M, Δmat2/3::LEU2-, leu1-32, ura4-D18, mam2::ura4* $^+$ (McCann, PhD Thesis, 2010) |
| JY1483 | *mat1-M, Δmat2/3::LEU2-, leu1-, ade6-M216, ura4-D18, cyr1-D51, rgs1::ura4*$^+$*, sxa2>Venus* (Croft, this study) |

TABLE 2.9: Standard names of *S. pombe* strains and their corresponding genotypes as used in this study.

#### 2.1.8.1 Integration Strains

Selection for the loss of *ura4*, upon replacement with sequence of interest was performed using AA medium containing limited uracil (450 $\mu$M) and 4.5 mM 5-fluoro-orotic acid (FOA, supplied by Toronto Research Chemicals Inc., Ontario, Canada). FOA is converted by Ura4 into the toxic uracil analogue 5-fluoro-uracil (Grimm et al., 1988).

### 2.1.9 Plasmids and Constructs

Table 2.10 lists the DNA constructs used in this thesis.

| Name | Construct (Selection) | Source |
|---|---|---|
| JD907 | Disruption construct for creating rgs1::ura4$^+$ | Watson et al., 1999 |
| JD1627 | pREP3x-Mam2 (*leu1*) | Ladds et al., 2005a |
| JD1634 | Disruption construct for creating gpa1::ura4$^+$ | Ladds and Davey, 2004 |
| JD1766 | pKS | |
| JD1771 | pKS-Gpa1 | Ladds et al., 2007 |
| JD1778 | pKS-GFP | Ladds and Davey, 2004 |
| JD2261 | pREP3x-GFP (*leu1*) | Ladds and Davey, 2004 |
| JD2332 | pREP3x-Gpa1 (*leu1*) | Ladds et al., 2007 |
| JD2375 | pREP3x-Gpa1$^{G243A}$ (*leu1*) | Ladds and Davey, 2004 |
| JD2388 | pREP4x-Rgs1 (*ura4*) | Ladds et al., 2007 |
| JD2434 | pREP3x-Rgs1-GFP (*leu1*) | Hill, PhD Thesis, 2008 |
| JD2455 | pREP3x-Mam2-Rgs1 (*leu1*) | Hill, PhD Thesis, 2008 |
| JD2554 | pREP3x (*leu1*) | Maundrell, 1993 |
| JD555 | pREP4x (*ura4*) | Forsburg, 1993 |
| JD2555 | pREP3x-Rgs1 (*leu1*) | Watson et al., 1999 |
| JD2637 | pREP3x-Gpa1$^{G223S}$ (*leu1*) | Ladds et al., 2007 |
| JD2733 | pREP3x-Gpa1$^{Q244L}$ (*leu1*) | Ladds et al., 2007 |
| JD2880 | pREP3x-Mam2$\Delta$tail (*leu1*) | Hill, PhD Thesis, 2008 |
| JD3196 | pREP3x-Gpa1$^{1-40}$-Rgs1-GFP (*leu1*) | Hill, PhD Thesis, 2008 |
| JD3346 | pREP3x-Gpa1-GFP (*leu1*) | Croft, this study |
| JD3353 | pREP3x-Gpa1$^{R218C}$ (*leu1*) | Croft, this study |
| JD3365 | pREP3x-Gpa1-linker (160) (*leu1*) | Croft, this study |
| JD3384 | pREP4x-Rgs1-GFP (*ura4*) | Hill, PhD Thesis, 2008 |
| JD3389 | pREP3x-Gpa1-linker-GFP (160) (*leu1*) | Croft, this study |
| JD3390 | pREP3x-Gpa1$^{G83L}$ (*leu1*) | Croft, this study |
| JD3391 | pREP3x-Gpa1$^{G83A}$ (*leu1*) | Croft, this study |
| JD3392 | pREP3x-Gpa1$^{G83S}$ (*leu1*) | Croft, this study |
| JD3444 | pREP3x-Gpa1-linker (132) (*leu1*) | Croft, this study |
| JD3448 | pREP3x-Gpa1-linker-GFP (132) (*leu1*) | Croft, this study |
| JD3453 | pKS-mCherry | Bond, University of Warwick, 2011 |
| JD3500 | pREP3x-Gpa1-TetCys (160) (*leu1*) | Croft, this study |
| JD3501 | pREP3x-Gpa1-TetCys (*leu1*) | Croft, this study |
| JD3590 | pREP3x-Mam2-mCherry (*leu1*) | Croft, this study |
| JD3621 | pREP3x-Mam2$\Delta$tail-mCherry (*leu1*) | Croft, this study |
| JD3713 | pREP4x-Mam2-mCherry (*ura4*) | Croft, this study |
| JD3714 | pREP4x-Mam2$\Delta$tail-mCherry (*ura4*) | Croft, this study |

TABLE 2.10: Names of DNA constructs used in this thesis.

Genes in the pREP expression vectors are under the control of the *nmt1* promoter (Maundrell, 1993). Growth in the presence of thiamine represses the promoter. Induction requires growth in minimal media lacking thiamine (Maundrell, 1990).

pREP3x constructs use *leu1* for selection (Maundrell, 1993); *Sz. pombe leu1* encodes a $\beta$-isopropylmalate dehydrogenase (Kikuchi et al., 1988) and disruption leads to auxotrophy. The *Sc. cerevisiae LEU2* gene complements for the loss of *leu1* and is contained within the plasmid (Maundrell, 1993).

pREP4x constructs use *ura4* for selection (Forsburg, 1993); *Sz. pombe ura4* encodes orotodine monophosphate decarboxylase (Bach, 1987) essential for biogenesis of uracil. *ura4* can be used for both positive and negative selection. Growth in the presence of 5' fluoro-orotic acid (FOA) causes cytotoxicity, whilst the absence of uracil leads to auxotrophy for *ura4* disruptants. pREP4x contains the *ura4* gene (Forsburg, 1993).

## 2.2 Methods

### 2.2.1 Creation of DNA Constructs

This section details the construction of plasmids for the expression of proteins under the control of the *nmt1* promoter of pREP3x (Maundrell, 1990) and pREP4x (Forsburg, 1993). These pREP vectors were constructed to allow controlled expression of exogenous genes in *S. pombe* from a promoter that can be readily induced. Expressing genes under the control of the *nmt1* (no message in thiamine) promoter allows control over the expression of the protein by the addition or removal of thiamine from the growth medium (Maundrell, 1993).

#### 2.2.1.1 Creation of Gpa1 Mutant Expression Constructs

Gpa1 mutants were created by inverse PCR using a pKS-Gpa1 template, in which the pKS vector has been modified to contain the pREP vector multi-cloning site (JD1766). Inverse PCR was performed using a sense oligonucleotide within the ORF and an antisense oligonucleotide beginning immediately 5' to the sense oligonucleotide. The sense oligonucleotide contains one or two non-complementary bases designed to introduce a specific mutated amino acid residue. The PCR product was digested with *Dpn*I to remove methylated template DNA (Sullivan and Folk, 1988) and ligated to reconstitute the circular vector containing the mutated Gpa1 ORF. This was then digested with *Eco*RV and *Bam*HI to give a fragment containing the Gpa1 ORF and ligated into *Eco*RV and *Bam*HI digested pREP3x (Figure 2.1). Sense and antisense oligonucleotide primer pairs used to create the specific mutations are presented in Table 2.11 with the altered nucleotide shown in lower case.

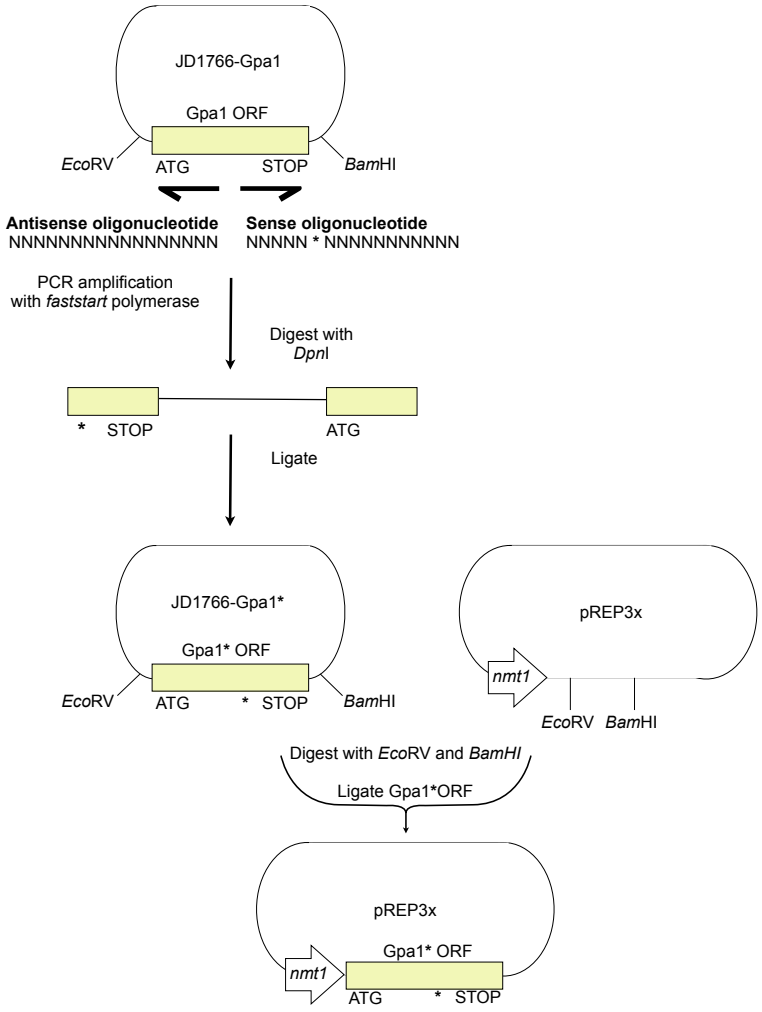


FIGURE 2.1: **Creating Gpa1 mutant expression constructs.** The mutations Gpa1$^{R218C}$, Gpa1$^{G83V}$, Gpa1$^{G83S}$,Gpa1$^{G83L}$ and Gpa1$^{G83A}$ were created using inverse PCR. PCR amplification was performed on pKS-Gpa1 using a sense oligonucleotide within the ORF and an antisense oligonucleotide beginning immediately 5' to the sense oligonucleotide, in which the sense oligonucleotide contains the desired point mutation, denoted by a * (Table 2.11). The product was then digested with *Dpn*I to remove template DNA and ligated to reconstitute the circularised vector. The Gpa1 mutant was obtained through digestion of the vector with *Eco*RV and *Bam*HI and ligated into *Eco*RV and *Bam*HI digested pREP3x.

| Gpa1 mutant | Sense oligonucleotide | Antisense oligonucleotide |
|---|---|---|
| Gpa1$^{R218C}$ | CTTCACTGT tGT ATCAAGACGACCGGT | GATATCTTGATCAGAAGG |
| Gpa1$^{G83V}$ | TTAGGCGCC GtT GATAGTGGGA | GAGCAAAACTTTAATGTCAT |
| Gpa1$^{G83S}$ | TTAGGCGCC aGT GATAGTGGGA | GAGCAAAACTTTAATGTCAT |
| Gpa1$^{G83L}$ | TTAGGCGCC ctT GATAGTGGGA | GAGCAAAACTTTAATGTCAT |
| Gpa1$^{G83A}$ | TTAGGCGCC GcT GATAGTGGGA | GAGCAAAACTTTAATGTCAT |

TABLE 2.11: **Oligonucleotides for introduction of point mutations in Gpa1 by inverse PCR.** The underlined bases are the codons introducing the amino acid change. Uppercase letters denote bases complimentary to template DNA and lowercase letters denote the non-complimentary bases to generate the mutation.

#### 2.2.1.2 Creation of Gpa1-GFP Fusion Expression Constructs

To allow visualisation of Gpa1, direct in-frame fusions of Gpa1 to GFP were made in expression vector pREP3x. These in-frame fusions were created at the C-terminus of Gpa1 and also with GFP inserted, flanked by a flexible linker sequence within the loop regions of the helical domain of Gpa1. To create the C-terminal fusion, Gpa1-GFP in pREP3x, a pKS-Gpa1-GFP construct was digested with *Spe*I and *Bam*HI to liberate the C-terminal fragment of Gpa1-GFP. This fragment was then ligated into *Spe*I and *Bam*HI digested pREP3x-Gpa1 to create the Gpa1-GFP C-terminal fusion in pREP3x (Figure 2.2).

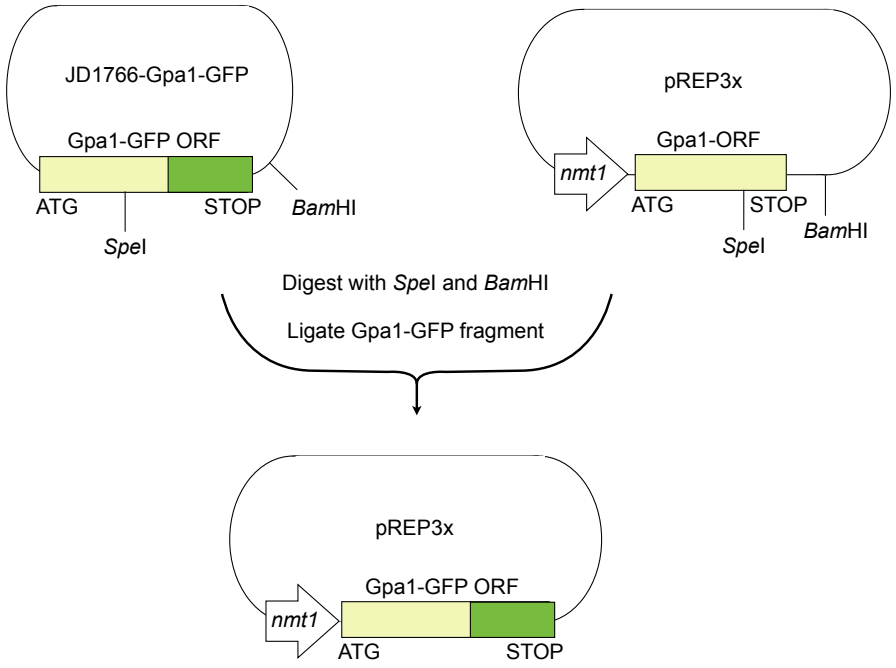


FIGURE 2.2: **Creating C-terminal Gpa1-GFP fusion expression constructs.** The pKS-Gpa1-GFP vector was digested with *Spe*I and *Bam*HI and the resulting fragment; C-terminus of Gpa1 fused to GFP was ligated into *Spe*I and *Bam*HI digested pREP3x-Gpa1 to create pREP3x-Gpa1-GFP.

The fusions, with GFP inserted in the middle of Gpa1, were created by making GFP flanked by a ser/gly repeat sequence flexible linker after amino acid residue 132 (Gpa1-GFP$^{(132)}$) and after amino acid residue 160 (Gpa1-GFP$^{(160)}$). The insertion positions were specifically selected based on homology to examples of similar fusions created in human G$\alpha$ subunits (discussed further in Chapter 3). Constructs with the flexible linker sequence containing *Bgl*II restriction enzyme sites within it were created by inverse PCR using a pKS-Gpa1 template. Inverse PCR was performed using a sense oligonucleotide within the ORF and an antisense oligonucleotide beginning immediately 5' to the sense oligonucleotide. Each primer introduces half of the flexible linker sequence and a single *Bgl*II site within it. The PCR product was then digested with *Dpn*I to remove methylated template

DNA and ligated to reconstitute the circular vector containing Gpa1 with inserted flexible linker sequence (1766-Gpa1-linker-Gpa1). GFP was liberated through *Bgl*II digest of a construct containing GFP flanked by *Bgl*II sites (1766-GFP) and ligated into *Bgl*II digested 1766-Gpa1-linker-Gpa1. The resulting construct contains GFP flanked by a flexible linker sequence within the Gpa1 ORF (1766-Gpa1-GFP-Gpa1). This was digested with *Eco*RV and *Bam*HI and the liberated Gpa1-GFP-Gpa1 construct was ligated into *Eco*RV and *Bam*HI digested pREP3x (Figure 2.3). The oligonucleotides used to place the linker region containing *Bgl*II sites after amino acid residue 132 (Gpa1-linker$^{132}$) and 160 (Gpa1$^{160}$) within the Gpa1 ORF are presented in Table 2.12.

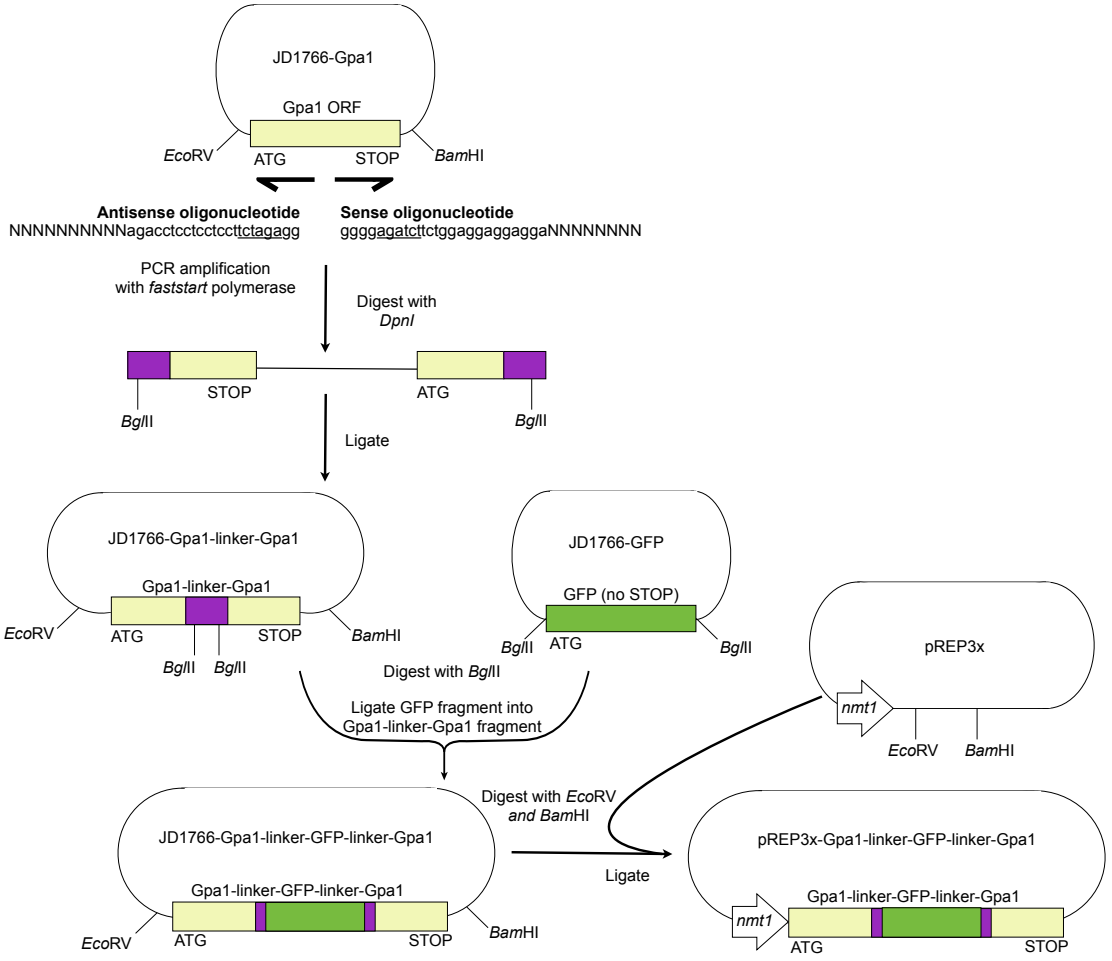


FIGURE 2.3: **Creating Gpa1-GFP fusion expression constructs through insertion of GFP.** Gpa1 with a ser/gly flexible linker sequence (purple) inserted after amino acid residue 132 (Gpa1-linker$^{132}$) and 160 (Gpa1-linker$^{160}$) were created by inverse PCR on pKS-Gpa1. Each oligonucleotide incorporates half of the flexible linker sequence and a *Bgl*II site (agatct) (Table 2.12). The PCR product was digested with *Dpn*I to remove template DNA and ligated to reconstitute the circularised vector. A GFP ORF lacking a STOP codon was obtained through *Bgl*II digest of a construct containing GFP flanked by *Bgl*II sites (1766-GFP) and ligated into *Bgl*II digested 1766-Gpa1-linker-Gpa1. The resulting construct was digested with *Eco*RV and *Bam*HI and the liberated Gpa1-GFP-Gpa1 construct was ligated into *Eco*RV and *Bam*HI digested pREP3x.

| Gpa1 created | Sense oligonucleotide | Antisense oligonucleotide |
|---|---|---|
| Gpa1-linker$^{132}$ | ggggagatcttctggaggaggaggaAATGTCT CTTTACTTCCGGAA | ggggagatcttcctcctcctccagaACTATTATC CATAGCTTCAAG |
| Gpa1-linker$^{160}$ | ggggagatcttctggaggaggaggaTCTCCAG AAATATATGAAGCT | ggggagatcttcctcctcctccagaAAATGGCT CATTGGGTTGA |

TABLE 2.12: **Oligonucleotides for introduction of a flexible linker sequence within Gpa1 by inverse PCR.** Bases introducing a *Bgl*II site are underlined, letters in uppercase denote bases complimentary to template DNA and letters in lowercase denote the non-complimentary bases, introducing the ser/gly linker and the *Bgl*II site.

#### 2.2.1.3 Creation of Gpa1-Tetra-cysteine Fusion Expression Constructs

To allow visualisation of Gpa1 by FLAsH labelling (discussed in Chapter3), direct in-frame fusions of Gpa1 to a tetra-cysteine motif (cys, cys, pro, gly, cys, cys) were made in expression vector pREP3x. These in-frame fusions were created at the C-terminus of Gpa1 (Gpa1-CCPGCC) and also with the motif inserted flanked by flexible linker sequence within a loop region of the helical domain of Gpa1 (Gpa1-CCPGCC-Gpa1). To create Gpa1-CCPGCC in pREP3x, inverse PCR was performed on a pKS-Gpa1 template. Inverse PCR was performed using a sense oligonucleotide complimentary to the STOP codon and sequence of the pKS vector within the ORF, and an antisense oligonucleotide beginning immediately 5' to the sense oligonucleotide. The PCR product was then digested with *Dpn*I to remove methylated template DNA and ligated to reconstitute the circular vector containing Gpa1 fused at its C-terminus to a ser/gly repeat flexible linker and the tetra-cysteine motif. This was digested with *Eco*RV and *Bam*HI and the liberated Gpa1-CCPGCC construct was ligated into *Eco*RV and *Bam*HI digested pREP3x (Figure 2.4).

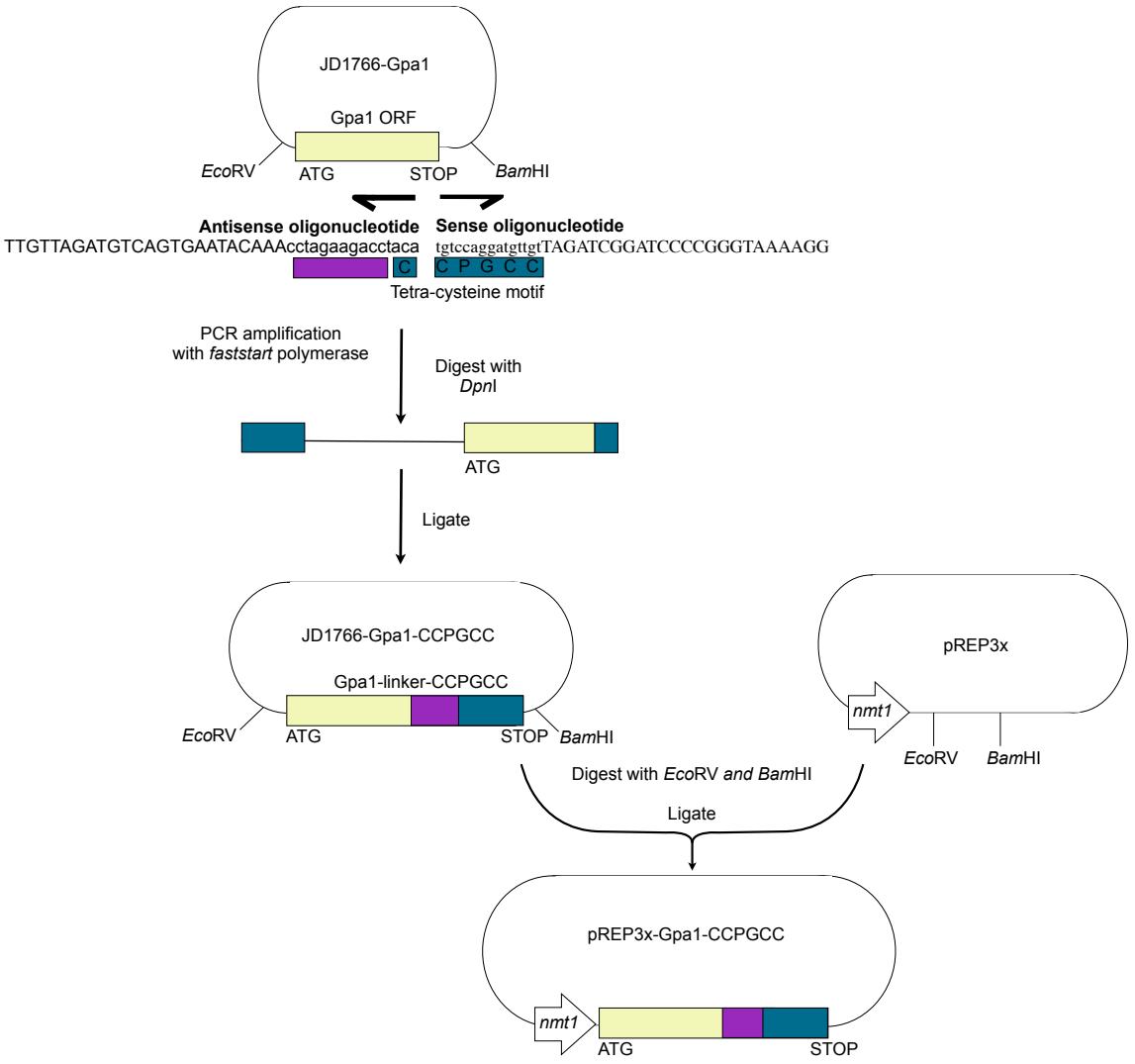


FIGURE 2.4: **Creating C-terminal Gpa1-tetra-cysteine fusion expression constructs.** Gpa1 fused at its C-terminus to a ser/gly flexible linker sequence (purple) followed by a tetra-cysteine (CCPGCC) motif (teal) was created by inverse PCR on pKS-Gpa1. The antisense oligonucleotide incorporates the flexible linker and the first C of the tetra-cysteine motif. The sense oligonucleotide incorporates the remaining CPGCC of the motif. The PCR product was digested with *Dpn*I to remove template DNA and ligated to reconstitute the circularised vector. This vector was digested with *Eco*RV and *Bam*HI to give the Gpa1-CCPGCC fragment and this was ligated into *Eco*RV and *Bam*HI digested pREP3x.

The fusion with the tetra-cysteine motif inserted within the helical domain of Gpa1 was created by making the tetra-cysteine motif flanked by a ser/gly repeat flexible linker after amino acid residue 160(Gpa1-CCPGCC-Gpa1). The construct with the tetra-cysteine motif flanked by a flexible linker sequence was created by inverse PCR using a pKS-Gpa1-linker[160] template. Inverse PCR was performed using a sense oligonucleotide within the ORF and an antisense oligonucleotide beginning immediately 5' to the sense oligonucleotide. The PCR product was then digested with *Dpn*I to remove methylated template DNA and ligated

to reconstitute the circular vector containing Gpa1-CCPGCC-Gpa1 (1766-Gpa1-CCPG-Gpa1). This was digested with *Eco*RV and *Bam*HI, and the liberated Gpa1-CCPGCC-Gpa1 construct was ligated into *Eco*RV and *Bam*HI digested pREP3x (Figure 2.5).

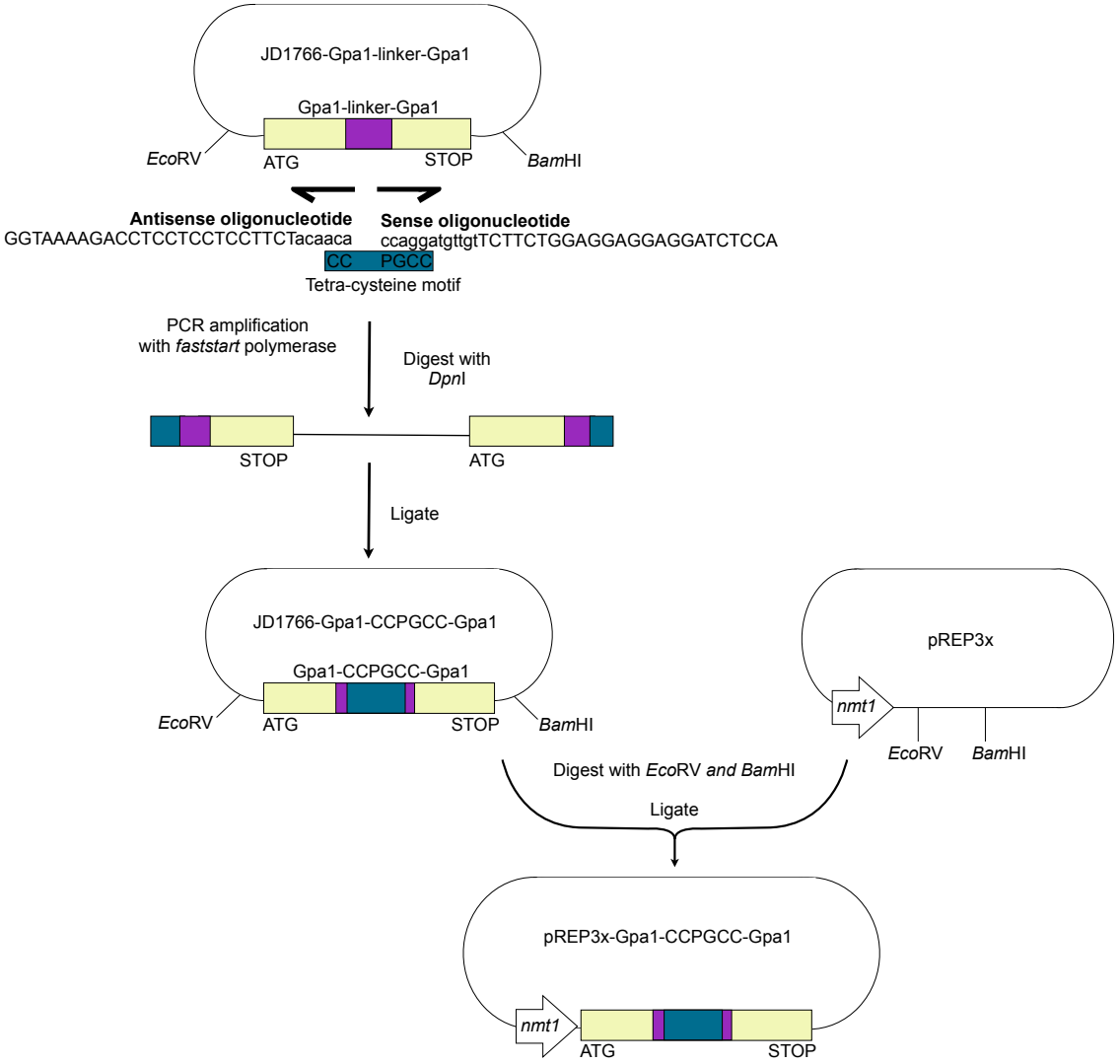


FIGURE 2.5: **Creating a Gpa1-tetra-cysteine fusion expression construct.** Gpa1 with a ser/gly flexible linker sequence (purple) flanking a tetra-cysteine (CCPGCC) motif (teal) inserted after amino acid residue 160 (Gpa1-CCPGCC-Gpa1) was created by inverse PCR on pKS-Gpa1-linker$^{160}$. Each primer incorporates part of the CCPGCC motif in the middle of the flexible linker sequence. The PCR product was digested with *Dpn*I to remove template DNA and ligated to reconstitute the circularised vector. This vector was digested with *Eco*RV and *Bam*HI to give the Gpa1-CCPGCC-Gpa1 fragment and this was ligated into *Eco*RV and *Bam*HI digested pREP3x.

#### 2.2.1.4 Creation of Mam2/Mam2Δtail-mCherry Fusion Constructs

To allow visualisation of Mam2 and Mam2 truncated for its C-terminal tail (Mam2Δtail), direct in-frame fusions of both Mam2 and Mam2Δtail to mCherry were made in expression vectors pREP3x and pREP4x.

To create Mam2-mCherry and Mam2Δtail-mCherry in pREP3x, Mam2 and Mam2Δtail lacking STOP codons were amplified by PCR on a template Mam2 ORF lacking a STOP codon. The amplified products were ligated into a *Pvu*II cut vector, specifically made for N or C-terminally tagging proteins with mCherry (Bond, University of Warwick, 2011). This ligation created direct in-frame fusions of Mam2 and Mam2Δtail to mCherry. Mam2-mCherry and Mam2Δtail-mCherry were liberated by digesting with *Xho*I and *BamHI* then ligating into *Xho*I and *BamHI* digested pREP3x (Figure 2.6).

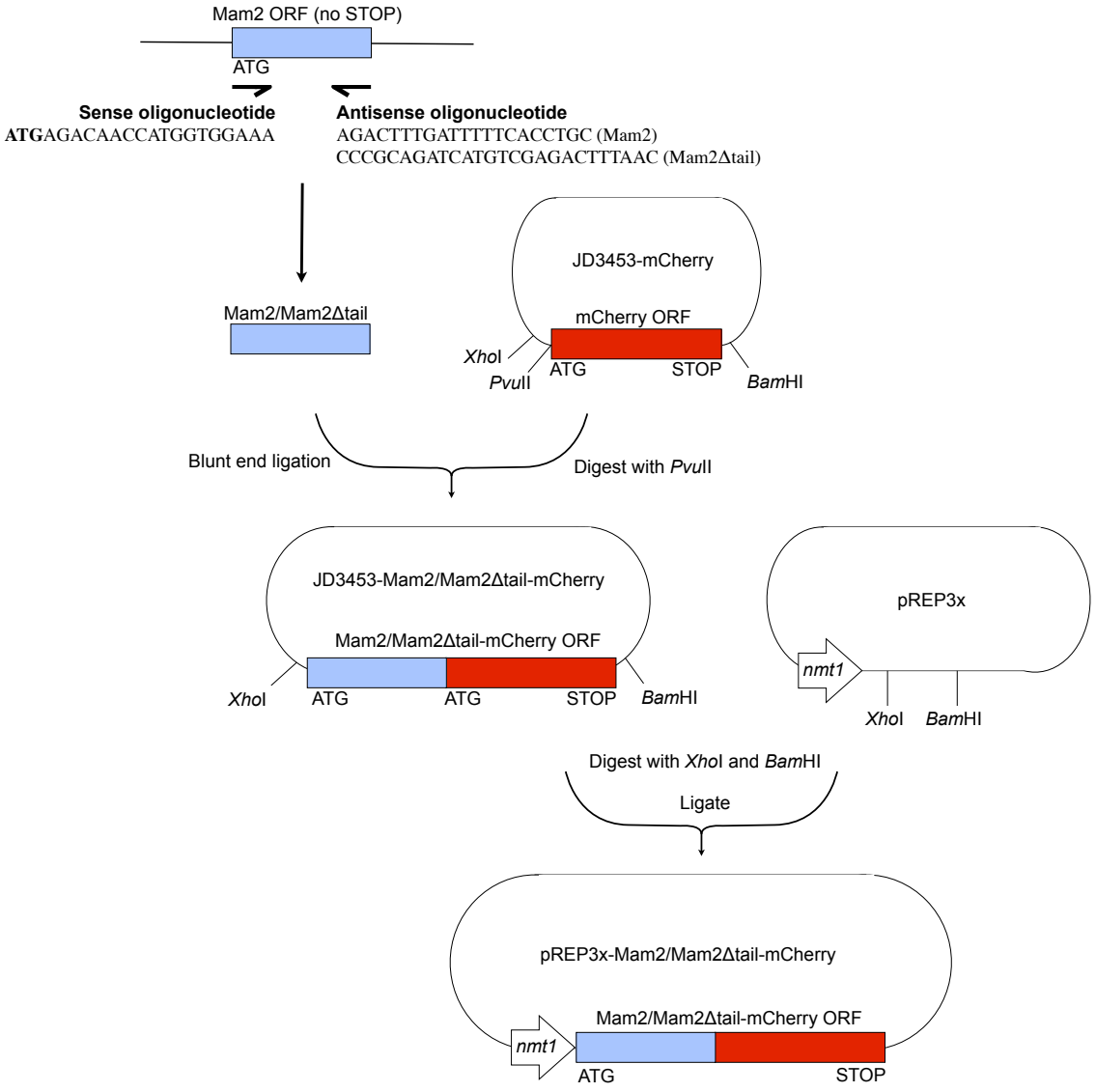


FIGURE 2.6: **Creating C-terminal Mam2/Mam2Δtail-mCherry fusion expression constructs.** Mam2 and Mam2Δtail C-terminal mCherry fusion constructs were created in pREP3x through the following steps. Mam2 and Mam2Δtail lacking a STOP codon were amplified by PCR on a template pKS vector containing the Mam2 ORF lacking a STOP codon. PCR products were ligated into a *PvuII* cut vector designed for C and N terminal fusion of proteins to mCherry (Bond, University of Warwick, 2011). The resulting vectors containing Mam2-mCherry and Mam2Δtail-mCherry were digested with *Xho*I and *Bam*HI to obtain Mam2-mCherry and Mam2Δtail-mCherry fragments. These were then ligated into *Xho*I and *Bam*HI digested pREP3x.

Both Mam2-mCherry and Mam2Δtail-mCherry were also subsequently created in expression vector pREP4x. The vectors pREP3x-Mam2-mCherry and pREP3x-Mam2Δtail-mCherry were digested with *Xho*I and *Mlu*I to liberate Mam2-mCherry and Mam2Δtail-mCherry fragments. These were then ligated into *Xho*I and *Mlu*I digested pREP4x (Figure 2.7).

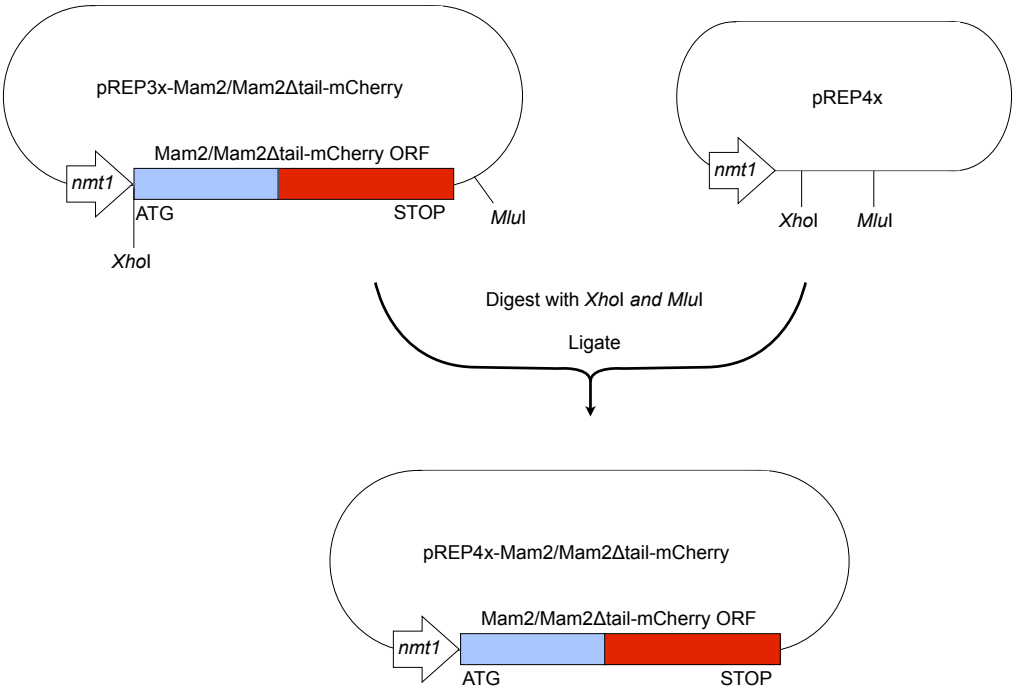


FIGURE 2.7: **Creating C-terminal Mam2/Mam2Δtail-mCherry fusion expression constructs in pREP4x.** pREP3x-Mam2-mCherry and pREP3x-Mam2Δtail-mCherry were digested with *Xho*I and *Mlu*I to obtain Mam2-mCherry and Mam2Δtail-mCherry fragments. These were then ligated into *Xho*I and *Mlu*I digested pREP4x (Figure 2.7).

### 2.2.2 Cloning Techniques

DNA manipulations were performed using standard methods (Sambrook et al., 1989). Restriction endonucleases were used according to manufacturer's recommendations. DNA fragments were analysed by electrophoresis on 1 % agarose gels stained with 0.5 $\mu$g/ml ethidium bromide. DNA fragments were recovered from agarose gels using the QIAquick Gel Extraction Kit (Qiagen, West Sussex, UK).

### 2.2.3 Transformation of *E. coli*

Chemically competent *E. coli* DH5$\alpha$ (Stratagene) were produced and transformed with plasmid DNA as described by (Sambrook et al., 1989).

### 2.2.4 Transformation of *Sz. pombe*

*Sz. pombe* was transformed with circularised plasmid DNA or linear DNA fragments using the lithium acetate method described by Okazaki et al., 1990.

### 2.2.5 Polymerase Chain Reaction

*Taq* DNA polymerase (Invitrogen Ltd) was used for screening bacterial colonies and yeast strains. FastStart high fidelity polymerase blend (Roche Diagnostics Ltd) was used for amplifying DNA fragments for cloning. All polymerases were used according to manufacturer recommendations.

#### 2.2.5.1 PCR Amplification of DNA for Cloning

Total reaction volume was typically 50 $\mu$l, and used 1 $\mu$g each of sense and antisense oligonucleotide primer, and 10-50 ng template DNA. Deoxyribonucleoside triphosphates (dNTPs) (dATP, dCTP, dGTP and dGTP; Fermentas, Hanover, MD, USA) were used at a final concentration of 0.2 mM. The PCR cycle consisted of a denaturation step of 94°C held for 30 s, followed by an annealing step (45-60°C held for 60 s). The extension step (72°C) was typically held for 60 s per 1000 bp of product. In general, 30 cycles of amplification were used per reaction. Reactions were concluded with a 7 min incubation at 72°C to complete product extension.

#### 2.2.5.2 Screening Plasmid DNA From Bacterial Cells

A single bacterial colony was suspended in 100 $\mu$l water and stored at 4°C. 1 $\mu$l of this suspension was used as the template in a 10 $\mu$l PCR reaction.

#### 2.2.5.3 Screening Yeast Genomic DNA

1 $\mu$l of yeast genomic DNA (200-400 ng) was used as the template in a 10 $\mu$l PCR reaction.

### 2.2.6 Double Stranded DNA Sequencing

Plasmid DNA was sequenced to confirm that no mutations were added during amplification in bacteria. Sequencing was performed by the Molecular Biology Service at the University of Warwick. Reactions were performed using Big Dye Terminator 3.1 Chemistry (Applied Biosystems, Foster City, CA, USA) and run on the 3100 Genetic Analyser (Applied Biosystems).

### 2.2.7 Preparation of Yeast Genomic DNA

Genomic DNA was isolated from yeast using the protocol from Hoffman and Winston, 1987. Strains were grown to a density of 1x$10^7$ cells/ml, harvested by centrifugation, washed once in distilled water and resuspended in 200 $\mu$l Blue Buffer (2 % Triton X-100, 1 % SDS, 100 mM NaCl, 10 mM Tris-HCl, pH 8.0 and 1 mM EDTA). 200 $\mu$l of a 1:1 phenol:chloroform mixture and 400 $\mu$l acid-washed glass beads (425-600 $\mu$m diameter) were added and the tubes vortexed for 3 min. 200 $\mu$l TE (pH 7.5) was added immediately and the tubes centrifuged for 5 min at 13,000 rpm, 4°C. The aqueous phase was transferred to 1 ml ice-cold ethanol, mixed by inversion and centrifuged for 2 min at 13,000 rpm. The pellet was washed with 70 % ethanol, dried and resuspended in 50 $\mu$l TE (pH 7.5). Preparation of genomic DNA by this method typically yields 10-20 $\mu$g DNA.

### 2.2.8 Cell Number and Size Analysis

Cell densities and mean cell volumes were determined using a Z2 Coulter® Particle count and Isoton II azide-free electrolyte, both supplied by Beckman Coulter (Luton, Bedfordshire, UK).

### 2.2.9 $\beta$-galactosidase Assays

Liquid $\beta$-galactosidase assays of *Sz. pombe* cultures were performed using a method modified from Dohlman et al., 1995. *Sz. pombe* cells were cultured to a density of ~5x$10^6$ cells/ml in DMM (lacking thiamine unless stated) and 500 $\mu$l aliquots transferred to 2 ml Safe-Lock Eppendorf tubes containing 5 $\mu$l P-factor pheromone diluted in HPLC-grade methanol. Tubes were incubated at 29°C for 16 h on a rotating wheel, and 50 $\mu$l transferred to 750 $\mu$l Z-buffer (Table 2.13) containing 2.25 mM o-nitrophenyl-D-galactoside (ONPG; purchased from Sigma-Aldrich Co. Ltd.) and incubated on a rotating wheel at 29°C for a further 90 min. Reactions were halted by addition of 200 $\mu$l 2 M sodium carbonate, and $\beta$-galactosidase production calculated as the ratio of ONPG product formed (detected by optical density (OD) measurement at 420 nm using an Ultrospec 3000; Pharmacia Biotech, Uppsala, Sweden) to assayed cells (determined using a Coulter Channelyser; Beckman Coulter, Luton, Bedfordshire, UK) using the formula $OD_{420}/10^6$ assayed cells.

Table 2.13: Z buffer

| | |
|---|---|
| $NaPO_4$ (pH 7.0) | 0.1 M |
| KCl | 10 mM |
| $MgSO_4$ | 1 mM |
| $\beta$-mercaptoethanol | 50 mM |
| (v/v) chloroform | 0.5 % |
| (w/v) SDS | 0.005 % |

#### 2.2.9.1 Analysis of Data from $\beta$-galactosidase Assays

Non-linear regression of dose-response data and statistical analysis was completed using GraphPad Prism software version 4.03 for Windows (GraphPad Software Inc., San Diego, CA, USA). Where possible, sigmoidal dose response curves were fit to dose-response data. Statistical significance was determined using un-paired $t$ tests.

### 2.2.10 Yeast Mating Efficiency Assays

Cells were cultured in liquid DMM to a density of $\sim$5x$10^6$ cells/ml. 200 $\mu$l of each mating type strain were mixed and harvested by centrifugation (2000 rpm for 3 min). Cells were resuspended in 10 $\mu$l of sterile water and spotted onto DMM plates containing 100-fold lower $NH_4Cl$ than detailed in section 2.1.6. Non-mixed controls were also spotted onto the plates. Following 72 h incubation at 29 $^o$C, each colony was collected from the spots and suspended in 1 ml of sterile water. Two separate 1 in 100 dilutions were then made from each 1 ml culture. One of these was plated onto separate YE plates at final dilution factors of 1 in 1,000 and 1 in 10,000 respectively. The other was placed in a 55$^o$C heat block for 10 min to kill everything except spores formed from mating events. This heat-treated sample was then also plated onto separate YE plates at final dilution factors of 1 in 1,000 and 1 in 10,000. Following 72 h incubation, the number of colonies on each plate were counted using a G:Box iChemi gel documentation system with GeneTool analysis software (Syngene, Cambridge, UK). The number of colonies as a percentage of the total (colony survival) can then be calculated for mated strains and controls, then the mating efficiency calculated as colony survival (mated strains) - colony survival (non mated control strain). This mating efficiency protocol was developed by Bond, University of Warwick, 2010.

### 2.2.11 Fluorescence Microscopy

Strains were cultured in the appropriate medium to a density of $\sim$5x$10^6$ cells/ml. 2 $\mu$l of cell culture was transferred directly to a solid DMM (2 % agarose) pad on a CoverWell$^{TM}$ imaging chamber (Grace Bio-Labs, Oregon, USA) and the residual liquid media was allowed

to dry. A coverslip was placed over the cells on the agar pad and sealed with a Vaseline, Lanolin and Paraffin equal parts by weight mixture (VALAP) to prevent drying of the sample. Images were then obtained using either a True Confocal Scanner Leica TCS SP5 microscope (Leica Microsystems Ltd., Milton Keynes, UK) or DeltaVision system wide-field deconvolution microscope. Image acquisition and subsequent deconvolution of images from the DeltaVision system was performed with softWoRx (applied precision) software. Deconvolution was performed with the following settings; Ratio = conservative, Number of cycles = 8 and Noise filtering = high.

### 2.2.12 Time-series Live-cell Imaging

Microscope slides for time-series imaging of live cells were prepared as in section 2.2.11. P-factor was added at the desired concentration to the DMM (2 % agarose) pad. Imaging was performed using a True Confocal Scanner Leica TCS SP5 microscope. Cells were imaged using a 63x objective lens taking a Z-stack at time = 0 h and subsequently every 15 min for a period of 16 h. The imaging procedure was set up such that cells were focused at 0 h and the Z position noted ($Z_{focus}$). The Z-stack was then defined such that 20 Z-slice images would be obtained from $Z_{focus}$ - 10 $\mu$m to $Z_{focus}$ + 10 $\mu$m to allow for drift in the focal plane over the course of the experiment. The time-series experiment was setup such that both light-field and fluorescence images were generated.

### 2.2.13 Flow Cytometry

Flow cytometry was performed using a Becton, Dickinson and Company (BD) LSR II flow cytometer (BD Biosciences, Oxford, UK).

#### 2.2.13.1 Flow Cytometry Analysis of Cell Fluorescence

Cells were grown in the relevant culture medium to a density of $\sim$1x10$^7$ cells/ml before analysis with the flow cytometer. Up to 30,000 particles were analysed for fluorescence intensity per sample. Excitation was achieved using a 488 nm laser, and emission detected using a 530/30 nm band pass filter with a 505 nm long pass filter.

#### 2.2.13.2 Flow Cytometry Analysis of Cell Cycle Position

Cells were grown in the relevant culture medium to a density of $\sim$1x10$^7$ cells/ml. 1 ml of culture was sonicated, harvested by centrifugation and fixed in 1 ml of ice cold 70 % ethanol overnight. 300 $\mu$l of fixed cells were then washed in 3 ml of 50 mM sodium citrate and resuspended in 500 $\mu$l of 50 mM sodium citrate containing 0.1 mg/ml RNase A. Cells were incubated at 37$^o$C for 2 h before the addition of 500 $\mu$l of 50 mM sodium citrate containing 8 g/ml propidium iodide. Up to 30,000 particles per sample were then analysed using the

flow cytometer, measuring the intensities of staining with propidium iodide. Excitation was achieved using a 488 nm laser, and emission detected using a 575/26 nm band pass filter with a 550 nm long pass filter.

### 2.2.14 Fluorescence Assays Using Multi-well Microplate-reader

24 well clear-bottom microplates were prepared by adding 1 % Agarose to DMM, heating and mixing until dissolved (making 1 % DMMA). This was allowed to cool to 50°C before adding and gently mixing the required amount of P-factor dissolved in methanol (not more than 10 % final volume of plug). Pheromone treated 1 % DMMA was added to each well (2.5 ml per well in a 24-well plate) under aseptic conditions and the plate allowed to dry for 2 h, maintained at a temperature of 30°C on a heat plate inside a flow cabinet. Fluorescence and $OD_{620}$ of each well of the 24-well plate was measured in triplicate using a Berthold Mithras LB940 BRET multi-mode microplate-reader (Berthold Technologies (UK) Ltd, Harpenden, Hertfordshire, UK) to determine the baseline.

*Sz. pombe* cell cultures were grown to mid-log phase at high density ($\sim 2 \times 10^8$ cells/ml) in DMM (minus selective amino acids, as required). 75 $\mu$l of cells were place onto the top of plugs in the prepared 24-well plates. An even spread of cells was ensured by manipulation of the plate and then the liquid was allowed to dry for 5 min inside the flow cabinet at a temperature of 30°C. Following this, the plate is installed in the measurement chamber or the Mithras LB940 microplate-reader and the measurement program initialised. The program maintains temperature at 30°C and measures fluorescence (at 530 nm for GFP and 535 nm for Venus) then $OD_{620}$ at 30 min intervals over the course of 16 h. For $OD_{620}$ and fluorescence measurements, lamp intensity was set to 12,500 intensity units with a measurement time of 0.5 s.

#### 2.2.14.1 Analysis of Multi-well Fluorescence Assay Data

Baseline fluorescence and $OD_{620}$ were subtracted from the measured fluorescence and $OD_{620}$, respectively. The corrected fluorescence measurements were then divided by the corrected $OD_{620}$ measurements to provide "Fluorescence units" that take into account cell size and volume.

GraphPad Prism software version 4.03 was used to plot time-dependent and dose-dependent data, where appropriate fitting nonlinear curves to the data for visual clarity. The regression method was selected based on the fit that would be most appropriate for the data-points observed.

### 2.2.15 Image Analysis

All image processing was performed using the open source software ImageJ (http://rsb.info.nih.gov/ij/). Cell segmentation and tracking was performed using the Quantitative Imaging of Membrane Proteins (QuimP) plugin for ImageJ, first described by Dormann et al., 2002 and further developed to quantify spatio-temporal patterns of fluorescently labelled proteins in the cortex of moving cells by Bosgraaf et al., 2009; Tyson et al., 2010 and Bosgraaf and Van Haastert, 2010. All images to be analysed with QuimP were processed by creating maximal projections from Z-stacks and subtracting background pixel intensity prior to analysis.

#### 2.2.15.1 Cell Segmentation and Tracking

QuimP software was used to segment individual cells within an image. Cell selection was where possible, randomised by using a random number generator to obtain a coordinate on the image and subsequently selecting the closest cell to this co-ordinate (based on distance to the closest cell edge).

#### 2.2.15.2 Single Cell Quantification

The image analysis software QuimP calculates fluorescence measurements from pixel intensities and cell size measurements based on the cell outline for each single time point image or for each frame of a given time-series set of images. This data was analysed further using bespoke program code written in Matlab and using GraphPad Prism software version 4.03.

### 2.2.16 Computational Methods

Modelling and simulation were performed using bespoke code written and implemented within Mathematica 7.0 and 8.0 (Wolfram Research Inc., USA, 2003). The *xCellerator* (California Institute of Technology, USA, 2005) free-ware add-on package for *Mathematica* was used to facilitate *in silico* experimentation and hypothesis modification. The package is able to take a reaction scheme as input and produce an equivalent system of ordinary differential equations (ODEs).

#### 2.2.16.1 Numerical Differential Equation Solver

Systems of ODE's were solved using the in-built *Mathematica* function `NDSolve` with the default options. This function has a range of available algorithms at its disposal and selects the most appropriate depending on the type of system being solved. It automatically adjusts step-size to achieve the specified accuracy and precision, which in all cases were set to `Automatic` and found to function without introducing any significant numerical errors.

#### 2.2.16.2 Simulation of Dose-response Curves

To simulate the addition of pheromone after a certain time, the ligand concentration was increased from zero up to a range of concentrations ($10^{-9}$M to $10^{-4}$M) corresponding approximately to the concentrations seen by cells in an assay. The system was allowed to reach steady state in the absence of ligand before it was added. The increase in ligand concentration was not quite instantaneous, instead a *tanh* function was used to avoid numerical errors that can occur at discontinuities, during the solving process. It is assumed that binding of ligand to receptor depletes the local availability of ligand. The output is taken to be the number of active effector complexes and is integrated over the duration of the simulated assay to mimic the accumulation of the reporter gene $\beta$-galactosidase, which in *Sz. pombe* is very stable. The accumulated quantity is plotted against the stimulating quantity of ligand to produce a simulated dose-response curve.

#### 2.2.16.3 Simulated Modified Strains

Modifications to the simulated *wild-type* strain were achieved either by altering the values used for reaction rate constants, usually setting some of them to zero to prevent the required reactions from occurring, or by altering the initial concentrations of some species to simulate additional plasmid-borne expression or gene deletions.

# Chapter 3

# Investigating G$\alpha$ Nucleotide Exchange

## 3.1 Background

The key, central regulatory process that determines whether a G protein will propagate a signal is the nucleotide bound state of the G$\alpha$ subunit. The G protein is a molecular switch, which is 'off' when GDP-bound and 'on' when GTP-bound, therefore the exchange of nucleotides provides high level control over the activation of downstream pathways and can coordinate the speed and amplitude of a signalling response (Ross, 2008). Steady state signal output is a balance between the rate of GTP binding and the rate of GTP hydrolysis. Nucleotide exchange can occur through the release of GDP by the activation of a GEF such as a ligand-occupied GPCR, resulting in subsequent attachment of GTP. The switch back to the GDP-bound state occurs through GTP hydrolysis, either very slowly through intrinsic GTPase activity, or rapidly through interaction with GAPs such as RGS proteins. In addition to GDP and GTP-bound states, transition states between the two are also possible, which provide added complexity. The Smith *et al.* kinetic model of the G protein cycle was built based on quantitative experimental data from the mating-response pathway in *S. pombe* (Smith et al., 2009) and it places significant importance on GTP hydrolysis of an inactive, but GTP-bound state of the G$\alpha$ in order to be able to reproduce the biological data.

To investigate the system level effects of altering nucleotide exchange events of G$\alpha$, a number of Gpa1 mutants (some previously uncharacterised) are quantified for their signalling activity in the mating-response of *S. pombe*. Furthermore, the Smith *et al.* model of the GTPase cycle is perturbed to investigate the sensitivity of reaction rate parameters and to compare model simulations to quantitative biological data to predict possible behaviours of the specific mutants.

## 3.2 Smith *et al.* Model of the G protein Cycle: A Positive Regulatory Effect of GTP Hydrolysis

The mating-response pathway in the fission yeast *S. pombe* has been used as a model system to study G protein mediated signalling in isolation. A nucleotide exchange event, more often associated with a dampening down of signalling response, was identified as having the opposite effect in the mating-response pathway (Smith et al., 2009). The RGS-catalysed hydrolysis of GTP->GDP is required to achieve maximal levels of signalling when the pathway is saturated with high ($\geq 10^{-7}$M) concentration of P-factor (Figure 3.1, A). This positive regulatory effect could only be simulated by introducing an additional state for the G$\alpha$ species, which was associated with GTP, yet remained inactive (inertG$\alpha_{\mathrm{GTP}}$). Hydrolysis of inertG$\alpha_{\mathrm{GTP}}$ is required to be released from this inactive state, therefore having a positive influence on signal transduction. The ODE model developed by Smith *et al.* introduces the concept of this additional G$\alpha$ state and is capable of reproducing this counterintuitive experimental data (Figure 3.1, B) (Smith et al., 2009). These initial model building efforts are summarised here to enhance reader understanding of the methods by which G protein signalling is being simulated and of the work presented in this chapter.

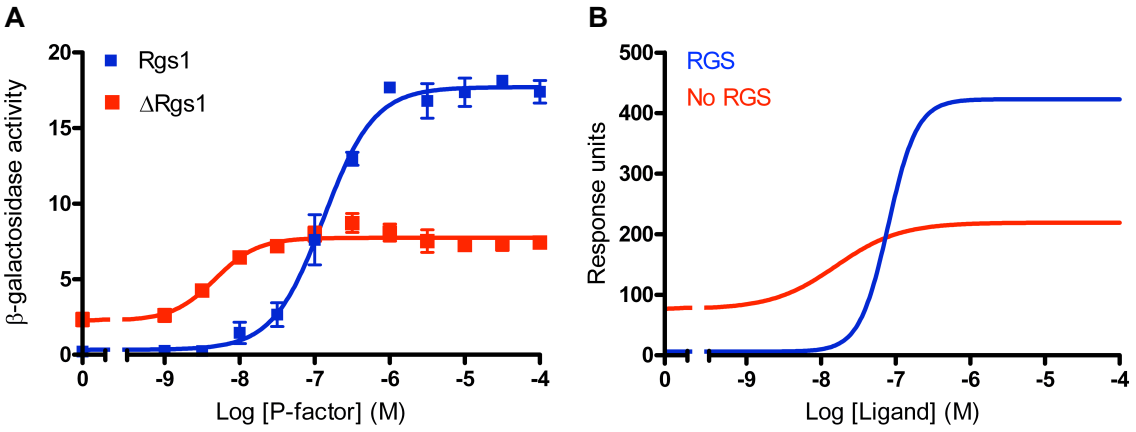


FIGURE 3.1: **The dual role of Rgs1.** A: *S. pombe* reporter strain JY544, which has endogenous Rgs1 present (Rgs1) and reporter strain JY630, which lacks endogenous Rgs1 (ΔRgs1) were cultured in minimal media to a density of ~5x10$^6$ cells/ml, before assaying for $\beta$-galactosidase activity. $\beta$-galactosidase activity was measured as OD$_{420}$/10$^6$ cells. Results are the means ± S.E.M. of triplicate determinations of three independent isolates. B: Simulations of the Smith *et al.* model (Table 3.1) with (RGS) and without (no RGS) an RGS species. The concentration of ligand in the simulation was varied over the range 0-100 $\mu$M following 16 h simulated induction. Output from the model shows the accumulation of activated G$\alpha_{GTP}$Effector complexes over the duration of the simulated assay. Figure adapted from Smith et al., 2009.

### 3.2.1 Model Reaction Scheme

The reaction scheme for this model includes the transition of G$\alpha_{\mathrm{GTP}}$ into inertG$\alpha_{\mathrm{GTP}}$ following activation of a single downstream effector species. The release from this state is by

intrinsic or RGS-catalysed hydrolysis of inert$G\alpha_{GTP}$ (Table 3.1). This model represents a conceptual advancement in the cycling of G proteins, but as yet the presence of the proposed inert state remains unproven.

| | | | |
|---|---|---|---|
| $L + R \rightarrow LR$ | $k_1$ | 0.0025 | $nM^{-1}h^{-1}$ |
| $G\alpha\beta\gamma + R \rightarrow RG\alpha\beta\gamma$ | $k_2$ | 0.005 | $nM^{-1}h^{-1}$ |
| $G\alpha\beta\gamma + LR \rightarrow LRG\alpha\beta\gamma$ | $k_3$ | 0.02 | $nM^{-1}h^{-1}$ |
| $L + RG\alpha\beta\gamma \rightarrow LRG\alpha\beta\gamma$ | $k_4$ | 0.005 | $nM^{-1}h^{-1}$ |
| $LRG\alpha\beta\gamma \rightarrow G\alpha_{GTP} + G\beta\gamma + LR$ | $k_5$ | 50 | $h^{-1}$ |
| $G\alpha\beta\gamma \rightarrow G\alpha_{GTP} + G\beta\gamma$ | $k_6$ | 0.2 | $h^{-1}$ |
| $G\alpha_{GTP} + RGS \rightarrow RGSG\alpha_{GTP}$ | $k_7$ | 500 | $nM^{-1}h^{-1}$ |
| $RGSG\alpha_{GTP} \rightarrow G\alpha_{GDPP} + RGS$ | $k_8$ | 2.5 | $h^{-1}$ |
| $G\alpha_{GTP} \rightarrow G\alpha_{GDPP}$ | $k_9$ | 0.005 | $h^{-1}$ |
| $Effector + G\alpha_{GTP} \rightarrow G\alpha_{GTP}Effector$ | $k_{10}$ | 10 | $nM^{-1}h^{-1}$ |
| $G\alpha_{GTP}Effector \rightarrow Effector + inertG\alpha_{GTP}$ | $k_{11}$ | 1 | $h^{-1}$ |
| $inertG\alpha_{GTP} + RGS \rightarrow RGSinertG\alpha_{GTP}$ | $k_{12}$ | 50 | $nM^{-1}h^{-1}$ |
| $RGSinertG\alpha_{GTP} \rightarrow RGS + G\alpha_{GDPP}$ | $k_{13}$ | 0.3 | $h^{-1}$ |
| $inertG\alpha_{GTP} \rightarrow G\alpha_{GDPP}$ | $k_{14}$ | 0.005 | $h^{-1}$ |
| $G\alpha_{GDPP} \rightarrow G\alpha_{GDP} + P$ | $k_{15}$ | 1000 | $h^{-1}$ |
| $G\alpha_{GDP} + G\beta\gamma \rightarrow G\alpha\beta\gamma$ | $k_{16}$ | 1000 | $nM^{-1}h^{-1}$ |
| $P \rightarrow \emptyset$ | $k_{17}$ | 10 | $h^{-1}$ |

TABLE 3.1: **Reaction scheme for Smith *et al.* model of the G protein cycle (Smith et al., 2009).** This reaction scheme contains all the basic elements of G protein activation and deactivation as proposed by Zhong et al., 2003; Hao et al., 2003; Kofahl and Klipp, 2004; Yildirim et al., 2004; Bornheimer et al., 2004 and Goryachev and Pokhilko, 2006 plus additional reactions describing spontaneous Gα activation and reactions involving an inert$G\alpha_{GTP}$ state proposed by Smith et al., 2009. Each of the 17 reactions are defined alongside their associated rate constant (k).

### 3.2.2 Model Equations

To run simulations of the model, in order to be able to simulate dose-response profiles such as in Figure 3.1, B that can closely represent the data from experimental assay, the reaction scheme has to be converted into a system of ODEs. This allows quantification of each species concentration over a given time period for a simulated assay, through solving the equations using a numerical differential equation solving algorithm. Some additional equations are also included in attempts to model the situation of cells in experimental assay.

#### 3.2.2.1 Ligand Addition

To simulate incubation of cells followed by stimulation with ligand, the initial ligand concentration (L(0)) is set to 0M for a period of time ($t_0$ = 14 h) to allow the system to pre-equilibrate. The ligand concentration is then very rapidly, but not discontinuously increased to the specified concentration (L($t_0$)) for the experiment, using the expression

$$L(t) = \frac{L(t_0)}{2}(\tanh(b * (t - t_0)) + \tanh(b * t_0))L(t_0). \tag{3.1}$$

The constant $b$ controls the sharpness of ligand addition, increasing this value makes the addition closer to a step-function. The value of $b$ used in the simulations was 100. This gives a close to instantaneous ligand application, although still sufficiently smooth that the numerical differential equation solving algorithm remains accurate in this region.

#### 3.2.2.2 Measuring Response

The *in vivo S. pombe* mating-response is measured by detecting the accumulated quantity of $\beta$-galactosidase through colourimetric assay (Didmon et al., 2002). This is simulated by measuring an integral, from t = 0 h up to a short time after the system reaches a new equilibrium following stimulation with ligand, $t_{assay}$. A cascade of linear relaxation elements (z1(t), z2(t) and z3(t)) is applied to the number of active effector molecules ($G\alpha_{GTP}$Effector), and $\int_0^{t_{assay}} z3(t)$ is the quantity measured as output response from the model. The cascade is applied by augmenting the system of differential equations with

$$z1(t)' = \alpha * G\alpha^*_{GTP}\text{Effector} - \alpha * z1(t). \tag{3.2}$$
$$z2(t)' = \alpha * z1(t) - \alpha * z2(t). \tag{3.3}$$
$$z3(t)' = \alpha * z2(t) - \alpha * z3(t). \tag{3.4}$$

This simplistically models all components downstream of the G protein and reflects the time difference between the rapid dynamics of the G protein cycle and the expression of the reporter protein. The delay parameter $\alpha$ was chosen based on time-course experiments; induction of $\beta$-galactosidase in response to P-factor becomes detectable between 2 h and 4 h (Smith et al., 2009). In the absence of detailed data for the *Sz. pombe* G protein cycle, the initial non-equilibrium G protein cycle dynamics are assumed to occur over a period of about an hour. This is close to the time taken for Sxa2 production (Imai and Yamamoto, 1992; Ladds et al., 1996b). To stretch the response time to that seen in the time-course experiment, a value of $\alpha = 3/2$ is used. The production of the P-factor inducible reporter gene, expressed from the *sxa2* promotor is essentially what is being measured in assays of reporter strains containing *sxa2>lacZ*. The ODE model aims to simulate this P-factor induced response.

#### 3.2.2.3 System of Ordinary Differential Equations

The system of ODEs generated from the reaction scheme (Table 3.1) is presented in Table 3.2. The model is initiated with species concentrations L = 0-100,000 nM, R = 205 nM, $G\alpha_{GDP}$ = 205 nM, $G\beta\gamma$ = 205 nM, RGS = 60 nM and Effector = 205 nM. Values for R, $G\alpha_{GDP}$, $G\beta\gamma$ and RGS are assumed the same as in published data for *S. cerevisiae* (Yildirim et al., 2004). All other species are initiated at 0 nM.

| | |
|---|---|
| Effector | Effector'(t) = - $k_{10}$Effector(t) $G\alpha_{GTP}$(t) + $k_{11}G\alpha_{GTP}$Effector(t) |
| $G\alpha\beta\gamma$ | $G\alpha\beta\gamma$'(t) = - $k_6G\alpha\beta\gamma$(t) - $k_2G\alpha\beta\gamma$(t) R(t) - $k_3G\alpha\beta\gamma$(t) LR(t) + $k_{16}G\beta\gamma$(t) $G\alpha_{GDP}$(t) |
| $G\beta\gamma$ | $G\beta\gamma$'(t) = $k_6G\alpha\beta\gamma$(t) + $k_5$LR$G\alpha\beta\gamma$(t) - $k_{16}G\beta\gamma$(t) $G\alpha_{GDP}$(t) |
| L | L'(t) = - $\frac{1}{2}$ $k_1$L(t) R(t) (Tanh($t_0$ b) - Tanh(b($t_0$ - t))) - $\frac{1}{2}$ $k_4$L(t) R$G\alpha\beta\gamma$(t) (Tanh($t_0$ b) - Tanh(b($t_0$ - t))) |
| P | P'(t) = - $k_{17}$P(t) + $k_{15}G\alpha_{GDPP}$(t) |
| R | R'(t) = - $k_2G\alpha\beta\gamma$(t) R(t) - $\frac{1}{2}$ $k_1$L(t) R(t) (Tanh($t_0$ b) - Tanh(b($t_0$ - t))) |
| R$G\alpha\beta\gamma$ | R$G\alpha\beta\gamma$'(t) = $k_2G\alpha\beta\gamma$(t) R(t) - $\frac{1}{2}$ $k_4$L(t) R$G\alpha\beta\gamma$(t) (Tanh($t_0$ b) - Tanh(b($t_0$ - t))) |
| LR$G\alpha\beta\gamma$ | LR$G\alpha\beta\gamma$'(t) = - $k_5$LR$G\alpha\beta\gamma$(t) + $k_3G\alpha\beta\gamma$(t) LR(t) + $\frac{1}{2}$ $k_4$L(t) R$G\alpha\beta\gamma$(t) (Tanh($t_0$ b) - Tanh(b($t_0$ - t))) |
| LR | LR'(t) = $k_5$LR$G\alpha\beta\gamma$(t) - $k_3G\alpha\beta\gamma$(t) LR(t) + $\frac{1}{2}$ $k_1$L(t) R(t) (Tanh($t_0$ b) - Tanh(b($t_0$ - t))) |
| $G\alpha_{GDP}$ | $G\alpha_{GDP}$'(t) = - $k_{16}G\beta\gamma$(t) $G\alpha_{GDP}$(t) + $k_{15}G\alpha_{GDPP}$(t) |
| $G\alpha_{GDPP}$ | $G\alpha_{GDPP}$'(t) = - $k_{15}G\alpha_{GDPP}$(t) + $k_9G\alpha_{GTP}$(t) + $k_{14}$inert$G\alpha_{GTP}$(t) + $k_8$RGS$G\alpha_{GTP}$(t) + $k_{13}$RGSinert$G\alpha_{GTP}$(t) |
| $G\alpha_{GTP}$ | $G\alpha_{GTP}$'(t) = $k_6G\alpha\beta\gamma$(t) + $k_5$LR$G\alpha\beta\gamma$(t) - $k_9G\alpha_{GTP}$(t) - $k_{10}$Effector(t) $G\alpha_{GTP}$(t) - $k_7G\alpha_{GTP}$(t) RGS(t) |
| $G\alpha_{GTP}$Effector | $G\alpha_{GTP}$Effector'(t) = $k_{10}$Effector(t) $G\alpha_{GTP}$(t) - $k_{11}G\alpha_{GTP}$Effector(t) |
| inert$G\alpha_{GTP}$ | inert$G\alpha_{GTP}$'(t) = $k_{11}G\alpha_{GTP}$Effector(t) - $k_{14}$inert$G\alpha_{GTP}$(t) - $k_{12}$inert$G\alpha_{GTP}$(t) RGS(t) |
| RGS | RGS'(t) = - $k_7G\alpha_{GTP}$(t) RGS(t) - $k_{12}$inert$G\alpha_{GTP}$(t) RGS(t) + $k_8$RGS$G\alpha_{GTP}$(t) + $k_{13}$RGSinert$G\alpha_{GTP}$(t) |
| RGS$G\alpha_{GTP}$ | RGS$G\alpha_{GTP}$'(t) = $k_7G\alpha_{GTP}$(t) RGS(t) - $k_8$RGS$G\alpha_{GTP}$(t) |
| RGSinert$G\alpha_{GTP}$ | RGSinert$G\alpha_{GTP}$'(t) = $k_{12}$inert$G\alpha_{GTP}$(t) RGS(t) - $k_{13}$RGSinert$G\alpha_{GTP}$(t) |
| z(1) | z(1)'(t) = $\frac{3}{2}$ Effector(t) $G\alpha_{GTP}$- $\frac{3}{2}$ z(1)(t) |
| z(2) | z(2)'(t) = $\frac{3}{2}$ z(1)(t) - $\frac{3}{2}$ z(2)(t) |
| z(3) | z(3)'(t) = $\frac{3}{2}$ z(2)(t) - $\frac{3}{2}$ z(3)(t) |

TABLE 3.2: **System of ODEs for simulating the Smith *et al.* model of the G protein cycle (Smith et al., 2009).** The table shows each species defined within the model and its associated differential equation describing the rate of change in that species concentration with time. The ODEs are generated from the reaction scheme in Table 3.1. For reaction rate constants (k) refer to Table 3.1. b = 100 (constant for ligand addition), $t_0$ = 14 (equilibration time before ligand application).

This modelling of the G protein cycle, based on the mating-response in *S. pombe* presents a conceptual advancement through the prediction of the inert$G\alpha_{GTP}$ state. The model itself, although incomplete in terms of signalling components, is used as a starting point in this thesis for further development. Additionally, the reaction rates for important regulatory nucleotide exchange events are largely unknown and have not been extensively investigated in either the biological system or the mathematical model. This chapter presents some of the work towards resolving these issues.

## 3.3 Tagging Gpa1

There were a number of motivations for tagging the G$\alpha$ subunit; Gpa1. Firstly, the Smith *et al.* model predicts an inert state for G$\alpha$ (Smith et al., 2009), but this is yet to be confirmed experimentally. By tagging Gpa1 with an epitope that has an associated selective antibody, the protein could be pulled-down and purified to be used in *in vitro* GTP turnover assays to gather evidence for the existence of the inert state. Additionally, the identity of the effector protein downstream of Gpa1 remains unconfirmed. Purification of Gpa1 in complex with binding partners and subsequent mass spectrometry analysis could lead to the identification of this effector protein and also the identification of binding partners specific to the GDP or GTP-bound forms of Gpa1. Another motivation was to improve the model by obtaining more accurate kinetics for protein-protein interactions involving Gpa1. Functional, C-terminal fluorescently tagged receptor (Mam2) and RGS (Rgs1) proteins have been constructed and if Gpa1 was also made with an appropriate fluorescent tag, then this would enable Fluorescent Resonance Energy Transfer (FRET) experiments to obtain protein-protein binding and dissociation rates. Additionally, a functional, fluorescent labelled protein would allow visualisation of Gpa1 cellular localisation under various physiological conditions.

### 3.3.1 Fluorescent Labelling

GFP was selected as the tag for Gpa1, as a GFP antibody was already available for use to purify the protein and for identification through western blotting. Additionally, GFP can be used in FRET experiments as the donor fluorophore (Pollok and Heim, 1999). A Gpa1 construct was made with GFP fused directly in frame to Gpa1 at the C-terminus. The C-terminus was preferred over the N-terminus due to the fact that Gpa1 undergoes post-translational modification, whereby the protein is cleaved after the N-terminal methionine residue, therefore making N-terminal tagging inappropriate (Godfrey, PhD Thesis, 2009). Gpa1 is coupled to the cell surface GPCR Mam2, and itself undergoes lipid modifications, therefore it is likely to be plasma membrane localised. Indeed previous studies have shown that the first 40 amino acid residues alone of Gpa1 are sufficient to direct plasma membrane localisation of the protein (Godfrey, PhD Thesis, 2009). This is most likely due to sites within this region for palmitoylation and myristoylation, which promote membrane association.

GFP and the Gpa1-GFP fusion protein were expressed from thiamine-repressible *nmt1* promoters on the pREP3x plasmid (Maundrell, 1993) in the $\beta$-galactosidase reporter strain JY1285(*sxa2>lacZ*, $\Delta$Gpa1). The pREP3x plasmid contains contains the LEU2 nutritional marker for the selection of transformants on minimal media growth plates lacking leucine.

Strains transformed with the plasmids were grown in minimal media lacking leucine for selection and thiamine for maximal protein expression levels before imaging with a DeltaVision wide-field microscope. Imaging confirmed that Gpa1-GFP is being expressed and predictably localises to the plasma membrane of the cell (Figure 3.2).

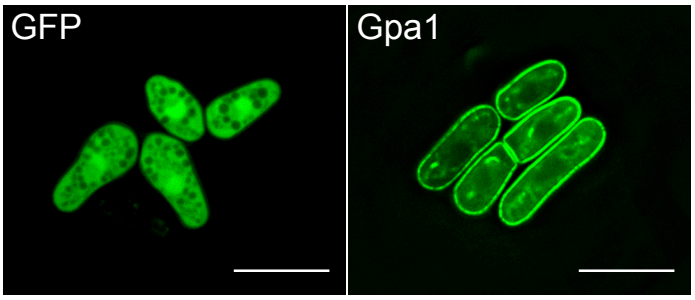


FIGURE 3.2: **GFP labelling of Gpa1.** Gpa1 was fused directly in frame to GFP at its C-terminus and expressed from expression vector pREP3x in strain JY1285 (ΔGpa1). Images were generated using a DeltaVision wide-field deconvolution microscope and are representative of three independent transformations. Scale bar = 10 $\mu$m

It is possible to measure the level of signalling through the mating-response pathway in *S. pombe* (Obara et al., 1991; Ladds et al., 2007). Replacement of a highly inducible and non-essential mating-response gene (*sxa2*) with a $\beta$-galactosidase reporter gene (*lacZ*), allows colourimetric determination of the quantity of signal transmitted through the pathway of M-type cells stimulated with the mating pheromone, P-factor (Didmon et al., 2002). For the Gpa1-GFP fusion protein to be useful in possible FRET experiments, purification and *in-vitro* assays of GTP turnover, it was necessary to assay its signalling activity to confirm functionality. Transformed strains were grown in minimal media lacking leucine and thiamine, incubated with P-factor at $10^{-5}$M or 0M for 16 h before assaying for induction of *sxa2>lacZ* (Figure 3.3).

The Gpa1-GFP fusion protein failed to give any P-factor induced signalling response and therefore was not functional (Figure 3.3). The C-terminal amino acids of G$\alpha$ proteins have been shown to be responsible for interaction with GPCRs (Dowell et al., 2002; Ladds et al., 2003), therefore the addition of GFP at the C-terminus of the protein could hinder the functionality of the protein through preventing interaction with Mam2.

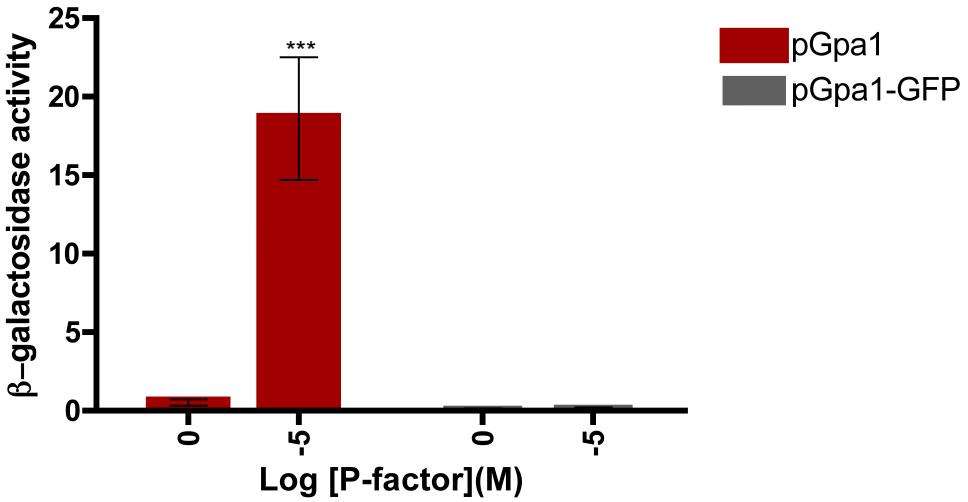


FIGURE 3.3: **Signalling activity of GFP labelled Gpa1.** Gpa1, and the C-terminal GFP fusion construct Gpa1-GFP were expressed from pREP3x in strain JY1285(*sxa2>lacZ*, ΔGpa1). Cells were cultured in minimal media lacking leucine to a density of ~5x10$^6$ cells/ml, incubated with 0 or $10^{-5}$M P-factor before assaying for $\beta$-galactosidase activity. $\beta$-galactosidase activity was measured as $OD_{420}/10^6$ cells. Results are the means ± S.E.M. from triplicate determinations of three independent isolates. Significant difference to 0M P-factor treatment is indicated with ***($p$<0.001), **($p$<0.01) or *($p$<0.05) as determined by unpaired $t$ test.

#### 3.3.1.1 Fluorescent Labelling Within the Helical Domain

Previously, human Gα proteins have been fluorescently labelled and have remained functional through inserting the tag within specific regions in the middle of the protein, flanked by flexible linker sequences so as to allow correct protein folding. A functional human $G\alpha_q$-GFP fusion protein was created by inserting GFP flanked by a 6 residue ser/gly flexible linker sequence (S-G-G-G-G-S) between residues 124 and 125 in the αB/αC loop of the helical domain (Figure 3.4) (Hughes et al., 2001). $G\alpha_i$ was another human Gα subunit successfully fused to a fluorescent protein, in this case for use in FRET experiments investigating $G\alpha_i$ activation (Bunemann et al., 2003). Here YFP was inserted between residues 91 and 92 of the protein, again in a loop region of the helical domain.

GFP was inserted flanked by a flexible linker sequence in both of these equivalent positions within Gpa1. The equivalent insertion points to $G\alpha_q$-GFP and $G\alpha_i$-GFP in Gpa1 were after amino acid residue 160 ($Gpa1^{(160)GFP}$) and 132 ($Gpa1^{(132)GFP}$) respectively.

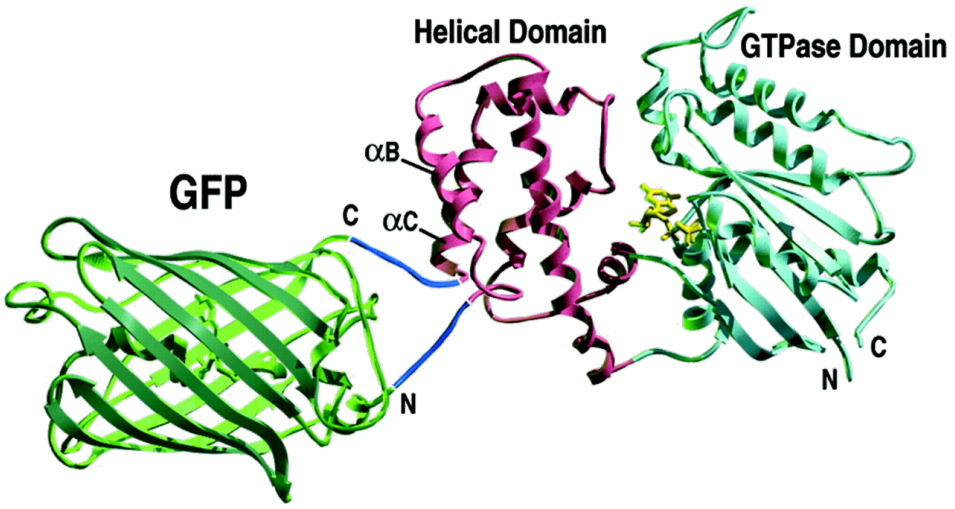


FIGURE 3.4: **Model of GFP labelling within the helical domain of Gα.** The GFP structure is shown in green. The Gα subunit structure is that of $G\alpha_q$GTPγS. The helical domain is pink and the GTPase domain is light blue. GTPγS is yellow. The SGGGGS linkers between GFP and the Gα subunit are shown schematically in dark blue. Figure from Hughes et al., 2001.

GFP alone and the Gpa1 GFP fusion constructs ($Gpa1^{(160)GFP}$ and $Gpa1^{(132)GFP}$) were expressed from pREP3x in the β-galactosidase reporter strain JY1285(*sxa2>lacZ*, ΔGpa1). Transformed strains were then grown in minimal media lacking leucine and thiamine before imaging with a DeltaVision wide-field microscope. This confirmed the fusions were being expressed and predictably localised to the plasma membrane (Figure 3.5).

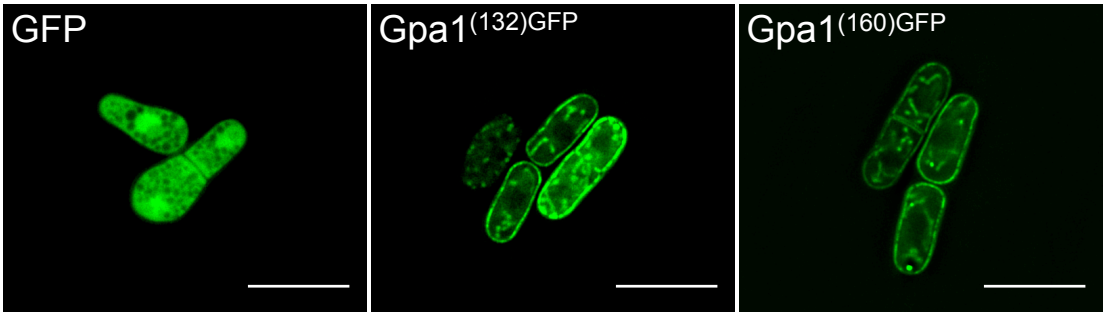


FIGURE 3.5: **GFP labelling Gpa1 within the helical domain.** Gpa1 constructs were made with GFP flanked by a serine and glycine flexible linker sequence (SGGGGS-GFP-SGGGGS) inserted after amino acid residue 132 ($Gpa1^{(132)GFP}$) and 160 ($Gpa1^{(160)GFP}$). These were expressed from vector pREP3x in strain JY1285(ΔGpa1). Images were generated using a DeltaVision wide-field deconvolution microscope and are representative of three independent transformations. Scale bar = 10 μm.

In the process of making the fusion constructs, constructs were also made with the linker alone inserted in the same positions ($Gpa1^{(160)linker}$ and $Gpa1^{(132)linker}$). These, along with the GFP fusions were expressed from pREP3x in the β-galactosidase reporter strain JY1285(*sxa2>lacZ*, ΔGpa1). Treatment of cells with increasing concentration of

P-factor, increases the number of GPCRs that become ligand bound and hence increases the subsequent ligand induced G protein activation. A dose-response profile is obtained by plotting the quantity of $\beta$-galactosidase/$10^6$ cells against the concentration of P-factor. Transformed strains were grown in minimal media lacking leucine and thiamine, incubated with P-factor at concentrations of 0M to $10^{-4}$M for 16 h before assaying for induction of *sxa2>lacZ* to test for functionality of the modified proteins (Figure 3.6).

GFP inserted within a flexible linker sequence after both positions 132 and 160 resulted in the loss of function of Gpa1. The only construct to show functionality was that with the flexible linker sequence inserted after position 160, although signalling was slightly reduced compared to *wild-type* Gpa1 (Figure 3.6). A fluorescent labelled and functional Gpa1 has not been obtained, and because of the lack of functionality these GFP fusion constructs were not deemed useful for any subsequent experiments.

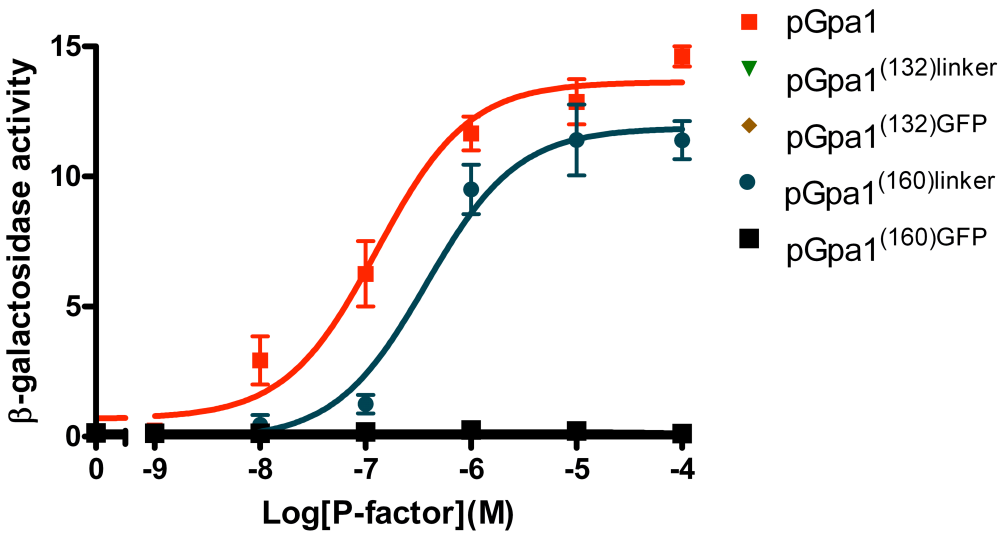


FIGURE 3.6: **Signalling activity of Gpa1 labelled with GFP within the helical domain.** Gpa1 constructs were made with a serine and glycine flexible linker sequence (SGGGGSSGGGGS) inserted after amino acid residue 132 (Gpa1$^{(132)linker}$) and 160 (Gpa1$^{(160)linker}$). Constructs were also made with GFP inserted in the middle of the linker sequence (SGGGGS-GFP-SGGGGS) at the same positions (Gpa1$^{(132)GFP}$ and Gpa1$^{(160)GFP}$). These and unmodified Gpa1 were expressed from pREP3x in strain JY1285(*sxa2>lacZ*, ΔGpa1). Cells were cultured in minimal media lacking leucine to a density of ~5x$10^6$ cells/ml, incubated with 0M to $10^{-4}$M P-factor before assaying for $\beta$-galactosidase activity. $\beta$-galactosidase activity was measured as $OD_{420}/10^6$ cells. Results are the means ± S.E.M. from triplicate determinations of three independent isolates.

### 3.3.2 FlAsH Tagging

One of the major problems with tagging a protein with GFP is the size of the tag. GFP is 238 amino acid residues in length and has a size of 26.9 kDa. This is over half the mass of

Gpa1 (46.2 kDa), therefore fusing it to Gpa1 or any other protein can often cause disruptions either in folding, or by blocking important interactions with binding partners, therefore reducing the proteins functionality (Zimmermann et al., 2003). A different method for achieving fluorescence of a specific protein is to use Fluorescein Arsenical Hairpin (FlAsH) tagging (Adams et al., 2002). The benefit of this being that the protein of interest only has to be modified by the addition of a six amino acid tetra-cysteine motif (Cys-Cys-Pro-Gly-Cys-Cys). This motif is specifically recognised by a membrane-permeable fluorescein derivative, FlAsH, which fluoresces only after the arsenics bind to the cysteine thiols (Figure 3.7). This technique has previously been used in live-cell imaging to study the glutamate analog $\alpha$-amino-3-hydroxy-5-methyl-4-isoxazolepropionic acid (AMPA) receptor in mammalian cells (Ju et al., 2004) and $\beta$-tubulin in yeast (Andresen et al., 2004). Although this technique would not allow for purification of the protein, the high affinity binding of FlAsH (24 pM Kd) leads to long term fluorescence of the protein, therefore time-series imaging and FRET experiments are possible (Chen and Ting, 2005).

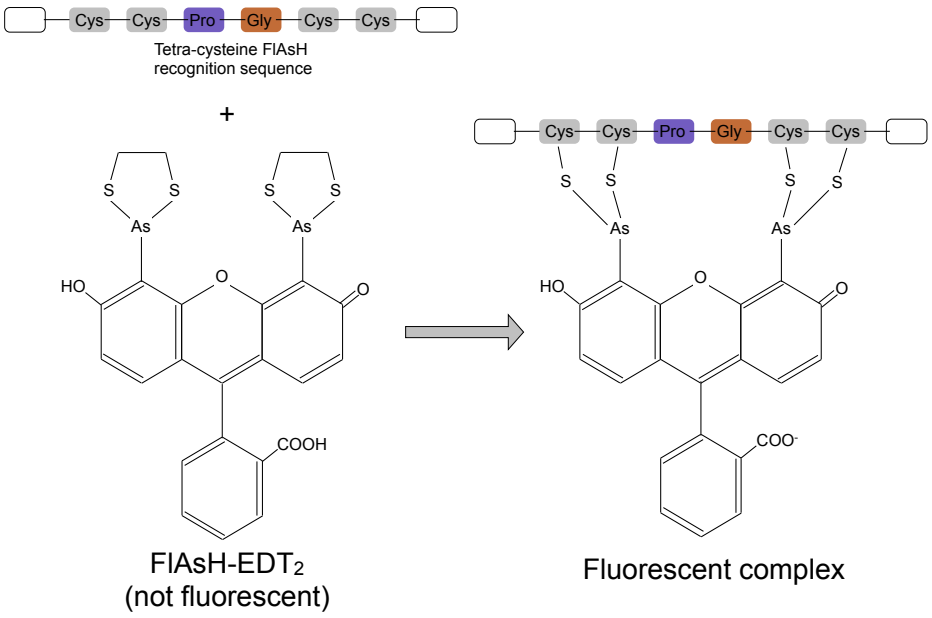


FIGURE 3.7: **Labelling proteins with FlAsH-EDT$_2$.** Upon binding of the bi-arsenical labelling reagent FlAsH-EDT$_2$ to recombinant proteins containing the tetra-cysteine motif Cys-Cys-Pro-Gly-Cys-Cys, EDT is displaced and the tag becomes highly fluorescent.

Gpa1 constructs were made with the tetra-cysteine motif flanked by the flexible linker sequence after amino acid residue 160 (Gpa1$^{(160)TetCys}$) and also at the C-terminus (Gpa1$^{(C-term)TetCys}$). The decision to try the motif at position 160 was based on the fact that previously, the linker sequence was placed here with little detrimental effect to protein function (Figure 3.6). Due to the small size of the motif making it less likely to interfere with protein functionality, it was also fused to the C-terminus. These

fusion constructs, along with unmodified Gpa1, were expressed from pREP3x in the β-galactosidase reporter strain JY1285(*sxa2>lacZ*, ΔGpa1). Transformed strains were grown in minimal media lacking leucine and thiamine, incubated with P-factor for 16 h before assaying for induction of *sxa2>lacZ* (Figure 3.8).

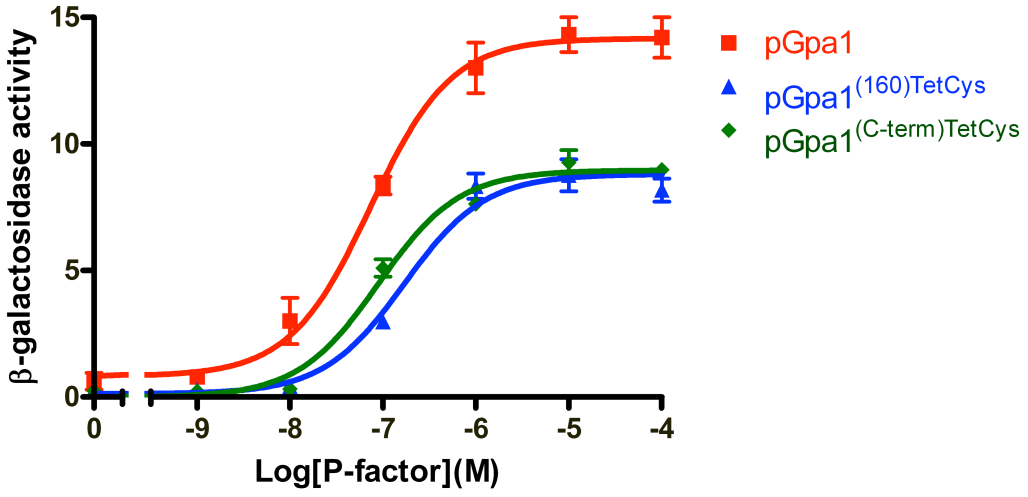


FIGURE 3.8: **Signalling activity of tetra-cysteine tagged Gpa1.** Gpa1 constructs were made with a tetra-cysteine tag flanked by a flexible linker sequence (SGGGGS-Cys-Cys-Pro-Gly-Cys-Cys-SGGGGS) after amino acid residue 160 (Gpa1$^{(160)TetCys}$) and at the C-terminus (Gpa1$^{(C-term)TetCys}$). These, and unmodified Gpa1 were expressed from pREP3x in strain JY1285(*sxa2>lacZ*, ΔGpa1). Cells were cultured in minimal media lacking leucine to a density of ∼5x10$^6$ cells/ml, incubated with 0M to $10^{-4}$M P-factor before assaying for β-galactosidase activity. β-galactosidase activity was measured as $OD_{420}/10^6$ cells. Results are the means ± S.E.M. from triplicate determinations of three independent isolates.

Gpa1 remains functional, in terms of signal propagation, when the tetra-cysteine motif is introduced after amino acid residue 160, and also at the C-terminus. Comparing to unmodified Gpa1, it seems the addition of the motif has a slight detrimental effect on signalling, but a ligand induced signalling response is still observed (Figure 3.8). Maximal signalling activity is reduced from 14.17 ± 0.37 for Gpa1 to 8.81 ± 0.30 for Gpa1$^{(160)TetCys}$ and 8.96 ± 0.23 for Gpa1$^{(C-term)TetCys}$. Sensitivity to ligand is lightly reduced from $pEC_{50}$ of 7.12 ± 0.09 for Gpa1 to 6.77 ± 0.10 for Gpa1$^{(160)TetCys}$ and 7.05 ± 0.08 for Gpa1$^{(C-term)TetCys}$. Having confirmed functionality of the tagged proteins, the transformed strains were then grown in minimal media lacking leucine and thiamine, incubated overnight with 4 μM FlAsH-$EDT_2$ and visualised with a DeltaVision wide-field microscope following the protocols used previously for FlAsH labelling proteins in yeast (Andresen et al., 2004). Imaging results indicate fluorescence localised to the vacuoles of the cells in both cells expressing unmodified Gpa1 and cells expressing the tetra-cysteine fusion proteins (Figure 3.9). This suggests that there was not any specific labelling of Gpa1 taking place.

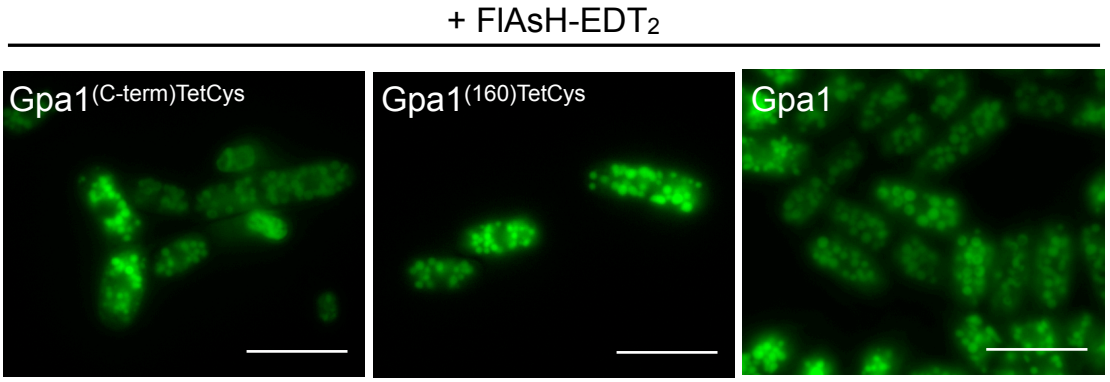


FIGURE 3.9: **Imaging of tetra-cysteine tagged Gpa1 treated with FlAsH-EDT$_2$.** Gpa1 constructs were made with a tetra-cysteine tag flanked by a flexible linker sequence (SGGGGS-Cys-Cys-Pro-Gly-Cys-Cys-SGGGGS) after amino acid residue 160 (Gpa1$^{(160)TetCys}$) and at the C-terminus (Gpa1$^{(C-term)TetCys}$). These, along with unmodified Gpa1 were expressed from expression vector pREP3x in strain JY1285(ΔGpa1) and incubated overnight with FlAsH-EDT$_2$ reagent before imaging. Images were generated using a DeltaVision wide-field deconvolution microscope and are representative of three independent transformations. Scale bar = 10 $\mu$m.

Tagging methods therefore failed to yield a labelled protein that could both be visualised and was functional. The problem of labelling with GFP is that it is likely to either inhibit correct protein folding or block important sites for binding with other signalling components and therefore is detrimental to protein function. Adding the much smaller tetra-cysteine motif did not abolish Gpa1 function, but the method for visualising the protein inside the cells using FlAsH-EDT$_2$ proved to be unsuccessful, as the tetra-cysteine labelled Gpa1 could not be visualised. As a result of not being able to obtain a functional protein that was labelled such that it could be purified and visualised, further experiments using a tagged Gpa1 protein were not pursued.

## 3.4 Characterisation of Gpa1 Nucleotide Exchange Mutants

To investigate the effect of altering the G$\alpha$ nucleotide exchange rate on signalling, a number of Gpa1 (the sole G$\alpha$ subunit in the *S. pombe* mating-response pathway) nucleotide cycling mutants were constructed (Table 3.3). These mutants are based on equivalent mutant human G proteins that have previously been characterised as having altered nucleotide exchange rates. Two residues have been identified as being necessary for GTPase activity. One is an arginine located within either the Switch I domains of the G$\alpha$ subunits of large G proteins or contributed by GAPs of small G proteins, often referred to as the 'arginine finger'. The other is a glutamine residue located in the Switch II domains of G$\alpha$ subunits (Majumdar et al., 2006). Mutations in either of these highly conserved residues severely compromise GTPase activity and moreover, have been associated with a variety of human tumours (Landis et al., 1989; Bourne, 1987; Weinstein et al., 1991). When compared to

each other in Gα transducin ($G\alpha_t$), the mutations were shown to have different effects on the ability to exchange GDP for GTP and on the proportions of the $G\alpha_t$ subunit in GTP, GDP and GDP-Pi-bound states, but both mutations showed similar inhibition of GTPase activity (Majumdar et al., 2006). The proportion of the Gα in various states is important for the level of signal transduction that could be achieved. The mutation of the Switch II region glutamine has been constructed previously in Gpa1 ($Gpa1^{Q244L}$) and signalling data indicated that it has reduced GTPase activity (Smith et al., 2009), although the mutant had not been extensively characterised. The equivalent arginine mutation in Gpa1 ($Gpa1^{R218C}$) had not previously been made or characterised, therefore its signalling activity was unknown.

Another previously uncharacterised series of mutants that have been constructed are the $Gpa1^{G83X}$ mutants , based on an equivalent mutation in the small monomeric G protein, Ras (Barbacid, 1987). Mutation of a glycine residue in this region renders the Ras GTPase domain insensitive to GAP activity, therefore making the protein fixed in the GTP-bound 'on' state and again this mutation is frequently found in human cancers and experimental cancer models (Barbacid, 1987; Bos, 1989). The equivalent glycine to valine mutation has also previously been investigated in *S. cerevisiae* Gpa1 because of this conserved residue being known to make contacts with the phosphates of GDP and GTP (Cismowski et al., 1999). The glycine in the *S. pombe* $Gpa1^{G83X}$ series of mutants has been replaced with four different amino acid residues, giving the mutants $Gpa1^{G83V}$, $Gpa1^{G83S}$, $Gpa1^{G83L}$ and $Gpa1^{G83A}$. All of the aforementioned mutations should give a Gα protein that is predominantly GTP-bound and have reduced capability to undergo the $G\alpha_{GTP}$ to $G\alpha_{GDP}$ transition. For comparison, an additional Gpa1 mutant ($Gpa1^{G243A}$) is investigated that has the opposite behaviour. This mutant is predominantly GDP-bound and therefore in the 'off' state, as it is incapable of exchanging GDP for GTP (Ladds et al., 2007). Table 3.3 summarises the mutants that are to be characterised.

| Mutant | Expected behaviour | Reference |
|---|---|---|
| $Gpa1^{Q244L}$ | Constitutively active - compromised GTPase activity | Obara et al., 1991; Majumdar et al., 2006; Smith et al., 2009 |
| $Gpa1^{G243A}$ | Inactive - unable to exchange GDP | Ladds et al., 2007 |
| $Gpa1^{R218C}$ | Compromised GTPase activity | Majumdar et al., 2006 |
| $Gpa1^{G83X}$ | Insensitive to GAP activity in small monomeric G proteins | Barbacid, 1987; Bos, 1989; Cismowski et al., 1999 |

TABLE 3.3: **Gpa1 nucleotide exchange mutants.** Summary of *S. pombe* Gpa1 nucleotide exchange mutants; $Gpa1^{Q244L}$, $Gpa1^{G243A}$, $Gpa1^{R218C}$ and $Gpa1^{G83X}$. The $Gpa1^{G83X}$ series of mutants consists of substitutions of glycine for valine, serine, leucine or alanine.

Gpa1$^{Q244L}$, Gpa1$^{G243A}$, Gpa1$^{R218C}$, the Gpa1$^{G83X}$ series of mutants and unmodified Gpa1 were expressed from the pREP3x plasmid in a number of different $\beta$-galactosidase reporter strains to investigate their signalling activity. Strains transformed with the plasmids were grown in minimal media lacking leucine and thiamine. These cultures could then be assayed for induction of *sxa2>lacZ* following 16 h with P-factor at concentrations ranging from 0M to $10^{-4}$M.

### 3.4.1 Spontaneous Activation

Spontaneous activation involves the release of GDP from the G$\alpha$, independently of any GEF activity. For *wild-type* G$\alpha$ subunits this usually occurs at a very slow rate, if at all, in order to reduce the unstimulated or unnecessary activation of downstream signalling pathways and to maintain sensitivity to ligand. The spontaneous activation is measured as the ability of the G$\alpha$ protein to activate the downstream signalling pathway independently of any ligand-activated receptors or any regulation by an RGS protein. To determine spontaneous activity of the Gpa1 mutants, Gpa1$^{Q244L}$, Gpa1$^{R218C}$, Gpa1$^{G243A}$ and the Gpa1$^{G83X}$ series of mutants were expressed from the pREP3x plasmid in a $\beta$-galactosidase reporter strain lacking endogenous Gpa1, Rgs1 and Mam2 (JY1286; *sxa2>lacZ*, ΔGpa1, ΔRgs1, ΔMam2). Strains transformed with the plasmids were grown in minimal media lacking leucine and thiamine then assayed for induction of *sxa2>lacZ* (Figure 3.10).

Data from investigating spontaneous activation (Figure 3.10) shows that Gpa1$^{Q244L}$ gives the highest level of spontaneous activation with a >3 fold increase in signalling compared to Gpa1, indicative of a high level of spontaneous activation and/or a compromised intrinsic GTP hydrolysis abilty. Gpa1$^{G243A}$ shows reduced spontaneous activation in keeping with its reduced ability to release GDP. Gpa1$^{R218C}$ gives slightly increased signalling (almost 2-fold increase compared to Gpa1), but lower than that seen for Gpa1$^{Q244L}$, indicating that this mutant could be an intermediate between Gpa1 and Gpa1$^{Q244L}$ in terms of its propensity to be in a GTP-bound state. Gpa1$^{G83X}$ mutants appear to have different characteristics in terms of spontaneous activity, depending on what the glycine residue has been replaced with (Figure 3.10). Gpa1$^{G83S}$ and Gpa1$^{G83L}$ have reduced spontaneous activation compared to Gpa1, with approximately half the levels of Gpa1. Gpa1$^{G83V}$ and Gpa1$^{G83L}$ give very little or no signalling activity indicating that replacing with valine or leucine at amino acid position 83 severely compromises Gpa1 functionality. Results appear to contradict the prediction that this mutation should render Gpa1 in a predominantly GTP-bound 'on' state, at least in terms of the proteins ability to activate in the absence of any ligand-activated GPCR.

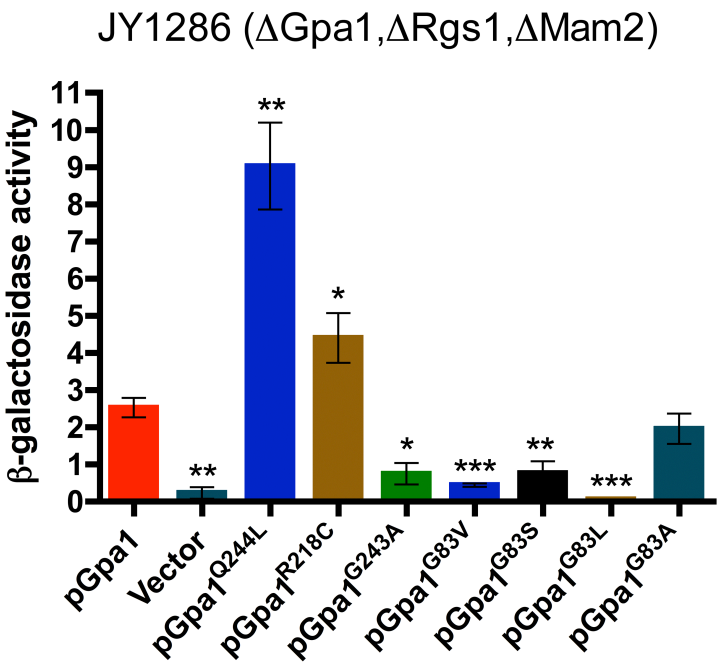


FIGURE 3.10: **Spontaneous activation of Gpa1 nucleotide exchange mutants.** Gpa1, Gpa1$^{Q244L}$, Gpa1$^{R218C}$, Gpa1$^{G243A}$, Gpa1$^{G83V}$, Gpa1$^{G83S}$, Gpa1$^{G83L}$ and Gpa1$^{G83A}$ were expressed from expression vector pREP3x in reporter strain JY1286(ΔGpa1,ΔRgs1,ΔMam2). Cells were cultured in minimal media lacking leucine to a density of ∼5x10$^6$ cells/ml, before assaying for $\beta$-galactosidase activity. $\beta$-galactosidase activity was measured as OD$_{420}$/10$^6$ cells. Results are the means ± S.E.M. of triplicate determinations from three independent isolates. Significant difference to pGpa1 is indicated with ***($p$<0.001), **($p$<0.01) or *($p$<0.05) as determined by unpaired $t$ test.

### 3.4.2 P-factor Induced Activation

A more efficient method of promoting GDP->GTP exchange on the G$\alpha$ subunit is through the activation of the GPCR it is coupled to, by the addition of a ligand. To gain insight into signalling behaviour when G$\alpha$ is the sole signal propagator, dose-response profiles were obtained for all Gpa1 mutants expressed in strains lacking endogenous Gpa1. Gpa1, Gpa1$^{Q244L}$, Gpa1$^{R218C}$, Gpa1$^{G243A}$ and the Gpa1$^{G83X}$ series of mutants were expressed from pREP3x in the $\beta$-galactosidase reporter strain containing Rgs1 (JY1285; *sxa2>lacZ*, ΔGpa1) and lacking Rgs1 (JY1287; *sxa2>lacZ*, ΔGpa1, ΔRgs1). Activity was investigated in the presence and absence of Rgs1, as Rgs1 is a key regulator of the G protein cycle by promoting GTP hydrolysis, therefore this will give insight into both the Rgs1-dependent and independent activity of the nucleotide exchange mutants. Transformed strains were then grown in minimal media lacking leucine and thiamine, incubated with P-factor at concentrations of 0M to 10$^{-4}$M for 16 h before assaying for induction of *sxa2>lacZ* (Figure 3.11 and Figure 3.12).

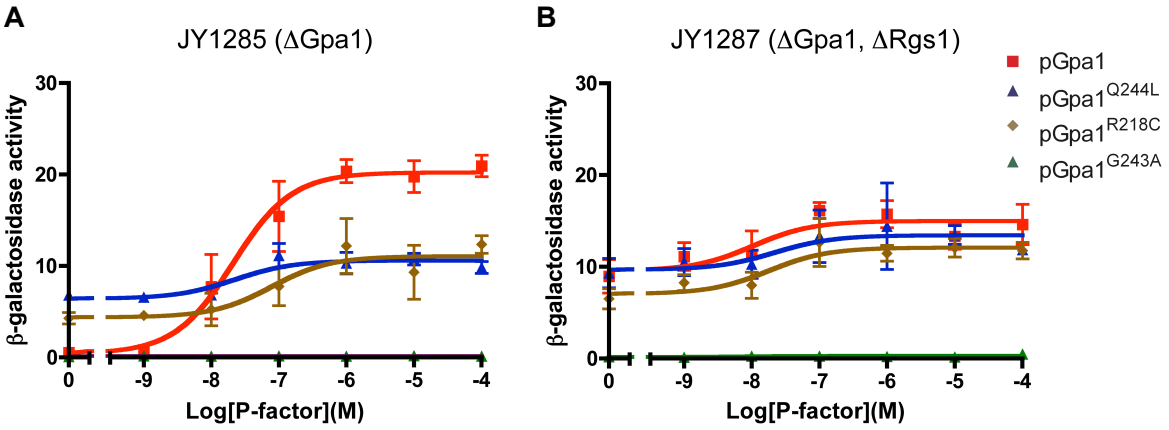


| | Basal | Maximal | $pEC_{50}$ |
|---|---|---|---|
| **JY1285 (ΔGpa1)** | | | |
| pGpa1 | 0.549 +/- 0.184 | 20.230 +/- 1.130 | 7.677 +/- 0.211 |
| $pGpa1^{Q244L}$ | 6.422 +/- 0.626 *** | 10.600 +/- 0.469 *** | 7.657 +/- 0.415 |
| $pGpa1^{R218C}$ | 4.386 +/- 1.084 ** | 11.080 +/- 1.134 ** | 7.110 +/- 0.558 |
| $pGpa1^{G243A}$ | 0.079 +/- 0.044 | 0.150 +/- 0.029 *** | N/A |
| **JY1287 (ΔGpa1, ΔRgs1)** | | | |
| pGpa1 | 8.959 +/- 1.826 | 14.990 +/- 0.943 | 7.979 +/- 0.623 |
| $pGpa1^{Q244L}$ | 9.671 +/- 1.373 | 13.430 +/- 1.145 | 7.666 +/- 1.022 |
| $pGpa1^{R218C}$ | 7.034 +/- 1.408 | 12.090 +/- 0.739 * | 7.752 +/- 0.540 |
| $pGpa1^{G243A}$ | 0.186 +/- 0.066 *** | 0.281 +/- 0.062 *** | N/A |

FIGURE 3.11: **Characterisation of Gpa1 nucleotide exchange mutants: $Gpa1^{Q244L}$, $Gpa1^{R218C}$ and $Gpa1^{G243A}$.** Gpa1, $Gpa1^{Q244L}$, $Gpa1^{R218C}$ and $Gpa1^{G243A}$ were expressed from vector pREP3x in reporter strains JY1285(ΔGpa1) (A) and JY1287(ΔGpa1,ΔRgs1) (B). Cells were cultured in minimal media lacking leucine to a density of ~5x$10^6$ cells/ml, incubated with 0M to $10^{-4}$M P-factor before assaying for $\beta$-galactosidase activity. $\beta$-galactosidase activity was measured as $OD_{420}/10^6$ cells. Results are the means ± S.E.M. of triplicate determinations from three independent isolates. The table summarises the mean basal, maximal and $pEC_{50}$ values ± S.E.M. for each profile. Values for mutants that are significantly different to pGpa1 are indicated with ***($p$<0.001), **($p$<0.01) or *($p$<0.05) as determined by unpaired $t$ test.

Signalling response in reporter strains expressing $Gpa1^{Q244L}$ is only slightly inducible with increasing P-factor concentration (Figure 3.11, A), and the removal of Rgs1 has little effect on the overall dose-response pattern other than to slightly raise the signalling levels at all concentrations (Figure 3.11, B), therefore suggesting a negative influence of Rgs1 that is independent of GAP activity. $Gpa1^{R218C}$ shows slight P-factor inducible response with similar sensitivity compared to Gpa1 ($pEC_{50}$ for $Gpa1^{R218C}$; 7.110 ± 0.558 vs Gpa1; 7.677 ± 0.211) (Figure 3.11, A). Removal of the negative regulation by Rgs1 again results in slightly increased signalling at low (0M) through to high ($10^{-4}$M) ligand concentration (compare Figure 3.11, A to Figure 3.11, B). The Gpa1 mutant unable to release GDP and therefore remaining inactive ($Gpa1^{G243A}$) shows no signalling activity.

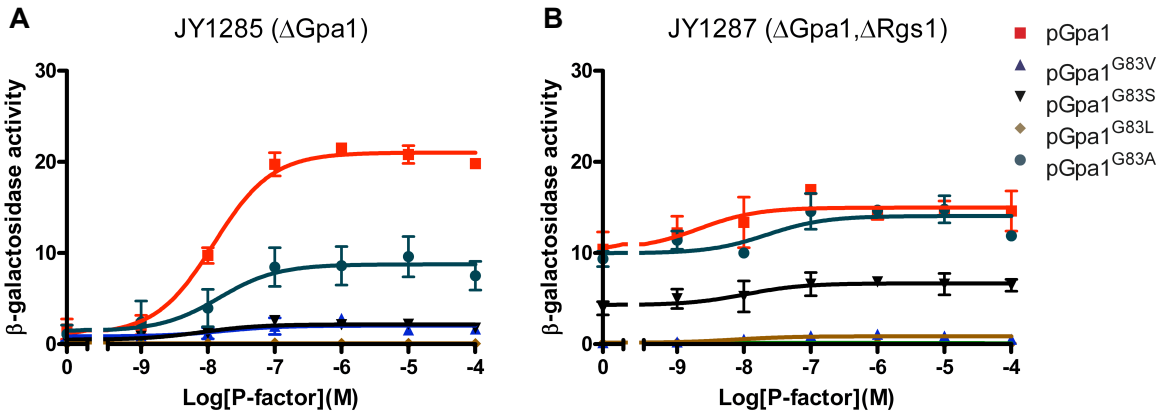


| | Basal | Maximal | $pEC_{50}$ |
|---|---|---|---|
| **JY1285 (ΔGpa1)** | | | |
| pGpa1 | 1.653 +/- 1.108 | 21.020 +/- 0.496 | 7.912 +/- 0.092 |
| $pGpa1^{G83V}$ | 0.901 +/- 0.587 | 2.035 +/- 0.306 *** | 7.794 +/- 0.946 |
| $pGpa1^{G83S}$ | 0.366 +/- 0.127 | 2.168 +/- 0.154 *** | 8.094 +/- 0.347 |
| $pGpa1^{G83L}$ | 0.073 +/- 0.073 | 0.121 +/- 0.056 *** | N/A |
| $pGpa1^{G83A}$ | 1.122 +/- 0.964 | 8.757 +/- 0.916 *** | 7.832 +/- 0.462 |
| **JY1287 (ΔGpa1, ΔRgs1)** | | | |
| pGpa1 | 10.419 +/- 1.900 | 14.980 +/- 0.785 | 8.668 +/- 0.819 |
| $pGpa1^{G83V}$ | 0.157 +/- 0.055 *** | 0.861 +/- 0.100 | N/A |
| $pGpa1^{G83S}$ | 3.936 +/- 0.716 * | 6.669 +/- 0.477 *** | 7.978 +/- 0.745 |
| $pGpa1^{G83L}$ | 0.091 +/- 0.042 *** | 0.097 +/- 0.068 *** | N/A |
| $pGpa1^{G83A}$ | 9.357 +/- 0.838 *** | 14.060 +/- 0.763 | 7.656 +/- 0.689 |

FIGURE 3.12: **Characterisation of Gpa1 nucleotide exchange mutants: $Gpa1^{G83X}$.** Gpa1, $Gpa1^{G83V}$, $Gpa1^{G83S}$, $Gpa1^{G83L}$ and $Gpa1^{G83A}$ were expressed from pREP3x in reporter strains JY1285(ΔGpa1) and JY1287(ΔGpa1,ΔRgs1). Cells were cultured in minimal media lacking leucine to a density of ~5x$10^6$ cells/ml, incubated with 0M to $10^{-4}$M P-factor before assaying for $\beta$-galactosidase activity. $\beta$-galactosidase activity was measured as $OD_{420}/10^6$ cells. Results are the means ± S.E.M. of triplicate determinations from three independent isolates. The table summarises the mean basal, maximal and $pEC_{50}$ values ± S.E.M. for each profile. Values for mutants that are significantly different to pGpa1 are indicated with ***($p$<0.001), **($p$<0.01) or *($p$<0.05) as determined by unpaired $t$ test.

Of all of the $Gpa1^{G83X}$ mutants, $Gpa1^{G83A}$ is the only variant which appears to show substantial P-factor induced signalling capability when expressed in place of the endogenous Gpa1 (Figure 3.12, A), although the level of maximal signalling in terms of $\beta$-galactosidase activity (8.757 ± 0.916) is significantly less than Gpa1(21.020 ± 0.496) (unpaired $t$, $p$<0.001). There appears to be only very slight P-factor induced signalling for $Gpa1^{G83S}$ and $Gpa1^{G83V}$ and mutating the glycine to a leucine ($Gpa1^{G83L}$) is a loss-of-function mutation (Figure 3.12, A). The removal of Rgs1 leads to increases in the level of signalling of $Gpa1^{G83A}$ and $Gpa1^{G83S}$ at all P-factor concentrations, but does not substantially effect signalling of $Gpa1^{G83V}$ or $Gpa1^{G83L}$ (compare Figure 3.12, A to Figure 3.12, B). For the mutant $Gpa1^{G83A}$, this indicates that it can propagate the signal, but must be highly sensitive to the negative regulation imposed by the presence of Rgs1. $Gpa1^{G83S}$ activity suggests it is a very weak Gpa1 with minimal capability for signal propagation, yet it is still sensitive to the removal of Rgs1.

### 3.4.3 P-factor Induced Morphology Response

The mating-response in *S. pombe* involves two main responses to P-factor stimulation of the signalling pathway; transcription of the genes required for mating and also the activation of proteins leading to a change in cell morphology (Figure 1.7). This morphology change is in the form of polarised cell elongation towards the source of the P-factor (shmoo). Both events occur downstream of the Gα subunit Gpa1 and are therefore influenced by Gpa1 activity. We can quantify this change in addition to the transcriptional response (induction of *sxa2>lacZ*) to provide further characterisation of the Gpa1 nucleotide exchange mutants. Cell size can be measured as the mean volume of a cell within the population using a Z2 Coulter channelyzer (Davey, 1991; Ladds et al., 2003, 2005b). Gpa1, Gpa1$^{Q244L}$, Gpa1$^{R218C}$, Gpa1$^{G243A}$ and the series of Gpa1$^{G83X}$ mutants were expressed from pREP3x in the β-galactosidase reporter strain lacking endogenous Gpa1; JY1285(*sxa2>lacZ*, ΔGpa1). Transformed strains were then grown in minimal media lacking leucine and thiamine, incubated with P-factor at concentrations of 0M to $10^{-4}$M for 16 h before assaying for cell volume (Figure 3.13, A and Figure 3.14, A). Similarly to the assays of transcriptional response, morphology response was also quantified for Gpa1 and the Gpa1 mutants in the β-galactosidase reporter strain lacking endogenous Gpa1 and endogenous Rgs1; JY1287(*sxa2>lacZ*, ΔGpa1, ΔRgs1) (Figure 3.13, B and Figure 3.14, B).

Data shows that with *wild-type* Gpa1 as the signal propagator, mean cell volume increases from 62.5 ± 1.5 fl at basal levels to a maximum of 96 ± 2.0 fl following induction by P-factor. Gpa1$^{R218C}$ shows a similar morphology response to this, although seemingly requiring a higher concentration of P-factor to induce a maximal response. Gpa1$^{Q244L}$ displays very little change in morphology in response to P-factor, but cells appear to generally be larger than with *wild-type* in the absence of any P-factor. The inactive mutant Gpa1$^{G243A}$ shows no P-factor induced cell size change, remaining at a basal level of ∼66.5 ± 3.5 fl (Figure 3.13, A). Removal of Rgs1 appears to have a similar effect on morphology as it does on P-factor induced transcription. Basal levels of Gpa1 and Gpa1$^{R218C}$ cell size are increased and maximal cell size is reduced, therefore giving less of a P-factor induced response. Morphology response for Gpa1$^{Q244L}$ and Gpa1$^{R218C}$ appears insensitive to the presence of Rgs1 (Figure 3.13, B). Interestingly at extreme P-factor concentration of $10^{-4}$M, this overstimulation has an adverse effect on cell size of Gpa1 and Gpa1$^{R218C}$ by reducing cell size compared to maximal levels, suggesting mechanisms for protecting against overstimulation (Weston *et al.,* in preparation) (Figure 3.13).

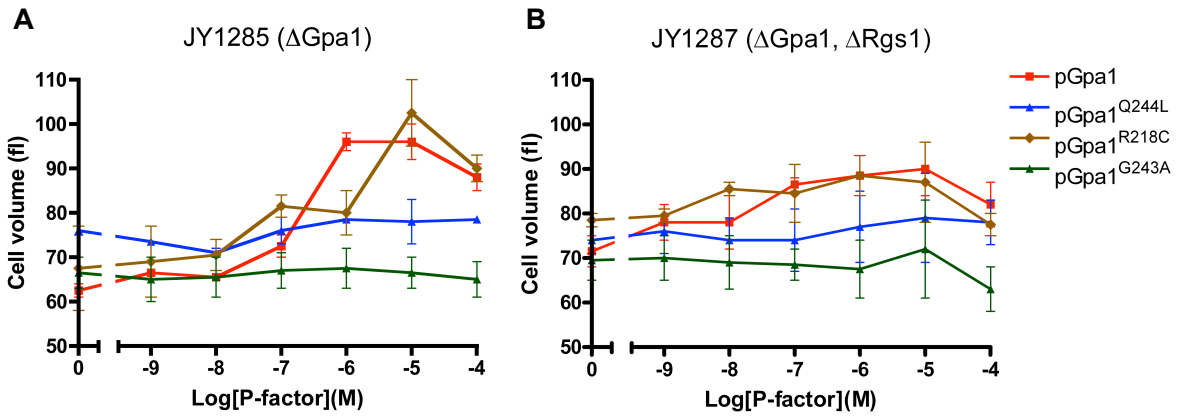


| | Basal (fl) | Maximal (fl) |
|---|---|---|
| **JY1285 (ΔGpa1)** | | |
| pGpa1 | 62.5 +/- 1.5 | 96.0 +/- 2.0 |
| pGpa1$^{Q244L}$ | 76.0 +/- 1.0 ** | 78.5 +/- 0.5 ** |
| pGpa1$^{R218C}$ | 67.5 +/- 9.5 | 102.5 +/- 7.5 |
| pGpa1$^{G243A}$ | 66.5 +/- 3.5 | 67.5 +/- 4.0 ** |
| **JY1287 (ΔGpa1, ΔRgs1)** | | |
| pGpa1 | 71.5 +/- 3.5 | 90.0 +/- 6.0 |
| pGpa1$^{Q244L}$ | 74.0 +/- 3.0 | 79.0 +/- 9.0 |
| pGpa1$^{R218C}$ | 78.5 +/- 1.5 | 88.5 +/- 4.5 |
| pGpa1$^{G243A}$ | 69.5 +/- 4.5 | 72.0 +/- 10.0 |

FIGURE 3.13: **Characterisation of Gpa1 nucleotide exchange mutants (morphology response): Gpa1$^{Q244L}$, Gpa1$^{R218C}$ and Gpa1$^{G243A}$.** Gpa1, Gpa1$^{Q244L}$, Gpa1$^{R218C}$ and Gpa1$^{G243A}$ were expressed from vector pREP3x in reporter strains JY1285(ΔGpa1) (A) and JY1287(ΔGpa1,ΔRgs1) (B). Cells were cultured in minimal media lacking leucine to a density of ~5x10$^6$ cells/ml, incubated with 0M to $10^{-4}$M P-factor before assaying for cell volume using a Coulter Size Analyser. Results are the means ± S.E.M. of triplicate determinations from three independent isolates. The table summarises the mean basal and maximal values ± S.E.M. for each Gpa1 variant. Values for mutants that are significantly different to pGpa1 are indicated with ***($p$<0.001), **($p$<0.01) or *($p$<0.05) as determined by unpaired $t$ test.

Of the Gpa1$^{G83X}$ mutants, Gpa1$^{G83L}$, Gpa1$^{G83S}$ and Gpa1$^{G83V}$ lack any P-factor induced change in cell size. Gpa1$^{G83A}$ displays some induction, but not to the same extent as seen for Gpa1 (Gpa1 max = 96.5 ± 2.5 fl, Gpa1$^{G83A}$ max = 82.5± 4.5 fl) (Figure 3.14, A). Removing regulation by Rgs1 results in reduction of maximal cell size of Gpa1$^{G83A}$, increased cell size across all concentrations for Gpa1$^{G83S}$ and has no effect on cell size for Gpa1$^{G83L}$ and Gpa1$^{G83V}$ (Figure 3.14, B). Generally the patterns observed for all mutants in P-factor induced change in cell size are similar to what was observed for the patterns observed for P-factor induced transcriptional response (compare Figure 3.11 and Figure 3.12 to Figure 3.13 and Figure 3.14).

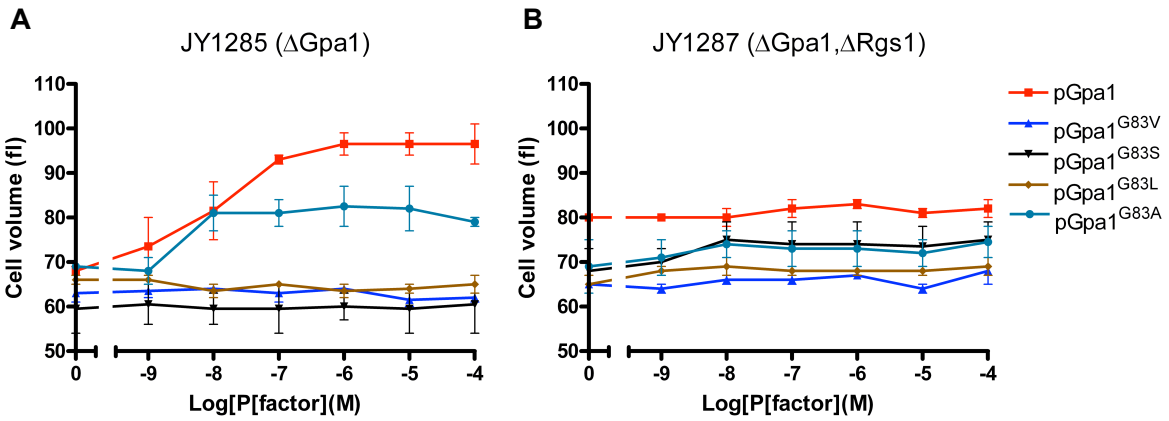


| | Basal (fl) | Maximal (fl) |
|---|---|---|
| **JY1285 (ΔGpa1)** | | |
| pGpa1 | 68.0 +/- 1.0 | 96.5 +/- 2.5 |
| pGpa1$^{G83V}$ | 63.0 +/- 2.0 | 64.0 +/- 1.0 *** |
| pGpa1$^{G83S}$ | 59.5 +/- 5.0 | 60.5 +/- 3.0 *** |
| pGpa1$^{G83L}$ | 66.0 +/- 1.0 | 66.0 +/- 1.0 *** |
| pGpa1$^{G83A}$ | 69.0 +/- 0 | 82.5 +/- 4.0 * |
| **JY1287 (ΔGpa1, ΔRgs1)** | | |
| pGpa1 | 80.0 +/- 0 | 83.0 +/- 1.0 |
| pGpa1$^{G83V}$ | 65.0 +/- 0.5 *** | 68.0 +/- 3.0 ** |
| pGpa1$^{G83S}$ | 68.0 +/- 5.0 | 75.0 +/- 5.0 |
| pGpa1$^{G83L}$ | 65.0 +/- 2.0 ** | 69.0 +/- 2.0 ** |
| pGpa1$^{G83A}$ | 65.0 +/- 2.0 ** | 74.5 +/- 3.5 |

FIGURE 3.14: **Characterisation of Gpa1 nucleotide exchange mutants (morphology response): Gpa1$^{G83X}$.** Gpa1, Gpa1$^{G83V}$, Gpa1$^{G83S}$, Gpa1$^{G83L}$ and Gpa1$^{G83A}$ were expressed from pREP3x in reporter strains JY1285(ΔGpa1) and JY1287(ΔGpa1,ΔRgs1). Cells were cultured in minimal media lacking leucine to a density of ~5x10$^6$ cells/ml, incubated with 0M to $10^{-4}$M P-factor before assaying for cell volume using a Coulter Size Analyser. Results are the means ± S.E.M. of triplicate determinations from three independent isolates. The table summarises the mean basal and maximal values ± S.E.M. for each Gpa1 variant. Values for mutants that are significantly different to pGpa1 are indicated with ***($p$<0.001), **($p$<0.01) or *($p$<0.05) as determined by unpaired $t$ test.

### 3.4.4 Dominant Activity

Through the addition of exogenous Gα subunits into a signalling system already containing endogenous Gα, further insight can be obtained. If the concentration of Gα in the system is a limiting factor then the addition of extra Gα that is identical to the endogenous protein should only serve to enhance the level of signal transduced through the pathway. Any exogenous Gα protein that does this is therefore likely to have similar characteristics to the endogenous protein. If the addition of a mutant Gα protein is detrimental to the signalling response then this points to the mutant having a negative effect, most likely through competing with endogenous Gα in binding events that would under normal circumstances lead to signal transduction. Additionally, this would suggest that the exogenous Gα mutant has different characteristics in terms of binding, activation or de-activation rates compared to

the endogenous protein. In the mating-response pathway, the concentration of Gpa1 has been shown to limit the possible maximal level of signalling response (Smith et al., 2009), therefore we are more interested in determining the mutants displaying dominant activity over the endogenous Gpa1. To characterise the dominant activity or lack of it, Gpa1, Gpa1$^{Q244L}$, Gpa1$^{R218C}$, Gpa1$^{G243A}$ and the Gpa1$^{G83X}$ mutants were expressed from the pREP3x plasmid in a *wild-type* $\beta$-galactosidase reporter strain that contains endogenous Gpa1; JY544(*sxa2>lacZ*). Transformed strains were grown in minimal media lacking leucine and thiamine, incubated with 0M to $10^{-4}$M P-factor for 16 h before assaying for induction of *sxa2>lacZ* (Figure 3.15). These transformed strains were also assayed for their ligand induced morphology response through measurement of mean cell volume (Figure 3.16).

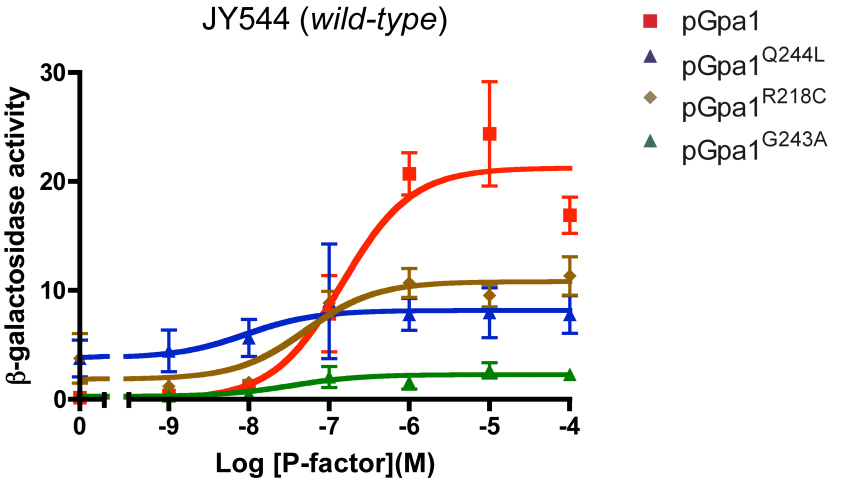


| | Basal | Maximal | pEC$_{50}$ |
|---|---|---|---|
| **JY544 (*wild-type*)** | | | |
| pGpa1 | 0.167 +/- 0.025 | 21.240 +/- 1.749 | 6.839 +/- 0.244 |
| pGpa1$^{Q244L}$ | 3.755 +/- 1.686 | 8.161 +/- 1.250 ** | 8.038 +/- 1.080 |
| pGpa1$^{R218C}$ | 1.842 +/- 0.979 | 10.810 +/- 0.879 ** | 7.291 +/- 0.328 |
| pGpa1$^{G243A}$ | 0.399 +/- 0.127 | 2.270 +/- 0.303 *** | 7.469 +/- 0.543 |

FIGURE 3.15: **Characterisation of dominant activity of Gpa1 nucleotide exchange mutants: Gpa1$^{Q244L}$, Gpa1$^{R218C}$ and Gpa1$^{G243A}$.** Gpa1, Gpa1$^{Q244L}$, Gpa1$^{R218C}$ and Gpa1$^{G243A}$ were expressed from vector pREP3x in reporter strain JY544(*wild-type*). Cells were cultured in minimal media lacking leucine to a density of ~5x10$^6$ cells/ml, incubated with 0M to $10^{-4}$M P-factor before assaying for $\beta$-galactosidase activity. $\beta$-galactosidase activity was measured as OD$_{420}$/10$^6$ cells. Results are the means $\pm$ S.E.M. of triplicate determinations from three independent isolates. The table summarises the mean basal, maximal and pEC$_{50}$ values $\pm$ S.E.M. for each profile. Values for mutants that are significantly different to pGpa1 are indicated with ***($p$<0.001), **($p$<0.01) or *($p$<0.05) as determined by unpaired $t$ test.

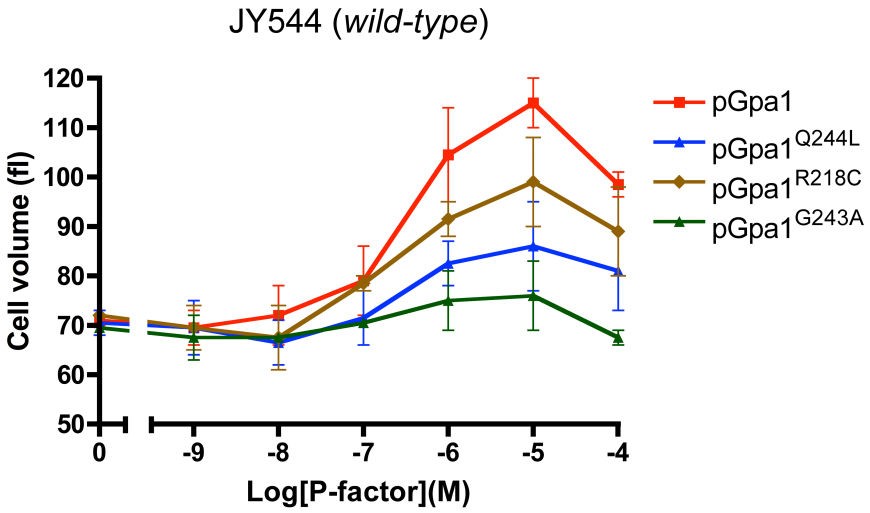


| | Basal (fl) | Maximal (fl) |
|---|---|---|
| **JY544 (*wild-type*)** | | |
| pGpa1 | 71.0 +/- 1.0 | 115.0 +/- 5.0 |
| pGpa1$^{Q244L}$ | 70.5 +/- 2.5 | 86.0 +/- 9.0 * |
| pGpa1$^{R218C}$ | 72.0 +/- 1.0 | 99.0 +/- 9.0 |
| pGpa1$^{G243A}$ | 69.5 +/- 0.5 | 76.0 +/- 7.0 * |

FIGURE 3.16: **Characterisation of dominant activity of Gpa1 nucleotide exchange mutants (morphology response): Gpa1$^{Q244L}$, Gpa1$^{R218C}$ and Gpa1$^{G243A}$.** Gpa1, Gpa1$^{Q244L}$, Gpa1$^{R218C}$ and Gpa1$^{G243A}$ were expressed from vector pREP3x in reporter strain JY544(*wild-type*). Cells were cultured in minimal media lacking leucine to a density of ~5x10$^6$ cells/ml, incubated with 0M to $10^{-4}$M P-factor before assaying for cell volume using a Coulter Size Analyser. Results are the means ± S.E.M. of triplicate determinations from three independent isolates. The table summarises the mean ± S.E.M. basal and maximal values. Values for mutants that are significantly different to pGpa1 are indicated with ***($p$<0.001), **($p$<0.01) or *($p$<0.05) as determined by unpaired $t$ test.

Previous assays of spontaneous activation (Figure 3.10) and ligand induced activation (Figure 3.11) have shown Gpa1$^{R218C}$ to have similar signalling activity to Gpa1$^{Q244L}$. Indeed, both Gpa1$^{Q244L}$ and Gpa1$^{R218C}$ are also similar in their ability to show dominance over endogenous Gpa1, through the reduction of maximal signalling (Figure 3.15). Both mutants significantly reduce maximal signalling (unpaired $t$, $p$<0.01), with Gpa1$^{Q244L}$ having the most dominant negative activity of the two, reducing maximal $\beta$-galactosidase activity in the presence of endogenous Gpa1 from 21.24 ± 0.025 to 8.161 ± 1.250 (Figure 3.15). One explanation for this could be that Gpa1$^{Q244L}$ and Gpa1$^{R218C}$ outcompete endogenous Gpa1 for interaction with the effector protein, thus saturating all available effectors. Results are consistent with these mutants being constitutively active (as previously demonstrated for Gpa1$^{Q244L}$ by Smith et al., 2009) and them having an inability to hydrolyse GTP. Gpa1$^{G243A}$ shows the most significant dominant activity over *wild-type* Gpa1 (unpaired $t$, $p$<0.001), reducing maximal $\beta$-galactosidase activity from 21.24 ± 0.025 to 2.70 ± 0.303 (Figure 3.15). This could be due to its constant GDP-bound state resulting in enhanced affinity for the GPCR, therefore saturating the available receptors by tightly

coupling them to an unactivatable G protein. This informs that despite a complete lack of capability for P-factor induced signal propagation (Figure 3.11 and Figure 3.13), Gpa1$^{G243A}$ must maintain the ability to bind to the receptor.

Quantification of cell size displays a similar pattern in the data (compare Figure 3.16 to Figure 3.15). Gpa1$^{Q244L}$, Gpa1$^{R218C}$ and Gpa1$^{G243A}$ show dominant negative activity over Gpa1, evident from reduced maximal cell volumes. The greatest reduction in the morphology response compared to *wild-type* Gpa1 is observed for Gpa1$^{G243A}$ (Figure 3.16).

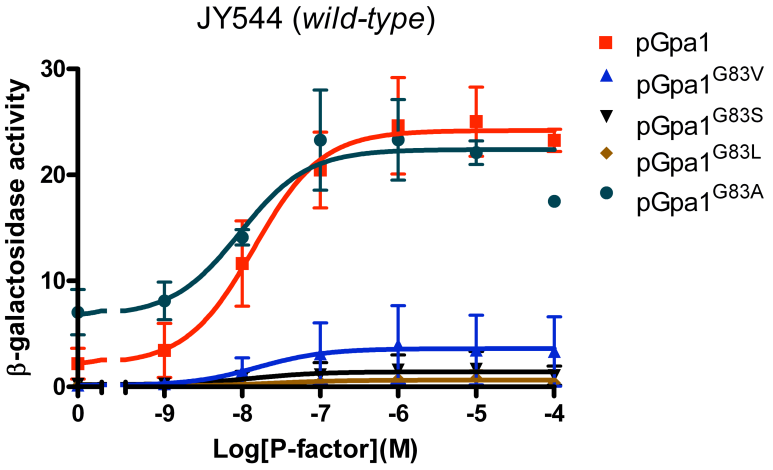


| | Basal | Maximal | $pEC_{50}$ |
|---|---|---|---|
| **JY544 (*wild-type*)** | | | |
| pGpa1 | 2.186 +/- 1.455 | 24.190 +/- 1.429 | 7.848 +/- 0.239 |
| pGpa1$^{G83V}$ | 0.155 +/- 0.144 | 3.604 +/- 1.137 *** | 7.801 +/- 1.202 |
| pGpa1$^{G83S}$ | 0.226 +/- 0.168 | 1.418 +/- 0.461 *** | N/A |
| pGpa1$^{G83L}$ | 0.134 +/- 0.116 | 0.633 +/- 0.194 *** | N/A |
| pGpa1$^{G83A}$ | 7.049 +/- 2.139 | 22.390 +/- 1.486 | 8.032 +/- 0.333 |

FIGURE 3.17: **Characterisation of Gpa1 nucleotide exchange mutants: Gpa1$^{G83X}$.** Gpa1, Gpa1$^{G83V}$, Gpa1$^{G83S}$, Gpa1$^{G83L}$ and Gpa1$^{G83A}$ were expressed from pREP3x in reporter strain JY544(*wild-type*). Cells were cultured in minimal media lacking leucine to a density of ~5x10$^6$ cells/ml, incubated with 0M to $10^{-4}$M P-factor before assaying for $\beta$-galactosidase activity. $\beta$-galactosidase activity was measured as $OD_{420}/10^6$ cells. Results are the means ± S.E.M. of triplicate determinations from three independent isolates. The table summarises the mean basal, maximal and $pEC_{50}$ values ± S.E.M. for each profile. Values for mutants that are significantly different to pGpa1 are indicated with ***($p$<0.001), **($p$<0.01) or *($p$<0.05) as determined by unpaired $t$ test.

Three out of the four Gpa1$^{G83X}$ mutants show dominant negative activity, significantly reducing maximal signalling in terms of $\beta$-galactosidase activity from 24.19 ± 1.429 (Gpa1) to 3.604 ± 1.137 (Gpa1$^{G83V}$), 1.418 ± 0.461 (Gpa1$^{G83S}$) and 0.633 ± 0.194 (Gpa1$^{G83L}$) (unpaired $t$, $p$<0.001). However, the point mutation of glycine to alanine (Gpa1$^{G83A}$) gives a mutant that appears to have some dominant positive activity over *wild-type* Gpa1, evident from increased basal $\beta$-galactosidase activity of 7.049 ± 2.139 compared to 2.186 ± 1.455. This dominant positive effect of Gpa1$^{G83A}$ is not observed at high P-factor concentrations

(>$10^{-7}$M), with maximal $\beta$-galactosidase activity of 22.39 ± 1.486 being similar to that of unmodified Gpa1 (Figure 3.17).

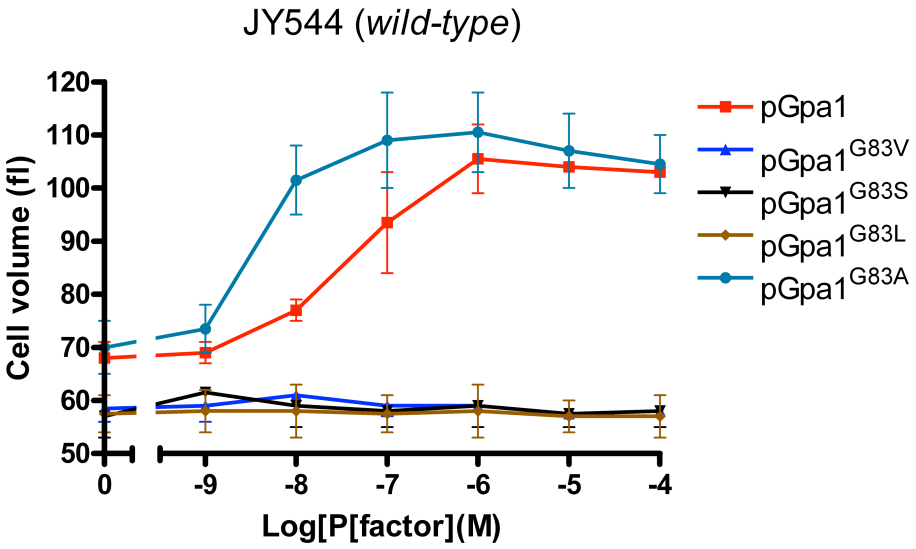


| | Basal (fl) | Maximal (fl) |
|---|---|---|
| **JY544 (*wild-type*)** | | |
| pGpa1 | 68.0 +/- 3.0 | 105.5 +/- 6.5 |
| pGpa1$^{G83V}$ | 58.5 +/- 2.5 | 61.0 +/- 2.0 ** |
| pGpa1$^{G83S}$ | 57.0 +/- 4.0 | 61.5 +/- 0.5 ** |
| pGpa1$^{G83L}$ | 57.5 +/- 3.5 | 58.0 +/- 4.0 ** |
| pGpa1$^{G83A}$ | 70.0 +/- 5.0 | 110.5 +/- 7.0 |

FIGURE 3.18: **Characterisation of Gpa1 nucleotide exchange mutants (morphology response): Gpa1$^{G83X}$.** Gpa1, Gpa1$^{G83V}$, Gpa1$^{G83S}$, Gpa1$^{G83L}$ and Gpa1$^{G83A}$ were expressed from pREP3x in reporter strain JY544(*wild-type*). Cells were cultured in minimal media lacking leucine to a density of ~5x$10^6$ cells/ml, incubated with 0M to $10^{-4}$M P-factor before assaying for cell volume using a Coulter Size Analyser. Results are the means ± S.E.M. of triplicate determinations from three independent isolates. The table summarises the mean ± S.E.M. basal and maximal values. Values for mutants that are significantly different to pGpa1 are indicated with ***($p$<0.001), **($p$<0.01) or *($p$<0.05) as determined by unpaired $t$ test.

Again, similar patterns are observed in the data for dominant activity in terms of both transcriptional and morphology response (compare Figure 3.18 to Figure 3.17). Gpa1$^{G83V}$, Gpa1$^{G83S}$ and Gpa1$^{G83L}$ are all dominant negative, whilst Gpa1$^{G83A}$ does not have a negative influence on P-factor induced morphology response. The addition of Gpa1$^{G83A}$ appears to enhance the sensitivity of the morphology response with cell volume of 101 ± 6.5 fl being reached at $10^{-8}$M compared to 77 ± 2.0 fl for Gpa1 at the same concentration. These data imply that the glycine residue at this position is important for signal transduction and strikingly different effects can be observed depending on the amino acid residue that glycine is replaced with. All mutants except for Gpa1$^{G83A}$ exert dominant negativity, possibly through out-competing *wild-type* Gpa1 for receptors or effectors, suggesting that this residue could be important for protein-protein interactions.

Of all the mutants now classified, we have observed that Gpa1 can be rendered unable to propagate a signal through mutating residue 243 ($Gpa1^{G243A}$) (shown previously by Ladds et al., 2007) and also through mutating residue 83 ($Gpa1^{G83V}$, $Gpa1^{G83S}$ and $Gpa1^{G83L}$). These two residues are therefore of importance for allowing nucleotide exchange in terms of activation of the protein. Other newly characterised Gpa1 mutants; $Gpa1^{R218C}$ and $Gpa1^{G83A}$ were found to have similar signalling activity in terms of P-factor induced transcriptional response to that of the GTPase deficient mutant $Gpa1^{Q244L}$, but with subtle differences in the basal levels of signalling between the different mutants. Slight differences were also observed in morphology response of these mutants, suggesting differing effects of the mutations on the morphology response pathway. One major difference between the mutants $Gpa1^{R218C}$, $Gpa1^{G83A}$ and $Gpa1^{Q244L}$ was observed through investigation of dominant activity over endogenous Gpa1. $Gpa1^{Q244L}$ and $Gpa1^{R218C}$ showed high degree of dominant negative activity by reducing maximal signalling, whilst this was not apparent for $Gpa1^{G83A}$.

### 3.4.5 A Fluorescent Reporter of Signalling

The temporal dynamics of nucleotide exchange of the different Gpa1 mutants are likely to have a significant effect on the resulting dose-response profiles observed. Using $\beta$-galactosidase reporters for characterisation of the Gpa1 mutants is limited by the fact that cells have to be lysed in order to obtain a readout for the signalling response, therefore making it impossible to investigate the temporal dynamics of ligand induced signalling response from live cells. To further characterise the Gpa1 mutants, an alternative reporter system had to be used, whereby signalling activity can be quantified from live cells in terms of the induction of a fluorescent reporter protein. The use of fluorescent reporter strains to quantify live-cell signalling response with time in both population-based assay and single cells is investigated more extensively later in Chapter 5.

Fluorescent reporters allow the signalling response to be quantified in real-time from living cells as they are responding, without the need for any cell lysis. A *S. pombe* strain (JY1325) containing the gene for GFP in the place of the P-factor inducible gene *sxa2* has previously been made (Smith, University of Warwick, 2008). Very little work has been completed using such fluorescent reporter strains as tools to quantify signalling through the mating-response pathway in *S. pombe*. To initially test the use of the reporter to quantify P-factor induced signalling response, the fluorescent reporter strain JY1325(*sxa2>GFP*) was grown in minimal media before being transferred on to agarose plugs made from growth media containing P-factor at concentrations of 0M to $10^{-5}$M plus 1 % agarose. Cells were incubated on the plugs for 16 h at 30°C before assaying for fluorescence intensity (relating to induction of *sxa2>GFP*) of the population on the plug, using a Berthold Mithras LB940 BRET multi-mode microplate-reader (Figure 3.19, A). A measure of fluorescence intensity

is obtained by detecting fluorescence at wavelength of 535 nm. Cells are able to grow on the agarose plugs containing P-factor, therefore time-series quantification of live cells can be obtained using the plate-reader to take measurements of population fluorescence at set time points during the 16 h assay (Figure 3.19, B). Due to cell growth, all fluorescence intensity measurements are corrected for cell number by dividing fluorescence intensity by a value indicative of the number of cells on the plug; optical density at 620 nm ($OD_{620}$). Fluorescence units are presented as fluorescence intensity/$OD_{620}$. The fluorescent reporter can be used to obtain a dose-response profile that is comparable to that obtained from a $\beta$-galactosidase assay in addition to information on the temporal dynamics of P-factor induced response from the cell population. Time-series data shows induction of *sxa2>GFP* occurring at ~2-3 h following initiation with P-factor. Fluorescence increases steadily before beginning to plateau after ~8 h, suggesting that transcription of *sxa2>GFP* has slowed or ceased at this time-point (Figure 3.19, B).

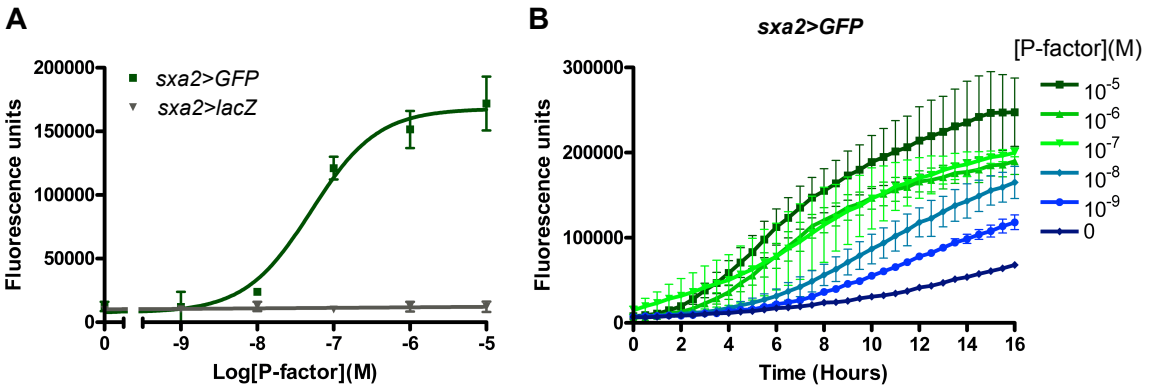


FIGURE 3.19: **A fluorescent reporter of signalling.** Cells from fluorescent reporter strain JY1325(*sxa2>GFP*) were cultured to a density of ~5x$10^6$ cells/ml and transferred onto minimal growth media agarose plugs containing 0M to $10^{-5}$M P-factor. P-factor induced transcription of *sxa2>GFP* was measured following 16 h induction with P-factor (A). time-series quantification was obtained through measuring P-factor induced transcription of *sxa2>GFP* every 30 min following addition of cell culture onto the P-factor containing agarose plugs at time = 0 h (B). Fluorescence units describe the fluorescence emitted from the cell population corrected for cell density (fluorescence intensity at 535 nm/$OD_{620}$). Results are means ± S.E.M. of duplicate determinations from two independent isolates.

The motivations for using the fluorescent reporter strains in addition to the $\beta$-galactosidase reporters for characterisation of the Gpa1 mutants are that by combining information from the two types of reporter it should provide a more accurate description of the mutants signalling behaviour, with the benefits of obtaining time-series data for better temporal dynamics and the possibility of performing fluorescence imaging experiments on strains expressing the mutant proteins. Additionally, it allows a direct comparison of the two reporters to assess their applicability for use in such characterisation experiments.

### 3.4.5.1 Construction of a Gpa1 Knockout in the *sxa2>GFP* Reporter Strain

To be able to further characterise the Gpa1 nucleotide exchange mutants using a fluorescent reporter strain, further modification had to be made to strain JY1325(*sxa2>GFP*) such that a fluorescent reporter could be created lacking endogenous Gpa1. This was accomplished by transforming JY1325 with a DNA construct containing the *ura4* cassette flanked by regions homologous to the 5' and 3' untranslated regions of *gpa1* (Figure 3.20). Transformants containing the *ura4* cassette were selected for by growth on selective media plates lacking uracil. To ensure insertion of the *ura4* cassette in the correct place in the genome at the *gpa1* locus, the resultant strain; JY1341(*sxa2>GFP*, ΔGpa1) was confirmed to be lacking endogenous Gpa1 by assaying for fluorescence intensity using a fluorescence plate-reader (Figure 3.21).

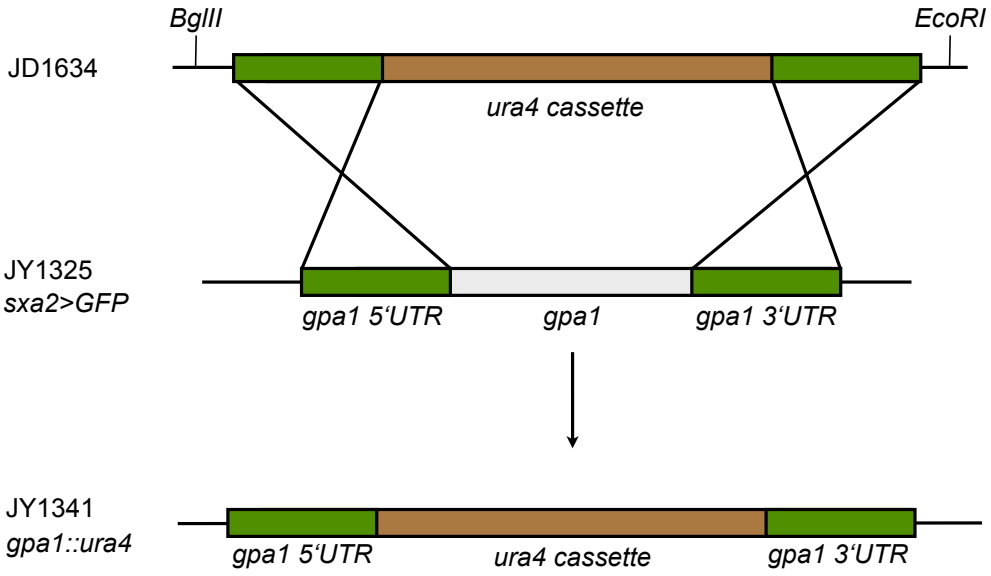


FIGURE 3.20: **Strain generation: Gpa1 knockout in *sxa2>GFP* reporter strain.** The integration fragment from JD1634 was liberated by a *BglII/EcoRI* digest and used to transform JY1325(*sxa2>GFP*) to produce JY1341(*sxa2>GFP, gpa1::ura4*). Transformants were selected by growth in the absence of uracil, which indicates the presence of the *ura4* cassette in the genome.

Gpa1 was expressed from the plasmid pREP3x in the *sxa2>GFP* reporter strain lacking endogenous Gpa1; JY1341(*sxa2>GFP, ΔGpa1*). Transformed strains were grown in minimal media lacking thiamine and leucine before incubation on 1 % agarose plugs containing the same minimal media + P-factor for a period of 16 h. Following incubation, fluorescence intensity of the cell population was measured using a Mithras LB940 BRET multi-mode microplate-reader. The *wild-type* reporter strain; JY1325 and the Gpa1 knockout reporter strain; JY1341 were also grown on P-factor containing agarose plugs (P-factor concentrations of 0M to $10^{-5}$M) for 16 h and assayed for comparison (Figure 3.21).

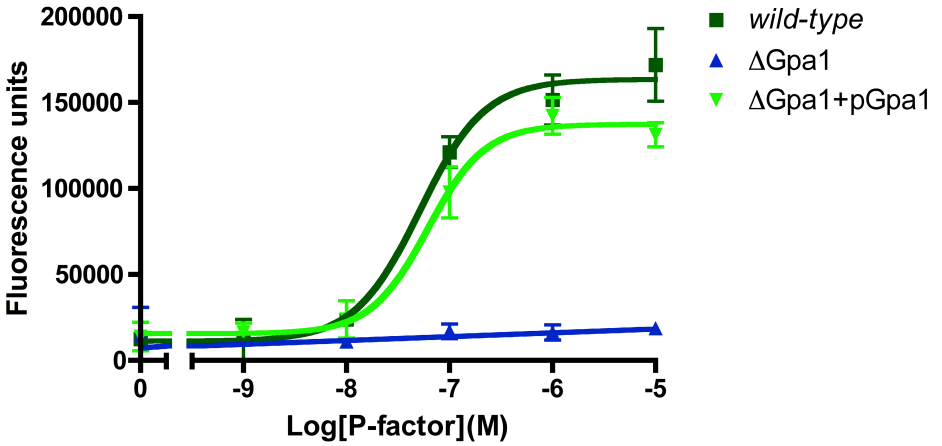


FIGURE 3.21: **Confirmation of Gpa1 knockout in *sxa2>GFP* reporter strain.** *S. pombe* strains JY1325 (*sxa2>GFP*), JY1341(*sxa2>GFP*, ΔGpa1), and JY1341 + pGpa1 (pREP3x-Gpa1) were cultured to a density of ∼5x10$^6$ cells/ml and transferred onto minimal media agarose plugs containing 0M to $10^{-5}$M P-factor. P-factor induced transcription of *sxa2>GFP* was measured following 16 h induction with P-factor. Fluorescence units describe the fluorescence emitted from the cell population corrected for cell density (fluorescence intensity at 535 nm/$OD_{620}$). Results are the means of duplicate measurements ± S.E.M. from two independent determinations.

The Gpa1 knockout strain; JY1341 displays a lack of P-factor induced response. Signalling is recovered to close to the levels observed for the *wild-type* reporter by the introduction of Gpa1 (Figure 3.21). This confirms that endogenous Gpa1 has been successfully removed from the genome in this strain.

### 3.4.6 Characterisation of Gpa1 Mutants Using the *sxa2>GFP* Reporter

A selection of the Gpa1 mutants were characterised further using the fluorescent reporter strains. Gpa1, Gpa1$^{Q244L}$, Gpa1$^{R218C}$ and Gpa1$^{G243A}$ were expressed from the vector pREP3x in reporter strains JY1341(*sxa2>GFP*, ΔGpa1) and JY1325(*sxa2>GFP*). Transformants were grown in minimal media before incubation on agarose plugs containing the same minimal media + P-factor at 0M to $10^{-5}$M for a period of 16 h. Following incubation, fluorescence intensity of the cell populations were measured using a Mithras LB940 BRET multi-mode microplate-reader. Dose-response profiles could then be obtained to analyse P-factor induction of *sxa2>GFP* (Figure 3.22) and to investigate dominant activity (Figure 3.23) of these mutants.

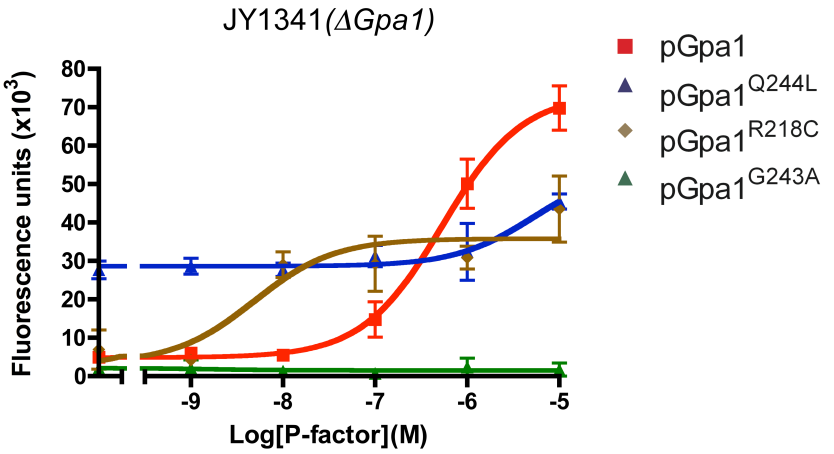


| | Basal (x10³) | Maximal (x10³) | pEC50 |
|---|---|---|---|
| **JY1341 (ΔGpa1)** | | | |
| pGpa1 | 4.94 +/- 1.18 | 73.56 +/- 4.02 | 6.269 +/- 0.118 |
| pGpa1$^{Q244L}$ | 27.69 +/- 2.30 *** | 54.50 +/- 17.02 * | 5.269 +/- 0.752 * |
| pGpa1$^{R218C}$ | 6.94 +/- 5.12 | 35.80 +/- 3.70 ** | 8.312 +/- 0.420 ** |
| pGpa1$^{G243A}$ | 2.02 +/- 0.68 | 2.15 +/- 1.74 *** | N/A |

FIGURE 3.22: **Characterisation of Gpa1 nucleotide exchange mutants using a *sxa2>GFP* reporter.** Gpa1, Gpa1$^{Q244L}$, Gpa1$^{R218C}$ and Gpa1$^{G243A}$ were expressed from pREP3x in reporter strain JY1341(*sxa2>GFP*, ΔGpa1). Cells were cultured to a density of ∼5x10$^6$ cells/ml and transferred onto minimal growth media agarose plugs containing 0M to $10^{-5}$M P-factor. P-factor induced transcription of *sxa2>GFP* was measured following 16 h induction with P-factor. Fluorescence units describe the fluorescence emitted from the cell population corrected for cell density (fluorescence intensity at 535 nm/$OD_{620}$). Results are the means of duplicate measurements ± S.E.M. from two independent determinations. The table summarises the mean basal, maximal and $pEC_{50}$ values ± S.E.M. for each profile. Values for mutants that are significantly different to pGpa1 are indicated with ***($p$<0.001), **($p$<0.01) or *($p$<0.05) as determined by unpaired $t$ test.

The patterns observed in the dose-response profiles for the mutants Gpa1$^{Q244L}$, Gpa1$^{G243A}$ and Gpa1$^{R218C}$ are consistent in both β-galactosidase *(sxa2>lacZ)* and fluorescent *(sxa2>gfp)* reporter strains lacking endogenous Gpa1 (compare Figure 3.11, A and Figure 3.22, A). In both of these reporter strains it was evident that Gpa1$^{Q244L}$ has a high and consistent signalling activity over all P-factor concentrations, Gpa1$^{R218C}$ is more sensitive than *wild-type* Gpa1 and Gpa1$^{G243A}$ is inactive. The increased sensitivity of Gpa1$^{R218C}$ is much more apparent in the fluorescent reporter strain with a $pEC_{50}$ of 7.517 ± 0.240 compared to 6.269 ± 0.118 for Gpa1 (Figure 3.22, A). In terms of dominant activity over *wild-type* Gpa1, data from the fluorescent reporter strain is in agreement with β-galactosidase assay data with Gpa1$^{Q244L}$, Gpa1$^{R218C}$ and to a greater extent Gpa1$^{G243A}$ showing dominant negative activity by reducing maximal signalling activity (compare Figure 3.23 and Figure 3.15).

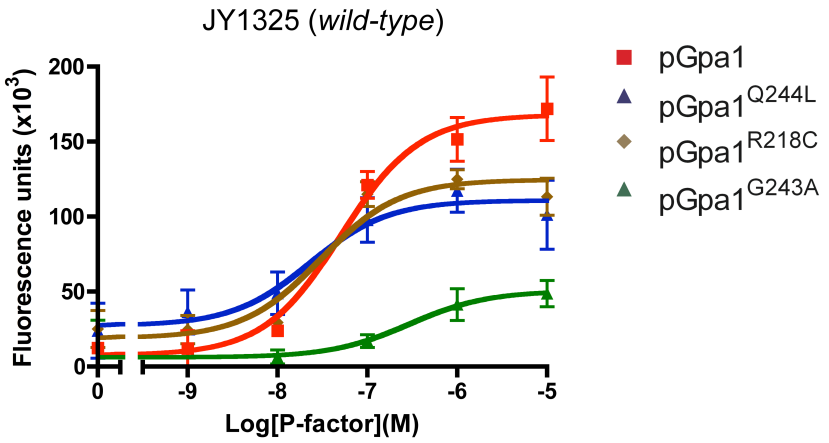


| | Basal (x10³) | Maximal (x10³) | pEC₅₀ |
|---|---|---|---|
| **JY1325 (*wild-type*)** | | | |
| pGpa1 | 12.42 +/- 3.67 | 167.92 +/- 8.83 | 7.291 +/- 0.154 |
| pGpa1$^{Q244L}$ | 23.94 +/- 18.38 | 110.83 +/- 10.28 * | 7.638 +/- 0.387 |
| pGpa1$^{R218C}$ | 18.87 +/- 8.33 | 124.60 +/- 8.29 * | 7.517 +/- 0.240 |
| pGpa1$^{G243A}$ | 14.66 +/- 16.21 | 50.52 +/- 8.74 *** | 6.533 +/- 0.454 |

FIGURE 3.23: **Characterisation of dominant activity of Gpa1 nucleotide exchange mutants using a *sxa2>GFP* reporter.** Gpa1, Gpa1$^{Q244L}$, Gpa1$^{R218C}$ and Gpa1$^{G243A}$ were expressed from pREP3x in reporter strain JY1325 *(sxa2>GFP)*. Cells were cultured to a density of ~5x10$^6$ cells/ml and transferred onto minimal growth media agarose plugs containing 0M to $10^{-5}$M P-factor. P-factor induced transcription of *sxa2>GFP* was measured following 16 h induction with P-factor. Fluorescence units describe the fluorescence emitted from the cell population corrected for cell density (fluorescence intensity at 535 nm/OD$_{620}$). Results are the means of duplicate measurements ± S.E.M. from two independent determinations. The table summarises the mean basal, maximal and pEC$_{50}$ values ± S.E.M. for each profile. Values for mutants that are significantly different to pGpa1 are indicated with ***($p$<0.001), **($p$<0.01) or *($p$<0.05) as determined by unpaired $t$ test.

### 3.4.6.1 Time-series Live-cell Signalling Response

Gpa1, Gpa1$^{Q244L}$, Gpa1$^{R218C}$ and Gpa1$^{G243A}$ were also characterised for their time-dependent signalling response to P-factor. These proteins were expressed from pREP3x in fluorescent reporter strain JY1341(*sxa2>GFP*, ΔGpa1). Transformants were grown in minimal media before being transferred to agarose plugs containing the same minimal media + P-factor at concentrations of 0M to $10^{-5}$M . Fluorescence intensity of the cell population was measured every 30 min for a 16 h period using a Mithras LB940 BRET multi-mode microplate-reader (Figure 3.24).

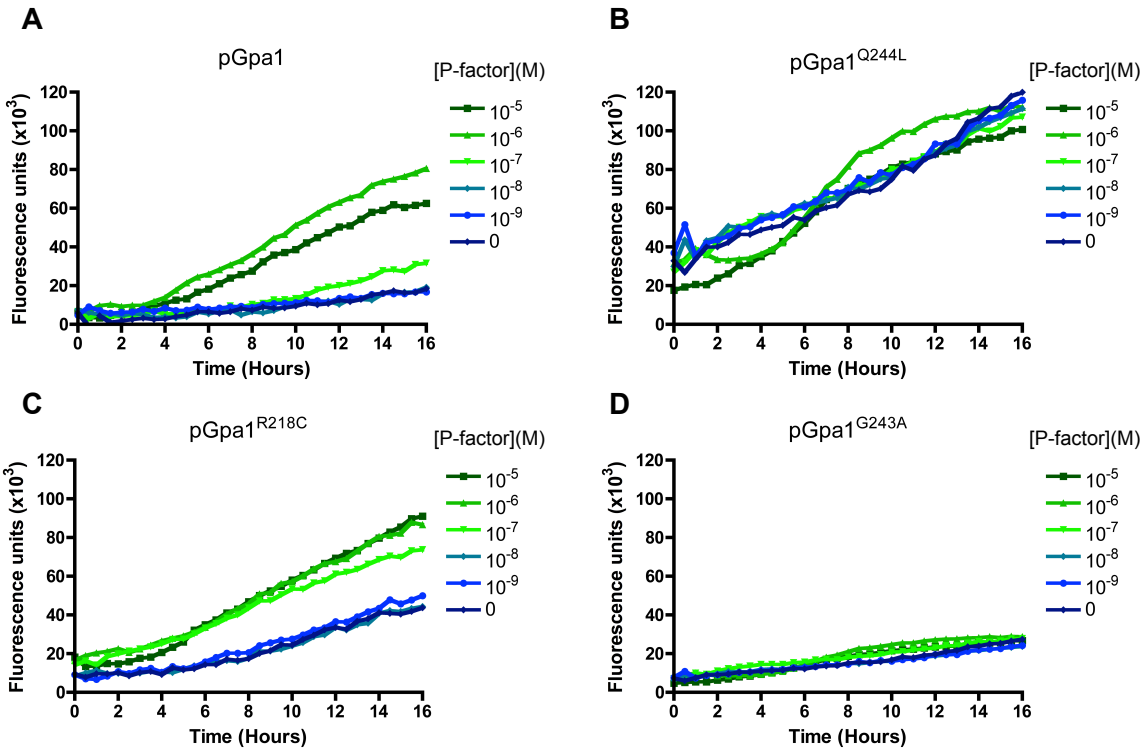


FIGURE 3.24: **Time-series characterisation of Gpa1 nucleotide exchange mutants: Gpa1$^{Q244L}$, Gpa1$^{R218C}$ and Gpa1$^{G243A}$.** Gpa1 (A), Gpa1$^{Q244L}$ (B), Gpa1$^{R218C}$ (C) and Gpa1$^{G243A}$ (D) were expressed from pREP3x in reporter strain JY1341(*sxa2>GFP*, ΔGpa1). Cells were cultured to a density of ~5x10$^6$ cells/ml and transferred onto minimal media agarose plugs containing 0M to 10$^{-5}$M P-factor at time 0. P-factor induced transcription of the GFP reporter was measured every 30 min for a 16 h period. Fluorescence units describe the fluorescence emitted from the cell population corrected for cell density (fluorescence intensity at 535 nm/OD$_{620}$).

Previous assays have demonstrated the Gpa1$^{Q244L}$ mutants to have raised basal signalling activity and not very substantial increases from this as a result of P-factor stimulation (Figure 3.11 and Figure 3.22). This is also apparent from the time-series data, as the time-series response is similar for all P-factor concentrations. Fluorescence measurements at 0 h are greater than those for any of the other Gpa1 variants (Figure 3.24, B), confirming its ability to spontaneously activate in the absence of ligand. The time-series signalling activity shows a very similar response profile for Gpa1 compared to Gpa1$^{R218C}$. There are however some notable differences, including that there appears to be slight induction with time for Gpa1$^{R218C}$ even in the absence of any P-factor, whereas this is not so apparent for Gpa1, suggesting increased spontaneous activation of Gpa1$^{R218C}$. Gpa1$^{R218C}$ also shows a more substantial response at the intermediate P-factor concentration of 10$^{-7}$M (compare Figure 3.24, A and C). With-time there is no P-factor induced increase in fluorescence for Gpa1$^{G243A}$, although there is a general slight increase in fluorescence with time, possibly due to increased cell numbers as the cells proliferate on the agarose plugs (Figure 3.24, D).

Time-dependent signalling data in Figure 3.24 can be analysed further to obtain estimates of the rate of fluorescence induction. This gives insight into the dynamics of the signalling response in terms of the speed the Gpa1 mutants are able to transfer ligand stimulation into gene expression. Ligand induced increase in fluorescence at high P-factor stimulation ($\geq 10^{-6}$M) is observable after 4 h and generally does not begin to show signs of plateau for the duration of the 16 h assay (pGpa1 in Figure 3.24). Fluorescence production rates for each Gpa1 variant are therefore calculated as the rate of change in fluorescence observed from 4-16 h (Figure 3.25).

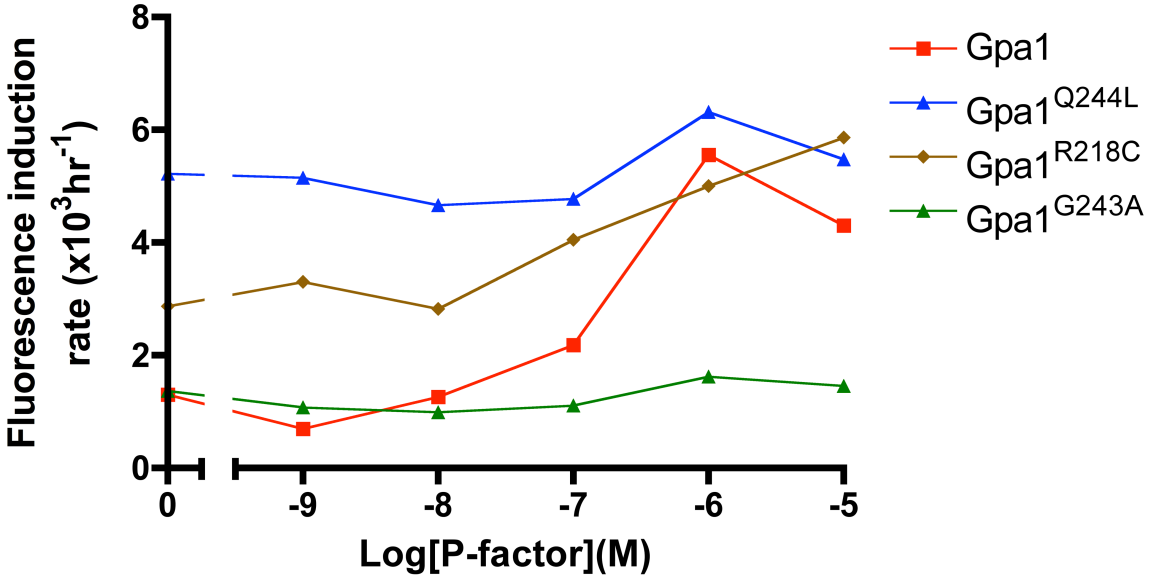


FIGURE 3.25: **Fluorescence induction rates of Gpa1 nucleotide exchange mutants: Gpa1$^{Q244L}$, Gpa1$^{R218C}$ and Gpa1$^{G243A}$.** Gpa1, Gpa1$^{Q244L}$, Gpa1$^{R218C}$ and Gpa1$^{G243A}$ were expressed from pREP3x in reporter strain JY1341(*sxa2>GFP*, ΔGpa1). Cells were cultured to a density of ~5x10$^6$ cells/ml and transferred onto minimal media agarose plugs containing 0M to $10^{-5}$M P-factor at time 0. P-factor induced transcription of *sxa2>GFP* was measured every 30 min for a 16 h period as in Figure 3.24. Induction rates are calculated within the time-frame of 4-16 h and presented are the rates of change in fluorescence calculated within this period.

Fluorescence induction rate data (Figure 3.25) indicates that the fluorescence production rates of Gpa1$^{Q244L}$ and Gpa1$^{R218C}$ are greater than that of Gpa1 even at low P-factor concentration, implying the increased spontaneous activation rates of these two mutants. The rate of fluorescence production for Gpa1 increases ~3-fold when P-factor concentration is increased from $10^{-7}$M to $10^{-6}$M suggesting a large P-factor induced effect on the rate of transcription of the fluorescent reporter. This highlights the difference between these two mutants, and again indicates that Gpa1$^{R218C}$ is an intermediate between Gpa1 and Gpa1$^{Q244L}$ in terms of its capability to become activated. P-factor induced increase in production rates are observed for Gpa1$^{R218C}$, but there is very little difference in the rates for Gpa1$^{Q244L}$ from a concentration of 0M to $10^{-5}$M. Given that the rate of fluorescence production for Gpa1$^{Q244L}$ at 0M (5.224x10$^3$ h$^{-1}$) is similar to the maximal rate achieved for

Gpa1 at $10^{-6}$M (5.556x$10^3$ $h^{-1}$), this implies that the constitutive activity of Gpa1$^{Q244L}$ is propagating the signal downstream of Gpa1 at a similar rate to the maximum rate achievable through ligand stimulation.

## 3.5 Modelling Effects of Nucleotide Exchange Rate Perturbation

Nucleotide exchange on the G$\alpha$ subunit is a regulatory event in switching the signal 'on' and 'off' and therefore is a critical control point in any model of the G protein cycle. All of the nucleotide exchange reactions, as defined in the Smith *et al.* model of the G protein cycle (Smith et al., 2009) (Table 3.1) are presented in Figure 3.26 as a schematic. In this model, a nucleotide exchange reaction is given further significance to enable the model simulations to reproduce the biological data. Here, nucleotide exchange is not only responsible for switching the G protein on (Figure 3.26, reactions a and b) and off (Figure 3.26, reactions d and e) in the traditional manner, but also for recycling the G$\alpha$ when it becomes trapped in an 'inert' state following the activation of a single downstream effector ( Figure 3.26, reactions f and g). This recycling is primarily through a GTP hydrolysis reaction, catalysed by an RGS species. All reaction rate parameters (k) in the Smith *et al.* model were originally chosen based on fitting to experimental dose-response data from $\beta$-galactosidase reporter strains, including time-course data showing the timings of regulatory influence by the RGS protein (Smith et al., 2009). These parameters have not been extensively analysed or subjected to any optimisation algorithms for model fitting. The influence on signalling output of the nucleotide exchange reactions in the Smith *et al.* model has been investigated here to determine their level of control on signalling response and to aid the modelling and characterisation of the Gpa1 mutants previously assayed.

The rates of the reactions presented in the schematic (Figure 3.26) are likely to be the reactions that are altered on a physiological level in the Gpa1 nucleotide exchange mutants previously assayed. These reaction rate constants ($k_5$ = 50 $h^{-1}$, $k_6$ = 0.2 $h^{-1}$ , $k_8$ = 2.5 $h^{-1}$, $k_9$ = 0.005 $h^{-1}$, $k_{10}$ = 10 $nM^{-1}$ $h^{-1}$, $k_{13}$ = 0.3 $h^{-1}$ and $k_{14}$ = 0.005 $h^{-1}$) can be perturbed to investigate model behaviour and the system-level response under these perturbed conditions. This will give predictions for the mechanisms, and the associated kinetics resulting in the previously observed signalling characteristics of the Gpa1 mutants.

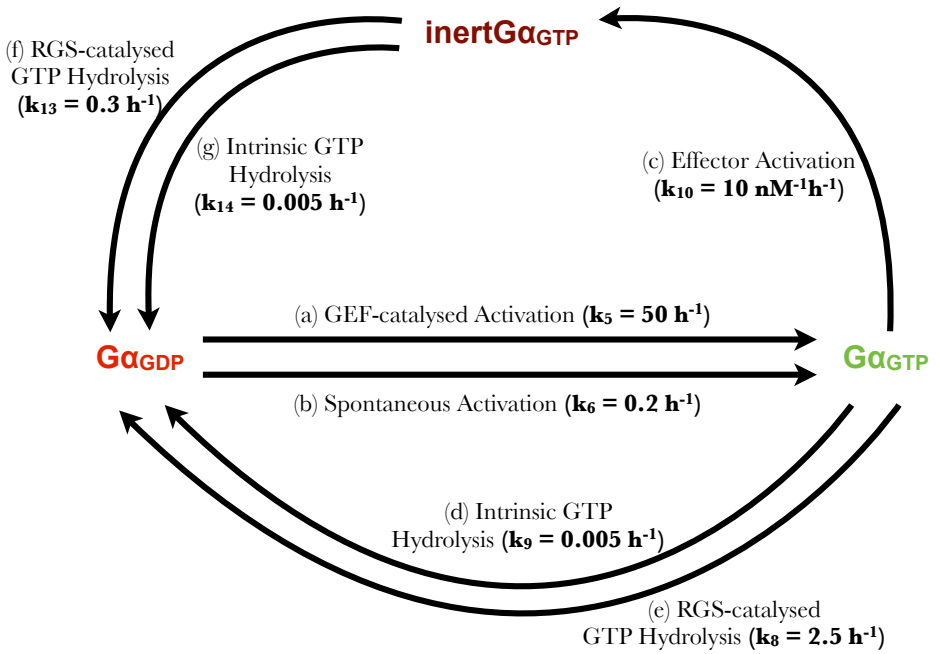


FIGURE 3.26: **Schematic of Gα states in the Smith *et al.* model of the G protein cycle.** Inactive $G\alpha_{GDP}$ can become activated and GTP-bound through GDP release catalysed by a Guanine Nucleotide Exchange Factor (GEF) (a) or Spontaneous GDP release (b). $G\alpha_{GTP}$ then propagates the signal through binding to a downstream effector (c), but subsequently enters into an inactive or inert state (inert$G\alpha_{GTP}$ ). Hydrolysis of $G\alpha_{GTP}$ reverts $G\alpha_{GTP}$ back to $G\alpha_{GDP}$ by the removal of a phosphate, either through intrinsic GTP hydrolysis (d) or GTP hydrolysis catalysed by a Regulator of G protein Signalling (RGS) (e). Hydrolysis can also occur on the inert $G\alpha_{GTP}$ returning it to $G\alpha_{GDP}$ again either by the RGS-catalysed reaction (f) or through intrinsic GTP hydrolysis (g). Reaction rate constants (k) as used in the Smith *et al.* model (Smith et al., 2009) are shown.

### 3.5.1 Gα Activation Reactions

There are three mechanisms in which Gα nucleotide exchange mutants may have altered activation kinetics. One is through a modified rate of $G\alpha_{GDP}$ -> $G\alpha_{GTP}$ through a GEF-catalysed reaction (i.e. more/less sensitive to activation by the GPCR) (Figure 3.26, (a)). The second is through the capability to spontaneously release GDP (Figure 3.26, (b)). Finally a possible mechanism for which a mutant may alter the signalling response could be through an altered rate of $G\alpha_{GTP}$ activation of the downstream Effector (Figure 3.26, (c)). This is not strictly a nucleotide exchange reaction, but it is included for investigation here as this reaction results in the $G\alpha_{GTP}$ transition into a different state (inert$G\alpha_{GTP}$), which physiologically could involve some form of nucleotide exchange. The reaction rate constants for each of these reactions ($k_5$, $k_6$ and $k_{10}$ respectively) were varied by increasing/decreasing each of them up to 1,000-fold from the *wild-type* Gα value and abolishing the reaction by setting the rate to zero. Varying these parameters in this way should give insight into the effect of activation dynamics on signalling response in the model.

#### 3.5.1.1 GEF-catalysed and Spontaneous Activation

Simulations of the model with perturbed GEF-catalysed activation of Gα ($k_5 = 50\ h^{-1}$) indicate that increasing the rate of this reaction up to 1,000-fold has no effect on the signalling activity and hence the dose-response profile is unchanged compared to that of a Gα with rates unmodified. Decreasing the rate of GEF-catalysed activation reduces maximal signalling from 438 for Gα to 18 response units for $G\alpha^{(0.001*k5)}$ and slightly decreases sensitivity to ligand (Figure 3.27, A). This suggests the GEF-catalysed activation rate is not limiting the achievable amplitude of the signalling response and is already at a close to optimal rate. Increasing the spontaneous activation rate of Gα ($k_6 = 0.2\ h^{-1}$) increases both basal and maximal signalling levels, whilst decreasing this rate decreases basal, but has no effect on maximal signalling response. This suggests the rate of spontaneous G protein activation limits the signalling response achievable at all ligand concentrations. The greatest effect of the spontaneous activation rate is on the basal level signalling, increasing the response from 9 for Gα to 698 response units for $G\alpha^{(1000*k6)}$. Maximal signalling is also increased from 438 for Gα to 698 response units for $G\alpha^{(1000*k6)}$ (Figure 3.27, B).

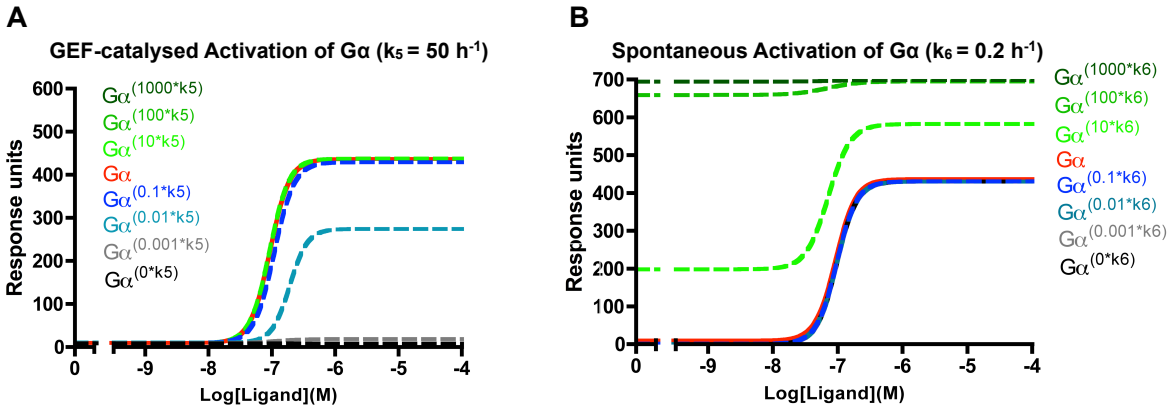


FIGURE 3.27: **Perturbation of GEF-catalysed and spontaneous activation rates.** Simulations of the Smith *et al.* model (Table 3.1) with Gα species having perturbed rates of GEF-catalysed activation (A) and spontaneous activation (B). The concentration of ligand in the simulation was varied over the range 0-100 $\mu$M following 16 h simulated induction. Output from the model shows the accumulation of activated $G\alpha_{GTP}$Effector complexes over the duration of the simulated assay.

#### 3.5.1.2 Effector Activation

Model simulations with perturbation of the rate of effector activation ($k_{10} = 10\ nM^{-1}h^{-1}$) by Gα effects basal signalling, maximal signalling and sensitivity to ligand. Increase of this rate results in increases in basal levels from 9 response units for Gα to 106 response units for $G\alpha^{(1000*k10)}$. Sensitivity can also be increased from $pEC_{50}$ of 7 for Gα to 7.3 for $G\alpha^{(1000*k10)}$. Maximal levels are also increased from 438 for Gα to 508 response units for $G\alpha^{(1000*k10)}$. Decreasing this rate decreases the basal, sensitivity and maximal levels and abolishing this reaction $G\alpha^{(0*k10)}$ eliminates any signalling response (Figure 3.28).

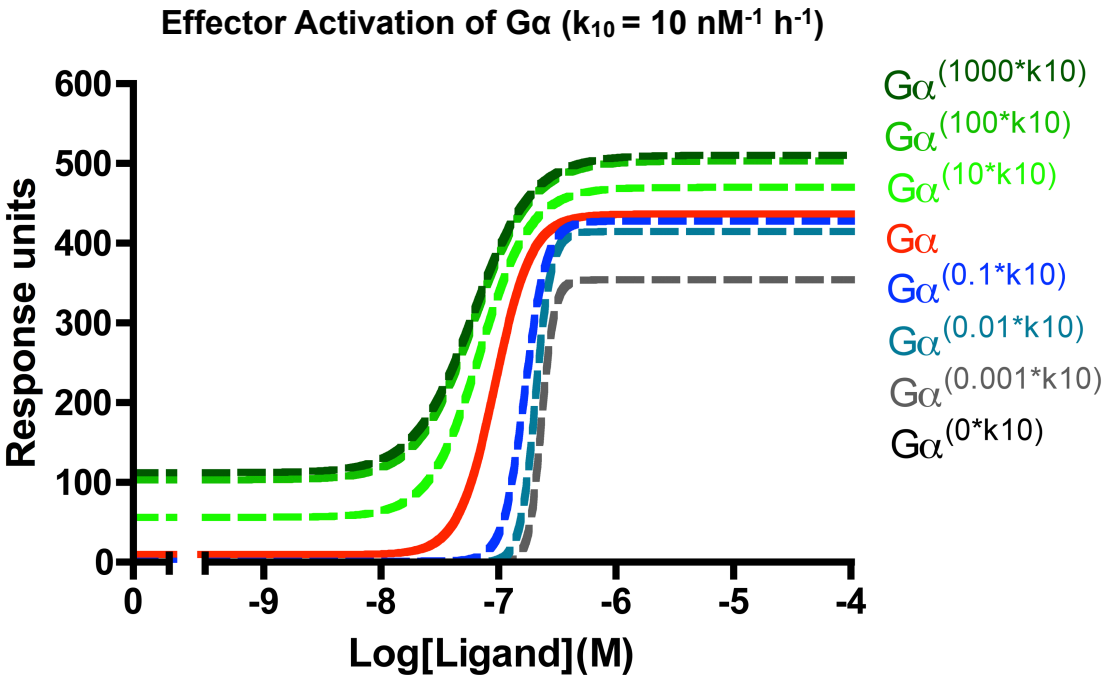


FIGURE 3.28: **Perturbation of Effector activation rate.** Simulations of the Smith *et al.* model (Table 3.1) with G$\alpha$ species having perturbed rates of Effector activation. The concentration of ligand in the simulation was varied over the range 0-100 $\mu$M following 16 h simulated induction. Output from the model shows the accumulation of activated G$\alpha_{GTP}$Effector complexes over the duration of the simulated assay.

Of the parameters tested governing activation, basal signalling response can be raised by increasing either spontaneous activation rate or effector activation rate. Maximal signalling levels can be decreased by decreasing the rate at which G$\alpha$ is activated by its GEF or by decreasing effector activation rate. Maximal signalling response can only be increased by increasing either the spontaneous activation rate or the effector activation rate. This suggests that when ligand concentration is sufficiently high, the rate of GEF-catalysed activation is already at the rate required to achieve maximum response. Increase or decrease in effector activation rate appears to either increase or decrease response in a similar manner across all ligand concentrations. The increased basal observed at low ligand concentration when effector activation is increased indicates that the increased rate is overriding the negative influence of RGS binding as effectors will become activated by G$\alpha_{\text{GTP}}$ before RGS species can have a blocking effect on this event.

### 3.5.2 GTP Hydrolysis Reactions

In the widely accepted view of a G protein cycle there are two main mechanisms for which a G$\alpha$ nucleotide exchange mutant may have altered GTP hydrolysis kinetics. One is through a modified rate of intrinsic GTPase activity (Figure 3.26, (d)) and the other is through a modified rate of GTP hydrolysis catalysed by RGS proteins (Figure 3.26, (e)). Additionally, the Smith *et al.* model proposes a conceptual advancement in that the G$\alpha$ enters into an

inactive GTP-bound state (inert$G\alpha_{GTP}$), with hydrolysis being required to release from this inactive state. This results in two other possible reactions whereby a G$\alpha$ nucleotide exchange mutant may have altered reaction rates; intrinsic GTP hydrolysis of inert$G\alpha_{GTP}$ (Figure 3.26, (g)) and RGS-catalysed hydrolysis of inert$G\alpha_{GTP}$ (Figure 3.26, (f)). The reaction rate constants for each of these reactions ($k_9$, $k_8$, $k_{14}$ and $k_{13}$ respectively) were varied by increasing/decreasing each of them up to 1,000-fold from the *wild-type* G$\alpha$ value and abolishing the reaction by setting the rate to zero in order to investigate effects on simulated signalling response.

#### 3.5.2.1 Hydrolysis of G$\alpha_{GTP}$

The model simulations with intrinsic $G\alpha_{GTP}$ hydrolysis rate ($k_9 = 0.005\ h^{-1}$) perturbed indicate that this parameter is very robust, in that reducing the rate to zero or increasing it 1,000-fold has no effect on the signalling response. A difference in the dose-response profiles only becomes apparent when this rate is increased $\geq$ 10,000,000-fold, which results in decreased basal response, maximal response and sensitivity to ligand (Figure 3.29, A). This suggests that intrinsic GTP hydrolysis is having minimal impact on the response characteristics. The model output is more sensitive to perturbation in the RGS-catalysed $G\alpha_{GTP}$ hydrolysis ($k_8 = 2.5\ h^{-1}$) in that reducing this reaction rate by 1000-fold reduces maximal signalling from 438 response units for G$\alpha$ to 169 response units for $G\alpha^{(0.001*k8)}$. Basal signalling is unaffected by any rate change, but there is a slight reduction in maximal response when the rate is increased (from 438 response units for G$\alpha$ to 423 response units for $G\alpha^{(1000*k8)}$) (Figure 3.29, B). This indicates that RGS-catalysed hydrolysis of $G\alpha_{GTP}$ dominates over intrinsic hydrolysis and shows the requirement for RGS-catalysed GTP hydrolysis to achieve *wild-type* maximal signalling response. The observation that reducing the rate of $G\alpha_{GTP}$ hydrolysis reduces maximal signalling (Figure 3.29, B) is counterintuitive, but when the species concentrations are considered, the reasoning for this result becomes clearer. The system is only initiated with 60 nM RGS species but 205 nM G protein, therefore as the hydrolysis rate of $G\alpha_{GTP}$ approaches zero, more RGS species are becoming sequestered bound to $G\alpha_{GTP}$. This leaves less free RGS to perform the subsequent hydrolysis of inert$G\alpha_{GTP}$ to promote the recycling of the G protein required to achieve maximal signalling.

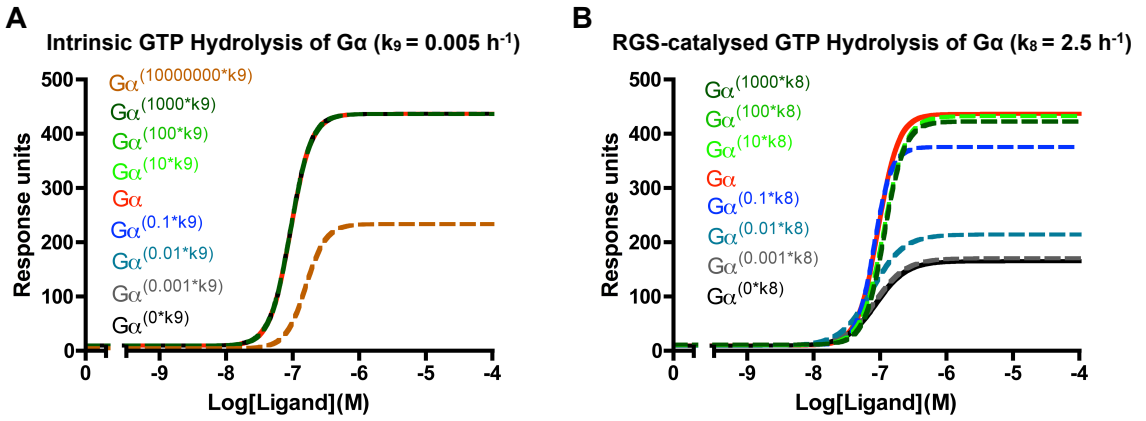


FIGURE 3.29: **Perturbation of G$\alpha$ hydrolysis rates.** Simulations of the Smith *et al.* model (Table 3.1) with G$\alpha$ species having perturbed rates of intrinsic GTP hydrolysis of G$\alpha$ (A), and RGS-catalysed GTP hydrolysis of G$\alpha$ (B). The concentration of ligand in the simulation was varied over the range 0-100 $\mu$M following 16 h simulated induction. Output from the model shows the accumulation of activated G$\alpha_{GTP}$Effector complexes over the duration of the simulated assay.

### 3.5.2.2 Hydrolysis of inertG$\alpha_{\mathbf{GTP}}$

Of the two possible GTP-bound states (G$\alpha_{GTP}$ and inertG$\alpha_{GTP}$), the hydrolysis reactions of inertG$\alpha_{GTP}$ have the most influence on the signalling response in the model. Whilst the rate of intrinsic GTP hydrolysis of G$\alpha_{GTP}$ seems to have very little effect, the intrinsic hydrolysis of inertG$\alpha_{GTP}$ ($k_{14} = 0.005$ h$^{-1}$) is a much more sensitive parameter in terms of response in the model. Reducing the rate of this reaction has no effect, but an increase results in a large increase in maximal signalling, increasing it > 3-fold from 438 response units for inertG$\alpha$ to 1442 response units for inertG$\alpha^{(1000*k14)}$ (Figure 3.30, A). The rate of RGS-catalysed hydrolysis of inertG$\alpha_{GTP}$ ($k_{13} = 0.3$ h$^{-1}$) is an even more sensitive parameter than that of the intrinsic hydrolysis of inertG$\alpha_{GTP}$ in terms of effects on maximal response. Increasing this reaction rate by just 10-fold results in a >3-fold increase in maximal signalling levels from 438 response units for inertG$\alpha$ to 1445 response units for inertG$\alpha^{(10*k13)}$. This appears to be a close to optimum rate as any further increase results in the level of maximal signalling decreasing from 1445 response units for inertG$\alpha^{(10*k13)}$ to 1260 response units for inertG$\alpha^{(1000*k13)}$ (Figure 3.30, B). All perturbations do not effect the basal level of signalling, but only a slight decrease in this rate is required to decrease the maximal signalling response units from 438 for inertG$\alpha$ to 236 for inertG$\alpha^{(0.1*k13)}$ (Figure 3.30, B). These data demonstrate that the rate of hydrolysis reactions on inertG$\alpha_{\mathrm{GTP}}$ is what limits the maximal level of response in the model and that rapid recycling of inertG$\alpha_{\mathrm{GTP}}$ can greatly enhance signal output.

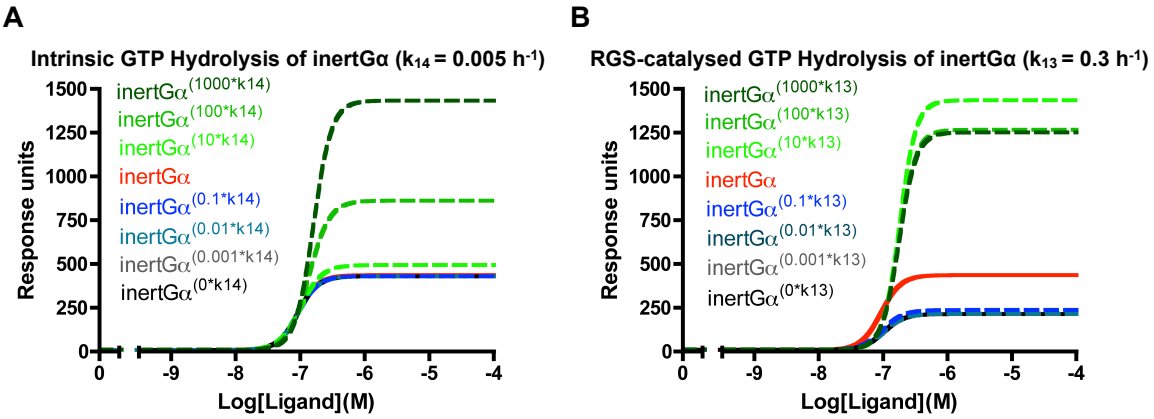


FIGURE 3.30: **Perturbation of inertG$\alpha$ hydrolysis rates.** Simulations of the Smith *et al.* model (Table 3.1) with G$\alpha$ species having perturbed rates of intrinsic GTP hydrolysis of inertG$\alpha$ (A) and RGS-catalysed GTP hydrolysis of inertG$\alpha$ (B). The concentration of ligand in the simulation was varied over the range 0-100 $\mu$M following 16 h simulated induction. Output from the model shows the accumulation of activated G$\alpha_{GTP}$Effector complexes over the duration of the simulated assay.

### 3.5.2.3 Combinatorial Hydrolysis Reactions

The overall influence of intrinsic hydrolysis compared to RGS-catalysed hydrolysis was investigated by equally perturbing the intrinsic hydrolysis rates of both G$\alpha_{\text{GTP}}$ ($k_9 = 0.005$ $h^{-1}$) and inertG$\alpha_{\text{GTP}}$ ($k_{14} = 0.005$ $h^{-1}$), and comparing to response when equally perturbing RGS-catalysed GTP hydrolysis rates of both G$\alpha_{\text{GTP}}$ ($k_8 = 2.5$ $h^{-1}$) and inertG$\alpha_{\text{GTP}}$ ($k_{13} = 0.3$ $h^{-1}$) (Figure 3.31). Results of the simulations indicate that perturbing intrinsic hydrolysis rates of both G$\alpha_{\text{GTP}}$ and inertG$\alpha_{\text{GTP}}$ has the same effect as that seen when perturbing this rate on inertG$\alpha_{\text{GTP}}$ alone (compare Figure 3.31, A to Figure 3.30, A). This suggests that intrinsic hydrolysis of inertG$\alpha_{\text{GTP}}$ dominates over intrinsic hydrolysis of G$\alpha_{\text{GTP}}$ in terms of controlling the response. Perturbing the RGS-catalysed hydrolysis rates of both G$\alpha_{\text{GTP}}$ and inertG$\alpha_{\text{GTP}}$ indicates that these two rates could be 'competing' with each other in terms of controlling the maximal signalling response (compare Figure 3.31, B to Figure 3.30, B and Figure 3.29, B). Whilst increasing the RGS-catalysed hydrolysis rate of inertG$\alpha_{\text{GTP}}$ alone was shown to have a substantial positive effect on maximal signalling, when this rate is increased along with RGS-catalysed hydrolysis of G$\alpha_{\text{GTP}}$ the increase in maximal signalling from *wild-type* levels is less substantial, reaching only 740 response units for G$\alpha^{(10*RGS\ Hydrolysis)}$. RGS-catalysed hydrolysis of G$\alpha_{\text{GTP}}$ therefore seems to counteract the effects of RGS-catalysed hydrolysis of inertG$\alpha_{\text{GTP}}$. This is to be expected because by increasing the rate of RGS-catalysed hydrolysis of G$\alpha_{\text{GTP}}$, this reduces the number of G$\alpha_{\text{GTP}}$ species that encounter the effectors and as a result reduces the number entering into the inertG$\alpha_{\text{GTP}}$ state.

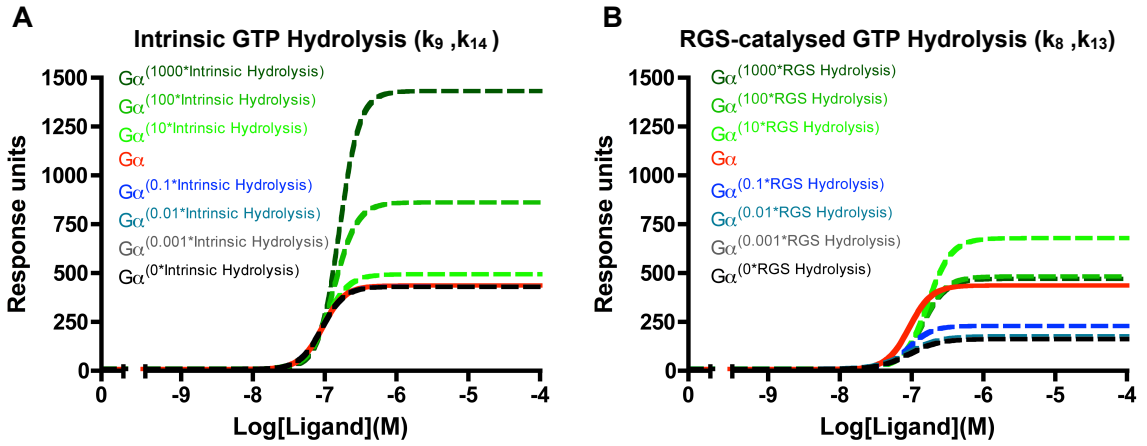


FIGURE 3.31: **Perturbation of GTP hydrolysis activity on Gα and inertGα combined.** Simulations of the Smith *et al.* model (Table 3.1) with Gα and inertGα species having equally perturbed rates of intrinsic GTP hydrolysis of Gα and inertGα ($k_9 = 0.005$ $h^{-1}$ and $k_{14} = 0.005$ $h^{-1}$) (A) and equally perturbed rates of RGS-catalysed GTP hydrolysis of Gα and inertGα ($k_8 = 2.5$ $h^{-1}$ and $k_{13} = 0.3$ $h^{-1}$) (B). The concentration of ligand in the simulation was varied over the range 0-100 $\mu$M following 16 h simulated induction. Output from the model shows the accumulation of activated $G\alpha_{GTP}$Effector complexes over the duration of the simulated assay.

Although it may be possible that a *Gα* nucleotide exchange mutant could behave differently in terms of its hydrolysis rates when in a $G\alpha_{GTP}$ state compared to the inert$G\alpha_{GTP}$ state, it is more likely that a mutant with perturbed GTPase activity would have similarly altered rates, irrespective of when in the two possible GTP-bound states. Additionally, if the mutation was to inhibit or enhance intrinsic GTP hydrolysis then it is likely to also inhibit or enhance RGS-catalysed hydrolysis. Considering these assumptions, a more general effect of perturbing all four hydrolysis rates (Figure 3.26, (d,e,f and g)) equally was investigated (Figure 3.32).

Simulations from the model, perturbed for all possible GTP hydrolysis reaction rates, return similar results to those when only the rate of RGS-catalysed hydrolysis of inert$G\alpha_{GTP}$ is perturbed (compare Figure 3.32 to Figure 3.30, B). This suggests that the level of signalling response is dominated by the rate of RGS-catalysed GTP hydrolysis of inert$G\alpha_{GTP}$ and also that this rate is a key sensitive parameter in the model. Perturbing all hydrolysis rates by just 10-fold results in an increase in maximal signalling response units from 438 for Gα to 696 for $G\alpha^{(10*GTPHydrolysis)}$. Similar to results seen in Figure 3.30, B, further increase in these GTP hydrolysis rates leads to a decrease in maximal signalling response units from 696 for $G\alpha^{(10*GTPHydrolysis)}$ to 473 response units for $G\alpha^{(1000*GTPHydrolysis)}$. Decreasing GTP hydrolysis rates by just 10-fold almost halves the maximal signalling response, reducing it from 438 response units for Gα to 221 for $G\alpha^{(0.1*GTPHydrolysis)}$ and abolishing all GTP hydrolysis reduces this further to 152 for $G\alpha^{(0*GTPHydrolysis)}$. Basal

signalling remains largely unaffected by all perturbations in GTP hydrolysis rates (Figure 3.32), which is possible due to low basal activity being maintained by a negative effect of RGS binding to Gα that is independent of GTPase activity.

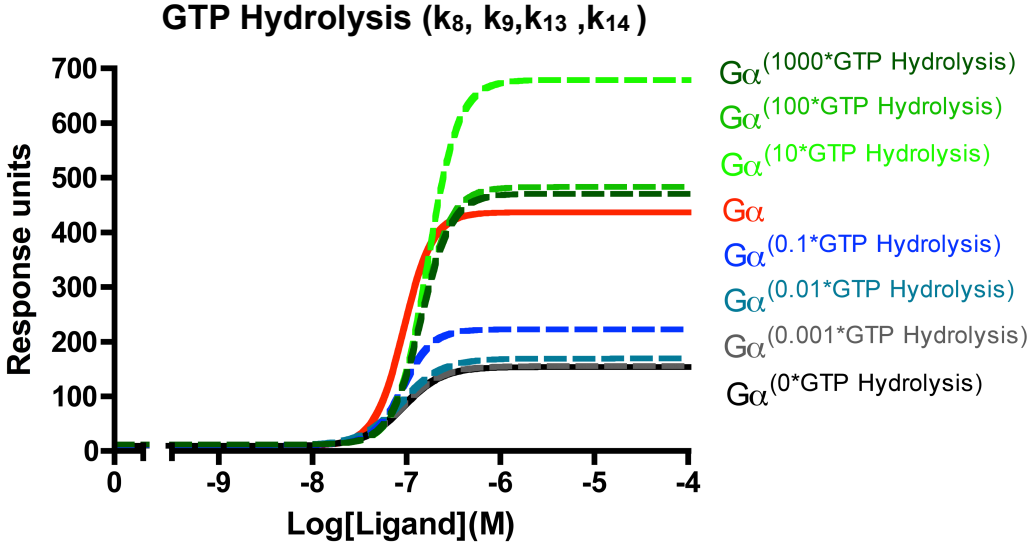


FIGURE 3.32: **Perturbation of all GTP hydrolysis activity.** Simulations of the Smith *et al.* model (Table 3.1) with Gα species having equally perturbed rates of intrinsic GTP hydrolysis of Gα ($k_9 = 0.005\ h^{-1}$), RGS-catalysed GTP hydrolysis of Gα ($k_8 = 2.5\ h^{-1}$), intrinsic GTP hydrolysis of inertGα ($k_{14} = 0.005\ h^{-1}$) and RGS-catalysed GTP hydrolysis of inertGα ($k_{13} = 0.3\ h^{-1}$). The concentration of ligand in the simulation was varied over the range 0-100 μM following 16 h simulated induction. Output from the model shows the accumulation of activated $G\alpha_{GTP}$Effector complexes over the duration of the simulated assay.

#### 3.5.2.4 Spontaneous Activation in GTPase Compromised Gα Species

Results from all simulations obtained through perturbations of nucleotide exchange reaction rates of the Gα species suggest that maximal signalling levels are most sensitive to changes in the RGS-catalysed GTP hydrolysis rate, whilst basal signalling levels are more sensitive to the spontaneous Gα activation rate. Some of the Gpa1 mutants ($Gpa1^{Q244L}$ and $Gpa1^{R218C}$) assayed previously display decreased maximal signalling levels, whilst having increased spontaneous activation compared to the unmodified Gpa1 protein (Figure 3.10 and Figure 3.11). To investigate the modelling of such mutants, simulations were obtained whereby all GTP hydrolysis rates were perturbed in combination with perturbation of the spontaneous activation rate. Additionally, as such mutants were assayed in the presence and absence of Rgs1 (Figure 3.11), the model simulations are obtained under equivalent conditions (Figure 3.33).

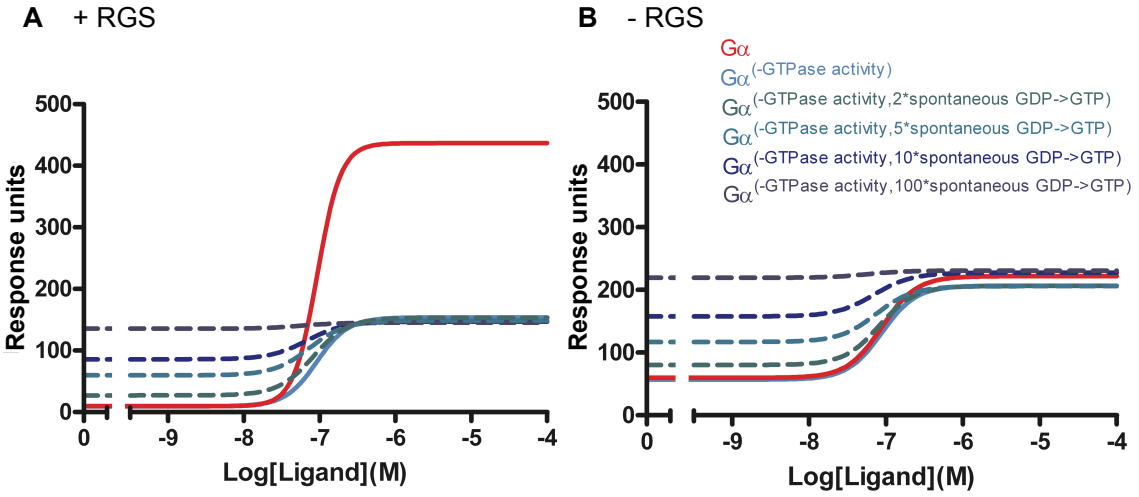


FIGURE 3.33: **Modelling increased basal signalling in GTPase compromised Gα species.** Simulations of the Smith *et al.* model (Table 3.1) with Gα species lacking the ability to hydrolyse GTP, but with increased ability to spontaneously activate itself. Simulations are of the model + RGS (A) and - RGS (B) species. The concentration of ligand in the simulation was varied over the range 0-100 $\mu$M following 16 h simulated induction. Output from the model shows the accumulation of activated $G\alpha_{GTP}$Effector complexes over the duration of the simulated assay.

Simulations suggest that basal signalling can be increased up to maximal levels in Gα species that are unable to hydrolyse GTP to give a dose-response profile showing lack of induced increase in signalling response (Figure 3.33). This suggests that the Gpa1 mutants; $Gpa1^{Q244L}$ and $Gpa1^{R218C}$ that have compromised GTP hydrolysis may also have a higher susceptibility to spontaneously activate. Results indicate another regulatory role for the RGS species in addition to that of catalysing the GTP hydrolysis reaction due to the fact that the removal of RGS leads to an increase in response across all ligand concentrations for Gα species that are incapable of hydrolysing GTP (compare $G\alpha^{(-GTPase\ activity)}$ in Figure 3.33, A and B). The model suggests RGS has a negative influence on signalling response independent of its role in catalysing the GTP hydrolysis reaction. Other mammalian RGS proteins have been identified as having negative regulatory roles, independent of GTPase activity by behaving as effector antagonists through competing with effector proteins for binding to $G\alpha_{GTP}$ (Willars, 2006). This effector antagonism is replicated in the model, with RGS species forming complexes with $G\alpha_{GTP}$ that hinders $G\alpha_{GTP}$ activation of its effector species. Different N and C-terminal domains of RGS proteins have also been implicated as having competing positive and negative regulatory roles on RGS function (Willars, 2006). Indeed *S. pombe* Rgs1 is one of the larger members of the RGS family and has N-terminal domains additional to the C-terminal RGS-fold that have been shown to influence signal transduction. The N terminal alone of Rgs1 has previously been shown to negatively regulate signalling despite it not containing the RGS-fold domain required for GTP hydrolysis (Hill, PhD Thesis, 2008).

## 3.6 Extending to Model Effects of Exogenous Gα Within the System

The Smith *et al.* model of the G protein cycle can be perturbed to investigate the effects of changing key parameters controlling nucleotide exchange reactions to simulate mutant G proteins, but it cannot be used to simulate the effects of adding additional G protein into the system to investigate dominant activity. Various Gpa1 mutants with differing nucleotide exchange capabilities have been characterised in both β-galactosidase and fluorescent reporter strains containing endogenous Gpa1. Assays have determined the effect that the addition of exogenous Gpa1 can have on signal output (Figure 3.15, Figure 3.17 and Figure 3.23). To be able to simulate such experiments, the model had to be extended to include an additional exogenous Gα species (pGα) that could be assigned different characteristics for reactions in which it undergoes nucleotide exchange. In the extended model the downstream Effector species now has the possibility of becoming activated through the active endogenous Gα species (Gα) or the exogenous Gα species (pGα). pGα is initiated in the system as its inactive $pG\alpha_{GDP}$ form at a concentration of 205 nM so that the system is initiated with the same initial concentration of endogenous and exogenous Gα species. All of the reactions involving pGα are the same as those involving Gα species therefore pGα can be converted to all the same states as for Gα. The rate constants are initiated with the same values, therefore initiating a *wild-type* system containing exogenous pGα that has all the same properties as Gα. The full reaction scheme for this model is presented in Table 3.4.

### 3.6.1 Model Equations

The system of ODEs to allow simulation of the model is presented in Table 3.5. The additional Gα species introduced into the system (pGα) is defined as having initial concentration of 205 nM, the same as the concentration of Gα.

This new model (Table 3.4) now allows investigation into the effects of the addition of mutant Gα species into a *wild-type* system, essentially simulating previous experiments whereby mutant Gpa1 is expressed in *wild-type* reporter strains JY544(*sxa2>lacZ*) and JY1325(*sxa2>GFP*) (Figures 3.15, 3.17 and 3.23).

| | | | | |
|---|---|---|---|---|
| Smith *et al.* | $L + R \rightarrow LR$ | $k_1$ | 0.0025 | $nM^{-1}h^{-1}$ |
| | $G\alpha\beta\gamma + R \rightarrow RG\alpha\beta\gamma$ | $k_2$ | 0.005 | $nM^{-1}h^{-1}$ |
| | $G\alpha\beta\gamma + LR \rightarrow LRG\alpha\beta\gamma$ | $k_3$ | 0.02 | $nM^{-1}h^{-1}$ |
| | $L + RG\alpha\beta\gamma \rightarrow LRG\alpha\beta\gamma$ | $k_4$ | 0.005 | $nM^{-1}h^{-1}$ |
| | $LRG\alpha\beta\gamma \rightarrow G\alpha_{GTP} + G\beta\gamma + LR$ | $k_5$ | 50 | $h^{-1}$ |
| | $G\alpha\beta\gamma \rightarrow G\alpha_{GTP} + G\beta\gamma$ | $k_6$ | 0.2 | $h^{-1}$ |
| | $G\alpha_{GTP} + RGS \rightarrow RGSG\alpha_{GTP}$ | $k_7$ | 500 | $nM^{-1}h^{-1}$ |
| | $RGSG\alpha_{GTP} \rightarrow G\alpha_{GDPP} + RGS$ | $k_8$ | 2.5 | $h^{-1}$ |
| | $G\alpha_{GTP} \rightarrow G\alpha_{GDPP}$ | $k_9$ | 0.005 | $h^{-1}$ |
| | $Effector + G\alpha_{GTP} \rightarrow G\alpha_{GTP}Effector$ | $k_{10}$ | 10 | $nM^{-1}h^{-1}$ |
| | $G\alpha_{GTP}Effector \rightarrow Effector + inertG\alpha_{GTP}$ | $k_{11}$ | 1 | $h^{-1}$ |
| | $inertG\alpha_{GTP} + RGS \rightarrow RGSinertG\alpha_{GTP}$ | $k_{12}$ | 50 | $nM^{-1}h^{-1}$ |
| | $RGSinertG\alpha_{GTP} \rightarrow RGS + G\alpha_{GDPP}$ | $k_{13}$ | 0.3 | $h^{-1}$ |
| | $inertG\alpha_{GTP} \rightarrow G\alpha_{GDPP}$ | $k_{14}$ | 0.005 | $h^{-1}$ |
| | $G\alpha_{GDPP} \rightarrow G\alpha_{GDP} + P$ | $k_{15}$ | 1000 | $h^{-1}$ |
| | $G\alpha_{GDP} + G\beta\gamma \rightarrow G\alpha\beta\gamma$ | $k_{16}$ | 1000 | $nM^{-1}h^{-1}$ |
| | $P \rightarrow \emptyset$ | $k_{17}$ | 10 | $h^{-1}$ |
| Modifications | $pG\alpha_{GDP} + G\beta\gamma \rightarrow G\alpha\beta\gamma$ | $k_{18}$ | 1000 | $nM^{-1}h^{-1}$ |
| | $pG\alpha\beta\gamma + R \rightarrow RpG\alpha\beta\gamma$ | $k_{19}$ | 0.005 | $nM^{-1}h^{-1}$ |
| | $pG\alpha\beta\gamma + LR \rightarrow LRpG\alpha\beta\gamma$ | $k_{20}$ | 0.02 | $nM^{-1}h^{-1}$ |
| | $L + RpG\alpha\beta\gamma \rightarrow LRpG\alpha\beta\gamma$ | $k_{21}$ | 0.005 | $nM^{-1}h^{-1}$ |
| | $LRpG\alpha\beta\gamma \rightarrow pG\alpha_{GTP} + G\beta\gamma + LR$ | $k_{22}$ | 50 | $h^{-1}$ |
| | $pG\alpha\beta\gamma \rightarrow pG\alpha_{GTP} + G\beta\gamma$ | $k_{23}$ | 0.2 | $h^{-1}$ |
| | $pG\alpha_{GTP} + RGS \rightarrow RGSpG\alpha_{GTP}$ | $k_{24}$ | 500 | $nM^{-1}h^{-1}$ |
| | $RGSpG\alpha_{GTP} \rightarrow pG\alpha_{GDPP} + RGS$ | $k_{25}$ | 2.5 | $h^{-1}$ |
| | $Effector + pG\alpha_{GTP} \rightarrow pG\alpha_{GTP}Effector$ | $k_{26}$ | 10 | $nM^{-1}h^{-1}$ |
| | $pG\alpha_{GTP}Effector \rightarrow Effector + inertpG\alpha_{GTP}$ | $k_{27}$ | 1 | $h^{-1}$ |
| | $inertpG\alpha_{GTP} + RGS \rightarrow RGSinertpG\alpha_{GTP}$ | $k_{28}$ | 50 | $nM^{-1}h^{-1}$ |
| | $RGSinertpG\alpha_{GTP} \rightarrow RGS + pG\alpha_{GDPP}$ | $k_{29}$ | 0.3 | $h^{-1}$ |
| | $inertpG\alpha_{GTP} \rightarrow pG\alpha_{GDPP}$ | $k_{30}$ | 0.005 | $h^{-1}$ |
| | $pG\alpha_{GDPP} \rightarrow pG\alpha_{GDP} + P$ | $k_{31}$ | 1000 | $h^{-1}$ |
| | $pG\alpha_{GTP} \rightarrow pG\alpha_{GDPP}$ | $k_{32}$ | 0.005 | $h^{-1}$ |

TABLE 3.4: **Reaction scheme of model extended to include exogenous Gα species.** This reaction scheme contains all the elements of G protein activation and deactivation as presented in Smith et al., 2009, but additionally it includes another Gα protein species (pGα), to model system behaviour when additional Gα variants are added into the system (Modifications). All reactions for pGα are the same as those for Gα with the same associated rate constant values defined.

| | |
|---|---|
| Effector | Effector'(t) = - $k_{10}$Effector(t) $G\alpha_{GTP}(t)$ + $k_{11}G\alpha_{GTP}$Effector(t) - $k_{26}$Effector(t) $pG\alpha_{GTP}(t)$ + $k_{27}pG\alpha_{GTP}$Effector(t) |
| $G\alpha\beta\gamma$ | $G\alpha\beta\gamma$'(t) = - $k_6G\alpha\beta\gamma(t)$ - $k_2G\alpha\beta\gamma(t)$ R(t) - $k_3G\alpha\beta\gamma(t)$ LR(t) + $k_{16}G\beta\gamma(t)$ $G\alpha_{GDP}(t)$ |
| $G\beta\gamma$ | $G\beta\gamma$'(t) = $k_6G\alpha\beta\gamma(t)$ + $k_{23}pG\alpha\beta\gamma(t)$ + $k_5LRG\alpha\beta\gamma(t)$ + $k_{22}LRpG\alpha\beta\gamma(t)$ - $k_{16}G\beta\gamma(t)$ $G\alpha_{GDP}(t)$ - $k_{18}pG\beta\gamma(t)$ $G\alpha_{GDP}(t)$ |
| L | L'(t) = - $\frac{1}{2}$ $k_1$L(t) R(t) (Tanh($t_0$ b) - Tanh(b($t_0$ - t))) - $\frac{1}{2}$ $k_4$L(t) $RG\alpha\beta\gamma(t)$ (Tanh($t_0$ b) - Tanh(b($t_0$ - t))) - $\frac{1}{2}$ $k_2$1L(t) $RpG\alpha\beta\gamma(t)$ (Tanh($t_0$ b) - Tanh(b($t_0$ - t))) |
| P | P'(t) = - $k_{17}$P(t) + $k_{15}G\alpha_{GDPP}(t)$ + $k_{31}pG\alpha_{GDPP}(t)$ |
| $pG\alpha\beta\gamma$ | $pG\alpha\beta\gamma$'(t) = - $k_{23}pG\alpha\beta\gamma(t)$ - $k_{19}pG\alpha\beta\gamma(t)$ R(t) - $k_{20}pG\alpha\beta\gamma(t)$ LR(t) + $k_{18}G\beta\gamma(t)$ $pG\alpha_{GDP}(t)$ |
| R | R'(t) = - $k_2G\alpha\beta\gamma(t)$ R(t) - $k_{19}pG\alpha\beta\gamma(t)$ R(t) - $\frac{1}{2}$ $k_1$L(t) R(t) (Tanh($t_0$ b) - Tanh(b($t_0$ - t))) |
| $RG\alpha\beta\gamma$ | $RG\alpha\beta\gamma$'(t) = $k_2G\alpha\beta\gamma(t)$ R(t) - $\frac{1}{2}$ $k_4$L(t) $RG\alpha\beta\gamma(t)$ (Tanh($t_0$ b) - Tanh(b($t_0$ - t))) |
| $LRG\alpha\beta\gamma$ | $LRG\alpha\beta\gamma$'(t) = - $k_5LRG\alpha\beta\gamma(t)$ + $k_3G\alpha\beta\gamma(t)$ LR(t) + $\frac{1}{2}$ $k_4$L(t) $RG\alpha\beta\gamma(t)$ (Tanh($t_0$ b) - Tanh(b($t_0$ - t))) |
| LR | LR'(t) = $k_5LRG\alpha\beta\gamma(t)$ - $k_3G\alpha\beta\gamma(t)$ LR(t) - $k_{20}pG\alpha\beta\gamma(t)$ LR(t) + $k_{22}LRpG\alpha\beta\gamma(t)$ + $\frac{1}{2}$ $k_1$L(t) R(t) (Tanh($t_0$ b) - Tanh(b($t_0$ - t))) |
| $RpG\alpha\beta\gamma$ | $RpG\alpha\beta\gamma$'(t) = $k_{19}G\alpha\beta\gamma(t)$ R(t) - $\frac{1}{2}$ $k_{21}$L(t) $RpG\alpha\beta\gamma(t)$ (Tanh($t_0$ b) - Tanh(b($t_0$ - t))) |
| $LRpG\alpha\beta\gamma$ | $LRpG\alpha\beta\gamma$'(t) = - $k_{22}LRpG\alpha\beta\gamma(t)$ + $k_{20}pG\alpha\beta\gamma(t)$ LR(t) + $\frac{1}{2}$ $k_{21}$L(t) $RpG\alpha\beta\gamma(t)$ (Tanh($t_0$ b) - Tanh(b($t_0$ - t))) |
| $G\alpha_{GDP}$ | $G\alpha_{GDP}$'(t) = - $k_{16}G\beta\gamma(t)$ $G\alpha_{GDP}(t)$ + $k_{15}G\alpha_{GDPP}(t)$ |
| $G\alpha_{GDPP}$ | $G\alpha_{GDPP}$'(t) = - $k_{15}G\alpha_{GDPP}(t)$ + $k_9G\alpha_{GTP}(t)$ + $k_{14}$inert$G\alpha_{GTP}(t)$ + $k_8RGSG\alpha_{GTP}(t)$ + $k_{13}RGSinertG\alpha_{GTP}(t)$ |
| $G\alpha_{GTP}$ | $G\alpha_{GTP}$'(t) = $k_6G\alpha\beta\gamma(t)$ + $k_5LRG\alpha\beta\gamma(t)$ - $k_9G\alpha_{GTP}(t)$ - $k_{10}$Effector(t) $G\alpha_{GTP}(t)$ - $k_7G\alpha_{GTP}(t)$ RGS(t) |
| $G\alpha_{GTP}$Effector | $G\alpha_{GTP}$Effector'(t) = $k_{10}$Effector(t) $G\alpha_{GTP}(t)$ - $k_{11}G\alpha_{GTP}$Effector(t) |
| inert$G\alpha_{GTP}$ | inert$G\alpha_{GTP}$'(t) = $k_{11}G\alpha_{GTP}$Effector(t) - $k_{14}$inert$G\alpha_{GTP}(t)$ - $k_{12}$inert$G\alpha_{GTP}(t)$ RGS(t) |
| inertp$G\alpha_{GTP}$ | inertp$G\alpha_{GTP}$'(t) = $k_{27}pG\alpha_{GTP}$Effector(t) - $k_{30}$inertp$G\alpha_{GTP}(t)$ - $k_{28}$inertp$G\alpha_{GTP}(t)$ RGS(t) |
| $pG\alpha_{GDP}$ | $pG\alpha_{GDP}$'(t) = - $k_{18}G\beta\gamma(t)$ $pG\alpha_{GDP}(t)$ + $k_{31}pG\alpha_{GDPP}(t)$ |
| $pG\alpha_{GDPP}$ | $pG\alpha_{GDPP}$'(t) = - $k_{31}pG\alpha_{GDPP}(t)$ + $k_{32}pG\alpha_{GTP}(t)$ + $k_{30}$inertp$G\alpha_{GTP}(t)$ + $k_{25}RGSpG\alpha_{GTP}(t)$ + $k_{29}RGSinertpG\alpha_{GTP}(t)$ |
| $pG\alpha_{GTP}$ | $pG\alpha_{GTP}$'(t) = $k_{23}pG\alpha\beta\gamma(t)$ + $k_{22}LRpG\alpha\beta\gamma(t)$ - $k_{32}pG\alpha_{GTP}(t)$ - $k_{26}$Effector(t) $pG\alpha_{GTP}(t)$ - $k_{24}pG\alpha_{GTP}(t)$ RGS(t) |
| $pG\alpha_{GTP}$Effector | $pG\alpha_{GTP}$Effector'(t) = $k_{26}$Effector(t) $pG\alpha_{GTP}(t)$ - $k_{27}pG\alpha_{GTP}$Effector(t) |
| RGS | RGS'(t) = - $k_7G\alpha_{GTP}(t)$ RGS(t) - $k_{12}$inert$G\alpha_{GTP}(t)$ RGS(t) - $k_{28}$inertp$G\alpha_{GTP}(t)$ RGS(t) - $k_{24}pG\alpha_{GTP}(t)$ RGS(t) + $k_8RGSG\alpha_{GTP}(t)$ + $k_{13}RGSinertG\alpha_{GTP}(t)$ + $k_{25}RGSpG\alpha_{GTP}(t)$ + $k_{29}RGSinertpG\alpha_{GTP}(t)$ |
| $RGSG\alpha_{GTP}$ | $RGSG\alpha_{GTP}$'(t) = $k_7G\alpha_{GTP}(t)$ RGS(t) - $k_8RGSG\alpha_{GTP}(t)$ |
| $RGSinertG\alpha_{GTP}$ | $RGSinertG\alpha_{GTP}$'(t) = $k_{12}$inert$G\alpha_{GTP}(t)$ RGS(t) - $k_{13}RGSinertG\alpha_{GTP}(t)$ |
| $RGSpG\alpha_{GTP}$ | $RGSpG\alpha_{GTP}$'(t) = $k_{24}pG\alpha_{GTP}(t)$ RGS(t) - $k_{25}RGSpG\alpha_{GTP}(t)$ |
| $RGSinertpG\alpha_{GTP}$ | $RGSinertpG\alpha_{GTP}$'(t) = $k_{28}$inertp$G\alpha_{GTP}(t)$ RGS(t) - $k_{29}RGSinertpG\alpha_{GTP}(t)$ |
| z(1) | z(1)'(t) = $\frac{3}{2}$ Effector(t) $G\alpha_{GTP}$+ $\frac{3}{2}$ Effector(t) $pG\alpha_{GTP}$- $\frac{3}{2}$ z(1)(t) |
| z(2) | z(2)'(t) = $\frac{3}{2}$ z(1)(t) - $\frac{3}{2}$ z(2)(t) |
| z(3) | z(3)'(t) = $\frac{3}{2}$ z(2)(t) - $\frac{3}{2}$ z(3)(t) |

TABLE 3.5: **System of ODEs for simulating the model with additional 'exogenous' Gα species** The table shows each species defined within the model and its associated differential equation describing the rate of change in that species concentration with time. The ODEs are generated from the reaction scheme in Table 3.4. For reaction rate constants (k) refer to Table 3.4. b = 100 (constant for ligand addition), $t_0$ = 14 (equilibration time before ligand application).

### 3.6.2 Simulations of the Addition of Exogenous Mutant Gα Species

To test the extended model, simulations are run with an unchanged Gα and three different types of Gα nucleotide exchange mutant added into the system (Figure 3.34). One mutant pGα is unable to exchange GDP for GTP ($k_{22} = 0\ h^{-1}$, $k_5 = 0\ h^{-1}$) ($pG\alpha^{(inactive)}$), another has an increased spontaneous activation rate ($k_{23} = k_{23}{*}10\ h^{-1}$) ($pG\alpha^{(incSpon)}$) and the third mutant is not able to hydrolyse GTP ($k_{25} = 0\ h^{-1}$, $k_{29} = 0\ h^{-1}$, $k_{30} = 0\ h^{-1}$, $k_{32} = 0\ h^{-1}$) ($pG\alpha^{-GTPase}$).

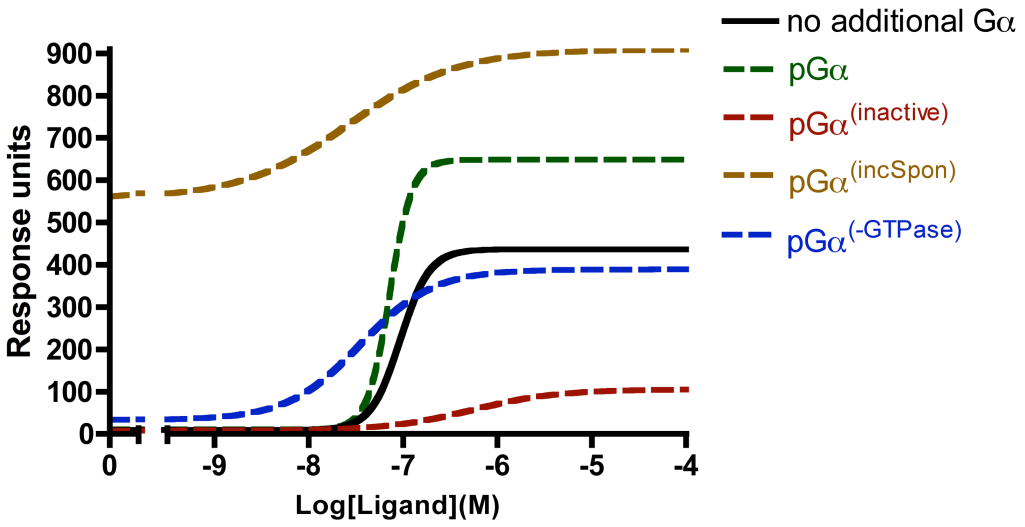


FIGURE 3.34: **Simulating addition of Gα to a *wild-type* system.** Simulations of a JY544(*sxa2>lacZ*) or JY1325(*sxa2>GFP*) equivalent system with additional Gα mutant variants introduced (Table 3.4). Mutant Gα species include a Gα that is unable to release GDP ($G\alpha^{inactive}$), a Gα with increased capability to spontaneously activate ($G\alpha^{incSpon}$) and a Gα unable to hydrolyse GTP ($G\alpha^{-GTPase}$). The concentration of ligand in the simulation was varied over the range 0-100 μM following 16 h simulated induction. Output from the model shows the accumulation of activated $G\alpha_{GTP}$Effector + $pG\alpha_{GTP}$Effector complexes over the duration of the simulated assay. The pGα species concentration was initiated at the same concentration as 'endogenous' Gα (205nM).

Results from simulations of the extended model, firstly show that the new model is still able to reproduce the classic response profile for a system containing a single unmodified Gα (see 'no additional Gα' in Figure 3.34). More importantly, the model is capable of reproducing some of the patterns observed in the equivalent assays of Gpa1 mutants. For example $Gpa1^{G243A}$, a Gα incapable of releasing GDP has been shown to be highly dominant negative over endogenous Gpa1 in previous assays (Figure 3.15 and Figure 3.23). This dominant negativity (reduction in maximal signalling compared to no-additional Gα) is also observed in simulations with a Gα mutant having rates of GDP release set to zero ($G\alpha^{inactive}$ in Figure 3.34). Similarly, but to a lesser extent, dominant negativity is observed from assays of $Gpa1^{Q244L}$ and $Gpa1^{R218C}$ (Figure 3.15 and Figure 3.23). Again this can be reproduced by the model when simulating the response with a mutant having all GTP hydrolysis rates set to zero ($G\alpha^{-GTPase}$ in Figure 3.34). Simulations of the other

mutant ($G\alpha^{incSpon}$), which has an increased spontaneous activation rate, predict that this would result in a large increase in basal signalling response and a large increase in maximal signalling, demonstrating that the concentration of $G\alpha$ is a limiting factor in the model. This prediction can not be validated against data from assays as no such equivalent Gpa1 mutant has been characterised.

## 3.7 Modelling Gpa1 Mutant Signalling Activity

Data from assays characterising the Gpa1 nucleotide exchange mutants can be used to test the Smith *et al.* model and the extended *wild-type* model to determine whether the models are able to reproduce some of the experimental data observed. Having already investigated model output under various perturbed conditions for the nucleotide exchange reactions (Figure 3.27, Figure 3.28, Figure 3.29, Figure 3.30, Figure 3.32, Figure 3.33 and Figure 3.34) this aids finding solutions in the models that can closely represent the experimental data. Simulations have been completed of the models to try to reproduce all of the previous experimental that has been obtained for all of the Gpa1 mutants. The Gpa1 mutants have been characterised under three different conditions; in *wild-type* strains, in the absence of endogenous Gpa1 and in the absence of endogenous Gpa1 and Rgs1. Simulations under equivalent conditions have been run in the models.

### 3.7.1 Modelling $Gpa1^{Q244L}$, $Gpa1^{R218C}$ and $Gpa1^{G243A}$ Mutants

The results of simulations from the Smith *et al.* model when simulating the experimental data for Gpa1, $Gpa1^{Q244L}$, $Gpa1^{R218C}$ and $Gpa1^{G243A}$ being expressed in a strain lacking endogenous Gpa1 or lacking endogenous Gpa1 and Rgs1 are presented in Figure 3.35. Patterns in dose-response profiles observed for mutants lacking the ability to hydrolyse GTP ($Gpa1^{Q244L}$), lacking the ability to release GDP ($Gpa1^{G243A}$) and showing compromised GTPase activity ($Gpa1^{R218C}$) could be reproduced in the model by adjusting parameters governing nucleotide exchange rates on $G\alpha$ (Figure 3.35). For mutants $Gpa1^{Q244L}$ and $Gpa1^{R218C}$, experimental data indicates a lack of GTPase capability due to reduced maximal signalling, reduced P-factor induction and increased basal signalling (Figure 3.11 and Figure 3.22). To achieve reduced maximal signalling in the simulations of these mutants, all GTP hydrolysis events ($k_8$,$k_9$,$k_{13}$,$k_{14}$) on $G\alpha$ were blocked. As seen in previous model perturbations, this reduces maximal signalling but has little effect on basal levels and on the extent of P-factor induced response (Figure 3.32). To more accurately reproduce the $Gpa1^{Q244L}$ and $Gpa1^{R218C}$ experimental data, additional changes had to be made to simulate effects on basal and P-factor induced signalling. Previous simulations show that increased basal and decreased extent of P-factor induced response can be achieved in $G\alpha$ species that are lacking GTPase capability through increasing their rate of spontaneous

activation (Figure 3.33). To achieve good qualitative agreement with the experimental data, the model predicts that Gpa1$^{Q244L}$ has a greatly enhanced spontaneous activation rate (10 x normal rate) and Gpa1$^{R218C}$ has a more modest enhanced rate (5 x normal rate) (Figure 3.35). The model prediction is in agreement with the experimental data looking at spontaneous activation of the Gpa1 mutants, with increased spontaneous activation being observed for Gpa1$^{Q244L}$ and Gpa1$^{R218C}$ (Figure 3.10). Modelling the data for Gpa1$^{G243A}$ is achieved by blocking any reactions on Gα that result in GDP being replaced by GTP. This results in a lack of any simulated signalling response (Figure 3.35). Simulating a lack of response for this mutant could also be achieved through blocking interaction of the Gα with the receptor, but experimental data showing dominant activity of Gpa1$^{G243A}$ over *wild-type* Gpa1 (Figure 3.15 and Figure 3.23) points to this mutant maintaining ability to bind the receptor.

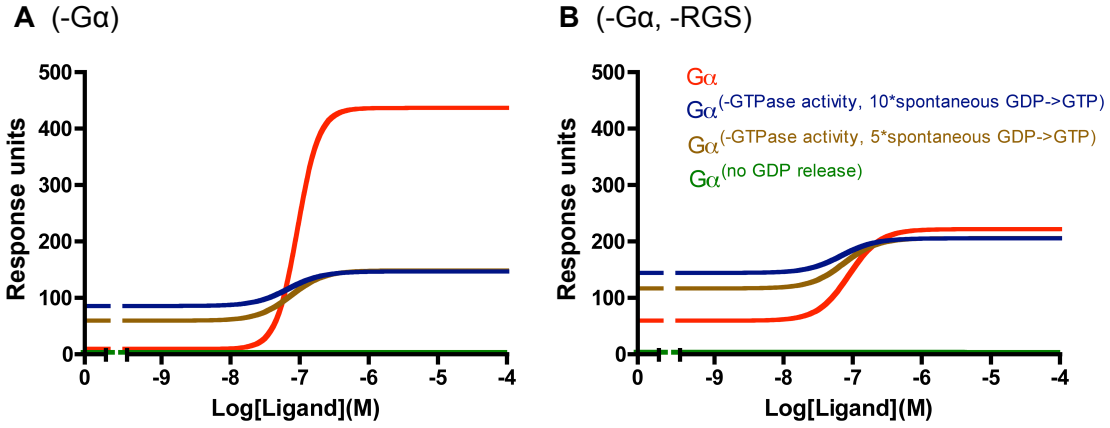


FIGURE 3.35: **Simulations of Gα mutants: Gpa1$^{Q244L}$, Gpa1$^{R218C}$ and Gpa1$^{G243A}$.** Simulations of the Smith *et al.* model (Table 3.1) of Gα species mutant variants in JY1285(ΔGpa1) (A) and JY1287(ΔGpa1,ΔRgs1) (B) equivalent systems. Simulations are of Gpa1 (Gα), Gpa1$^{Q244L}$ (Gα$^{(-GTPase\ activity,\ 10*spontaneous\ GDP->GTP)}$), Gpa1$^{R218C}$ (Gα$^{(-GTPase\ activity,\ 5*spontaneous\ GDP->GTP)}$) and Gpa1$^{G243A}$ (Gα$^{(no\ GDP\ release)}$). The concentration of ligand in the simulation was varied over the range 0-100 μM following 16 h simulated induction. Output from the model shows the accumulation of activated $G\alpha_{GTP}$Effector complexes over the duration of the simulated assay.

For simulations of experimental data investigating dominant activity of Gpa1$^{Q244L}$, Gpa1$^{R218C}$ and Gpa1$^{G243A}$, the *wild-type* model from Table 3.4 was simulated when containing additional pGα species that have modified nucleotide exchange rates as determined from the previous simulations of Gpa1$^{Q244L}$, Gpa1$^{R218C}$ and Gpa1$^{G243A}$ (Figure 3.35). The simulations show some patterns consistent with experimental data in that dominant negative activity is observed when the reaction exchanging GDP for GTP is blocked on the pGα species (Gpa1$^{G243A}$ equivalent). The simulations for pGα species with no GTPase activity and 10 x spontaneous activation (Gpa1$^{Q244L}$ equivalent) and no GTPase activity and 5 x spontaneous activity (Gpa1$^{R218C}$ equivalent) show some agreement with the experimental data. Simulations suggest that both of these mutants should have the same behaviour

in that they show some dominant negativity in terms of reducing maximal signalling but retain an increased level of basal signalling (Figure 3.36). Comparing simulations to reporter assay data indicates good qualitative agreement for Gpa1$^{Q244L}$ and Gpa1$^{R218C}$, as experimental data suggests dominant negativity for this mutant (compare Figure 3.36 to Figure 3.15 and Figure 3.23). The data suggests that Gpa1$^{Q244L}$ and Gpa1$^{R218C}$ influence signalling differently in terms of basal levels, whilst simulations predict basal activity should be similar in a strain containing an endogenous Gα (compare Figure 3.36 to Figure 3.15 and Figure 3.23).

The simulated dominant activity of Gpa1$^{Q244L}$ and Gpa1$^{R218C}$ is a result of the fact that in the model the RGS species will bind to pG$\alpha_{GTP}$ and inertpG$\alpha_{GTP}$ ,but as the hydrolysis reaction cannot occur, RGS remains bound in these complexes and is therefore sequestered such that less free RGS is available to recycle the *wild-type* inertG$\alpha_{GTP}$. As these simulations closely reproduce the dominant activity observed in the experimental data, it is reasonable to predict that in the physiological system the dominant activity of Gpa1$^{Q244L}$ and Gpa1$^{R218C}$ resulting in reduction in maximal signalling is a result of Rgs1 being sequestered by these mutants, due to these mutants having increased propensity to remain in Gpa1$_{GTP}$ and inertGpa1$_{GTP}$ states.

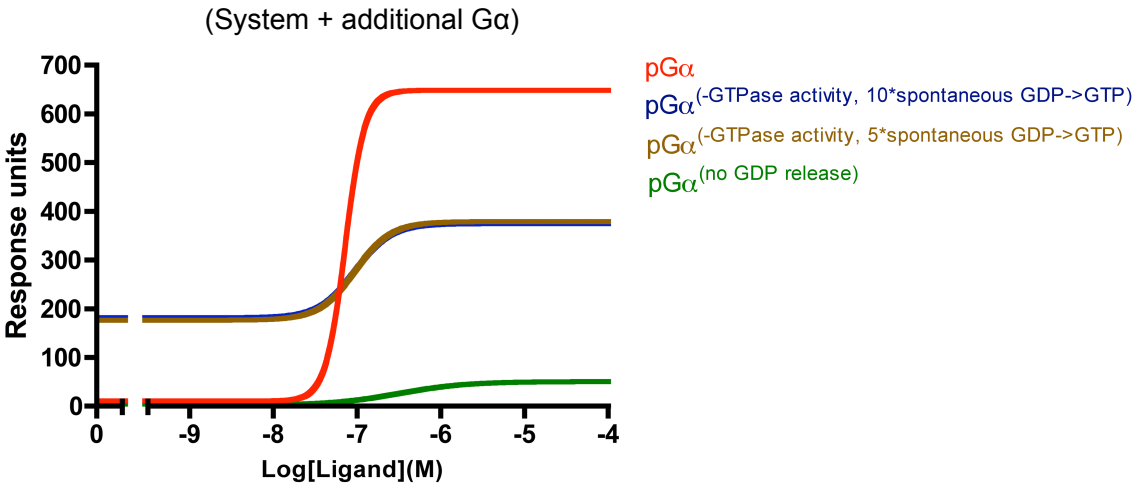


FIGURE 3.36: **Simulations of dominant activity of Gα mutants: Gpa1$^{Q244L}$, Gpa1$^{R218C}$ and Gpa1$^{G243A}$.** Simulations of the extended model (Table 3.4) with Gα species mutant variants introduced into JY544(*sxa2>lacZ*) and JY1325(*sxa2>GFP*) equivalent systems. Simulations are of Gpa1 (Gα), Gpa1$^{Q244L}$ (G$\alpha^{(-GTPase\ activity,\ 10*spontaneous\ GDP->GTP)}$), Gpa1$^{R218C}$ (G$\alpha^{(-GTPase\ activity,\ 5*spontaneous\ GDP->GTP)}$) and Gpa1$^{G243A}$ (G$\alpha^{(no\ GDP\ release)}$). The concentration of ligand in the simulation was varied over the range 0-100 $\mu$M following 16 h simulated induction. Output from the model shows the accumulation of activated G$\alpha_{GTP}$Effector + pG$\alpha_{GTP}$Effector complexes over the duration of the simulated assay.

Simulations of Gpa1, Gpa1$^{Q244L}$, Gpa1$^{R218C}$ and Gpa1$^{G243A}$ qualitatively agree with the majority of the dose-response profiles observed in the equivalent $\beta$-galactosidase and fluorescent reporter assays of Gpa1 mutants (compare model simulations; Figure 3.35 and

Figure 3.36 with quantitative assay data; Figure 3.11, Figure 3.22, Figure 3.15 and Figure 3.23). The fact that the model(s) are able to qualitatively reproduce much of this new experimental data provides further validation for the model and also allows further insight into the predicted behaviour of the Gpa1 mutants that could not be obtained from experimental data alone.

### 3.7.2 Modelling Gpa1$^{G83X}$ Series of Mutants

The results of simulations from the Smith *et al.* model when modelling the experimental data for Gpa1, Gpa1$^{G83V}$, Gpa1$^{G83S}$, Gpa1$^{G83L}$ and Gpa1$^{G83A}$ being expressed in a strain lacking endogenous Gpa1 or lacking endogenous Gpa1 and Rgs1 are shown in Figure 3.37. To simulate experimental data for Gpa1$^{G83A}$, GTPase capability was blocked (modelled by defining: $k_8 = 0\ h^{-1}$, $k_9 = 0\ h^{-1}$, $k_{13} = 0\ h^{-1}$, $k_{14} = 0\ h^{-1}$) but activation rates were left unchanged as basal signalling did not appear to be increased (Figure 3.12). Experimental data for Gpa1$^{G83V}$ and Gpa1$^{G83S}$ suggests that these mutants gave similar dose-response profiles, both showing minimal P-factor induced response, but they differed in their apparent sensitivity to negative regulation by Rgs1, with signalling levels increasing for Gpa1$^{G83S}$ when Rgs1 is removed but remaining the same for Gpa1$^{G83V}$ (Figure 3.12). To simulate these results for Gpa1$^{G83S}$ required blocking GTPase activity and reducing the ability of the Gα to become activated, but also for Gpa1$^{G83V}$, hindering its ability to interact with RGS, therefore making it less sensitive to the presence or absence of RGS. The simulated equivalent of Gpa1$^{G83S}$; G$\alpha^{(-GTPase,\ \downarrow activation)}$ is obtained by blocking all GTP hydrolysis reactions, reducing GEF-catalysed activation from 50 $h^{-1}$ to 0.025 $h^{-1}$ and halving the spontaneous activation rate (modelled by defining: $k_8 = 0\ h^{-1}$, $k_9 = 0\ h^{-1}$, $k_{13} = 0\ h^{-1}$, $k_{14} = 0\ h^{-1}$, $k_5 = 0.025\ h^{-1}$, $k_6 = 0.1\ h^{-1}$). The simulated equivalent of Gpa1$^{G83V}$; G$\alpha^{(-GTPase,\ \downarrow activation,\ \downarrow RGS\ binding)}$ is obtained by blocking all GTP hydrolysis reactions, reducing GEF-catalysed activation to $0.01 hr^{-1}$, reducing the spontaneous activation rate 1000-fold and blocking any RGS binding (modelled by defining: $k_8 = 0\ h^{-1}$, $k_9 = 0\ h^{-1}$, $k_{13} = 0\ h^{-1}$, $k_{14} = 0\ h^{-1}$, $k_5 = 0.01\ h^{-1}$, $k_6 = 0.0002\ h^{-1}$, $k_7 = 0\ nM^{-1}h^{-1}$, $k_{12} = 0\ nM^{-1}h^{-1}$) (Figure 3.37). The model therefore predicts that mutating the glycine to serine or valine at position 83 not only blocks GTP hydrolysis, but can also interfere with activation and ability to bind RGS. Experimental data for Gpa1$^{G83L}$ showed this particular mutant to be completely inactive, therefore it was modelled in the same way as for Gpa1$^{G243A}$ by blocking any capability to exchange GDP for GTP (modelled by defining: $k_5 = 0\ h^{-1}$, $k_6 = 0\ h^{-1}$) (G$\alpha^{(un-activatable)}$) (Figure 3.37).

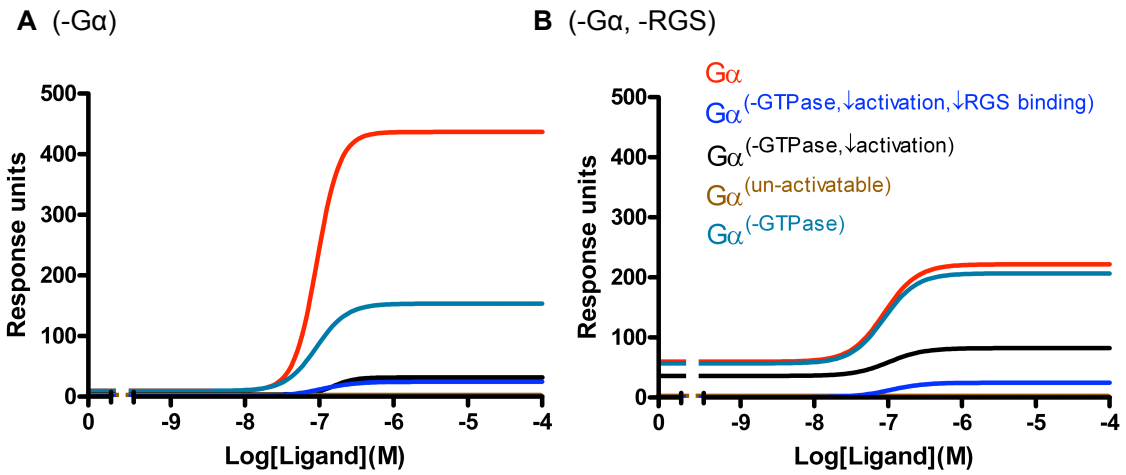


FIGURE 3.37: **Simulations of Gα mutants: Gpa1$^{G83X}$.** Simulations of the Smith *et al.* model (Table 3.1) of Gα species mutant variants in JY1285(ΔGpa1) (A) and JY1287(ΔGpa1,ΔRgs1) (B) equivalent systems. Simulations are of Gpa1 (Gα), Gpa1$^{G83V}$ (G$\alpha^{(-GTPase,\ \downarrow activation,\ \downarrow RGS\ binding)}$), Gpa1$^{G83S}$ (G$\alpha^{(-GTPase,\ \downarrow activation)}$), Gpa1$^{G83L}$ (G$\alpha^{(un-activatable)}$) and Gpa1$^{G83A}$ (G$\alpha^{(-GTPase)}$). The concentration of ligand in the simulation was varied over the range 0-100 μM following 16 h simulated induction. Output from the model shows the accumulation of activated G$\alpha_{GTP}$Effector complexes over the duration of the simulated assay.

Having simulated dose-responses for all Gpa1$^{G83X}$ mutants with reasonably close qualitative agreement, these mutants were than simulated in a *wild-type* model, to investigate behaviour in the presence of endogenous Gα (Figure 3.38). Experimental data suggests that all Gpa1$^{G83X}$ mutants except for Gpa1$^{G83A}$ show dominant negativity over *wild-type* Gpa1 and to a similar extent (Figure 3.17). Simulations from the model are not able to reproduce this result, as the model predicts that all mutants have dominant negative activity, including Gpa1$^{G83A}$, and the extent to which this occurs varies between the mutants. The simulations of Gpa1$^{G83L}$ and Gpa1$^{G83V}$ equivalent mutants (G$\alpha^{(un-activatable)}$ and G$\alpha^{(-GTPase,\ \downarrow activation,\ \downarrow RGS\ binding)}$ respectively) show the most dominant negativity and are the closest qualitative matches to the experimental data (compare Figure 3.38 to Figure 3.17). Simulations of the Gpa1$^{G83S}$ and Gpa1$^{G83A}$ equivalent mutants (G$\alpha^{(-GTPase,\ \downarrow activation)}$ and G$\alpha^{(-GTPase)}$ respectively) do not show very good agreement with experimental data (compare Figure 3.38 to Figure 3.17). The lack of good agreement with the data here highlights the limitation of the model as these particular mutations may be having additional effects on signalling reactions, which are not represented in the model.

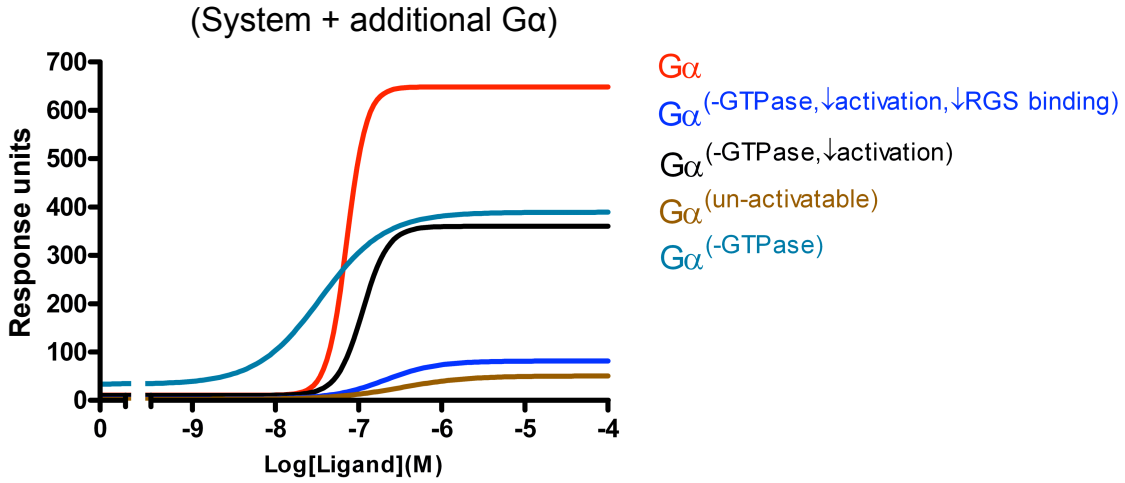


FIGURE 3.38: **Simulations of dominant activity of Gα mutants: Gpa1$^{G83X}$.** Simulations of the extended model (Table 3.4) with Gα species mutant variants introduced into JY544(*sxa2>lacZ*) and JY1325(*sxa2>GFP*) equivalent systems. Simulations are of Gpa1 (Gα), Gpa1$^{G83V}$ (G$\alpha^{(-GTPase,\ \downarrow activation,\ \downarrow RGS\ binding)}$), Gpa1$^{G83S}$ (G$\alpha^{(-GTPase,\ \downarrow activation)}$), Gpa1$^{G83L}$ (G$\alpha^{(un-activatable)}$) and Gpa1$^{G83A}$ (G$\alpha^{(-GTPase)}$). The concentration of ligand in the simulation was varied over the range 0-100 $\mu$M following 16 h simulated induction. Output from the model shows the accumulation of activated G$\alpha_{GTP}$Effector + pG$\alpha_{GTP}$Effector complexes over the duration of the simulated assay.

Simulations of the Gpa1$^{G83X}$ mutants are good qualitative matches in terms of the signalling response in strains lacking endogenous Gα and strains lacking endogenous Gα and RGS, but to achieve agreement, the model assumes that the mutation can alter activation capability and RGS binding in addition to the predicted effect of blocking GTP hydrolysis (Barbacid, 1987; Bos, 1989) (compare Figure 3.37 to Figure 3.12). Not such a good agreement with the data is obtained when simulating the mutants in a strain containing endogenous Gα, with the most difficult mutants to model being Gpa1$^{G83A}$ and Gpa1$^{G83S}$ (compare Figure 3.38 to Figure 3.17). Experimental data in strains lacking endogenous Gpa1 suggest that Gpa1$^{G83A}$ has compromised GTPase capability similar to that seen previously for Gpa1$^{Q244L}$ (compare Figure 3.11 to Figure 3.12), but whilst Gpa1$^{Q244L}$ displays dominant negativity, Gpa1$^{G83A}$ does not (compare Figure 3.15 to Figure 3.17). This suggests subtle differences between these GTPase compromised mutants in terms of their ability to compete with endogenous Gpa1 for binding partners, therefore making it difficult to simulate this result. Simulations of Gpa1$^{G83S}$ dominant negative activity have also proved difficult as this mutant is slightly activatable and sensitive to Rgs1 (Figure 3.12), yet to achieve the dominant negative activity in simulation requires an unactivatable mutant or reduced activation and a lack of sensitivity to RGS (Figure 3.38).

### 3.7.3 Modelling Time-series Data

In all previous simulations, the output from the model has been given as the accumulated concentration of activated $G\alpha_{GTP}$Effector complexes over 16 h of simulated response following the addition of ligand. This endpoint simulated response can be compared to endpoint data from $\beta$-galactosidase assays. It is this comparing of simulated signalling response to endpoint experimental data that has primarily been used in the development and testing of the current model(s). The development of fluorescent reporter strains, allowing time-series measurement of signalling response has enabled a further avenue for developing and testing the model using time-series response. Gpa1, Gpa1$^{Q244L}$, Gpa1$^{R218C}$ and Gpa1$^{G243A}$ have all been assayed in a *sxa2>GFP* reporter strain lacking endogenous Gpa1 to investigate their signalling response with time (Figure 3.24). The modified Gα species deemed equivalent to these Gpa1 variants have been simulated for their response with time to allow comparison of simulated time-series response from the model to time-series experimental data (compare Figure 3.39 to Figure 3.24). The time-series response is given as the accumulated $G\alpha_{GTP}$Effector complexes over 16 h following the addition of ligand at time zero (Figure 3.39).

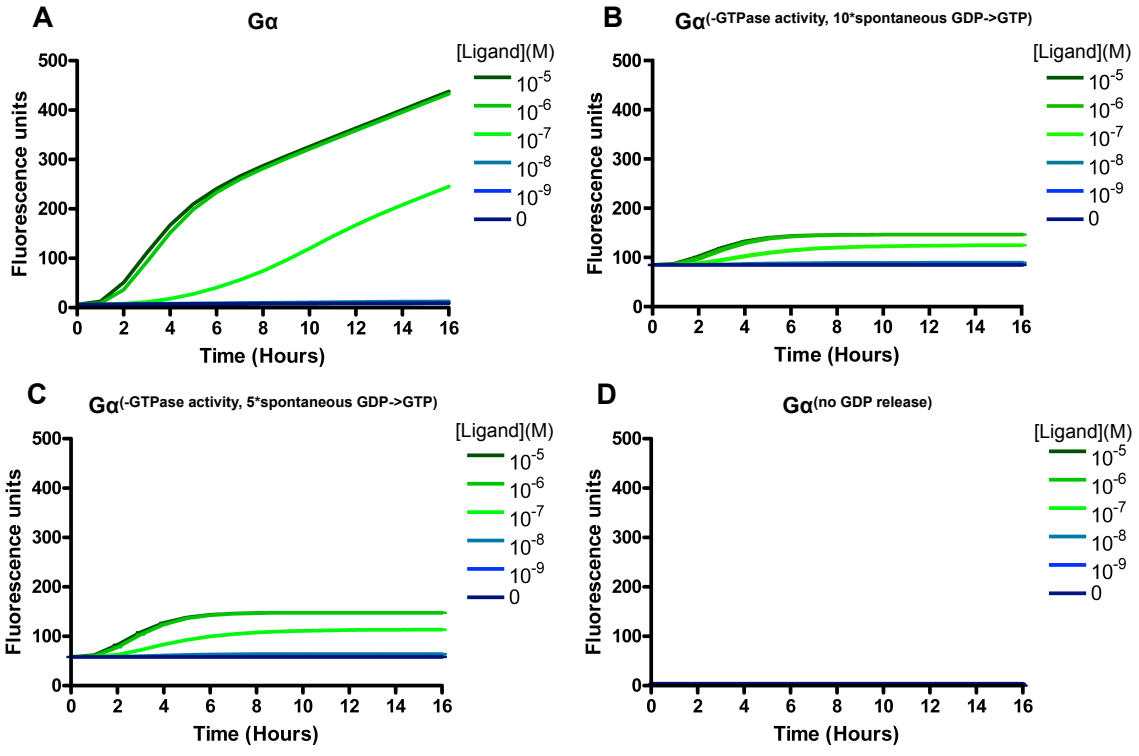


FIGURE 3.39: **Time-series simulations of Gα mutants: Gpa1$^{Q244L}$, Gpa1$^{R218C}$ and Gpa1$^{G243A}$.** Time-series simulations of the Smith *et al.* model (Table 3.1) of Gα species mutants in a JY1341(*sxa2>GFP*,ΔGpa1) equivalent strain. Simulations are of Gpa1 (Gα) (A), Gpa1$^{Q244L}$ (G$\alpha^{(-GTPase\ activity,\ 10*spontaneous\ GDP->GTP)}$) (B), Gpa1$^{R218C}$ (G$\alpha^{(-GTPase\ activity,\ 5*spontaneous\ GDP->GTP)}$) (C) and Gpa1$^{G243A}$ (G$\alpha^{(no\ GDP\ release)}$) (D). The concentration of ligand in the simulation was varied over the range 0-100 $\mu$M following and output from the model shows the accumulation of activated $G\alpha_{GTP}$Effector complexes over the duration of the simulated 16 h assay.

In comparing output from the model to experimental data for *wild-type* Gpa1 (compare Figure 3.39, A to Figure 3.24, A) the time-series simulated response is in reasonable agreement with the experimental data. The model is deterministic, therefore it is unable to encompass the variability observed in the experimental data, which is why there is no gradual increase in response at ligand concentrations of 0M, $10^{-9}$M and $10^{-8}$M. The general pattern observed in experimental data (Figure 3.24, A) of a greater response at ligand concentrations of $10^{-5}$M and $10^{-6}$M compared to the response at $10^{-7}$M, is reproduced in the simulation, as is the more rapid induction of a response at concentrations of $10^{-5}$M and $10^{-6}$M following addition of ligand. The simulated response with time for Gpa1$^{Q244L}$ is not in very good agreement with the experimental data as there is no gradual increase in response with time for all concentrations, although the model output does maintain that there is minimal effect of varying ligand concentration on the level of response (compare Figure 3.39, B to Figure 3.24, B). It is possible that this difference is due to no further response being able to occur in both the simulation and the experimental data as all G$\alpha$ is trapped in the inert state, the difference possibly being due to the effects of a very stable GFP protein and cell growth giving a gradual increase in fluorescence intensity. Simulations of Gpa1$^{R218C}$ displays an induced response with time at ligand concentrations of $10^{-5}$M, $10^{-6}$M and $10^{-7}$M, which rapidly plateaus after 6 h suggesting no further response after this time (Figure 3.39, C). This is similar to what is observed in the experimental data, although there is the gradual increase in response again at all concentrations that is a common effect in the fluorescence assays (compare Figure 3.39, C to Figure 3.24, C). The simulations for Gpa1$^{Q244L}$ and Gpa1$^{R218C}$ suggest that whilst the majority of the G$\alpha$ species are already trapped in the inert state for Gpa1$^{Q244L}$ prior to the addition of any ligand, some Gpa1$^{R218C}$ must be in an activateble form. Simulations of Gpa1$^{G243A}$ show a lack of response with time, as expected from a mutant that cannot become activated. The non-signalling induced increase in fluorescence intensity in the experimental data is most evident for this mutant (compare Figure 3.39, D to Figure 3.24, D). It appears that if fluorescence change due to non-signalling events could be removed from the experimental data, then the simulations would be in good agreement with the data. A limitation of modelling the time-series data with the current model(s) is that there is no mechanism for having the response decrease with time, as the output is integrated over the number of activated G$\alpha^{GTP}$Effector complexes and the model(s) lack mechanisms for terminating the response other than GTP hydrolysis events, therefore limiting the modelling of recovery from response to observing a plateau in the simulated response.

### 3.7.4 Modelling Limitations

Whilst all mutants have been extensively characterised through both assays of transcriptional and morphological signalling response, the model(s) are limited to simulating endpoint data from transcriptional assay and to a lesser extent, time-series transcriptional data. Unlike in the experimental assays whereby a morphology readout can be obtained through the measurement of cell volume, there is no such readout in the current model(s).

Additionally, due to the deterministic nature of the model(s) and the stochastic nature of molecular interactions, the reactions defined in the model(s) are only approximations of the reactions occurring physiologically. Further modelling considerations are addressed later in Chapter 6.

### 3.7.5 The Simulated Nucleotide Exchange Mutants

To reproduce the signalling profiles for the Gpa1 nucleotide exchange mutants required the modification of various reactions rates in the model(s), therefore giving G$\alpha$ species in the model with the behaviour that is predicted to occur as a result of the specific mutation. A summary of all the rates associated with each simulated mutant is given in Table 3.6. The mutant rates can be compared to *wild-type* Gpa1 rates to see how the mutant differs from its unmodified counterpart. Gpa1$^{Q244L}$ has previously been shown to be a mutation causing a lack of GTPase capability (Obara et al., 1991; Majumdar et al., 2006; Smith et al., 2009). To achieve this in the model, all rates for GTP hydrolysis reactions were set to zero. This was not sufficient to accurately reproduce the experimental in terms of a raised basal signalling activity and a lack of ligand induced response, therefore the spontaneous activation rate had to be increased 10-fold to obtain a good qualitative agreement between simulation and experimental data. The model therefore predicts that this particular mutant has no GTPase activity, but additionally has an increased ability to spontaneously activate. Gpa1$^{R218C}$ is suggested to be a similar mutant to Gpa1$^{Q244L}$ in that it has compromised GTP hydrolysis capability (Majumdar et al., 2006) and the assays confirm this in that Gpa1$^{R218C}$ shows reduced maximal signalling that is comparable to Gpa1$^{Q244L}$. The difference is that Gpa1$^{R218C}$ has lower basal signalling and is therefore inducible by P-factor. Basal levels, although lower than Gpa1$^{Q244L}$, are still higher than those for Gpa1, therefore this mutant is modelled by blocking all GTP hydrolysis reactions plus having a more modest 5-fold increase in spontaneous activation rate. Gpa1$^{G243A}$, a mutant unable to release GDP and therefore unable to become activated (Ladds et al., 2007) could be modelled by blocking GDP->GTP exchange through blocking both spontaneous activation and GEF-catalysed activation by an activated GPCR. The Gpa1$^{G83X}$ mutation is again predicted to have compromised GTPase capability through an insensitivity to GAP activity (Barbacid, 1987; Bos, 1989), although different Gpa1$^{G83X}$ mutants had to be modelled in different ways due to differences in signalling behaviour, dependent on which amino acid was used

to replace the glycine. All Gpa1$^{G83X}$ mutants were modelled by blocking GTP hydrolysis reactions, but then alterations were made to other reactions to achieve as close as possible agreement to experimental data. Gpa1$^{G83V}$ additionally has reduced GEF-catalysed and spontaneous activation rates as well as an inability to bind to RGS species, Gpa1$^{G83S}$ has reduced GEF-catalysed and spontaneous activation rates to a lesser extent, but remains sensitive to RGS binding and Gpa1$^{G83L}$ is rendered non activatable by blocking any GDP -> GTP exchange reactions (Table 3.6).

| Gα | GEF-catalysed Activation Rate ($k_5$) ($h^{-1}$) | Spontaneous Activation Rate ($k_6$) ($h^{-1}$) | GTP Hydrolysis Rates ($k_8$, $k_9$, $k_{13}$, $k_{14}$) ($h^{-1}$) | RGS Binding Rates ($k_7$, $k_{12}$)($nM^{-1}h^{-1}$) |
|---|---|---|---|---|
| Gpa1 | 50 | 0.2 | 2.5, 0.005, 0.3, 0.005 | 500, 50 |
| Gpa1$^{Q244L}$ | 50 | 2 | 0, 0, 0, 0 | 500, 50 |
| Gpa1$^{R218C}$ | 50 | 1 | 0, 0, 0, 0 | 500, 50 |
| Gpa1$^{G243A}$ | 50 | 2 | 2.5, 0.005, 0.3, 0.005 | 500, 50 |
| Gpa1$^{G83V}$ | 0.01 | 0.0002 | 0, 0, 0, 0 | 0, 0 |
| Gpa1$^{G83S}$ | 0.025 | 0.1 | 0, 0, 0, 0 | 500, 50 |
| Gpa1$^{G83L}$ | 0 | 0 | 0, 0, 0, 0 | 500, 50 |
| Gpa1$^{G83A}$ | 50 | 0.2 | 0, 0, 0, 0 | 500, 50 |

TABLE 3.6: **Simulated Gpa1 nucleotide exchange mutant reaction rates.** The rates required to model the signalling activity of the Gα nucleotide exchange mutants; Gpa1$^{Q244L}$, Gpa1$^{R218C}$, Gpa1$^{G243A}$, Gpa1$^{G83V}$, Gpa1$^{G83S}$, Gpa1$^{G83L}$, Gpa1$^{G83A}$ are presented. Rates of the unmodified Gα species (Gpa1) are given for comparison.

## 3.8 Summary

A number of Gpa1 fusion constructs have been made and tested for their ability to function and be visualised within the cell. Tagging with GFP at the C-terminus, after amino acid residue 132 and after amino acid residue 160 allowed visualisation of the fusion protein at the plasma membrane of cells, but all of these modifications rendered the protein non-functional. Tagging with a tetra-cysteine motif for FLAsH labelling at the C-terminus and after amino acid residue 160 resulted in functional fusion proteins but initial attempts at visualising these proteins were unsuccessful.

A number of different Gpa1 nucleotide exchange mutants have been characterised using a combination of assays from *sxa2>lacZ* reporters, *sxa2>GFP* reporters and through perturbations of the Smith *et al.* model of the G protein cycle. Investigations into nucleotide exchange reaction rates in the model have shown that GTP hydrolysis of the inertGαGTP species is a highly sensitive parameter governing system level signalling output.

The model has been extended to enable simulations of the system whereby additional Gα species, having modified kinetics can be introduced to investigate how this effects signalling response. This allows comparison of model output to the results of assays of reporter strains expressing additional Gα species, which was not possible with the previous model.

Simulations from the models can qualitatively reproduce much of the biological data from assays of Gpa1 nucleotide exchange mutants, thus providing further model validation. Through simulation of the Gpa1 nucleotide exchange mutants to reproduce experimental data, the models predict that in addition to an inability to hydrolyse GTP, the $Gpa1^{Q244L}$ and $Gpa1^{R218C}$ mutants display increased rates of spontaneous activation, $Gpa1^{G83V}$ and $Gpa1^{G83S}$ have reduced capability to become activated, $Gpa1^{G83V}$ is unable to bind to Rgs1 and $Gpa1^{G83L}$ is inactive.

Assays and modelling of a system containing a Gα protein unable to hydrolyse GTP in the presence and absence of an RGS species has indicated that there is an additional negative regulatory role of Rgs1 that is independent of its more common function of catalysing GTP hydrolysis.

# Chapter 4

# Integrating Biological and Mathematical Approaches: Spatial Regulation of RGS

## 4.1 Background

RGS proteins are important regulators of G protein-mediated signalling pathways and are united by the presence of the RGS domain, which in the majority of cases, serves as a GAP for G$\alpha$ subunits of heterotrimeric G proteins. This mechanism, common to all RGS proteins allows them to regulate the signalling of numerous GPCRs. In addition to the catalysis of GTPase reactions, it is becoming increasingly evident that RGS proteins have other non-canonical functions, due to the presence of diverse regions of various lengths other than the RGS domain (Willars, 2006; Sethakorn et al., 2010). Some of these regions providing additional levels of regulation of G protein signalling by determining intracellular localisation, receptor selectivity and interactions with other signalling partners.

The *S. pombe* RGS protein Rgs1, has an unusual role in regulation of signalling, in that it has been shown to have both a positive and negative impact on signal transduction, that is dependent on the level of ligand stimulation (Smith et al., 2009). This behaviour has been the subject of a mathematical model by Smith *et al.* (described in Chapter 3, Table 3.1) that provides a theory as to the mechanisms of this dual regulation. Additional evidence from experimental data that is unexplainable with the Smith *et al.* model has provided added complexity, and a possible additional higher level of regulation on RGS function and hence the overall regulation of the signalling pathway. These experiments implied an interaction between the GPCR Mam2, and Rgs1, that is key to the regulation of signalling.

Other RGS proteins have been shown to interact with specific GPCRs with a functional consequence on signal regulation, namely the *S. cerevisiae* RGS protein SST2, which regulates *S. cerevisiae* mating-response, can interact with its cognate GPCR STE2, via an N-terminal DEP domain in SST2 (Ballon et al., 2006). Rgs1 contains two of these conserved DEP domains in its N-terminus (Figure 4.1).


FIGURE 4.1: **Conserved domains within *S. pombe* Rgs1.** The *S. pombe* Rgs1 protein consists of 481 residues and contains conserved domains. The N-terminus incorporates residues 1-309 and contains two DEP domains; DEP-A (residues 114-156) and DEP-B (residues 250-309). The C-terminus incorporates residues 310-481 and contains the RGS-fold (residues 345-474).

## 4.2 GPCR-RGS Interaction Model Development

The interaction between Mam2 and Rgs1 specifically involves the C-terminal tail of Mam2, which comprises of the last 45 amino acid residues of the protein (Figure 4.2). GPCR C-terminal tails have been implicated in many aspects of GPCR behaviour (reviewed by Bockaert et al., 2003), including regulation of receptor localisation, trafficking to the plasma membrane (PM) and desensitisation to prolonged stimulation through promoting internalisation. There are a number of lysine and serine/tyrosine residues in the tail of Mam2, which may be (but not confirmed to be) ubiquitinated or phosphorylated to target the receptor for degradation and internalisation. Crucially, the C-terminal tail could also dictate the level and nature of the signalling response by providing a scaffold for downstream signalling components such as RGS proteins (Hepler, 1999, 2003). Indeed in the *S. cerevisiae* mating-response pathway it is the cytoplasmic C-terminal tail of the GPCR that provides a docking site for the RGS protein SST2 (Ballon et al., 2006).

One method of testing for direct interactions between proteins is through yeast two-hybrid analysis (Fields and Song, 1989). The interaction between the Mam2 tail and Rgs1 was confirmed as being a strong interaction by yeast two-hybrid experiments (McCann, PhD Thesis, 2010) (Figure 4.3, A). To assay signalling activity, full length Mam2 and Mam2 truncated for its C-terminal tail (Mam2$\Delta$tail) were expressed from vector pREP3x in reporter strain JY1169(*sxa2>lacZ*, $\Delta$Mam2). These transformed strains, and a reporter strain lacking endogenous Rgs1; JY630(*sxa2>lacZ*, $\Delta$Rgs), were grown in minimal media, incubated with P-factor at concentrations of 0M to $10^{-4}$M for 16 h before assaying for induction of *sxa2>lacZ* (Figure 4.3, B).

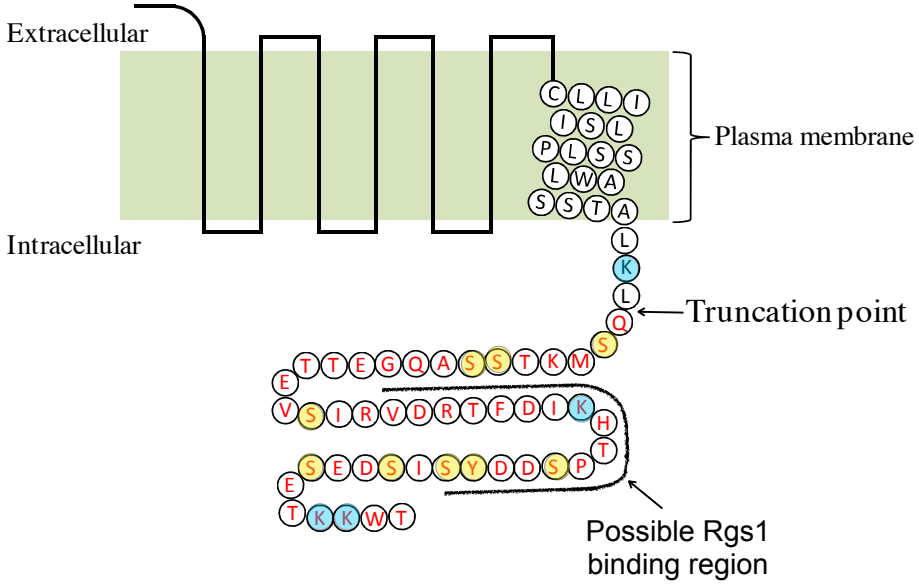


FIGURE 4.2: **Mam2 C-terminal tail.** The amino acid sequence of the C-terminal region of Mam2 is shown including the predicted transmembrane domain 7 (as predicted by NCBI Protein). The truncation is depicted with the proposed 45-residue C-terminal tail of Mam2 shown in red. Possible lysine residues that could be involved in protein ubiquitination to target the protein for degradation are highlighted in blue and possible tyrosine/serine phosphorylation targets for recognition by cellular internalisation machinery are highlighted in yellow. The estimated Rgs1 binding region as determined by truncation studies (McCann, PhD thesis, 2010) is also labelled.

Similarities in the dose-response profiles of the strain expressing Mam2Δtail and the ΔRgs1 strain include a raised basal $\beta$-galactosidase activity (Mam2Δtail; 2.123 ± 0.44) compared to when full length receptor is present (Mam2; 0.339 ± 0.382 ), increased sensitivity to ligand (Mam2Δtail $pEC_{50}$; 8.319 ± 0.108 vs Mam2 $pEC_{50}$; 6.882 ± 0.05 ) and reduced maximal signalling activity (Mam2Δtail; 7.031 ± 0.194 vs Mam2; 17.71 ± 0.382) (Figure 4.3). Signalling activity in reporter strains expressing a receptor lacking its tail (Mam2Δtail) and therefore incapable of the Mam2-Rgs1 interaction is characteristic of signalling observed in strains lacking any Rgs1 (ΔRgs1) (Figure 4.3, B). This result points to a possible role for the tail of Mam2 in regulating the signalling response via an interaction with Rgs1.

The experimental data concerning the loss of a GPCR-RGS interaction (pMam2Δtail in Figure 4.3, B) cannot be simulated by the Smith *et al.* model, as this model does not include any reactions for GPCR-RGS interactions (see Chapter 3, Table 3.1), therefore this model is missing a key regulatory mechanism controlling the G protein cycle.

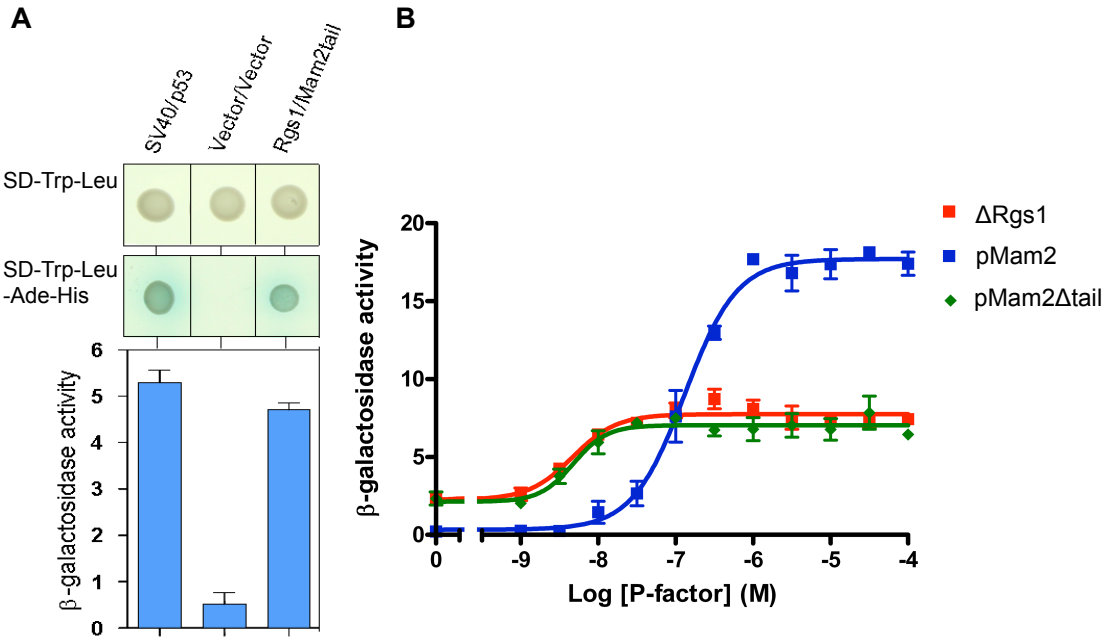


| | Basal | Maximal | $pEC_{50}$ |
|---|---|---|---|
| ΔRgs1 | 2.249 +/- 0.418 * | 7.740 +/- 0.169 *** | 8.328 +/- 0.100 *** |
| pMam2 | 0.331 +/- 0.383 | 17.710 +/- 0.357 | 6.882 +/- 0.049 |
| pMam2Δtail | 2.123 +/- 0.440 * | 7.031 +/- 0.194 *** | -8.319 +/- 0.108 *** |

FIGURE 4.3: **A Mam2-Rgs1 interaction with a possible functional consequence on signalling.** *S. cerevisiae* yeast two-hybrid transformants expressing Mam2tail with Rgs1 from vectors pGBKT7 and pGADT7 respectively were capable of growth on SD-leu-trp and on SD-leu-trp-his-ade + X-$\alpha$-gal confirming an interaction between the tail of Mam2 and Rgs1 resulting in the expression of the HIS3, ADE2 and MEL1 reporter genes and the formation of blue colonies. Control strains expressing the strongly interacting SV40-T antigen and p53 or the non-interacting vectors are included for comparison. A liquid based $\beta$-galactosidase assay indicated that the Mam2tail-Rgs1 interaction was a strong one (A) (McCann, PhD Thesis, 2010). Reporter strain JY1169($\Delta$Mam2) was transformed with expression vectors pREP3x-Mam2 (pMam2), and pREP3x-Mam2$\Delta$tail (pMam2$\Delta$tail). Reporter strain JY630($\Delta$Rgs1) was assayed for comparison ($\Delta$Rgs1). Cells were cultured in minimal media to a density of $\sim$5x$10^6$ cells/ml, incubated with 0M to $10^{-4}$M P-factor before assaying for $\beta$-galactosidase activity. $\beta$-galactosidase activity was measured as $OD_{420}/10^6$ cells. Results are the means $\pm$ S.E.M. from triplicate determinations of three independent isolates.

This chapter describes an iterative approach of experimental data gathering and mathematical modelling of the signalling pathway, that has enabled the Smith *et al.* model to be developed and extended further to investigate the role this interaction is having in regulating G protein-mediated signalling.

### 4.2.1 Mating Efficiency of Mam2$\Delta$tail and $\Delta$Rgs1 Strains

The C-terminal tail of Mam2 has previously been demonstrated to be involved in an interaction with Rgs1 (McCann, PhD Thesis, 2010) and also confirmed as having an effect on the level of signal transduced through the pathway following stimulation with P-factor (Figure 4.3). As the physiological purpose of the cell's signalling response to P-factor is

to promote cell elongation and fusion with a mating partner, it was necessary to also investigate the requirement of the receptor tail in terms of a cell's ability to mate. The contribution of the Mam2 C-terminal tail to the mating-response has been investigated previously in a non-quantitative mating assay. Mating was found to be reduced, but not abolished in strains expressing a single copy of Mam2Δtail (McCann, PhD Thesis, 2010). It is possible that this negative effect is due to the dysregulation of the signalling pathway as a result of a lack of interaction between Mam2 and Rgs1 when the tail is removed.

To determine the role of the Mam2 tail in the efficiency of mating, and to compare to the mating efficiency of a strain lacking endogenous Rgs1, a quantitative mating assay is used (Bond, University of Warwick, 2010). In this assay, cells of opposite mating types: M and P are mixed and cultured on a nitrogen limited plate to induce mating. The colony is then collected and heat-treated at 55$^o$C to induce cell death such that only the spores produced from cells that have mated will survive due to their increased tolerance to temperature change. The heat-treated cell culture is then plated onto a nitrogen rich plate and quantified for the number of colonies that recover. For these assays, non-sterile strains are used that contain Sxa2 (Imai and Yamamoto, 1992).

The *wild-type* P-cell (JY1025) was cultured in minimal media and mixed with cultures of the *wild-type* M-cell (JY444), M-cells deleted for Rgs1(JY478), M-cells deleted for Rgs1 but expressing Rgs1 from vector pREP3x, M cells deleted for Mam2 (JY1353) and M cells deleted for Mam2 but expressing either Mam2 or Mam2Δtail from pREP3x. Following growth on nitrogen limited plates to induce mating, heat-treatment to kill all but spores and re-plating on nitrogen rich plates, the number of recovered colonies was quantified (Figure 4.4).

Strains lacking Mam2 (ΔMam2) are sterile, but this can be overcome to near *wild-type* levels (24.37 ± 1.23 %) by expressing Mam2 from an inducible plasmid (pMam2; 17.33 ± 2.27 %). The expression of Mam2Δtail does not completely recover the sterility of a ΔMam2 strain (2.23 ± 1.24 %). Reduced mating efficiency compared to *wild-type* is also observed when Rgs1 is expressed from a vector (pRgs1; 10.22 ± 0.99 %) and is significantly reduced when Rgs1 is deleted (ΔRgs; 0.07 ± 0.03 %) (unpaired $t$, $p<0.001$). The absolute requirement of Rgs1 for mating has been described previously by Watson et al., 1999. When comparing the mating efficiencies of a strain lacking a receptor tail to those of a strain lacking Rgs1, both strains have significantly hampered ability to mate (unpaired $t$, $p<0.001$). These results prove a functional role for the C-terminal tail of Mam2 in facilitating mating and suggest that it could be the reduced functionality of Rgs1 as a result of no interaction with the receptor that is causing the reduction in a cells ability to mate.

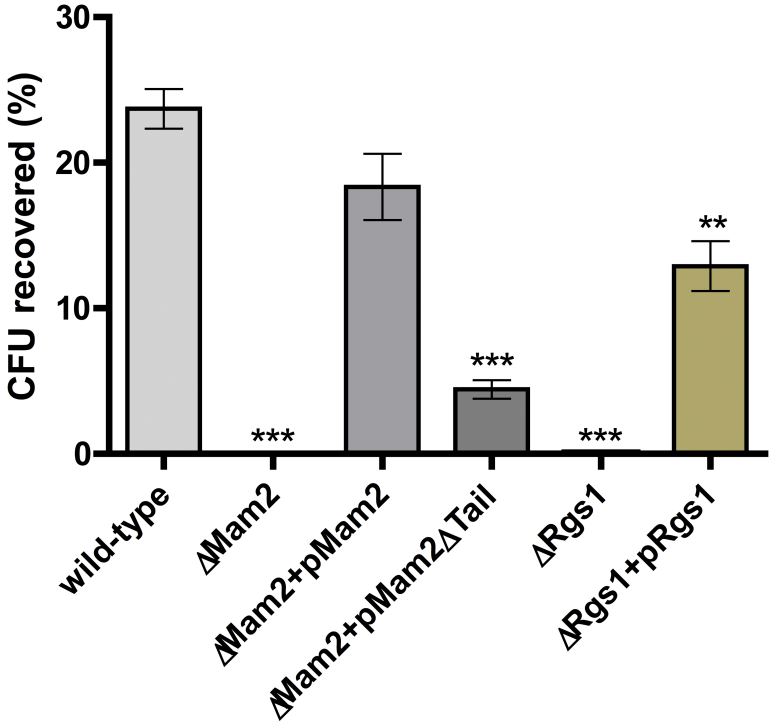


FIGURE 4.4: **Mating efficiencies: Mam2Δtail vs ΔRgs1.** The *wild-type* non sterile P cell; JY1025 was mated with *wild-type* non sterile M cell; JY444 (*wild-type*), an M cell lacking endogenous Mam2; JY1353 (ΔMam2), JY1353 expressing Mam2 from vector pREP3x (pMam2), JY1353 expressing Mam2Δtail from pREP3x (pMam2Δtail), an M cell lacking endogenous Rgs1; JY478 (ΔRgs1) and JY478 expressing Rgs1 from vector pREP3x (pRgs1). The mixed strains were cultured in minimal media to mid-exponential phase, spotted onto a nitrogen limited plate before heat treating and re-plating onto a nitrogen rich plate. Mating efficiency is quantified as the mean ± S.E.M. percentage of colony forming units recovered from three independent experiments. Significant difference from *wild-type* is indicated with ***($p$<0.001), **($p$<0.01) or *(P< 0.05) as determined by unpaired $t$ test.

### 4.2.2 Rgs1 localisation and function

RGS proteins possess GAP activity, which requires close proximity to G$\alpha$ subunits in order to catalyse the GTP hydrolysis reaction. This would suggest that generally they should be localised to the PM of the cell where the G$\alpha$ subunits reside, but despite this, the vast majority of RGS proteins are localised to the cytosol or the nucleus (De Vries et al., 2000; Chatterjee and Fisher, 2000). Previous studies using confocal microscopy has indicated that *S. pombe* Rgs1 also localises to the nucleus (Pereira and Jones, 2001). Despite these findings, it is plausible that Rgs1 and other RGS proteins only become PM localised when absolutely required, and that there is some signal to promote membrane localisation, or it is possible that the concentration needed at the PM is very small, therefore it is not easily detected using less sensitive microscopy techniques. With the aid of a more sensitive DeltaVision wide-field deconvolution microscope, localisation of Rgs1 has been investigated.

Rgs1, with GFP fused to its C-terminus was expressed from vector pREP3x in the reporter strain JY630(*sxa2>lacZ*, ΔRgs1) and assayed to confirm its expression and functionality. The reporter strains JY630 and JY630 expressing Rgs1 or Rgs1-GFP from vector pREP3x were grown in minimal media and incubated with P-factor at concentrations of 0M to $10^{-4}$M for 16 h before assaying for the induction of *sxa2>lacZ* (Figure 4.5, A). Following confirmation of protein function, the strain expressing Rgs1-GFP was grown in minimal media before imaging to investigate cellular localisation of the protein (Figure 4.5, B).

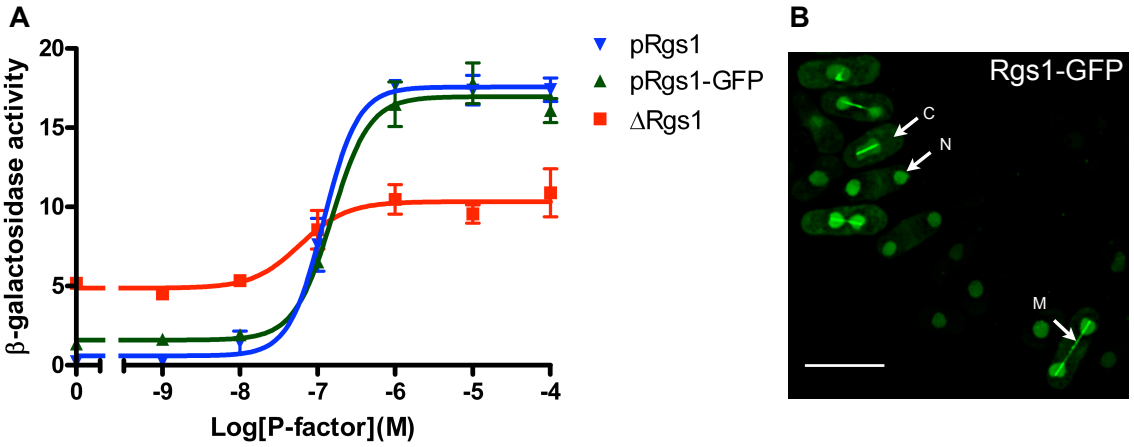


| | Basal | Maximal | $pEC_{50}$ |
|---|---|---|---|
| pRgs1 | 1.878 +/- 0.319 | 16.611 +/- 0.524 | 6.96 +/- 0.093 |
| pRgs1-GFP | 0.61 +/- 0.462 | 17.528 +/- 0.422 | 6.889 +/- 0.087 |
| ΔRgs1 | 4.869 +/- 0.514 | 9.366 +/- 0.613 | 7.215 +/- 0.091 |

FIGURE 4.5: **Rgs1-GFP localisation and functionality.** Reporter strains JY630 (ΔRgs1) and JY630 containing the expression vector pREP3x expressing Rgs1-GFP (pRgs1-GFP) or Rgs1 (pRgs1) were cultured in minimal media to a density of ~5x$10^6$ cells/ml, incubated with 0M to $10^{-4}$M P-factor before assaying for $\beta$-galactosidase activity. $\beta$-galactosidase activity was measured as $OD_{420}/10^6$ cells. Results are the means of triplicate determinations from three independent isolates ± S.E.M. (A). Rgs1 with GFP fused to its C-terminus was expressed from expression vector pREP3x in strain JY630 (ΔRgs1). Images were generated using a DeltaVision wide-field deconvolution microscope and are representative of three independent transformations (B). N = Nucleus, C = Cytoplasm, M = Microtubules. Scale bar = 10 $\mu$m.

Fusing GFP to the C-terminus of Rgs1 has no observable detrimental effect on its function in signalling regulation. The C-terminal fusion protein results in a similar signalling profile to that observed for Rgs1. In comparison to ΔRgs1 strains, expression of Rgs1-GFP reduces basal $\beta$-galactosidase activity to 0.61 ± 0.462 and increases maximal activity to 17.528 ± 0.422. Similarly, expression of Rgs1 reduces basal $\beta$-galactosidase activity to 1.878 ± 0.319 and increases maximal to 16.611± 0.524. Sensitivity to P-factor was also similar for Rgs1-GFP compared to Rgs1 with $pEC_{50}$ values of 6.889 ± 0.087 and 6.96 ± 0.093 respectively (Figure 4.5, A). Imaging failed to show clear PM localisation of Rgs1, indeed it was detected in the nucleus and the cytosol of the cell. In cells undergoing cell division at the point in their life cycle whereby nuclear separation is/has occurred but prior to cytokinesis, Rgs1 appears to be associated with the microtubules (Figure 4.5: B).

The substrate for Rgs1 is the G$\alpha$ protein Gpa1, and Gpa1 has been demonstrated in Chapter 3 to be localised at the PM. Despite this, Rgs1 is observed predominantly in the nucleus of the cell (Figure 4.5, B). A possible explanation for this could be that Rgs1 is not required to localise at the PM until the signalling pathway is triggered through ligand stimulation. This is a reasonable assumption, given that the substrate for Rgs1 is the activated, GTP-bound form of Gpa1, hence Rgs1 may only be required at the PM when Gpa1 is being activated through P-factor stimulation of the pathway.

Physiologically, Rgs1 is not expressed in high levels until the mating-response is stimulated by P-factor (Mata and Bähler, 2006; Xue-Franzén et al., 2006), but we have evidence for an interaction of Rgs1 with Mam2, that is required for Rgs1 functionality (Figure 4.3 and Figure 4.4). Considering this, the lack of observable Rgs1 at the PM may be due to insufficient Mam2 concentration to tether Rgs1 at this localisation. Both Rgs1 and Mam2 are known to be up-regulated in response to P-factor. Upon P-factor stimulation, mean fold-increase in expression of Rgs1 and Mam2 is 11.2 and 28.4 respectively (Xue-Franzén et al., 2006), therefore it is possible that Rgs1 can only be detected at the PM when the concentration of Mam2 has increased sufficiently, due to stimulation of the signalling pathway. Increased Mam2 could then promote trafficking of Rgs1 to the membrane through interactions with its C-terminal tail. To investigate this possibility, Mam2 was overexpressed in strains containing Rgs1-GFP.

#### 4.2.2.1 Overexpressing Mam2 and Mam2$\Delta$tail in Strains Expressing Rgs1-GFP

Having a greater concentration of full length Mam2 could encourage more interactions of Mam2 with Rgs1 via the Mam2 tail, therefore tethering Rgs1 at the PM in large enough quantities to be detected. Cells expressing Rgs1-GFP from the *nmt1* promotor on the pREP4x vector (uracil selection) (Forsburg, 1993), were transformed with plasmids expressing either Mam2 or Mam2$\Delta$tail from pREP3x (leucine selection) and selected on media lacking both leucine and uracil to ensure the selection of both inducible plasmids. The transformed strains were grown in minimal media before imaging with a DeltaVision wide-field deconvolution microscope (Figure 4.6).

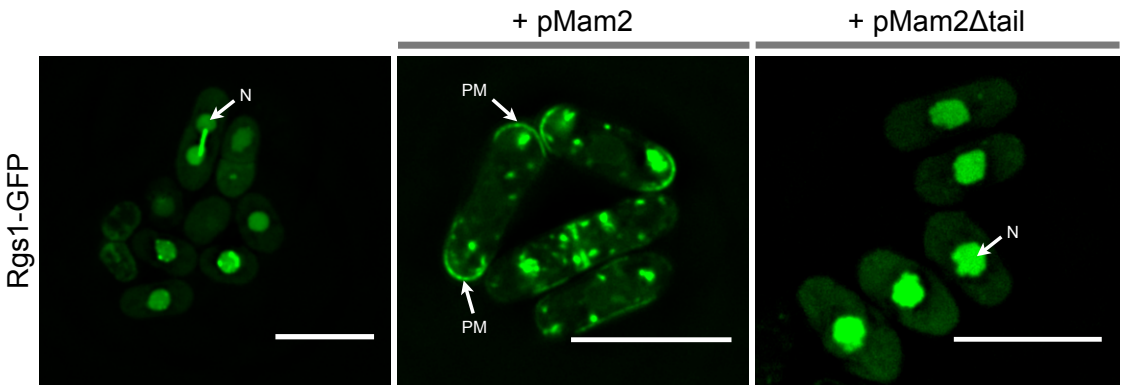


FIGURE 4.6: **Rgs1-GFP localisation when over-expressing Mam2 or Mam2Δtail.** Rgs1 with GFP fused to its C-terminus was expressed from expression vector pREP4x in strain JY1291(ΔMam2, ΔRgs1). This transformed strain was then further transformed to over-express either Mam2 (+ pMam2) or Mam2 truncated for its C-terminal tail (+ pMam2Δtail) from expression vector pREP3x. Images were generated using a DeltaVision wide-field deconvolution microscope and are representative of three independent transformations. N = Nucleus, PM = Plasma Membrane and scale bar = 10 $\mu$m.

Imaging data revealed that in strains co-expressing Rgs1-GFP from pREP4x and Mam2 from pREP3x, Rgs1 was detected at the PM of the cell, mostly at the tips. Some internal detection is seen, but little is detected within the cell nucleus (+ pMam2 in Figure 4.6). In strains co-expressing Rgs1-GFP from pREP4x and Mam2Δtail from pREP3x, Rgs1 is only detected within the cytosol and primarily the nucleus of the cell (+ pMam2Δtail in Figure 4.6). These images suggest that overexpressing Mam2 can promote PM localisation of Rgs1, and furthermore that the PM recruitment of Rgs1 requires the receptor tail. This supports the hypothesis that increased expression of Mam2 results in the accumulation of Rgs1 at the PM.

### 4.2.3 Mam2 and Mam2Δtail Localisation and Function

Having demonstrated that an increased expression of Mam2 will promote Rgs1 translocation to the PM, we next sought to confirm that Mam2 and Mam2Δtail display PM localisation. C-terminal fusions of Mam2 to mCherry and Mam2Δtail to mCherry were expressed from vector pREP3x in a reporter strain lacking the endogenous Mam2; JY1169(ΔMam2). The transformed strains were grown in minimal media before imaging using a DeltaVision wide-field deconvolution microscope (Figure 4.7, A). These transformed strains were also assayed for signalling activity to confirm functionality of the labelled proteins. Reporter strain JY1169(ΔMam2) and JY1169 expressing Mam2, Mam2-mCherry, Mam2Δtail or Mam2Δtail-mCherry from expression vector pREP3x were grown in minimal media and incubated with P-factor at concentrations 0M to $10^{-4}$M for 16 h before assaying for induction of *sxa2>lacZ* (Figure 4.7, B).

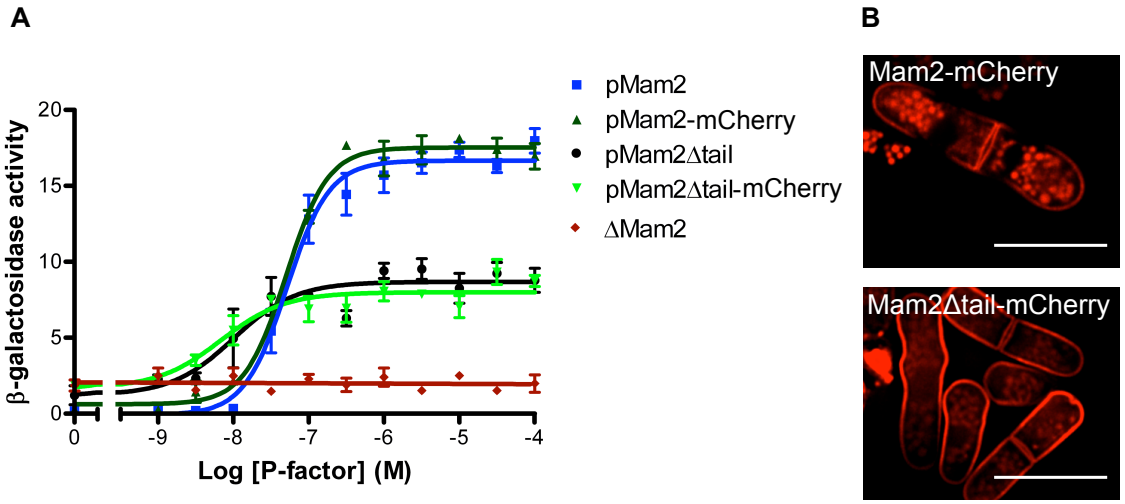


| | Basal | Maximal | $pEC_{50}$ |
|---|---|---|---|
| pMam2 | 0.090 +/- 0.516 | 16.660 +/- 0.391 | 7.291 +/- 0.058 |
| pMam2-mCherry | 0.622 +/- 0.355 | 17.520 +/- 0.269 | 7.302 +/- 0.039 |
| pMam2Δtail | 1.679 +/- 0.713 | 7.995 +/- 0.283 | 8.164 +/- 0.181 |
| pMam2Δtail-mCherry | 1.954 +/- 0.379 | 7.748 +/- 0.179 | 8.313 +/- 0.078 |
| ΔMam2 | 2.112 +/- 0.361 | 2.112 +/- 0.361 | N/A |

FIGURE 4.7: **Mam2-mCherry and Mam2Δtail-mCherry localisation and functionality.** Reporter strains JY1169 (ΔMam2), and JY1169 containing the expressions vector pREP3x expressing Mam2 (pMam2), Mam2-mCherry (pMam2-mCherry), Mam2Δtail (pMam2Δtail) or Mam2Δtail-mCherry (pMam2Δtail-mCherry) were cultured in minimal media to a density of ~5x$10^6$ cells/ml, incubated with 0M to $10^{-4}$M P-factor before assaying for $\beta$-galactosidase activity. $\beta$-galactosidase activity was measured as $OD_{420}/10^6$ cells. Results are the means ± S.E.M. of triplicate determinations from three independent isolates (A). Constructs with full length Mam2 and Mam2 truncated for its C-terminal tail (Mam2Δtail) fused to mCherry at their C-terminus were expressed from expression vector pREP3x in reporter strain JY1169 (ΔMam2). Images were generated using a DeltaVision wide-field deconvolution microscope and are representative of three independent transformations (B). Scale bar = 10 $\mu$m.

The C-terminal fusion of mCherry does not interfere with signalling functionality of either Mam2 or Mam2Δtail as indicated by the similarities in the dose-response profiles of the labelled and unlabelled versions of the proteins (Figure 4.7, A). Both Mam2 and Mam2-mCherry dose-response profiles show similar ligand-independent signalling (0.09 ± 0.516 vs 0.622 ± 0.355), maximal signalling activity (16.66 ± 0.391 vs 17.52 ± 0.269) and sensitivity to ligand ($pEC_{50}$; 7.291 ± 0.058 vs 7.302 ± 0.039). Fusing mCherry to the C-terminal tail of Mam2Δtail did not result in a compromise of its activity (compare basal signalling, maximal signalling and $pEC_{50}$ of Mam2Δtail-mCherry to Mam2Δtail). Imaging data shows that Mam2 is detected at the PM of the cell, predominantly at the cell tips and also at the septum of a dividing cell. There is also some detection of punctate structures within the cytosol. This is in agreement with previous work identifying the localisation of Mam2 (Matsuyama et al., 2006). Mam2Δtail is more prominently localised at the PM and has a more uniform distribution at the cell periphery compared to Mam2. Mam2Δtail is detected at the septum but there is a reduction in detection within the cytosol (Figure 4.7,

B). These data show that both Mam2 and Mam2Δtail C-terminally fused to mCherry remain functional and are localised at the PM. Given the previous data demonstrating overexpression of Mam2, but not Mam2Δtail, to promote PM localisation of Rgs1-GFP (Figure 4.6), this suggests that if the C-terminal tail is present for interaction with Rgs1, then Rgs1 and Mam2 can colocalise at the PM.

### 4.2.4 Co-localisation Investigations of Rgs1 with Mam2 and Mam2Δtail

Co-localisation studies of Rgs1 and Mam2/Mam2Δtail have not been attempted previously. Separate imaging experiments of Rgs1 (Figure 4.5, B) and Mam2/Mam2Δtail (Figure 4.7, B) would suggest that these proteins do not show a high degree of co-localisation in 'resting' cell conditions (i.e. not stimulated to increase expression levels of Mam2), but as there is sufficient data indicating an interaction (Figure 4.3), and overexpression of Mam2 has been shown to promote PM localisation of Rgs1-GFP (Figure 4.6), it was decided to persist with investigations into co-localisation by imaging both Rgs1 and Mam2/Mam2Δtail in the same cell. Evidence of co-localisation under physiological conditions would provide further support for a physiological interaction between Rgs1 and Mam2.

#### 4.2.4.1 Co-expressing Rgs1-GFP and Mam2/Mam2Δtail-mCherry

The red fluorescent protein mCherry excites at wavelength 587 nm and emits at 610 nm, whilst GFP excites at 488 nm and emits at 507 nm (Shaner et al., 2005), therefore these two fluorescent markers can be distinguished when in the same cell. To confirm functionality in terms of signal transduction the *sxa2>lacZ* reporter strain JY1291(ΔMam2, ΔRgs1) was co-transformed with Rgs1-GFP and Mam2-mCherry or with Rgs1-GFP and Mam2Δtail-mCherry, assayed for signalling activity and compared to assays of the same strain co-transformed with the un-labelled form of the proteins. These strains were grown in minimal media and incubated with P-factor at concentrations 0M to $10^{-4}$M for 16 h before assaying for the induction of *sxa2>lacZ* (Figure 4.8, A). The strains co-expressing Rgs1-GFP and Mam2-mCherry or Rgs1-GFP and Mam2Δtail-mCherry were investigated for co-localisation by culturing in minimal media before imaging with a DeltaVision wide-field deconvolution microscope (Figure 4.8, B).

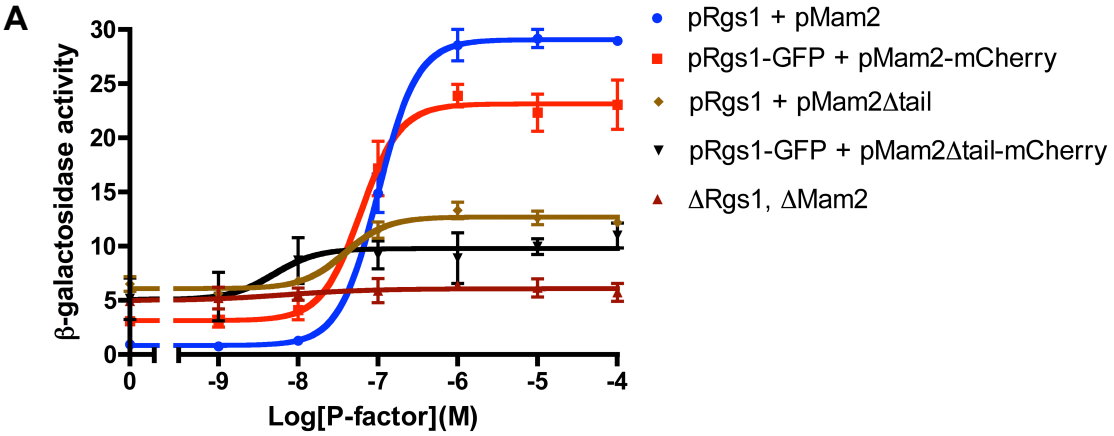


| | Basal | Maximal | $pEC_{50}$ |
|---|---|---|---|
| pRgs1 + pMam2 | 0.839 +/- 0.511 | 29.060 +/- 0.512 | 6.998 +/- 0.030 |
| pRgs1-GFP + pMam2-mCherry | 3.135 +/- 0.965 | 23.130 +/- 0.797 | 7.216 +/- 0.137 |
| pRgs1 + pMam2Δtail | 6.091 +/- 0.434 | 12.700 +/- 0.352 | 7.412 +/- 0.181 |
| pRgs1-GFP + pMam2Δtail-mCherry | 5.079 +/- 1.661 | 9.783 +/- 0.803 | 8.304 +/- 0.740 |
| ΔRgs1, ΔMam2 | 4.944 +/- 0.992 | 6.078 +/- 0.425 | 8.180 +/- 1.766 |

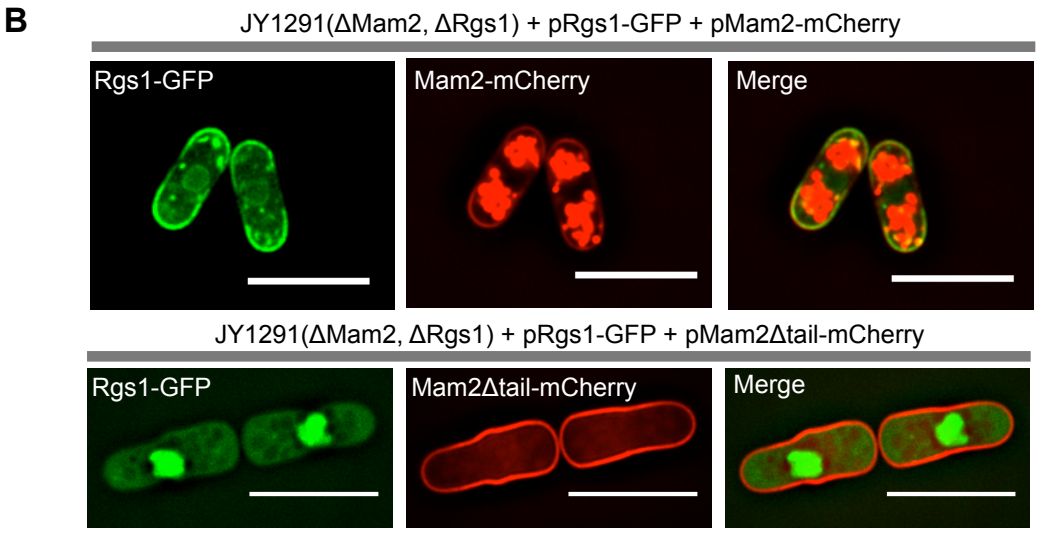


FIGURE 4.8: **Co-expression of Rgs1-GFP and Mam2/Mam2Δtail-mCherry.** Reporter strain JY1291(ΔMam2, ΔRgs1) was co-transformed with Rgs1-GFP expressed from vector pREP4x and either Mam2-mCherry expressed from pREP3x (JY1291 + pRgs1-GFP + pMam2-mCherry) or Mam2Δtail-mCherry expressed from pREP3x (JY1291(ΔMam2, ΔRgs1) + pRgs1-GFP + pMam2Δtail-mCherry). JY1291 was also transformed with vectors expressing the same combinations of the un-labelled proteins. JY1291 and all transformed strains were cultured in minimal media to a density of ~5x$10^6$ cells/ml, incubated with 0M to $10^{-4}$M P-factor before assaying for $\beta$-galactosidase activity. $\beta$-galactosidase activity was measured as $OD_{420}/10^6$ cells. Results are the means ± S.E.M. of triplicate determinations from three independent isolates (A). Co-transformed strains were imaged in the GFP channel and mCherry channel using a DeltaVision wide-field deconvolution microscope and are representative of three independent transformations (B). Yellow colour on the merged images indicate regions of co-localisation. Scale bar = 10 $\mu$m.

Data from reporter assays indicate that the strains co-transformed with the fluorescently labelled proteins signal in a similar manner to the equivalent co-transformed strains expressing the unlabelled proteins, although there are some slight differences in dose-response profiles (Figure 4.8, A). Strains co-expressing Mam2-mCherry + Rgs1-GFP show a P-factor induced signalling response but with raised basal activity of 3.135 ± 0.965 compared to 0.839 ± 0.511 for Mam2 + Rgs1. The maximal signalling activity is at a reduced level of 23.13 ± 0.965 for Mam2-mCherry + Rgs1-GFP compared to 29.06 ± 0.512 for the unlabelled proteins (compare pRgs1-GFP + pMam2-mCherry profile to pRgs1 + pMam2 profile in Figure 4.8, A). Strains co-expressing Mam2Δtail-mCherry and Rgs1-GFP display the characteristic response for a strain lacking the tail of the receptor, with raised basal activity (5.079 ± 1.661) and a slight P-factor induced signalling response to approximately half the maximal levels achieved in a strain containing full length Mam2 (9.783 ± 0.803) (compare pRgs1-GFP + pMam2Δtail-mCherry and pRgs1 + pMam2Δtail in Figure 4.8, A).

This result indicates that fluorescent labelling of both Mam2 and Rgs1 in the cells, has only minimal effects on the functionality of the proteins and their capability for facilitating signal transduction and signalling regulation.

Imaging indicates that when expressed in the same cell as Mam2-mCherry, Rgs1-GFP is now detectable at the PM of the cell. It is mainly detected at the cell tips, but some is also observed in the cytosol and nucleus. Mam2-mCherry is detected at the PM of the cell, predominantly at the cell tips, but also within internal spherical structures (Figure 4.8, B). The size and apparent number of these internal structures indicate that they are the cell vacuoles (Takegawa et al., 2003; Ladds et al., 2005a). The merged image shows qualitatively a high degree of co-localisation occurring between Rgs1-GFP and Mam2-mCherry on the PM of the cell at the cell tips, as indicated by the yellow colour in the merged image (Figure 4.8, B). Imaging confirms that in the presence of Mam2-mCherry, Rgs1-GFP localises at the PM, displaying high co-localisation with Mam2-mCherry at the tips of the cell, whereas in the presence of Mam2Δtail-mCherry, Rgs1-GFP is detected in the cytosol and nucleus, but shows a lack of PM localisation and minimal co-localisation with Mam2Δtail-mCherry (Figure 4.8, B). These images provide further evidence for the Mam2-Rgs1 interaction and suggest the absolute requirement for the tail of Mam2 to promote PM localisation of Rgs1.

### 4.2.5 Initial Hypothesis: GPCR-RGS Interaction Required for RGS Function

As it is the RGS-catalysed hydrolysis of $G\alpha_{GTP}$ that is required to regulate signalling and hence observe a wild-type dose-response profile (pMam2 in Figure 4.3, B), one assumption drawn from the data in Figure 4.3 could be that the Rgs1 interaction with the Mam2 tail is an absolute requirement for Rgs1 to function as a GAP. Therefore, removing this interaction, through removal of the receptor tail, eliminates this function and results in a

ΔRgs1 comparable signalling response. The Smith *et al.* model was extended to test this initial hypothesis. A simple way to do this was to include a separate RGS species in the model, one which is inactive ($RGS_i$) and one which is active ($RGS_a$). $RGS_a$ is the only active species as it is the only RGS species that is capable of GTP hydrolysis reactions on G$\alpha$. The requirement for an interaction with the GPCR (R) for RGS to function is included through a simple reaction converting inactive $RGS_i$ to active $RGS_a$, via an interaction with R (R + $RGS_i$ -> R + $RGS_a$) (Table 4.1). The rate for this reaction is unknown therefore it was given an arbitrary value and hand-tuned to best fit the experimental data.

| | | | | |
|---|---|---|---|---|
| Smith *et al.* | $L + R \rightarrow LR$ | $k_1$ | 0.0025 | $nM^{-1}h^{-1}$ |
| | $G\alpha\beta\gamma + R \rightarrow RG\alpha\beta\gamma$ | $k_2$ | 0.005 | $nM^{-1}h^{-1}$ |
| | $G\alpha\beta\gamma + LR \rightarrow LRG\alpha\beta\gamma$ | $k_3$ | 0.02 | $nM^{-1}h^{-1}$ |
| | $L + RG\alpha\beta\gamma \rightarrow LRG\alpha\beta\gamma$ | $k_4$ | 0.005 | $nM^{-1}h^{-1}$ |
| | $LRG\alpha\beta\gamma \rightarrow G\alpha_{GTP} + G\beta\gamma + LR$ | $k_5$ | 50 | $h^{-1}$ |
| | $G\alpha\beta\gamma \rightarrow G\alpha_{GTP} + G\beta\gamma$ | $k_6$ | 0.2 | $h^{-1}$ |
| | $G\alpha_{GTP} + RGS_a \rightarrow RGS_aG\alpha_{GTP}$ | $k_7$ | 500 | $nM^{-1}h^{-1}$ |
| | $RGS_aG\alpha_{GTP} \rightarrow G\alpha_{GDP} + RGS_a$ | $k_8$ | 2.5 | $h^{-1}$ |
| | $G\alpha_{GTP} \rightarrow G\alpha_{GDPP}$ | $k_9$ | 0.005 | $h^{-1}$ |
| | $Effector + G\alpha_{GTP} \rightarrow G\alpha_{GTP}Effector$ | $k_{10}$ | 10 | $nM^{-1}h^{-1}$ |
| | $G\alpha_{GTP}Effector \rightarrow Effector + inertG\alpha_{GTP}$ | $k_{11}$ | 1 | $h^{-1}$ |
| | $inertG\alpha_{GTP} + RGS_a \rightarrow RGS_ainertG\alpha_{GTP}$ | $k_{12}$ | 50 | $nM^{-1}h^{-1}$ |
| | $RGS_ainertG\alpha_{GTP} \rightarrow RGS_a + G\alpha_{GDP}$ | $k_{13}$ | 0.3 | $h^{-1}$ |
| | $inertG\alpha_{GTP} \rightarrow G\alpha_{GDPP}$ | $k_{14}$ | 0.005 | $h^{-1}$ |
| | $G\alpha_{GDPP} \rightarrow G\alpha_{GDP} + P$ | $k_{15}$ | 1000 | $h^{-1}$ |
| | $G\alpha_{GDP} + G\beta\gamma \rightarrow G\alpha\beta\gamma$ | $k_{16}$ | 1000 | $nM^{-1}h^{-1}$ |
| | $P \rightarrow \emptyset$ | $k_{17}$ | 10 | $h^{-1}$ |
| Modification | $R + RGS_i \rightarrow R + RGS_a$ | $k_{18}$ | 0.1 | $nM^{-1}h^{-1}$ |

TABLE 4.1: **Initial hypothesis model: GPCR-RGS interaction required for RGS function.** A single additional reaction (reaction 18) is added to the original Smith *et al.* model of the G protein cycle, whereby the GPCR (R) can interact with the inactive RGS species ($RGS_i$), therefore converting it into the active species ($RGS_a$). Each of the 18 reactions are defined alongside their associated rate constant (k).

The system of ODEs generated from the reaction scheme in Table 4.1 is presented in Table 4.2. The model is initiated with species concentrations L = 0-100,000 nM, R = 205 nM, $G\alpha_{GDP}$ = 205 nM, $G\beta\gamma$ = 205 nM, $RGS_i$ = 60 nM and Effector = 205 nM. Values for R, $G\alpha_{GDP}$, $G\beta\gamma$ and $RGS_i$ are assumed the same as in published data for *S. cerevisiae* (Yildirim et al., 2004). All other species are initiated at 0 nM.

| | |
|---|---|
| Effector | $Effector'(t) = - k_{10}Effector(t)\ G\alpha_{GTP}(t) + k_{11}G\alpha_{GTP}Effector(t)$ |
| $G\alpha\beta\gamma$ | $G\alpha\beta\gamma'(t) = - k_6G\alpha\beta\gamma(t) - k_2G\alpha\beta\gamma(t)\ R(t) - k_3G\alpha\beta\gamma(t)\ LR(t) + k_{16}G\beta\gamma(t)\ G\alpha_{GDP}(t)$ |
| $G\beta\gamma$ | $G\beta\gamma'(t) = k_6G\alpha\beta\gamma(t) + k_5LRG\alpha\beta\gamma(t) - k_{16}G\beta\gamma(t)\ G\alpha_{GDP}(t)$ |
| L | $L'(t) = -\frac{1}{2}k_1L(t)\ R(t)\ (Tanh(t_0\ b) - Tanh(b(t_0 - t))) - \frac{1}{2}k_4L(t)\ RG\alpha\beta\gamma(t)\ (Tanh(t_0\ b) - Tanh(b(t_0 - t)))$ |
| P | $P'(t) = - k_{17}P(t) + k_{15}G\alpha_{GDPP}(t)$ |
| R | $R'(t) = - k_2G\alpha\beta\gamma(t)\ R(t) - \frac{1}{2}k_1L(t)\ R(t)\ (Tanh(t_0\ b) - Tanh(b(t_0 - t)))$ |
| $RG\alpha\beta\gamma$ | $RG\alpha\beta\gamma'(t) = k_2G\alpha\beta\gamma(t)\ R(t) - \frac{1}{2}k_4L(t)\ RG\alpha\beta\gamma(t)\ (Tanh(t_0\ b) - Tanh(b(t_0 - t)))$ |
| $LRG\alpha\beta\gamma$ | $LRG\alpha\beta\gamma'(t) = - k_5LRG\alpha\beta\gamma(t) + k_3G\alpha\beta\gamma(t)\ LR(t) + \frac{1}{2}k_4L(t)\ RG\alpha\beta\gamma(t)\ (Tanh(t_0\ b) - Tanh(b(t_0 - t)))$ |
| LR | $LR'(t) = k_5LRG\alpha\beta\gamma(t) - k_3G\alpha\beta\gamma(t)\ LR(t) + \frac{1}{2}k_1L(t)\ R(t)\ (Tanh(t_0\ b) - Tanh(b(t_0 - t)))$ |
| $G\alpha_{GDP}$ | $G\alpha_{GDP}'(t) = - k_{16}G\beta\gamma(t)\ G\alpha_{GDP}(t) + k_{15}G\alpha_{GDPP}(t)$ |
| $G\alpha_{GDPP}$ | $G\alpha_{GDPP}'(t) = - k_{15}G\alpha_{GDPP}(t) + k_9G\alpha_{GTP}(t) + k_{14}inertG\alpha_{GTP}(t) + k_8RGS_aG\alpha_{GTP}(t) + k_{13}RGS_ainertG\alpha_{GTP}(t)$ |
| $G\alpha_{GTP}$ | $G\alpha_{GTP}'(t) = k_6G\alpha\beta\gamma(t) + k_5LRG\alpha\beta\gamma(t) - k_9G\alpha_{GTP}(t) - k_{10}Effector(t)\ G\alpha_{GTP}(t) - k_7G\alpha_{GTP}(t)\ RGS_a(t)$ |
| $G\alpha_{GTP}$Effector | $G\alpha_{GTP}Effector'(t) = k_{10}Effector(t)\ G\alpha_{GTP}(t) - k_{11}G\alpha_{GTP}Effector(t)$ |
| $inertG\alpha_{GTP}$ | $inertG\alpha_{GTP}'(t) = k_{11}G\alpha_{GTP}Effector(t) - k_{14}inertG\alpha_{GTP}(t) - k_{12}inertG\alpha_{GTP}(t)\ RGS_a(t)$ |
| $RGS_a$ | $RGS_a'(t) = - k_7G\alpha_{GTP}(t)\ RGS_a(t) - k_{12}inertG\alpha_{GTP}(t)\ RGS_a(t) + k_8RGS_aG\alpha_{GTP}(t) + k_{13}RGS_ainertG\alpha_{GTP}(t) + k_{18}R(t)\ RGS_i(t)$ |
| $RGS_aG\alpha_{GTP}$ | $RGS_aG\alpha_{GTP}'(t) = k_8G\alpha_{GTP}(t)\ RGS_a(t) - k_8RGS_aG\alpha_{GTP}(t)$ |
| $RGS_ainertG\alpha_{GTP}$ | $RGS_ainertG\alpha_{GTP}'(t) = k_{12}inertG\alpha_{GTP}(t)\ RGS_a(t) - k_{13}RGS_ainertG\alpha_{GTP}(t)$ |
| $RGS_i$ | $RGS_i'(t) = - k_{18}R(t)\ RGS_i(t)$ |
| z(1) | $z(1)'(t) = \frac{3}{2}Effector(t)\ G\alpha_{GTP} - \frac{3}{2}z(1)(t)$ |
| z(2) | $z(2)'(t) = \frac{3}{2}z(1)(t) - \frac{3}{2}z(2)(t)$ |
| z(3) | $z(3)'(t) = \frac{3}{2}z(2)(t) - \frac{3}{2}z(3)(t)$ |

TABLE 4.2: **System of ODEs for simulating the initial hypothesis model.** The table shows each species defined within the initial hypothesis model and its associated differential equation describing the rate of change in that species concentration with time. The ODEs are generated from the reaction scheme in Table 4.1. For reaction rate constants (k) refer to Table 4.1. b = 100 (constant for ligand addition), $t_0$ = 14 (equilibration time before ligand application).

Through the simple modification to the Smith *et al.* model, simulations of signalling response in a system lacking GPCR-RGS interaction as in strains expressing Mam2Δtail are possible. This can be achieved by blocking the interaction between R and RGS species by defining reaction rate constant $k_{18} = 0\ nM^{-1}h^{-1}$.

#### 4.2.5.1 Initial Hypothesis Testing: Signalling Without a GPCR-RGS Interaction

Qualitatively, the initial hypothesis model (Table 4.1) can now reproduce the experimental data regarding signalling response when the tail of the receptor is removed (compare Figure 4.9 to Figure 4.3, B). Simulated output when the interaction is blocked by defining $k_{18} = 0\ nM^{-1}h^{-1}$ ($GPCR^{(-RGS\ interaction)}$) results in the active $RGS_a$ species not being formed, which causes the simulated output to be identical to that of the system with RGS removed (No RGS), therefore basal signalling is increased and maximal signalling is approximately half that of the unchanged system(GPCR) (Figure 4.9).

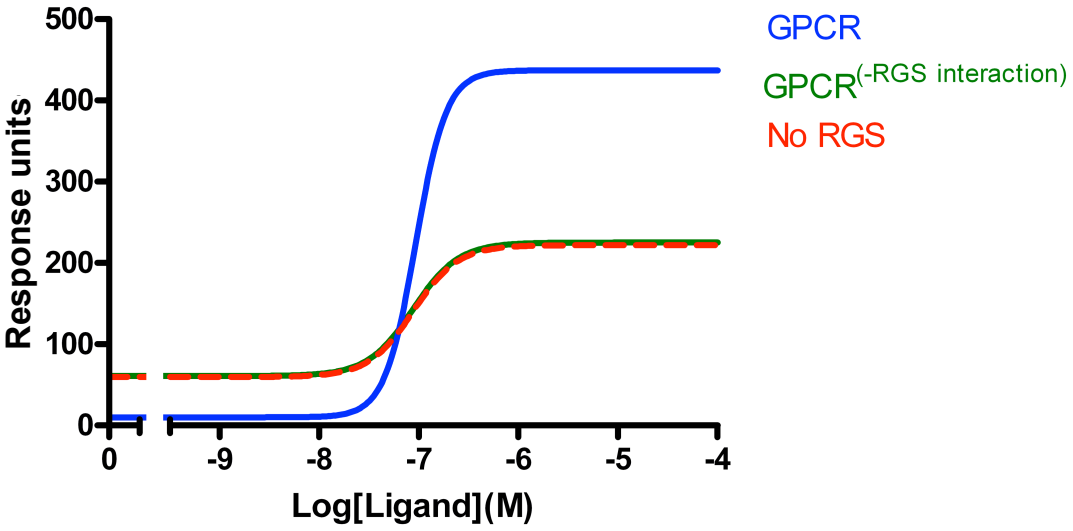


FIGURE 4.9: **Simulation of initial hypothesis model: System response lacking GPCR-RGS interaction** Simulations of the GPCR-RGS interaction model (Table 4.1). Simulations are of the system whereby all parameters are unmodified (GPCR), the GPCR-RGS interaction is blocked by setting reaction rate $k_{18} = 0$ $nM^{-1}h^{-1}$ ($GPCR^{(-RGS\ interaction)}$) and when RGS species are removed by defining initial concentrations $RGS_i = 0$ nM and $RGS_a = 0$ nM (No RGS). The concentration of ligand in the simulation was varied over the range 0-100 $\mu$M following 16 h simulated induction. Output from the model shows the accumulation of activated $G\alpha_{GTP}$Effector complexes over the duration of the simulated assay.

#### 4.2.5.2 Initial Hypothesis Testing: Signalling in the Absence of a Receptor

This initial model hypothesis was investigated further through $\beta$-galactosidase assay of basal signalling levels in strains expressing varying Rgs1 concentration, but lacking an endogenous receptor (Figure 4.10, A). This would indicate whether or not Rgs1 is capable of a regulatory effect on signalling in the absence of its interaction with the receptor. The reporter strains lacking endogenous Mam2 (JY1169) and the reporter strain lacking both endogenous Mam2 and Rgs1 (JY1291) were grown in minimal media. JY1291 was assayed for induction of *sxa2>lacZ* to quantify signalling in the absence of an Rgs1 ($\Delta$Rgs1 in Figure 4.10). Induction of *sxa2>lacZ* was also quantified having added Rgs1 back into these strains, expressed from the *nmt1* promotors of pREP3x and pREP4x. 1 x Rgs1 = JY1291 + pREP3x-Rgs1, 2 x Rgs1 = JY1169 ($Rgs1^+$) + pREP3x-Rgs1 and 3 x Rgs1 = JY1169 ($Rgs1^+$) + pREP3x-Rgs1 + pREP4x-Rgs1. This enables insight into whether the interaction with Mam2 is an absolute requirement for Rgs1 function. As there is no receptor present, there is no ligand induced activation through the receptor and therefore any signalling activity is due to basal levels through the spontaneous activation of Gpa1 (see Chapter 3).

For comparison to the biological data, the initial hypothesis model was tested under the equivalent simulated conditions by varying the RGS species concentration in the model system lacking any receptor. Simulations were completed with receptor (R) concentration

set to 0 nM and with various inactive RGS ($RGS_i$) concentrations initiated at 0 nM (No RGS), 60 nM (1 x RGS), 120 nM (2 x RGS) and 180 nM (3 x RGS) (Figure 4.10, B). These simulations are analogous to those presented in Smith et al., 2009.

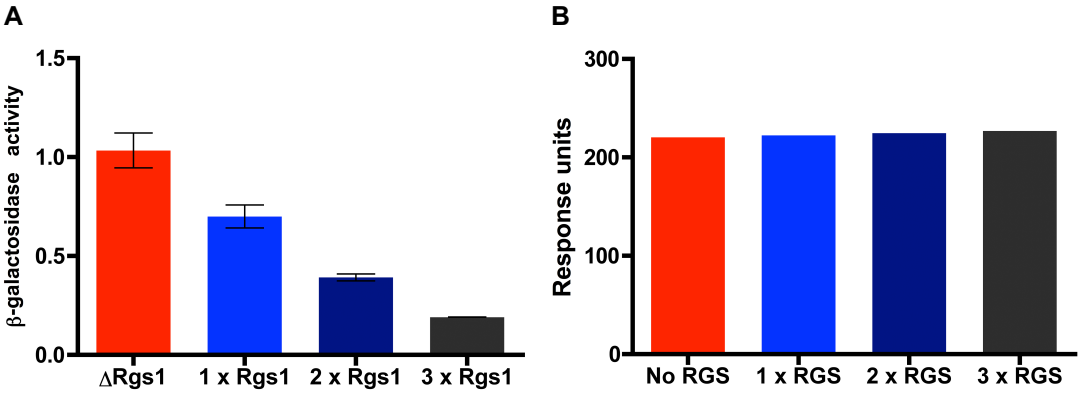


FIGURE 4.10: **Receptor-independent Rgs1 activity.** A: Transcription of $\beta$-galactosidase expressed from the *sxa2>lacZ* reporter construct was measured in strains deleted for the chromosomal copy of Mam2 when expressing varying levels of Rgs1. Strains included when no Rgs1 was present ($\Delta$Rgs1), when Rgs1 was expressed from expression vector pREP3x in strain JY1291($\Delta$Rgs1,$\Delta$Mam2) (1 x Rgs1), when Rgs1 was expressed from pREP3x in strain JY1169($\Delta$Mam2) (2 x Rgs1) and when Rgs1 was expressed from both expression vectors pREP3x and pREP4x in strain JY1169($\Delta$Mam2) (3 x Rgs1) Cells were cultured in minimal media to a density of $\sim 5x10^6$ cells/ml, before assaying for $\beta$-galactosidase activity. $\beta$-galactosidase activity was measured as $OD_{420}/10^6$ cells. Results are the means $\pm$ S.E.M. of triplicate determinations from three independent isolates. B: Simulations of the GPCR-RGS interaction model (Table 4.1). Simulations are of basal signalling response in the system lacking the GPCR (concentration of R = 0 nM) and whereby initial concentration of RGS species are defined as $RGS_i$ = 0 nM (No RGS) , $RGS_i$ = 60 nM (1 x RGS) , $RGS_i$ = 120 nM (2 x RGS) , $RGS_i$ = 180 nM (3 x RGS). Output from the model shows the accumulation of activated $G\alpha_{GTP}$Effector complexes over the duration of the simulated assay.

The experimental data (Figure 4.10, A) suggests the initial hypothesis to be incorrect. Data indicates that basal signalling activity decreases with increasing Rgs1 concentration from 1.033 $\pm$ 0.088 for $\Delta$Rgs1 to 0.191 $\pm$ 0.0006 for 3 x Rgs1, therefore Rgs1 is able to down-regulate signalling, without the requirement for a receptor interaction (Figure 4.10, A). The simulated assay showed that basal simulated response remained unchanged with increasing RGS concentration, therefore the model disagrees with the experimental data (compare Figure 4.10, A to B). The initial hypothesis model is therefore not an accurate representation of the true physiological mechanisms, therefore the initial hypothesis that an interaction is absolutely required for RGS function should be rejected as Rgs1 is able to negatively regulate signalling independently of the receptor.

### 4.2.6 New Hypothesis: Plasma Membrane Trafficking of RGS

The substrate for Rgs1 is the G$\alpha$ subunit Gpa1 when in a GTP-bound form. G$\alpha$ proteins couple to GPCRs and are therefore primarily localised at the PM. For Gpa1 this was also

shown through imaging experiments of fluorescently labelled Gpa1 (Chapter 3, Figure 3.2). Considering this, the data from transcriptional assays (Figure 4.3, B, Figure 4.10) and imaging, suggesting a regulatory effect of the Mam2 tail on Rgs1 subcellular localisation (Figure 4.6 and Figure 4.8, B), an alternative hypothesis involving spatial regulation of Rgs1 could be plausible. This new hypothesis is that the interaction of RGS with the GPCR is required for the correct spatial regulation of RGS within the cell. Rather than the interaction being explicitly required to activate RGS, an alternative is that the interaction facilitates the accumulation of RGS in the appropriate sub-cellular location. It is possible that the interaction is required to target and tether RGS at the PM, thus generating a pool of RGS proteins maintained in close proximity to their substrate G$\alpha_{GTP}$.

#### 4.2.6.1 Achieving Plasma Membrane localisation of Rgs1

To achieve sufficient proximity between Rgs1 and Gpa1, Rgs1 must be able to traffic to the PM. Despite a requirement for PM localisation, many RGS proteins are predicted to be, or have been detected, in the nucleus and the cytoplasm. Having said this, some cellular mechanisms contributing to membrane targeting of RGS proteins have also been identified. RGS4 has been shown to be recruited by its activated G$\alpha$ subunit target protein (Druey et al., 1998). Other mechanisms include covalent lipid modifications such as palmitoylation that assist membrane attachment (De Vries et al., 1996), domains essential for electrostatic interactions with membranes (Srinivasa et al., 1998) and scaffold proteins that assemble RGS proteins with their receptor and G protein have also been proposed (Xu et al., 1999). Some RGS proteins can interact directly with GPCRs to dictate specific RGS-G$\alpha$ interactions. This could be directed via DEP domains in the RGS protein that have been shown to contribute to PM localisation in a number of unrelated signalling proteins (Ponting and Bork, 1996). Rgs1 contains two N-terminal DEP domains that could possibly facilitate attachment to the tail of the receptor, similar to what has been described for the *S. cerevisiae* RGS protein SST2 (Ballon et al., 2006). Rgs1 is not known to have any specific sites for lipid modifications to aid membrane targeting other than its DEP domains, nor is it known to interact with any PM localised proteins other than Mam2. Therefore, simplistically it could achieve PM localisation through the three following mechanisms: direct binding to $Gpa1_{GTP}$, binding to the C-terminal tail of Mam2 and through random diffusion (Figure 4.11). The contribution to sustaining Rgs1 at the PM is likely to be different for these different mechanisms. Intuitively, the interactions of Rgs1 with both the receptor tail and the G protein are likely to make a greater contribution than PM localisation due to random diffusion, although DEP domains can also contribute to interactions directly with the membrane, through putative membrane binding regions (Wong et al., 2000).

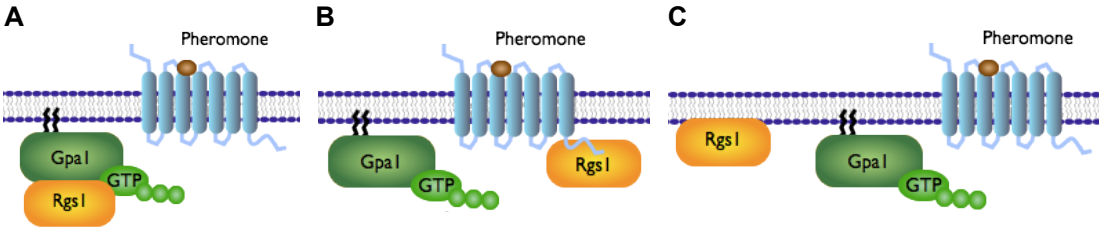


FIGURE 4.11: **Schematic of Rgs1 trafficking to the plasma membrane.** Rgs1 could achieve plasma membrane localisation in three ways; through binding to $Gpa1_{GTP}$, which is already docked at the plasma membrane through lipid attachments (A), through binding to the C-terminal tail of the receptor (B) and through random diffusion/brownian motion (C).

#### 4.2.6.2 Plasma Membrane Trafficking of RGS Model

Trafficking of RGS to-and-from the PM can be modelled by having two separate RGS species representing pools of RGS in separate cellular compartments. These include cytoplasmic (or non-PM) localised RGS ($RGS_c$) and PM localised RGS ($RGS_m$). Only the $RGS_m$ species is given the capacity to function as a GAP on $G\alpha_{GTP}$, as it is regarded as being in sufficient proximity to interact with its substrate. Given the stochastic nature of molecular movement, and interactions within the cell, the hypothesis incorporates RGS becoming PM localised in three ways: by associating with $G\alpha_{GTP}$ at the PM, by random movements such as through diffusion/brownian motion and by binding to the tail of the receptor. A model was built to incorporate the PM trafficking of RGS hypothesis by including these possible reactions involving RGS trafficking to-and-from the PM (Table 4.3).

For clarity, the PM trafficking of RGS model is split into 4 sections (Table 4.3). The first section, labelled 'Smith *et al.*', is the basic model of the G protein cycle. The 'Random movement' section includes reactions describing the random movement of RGS, therefore enabling RGS to switch between a membrane-bound and non-membrane-bound state without the requirement for any interactions (reactions $k_{18}$ and $k_{19}$). Reactions $k_{20}$-$k_{27}$ describe the 'Receptor-RGS interactions', which include the binding and dissociation reactions of RGS to the receptor (R) and complexes of the receptor, ligand (L) and G protein. This models the capability of RGS to become membrane-bound through association with the receptor. The final section, 'Interaction with GTP-bound G$\alpha$' involving reactions $k_{28}$-$k_{29}$, describes the final mechanism for RGS trafficking to the PM through RGS interaction with $G\alpha_{GTP}$ or $inertG\alpha_{GTP}$. All of the reaction rate constants for these additional reactions are unknown and therefore had to be hand-tuned to best fit experimental data.

| | | | | |
|---|---|---|---|---|
| $L + R \rightarrow LR$ | $k_1$ | 0.0025 | $nM^{-1}h^{-1}$ | Smith *et al.* |
| $G\alpha\beta\gamma + R \rightarrow RG\alpha\beta\gamma$ | $k_2$ | 0.005 | $nM^{-1}h^{-1}$ | |
| $G\alpha\beta\gamma + LR \rightarrow LRG\alpha\beta\gamma$ | $k_3$ | 0.02 | $nM^{-1}h^{-1}$ | |
| $L + RG\alpha\beta\gamma \rightarrow LRG\alpha\beta\gamma$ | $k_4$ | 0.005 | $nM^{-1}h^{-1}$ | |
| $LRG\alpha\beta\gamma \rightarrow G\alpha_{GTP} + G\beta\gamma + LR$ | $k_5$ | 50 | $h^{-1}$ | |
| $G\alpha\beta\gamma \rightarrow G\alpha_{GTP} + G\beta\gamma$ | $k_6$ | 0.2 | $h^{-1}$ | |
| $G\alpha_{GTP} + RGS_m \rightarrow RGS_mG\alpha_{GTP}$ | $k_7$ | 500 | $nM^{-1}h^{-1}$ | |
| $RGS_mG\alpha_{GTP} \rightarrow G\alpha_{GDPP} + RGS_c$ | $k_8$ | 2.5 | $h^{-1}$ | |
| $G\alpha_{GTP} \rightarrow G\alpha_{GDPP}$ | $k_9$ | 0.005 | $h^{-1}$ | |
| $Effector + G\alpha_{GTP} \rightarrow G\alpha_{GTP}Effector$ | $k_{10}$ | 10 | $nM^{-1}h^{-1}$ | |
| $G\alpha_{GTP}Effector \rightarrow Effector + inertG\alpha_{GTP}$ | $k_{11}$ | 1 | $h^{-1}$ | |
| $inertG\alpha_{GTP} + RGS_m \rightarrow RGS_minertG\alpha_{GTP}$ | $k_{12}$ | 50 | $nM^{-1}h^{-1}$ | |
| $RGS_minertG\alpha_{GTP} \rightarrow RGS_c + G\alpha_{GDPP}$ | $k_{13}$ | 0.3 | $h^{-1}$ | |
| $inertG\alpha_{GTP} \rightarrow G\alpha_{GDPP}$ | $k_{14}$ | 0.005 | $h^{-1}$ | |
| $G\alpha_{GDPP} \rightarrow G\alpha_{GDP} + P$ | $k_{15}$ | 1000 | $h^{-1}$ | |
| $G\alpha_{GDP} + G\beta\gamma \rightarrow G\alpha\beta\gamma$ | $k_{16}$ | 1000 | $nM^{-1}h^{-1}$ | |
| $P \rightarrow \emptyset$ | $k_{17}$ | 10 | $h^{-1}$ | |
| $RGS_c \rightarrow RGS_m$ | $k_{18}$ | 0.0005 | $h^{-1}$ | Random movement |
| $RGS_m \rightarrow RGS_c$ | $k_{19}$ | 0.005 | $h^{-1}$ | |
| $RG\alpha\beta\gamma + RGS_c \rightarrow RRGS_mG\alpha\beta\gamma$ | $k_{20}$ | 0.1 | $nM^{-1}h^{-1}$ | Receptor-RGS interactions |
| $RRGS_mG\alpha\beta\gamma \rightarrow RG\alpha\beta\gamma + RGS_m$ | $k_{21}$ | 0.1 | $h^{-1}$ | |
| $LR + RGS_c \rightarrow LRRGS_m$ | $k_{22}$ | 0.1 | $nM^{-1}h^{-1}$ | |
| $R + RGS_c \rightarrow RRGS_m$ | $k_{23}$ | 0.1 | $nM^{-1}h^{-1}$ | |
| $LRRGS_m \rightarrow LR + RGS_m$ | $k_{24}$ | 100 | $h^{-1}$ | |
| $RRGS_m \rightarrow R + RGS_m$ | $k_{25}$ | 100 | $h^{-1}$ | |
| $G\alpha_{GTP} + RGS_c \rightarrow RGS_mG\alpha_{GTP}$ | $k_{26}$ | 60 | $nM^{-1}h^{-1}$ | Interaction with GTP-bound Gα |
| $inertG\alpha_{GTP} + RGS_c \rightarrow RGS_minertG\alpha_{GTP}$ | $k_{27}$ | 0.0001 | $nM^{-1}h^{-1}$ | |

TABLE 4.3: **New hypothesis model: Plasma membrane trafficking of RGS.** Additional reactions are now included for GPCR complexes interacting with RGSc to promote its plasma membrane localisation to convert to RGSm (reactions: $k_{20}$, $k_{22}$ and $k_{23}$). RGSc can also become plasma membrane localised through random diffusion (reaction $k_{18}$) or through interaction with GTP-bound G$\alpha$ (reactions $k_{26}$ and $k_{27}$).

A system of ODEs that describes the new PM trafficking of RGS hypothesis model (Table 4.3) is shown in Table 4.4. It is suggested that RGS can only function as a GAP for $G\alpha_{GTP}$ and $inertG\alpha_{GTP}$ when it is localised in close proximity to G$\alpha$ at the PM ($RGS_m$ species). The model is initiated with species concentrations L = 0-100,000 nM, R = 205 nM, $G\alpha_{GDP}$ = 205 nM, G$\beta\gamma$ = 205 nM, $RGS_c$ = 60 nM and Effector = 205 nM. Values for R, $G\alpha_{GDP}$, G$\beta\gamma$ and $RGS_c$ are assumed the same as in published data for *S. cerevisiae* (Yildirim et al., 2004). All other species are initiated at 0 nM.

| | |
|---|---|
| Effector | Effector'(t) = - $k_{10}$Effector(t) $G\alpha_{GTP}$(t) + $k_{11}G\alpha_{GTP}$Effector(t) |
| $G\alpha\beta\gamma$ | $G\alpha\beta\gamma$'(t) = - $k_6G\alpha\beta\gamma$(t) - $k_2G\alpha\beta\gamma$(t) R(t) - $k_3G\alpha\beta\gamma$(t) LR(t) + $k_{16}G\beta\gamma$(t) $G\alpha_{GDP}$(t) |
| $G\beta\gamma$ | $G\beta\gamma$'(t) = $k_6G\alpha\beta\gamma$(t) + $k_5$LR$G\alpha\beta\gamma$(t) - $k_{16}G\beta\gamma$(t) $G\alpha_{GDP}$(t) |
| L | L'(t) = - $\frac{1}{2}$ $k_1$L(t) R(t) (Tanh($t_0$ b) - Tanh(b($t_0$ - t))) - $\frac{1}{2}$ $k_4$L(t) R$G\alpha\beta\gamma$(t) (Tanh($t_0$ b) - Tanh(b($t_0$ - t))) |
| P | P'(t) = - $k_{17}$P(t) + $k_{15}G\alpha_{GDPP}$(t) |
| R | R'(t) = - $k_2G\alpha\beta\gamma$(t) R(t) - $\frac{1}{2}$ $k_1$L(t) R(t) (Tanh($t_0$ b) - Tanh(b($t_0$ - t))) -$k_{23}$R(t) $RGS_c$(t) + $k_{25}$R$RGS_m$(t) |
| R$G\alpha\beta\gamma$ | R$G\alpha\beta\gamma$'(t) = $k_2G\alpha\beta\gamma$(t) R(t) - $\frac{1}{2}$ $k_4$L(t) R$G\alpha\beta\gamma$(t) (Tanh($t_0$ b) - Tanh(b($t_0$ - t))) - $k_{20}$R$G\alpha\beta\gamma$(t) $RGS_c$(t) + $k_{21}$R$RGS_mG\alpha\beta\gamma$(t) |
| LR$G\alpha\beta\gamma$ | LR$G\alpha\beta\gamma$'(t) = - $k_5$LR$G\alpha\beta\gamma$(t) + $k_3G\alpha\beta\gamma$(t) LR(t) + $\frac{1}{2}$ $k_4$L(t) R$G\alpha\beta\gamma$(t) (Tanh($t_0$ b) - Tanh(b($t_0$ - t))) |
| LR | LR'(t) = $k_5$LR$G\alpha\beta\gamma$(t) - $k_3G\alpha\beta\gamma$(t) LR(t) + $\frac{1}{2}$ $k_1$L(t) R(t) (Tanh($t_0$ b) - Tanh(b($t_0$ - t))) - $k_{22}$LR(t) $RGS_c$(t) + $k_{24}$LR$RGS_m$(t) |
| $G\alpha_{GDP}$ | $G\alpha_{GDP}$'(t) = - $k_{16}G\beta\gamma$(t) $G\alpha_{GDP}$(t) + $k_{15}G\alpha_{GDPP}$(t) |
| $G\alpha_{GDPP}$ | $G\alpha_{GDPP}$'(t) = - $k_{15}G\alpha_{GDPP}$(t) + $k_9G\alpha_{GTP}$(t) + $k_{14}$inert$G\alpha_{GTP}$(t) + $k_8$R$GS_mG\alpha_{GTP}$(t) + $k_{13}$R$GS_m$inert$G\alpha_{GTP}$(t) |
| $G\alpha_{GTP}$ | $G\alpha_{GTP}$'(t) = $k_6G\alpha\beta\gamma$(t) + $k_5$LR$G\alpha\beta\gamma$(t) - $k_9G\alpha_{GTP}$(t) - $k_{10}$Effector(t) $G\alpha_{GTP}$(t) - $k_{26}G\alpha_{GTP}$(t) $RGS_c$(t) - $k_7G\alpha_{GTP}$(t) $RGS_m$(t) |
| $G\alpha_{GTP}$Effector | $G\alpha_{GTP}$Effector'(t) = $k_{10}$Effector(t) $G\alpha_{GTP}$(t) - $k_{11}G\alpha_{GTP}$Effector(t) |
| inert$G\alpha_{GTP}$ | inert$G\alpha_{GTP}$'(t) = $k_{11}G\alpha_{GTP}$Effector(t) - $k_{14}$inert$G\alpha_{GTP}$(t) - $k_{27}$inert$G\alpha_{GTP}$(t) $RGS_c$ - $k_{12}$inert$G\alpha_{GTP}$(t) $RGS_m$(t) |
| $RGS_c$ | $RGS_c$'(t) = - $k_{18}RGS_c$(t) - $k_{23}$R(t) $RGS_c$(t) - $k_{20}$R$G\alpha\beta\gamma$(t) $RGS_c$(t) - $k_{22}$LR(t) $RGS_c$ - $k_{26}G\alpha_{GTP}$(t) $RGS_c$(t) - $k_{27}$inert$G\alpha_{GTP}$(t) $RGS_c$(t) + $k_{19}RGS_m$(t) + $k_8$R$GS_mG\alpha_{GTP}$(t) + $k_{13}$R$GS_m$inert$G\alpha_{GTP}$(t) |
| $RGS_m$ | $RGS_m$'(t) = $k_{18}RGS_c$(t) - $k_{19}RGS_m$(t) - $k_7G\alpha_{GTP}$(t) $RGS_m$(t) - $k_{12}$inert$G\alpha_{GTP}$(t) $RGS_m$(t) + $k_{21}$ R$RGS_mG\alpha\beta\gamma$(t) + k25R$RGS_m$ + $k_{24}$L$RRGS_m$ |
| R$GS_mG\alpha_{GTP}$ | R$GS_mG\alpha_{GTP}$'(t) = $k_{26}G\alpha_{GTP}$(t) $RGS_c$(t) + $k_7G\alpha_{GTP}$(t) $RGS_m$(t) - $k_8$R$GS_mG\alpha_{GTP}$(t) |
| R$GS_m$inert$G\alpha_{GTP}$ | R$GS_m$inert$G\alpha_{GTP}$'(t) = $k_{27}$inert$G\alpha_{GTP}$(t) $RGS_c$(t) + $k_{12}$inert$G\alpha_{GTP}$(t) $RGS_m$(t) - $k_{13}$R$GS_m$inert$G\alpha_{GTP}$(t) |
| R$RGS_mG\alpha\beta\gamma$ | R$RGS_mG\alpha\beta\gamma$'(t) = $k_{20}$R$G\alpha\beta\gamma$(t) $RGS_c$(t) - $k_{21}$R$RGS_mG\alpha\beta\gamma$(t) |
| R$RGS_m$ | R$RGS_m$'(t) = $k_{23}$R(t) $RGS_c$(t) - $k_{25}$R$RGS_m$(t) |
| LR$RGS_m$ | LR$RGS_m$'(t) = $k_{22}$LR(t) $RGS_c$(t) - $k_{24}$LR$RGS_m$(t) |
| z(1) | z(1)'(t) = $\frac{3}{2}$ Effector(t) $G\alpha_{GTP}$- $\frac{3}{2}$ z(1)(t) |
| z(2) | z(2)'(t) = $\frac{3}{2}$ z(1)(t) - $\frac{3}{2}$ z(2)(t) |
| z(3) | z(3)'(t) = $\frac{3}{2}$ z(2)(t) - $\frac{3}{2}$ z(3)(t) |

TABLE 4.4: **System of ODEs for simulating the new hypothesis: Plasma membrane trafficking of RGS model.** The table shows each species defined within the new hypothesis model and its associated differential equation describing the rate of change in that species concentration with time. For reaction rate constants (k) refer to Table 4.3. b = 100 (constant for ligand addition), $t_0$ = 14 (equilibration time before ligand application).

The difference in this model compared to the initial hypothesis (Table 4.1) is that some RGS species should achieve PM localisation independently of an interaction with the GPCR through binding $G\alpha_{GTP}$/inert$G\alpha_{GTP}$ or through random diffusion, therefore this model should now be capable of reproducing the negative effect of Rgs1 on signalling observed in strains lacking Mam2 (Figure 4.10, A).

#### 4.2.6.3 Testing Plasma Membrane Trafficking of RGS Model Against Experimental Data

To test the new model to confirm that the RGS species in the model can impose negative regulation on signalling, independently of the receptor as observed previously through experimental assay, the RGS species concentration was varied in a system lacking any receptor. The experimental data is compared to simulations from the new model (Figure 4.12). To accomplish this, simulations were completed with R concentration set to 0 nM along with $RGS_c$ concentration set to 0 nM (No RGS), 60 nM (1 x RGS), 120 nM (2 x RGS) and 180 nM (3 x RGS).

The simulated assay demonstrated that response decreased with increasing RGS concentration in a similar stepwise manner to that observed in the experimental data, therefore the model agrees with the experimental data (Figure 4.12).

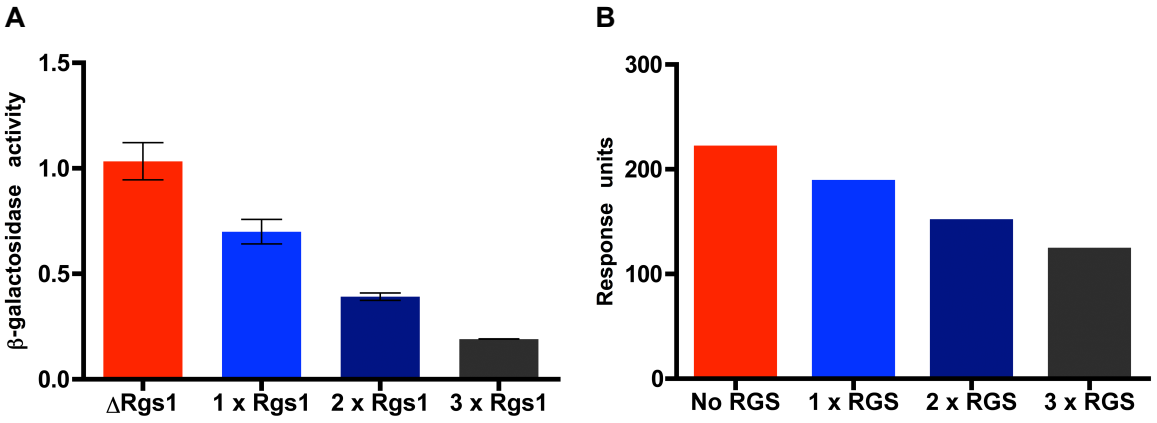


FIGURE 4.12: **Simulation of new hypothesis model: RGS activity independent of a GPCR-RGS interaction.** The data from $\beta$-galactosidase assay showing negative regulation by Rgs1 independent of a receptor (A) is compared to the equivalent simulated experiment from the plasma membrane trafficking of RGS model (Table 4.3) (B). Simulations are of basal signalling response in the system lacking the GPCR (initial R concentration = 0nM) and whereby initial concentration of RGS species is defined as $RGS_c = 0$ nM (No RGS) , $RGS_c = 60$ nM (RGS) , $RGS_c = 120$ nM (2 x RGS) , $RGS_c = 180$ nM (3 x RGS). Output from the model shows the accumulation of activated $G\alpha_{GTP}$Effector complexes over the duration of the simulated assay.

The new model also had to be validated against the key experimental data indicating the importance of the GPCR-RGS interaction for the regulation of P-factor induced signalling response. Simulations from the model having blocked any possible R-RGS interaction are a good qualitative match to the experimental data (compare Figure 4.13 to Figure 4.3, B). Blocking R-RGS interaction was simulated by defining any reaction rate for R-RGS interactions as zero ($k_{20} = 0\ nM^{-1}h^{-1}$, $k_{22} = 0\ nM^{-1}h^{-1}$, $k_{23} = 0\ nM^{-1}h^{-1}$). The simulated response when the interaction was blocked ($GPCR^{(-RGSinteraction)}$) increases basal response compared to the unmodified system (GPCR), although not to the same extent observed when RGS is removed (No RGS), but does decrease maximal response to the same level as

a system lacking RGS (Figure 4.13). The fact that the simulations qualitatively can closely reproduce both the negative regulation by Rgs1 independently of Mam2, and the dose-response observed for Mam2Δtail, suggests that the model maintains the requirement for interactions with the GPCR as sensitive parameters governing signalling response despite allowing some RGS to achieve PM localisation through the other mechanisms of diffusion and binding to G$\alpha_{GTP}$/inertG$\alpha_{GTP}$. This new PM trafficking of RGS hypothesis model (Table 4.3), that includes multiple mechanisms for achieving active RGS species at the PM, agrees with the biological data, suggesting this hypothesis to be correct.

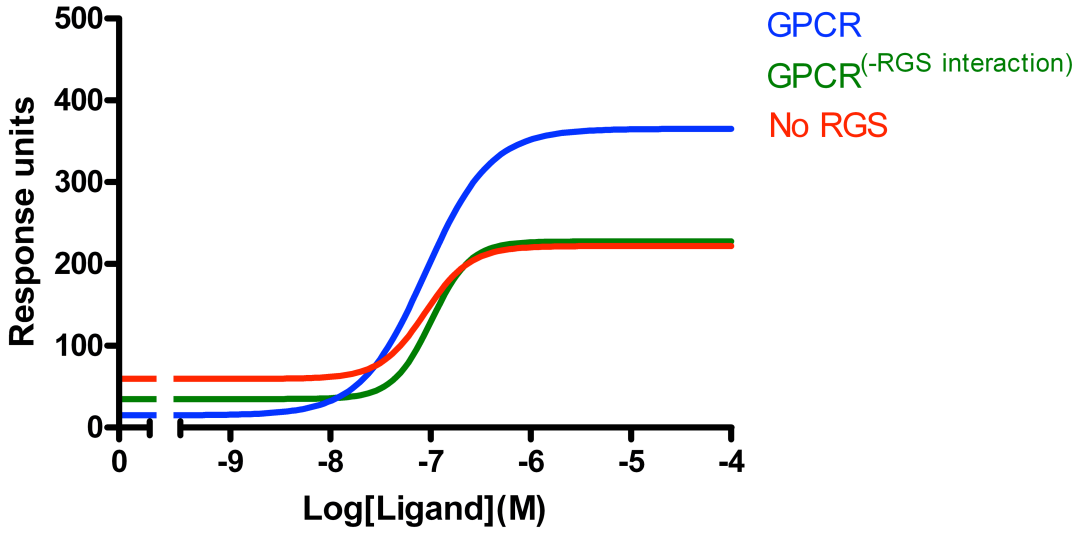


FIGURE 4.13: **Simulation of new hypothesis model: System response lacking GPCR-RGS interaction.** Simulations of the plasma membrane trafficking of RGS model (Table 4.3). Simulations are of the system whereby all parameters are unmodified (GPCR), the GPCR-RGS interaction is blocked by setting reaction rates $k_{20} = 0$ nM$^{-1}$, $k_{22} = 0$ nM$^{-1}$, $k_{23} = 0$ nM$^{-1}$, $k_{26} = 0$ nM$^{-1}$ (GPCR$^{(-RGS\ interaction)}$) and when RGS species are removed by defining initial concentrations $RGS_c = 0$ nM, $RGS_m = 0$ nM (No RGS). The concentration of ligand in the simulation was varied over the range 0-100 $\mu$M following 16 h simulated induction. Output from the model shows the accumulation of activated G$\alpha_{GTP}$Effector complexes over the duration of the simulated assay.

The new model places importance on the interaction between the GPCR and RGS species for regulation of signalling. One method for forcing interaction between two proteins is to fuse them together. To further probe this model, and to investigate the influence of interaction between the GPCR; Mam2 and RGS; Rgs1, a Mam2-Rgs1 fusion protein was expressed in *S. pombe* reporter cells.

### 4.2.7 GPCR-RGS Fusions

Data supporting the interaction between the tail of Mam2 and Rgs1 include yeast two-hybrid experiments expressing Rgs1 and Mam2tail in the budding yeast *S. cerevisiae* (Figure 4.3) and imaging work indicating co-localisation (Figure 4.8). Although these data give

strong evidence of an interaction, a limitation of the yeast two-hybrid is that the proteins are not in their physiological environment, therefore it does not confirm an interaction under physiological conditions. The co-localisation of Mam2 and Rgs1 observed through fluorescence imaging is in the native environment within the cell and this strengthens the argument for an interaction, but does not confirm one, as it is possible that localisation of Rgs1 at the PM could be a secondary effect of another function of the receptor tail, and not a result of a direct interaction. One method of forcing an interaction in the cell is to fuse the two proteins together and express them in *S. pombe*. If the fusion construct could facilitate a signalling response similar to the normal conditions when Mam2 and Rgs1 are not fused, then this would confirm that the proteins are able to function in a complex and suggest that they do indeed interact under physiological conditions.

An added consideration in fusing these proteins is that the concentrations of Mam2 and Rgs1 will be forced into a 1:1 ratio. Cellular Rgs1 concentration in *S. pombe* has not been quantified, but is assumed to be in the region of 60 nM based on similarities to the mating-response signalling in budding yeast *S. cerevisiae* (Yildirim et al., 2004). Mam2 concentration is greater at 205 nM (Ladds et al., 2003), again this is similar to budding yeast. If these estimates are correct then in a *wild-type* cell, the ratio of Mam2 to Rgs1 concentration would normally be in the region of 3-4:1. This could also provide a possible explanation for why a doubling of the Rgs1 concentration in cells results in seemingly optimal Rgs1 functionality, apparent from reduced basal signalling, decreased sensitivity and increased maximal signalling levels compared to a *wild-type* strain (Smith et al., 2009). The GPCR Mam2, has been suggested to be able to form dimers (Ladds et al., 2005a), therefore if Rgs1 was only able to bind to a Mam2 dimer and not the monomer, then given the predicted concentrations of Rgs1 and Mam2, this would mean that doubling the Rgs1 concentration to ∼120 nM would give a concentration of Rgs1 similar to that of the active Mam2 dimer (102.5 nM). This would be close to a 1:1 ratio between Rgs1 and the dimer, therefore ideal molecule numbers for Rgs1 binding to Mam2 dimers and efficient relative concentrations for Rgs1 PM recruitment.

A fusion construct containing the full length Mam2 fused at its C-terminus to Rgs1 (Hill, PhD Thesis, 2008) was expressed from vector pREP3x in a reporter strain lacking endogenous Mam2 and Rgs1; JY1291(ΔMam2, ΔRgs1). JY1291 was also transformed with vector pREP3x expressing Mam2 or transformed with both pREP3x expressing Mam2 and pREP4x expressing Rgs1. The *wild-type* reporter strain containing endogenous Mam2 and Rgs1 (JY544) and the transformed strains were grown in minimal media, incubated with 0M to $10^{-4}$M P-factor for 16 h and then assayed for the induction of *sxa2>lacZ* (Figure 4.14).

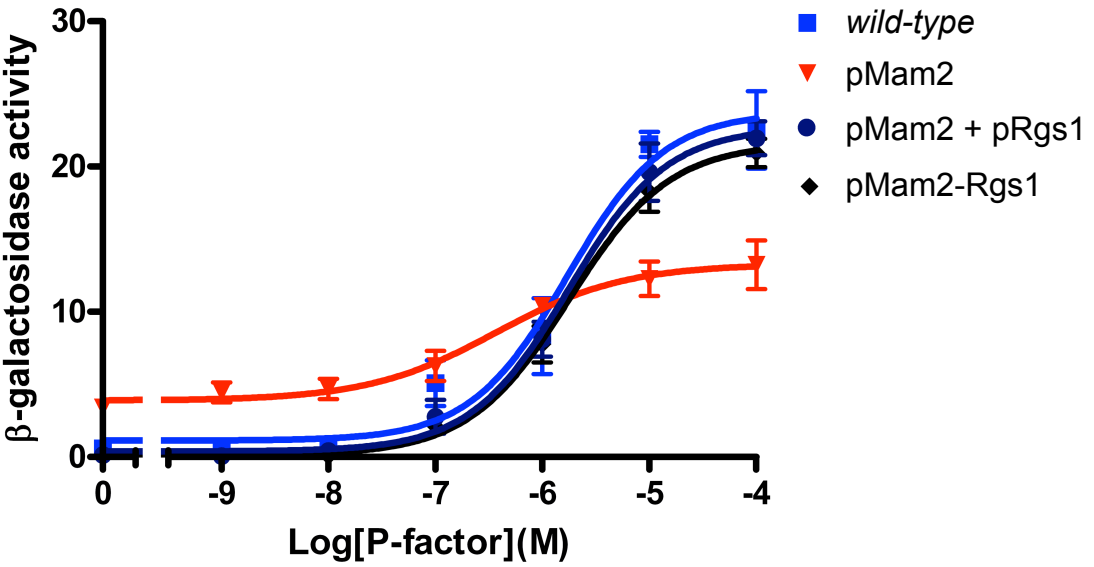


| | Basal | Maximal | $pEC_{50}$ |
|---|---|---|---|
| *wild-type* | 1.125 +/- 0.976 | 23.750 +/- 2.170 | 5.767 +/- 0.184 |
| pMam2 | 3.871 +/- 0.671 | 13.290 +/- 0.986 | 6.431 +/- 0.268 |
| pMam2 + pRgs1 | 0.378 +/- 0.596 | 22.720 +/- 1.347 | 5.754 +/- 0.116 |
| pMam2-Rgs1 | 0.130 +/- 0.449 | 21.600 +/- 1.027 | 5.750 +/- 0.092 |

FIGURE 4.14: **Signalling of Mam2-Rgs1 fusion.** Reporter strain JY1291(ΔMam2, ΔRgs1) was transformed with expression vectors pREP3x-Mam2 + pREP4x (pMam2), pREP3x-Mam2-Rgs1 (fusion protein) + pREP4x (pMam2-Rgs1) and both pREP3x-Mam2 + pREP4x-Rgs1 together (pMam2 + pRgs1). Cells were cultured in minimal media lacking leucine and uracil to a density of ~5x$10^6$ cells/ml, incubated with 0M to $10^{-4}$M P-factor before assaying for $\beta$-galactosidase activity. $\beta$-galactosidase activity was measured as $OD_{420}/10^6$ cells. The *wild-type* reporter strain JY544(*sxa2>lacZ*) was also assayed for comparison (*wild-type*). Results are the means ± S.E.M. of triplicate determinations from three independent isolates.

Data from the assay indicates that there is minimal difference in signalling response when Mam2 and Rgs1 are fused together compared to when they are not (compare profiles for pMam2-Rgs1 to pMam2 + pRgs1 and *wild-type* in Figure 4.14). Both Mam2 and Rgs1 are able to function without obvious hindrance when the two proteins are fused together, therefore suggesting that these two proteins may function in a complex, possibly in the same subcellular localisation. The experimental data of the fusion species showing no detriment to signalling, implies that it must be possible for a number of reactions to be able to occur physiologically when Mam2 is in complex with Rgs1. Mam2-Rgs1 must be capable of P-factor and $Gpa1_{GDP}$ binding and activation. Additionally, it must be possible for a Mam2-Rgs1 complex to bind to $Gpa1_{GTP}$ and the predicted inert$Gpa1_{GTP}$ to catalyse GTP hydrolysis reactions. The fused proteins must be capable of these reactions otherwise the *wild-type* signalling profile seen for the fusion protein in assays (Figure 4.14) would not be achievable. The PM trafficking of RGS model (Table 4.3) does not include all such interactions when the GPCR and RGS are in a complex, therefore this model does not represent all the possible reactions that occur physiologically.

#### 4.2.7.1 GPCR-RGS Fusion Model

To be able to simulate the Mam2-Rgs1 fusion data, a model was developed that contained a fusion of the R and RGS species. This model was built based on the reaction scheme for the PM trafficking of RGS model (Table 4.3) but removing any RGS trafficking events, as RGS is assumed constantly membrane localised due to being continuously fused to the receptor (RRGS). The reaction scheme for the GPCR-RGS fusion model is presented in Table 4.5.

| | | | |
|---|---|---|---|
| $L + RRGS \rightarrow LRRGS$ | $k_1$ | 0.0025 | $nM^{-1}h^{-1}$ |
| $G\alpha\beta\gamma + RRGS \rightarrow RRGSG\alpha\beta\gamma$ | $k_2$ | 0.005 | $nM^{-1}h^{-1}$ |
| $G\alpha\beta\gamma + LRRGS \rightarrow LRRGSG\alpha\beta\gamma$ | $k_3$ | 0.02 | $nM^{-1}h^{-1}$ |
| $L + RRGSG\alpha\beta\gamma \rightarrow LRRGSG\alpha\beta\gamma$ | $k_4$ | 0.005 | $nM^{-1}h^{-1}$ |
| $LRRGSG\alpha\beta\gamma \rightarrow G\alpha_{GTP} + G\beta\gamma + LRRGS$ | $k_5$ | 50 | $h^{-1}$ |
| $G\alpha\beta\gamma \rightarrow G\alpha_{GTP} + G\beta\gamma$ | $k_6$ | 0.2 | $h^{-1}$ |
| $G\alpha_{GTP} + RRGS \rightarrow RRGSG\alpha_{GTP}$ | $k_7$ | 500 | $nM^{-1}h^{-1}$ |
| $RRGSG\alpha_{GTP} \rightarrow G\alpha_{GDPP} + RRGS$ | $k_8$ | 2.5 | $h^{-1}$ |
| $G\alpha_{GTP} \rightarrow G\alpha_{GDPP}$ | $k_9$ | 0.005 | $h^{-1}$ |
| $Effector + G\alpha_{GTP} \rightarrow G\alpha_{GTP}Effector$ | $k_{10}$ | 10 | $nM^{-1}h^{-1}$ |
| $G\alpha_{GTP}Effector \rightarrow Effector + inertG\alpha_{GTP}$ | $k_{11}$ | 1 | $h^{-1}$ |
| $inertG\alpha_{GTP} + RRGS \rightarrow RRGSinertG\alpha_{GTP}$ | $k_{12}$ | 50 | $nM^{-1}h^{-1}$ |
| $RRGSinertG\alpha_{GTP} \rightarrow RRGS + G\alpha_{GDPP}$ | $k_{13}$ | 0.3 | $h^{-1}$ |
| $inertG\alpha_{GTP} \rightarrow G\alpha_{GDPP}$ | $k_{14}$ | 0.005 | $h^{-1}$ |
| $G\alpha_{GDPP} \rightarrow G\alpha_{GDP} + P$ | $k_{15}$ | 1000 | $h^{-1}$ |
| $G\alpha_{GDP} + G\beta\gamma \rightarrow G\alpha\beta\gamma$ | $k_{16}$ | 1000 | $nM^{-1}h^{-1}$ |
| $P \rightarrow \emptyset$ | $k_{17}$ | 10 | $h^{-1}$ |
| $G\alpha_{GTP} + LRRGS \rightarrow LRRGSG\alpha_{GTP}$ | $k_{18}$ | 100 | $nM^{-1}h^{-1}$ |
| $LRRGSG\alpha_{GTP} \rightarrow G\alpha_{GDPP} + LRRGS$ | $k_{19}$ | 2.5 | $h^{-1}$ |
| $inertG\alpha_{GTP} + LRRGS \rightarrow LRRGSinertG\alpha_{GTP}$ | $k_{20}$ | 50 | $nM^{-1}h^{-1}$ |
| $LRRGSinertG\alpha_{GTP} \rightarrow G\alpha_{GDPP} + LRRGS$ | $k_{21}$ | 0.3 | $h^{-1}$ |

TABLE 4.5: **GPCR-RGS fusion model.** The model was constructed based on modifying the plasma membrane trafficking of RGS model (Table 4.3) such that all R and RGS species are replaced with the fusion species (RRGS). The rates of these particular reactions remain unchanged. RGS is now effectively constantly membrane localised as it is fused to the membrane localised receptor species.

The fusion model (Table 4.5) includes additional reactions that were assumed not to occur in the previous PM trafficking of RGS model. These reactions include the G protein being able to become activated through ligand binding to a complex of the receptor, RGS and G protein (reactions $k_4$ and $k_5$), a complex of the receptor and RGS (RRGS) being capable of GAP activity on $G\alpha_{GTP}$ (reactions $k_7$ and $k_8$) and inert $G\alpha_{GTP}$ (reactions $k_{12}$ and $k_{13}$). RGS is also given the capability of GAP activity on $G\alpha_{GTP}$ and inert $G\alpha_{GTP}$ when in complex with a ligand-bound receptor (LRRGS) (reactions $k_{18-21}$).

The system of ODEs generated from the GPCR-RGS fusion model (Table 4.5) is given in Table 4.6. The fusion species $RRGS_m$ is initiated at 205 nM, the same concentration used in previous models for the receptor species R.

| | |
|---|---|
| Effector | Effector'(t) = - $k_{10}$Effector(t) $G\alpha_{GTP}$(t) + $k_{11}G\alpha_{GTP}$Effector(t) |
| $G\alpha\beta\gamma$ | $G\alpha\beta\gamma$'(t) = - $k_6G\alpha\beta\gamma$(t) - $k_2G\alpha\beta\gamma$(t) RRGS(t) - $k_3G\alpha\beta\gamma$(t) LRRGS(t) + $k_{16}G\beta\gamma$(t) $G\alpha_{GDP}$(t) |
| $G\beta\gamma$ | $G\beta\gamma$'(t) = $k_6G\alpha\beta\gamma$(t) + $k_5$LRRGS$G\alpha\beta\gamma$(t) - $k_{16}G\beta\gamma$(t) $G\alpha_{GDP}$(t) |
| L | L'(t) = - $\frac{1}{2}$ $k_1$L(t) RRGS(t) (Tanh($t_0$ b) - Tanh(b($t_0$ - t))) - $\frac{1}{2}$ $k_4$L(t) RRGS$G\alpha\beta\gamma$(t) (Tanh($t_0$ b) - Tanh(b($t_0$ - t))) |
| P | P'(t) = - $k_{17}$P(t) + $k_{15}G\alpha_{GDPP}$(t) |
| RRGS | RRGS'(t) = - $k_2G\alpha\beta\gamma$(t) RRGS(t) - $\frac{1}{2}$ $k_1$L(t) RRGS(t) (Tanh($t_0$ b) - Tanh(b($t_0$ - t))) - $k_7$RRGS(t) $G\alpha_{GTP}$(t) - $k_{12}$RRGS(t) inert$G\alpha_{GTP}$(t) + $k_8$RRGS$G\alpha_{GTP}$(t) + $k_{13}$RRGSinert$G\alpha_{GTP}$(t) |
| RRGS$G\alpha\beta\gamma$ | RRGS$G\alpha\beta\gamma$'(t) = $k_2G\alpha\beta\gamma$(t) RRGS(t) - $\frac{1}{2}$ $k_4$L(t) RRGS$G\alpha\beta\gamma$(t) (Tanh($t_0$ b) - Tanh(b($t_0$ - t))) |
| LRRGS$G\alpha\beta\gamma$ | LRRGS$G\alpha\beta\gamma$'(t) = - $k_5$LRRGS$G\alpha\beta\gamma$(t) + $k_3G\alpha\beta\gamma$(t) LRRGS(t) + $\frac{1}{2}$ $k_4$L(t) RRGS$G\alpha\beta\gamma$(t) (Tanh($t_0$ b) - Tanh(b($t_0$ - t))) |
| LRRGS | LRRGS'(t) = $k_5$LRRGS$G\alpha\beta\gamma$(t) - $k_3G\alpha\beta\gamma$(t) LRRGS(t) + $\frac{1}{2}$ $k_1$L(t) RRGS(t) (Tanh($t_0$ b) - Tanh(b($t_0$ - t))) - $k_{18}$LRRGS(t) $G\alpha_{GTP}$(t) - $k_{20}$LRRGS(t) inert$G\alpha_{GTP}$(t) + $k_{19}$LRRGS$G\alpha_{GTP}$(t) + $k_{21}$LRRGSinert$G\alpha_{GTP}$(t) |
| $G\alpha_{GDP}$ | $G\alpha_{GDP}$'(t) = - $k_{16}G\beta\gamma$(t) $G\alpha_{GDP}$(t) + $k_{15}G\alpha_{GDPP}$(t) |
| $G\alpha_{GDPP}$ | $G\alpha_{GDPP}$'(t) = - $k_{15}G\alpha_{GDPP}$(t) + $k_9G\alpha_{GTP}$(t) + $k_{14}$inert$G\alpha_{GTP}$(t) + $k_8$RRGS$G\alpha_{GTP}$(t) + $k_{13}$RRGSinert$G\alpha_{GTP}$(t) + $k_{19}$LRRGS$G\alpha_{GTP}$(t) + $k_{21}$LRRGSinert$G\alpha_{GTP}$(t) |
| $G\alpha_{GTP}$ | $G\alpha_{GTP}$'(t) = $k_6G\alpha\beta\gamma$(t) + $k_5$LRRGS$G\alpha\beta\gamma$(t) - $k_9G\alpha_{GTP}$(t) - $k_{10}$Effector(t) $G\alpha_{GTP}$(t) - $k_7$RRGS(t) $G\alpha_{GTP}$(t) - $k_{18}$LRRGS(t) $G\alpha_{GTP}$(t) |
| $G\alpha_{GTP}$Effector | $G\alpha_{GTP}$Effector'(t) = $k_{10}$Effector(t) $G\alpha_{GTP}$(t) - $k_{11}G\alpha_{GTP}$Effector(t) |
| inert$G\alpha_{GTP}$ | inert$G\alpha_{GTP}$'(t) = $k_{11}G\alpha_{GTP}$Effector(t) - $k_{14}$inert$G\alpha_{GTP}$(t) - $k_{12}$RRGS(t) inert$G\alpha_{GTP}$(t) - $k_{20}$LRRGS(t) inert$G\alpha_{GTP}$(t) |
| RRGS$G\alpha_{GTP}$ | RRGS$G\alpha_{GTP}$'(t) = $k_7$RRGS(t) $G\alpha_{GTP}$(t) - $k_8$RRGS$G\alpha_{GTP}$(t) |
| RRGSinert$G\alpha_{GTP}$ | RRGSinert$G\alpha_{GTP}$'(t) = $k_{12}$RRGS(t) inert$G\alpha_{GTP}$(t) - $k_{13}$RRGSinert$G\alpha_{GTP}$(t) |
| LRRGS$G\alpha_{GTP}$ | LRRGS$G\alpha_{GTP}$'(t) = $k_{18}$LRRGS(t) $G\alpha_{GTP}$(t) - $k_{19}$LRRGS$G\alpha_{GTP}$(t) |
| LRRGSinert$G\alpha_{GTP}$ | LRRGSinert$G\alpha_{GTP}$'(t) = $k_{20}$LRRGS(t) inert$G\alpha_{GTP}$(t) - $k_{21}$LRRGSinert$G\alpha_{GTP}$(t) |
| z(1) | z(1)'(t) = $\frac{3}{2}$ Effector(t) $G\alpha_{GTP}$- $\frac{3}{2}$ z(1)(t) |
| z(2) | z(2)'(t) = $\frac{3}{2}$ z(1)(t) - $\frac{3}{2}$ z(2)(t) |
| z(3) | z(3)'(t) = $\frac{3}{2}$ z(2)(t) - $\frac{3}{2}$ z(3)(t) |

TABLE 4.6: **System of ODEs for simulating the GPCR-RGS fusion model.** The table shows each species defined within the initial GPCR-RGS fusion model and its associated differential equation describing the rate of change in that species concentration with time. For reaction rate constants (k) refer to Table 4.5. b = 100 (constant for ligand addition), $t_0$ = 14 (equilibration time before ligand application).

#### 4.2.7.2 Testing GPCR-RGS Fusion Model

Simulations of the GPCR-RGS fusion model generated a signalling profile almost identical to that observed through simulations of the PM trafficking of RGS model (compare R-RGS fusion to RGS in Figure 4.15). Simulation of the PM trafficking of RGS model system lacking any RGS is included to highlight the fact that the simulated response from the fusion allows a fully functional RGS species, as shown by the decreased basal and increased maximal of the R-RGS fusion profile compared to the No RGS profile (Figure 4.15). The

GPCR-RGS fusion model is therefore able to qualitatively reproduce the experimental fusion data (compare Figure 4.15 to Figure 4.14).

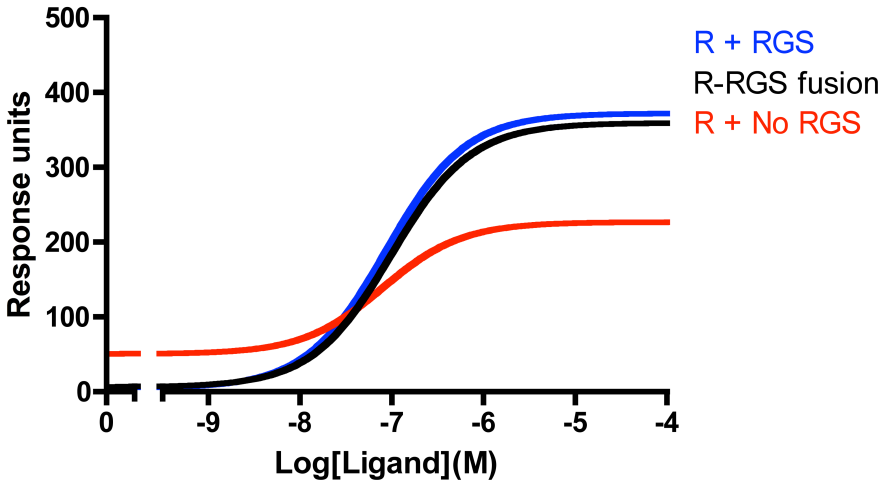


FIGURE 4.15: **Simulations of signalling response of a GPCR-RGS fusion.** Simulations are of the GPCR-RGS fusion model (Table 4.5). For comparison, simulated response from the GPCR-RGS fusion model (R-RGS fusion) is compared to the simulated response from the unmodified plasma membrane trafficking of RGS model (Table 4.3) (R + RGS) and when initial RGS concentration in this model is set to 0 nM (R + No RGS). The concentration of ligand in the simulation was varied over the range 0-100 $\mu$M following 16 h simulated induction. Output from the model shows the accumulation of activated $G\alpha_{GTP}$Effector complexes over the duration of the simulated assay.

Given the experimental data from the Mam2-Rgs1 fusion (Figure 4.14) and the success of the GPCR-RGS fusion model (Figure 4.15) we can identify the reactions that have to be added to the PM trafficking of RGS model to give a more accurate representation of the possible reactions that can occur when the GPCR and RGS species are in a complex.

### 4.2.8 Finalised Plasma Membrane Trafficking Model of RGS Function

Given the realisation that it is possible for further reactions to occur other than those already defined in the reaction scheme for the PM trafficking of RGS model (Table 4.3), modifications were made to this model to include reactions involving R-RGS complexes that experimental data suggests must be possible physiologically. The modifications resulted in the generation of the final PM trafficking model of RGS function (reaction scheme in Table 4.7; system of ODEs in Table 4.8). Modifications include additional reactions allowing R-RGS complexes to function in place of reactions involving R alone, and reactions involving RGS alone. Additional reactions include; ligand and G protein subunits binding to a R-RGS complex (Table 4.7, reactions $k_5$, $k_6$, $k_7$ and $k_8$) and enabling $G\alpha_{GTP}$ and inert$G\alpha_{GTP}$ to interact with RGS that is in complex with ligand-bound and non-ligand-bound R to promote GTP hydrolysis (Table 4.7, reactions $k_{29}$, $k_{30}$, $k_{31}$, $k_{32}$, $k_{36}$ and $k_{37}$). For clarity, the reactions have been grouped into the key events of the signalling pathway. These being;

ligand/G protein binding (reactions $k_{1-8}$), G protein activation (reactions $k_{9-12}$), RGS trafficking (reactions $k_{13-24}$) and switching off/recycling the G protein (reactions $k_{25-40}$). Where possible, the additional reactions involving fusion complexes are assumed to occur at the same reaction rates as the equivalent reactions involving the free R and RGS species. If this is not possible then reaction rate constants are defined based on best fit to experimental data.

| | | | | |
|---|---|---|---|---|
| ligand / G protein binding | $L + R \rightarrow LR$ | $k_1$ | 0.0025 | $nM^{-1}h^{-1}$ |
| | $G\alpha\beta\gamma + R \rightarrow RG\alpha\beta\gamma$ | $k_2$ | 0.005 | $nM^{-1}h^{-1}$ |
| | $G\alpha\beta\gamma + LR \rightarrow LRG\alpha\beta\gamma$ | $k_3$ | 0.02 | $nM^{-1}h^{-1}$ |
| | $L + RG\alpha\beta\gamma \rightarrow LRG\alpha\beta\gamma$ | $k_4$ | 0.005 | $nM^{-1}h^{-1}$ |
| | $L + RRGS_m \rightarrow LRRGS_m$ | $k_5$ | 0.005 | $nM^{-1}h^{-1}$ |
| | $G\alpha\beta\gamma + RRGS_m \rightarrow RRGS_mG\alpha\beta\gamma$ | $k_6$ | 0.005 | $nM^{-1}h^{-1}$ |
| | $G\alpha\beta\gamma + LRRGS_m \rightarrow LRRGS_mG\alpha\beta\gamma$ | $k_7$ | 0.02 | $nM^{-1}h^{-1}$ |
| | $L + RRGS_mG\alpha\beta\gamma \rightarrow LRRGS_mG\alpha\beta\gamma$ | $k_8$ | 0.005 | $nM^{-1}h^{-1}$ |
| G protein activation | $LRG\alpha\beta\gamma \rightarrow G\alpha_{GTP} + G\beta\gamma + LR$ | $k_9$ | 50 | $h^{-1}$ |
| | $G\alpha\beta\gamma \rightarrow G\alpha_{GTP} + G\beta\gamma$ | $k_{10}$ | 0.2 | $h^{-1}$ |
| | $LRRGS_mG\alpha\beta\gamma \rightarrow G\alpha_{GTP} + G\beta\gamma + LRRGS_m$ | $k_{11}$ | 40 | $h^{-1}$ |
| | $Effector + G\alpha_{GTP} \rightarrow G\alpha_{GTP}Effector$ | $k_{12}$ | 10 | $nM^{-1}h^{-1}$ |
| RGS trafficking | $RGS_c \rightarrow RGS_m$ | $k_{13}$ | 0.0005 | $h^{-1}$ |
| | $RGS_m \rightarrow RGS_c$ | $k_{14}$ | 0.005 | $h^{-1}$ |
| | $R + RGS_c \rightarrow RRGS_m$ | $k_{15}$ | 0.1 | $nM^{-1}h^{-1}$ |
| | $RRGS_m \rightarrow R + RGS_m$ | $k_{16}$ | 100 | $h^{-1}$ |
| | $LR + RGS_c \rightarrow LRRGS_m$ | $k_{17}$ | 0.1 | $nM^{-1}h^{-1}$ |
| | $LRRGS_m \rightarrow LR + RGS_m$ | $k_{18}$ | 100 | $h^{-1}$ |
| | $RG\alpha\beta\gamma + RGS_c \rightarrow RRGS_mG\alpha\beta\gamma$ | $k_{19}$ | 0.1 | $nM^{-1}h^{-1}$ |
| | $RRGS_mG\alpha\beta\gamma \rightarrow RG\alpha\beta\gamma + RGS_m$ | $k_{20}$ | 0.1 | $h^{-1}$ |
| | $LRG\alpha\beta\gamma + RGS_c \rightarrow LRRGS_mG\alpha\beta\gamma$ | $k_{21}$ | 0.1 | $nM^{-1}h^{-1}$ |
| | $G\alpha_{GTP} + \mathit{RGS}_c \rightarrow RGS_mG\alpha_{GTP}$ | $k_{22}$ | 60 | $nM^{-1}h^{-1}$ |
| | $RGS_mG\alpha_{GTP} \rightarrow G\alpha_{GTP} + RGS_c$ | $k_{23}$ | 0.05 | $h^{-1}$ |
| | $inertG\alpha_{GTP} + RGS_c \rightarrow RGS_minertG\alpha_{GTP}$ | $k_{24}$ | 0.0001 | $nM^{-1}h^{-1}$ |
| switching off / recycling G protein | $G\alpha_{GTP}Effector \rightarrow Effector + inertG\alpha_{GTP}$ | $k_{25}$ | 1 | $h^{-1}$ |
| | $G\alpha_{GTP} \rightarrow G\alpha_{GDPP}$ | $k_{26}$ | 0.005 | $h^{-1}$ |
| | $G\alpha_{GTP} + RGS_m \rightarrow RGS_mG\alpha_{GTP}$ | $k_{27}$ | 500 | $nM^{-1}h^{-1}$ |
| | $RGS_mG\alpha_{GTP} \rightarrow G\alpha_{GDPP} + RGS_c$ | $k_{28}$ | 2.5 | $h^{-1}$ |
| | $G\alpha_{GTP} + LRRGS_m \rightarrow LRRGS_mG\alpha_{GTP}$ | $k_{29}$ | 100 | $nM^{-1}h^{-1}$ |
| | $LRRGS_mG\alpha_{GTP} \rightarrow G\alpha_{GDPP} + LRRGS_m$ | $k_{30}$ | 2.5 | $h^{-1}$ |
| | $G\alpha_{GTP} + \mathit{RRGS}_m \rightarrow RRGS_mG\alpha_{GTP}$ | $k_{31}$ | 0.5 | $nM^{-1}h^{-1}$ |
| | $RRGS_mG\alpha_{GTP} \rightarrow G\alpha_{GDPP} + RRGS_m$ | $k_{32}$ | 0.5 | $h^{-1}$ |
| | $inertG\alpha_{GTP} \rightarrow G\alpha_{GDPP}$ | $k_{33}$ | 0.005 | $h^{-1}$ |
| | $inertG\alpha_{GTP} + RGS_m \rightarrow RGS_minertG\alpha_{GTP}$ | $k_{34}$ | 50 | $nM^{-1}h^{-1}$ |
| | $RGS_minertG\alpha_{GTP} \rightarrow G\alpha_{GDPP} + RGS_c$ | $k_{35}$ | 0.3 | $h^{-1}$ |
| | $inertG\alpha_{GTP} + LRRGS_m \rightarrow LRRGS_minertG\alpha_{GTP}$ | $k_{36}$ | 50 | $nM^{-1}h^{-1}$ |
| | $LRRGS_minertG\alpha_{GTP} \rightarrow G\alpha_{GDPP} + LRRGS_m$ | $k_{37}$ | 0.3 | $h^{-1}$ |
| | $G\alpha_{GDPP} \rightarrow G\alpha_{GDP} + P$ | $k_{38}$ | 1000 | $h^{-1}$ |
| | $G\alpha_{GDP} + G\beta\gamma \rightarrow G\alpha\beta\gamma$ | $k_{39}$ | 1000 | $nM^{-1}h^{-1}$ |
| | $P \rightarrow \emptyset$ | $k_{40}$ | 10 | $h^{-1}$ |

TABLE 4.7: **Final plasma membrane trafficking model of RGS function.** Additional reactions are included based on assumptions from the GPCR-RGS fusion data/-model and to allow better fit to experimental data. Ligand and G protein subunits are capable of binding to a complex of the R and RGS (reactions $k_{5-8}$). It is possible for RGS to 'fall off' G$\alpha$ without having promoted $G\alpha_{GTP}$ hydrolysis (reaction $k_{23}$). $G\alpha_{GTP}$ and $inertG\alpha_{GTP}$ can interact with RGS that is in complex with the ligand bound and non-ligand bound GPCR to promote GTP hydrolysis (reactions $k_{29-32}$ and $k_{36-37}$).

| | |
|---|---|
| Effector | Effector'(t) = - $k_{12}$Effector(t) $G\alpha_{GTP}$(t) + $k_{25}G\alpha_{GTP}$Effector(t) |
| $G\alpha\beta\gamma$ | $G\alpha\beta\gamma$'(t) = - $k_{10}G\alpha\beta\gamma$(t) - $k_3G\alpha\beta\gamma$(t) LR(t) - $k_2G\alpha\beta\gamma$(t) R(t) + $k_{39}G\beta\gamma$(t) $G\alpha_{GDP}$(t) - $k_7G\alpha\beta\gamma$(t) LRRGS$_m$(t) - $k_6G\alpha\beta\gamma$(t) RRGS$_m$(t) |
| $G\beta\gamma$ | $G\beta\gamma$'(t) = $k_{10}G\alpha\beta\gamma$(t) + $k_9$LR$G\alpha\beta\gamma$(t) - $k_{39}G\beta\gamma$(t) $G\alpha_{GDP}$(t) + $k_{11}$LRRGS$_m G\alpha\beta\gamma$(t) |
| L | L'(t) = - $\frac{1}{2}$ $k_1$L(t) R(t) (Tanh($t_0$ b) - Tanh(b($t_0$ - t))) - $\frac{1}{2}$ $k_4$L(t) R$G\alpha\beta\gamma$(t) (Tanh($t_0$ b) - Tanh(b($t_0$ - t))) - $\frac{1}{2}$ $k_5$L(t) (Tanh($t_0$ b) - Tanh(b($t_0$ - t))) RRGS$_m$(t) - $\frac{1}{2}$ $k_8$L(t) (Tanh($t_0$ b) - Tanh(b($t_0$ - t))) RRGS$_m G\alpha\beta\gamma$(t) |
| LR | LR'(t) = - $k_3G\alpha\beta\gamma$(t) LR(t) + $k_9$LR$G\alpha\beta\gamma$(t) + $\frac{1}{2}$ $k_1$L(t) R(t) (Tanh($t_0$ b) - Tanh(b($t_0$ - t))) + $k_{18}$LRRGS$_m$(t) - $k_{17}$LR(t) RGS$_c$(t) |
| LR$G\alpha\beta\gamma$ | LR$G\alpha\beta\gamma$'(t) = $k_3G\alpha\beta\gamma$(t) LR(t) - $k_9$LR$G\alpha\beta\gamma$(t) + $\frac{1}{2}$ k4L(t) R$G\alpha\beta\gamma$(t) (Tanh($t_0$ b) - Tanh(b($t_0$ - t))) - $k_{21}$ LR$G\alpha\beta\gamma$(t) RGS$_c$(t) |
| P | P'(t) = - $k_{40}$P(t) + $k_{38}G\alpha_{GDPP}$(t) |
| R | R'(t) = - $k_2G\alpha\beta\gamma$(t) R(t) - $\frac{1}{2}$ $k_1$L(t) R(t) (Tanh($t_0$ b) - Tanh(b($t_0$ - t))) - $k_{15}$R(t) RGS$_c$(t) + $k_{16}$RRGS$_m$(t) |
| R$G\alpha\beta\gamma$ | R$G\alpha\beta\gamma$'(t) = $k_2G\alpha\beta\gamma$(t) R(t) - $\frac{1}{2}$ k4L(t) R$G\alpha\beta\gamma$(t) (Tanh($t_0$ b) - Tanh(b($t_0$ - t))) - $k_{19}$R$G\alpha\beta\gamma$(t) RGS$_c$(t) + $k_{20}$RRGS$_m G\alpha\beta\gamma$(t) |
| $G\alpha_{GDP}$ | $G\alpha_{GDP}$'(t) = - $k_{39}G\beta\gamma$(t) $G\alpha_{GDP}$(t) + $k_{38}G\alpha_{GDPP}$(t) |
| $G\alpha_{GDPP}$ | $G\alpha_{GDPP}$'(t) = - $k_{38}G\alpha_{GDPP}$(t) + $k_{26}G\alpha_{GTP}$(t) + $k_{33}$inert$G\alpha_{GTP}$(t) + $k_{30}$LRRGS$_m G\alpha_{GTP}$(t) + $k_{37}$LRRGS$_m$inert$G\alpha_{GTP}$(t) + $k_{28}$RGS$_m G\alpha_{GTP}$(t) + $k_{35}$RGS$_m$inert$G\alpha_{GTP}$(t) + $k_{32}$RRGS$_m G\alpha_{GTP}$(t) |
| $G\alpha_{GTP}$ | $G\alpha_{GTP}$'(t) = $k_{10}G\alpha\beta\gamma$(t) + $k_9$LR$G\alpha\beta\gamma$(t) - $k_{26}G\alpha_{GTP}$(t) - $k_{12}$Effector(t) $G\alpha_{GTP}$(t) - $k_{29}G\alpha_{GTP}$(t) LRRGS$_m$ + $k_{11}$LRRGS$_m G\alpha\beta\gamma$(t) - $k_{22}G\alpha_{GTP}$(t) RGS$_c$(t) - $k_{27}G\alpha_{GTP}$(t) RGS$_m$(t) + $k_{23}$RGS$_m G\alpha_{GTP}$(t) - $k_{31}G\alpha_{GTP}$(t) RRGS$_m$(t) |
| $G\alpha_{GTP}$Effector | $G\alpha_{GTP}$Effector'(t) = $k_{12}$Effector(t) $G\alpha_{GTP}$(t) - $k_{25}G\alpha_{GTP}$Effector(t) |
| inert$G\alpha_{GTP}$ | inert$G\alpha_{GTP}$'(t) = $k_{25}G\alpha_{GTP}$Effector(t) - $k_{33}$inert$G\alpha_{GTP}$(t) - $k_{36}$inert$G\alpha_{GTP}$(t) LRRGS$_m$(t) - $k_{24}$inert$G\alpha_{GTP}$(t) RGS$_c$(t) - $k_{34}$inert$G\alpha_{GTP}$(t) RGS$_m$(t) |
| LRRGS$_m$ | LRRGS$_m$'(t) = - $k_{18}$ LRRGS$_m$(t) - $k_7G\alpha\beta\gamma$(t) LRRGS$_m$(t) - $k_{29}G\alpha_{GTP}$(t) LRRGS$_m$(t) - $k_{36}$inert$G\alpha_{GTP}$(t) LRRGS$_m$(t) + $k_{11}$LRRGS$_m G\alpha\beta\gamma$(t) + $k_{30}$LRRS$_m G\alpha_{GTP}$(t) + $k_{37}$LRRGS$_m$inert$G\alpha_{GTP}$(t) + $k_{17}$LR(t) RGS$_c$(t) + $\frac{1}{2}$ $k_5$L(t) (Tanh($t_0$ b) - Tanh(b($t_0$ - t))) RRGS$_m$(t) |
| LRRGS$_m G\alpha\beta\gamma$ | LRRGS$_m G\alpha\beta\gamma$'(t) = $k_7G\alpha\beta\gamma$(t) LRRGS$_m$(t) - $k_{11}$LRRGS$_m G\alpha\beta\gamma$(t) + $k_{21}$LR$G\alpha\beta\gamma$(t) RGS$_c$(t) + $\frac{1}{2}$ $k_8$L(t) (Tanh($t_0$ b) - Tanh(b($t_0$ - t))) RRGS$_m G\alpha\beta\gamma$(t) |
| LRRGS$_m G\alpha_{GTP}$ | LRRGS$_m G\alpha_{GTP}$'(t) = $k_{29}G\alpha_{GTP}$(t) LRRGS$_m$(t) - $k_{30}$LRRGS$_m$inert$G\alpha_{GTP}$(t) |
| LRRGS$_m$inert$G\alpha_{GTP}$ | LRRGS$_m$inert$G\alpha_{GTP}$'(t) = $k_{36}$inert$G\alpha_{GTP}$(t) LRRGS$_m$(t) - $k_{37}$LRRGS$_m$inert$G\alpha_{GTP}$(t) |
| RGS$_c$ | RGS$_c$'(t) = - $k_{13}$RGS$_c$(t) - $k_{17}$LR(t) RGS$_c$(t) - $k_{21}$LR$G\alpha\beta\gamma$(t) RGS$_c$(t) - $k_{15}$R(t) RGS$_c$(t) - $k_{19}$R$G\alpha\beta\gamma$(t) RGS$_c$(t) - $k_{22}G\alpha_{GTP}$(t) RGS$_c$(t) - $k_{24}$inert$G\alpha_{GTP}$(t) RGS$_c$(t) + $k_{14}$RGS$_m$(t) + $k_{23}$RGS$_m G\alpha_{GTP}$(t) + $k_{28}$RGS$_m G\alpha_{GTP}$(t) + $k_{35}$RGS$_m$inert$G\alpha_{GTP}$(t) |
| RGS$_m$ | RGS$_m$'(t) = $k_{18}$LRRGS$_m$(t) + $k_{13}$RGS$_c$(t) - $k_{14}$RGS$_m$(t) - $k_{27}G\alpha_{GTP}$(t) RGS$_m$(t) - $k_{34}$inert$G\alpha_{GTP}$(t) RGS$_m$(t) + $k_{16}$RRGS$_m$(t) + $k_{20}$RRGS$_m G\alpha\beta\gamma$(t) |
| RGS$_m G\alpha_{GTP}$ | RGS$_m G\alpha_{GTP}$'(t) = $k_{22}G\alpha_{GTP}$(t) RGS$_c$(t) + $k_{27}G\alpha_{GTP}$(t) RGS$_m$(t) - $k_{23}$RGS$_m G\alpha_{GTP}$(t) - $k_{28}$RGS$_m G\alpha_{GTP}$(t) |
| RGS$_m$inert$G\alpha_{GTP}$ | RGS$_m$inert$G\alpha_{GTP}$'(t) = $k_{24}$inert$G\alpha_{GTP}$(t) RGS$_c$(t) + $k_{34}$inert$G\alpha_{GTP}$(t) RGS$_m$(t) - $k_{35}$RGS$_m$inert$G\alpha_{GTP}$(t) |
| RRGS$_m$ | RRGS$_m$'(t) = $k_{15}$R(t) RGS$_c$(t) - $k_{16}$RRGS$_m$(t) - $k_6G\alpha\beta\gamma$(t) RRGS$_m$(t) - $\frac{1}{2}$ $k_5$ L(t) (Tanh($t_0$ b) - Tanh(b($t_0$ - t))) RRGS$_m$(t) - $k_{31}G\alpha_{GTP}$(t) RRGS$_m$(t) + $k_{32}$RRGS$_m G\alpha_{GTP}$(t) |
| RRGS$_m G\alpha\beta\gamma$ | RRGS$_m G\alpha\beta\gamma$'(t) = $k_{19}$R$G\alpha\beta\gamma$(t) RGS$_c$(t) + $k_6G\alpha\beta\gamma$(t) RRGS$_m$(t) - $k_{20}$RRGS$_m G\alpha\beta\gamma$(t) - $\frac{1}{2}$ $k_8$ L(t) (Tanh($t_0$ b) - Tanh(b($t_0$ - t))) RRGS$_m G\alpha\beta\gamma$(t) |
| RRGS$_m G\alpha_{GTP}$ | RRGS$_m G\alpha_{GTP}$'(t) = $k_{31}G\alpha_{GTP}$(t) RRGS$_m$(t) - $k_{32}$RRGS$_m G\alpha_{GTP}$(t) |
| z(1) | z(1)'(t) = $\frac{3}{2}$ Effector(t) $G\alpha_{GTP}$- $\frac{3}{2}$ z(1)(t) |
| z(2) | z(2)'(t) = $\frac{3}{2}$ z(1)(t) - $\frac{3}{2}$ z(2)(t) |
| z(3) | z(3)'(t) = $\frac{3}{2}$ z(2)(t) - $\frac{3}{2}$ z(3)(t) |

TABLE 4.8: **System of ODEs for simulating the final plasma membrane trafficking model of RGS function.** The table shows each species defined within the plasma membrane trafficking of RGS model and its associated differential equation describing the rate of change in that species concentration with time. For reaction rate constants (k) refer to Table 4.7. b = 100 (constant for ligand addition), $t_0$ = 14 (equilibration time before ligand application).

## 4.3 Validation of the Final Plasma Membrane Trafficking Model of RGS Function

The development of the mathematical model from Smith et al., 2009 to include GPCR-RGS interactions and spatial regulation of RGS has resulted in quite substantial changes to the reaction scheme (although not compromising the key elements of G protein cycling). As a result, validation of the final PM trafficking model of RGS function (Table 4.7) was required to ensure the new model remains able to reproduce all of the biological data that the original model could simulate. Validation should provide greater confidence in the core hypothesis built into the model and subsequently in using the model as a predictive tool.

### 4.3.1 Blocking the GPCR-RGS Interaction

The new model was primarily built to explain data which the original Smith *et al.* model was unable to reproduce; signalling activity when the tail of the receptor is removed (Figure 4.3, B and Figure 4.16, A). The new model is able to qualitatively reproduce some of the patterns observed in these data (Figure 4.16). All evidence suggests the receptor tail is required for an interaction with Rgs1 (Figure 4.3, A, Figure 4.6 and Figure 4.8) therefore an equivalent to Mam2$\Delta$tail is simulated in the model by blocking any interaction of R with RGS ($GPCR^{(-RGS\ interaction)}$ in Figure 4.16, B). This is achieved by setting all R-RGS interaction reaction rate constants to 0 $nM^{-1}h^{-1}$ (Table 4.7, reactions $k_{15}$, $k_{17}$, $k_{19}$, $k_{21}$).

The simulations qualitatively reproduce experimental data, as blocking R-RGS interaction reduces maximal signalling, increases basal signalling (although not substantially) and gives a signalling profile similar to that of the simulated system lacking any RGS. The one aspect of the Mam2$\Delta$tail data, which proves difficult to reproduce in the model is the increased sensitivity to ligand stimulation ($pEC_{50}$; 8.313 $\pm$ 0.07 for Mam2$\Delta$tail vs $pEC_{50}$; 7.044 $\pm$ 0.112 for $GPCR^{(-RGS\ interaction)}$) (Figure 4.16). Similarly, the increased sensitivity observed from experimental data of $\Delta$Rgs1 strains is also difficult to reproduce in this model.

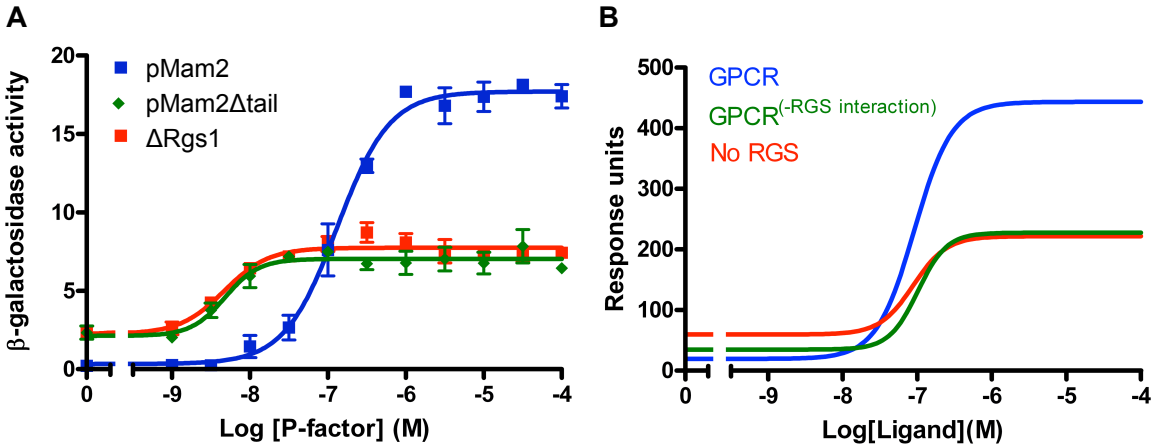


FIGURE 4.16: **Model testing: Removal of the receptor tail.** Experimental data (A) from assays of reporter strains JY1169(ΔMam2) expressing the full length receptor from vector pREP3x (pMam2), JY1169 expressing a receptor truncated for its C-terminal tail from pREP3x (pMam2Δtail) and reporter strain JY630 (ΔRgs1) is compared to simulated assays of the equivalent model system from Table 4.7 (B). Simulations are of an unmodified system (GPCR) when all GPCR-RGS interaction reactions are blocked ($GPCR^{(-RGS\ interaction)}$) and when RGS is removed. For experimental data cells were cultured in minimal media to a density of ~5x$10^6$ cells/ml, incubated with 0M to $10^{-4}$M P-factor before assaying for $\beta$-galactosidase activity. $\beta$-galactosidase activity was measured as $OD_{420}/10^6$ cells. Results are the means ± S.E.M. of triplicate determinations from three independent isolates. For the simulations the concentration of ligand was varied over the range 0-100 $\mu$M following 16 h simulated induction. Output from the model shows the accumulation of activated $G\alpha_{GTP}$Effector complexes over the duration of the simulated assay.

### 4.3.2 Negative Role of RGS in the Absence of a GPCR-RGS Interaction

The final model (Table 4.7) was also tested for whether it could reproduce the experimental data seen previously showing a negative influence of Rgs1 on basal signalling levels (Figure 4.10, A). To compare output from the model to this result, a simulated response was obtained in the model that has no receptor and with increasing concentration of RGS species (0 nM = No RGS, 60 nM = 1 x RGS, 120 nM = 2 x RGS and 180 nM = 3 x RGS) to observe the effect of more RGS on basal response.

The simulated response qualitatively reproduce the pattern observed in experimental data, with increasing RGS species resulting in a decrease in response (Figure 4.17). The final PM trafficking model of RGS function therefore correctly maintains the negative regulatory influence of RGS in the absence of a receptor and therefore the absence of a GPCR-RGS interaction.

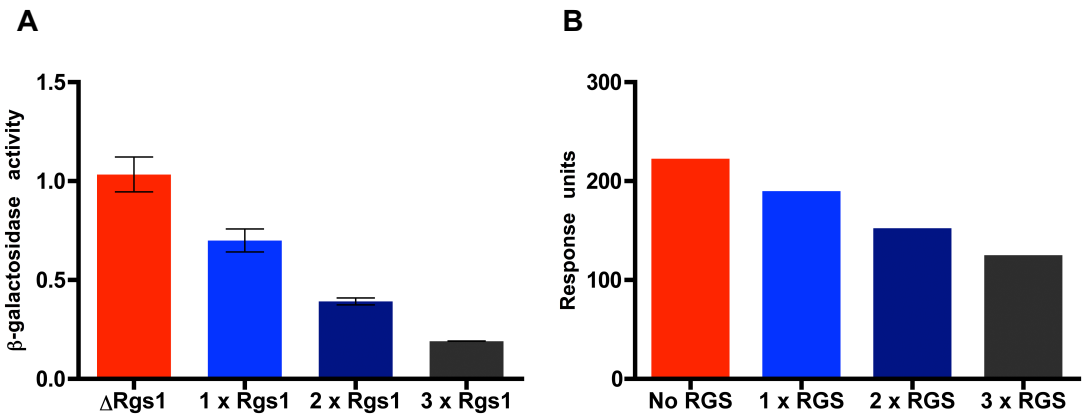


FIGURE 4.17: **Model testing: RGS influence in the absence of a receptor.** Experimental data (A) from assays of $\beta$-galactosidase expressed from the *sxa2>lacZ* reporter in strains deleted for the chromosomal copy of Mam2 when expressing varying levels of Rgs1 is compared to simulated assays of the equivalent model system from Table 4.7 (B). Strains include when no Rgs1 was present ($\Delta$Rgs1), when Rgs1 was expressed from vector pREP3x in reporter strain JY1291($\Delta$Rgs1,$\Delta$Mam2) (1 x Rgs1), when Rgs1 was expressed from pREP3x in reporter strain JY1169($\Delta$Mam2) (2 x Rgs1) and when Rgs1 was expressed from both vectors pREP3x and pREP4x in reporter strain JY1169($\Delta$Mam2) (3 x Rgs1). Cells were cultured in minimal media to a density of $\sim$5x10$^6$ cells/ml, before assaying for $\beta$-galactosidase activity. $\beta$-galactosidase activity was measured as OD$_{420}$/10$^6$ cells. Results are the means $\pm$ S.E.M. of triplicate determinations from three independent isolates (A). For the simulations the concentration of ligand was varied over the range 0-100 $\mu$M following 16 h simulated induction. Output from the model shows the accumulation of activated G$\alpha_{GTP}$Effector complexes over the duration of the simulated assay (B).

### 4.3.3 Dependence on RGS Concentration

In a system whereby G$\alpha_{\text{GTP}}$ is the signal propagator the concentration of free G$\alpha_{\text{GTP}}$ is likely to be be a critical control point. RGS proteins accelerate the hydrolysis of G$\alpha_{\text{GTP}}$ and therefore, are key regulators of the signal transduction. As a result, signalling output should be sensitive to the concentration of RGS protein. Indeed this was shown to be true in the *S. pombe* mating-response pathway by Smith et al., 2009, where the response was shown to be highly dependent on Rgs1 concentration. Experimental data shows that the basal signalling, maximal signalling and signal sensitivity are all dependent on the concentration of Rgs1 (Figure 4.18, A). Doubling the Rgs1 concentration increases maximal signalling activity from 17.71 $\pm$ 0.357 to 26.84 $\pm$ 0.6822 and decreases sensitivity from pEC$_{50}$ of 6.882 $\pm$ 0.049 to 6.086 $\pm$ 0.051, whilst trebling Rgs1 concentration reduces sensitivity further to 5.885 $\pm$ 0.098, but also reduces maximal signalling activity to 11.62 $\pm$ 0.6 (Figure 4.18). This clearly shows the dual positive and negative roles that Rgs1 can have on signalling, dependent on the level of ligand stimulation and the concentration of Rgs1 in the system. This key, counterintuitive result was the basis of the initial Smith *et al.* model hypothesis and could only be reproduced in the original model through the inclusion of an inert state for G$\alpha_{\text{GTP}}$ following effector activation, as discussed by Smith et al., 2009. This result therefore provides a good test for the final PM trafficking model of RGS function to determine

if the model maintains the positive and negative regulatory influence of RGS observed in the experimental data. To validate the new model in terms of dependence on RGS concentration, the equivalent *in silico* experiment was completed (Figure 4.18).

The core reactions involving cycling of G$\alpha$ through the GTP-bound active state, GTP-bound inert state and the GDP-bound inactive state remain largely unmodified in our final model. Given this, it is unlikely that the addition of another level of regulation through PM trafficking of RGS will disrupt the ability of the new model to reproduce the same qualitative agreement with experimental data as observed previously for the original Smith *et al.* model.

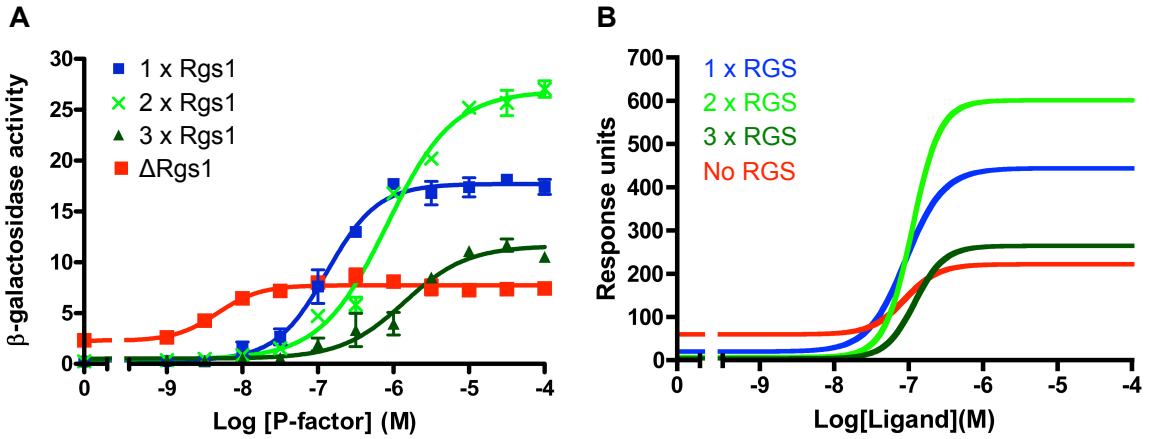


FIGURE 4.18: **Model testing: Dependence on Rgs1 concentration.** Experimental data (A) from reporter strains lacking endogenous Rgs1 (ΔRgs1), containing a single chromosomal copy (1 x Rgs1), containing one extra copy of Rgs1 from expression vector pREP3x (2 x Rgs1) and containing two extra copies of Rgs1 from expression vectors pREP3x and pREP4x (3 x Rgs1) is compared to simulated assays of the equivalent simulated assay using the final plasma membrane trafficking model of RGS function (Table 4.7) (B). Simulations are of the system initiated with $RGS_c$ concentration of 0 nM (No RGS), 60 nM (1 x RGS), 120 nM (2 x RGS) and 180 nM (3 x RGS). For experimental data, cells were cultured in minimal media to a density of $\sim 5x10^6$ cells/ml, incubated with 0M to $10^{-4}$M P-factor before assaying for $\beta$-galactosidase activity, measured as $OD_{420}/10^6$ cells. Results are the means ± S.E.M. of triplicate determinations from three independent isolates. Experimental data from Smith et al., 2009. For the simulations the concentration of ligand was varied over the range 0-100 $\mu$M following 16 h simulated induction. Output from the model shows the accumulation of activated $G\alpha_{GTP}$Effector complexes over the duration of the simulated assay.

Simulations demonstrated the model is able to qualitatively reproduce most of the relationships observed in the experimental data (compare Figure 4.18, A to B). Removal of RGS results in increased basal and decreased maximal response compared to 1 x RGS, doubling RGS concentration reduces basal but increases maximal response and 3 x RGS renders the RGS to only have a negative influence by decreasing both basal and maximal response. Simulations from the model are able to reproduce the pattern observed in the data in terms of increasing RGS concentration resulting in a decreased sensitivity to ligand, but the extent of the decrease in sensitivity due to change in RGS concentration is much

more modest than that observed in experimental data ($pEC_{50}$; No RGS = 7.106 ± 0.102, 1 x RGS = 7.081 ± 0.091, 2 x RGS = 6.958 ± 0.111 and 3 x RGS = 6.912 ± 0.106). The inclusion of PM trafficking of RGS to the Smith *et al.* model has therefore managed to maintain the relationship between RGS concentration and signalling response.

Additional validations of the final PM trafficking model of RGS function against experimental data were conducted. The model was found to qualitatively agree with experimental data from a range of experiments including conditions of Gpa1 overexpression, Mam2 overexpression and when expressing an Rgs1 insensitive Gpa1 (Appendix A).

### 4.3.4 Nucleotide Exchange Mutants

Gpa1 mutants that display altered nucleotide cycling capabilities have been characterised fully in Chapter 3 of this thesis. These mutants include $Gpa1^{Q244L}$, $Gpa1^{R218C}$ $Gpa1^{G243A}$ and the $Gpa1^{G83X}$ series of mutants. $Gpa1^{Q244L}$ is GTPase deficient (Dohlman and Thorner, 1997; Obara et al., 1991), displaying constitutive activity with increased basal signalling and maximal signalling approximately half that of *wild-type* levels (Chapter 3, Figure 3.11). Mutation of the 'arginine finger' of G$\alpha$ proteins is predicted to have compromised GTPase activity (Majumdar et al., 2006) and an equivalent mutation in Gpa1, $Gpa1^{R218C}$ has been shown to have similar activity to $Gpa1^{Q244L}$, being GTPase deficient but having reduced spontaneous activation, therefore reduced basal signalling (Chapter 3, Figure 3.11). $Gpa1^{G243A}$ is unable to exchange GDP for GTP and therefore remains inactive (Ladds et al., 2007) (Chapter 3, Figure 3.11). $Gpa1^{G83X}$ is an equivalent mutation of the Glycine residue that showed insensitivity to GAP activity in small monomeric G proteins (Barbacid, 1987; Bos, 1989). $Gpa1^{G83X}$ mutants showed different signalling characteristics depending on what the Glycine residue was replaced with (Chapter 3, Figure 3.12). The final PM trafficking model of RGS function (Table 4.7) has been investigated to determine if it can simulate the signalling response observed for all of these mutants in the presence and absence of an RGS species. For each mutant G$\alpha$, the values for the reaction rate constants used to model the specific behaviours are the same as those identified when simulating the mutants using the Smith *et al.* model (Chapter 3: Table 3.6).

Simulations of $Gpa1^{Q244L}$ ($G\alpha^{(-GTPase,\ 10*spontaneous\ GDP->GTP)}$), $Gpa1^{R218C}$ ($G\alpha^{(-GTPase,\ 5*spontaneous\ GDP->GTP)}$) and $Gpa1^{G243A}$ ($G\alpha^{(no\ GDP\ release)}$) show good qualitative agreement with experimental data observed (compare Figure 4.19 to Figure 3.11).

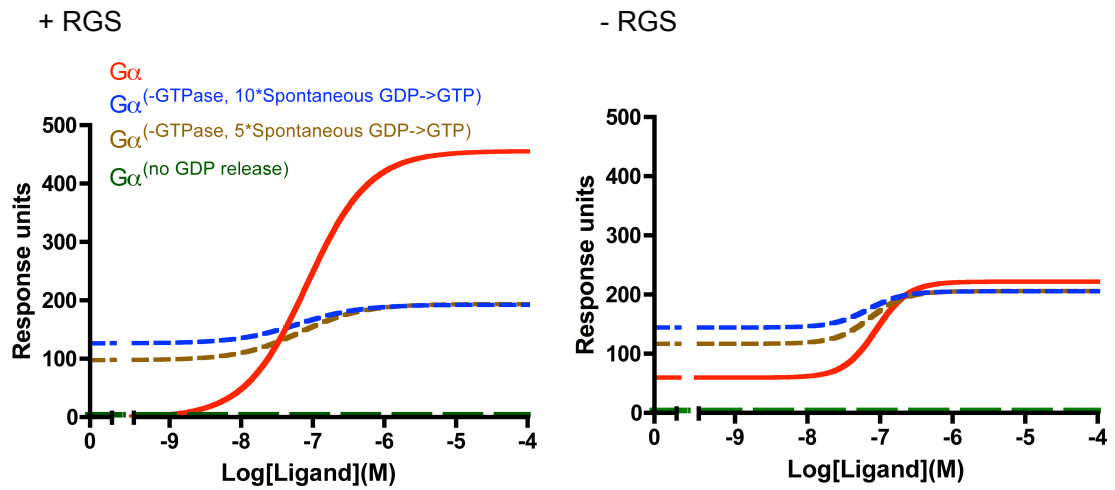


FIGURE 4.19: **Model testing: Gpa1 nucleotide exchange mutants.** Simulations from the model in Table 4.7 of G$\alpha$ species mutant variants in JY1285($\Delta$Gpa1) (+ RGS) and JY1287($\Delta$Gpa1,$\Delta$Rgs1) (-RGS) equivalent systems. Simulations are of Gpa1 (G$\alpha$), Gpa1$^{Q244L}$ (G$\alpha^{(-GTPase\ activity,\ 10*spontaneous\ GDP->GTP)}$), Gpa1$^{R218C}$ (G$\alpha^{(-GTPase\ activity,\ 5*spontaneous\ GDP->GTP)}$) and Gpa1$^{G243A}$ (G$\alpha^{(no\ GDP\ release)}$). The concentration of ligand in the simulation was varied over the range 0-100 $\mu$M following 16 h simulated induction. Output from the model shows the accumulation of activated G$\alpha_{GTP}$Effector complexes over the duration of the simulated assay.

Simulations of the Gpa1$^{G83X}$ mutants; Gpa1$^{G83V}$ (G$\alpha^{(-GTPase,\ \downarrow activation,\ \downarrow RGSbinding)}$), Gpa1$^{G83S}$ (G$\alpha^{(-GTPase,\ \downarrow activation)}$), Gpa1$^{G83L}$ (G$\alpha^{(un-activatable)}$), Gpa1$^{G83A}$ (G$\alpha^{(-GTPase)}$) again showed reasonable qualitative agreement with experimental data (compare Figure 4.20 to Chapter 3: Figure 3.12).

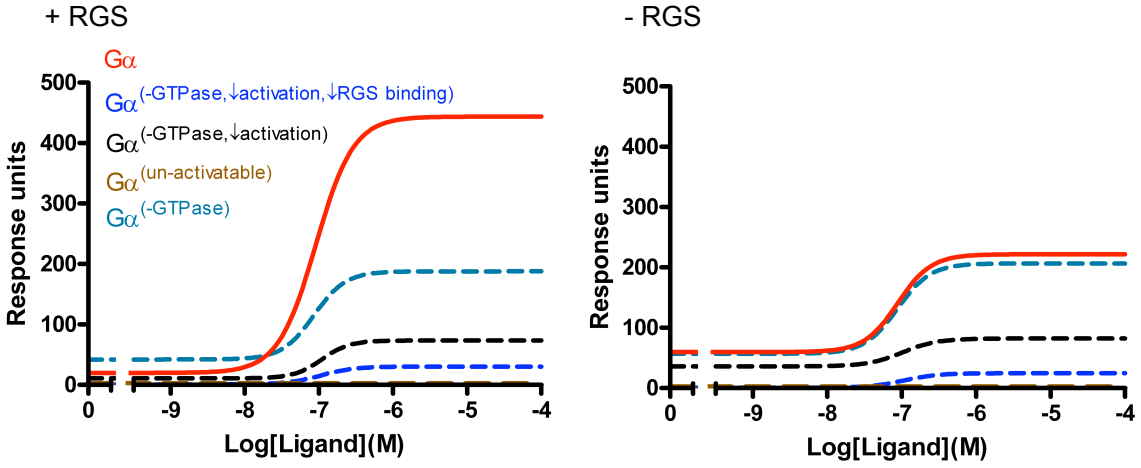


FIGURE 4.20: **Model testing: Gpa1 nucleotide exchange mutants (Gpa1$^{G83X}$).** Simulations from the model in Table 4.7 of G$\alpha$ species mutant variants in JY1285($\Delta$Gpa1) (+ RGS) and JY1287($\Delta$Gpa1,$\Delta$Rgs1) (- RGS) equivalent systems. Simulations are of Gpa1 (G$\alpha$), Gpa1$^{G83V}$ (G$\alpha^{(-GTPase,\ \downarrow activation,\ \downarrow RGS\ binding)}$), Gpa1$^{G83S}$ (G$\alpha^{(-GTPase,\ \downarrow activation)}$), Gpa1$^{G83L}$ (G$\alpha^{(un-activatable)}$) and Gpa1$^{G83A}$ (G$\alpha^{(-GTPase)}$). The concentration of ligand in the simulation was varied over the range 0-100 $\mu$M following 16 h simulated induction. Output from the model shows the accumulation of activated G$\alpha_{GTP}$Effector complexes over the duration of the simulated assay.

As the final PM trafficking model of RGS function is capable of reproducing much of the experimental data regarding G$\alpha$ mutants, this makes it very useful as a tool for predicting G$\alpha$ mutants characteristics and the model can be used to speculate exactly how particular mutants are influencing signalling response. It also suggests that the final model maintains a good agreement with the physiological events and dynamics surrounding the core element of the model, which is the nucleotide cycling of the G protein.

### 4.3.5 G$\beta\gamma$ as the Signal Propagator

A major strength of any cell signalling model is if it can be generalised to accurately simulate signalling data from different organisms and not just data from the signalling system used to develop the model. In some GPCR signalling systems it is the G$\beta\gamma$ dimer that is the propagator of a downstream signalling response rather than the G$\alpha_{\mathrm{GTP}}$. One such system is the mating-response pathway in budding yeast *S. cerevisiae* (Dohlman, 2002). We investigated whether the PM trafficking model of RGS function (Table 4.7) was capable of simulating such a G$\beta\gamma$-mediated signalling pathway when appropriately modified making G$\beta\gamma$ the signal propagator (Table 4.9). To convert our model to having G$\beta\gamma$ as the signal propagator, the reaction scheme was changed such that the downstream Effector species is activated by G$\beta\gamma$ rather than G$\alpha_{\mathrm{GTP}}$ (Table 4.9, reaction $k_{12}$). Additionally, reactions involving inertG$\alpha_{\mathrm{GTP}}$ are removed as inertG$\alpha_{\mathrm{GTP}}$ cannot be formed, therefore such reactions would have no contribution to the simulated response.

The plasma membrane trafficking model of RGS function with G$\beta\gamma$ as the signal propagator (Table 4.9) was simulated with RGS species concentration unchanged at 60 nM (RGS), doubled to 120 nM (2 x RGS), with RGS species concentration at 0 nM (No RGS) and with a G$\alpha$ species unable to hydrolyse GTP (G$\alpha^{(-GTPase)}$) (Figure 4.21).

| | | | | |
|---|---|---|---|---|
| ligand / G protein binding | $L + R \rightarrow LR$ | $k_1$ | 0.0025 | $nM^{-1}h^{-1}$ |
| | $G\alpha\beta\gamma + R \rightarrow RG\alpha\beta\gamma$ | $k_2$ | 0.005 | $nM^{-1}h^{-1}$ |
| | $G\alpha\beta\gamma + LR \rightarrow LRG\alpha\beta\gamma$ | $k_3$ | 0.02 | $nM^{-1}h^{-1}$ |
| | $L + RG\alpha\beta\gamma \rightarrow LRG\alpha\beta\gamma$ | $k_4$ | 0.005 | $nM^{-1}h^{-1}$ |
| | $L + RRGS_m \rightarrow LRRGS_m$ | $k_5$ | 0.005 | $nM^{-1}h^{-1}$ |
| | $G\alpha\beta\gamma + RRGS_m \rightarrow RRGS_mG\alpha\beta\gamma$ | $k_6$ | 0.005 | $nM^{-1}h^{-1}$ |
| | $G\alpha\beta\gamma + LRRGS_m \rightarrow LRRGS_mG\alpha\beta\gamma$ | $k_7$ | 0.02 | $nM^{-1}h^{-1}$ |
| | $L + RRGS_mG\alpha\beta\gamma \rightarrow LRRGS_mG\alpha\beta\gamma$ | $k_8$ | 0.005 | $nM^{-1}h^{-1}$ |
| G protein activation | $LRG\alpha\beta\gamma \rightarrow G\alpha_{GTP} + G\beta\gamma + LR$ | $k_9$ | 50 | $h^{-1}$ |
| | $G\alpha\beta\gamma \rightarrow G\alpha_{GTP} + G\beta\gamma$ | $k_{10}$ | 0.2 | $h^{-1}$ |
| | $LRRGS_mG\alpha\beta\gamma \rightarrow G\alpha_{GTP} + G\beta\gamma + LRRGS_m$ | $k_{11}$ | 40 | $h^{-1}$ |
| | $Effector + G\beta\gamma \rightarrow G\beta\gamma Effector$ | $k_{12}$ | 10 | $nM^{-1}h^{-1}$ |
| RGS trafficking | $RGS_c \rightarrow RGS_m$ | $k_{13}$ | 0.0005 | $h^{-1}$ |
| | $RGS_m \rightarrow RGS_c$ | $k_{14}$ | 0.005 | $h^{-1}$ |
| | $R + RGS_c \rightarrow RRGS_m$ | $k_{15}$ | 0.1 | $nM^{-1}h^{-1}$ |
| | $RRGS_m \rightarrow R + RGS_m$ | $k_{16}$ | 100 | $h^{-1}$ |
| | $LR + RGS_c \rightarrow LRRGS_m$ | $k_{17}$ | 0.1 | $nM^{-1}h^{-1}$ |
| | $LRRGS_m \rightarrow LR + RGS_m$ | $k_{18}$ | 100 | $h^{-1}$ |
| | $RG\alpha\beta\gamma + RGS_c \rightarrow RRGS_mG\alpha\beta\gamma$ | $k_{19}$ | 0.1 | $nM^{-1}h^{-1}$ |
| | $RRGS_mG\alpha\beta\gamma \rightarrow RG\alpha\beta\gamma + RGS_m$ | $k_{20}$ | 0.1 | $h^{-1}$ |
| | $LRG\alpha\beta\gamma + RGS_c \rightarrow LRRGS_mG\alpha\beta\gamma$ | $k_{21}$ | 0.1 | $nM^{-1}h^{-1}$ |
| | $G\alpha_{GTP} + RGS_c \rightarrow RGS_mG\alpha_{GTP}$ | $k_{22}$ | 60 | $nM^{-1}h^{-1}$ |
| | $RGS_mG\alpha_{GTP} \rightarrow G\alpha_{GTP} + RGS_c$ | $k_{23}$ | 0.05 | $h^{-1}$ |
| switching off / recycling G protein | $G\beta\gamma Effector \rightarrow G\beta\gamma + Effector$ | $k_{24}$ | 1 | $h^{-1}$ |
| | $G\alpha_{GTP} \rightarrow G\alpha_{GDPP}$ | $k_{25}$ | 0.005 | $h^{-1}$ |
| | $G\alpha_{GTP} + RGS_m \rightarrow RGS_mG\alpha_{GTP}$ | $k_{26}$ | 500 | $nM^{-1}h^{-1}$ |
| | $RGS_mG\alpha_{GTP} \rightarrow G\alpha_{GDPP} + RGS_c$ | $k_{27}$ | 2.5 | $h^{-1}$ |
| | $G\alpha_{GTP} + LRRGS_m \rightarrow LRRGS_mG\alpha_{GTP}$ | $k_{28}$ | 100 | $nM^{-1}h^{-1}$ |
| | $LRRGS_mG\alpha_{GTP} \rightarrow G\alpha_{GDPP} + LRRGS_m$ | $k_{29}$ | 2.5 | $h^{-1}$ |
| | $G\alpha_{GTP} + RRGS_m \rightarrow RRGS_mG\alpha_{GTP}$ | $k_{30}$ | 0.5 | $nM^{-1}h^{-1}$ |
| | $RRGS_mG\alpha_{GTP} \rightarrow G\alpha_{GDPP} + RRGS_m$ | $k_{31}$ | 0.5 | $h^{-1}$ |
| | $G\alpha_{GDPP} \rightarrow G\alpha_{GDP} + P$ | $k_{32}$ | 1000 | $h^{-1}$ |
| | $G\alpha_{GDP} + G\beta\gamma \rightarrow G\alpha\beta\gamma$ | $k_{33}$ | 1000 | $nM^{-1}h^{-1}$ |
| | $P \rightarrow \emptyset$ | $k_{34}$ | 10 | $h^{-1}$ |

TABLE 4.9: **Final plasma membrane trafficking model of RGS function with G$\beta\gamma$ as the signal propagator.** This reaction scheme has been adapted from Table 4.7 to signal through G$\beta\gamma$. G$\beta\gamma$ interacts with the downstream Effector species instead of G$\alpha_{GTP}$ (reaction $k_{12}$). As G$\alpha_{GTP}$ never contacts an Effector species, inertG$\alpha_{GTP}$ does not form, therefore reactions involving inertG$\alpha_{GTP}$are omitted from this model.

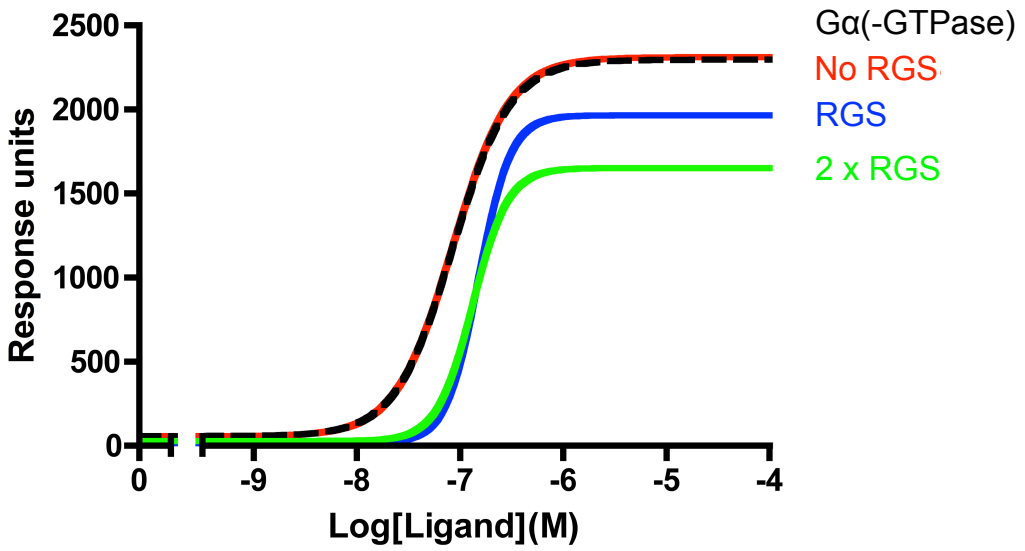


FIGURE 4.21: **Model testing: G$\beta\gamma$ as signal propagator.** Simulations are of the final plasma membrane trafficking model of RGS function, modified such that G$\beta\gamma$ is the signal propagator (Table 4.9). The model is simulated with RGS concentration at 60 nM (RGS), with RGS concentration at 120 nM (2 x RGS), without RGS (No RGS) and with a G$\alpha$ species that is unable to hydrolyse GTP (G$\alpha^{-GTPase}$). For simulations, the concentration of ligand was varied over the range 0-100 $\mu$M following 16 h simulated induction. Output from the model shows the accumulation of activated G$\beta\gamma$Effector complexes over the duration of the simulated assay.

Removing RGS, or blocking GTP hydrolysis of G$\alpha$ has the same effect, increasing basal and maximal response and ligand sensitivity (Figure 4.21). Doubling the RGS concentration results in additional negative regulation of signalling through reduction in maximal response. The results of these simulations are in close agreement with published data (Dohlman, 2002) and they indicate that in systems where G$\beta\gamma$ is the signal propagator RGS proteins can only negatively regulate signalling.

## 4.4 Use of the Model as a Predictive Tool

Extensive testing of the PM trafficking model of RGS function has been completed by comparing model output against a large bank of experimental data. Imaging work with fluorescently labelled GPCR and RGS proteins has also provided further evidence to support the hypothesis of this model. Given this confidence in the model, we could then use it to predict system level signalling behaviour under perturbed conditions of interest.

### 4.4.1 Increasing RGS Concentration at the Plasma Membrane

The PM trafficking model of RGS function places large emphasis on a requirement for RGS to be localised in the correct subcellular compartment at the PM for it to be able to exert GAP activity on G$\alpha_{\text{GTP}}$. The main role of the interaction between the R and RGS species

is to promote this PM localisation by tethering RGS in close proximity to G$\alpha$. If PM localisation is an absolute requirement for RGS to function and the overriding purpose of the R-RGS interaction is in promoting this localisation, then the effects on signalling seen when the interaction is blocked should be compensated for by increasing RGS at the PM through other mechanisms.

#### 4.4.1.1 Modelling an Increase in RGS at the Plasma Membrane

To simulate increased RGS at the PM, the reaction rate of RGS trafficking to the membrane by diffusion ($RGS_c \rightarrow RGS_m$) can be increased. In the unmodified system, the rate of this reaction (Table 4.7, $k_{13}$) is just 0.0005 $h^{-1}$. To increase RGS at the membrane, this reaction rate is increased 10,000-fold so that $k_{13} = 5\ h^{-1}$. Simulations of this modified system indicate that increased membrane localisation of RGS has little effect on the signalling profile other than to slightly increase the maximal signalling output (Figure 4.23, A). The model therefore predicts that the only effect of increasing Rgs1 concentration in a *wild-type* cell would be to enhance maximal signalling activity. To test this prediction through experimental assay of reporter strains requires modifications that would enhance the PM localisation of Rgs1.

#### 4.4.1.2 Enhancing Plasma Membrane Localisation of Rgs1

Testing the model prediction that increasing PM localisation of RGS will enhance maximal signalling was achievable through modifications to the Rgs1 protein. To increase PM localisation of Rgs1, the protein had to be modified to contain PM targeting regions. The *S. pombe* G$\alpha$ subunit, Gpa1 has been observed at a PM localisation (Figure 4.22, Gpa1-GFP). Furthermore, truncated versions of Gpa1 have previously been investigated for their localisation to reveal the region responsible for membrane targeting. The N-terminal region of Gpa1 contains myristoylation and palmitoylation sites that target the protein to the PM and the first 40 amino acids of Gpa1 alone have been found to be sufficient to target cytosolic proteins to the PM in *S. pombe* (Godfrey, PhD Thesis, 2009) (Figure 4.22, $^{1-40}$*Gpa*1-GFP). By fusing the first 40 amino acids of Gpa1 ($^{1-40}$*Gpa*1) to Rgs1-GFP in frame at the N-terminus, an Rgs1 protein is created that should have increased PM localisation. To confirm this, the *sxa2>lacZ* reporter strain lacking Mam2 (removing the possibility of Mam2 driven Rgs1 localisation) JY1291(ΔMam2, ΔRgs1) was transformed with the vector pREP3x expressing $^{1-40}$Gpa1-Rgs1-GFP or pREP3x expressing Rgs1-GFP. These transformed strains were grown in minimal media before imaging with a DeltaVision wide-field deconvolution microscope (Figure 4.22).

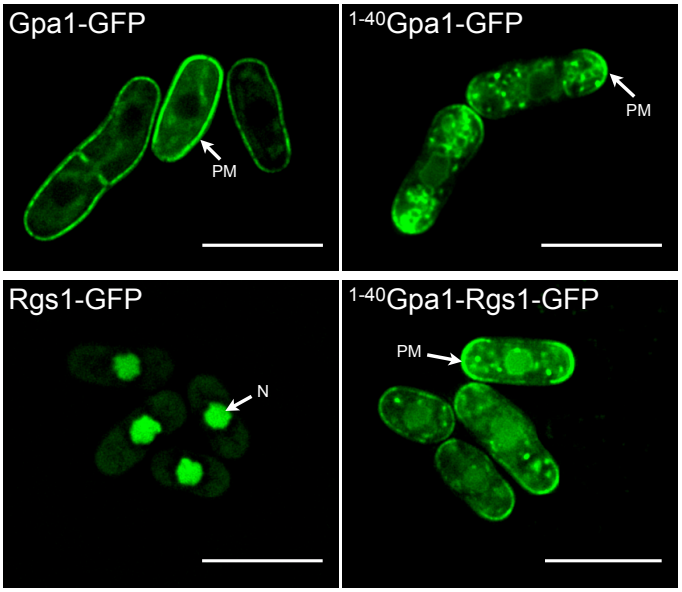


FIGURE 4.22: **Increasing Rgs1 plasma membrane localisation.** Strains lacking endogenous Gpa1 were transformed with vector pREP3x expressing either full length Gpa1 (Gpa1-GFP) or the first 40 amino acids of Gpa1 ($^{1-40}$Gpa1-GFP) fused at their C-terminus to GFP. Strains lacking endogenous Rgs1 and endogenous Mam2 were transformed with vector pREP3x expressing either Rgs1 fused at the C-teminus to GFP (Rgs1-GFP) or Rgs1-GFP fused at the N-terminus to the first 40 amino acids of Gpa1 ($^{1-40}$Gpa1-Rgs1-GFP). Cells were cultured in minimal media before imaging using a DeltaVision wide-field deconvolution microscope. Images are representative of three independent transformations, N = Nucleus, PM = Plasma Membrane and scale bar = 10 $\mu$m.

Imaging shows that $^{1-40}$Gpa1-Rgs1-GFP is detected in the nucleus, cytosol and also at the PM, whilst Rgs1-GFP is only detected in the nucleus and the cystosol in strains lacking endogenous Rgs1 and Mam2 (Figure 4.22). Fusing the first 40 amino acids of Gpa1 to Rgs1 is therefore able to promote increased PM localisation of Rgs1 even in the absence of any receptors.

Having achieved an Rgs1 that has enhanced PM localisation, the prediction of the model that increasing PM localisation of RGS should increase maximal response could be tested. The *sxa2>lacZ* reporter strain JY630(ΔRgs1) was transformed with the vector pREP3x expressing $^{1-40}$Gpa1-Rgs1-GFP and with pREP3x expressing Rgs1-GFP. The transformed strains were grown in minimal media, incubated with P-factor at concentrations of 0M to $10^{-4}$M and assayed for induction of the *sxa2>lacZ* reporter (Figure 4.23, B).

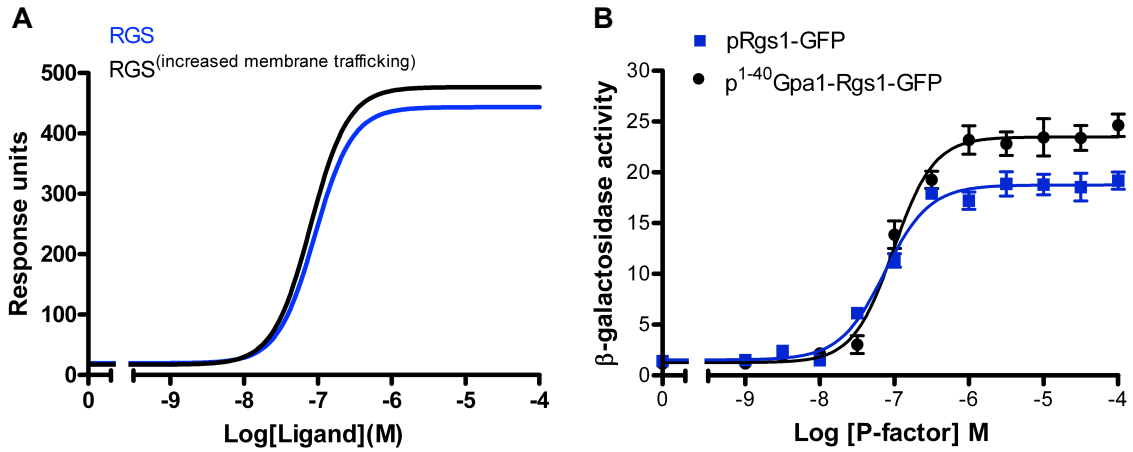


| | Basal | Maximal | $pEC_{50}$ |
|---|---|---|---|
| pRgs1-GFP | 1.535 +/- 0.440 | 18.750 +/- 0.359 | 7.131 +/- 0.051 |
| $p^{1-40}$Gpa1-Rgs1-GFP | 1.257 +/- 0.549 | 23.490 +/- 0.481** | 7.013 +/- 0.048 |

FIGURE 4.23: **Signalling activity with increased plasma membrane localisation of RGS.** Simulations are from the PM trafficking model of RGS function (Table 4.7) with an unmodified RGS species (RGS) and an RGS species that has increased capacity to become membrane localised through increasing the reaction rate for $RGS_c \rightarrow RGS_m$ 10,000-fold ($RGS^{(increased\ membrane\ trafficking)}$). The concentration of ligand was varied over the range 0-100 $\mu$M following 16 h simulated induction and output from the model shows the accumulation of activated $G\alpha_{GTP}$Effector complexes over the duration of the simulated assay (A). Reporter strain JY630($\Delta$Rgs1) was transformed with vector pREP3x expressing either Rgs1 fused at the C-teminus to GFP (pRgs1-GFP) or Rgs1-GFP fused at the N-terminus to the first 40 amino acids of Gpa1 ($p^{1-40}$Gpa1-Rgs1-GFP). Cells were cultured in minimal media to a density of $\sim$5x$10^6$ cells/ml, incubated with 0M to $10^{-4}$M P-factor before assaying for $\beta$-galactosidase activity, measured as $OD_{420}/10^6$ cells (B). Results are the means $\pm$ S.E.M. of triplicate determinations from three independent isolates. The table summarises the mean $\pm$ S.E.M. basal, maximal and $pEC_{50}$ values from B and significant difference to pRgs1-GFP is indicated with **($p$<0.01) as determined by unpaired $t$ test.

Data from the *in vivo* assay (Figure 4.23, B) proves the model prediction to be correct, with maximal $\beta$-galactosidase activity increasing significantly from 18.750 $\pm$ 0.359 for Rgs1-GFP to 23.490 $\pm$ 0.481 for $^{1-40}$Gpa1-Rgs1-GFP (unpaired $t$, $p$<0.01). There is no additional significant effect on either basal signalling or sensitivity to ligand, suggesting that increasing PM localisation only has influence on enhancing the positive regulatory role of Rgs1. As the positive role of Rgs1 is facilitated through the recycling of the inert state $G\alpha_{GTP}$, this suggests that following ligand induced G protein activation, the G$\alpha$ subunit remains at the PM, therefore increasing Rgs1 at the PM could result in more efficient recycling of inert $G\alpha_{GTP}$.

#### 4.4.1.3 Increasing Plasma Membrane Localisation of RGS to Compensate for a Lack of GPCR-RGS Interaction

It has been demonstrated that increasing the PM localisation of RGS effects signalling response when RGS remains still capable of interacting with the receptor, both through simulation of the model and through assay of $^{1-40}$Gpa1-Rgs1-GFP (Figure 4.23). The final

PM trafficking model of RGS function (Table 4.7) predicts PM localisation of Rgs1 to be required for it to function as a GAP on G$\alpha$ and interaction with the tail of Mam2 has been shown through fluorescence imaging to be a major facilitator of this PM localisation. To further investigate the importance of PM localisation of RGS, the model was used to test whether increasing the concentration of RGS species at the PM could compensate for a lack of R-RGS interaction. To achieve this, the model was simulated having increased the rate of reactions trafficking RGS to the membrane by random diffusion ($k_{13} = k_{13}$ *10,000 $h^{-1}$), but in the same simulation also blocking any interaction of R with RGS ($k_{15} = 0$ $nM^{-1}h^{-1}$, $k_{17} = 0$ $nM^{-1}h^{-1}$, $k_{19} = 0$ $nM^{-1}h^{-1}$, $k_{21} = 0$ $nM^{-1}h^{-1}$). For comparison, the simulated response of this system having no R-RGS interactions, but increased rate of trafficking RGS to the PM (No interaction + $RGS^{(increased\ membrane\ trafficking)}$), is compared to the unmodified system response (RGS) and the response when R-RGS interaction is blocked, but RGS trafficking is unchanged (No interaction + RGS) (Figure 4.24).

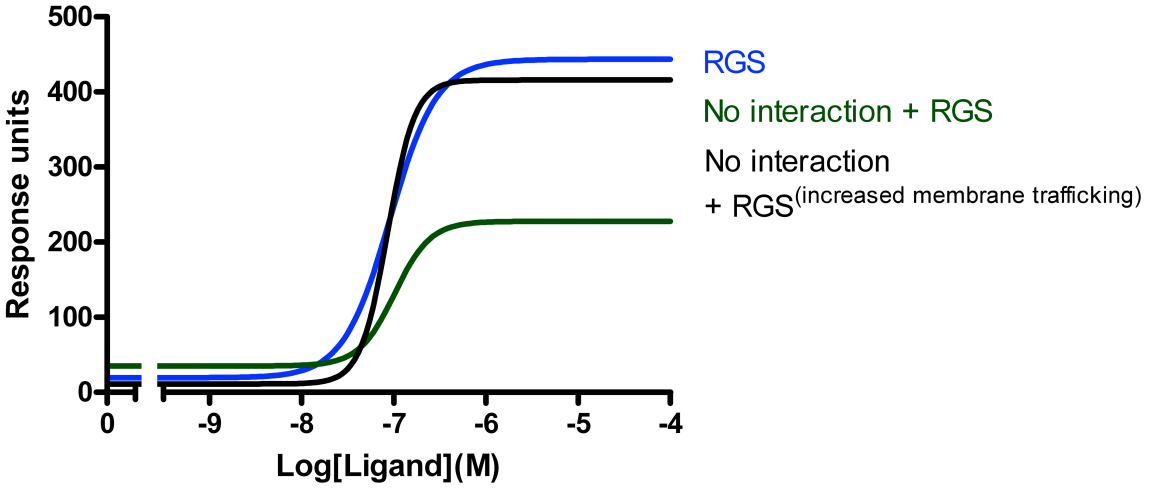


FIGURE 4.24: **Model simulation: Compensating for a lack of interaction by increased membrane trafficking of RGS.** Simulations are from the plasma membrane trafficking model of RGS function (Table 4.7) with an unmodified RGS species (RGS), the systems whereby GPCR-RGS interaction is blocked (No interaction + RGS) and the system whereby the GPCR-RGS interaction is blocked, but RGS has increased capability to become plasma membrane localised independently of an interaction (No interaction + $RGS^{(increased\ membrane\ trafficking)}$). The concentration of ligand was varied over the range 0-100 $\mu$M following 16 h simulated induction and output from the model shows the accumulation of activated $G\alpha_{GTP}$Effector complexes over the duration of the simulated assay.

Simulated responses predict that the lack of an interaction between the receptor and the RGS protein can be overcome by simulating more RGS at the PM. In doing this, although there is no interaction, basal and maximal signalling response is returned to close to the *wild-type* levels (Figure 4.24). The model therefore predicts PM localisation is sufficient for RGS function and that the role of the interaction is to place RGS at the PM to facilitate its function.

To experimentally test the prediction of the model required the expression of an Rgs1 protein targeted to the PM in a strain lacking the C-terminal tail of Mam2. Initially, activity of fluorescently labelled Rgs1 (Rgs1-GFP) and the membrane targeted Rgs1 ($Gpa1^{1-40}$Rgs1-GFP) was characterised when co-expressed with a fluorescently labelled full length receptor (Mam2-mCherry). A reporter strain lacking endogenous Rgs1 and Mam2; JY1291(ΔRgs1, ΔMam2) was co-transformed with pREP4xMam2-mCherry and pREP3xRgs1-GFP or pREP4xMam2-mCherry and pREP3x$Gpa1^{1-40}$Rgs1-GFP. These two transformed strains were grown in minimal media before imaging with a DeltaVision wide-field deconvolution microscope (Figure 4.25, A). Signalling activity of these strains was also characterised by incubating with P-factor at concentrations of 0M to $10^{-4}$M and assaying for induction of the *sxa2>lacZ* reporter (Figure 4.25, B).

Images results (Figure 4.25, A) confirm that in the presence of the C-terminal tail of Mam2, Rgs1-GFP and $Gpa1^{1-40}$Rgs1-GFP will colocalise with Mam2 at the PM. Assay of signalling activity (Figure 4.25, B) indicates that these co-expressed strains are capable of P-factor induced signalling response, therefore confirming the functionality of the labelled proteins.

We have determined through assays of signalling activity (Figure 4.25, B) that in the presence of a full length receptor, both Rgs1 and $Gpa1^{1-40}$Rgs1 are functional in terms of regulating the signalling response, but it is unproven whether this regulation can be recovered when Rgs1 is targeted to the PM in strains lacking the C-terminal tail of Mam2. To investigate this, reporter strain JY1291(ΔRgs1, ΔMam2) was co-transformed with pREP4xMam2Δtail-mCherry and pREP3xRgs1-GFP or pREP4xMam2Δtail-mCherry and pREP3x$Gpa1^{1-40}$Rgs1-GFP. Transformed strains were grown in minimal media before imaging with a DeltaVision wide-field deconvolution microscope (Figure 4.26, A). Signalling activity of these strains was also characterised by incubating with 0M to $10^{-4}$M P-factor and assaying for induction of the *sxa2>lacZ* reporter (Figure 4.26, B).

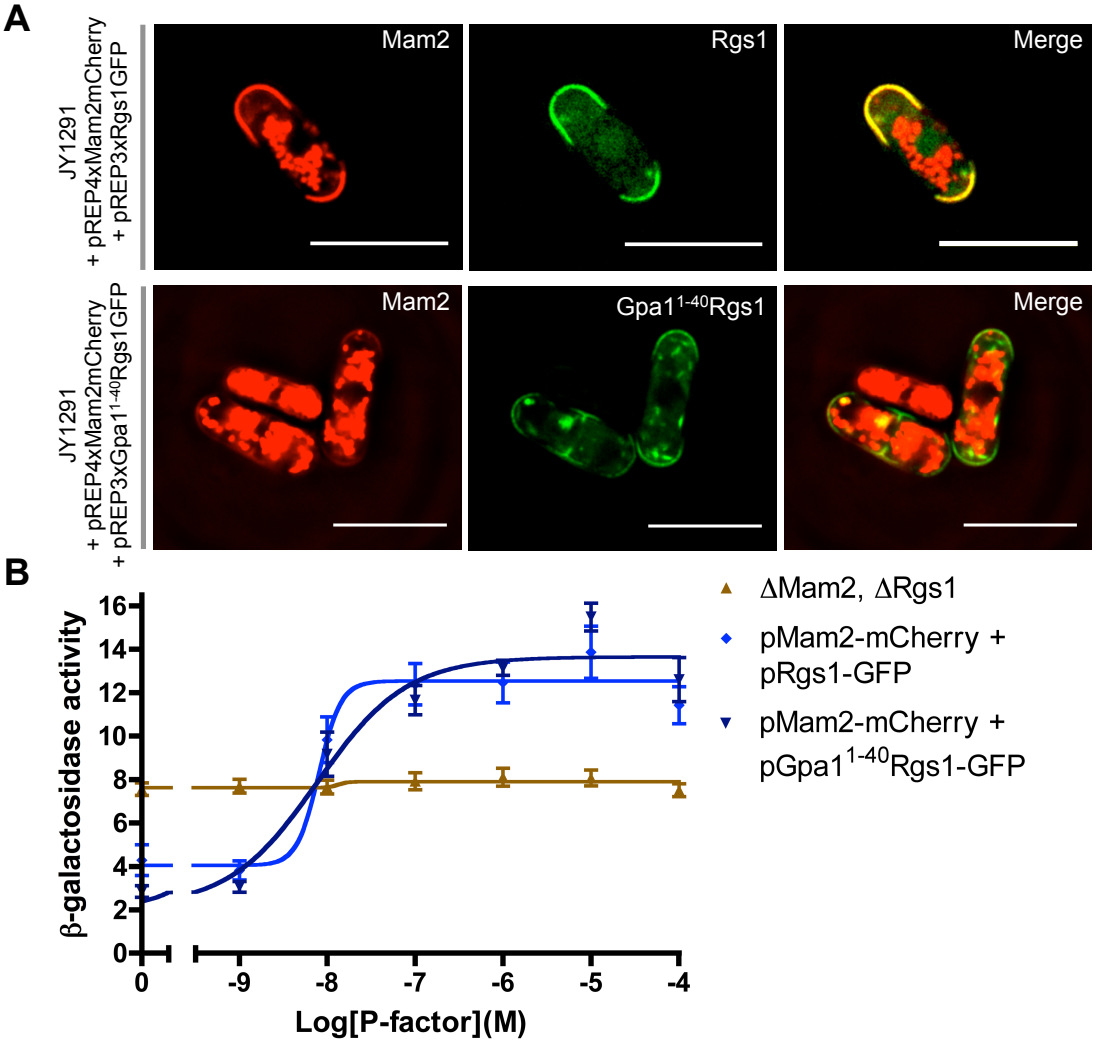


| | Basal | Maximal | $pEC_{50}$ |
|---|---|---|---|
| ΔMam2, ΔRgs1 | 7.621 +/- 0.236 | 7.901 +/- 0.193 | N/A |
| pMam2-mCherry + pRgs1-GFP | 4.045 +/- 0.914 | 12.530 +/- 0.470 | 8.095 +/- 2.117 |
| pMam2-mCherry + pGpa1$^{1-40}$Rgs1-GFP | 2.123 +/- 1.134 | 13.650 +/- 0.541 | 8.110 +/- 0.197 |

FIGURE 4.25: **Enhancing plasma membrane localisation of Rgs1 in the presence of full length Mam2.** Reporter strain JY1291(ΔRgs1, ΔMam2) was co-transformed with Mam2-mCherry expressed from vector pREP4x and either Rgs1-GFP or Gpa1$^{1-40}$Rgs1-GFP expressed from vector pREP3x. These two transformed strains were grown in minimal media and imaged using a DeltaVision wide-field deconvolution microscope (A). Cells from strain JY1291 and the two transformed strains were cultured in minimal media to a density of ~5x10$^6$ cells/ml, incubated with 0M to $10^{-4}$M P-factor before assaying for $\beta$-galactosidase activity, measured as $OD_{420}/10^6$ cells. Results are the means ± S.E.M. of triplicate determinations from three independent isolates (B). The table summarises the mean ± S.E.M. basal, maximal and $pEC_{50}$ values.

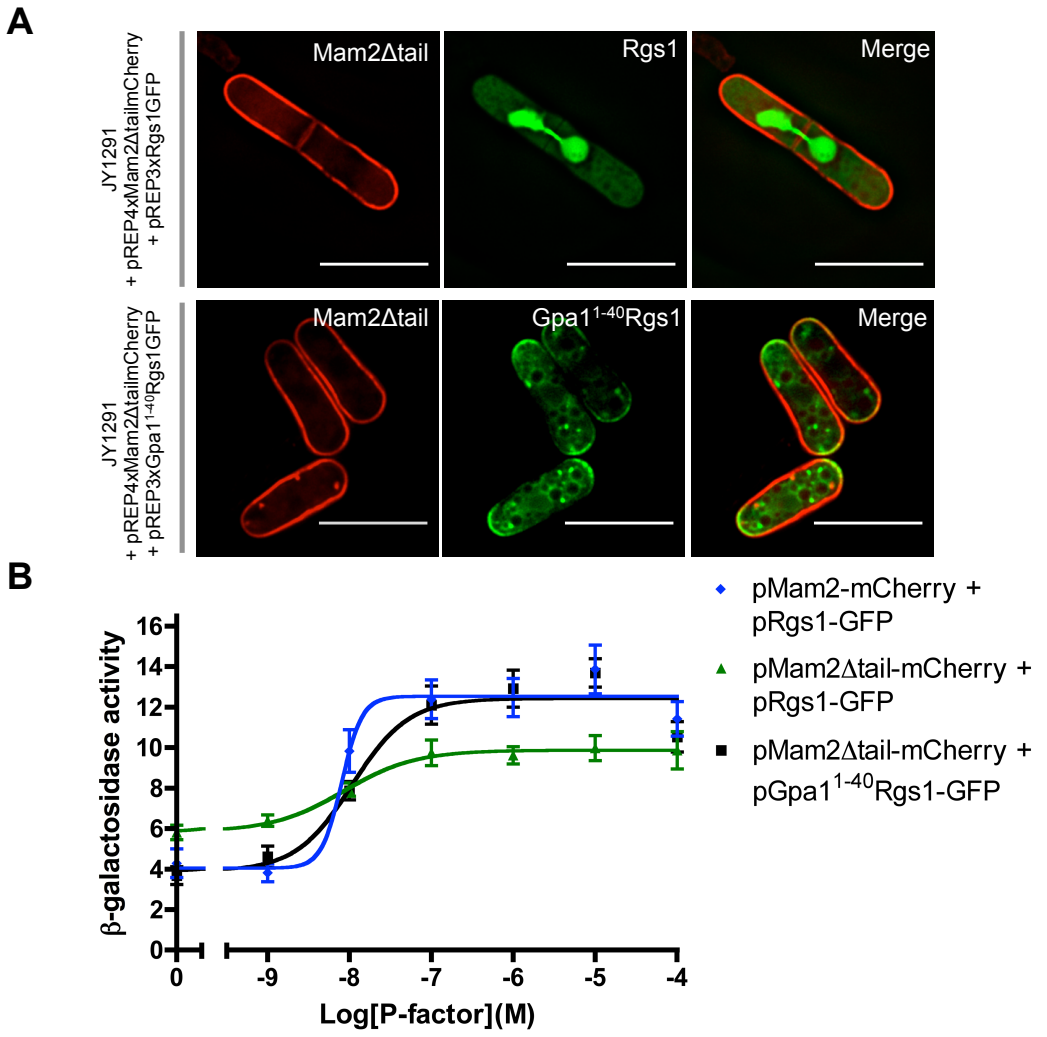


| | Basal | Maximal | $pEC_{50}$ |
|---|---|---|---|
| pMam2-mCherry + pRgs1-GFP | 4.045 +/- 0.914 | 12.530 +/- 0.470 | 8.095 +/- 2.117 |
| pMam2Δtail-mCherry + pRgs1-GFP | 5.843 +/- 0.575 | 9.873 +/- 0.302 | 8.070 +/- 0.273 |
| pMam2Δtail-mCherry + $p^{1\text{-}40}$Gpa1-Rgs1-GFP | 3.907 +/- 0.787 | 12.420 +/- 0.500 | 7.967 +/- 0.160 |

FIGURE 4.26: **Enhancing plasma membrane localisation of Rgs1 in the absence of the Mam2 C-terminal tail.** Reporter strain JY1291(ΔRgs1, ΔMam2) was co-transformed with Mam2Δ-mCherry expressed from vector pREP4x and either Rgs1-GFP or $Gpa1^{1-40}$Rgs1-GFP expressed from vector pREP3x. These two transformed strains were grown in minimal media and imaged using a DeltaVision wide-field deconvolution microscope (A). Cells from strain JY1291 and the two transformed strains were cultured in minimal media to a density of ~5x$10^6$ cells/ml, incubated with 0M to $10^{-4}$M P-factor before assaying for $\beta$-galactosidase activity, measured as $OD_{420}/10^6$ cells. Results are the means ± S.E.M. of triplicate determinations from three independent isolates (B). The table summarises the mean ± S.E.M. basal, maximal and $pEC_{50}$ values.

Imaging data (Figure 4.26, A) indicates that PM localisation of Rgs1 is maintained through the attachment of the first 40 amino acids of Gpa1, even in the absence of the receptor tail. The *wild-type* Rgs1 protein no longer localises at the PM upon removal of the tail. Assays of these strains show that in the absence of the receptor tail, a strain containing the membrane targeted Rgs1 ($Gpa1^{1-40}$Rgs1-GFP) displays reduced basal signalling and

increased maximal signalling, similar to a strain containing full length Mam2 and Rgs1. The imaging and assay data taken together indicate that PM localisation is sufficient to recover Rgs1 regulation of signalling, even in the absence of the receptor tail. These data therefore confirm the model prediction that PM localisation is vital for Rgs1 function and it is the tail of the Mam2 that is required to facilitate this PM localisation.

#### 4.4.1.4 Increasing RGS Concentration When Lacking a GPCR-RGS Interaction

The final PM trafficking model of RGS function allows some RGS species to become localised at the PM through mechanisms other than the interaction with the receptor. Given this, and the knowledge that molecules within the cell exist in a very crowded environment, and diffuse in a stochastic manner, we investigated whether the compensation observed for a lack of GPCR-RGS interaction, achieved by promoting more PM attachment of RGS could also be achieved simply by increasing the concentration of RGS within the cell. Through increasing the number of RGS molecules inside the cell, this would possibly force more collisions between RGS and $G\alpha_{GTP}$ at the PM. To test this theory in the model, simulations were completed of the unchanged model (GPCR) and the model having blocked any R-RGS interaction (described previously) at the same time as varying the RGS concentration in the system from 0 nM (No RGS) to 180 nM (3 x RGS) (Figure 4.27).

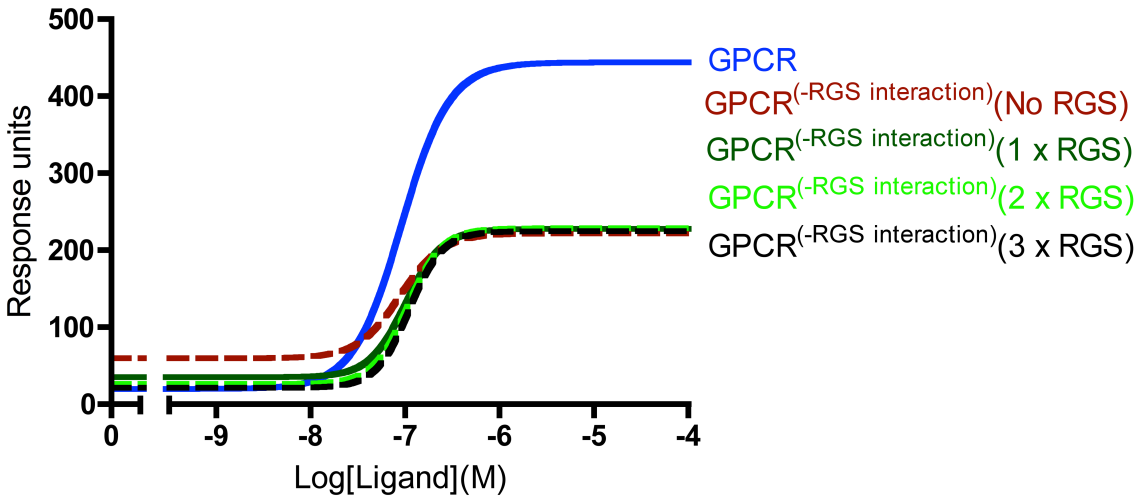


FIGURE 4.27: **Model simulation: Increasing RGS concentration in a system lacking GPCR-RGS interaction.** Simulations of the model system in Table 4.7 with an unmodified system (GPCR) and whereby GPCR-RGS interaction is blocked along with setting RGS concentration to RGS=0 ($GPCR^{(-RGSinteraction)}$(No RGS)), RGS = 60 nM ($GPCR^{(-RGSinteraction)}$(1 x RGS)), RGS = 120 nM ($GPCR^{(-RGSinteraction)}$(2 x RGS)) and RGS = 180 nM ($GPCR^{(-RGSinteraction)}$(3 x RGS)). The concentration of ligand was varied over the range 0-100 $\mu$M following 16 h simulated induction and output from the model shows the accumulation of activated $G\alpha_{GTP}$Effector complexes over the duration of the simulated assay.

Simulations of the model (Figure 4.27) predict that the only effect on signalling of increasing the RGS concentration in a system lacking a GPCR-RGS interaction is to reduce ligand-independent response. This suggests, that to compensate for a lack of interaction, it is not sufficient to simply increase concentration of RGS and implies that compensation requires RGS to be tethered to the PM. It is possible that the temporal regulation of RGS at the PM plays an important role, in that the RGS species has to be maintained at the membrane for a period of time, sufficient for it to function efficiently, enabling the recycling of the G protein, thus generating high maximal signalling response.

## 4.5 Additional Role for the Mam2 C-terminal Tail

We have observed through assays of reporter strains, imaging and supported by a mathematical model that an interaction of RGS with the C-terminal tail of a GPCR can be a key regulatory event in signalling through a GPCR. The tail of Mam2 influences signalling response through directing the spatial regulation of Rgs1, but this is not likely to be the only role for the tail.

### 4.5.1 Mam2Δtail-Rgs1 Fusion

Further evidence for the influence of the receptor tail on signalling that is independent of its role in directing PM localisation of Rgs1, can be gleaned by assaying the signalling activity of Mam2Δtail fused to Rgs1. Reporter strain JY1291 (ΔRgs1, ΔMam2) was transformed with expression vectors expressing both Mam2 and Rgs1 (pREP3xMam2 + pREP4xRgs1), both Mam2Δtail and Rgs1 (pREP3xMam2Δtail + pREP4xRgs1), the Mam2-Rgs1 fusion complex (pREP3xMam2-Rgs1) and a complex of Mam2 lacking its C-terminal tail fused in frame to Rgs1 (pREP3xMam2Δtail-Rgs1). These strains were grown in minimal media and incubated with P-factor at concentrations of 0M to $10^{-4}$M before assaying for induction of *sxa2>lacZ* (Figure 4.28).

The Mam2Δtail-Rgs1 fusion data (Figure 4.28) indicates that fusing Rgs1 to Mam2Δ tail can compensate for the lack of the tail, resuming a close to *wild-type* dose-response profile in terms of basal and maximal signalling activity (pMam2Δtail-Rgs1 in Figure 4.28). Comparing signalling profiles for the two fusion proteins Mam2Δtail-Rgs1 and Mam2-Rgs1, indicates that the fusion lacking the C-terminal receptor tail has increased P-factor sensitivity ($pEC_{50}$; pMam2Δtail-Rgs1 = 7.060 ± 0.089 vs pMam2-Rgs1 = 6.171 ± 0.073). This not only provides additional support for our model, implying the requirement for interaction of Mam2 with Rgs1, but also implies an additional role of the C-terminal receptor tail in controlling sensitivity of signalling response to ligand. GPCR C-terminal tails are known to also control receptor trafficking, therefore it is possible that the increased sensitivity observed when the tail is removed is a result of a lack of the desensitisation mechanism, usually

achieved through receptor tail promoted internalisation. Such a desensitisation mechanism protects against ligand overstimulation through internalising the receptor, therefore removing the possibility of any further receptor stimulation. The C-terminal tail of a GPCR can contribute to this by providing sites that become phosphorylated through the activity of receptor kinases in response to ligand stimulation. Phosphorylation then triggers receptor internalisation.

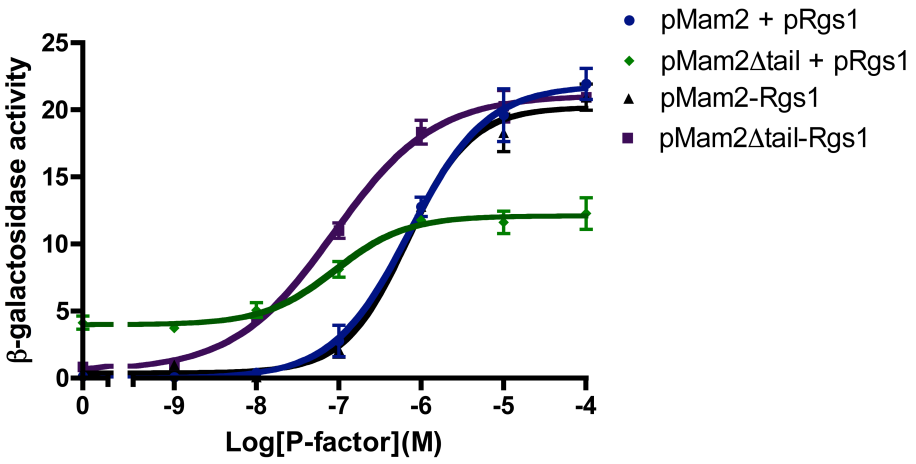


| | Basal | Maximal | $pEC_{50}$ |
|---|---|---|---|
| pMam2 + pRgs1 | 0.007 +/- 0.596 | 21.840 +/- 0.956 | 6.139 +/- 0.095 |
| pMam2Δtail + pRgs1 | 3.987 +/- 0.481 ** | 12.100 +/- 0.462 *** | 7.050 +/- 0.153 ** |
| pMam2-Rgs1 | 0.389 +/- 0.474 | 20.190 +/- 0.679 | 6.171 +/- 0.073 |
| pMam2Δtail-Rgs1 | 0.524 +/- 0.619 | 21.100 +/- 0.593 | 7.060 +/- 0.089 ** |

FIGURE 4.28: **Signalling activity of a Mam2Δtail-Rgs1 fusion.** Reporter strain JY1291(ΔRgs1, ΔMam2) was transformed with vectors expressing both Mam2 and Rgs1 (pMam2 + pRgs1), both Mam2Δtail and Rgs1 (pMam2Δtail + pRgs1), the Mam2-Rgs1 fusion complex (pMam2-Rgs1) and a complex of Mam2 lacking its C-terminal tail fused in frame to Rgs1 (pMam2Δtail-Rgs1). These strains were grown in minimal media to a density of ~5x$10^6$ cells/ml, incubated with 0M to $10^{-4}$M P-factor before assaying for $\beta$-galactosidase activity, measured as $OD_{420}/10^6$ cells. Results are the means ± S.E.M. of triplicate determinations from three independent isolates. The table summarises the mean ± S.E.M. basal, maximal and $pEC_{50}$ values. Significant difference to pMam2 + pRgs1 is indicated with ***($p$<0.001), **($p$<0.01) or *($p$<0.05) as determined by unpaired $t$ test.

The influence of the tail of Mam2 on internalisation was investigated by expressing Mam2-GFP or Mam2Δtail-GFP from pREP3x in a strain lacking endogenous Mam2; JY1169(ΔMam2). These transformed strains were grown in minimal media, incubated with $10^{-5}$M P-factor for 6 h before imaging with a DeltaVision wide-field deconvolution microscope (Figure 4.29).

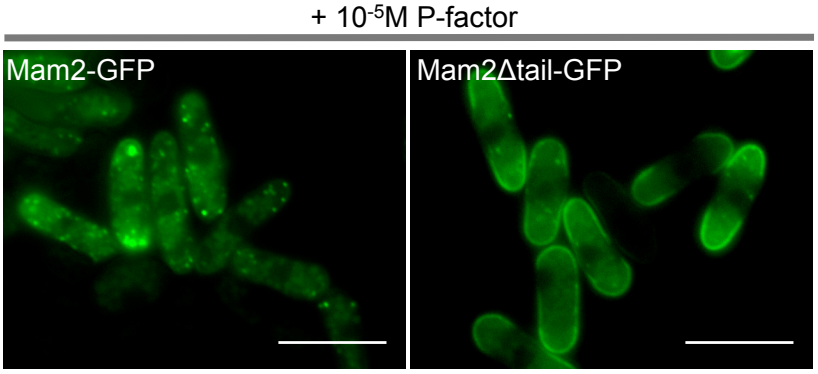


FIGURE 4.29: **Receptor internalisation: Mam2-GFP vs Mam2Δtail-GFP.** A strain deleted for its chromosomal copy of Mam2 (JY1169; ΔMam2) was transformed with the vector pREP3x expressing either full length Mam2 fused at the C-terminus to GFP (Mam2-GFP) or Mam2 truncated for its C-terminal tail fused to GFP (Mam2Δtail-GFP). Cells were grown in minimal media and incubated with P-factor at a concentration of $10^{-5}$M for a period of 6 h and images were then generated using a DeltaVision wide-field deconvolution microscope. Images are representative of three independent transformations and scale bar = 10 $\mu$m.

Imaging indicate that after induction with P-factor, Mam2-GFP is not detected on the PM, but in the cytoplasm and punctate structures on the inside of the cell. Mam2 lacking its C-terminal tail however, is clearly detected on the PM of the cell, primarily at the cell tips (Figure 4.29). This indicates that the tail is having a role in promoting P-factor induced internalisation of Mam2. This lack of internalisation for Mam2Δtail could explain the increased sensitivity observed for the Mam2Δtail-Rgs1 fusion protein (Figure 4.28).

## 4.6 Summary

An additional higher level of regulation of the mating-response in *S. pombe* has been identified, involving a probable interaction between the C-terminal tail of the GPCR Mam2, and the RGS protein Rgs1. Through quantitative assays using $\beta$-galactosidase reporter strains and mating efficiency assays, the removal of the tail has been demonstrated to have similar effects on signal transduction and mating efficiency to the removal of Rgs1, thus implicating a role for interaction between the Mam2 tail and Rgs1 in regulating Rgs1 function. Loss of the interaction through removal of the tail has a functional consequence in reducing a cells ability to mate.

Through fluorescence microscopy, the receptor tail has been implicated in the spatial regulation of Rgs1 within the cell. The tail of the receptor is confirmed as being required to localise Rgs1 at the PM of the cell, therefore placing Rgs1 in close proximity to its substrate G$\alpha$ protein Gpa1. Colocalisation of Mam2 and Rgs1 at the PM is only observed when full length Mam2 is being expressed and not when Mam2Δtail is expressed.

An iterative cycle of experimental data and mathematical modelling resulted in the Smith *et al.* ODE model (Smith et al., 2009) being extended to include an additional layer of regulation of the G protein mediated-signalling pathway, by including reactions for interactions between the GPCR and RGS species, and PM trafficking of RGS. The hypothesis built into the developing model was that PM localisation of RGS is essential for RGS to function as a GAP for GTP-bound G$\alpha$ species. To achieve agreement between experimental data and model simulations, this PM localisation of the RGS species was defined to occur through three mechanisms: RGS binding to the GPCR, RGS binding to GTP-bound G$\alpha$s and direct membrane contacts through random diffusion.

Additional data demonstrated that a fusion protein of Mam2-Rgs1 (thus forcing interaction within a cell) resulted in a *wild-type* signalling profile, which suggested that both Mam2 and Rgs1 can perform all their required roles when in a complex together. This result, along with the development of an additional GPCR-RGS fusion model of an equivalent system containing a fused GPCR-RGS species, prompted further refinements of the model to generate the final PM trafficking model of RGS function. This model includes additional reactions identified from experimental data and the GPCR-RGS fusion model that must be possible when the GPCR and RGS proteins are interacting.

Simulations from the final PM trafficking model of RGS function were compared to a bank of experimental data from $\beta$-galactosidase assays. The model could qualitatively reproduce all of the data that was also reproduced by the original Smith *et al.* model, including signalling activity of the Gpa1 nucleotide exchange mutants, characterised in Chapter 3. Additionally, the final model was able to reproduce signalling data from a different G protein-mediated signalling pathway in budding yeast, where G$\beta\gamma$ rather than G$\alpha$ is the signal propagator.

The model predicts that RGS regulatory activity that is lost when interaction with the receptor is blocked, could be recovered through increasing RGS concentration at the PM in a system with no GPCR-RGS interaction. To test the prediction, increased Rgs1 PM localisation was achieved in Mam2$\Delta$tail strains through fusion of Rgs1 to a 40 amino acid residue region of Gpa1 that targets to the PM. Increasing Rgs1 at the PM recovered the regulatory activity of Rgs1 in the absence of a Mam2-Rgs1 interaction, therefore implicating that PM localisation of Rgs1, primarily facilitated by the Mam2 tail is required for Rgs1 function.

Fusing Mam2$\Delta$tail to Rgs1 gives a signalling profile similar to the Mam2-Rgs1 fusion, but with increased sensitivity to ligand. This result suggests a role for the receptor tail, additional to its role in PM trafficking of Rgs1, that influences ligand sensitivity. The tail of Mam2 was observed to be required to promote receptor internalisation in response to P-factor stimulation, thereby implicating the tails involvement in desensitisation mechanisms. The increased sensitivity of Mam2$\Delta$tail, possibly as a result of a lack of receptor

internalisation can not be reproduced by the final model, therefore providing a possible avenue for future model development.

# Chapter 5

# Fluorescent Reporters of Signalling - From Population to Single Cell

## 5.1 Background

Previously, reporter systems have been used that contain a $\beta$-galactosidase gene in place of a non-essential pheromone-inducible gene (*sxa2*) (Didmon et al., 2002). This allows colourimetric determination of the quantity of signalling transmitted through the pathway of M-type cells following stimulation with the mating pheromone; P-factor. One limitation of this method is that cell lysis is required to release $\beta$-galactosidase to obtain a quantitative measure of signalling, therefore making time-series quantification from live cells impossible. Time-series quantification of live cells is possible using an alternative reporter system whereby *sxa2* is replaced with *mel1*, a gene encoding the secreted $\alpha$-galactosidase. This type of reporter has previously been used, but only for semi-quantitative plate based assays (Goddard et al., 2005). Another alternative is to use a fluorescent reporter gene in place of *sxa2*, which allows quantification through the measurement of fluorescence intensity resulting from accumulation of the fluorescent protein. Assays of cellular signalling responses to specific ligands are usually performed on a population of genetically identical cells, and the cell line is often engineered such that it will produce a quantifiable response to the stimulus. When performing such assays, measured is the average response of the entire population of cells. Previously, signalling data for the P-factor induced mating-response in *S. pombe* has been obtained by assays on populations by either colourimetric assay of $\beta$-galactosidase reporters (Didmon et al., 2002; Ladds et al., 2003, 2007) or fluorescence plate-reader assays of fluorescent reporter strains (Chapter 3 and Smith, PhD Thesis, 2010). In order to investigate cell-cell variation in the signalling response, and to obtain temporal dynamics for the initiation, length of time and termination of the signalling response it is necessary to quantify signalling response at the single cell level.

## 5.2 A Comparison of Two Different Fluorescent Reporters

The characteristics of a particular fluorescent protein used as a reporter of signalling can affect the sensitivity and interpretability of data obtained from fluorescent reporter assays. The *sxa2>GFP* reporter (JY1325) has been characterised (Smith, PhD Thesis, 2010) and its use as a reporter to characterise mutant signalling protein behaviour has been demonstrated in Chapter 3. The folding time, stability and brightness of the fluorescent reporter protein are possibly three major factors that implicate its suitability for use as a transcriptional reporter. GFP gives a very bright signal, but has a slow maturation time (Shaner et al., 2005), which can hinder the ability to evaluate processes occurring on a short time scale such as within a single cell cycle. Additionally, GFP is very stable, therefore making it difficult to evaluate when the signalling response is terminated following initial stimulation. An alternative fluorescent reporter strain has been generated that has the yellow fluorescent protein Venus in place of *sxa2* within the *S. pombe* genome; JY1337(*sxa2>Venus*). Venus is a GFP derivative made from YFP and contains mutations that greatly accelerate the maturation of the fluorescent protein at 37$^{o}$C. It is also reported to show 10 to 100-fold stronger fluorescence than YFP in mammalian cells (Nagai, 2002). Given this enhanced maturation time, it was thought that this reporter may achieve more accurate temporal resolution of the signalling response and it was therefore characterised and compared to the *sxa2>GFP* reporter strain.

### 5.2.1 End-point Ligand Induced Response

The fluorescent reporter strains containing either GFP or Venus in place of *sxa2* in the *S. pombe* genome were assayed for their fluorescence intensity in response to P-factor stimulation. The two strains were grown in minimal media before being transferred on to growth media agarose plugs containing 0M to $10^{-5}$M P-factor. Cells were incubated on the plugs for 16 h at 30$^{o}$C before assaying for fluorescence intensity (relating to induction of *sxa2>GFP* or *sxa2>Venus*) of the population on the plug, using a Berthold Mithras fluorescence microplate-reader (Figure 5.1, A and B). Fluorescence units are calculated by correcting fluorescence intensity at given wavelengths for GFP and Venus detection by a measure of cell number calculated by the OD at 620 nm (GFP fluorescence units = fluorescence intensity at 535 nm/$OD_{620}$ ; Venus fluorescence units = fluorescence intensity at 530 nm/$OD_{620}$).

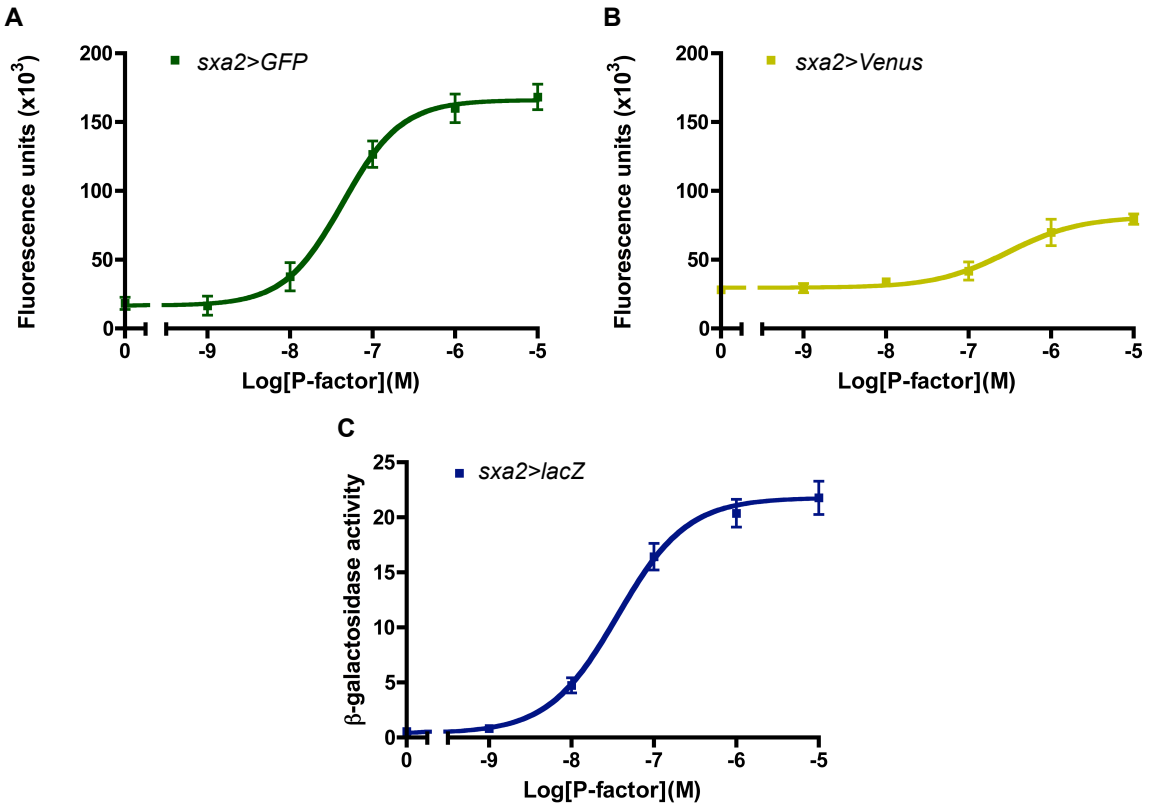


| | Basal | Maximal | $pEC_{50}$ |
|---|---|---|---|
| *sxa2>GFP* | 16.664 x10³ +/- 6.258 x10³ | 166.061 x10³ +/- 6.435 x10³ | 7.360 +/- 0.110 |
| *sxa2>Venus* | 29.708 x10³ +/- 3307 x10³ | 81.288 x10³ +/- 7.013 x10³ | 6.524 +/- 0.252 |
| *sxa2>lacZ* | 0.379 +/- 0.806 | 21.780 +/- 0.634 | 7.440 +/- 0.010 |

FIGURE 5.1: **GFP vs Venus: Dose-response assays.** Cells from the GFP fluorescent reporter strain; JY1325(*sxa2>GFP*) (A) and Venus fluorescent reporter strain; JY1337(*sxa2>Venus*) (B) were cultured to a density of ~5x$10^6$ cells/ml and transferred onto minimal growth media agarose plugs containing 0M to $10^{-5}$M P-factor. P-factor induced transcription of the fluorescent reporter was measured following 16 h induction with P-factor. Fluorescence units describe the fluorescence emitted from the cell population corrected for cell density (*sxa2>GFP* = fluorescence intensity at 535 nm/$OD_{620}$, *sxa2>Venus* = fluorescence intensity at 530 nm/$OD_{620}$). A *wild-type* dose-response profile from colourimetric assay of a $\beta$-galactosidase reporter strain (C) is included for comparison Results are means ± S.E.M. of duplicate determinations from two independent isolates. The table summarises the mean ± S.E.M. basal, maximal and $pEC_{50}$ values.

Dose-response assays (Figure 5.1) indicate some differences between the fluorescent genes used as *sxa2* reporters. Both reporters give sigmoidal dose-response profiles, but using Venus as a transcriptional reporter results in an increased basal fluorescence compared to GFP (29.708 ± 3.307x$10^3$ fluorescence units vs 16.664 ± 6.258x$10^3$ fluorescence units), a decreased maximal fluorescence (81.288 ± 7.013x$10^3$ fluorescence units vs 16.6061 ± 6.435x$10^3$ fluorescence units) and a decreased sensitivity to ligand ($pEC_{50}$; 6.524 ± 0.252 vs 7.360 ± 0.110). This suggests that the two fluorescent reporters have different properties, therefore resulting in differences in the dose-response profiles. In comparing dose-responses from the fluorescent reporter strains to the $\beta$-galactosidase reporter (Figure 5.1, C), the *sxa2>GFP* reporter strain bares the most similarity, whereas the *sxa2>Venus* reporter

strain displays a less sensitive response. Additionally the signal from the *sxa2>Venus* reporter cells is relatively low, indicating that Venus may not fluoresce as brightly as GFP in *S. pombe*.

### 5.2.2 Monitoring Signalling Response With Time

In addition to using the reporters to quantify dose-dependent signalling response of the population at a specific end-point, time-series quantification of response is also possible. The *sxa2>GFP* and *sxa2>Venus* reporter strains were grown in minimal media before being transferred to growth media agarose plugs containing 0M to $10^{-5}$M P-factor. Cells were incubated on the plugs at 30°C for 16 h inside a Berthold Mithras fluorescence microplate-reader. The fluorescence intensity from the cell population on the plugs was measured at 30 min intervals starting at 0 h (Figure 5.2).

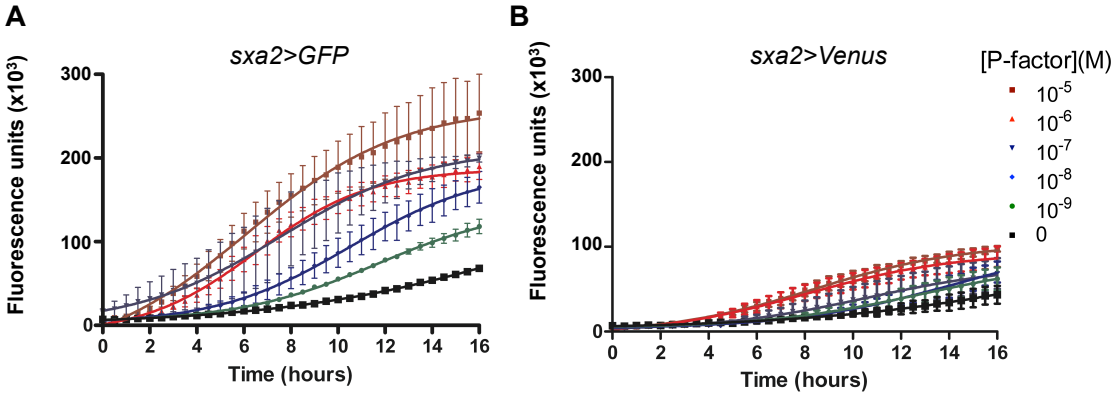


FIGURE 5.2: **GFP vs Venus: Time-series assays.** Cells from the GFP reporter strain; JY1325(*sxa2>GFP*) (A) and Venus reporter strain; JY1337(*sxa2>Venus*) (B) were cultured to a density of ~5x$10^6$ cells/ml and transferred onto minimal growth media agarose plugs containing 0M to $10^{-5}$M P-factor. P-factor induced transcription of the fluorescent reporter was measured at time = 0 h and every 30 min following addition of cell culture onto the P-factor containing agarose plugs. Fluorescence units describe the fluorescence emitted from the cell population corrected for cell density (*sxa2>GFP* = fluorescence intensity at 535 nm/$OD_{620}$, *sxa2>Venus* = fluorescence intensity at 530 nm/$OD_{620}$). Results are means ± S.E.M. of duplicate determinations from two independent isolates.

Comparing the time-series response of the *sxa2>Venus* reporter population to the *sxa2>GFP* reporter population again indicates a far brighter fluorescence from the *sxa2>GFP* reporter. The proposed enhanced maturation time of Venus (Nagai, 2002) is not apparent here, with induction of a response occurring at ~2 h for the *sxa2>Venus* reporter at maximal P-factor concentration of $10^{-5}$M (Figure 5.2).

Fluorescent reporters have the added benefit of allowing signalling response of a cell population to be visualised using fluorescence microscopy. Imaging of the *sxa2>Venus* and *sxa2>GFP* reporter strains was compared at different time-points following the addition of a high concentration ($10^{-5}$M) of P-factor (Figure 5.3). The two reporter strains were grown in minimal media containing $10^{-5}$M P-factor for a period of 10 h. Samples of the

cell cultures were removed every 2 h and imaged using a Leica SP5 scanning confocal microscope.

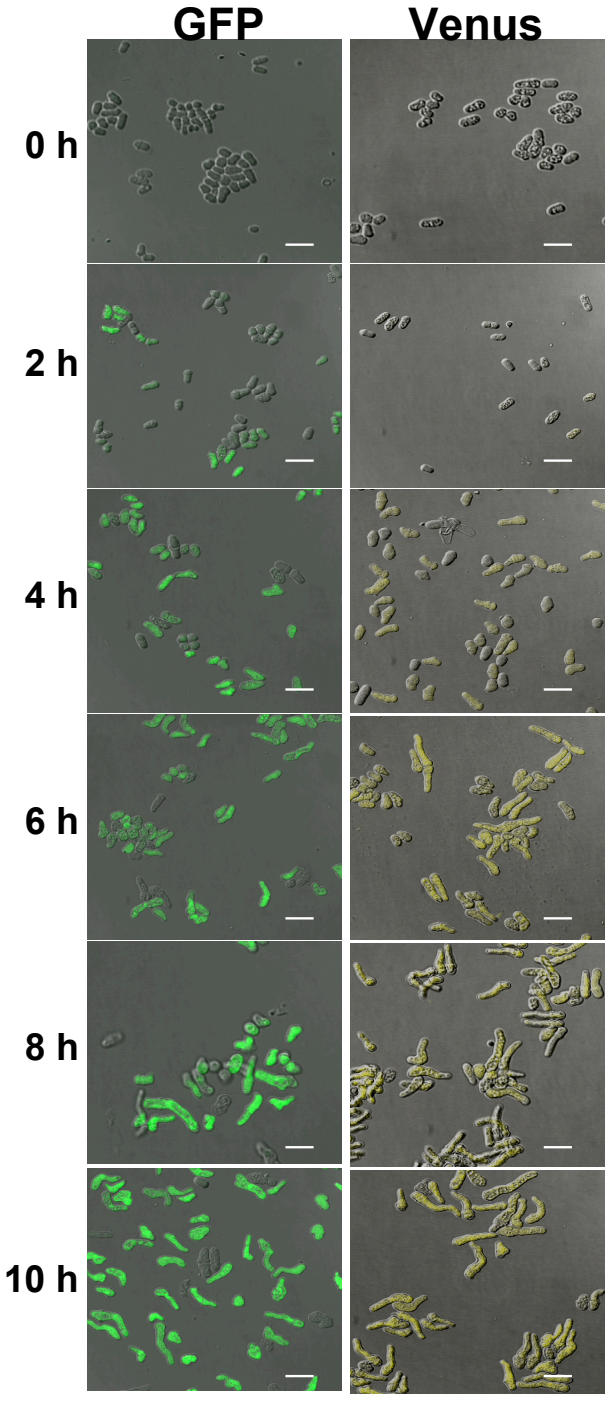


FIGURE 5.3: **Temporal response: GFP vs Venus endpoint fluorescence imaging.** Cells from the GFP reporter strain; JY1325(*sxa2>GFP*) and Venus reporter strain; JY1337(*sxa2>Venus*) were cultured to a density of ~5x10$^6$ cells/ml and incubated with P-factor at a concentration of $10^{-5}$M. A sample from each cell culture was removed and imaged every 2 h following the addition of P-factor for a period of 10 h. P-factor induced fluorescence of a randomly selected proportion of the cell population was captured using a Leica SP5 scanning microscope. Presented are overlays of the fluorescence and light-field images. Scale bar = 10 $\mu$m.

Results of the imaging experiment (Figure 5.3) indicate that both the *sxa2>Venus* and *sxa2>GFP* reporter strains have observably increased fluorescence with time following P-factor stimulation. Fluorescent cells can be seen from 2 h following stimulation, with Venus fluorescence appearing weaker in intensity compared to GFP. The main observable difference between the two reporters is the brightness in fluorescence, with GFP showing greater fluorescence intensity observable in the assays and imaging experiments of the fluorescent reporter strains.

Both the *sxa2>GFP* and *sxa2>Venus* reporter strains are capable of giving quantitative readouts of signal transduction through the mating-response pathway. They generate dose-response profiles that are similar to those obtained from $\beta$-galactosidase reporters (compare Figure 5.1, A and B to C). In addition to this, both fluorescent reporter strains (JY1325 and JY1337) give additional information on the time-dependent P-factor induced response and allow further qualitative data in terms of imaging the response. The purpose of the work presented in this chapter is to demonstrate improved quality and quantity of informative and quantitative data that can be gathered through new assays of signalling response using single cell measurements, and to highlight the insight this gives into cellular mechanisms involved in the regulation of signalling. As the *sxa2>GFP* reporter proved to give a more easily detectable P-factor induced response in terms of the intensity of fluorescence, this reporter strains was, for the most part, used in the rest of the work presented here.

## 5.3 Limitations of Population-based Assays

Population-based assays such as the colourimetric assay of the $\beta$-galactosidase reporter and fluorescence plate-reader assay of fluorescent reporters, measure an average response from the entire population of cells. Although this is a good way of quantifying signalling response on a population level, it has limitations in what can be learnt from the data. As these population-based assays do not quantify the response from individual cells within the population, it is difficult to obtain any insight into the distribution of response or the cell-to-cell variability within the population. Biological processes are inherently stochastic, therefore one cell's signalling response will never be identical to another. As well as there being variability in the amplitude of a signalling response, there is also variability in the timing of a response. Different cells will initiate a response at varying times following addition of P-factor and continue that response for varied durations. These factors contribute to population-based assays not being able to give a true reflection of the G protein-mediated signalling response at single cell level. Considering this, it would be advantageous to be able to quantify response from single cells rather than a whole population. One of the techniques by which single cell measurements can be obtained from fluorescent reporters is through flow cytometry (Jaroszeski and Radcliff, 1999). Flow cytometry is a tool that

allows the optical analysis of many thousands of individual particles (Jaroszeski and Radcliff, 1999). Included in the types of particle that can be measured are whole cells, as a result, this technology is used widely in biological and medical studies.

## 5.4 Flow Cytometry to Measure Population Distribution of Response

In order to obtain a more detailed understanding of signalling activity of the mating-response pathway, the *sxa2>GFP* reporter strain was subjected to analysis using a LSRII flow cytometer (BD Biosciences). The reporter strain JY1325(*sxa2>GFP*) was grown in minimal media and incubated with a range of P-factor concentrations from 0M to $10^{-5}$M. An aliquot of cell culture was removed every 1 h for 12 h following the addition of P-factor and analysed by flow cytometry. For each sample, 30,000 particles were counted and quantified for their induction of *sxa2>GFP* through measurement of the fluorescence intensity of the particle. Fluorescence is measured using the FITC flow cytometer settings (488 nm laser for excitation and emission detected with a 530 nm band pass filter and 505 nm long pass filter). The distributions of the populations at 12 h following P-factor addition are shown as histograms of fluorescence intensity vs frequency (Figure 5.4).

The main peak of the distribution shifts towards a greater fluorescence intensity as the P-factor concentration increases, indicating increased fluorescence intensity of the majority of the population with increased P-factor concentration (Figure 5.4). A shoulder is evident at each concentration at very low fluorescence intensity (FITC of ∼0-200), which indicates the presence of some dead cells within the population. The count of these dead cells increases as P-factor concentration increases. Overstimulation of the mating-response pathway is known to be a cause of increased cell death within a cell population (Weston *et al.,* in preparation). Addition of P-factor results in a 'narrowing' of the major distribution peak compared to 0M P-factor, confirming that P-factor is causing some synchronisation of the cells within the population. The addition of the mating pheromone P-factor has been shown previously to synchronise a population of *S. pombe* cells by promoting arrest in $G_1$ phase of the cell cycle (Davey and Nielsen, 1994).

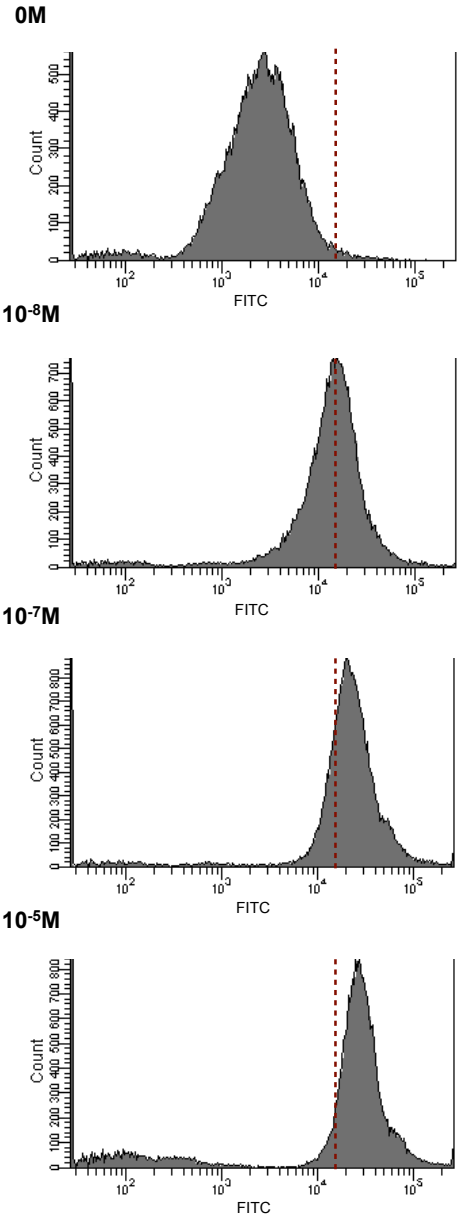


FIGURE 5.4: **Population-wide view of signalling response through flow cytometry analysis.** Fluorescent reporter strain JY1325(*sxa2>GFP*) was grown in minimal media and incubated with 0M to $10^{-5}$M P-factor for a period of 12 h before single cell analysis using a LSRII flow cytometer. A sample of the cell culture was analysed, quantifying the fluorescence intensity in the GFP channel (FITC) for 3x$10^4$ events. The graphs show fluorescence intensity vs frequency for each ligand concentration. The red dashed line represents a threshold set based on the data for 0M to segment the population into non-signalling cells (left of the line) and cells displaying a signalling response (right of the line).

The single particle measurements obtained through flow cytometry could be used to obtain an end-point quantification dose-response profile similar to that obtained from plate-reader-based population assays (Figure 5.1) through calculating the mean ±S.E.M. from the particle measurements at the final time-point in the experiments (12 h). An advantage of flow cytometry over plate-reader assay is that the cells identified as dead can be excluded

from the analysis. The population mean ±S.E.M. is calculated using only the estimated live-cell population (FITC >200) (Figure 5.5). A sigmoidal response profile is observed from 0M to $10^{-5}$M that is similar to that observed from plate-reader-based assays of the *sxa2>GFP* reporter strain, although data from the flow cytometry analysis shows a greater sensitivity to P-factor, possibly due to more accurate/sensitive measurement achieved through single particle measurements (compare Figure 5.5 to Figure 5.1, A).

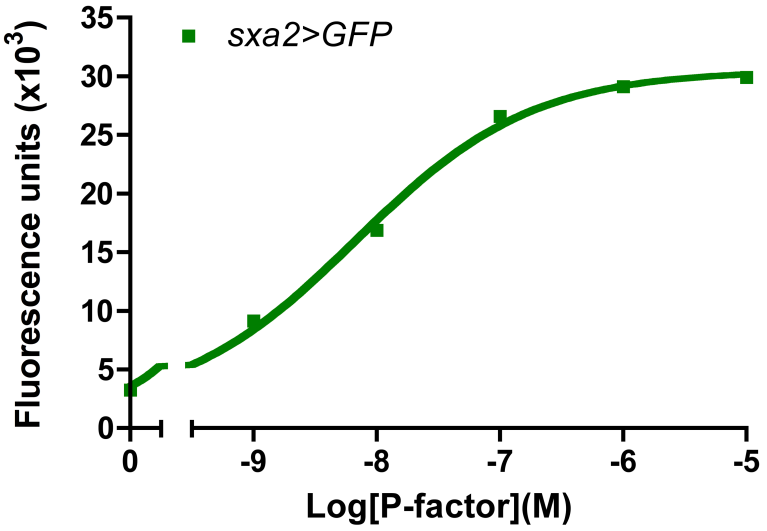


| | Basal (x10³) | Maximal (x10³) | pEC₅₀ |
|---|---|---|---|
| *sxa2>GFP* | 2.523 +/- 0.215 | 30.500 +/- 0.108 | 8.226 +/- 0.01638 |

FIGURE 5.5: **Ligand-dependent signalling response: Flow cytometry analysis of cell fluorescence.** Reporter strain JY1325(*sxa2>GFP*) was grown in minimal media and incubated with 0M to $10^{-5}$M P-factor for a period of 12 h before single cell analysis using a LSRII flow cytometer. A sample of the cell culture was analysed, quantifying the fluorescence intensity in the GFP channel (FITC) for $3x10^4$ events. From these events, the estimated live-cell population was identified (FITC>200). The table shows the mean ± S.E.M. of the basal and maximal fluorescence intensity from the estimated live-cell population.

Time-series population-based analysis of live-cell signalling response of fluorescent reporters is achievable through assays on the fluorescence plate-reader (Figure 5.2, A). Time-series analysis of population signalling response was also achieved by flow cytometry analysis, although flow cytometry is limited in that a different population of cells has to be analysed at each time-point due to sampling. Despite this limitation, this type of analysis allows detailed insight into population distribution change with time and average population signalling response with time that is comparable to data from plate-reader assays (compare Figure 5.6 to Figure 5.3, A).

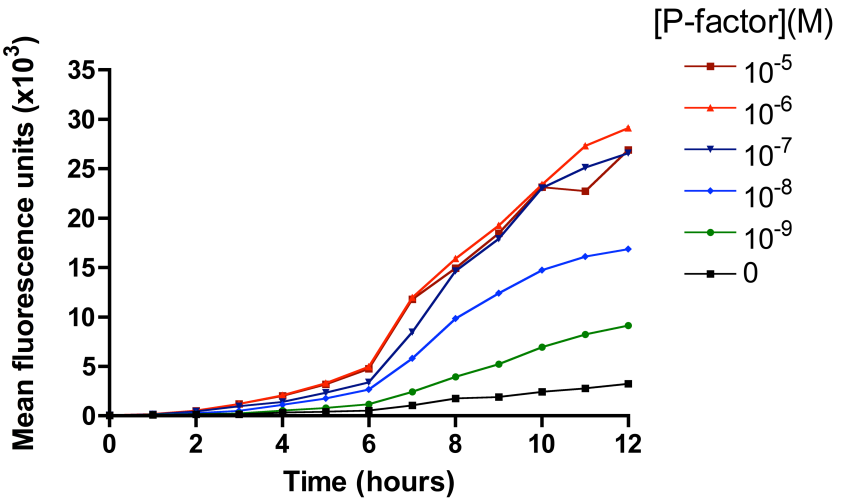


FIGURE 5.6: **Time-series signalling response: Flow cytometry analysis of cell fluorescence.** Reporter strain JY1325(*sxa2>GFP*) was grown in minimal media and incubated with 0M to $10^{-5}$M P-factor. Samples of the cell cultures were removed at 0 h and subsequently every hour for a period of 12 h to be analysed using a LSRII flow cytometer. For each cell culture sample at each time-point, the fluorescence intensity in the GFP channel (FITC) for $3x10^4$ individual events was calculated. From this the estimated live-cell population was identified (FITC>200). Results are the means ± S.E.M. from all events defined as being in the live-cell population.

Data from the time-course flow cytometry analysis (Figure 5.6) indicates a very similar mean transcriptional response pattern for P-factor concentrations from $10^{-7}$M to $10^{-5}$M in terms of both timing and amplitude, suggesting that the upper limits of the transcriptional response can be reached at $10^{-7}$M and any subsequent increase in P-factor concentration has little effect on this response. Transcriptional response at low ($10^{-9}$M) and intermediate ($10^{-8}$M) P-factor concentration appears to increase in a slightly graded fashion and gradual increase with time is also observed in the absence of any P-factor stimulation, probably as a result of the high stability of the GFP molecules.

Given the nature of the data from the flow cytometry analysis, it is possible to apply thresholds to the data to obtain estimates of the proportion of the population that have committed to a signalling response in terms of increased fluorescence intensity resulting from induction of *sxa2>GFP*. A threshold level of fluorescence intensity was set based on the population of non-responding cells (red dashed line in Figure 5.4, 0M). A cell is defined as having induced production of *sxa2>GFP*, and therefore having responded to P-factor, if its fluorescence value is greater than this defined threshold level. Of the 30,000 particles analysed, for each sample and at each time-point, it is then possible to identify cells that have responded and to quantify the responded cells as a percentage of the entire population. This gives insight into the timing of response and the effect of ligand concentration on the proportion of cells committing to a signalling response (Figure 5.7).

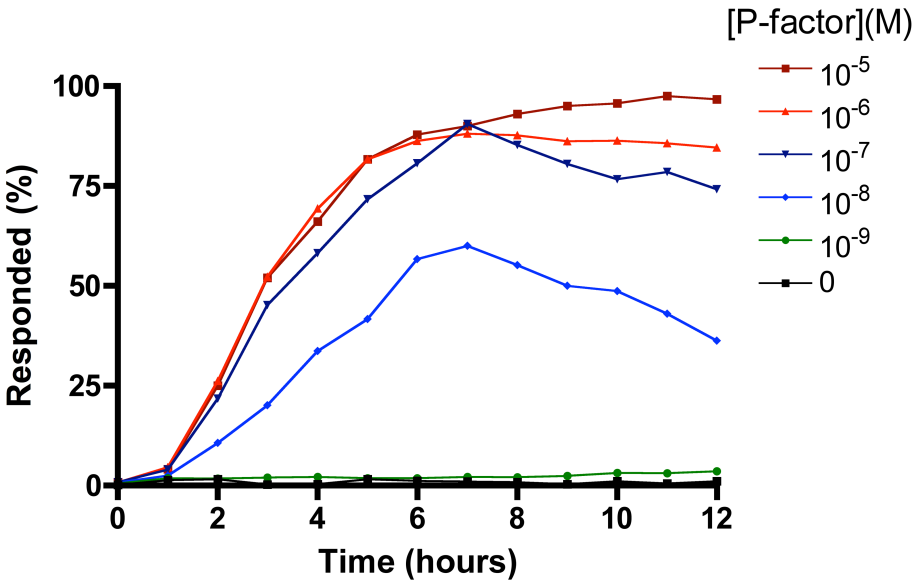


FIGURE 5.7: **Segmenting the signalling population with time: Flow cytometry analysis of cell fluorescence.** Reporter strain JY1325(*sxa2>GFP*) was grown in minimal media and incubated with 0M to $10^{-5}$M P-factor. Samples of the cell cultures were removed at 0 h and subsequently every hour for a period of 12 h to be analysed using a LSR II flow cytometer. For each cell culture sample at each time-point, the fluorescence intensity in the GFP channel (FITC) for $3x10^4$ individual events was calculated. The cell population was segmented into non-signalling and signalling cells as in Figure 5.4 to calculate the percentage of the cell population showing characteristics of a signalling response at each time-point.

Data indicates that the concentration of ligand influences the number of individual cells within the population that commit to the signalling response (Figure 5.7). Increasing ligand concentration from 0M to $10^{-8}$M results in a large increase in the proportion of the population that has responded (0M = 1.1 %, $10^{-8}$M = 36.3 % at 12 h). Increasing ligand concentration further to $10^{-7}$M results in another large increase in the percentage of the population that has responded ($10^{-7}$M = 74.2 % at 12 h). Increased concentration from $10^{-7}$M to $10^{-5}$M results in additional increase to close to the entire cell population responding at $10^{-5}$M.

These data suggest that at the single cell level there is a cell-fate 'decision' process that determines whether to commit to a signalling response or not, which relies on sensing the P-factor concentration gradient within the cell's environment. Increased concentration results in a larger number of cells committing to the response. The percentage of cells within the population that respond has a bearing on the average response quantified from the whole cell population, therefore the population level response has to be a combination of the number of cells that are signalling and the amplitude of that particular response.

Of the cells that respond, the timings of increase in percentage suggest that a response is triggered within 2 h of exposure to P-factor. The temporal dynamics of the signalling cascade from receptor activation through to initiation of gene transcription is likely to

occur in a much shorter timescale (seconds or minutes, rather than hours), but we can only observe the response once the fluorescent reporter protein has been transcribed, translated and matured, which is likely taking between 1-2 h to occur following stimulation.

Another method of investigating the dynamics of initiation of signalling response could be to quantify the cells that have arrested in $G_1$ phase of the cell cycle, as one of the cellular responses to P-factor is to arrest in $G_1$ phase in preparation for mating (Davey and Nielsen, 1994). By quantifying cells arrested in $G_1$ phase, this could give better temporal resolution on the initiation of a response that is not hampered by the long maturation times of a transcriptional reporter protein.

### 5.4.1 Time-series Analysis of $G_1$-arrest

Thus far, the response to P-factor stimulation has only been measured in terms of a transcriptional response from the *sxa2* promotor or change in cell morphology in terms of cell volume (Chapter 3). The mating-response in *S. pombe* provides an additional measurable feature to quantify signalling response, through the complement of genetic material within the cell. Staining cells with the DNA fluorochrome propidium iodide and subsequent flow cytometry analysis, can identify cells in $G_1$ phase of their cell cycle (Hutter and Eipel, 1978). The *sxa2>GFP* reporter strain was subjected to a time-series $G_1$-arrest assay to calculate the proportion of the population that becomes arrested in $G_1$ in response to P-factor stimulation.

The *sxa2>GFP* reporter strain was grown in minimal media and incubated with P-factor concentrations from 0M to $10^{-5}$M. An aliquot of cell culture was removed every hour for 12 h following the addition of P-factor, fixed with 70 % ethanol, chilled overnight and stained with propidium iodide before analysis using a LSR II flow cytometer. Excitation was achieved using a 488 nm laser, and emission detected using a 575/26 nm band pass filter with a 550 nm long pass filter. For each sample 30,000 particles were counted and quantified for their extent of staining (PE-A). Compensation was applied to remove the influence of any GFP fluorescence from the signal (He et al., 2003). The cells with one copy of the genetic material ($G_1$) are distinguished from cells with two copies of the genetic material ($G_2$) through the separation of peaks on the resulting frequency distribution histograms (Figure 5.8).

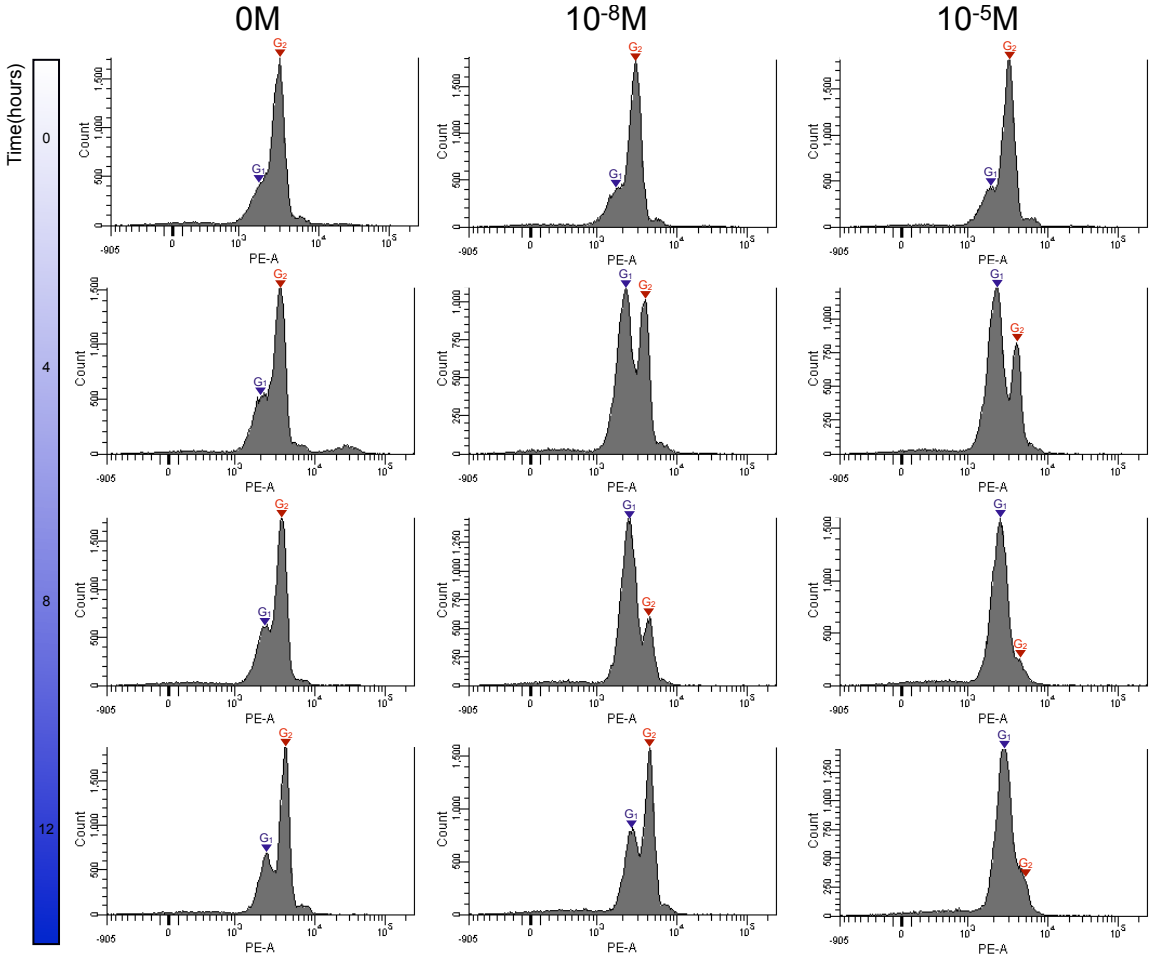


FIGURE 5.8: **Determination of cell phase through flow cytometry analysis.** Reporter strain JY1325(*sxa2>GFP*) was grown in minimal media and incubated with 0M to $10^{-5}$M P-factor. A sample from the cell cultures was removed at 0 h and subsequently every hour for a period of 12 h to be analysed by flow cytometry. For each cell culture sample at each time-point, the sample culture was stained with the DNA fluorochrome propidium iodide. Staining results in peaks at different intensity (PE-A) depending on the complement of chromosomes in the cell. The cell culture sample was analysed through flow cytometry, recording 3x$10^4$ events to produce histograms of PE-A vs frequency. The left peak represents cells with a single copy of genomic material ($G_1$ phase cells) and the right peak represents cells with two copies of the genomic material ($G_2$ phase cells). Data presented is from flow cytometry analysis of cells treated with a low (0M), intermediate ($10^{-8}$M) and high ($10^{-5}$M) P-factor concentration at every 4 h interval following P-factor addition from 0-12 h.

Data from the $G_1$-arrest assay (Figure 5.8) present the distributions of the populations in the absence of P-factor (0M), intermediate ($10^{-8}$M) and high ($10^{-5}$M) P-factor concentration into $G_1$ or $G_2$ phase cells at 4 h intervals following P-factor addition. In the absence of P-factor, the distribution of $G_1$ and $G_2$ phase cells remains relatively unchanged with time. At $10^{-8}$M P-factor concentration, the frequency of $G_1$ cells increases from 0 h to 8 h before decreasing again at 12 h, indicating an initial P-factor induced increase in $G_1$-arrest, then a recovery from this arrest. At high P-factor concentration ($10^{-5}$M), the frequency of $G_1$ phase cells increases from 0 h through to 12 h, showing no sign of any recovery. This

suggests that high P-factor stimulation can synchronise and maintain the majority of the cell population in $G_1$ phase of the cell cycle with time.

An estimate of the percentage of the population arrested in $G_1$ phase can be obtained from the histogram data by gating based on the $G_1$ peak and counting the number of cells that fall into the category of $G_1$ phase cells. This was completed for each P-factor concentration and at each time-point in the experiment, giving the ligand induced percentage $G_1$-arrested cell population with time (Figure 5.9).

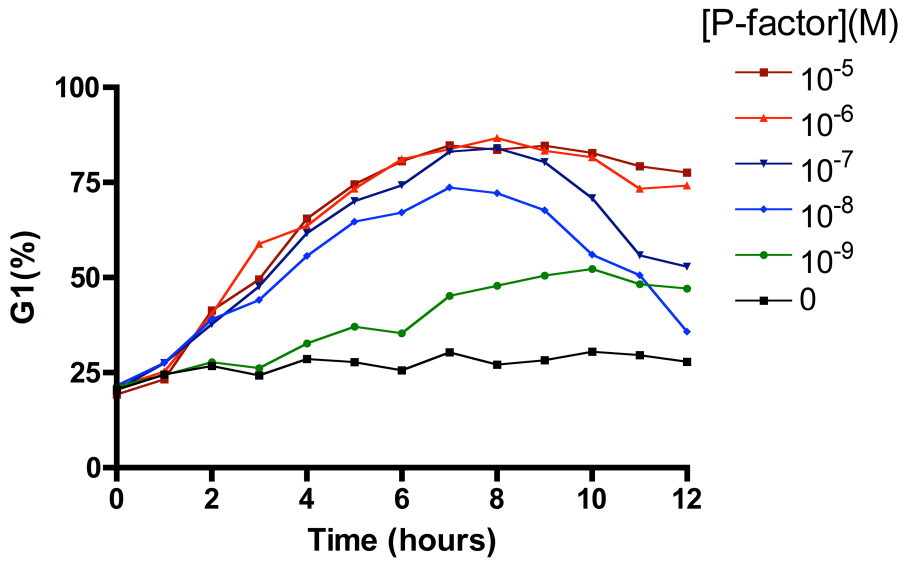


FIGURE 5.9: **Time-series $G_1$-arrest: Flow cytometry analysis of chromosome complement.** Fluorescent reporter strain JY1325(*sxa2>GFP*) was grown in minimal media and incubated with 0M to $10^{-5}$M P-factor. A sample of the cell cultures was removed at 0 h and subsequently every hour for a period of 12 h to be analysed by flow cytometry. For each cell culture sample at each time-point, the sample culture was stained with the DNA fluorochrome propidium iodide to allow identification of chromosome complement and cells in $G_1/G_2$ phase of their cell cycle (as in Figure 5.8). The cell culture sample was analysed through flow cytometry, recording $3x10^4$ events to produce histograms of propidium iodide staining intensity (PE-A) vs frequency. These data were analysed through gating of the $G_1$ peak to estimate the percentage of the analysed cell population that was in $G_1$ phase at each time-point and for each concentration of P-factor treatment.

Data from the $G_1$-arrest assay (Figure 5.9) indicates that at 0 h, all cell populations have ~25 % in $G_1$ phase of the cell cycle. The reason for this is that all reporter strains used are deleted for Cyr1 to enable P-factor induced mating-response without having to starve the cells of nutrients (Davey and Nielsen, 1994). As discussed in Chapter 1, nutrient limitation causes the loss of Cyr1 activity and a higher propensity for cells to enter $G_1$-arrest. The modified strains deleted for Cyr1 therefore have a relatively high percentage of cells already in $G_1$ arrest. Further $G_1$ arrest is a result of stimulation with P-factor. At P-factor concentrations $10^{-8}$M to $10^{-5}$M, the percentage of the cell population in the $G_1$ phase increases in a similar pattern from 0 - 8 h. Beyond 8 h, for intermediate P-factor concentrations of $10^{-8}$M and $10^{-7}$M, the percentage in $G_1$ decreases to ~30-50 %, whilst

at high P-factor stimulation ($10^{-6}$M and $10^{-5}$M) it remains fairly constant at ∼75 %. This could indicate the start of a recovery back to normal vegetative growth at intermediate P-factor concentration, which does not occur at high P-factor concentrations. At low P-factor concentration ($10^{-9}$M) there is a delayed, but gradual increase in cells in $G_1$ phase over the course of the assay, therefore $10^{-9}$M P-factor is a sufficient concentration for some cells to become arrested. Despite some cell cycle arrest occurring, fluorescence data suggests that this concentration is not sufficient to promote the induction of *sxa2>GFP* (Figure 5.7). In comparing the time after P-factor addition that increase in $G_1$ phase cells is observed to the time increase in percentage responding cells is observed, this is very similar, with both occurring at ∼1-2 h. Initiation of $G_1$-arrest and P-factor induced transcription therefore appears to occur within a very short time-frame of each other (compare Figures 5.9 to 5.7 and 5.6).

Analysis of the *sxa2>GFP* reporter strain through flow cytometry has given a more detailed understanding of the population-wide signalling response through the quantification of single cell signalling response in terms of the P-factor induced distribution of the response within the cell population, but it does not allow monitoring of live-cell signalling response of the same cells or cell population with time. Population-based assays on the fluorescence plate-readers can provide data on the mean transcriptional signalling response of the same population of live cells with time, but do not allow single cell measurements. Given the limitations of population-based assays mentioned previously, and the drawbacks of these two techniques in particular, we sought a method of monitoring and quantifying single live-cell signalling response with time. The benefits of such a method would enable more accurate insight into the temporal dynamics of signalling at the single cell level. One possible method that would combine the benefits of time-series monitoring of live cells, and single cell measurements of signalling response, would be to track and quantify single cell characteristics with time via fluorescence microscopy and subsequent image analysis.

## 5.5 Time-series Live-cell Imaging

Previously, all imaging work on *S. pombe* cells was end-point imaging and time-series imaging of live *S. pombe* cells had not been achieved. The main stumbling block was providing an environment on a microscope slide that allowed cells to remain viable for long periods of time. This problem was overcome by making 2 mm thick agarose pads from a mixture of growth media and 1% agarose on the microscope slides. Cells could then be placed on this pad underneath a coverslip, sealed, and imaged. Cells on these agarose pads could proliferate normally and remain viable for prolonged time periods, in excess of 24 h. To demonstrate the viability of cells imaged with time on these agarose pads, the *sxa2>GFP* reporter strain was grown in minimal media before transferring onto an agarose pad for

imaging. Cells were imaged using light-field on a Leica SP5 scanning confocal microscope for a period of 14 h, with images being taken every 15 min (Figure 5.10).

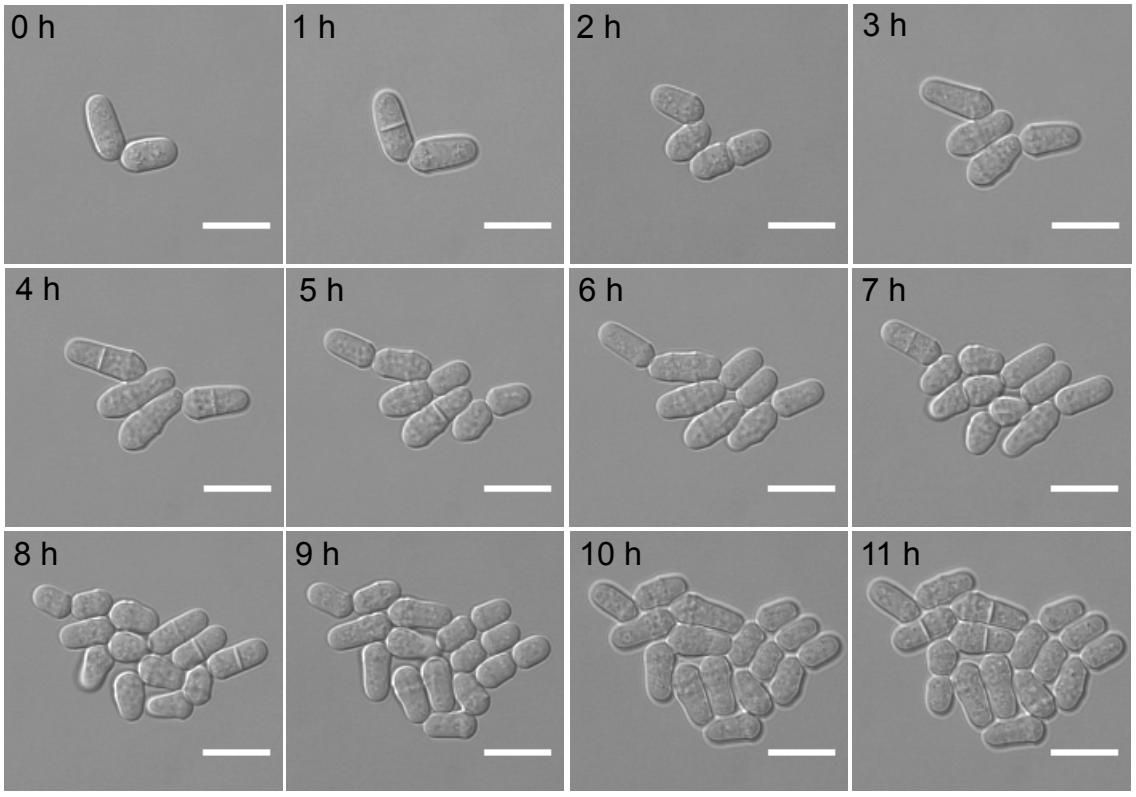


FIGURE 5.10: **Time-series live-cell imaging.** Cells from the *wild-type* reporter strain; JY1325(*sxa2>GFP*) were cultured to a density of ~5x10$^6$ cells/ml before transferring onto a minimal media + agarose pad on a microscope slide prepared for time-series live-cell imaging. Dividing cells were imaged using a light-field microscope, taking images every 15 min for a period of 14 h. For clarity, only the images at every hour mark are presented from 0-11 h. Scale bar = 10 $\mu$m.

Imaging shows that cells can undergo normal vegetative cell growth on the growth media + agarose pads with no obvious problems, therefore allowing for the monitoring of live *S. pombe* cells over prolonged time periods through imaging.

### 5.5.1 Imaging of Single Cell Signalling Response

Given that we could now monitor live cells in real-time through time-series imaging, the next step towards quantification of single cell response was to image cells as they respond to P-factor. To accomplish this required the addition of P-factor to the agarose pads to give an environment for the cells where they were viable, and could detect P-factor. P-factor was added to the agarose + growth media mix before constructing the agarose pads on microscope slides. The *sxa2>GFP* reporter strain was grown in minimal media before transferring to the agarose pads containing P-factor at concentrations from 0M to $10^{-5}$M.

The cells were then imaged for 14 h using a Leica SP5 scanning confocal microscope, taking fluorescence and light-field images every 15 min (Figure 5.11).

All time-series imaging experiments on live cells presented in this chapter were obtained by taking Z-slices through the cells at each time-point. The lower and upper limits of the Z-plane were defined 10 $\mu$m below and 10 $\mu$m above the bottom and top of the cells respectively at time = 0 h to account for the problem of microscope drift over the course of the experiment. Z-slices were obtained every 1 $\mu$m. *S. pombe* cells are approximately 4 $\mu$m in depth, therefore this achieved ~4 slices through a cell. For the purpose of presentation of any overlaid light-field and fluorescence images a single Z slice is presented.

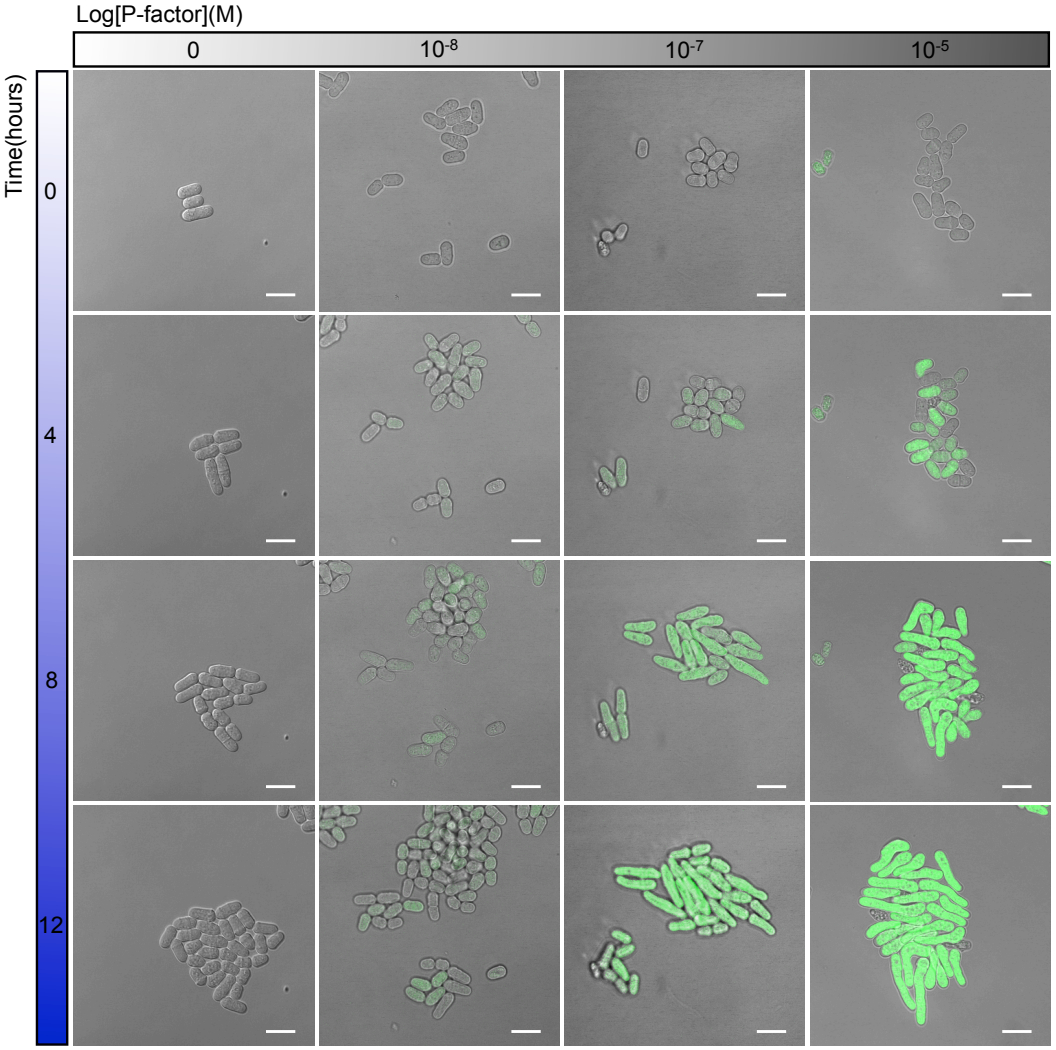


FIGURE 5.11: **Time-series live-cell imaging of P-factor treated fluorescent reporter cells.** Cells from the *wild-type* reporter strain; JY1325(*sxa2>GFP*) were cultured to a density of ~5x$10^6$ cells/ml before transferring onto minimal media + agarose pads containing 0M to $10^{-5}$M P-factor. The pads were constructed on a microscope slide prepared for time-series live-cell imaging. Starting from a randomly selected field of view containing enough cells to monitor the response, a light-field and fluorescence image was taken every 15 min for a period of 14 h. Images presented here are the overlays of light-field and fluorescence images from a representative subset of the population at every 2 h time-point from 0 - 12 h. Scale bar = 10 $\mu$m.

Time-series imaging of live *sxa2>GFP* reporter cells treated with P-factor confirms that cells will respond to the P-factor added to the agarose pads in a manner dependent on the concentration of P-factor in the pad (Figure 5.11). Qualitatively, we can observe in the images, both the transcriptional and morphology response of single cells following P-factor stimulation with time. At concentrations where some cells will commit to a signalling response ($10^{-8}$M to $10^{-5}$M), increased fluorescence becomes apparent from ~2 h. Cell-to-cell variability is observable within the population in terms of timings of a response, the extent of induction of *sxa2>GFP* and the extent of a morphology response in terms of how elongated cells become upon shmoo formation. Cells treated with $\geq 10^{-7}$M P-factor appear to undergo a similar level of transcriptional response to cells at $10^{-5}$M in terms of cell fluorescence, but cells at $10^{-5}$M become more elongated. This live-cell imaging gives more qualitative insights into the transcriptional and morphology signalling responses, the effect of cell cycle position on initiation of response, recovery from ligand stimulation and the ability of cells to prolong the response through subsequent generations.

## 5.6 Characterisation of Transcriptional and Morphology Response Within a Population Using Single Cell Measurements

Observing the response at the single cell level through time-series imaging of live fluorescent reporter cells gives good qualitative insight into the signalling response, but to understand it in a more detailed manner, and to enable more in-depth analysis of the signalling response, we have to be able to quantify the response from individual cells. To achieve this using images such as those in Figure 5.11, requires image processing and image analysis software that will enable the tracking of multiple single cells within the imaged population through time-frames. The image analysis software used for this purpose is the quantitative imaging software QuimP, first developed by Dormann et al., 2002.

Prior to quantification using QuimP all fluorescence images are processed in ImageJ by applying maximal projection through all of the Z-slices at each time-point and subjecting each image to background subtraction to remove noise.

### 5.6.1 Cell Segmentation and Tracking with Image Analysis Software QuimP

The QuimP software is a set of plugins for ImageJ that was developed to quantify spatio-temporal patterns of fluorescently labelled proteins in the cortex of moving cells (Bosgraaf et al., 2009; Tyson et al., 2010; Bosgraaf and Van Haastert, 2010). The software enables automated segmentation of multiple single cells from an image and the automated tracking of these cells through each frame of time-series images. An example of using this software

to track single fluorescent *S. pombe* reporter cells is shown in Figure 5.12. In the example the *sxa2>GFP* reporter strain was grown in minimal media, cells were transferred onto an agarose pad containing $10^{-5}$M P-factor before imaging on a Leica SP5 scanning confocal microscope for a period of 14 h, taking an image every 15 min. Two single cells from the resulting images were selected at frame 1 and analysed using QuimP to locate the cell contours and track the cell movement/growth through all of the remaining frames.

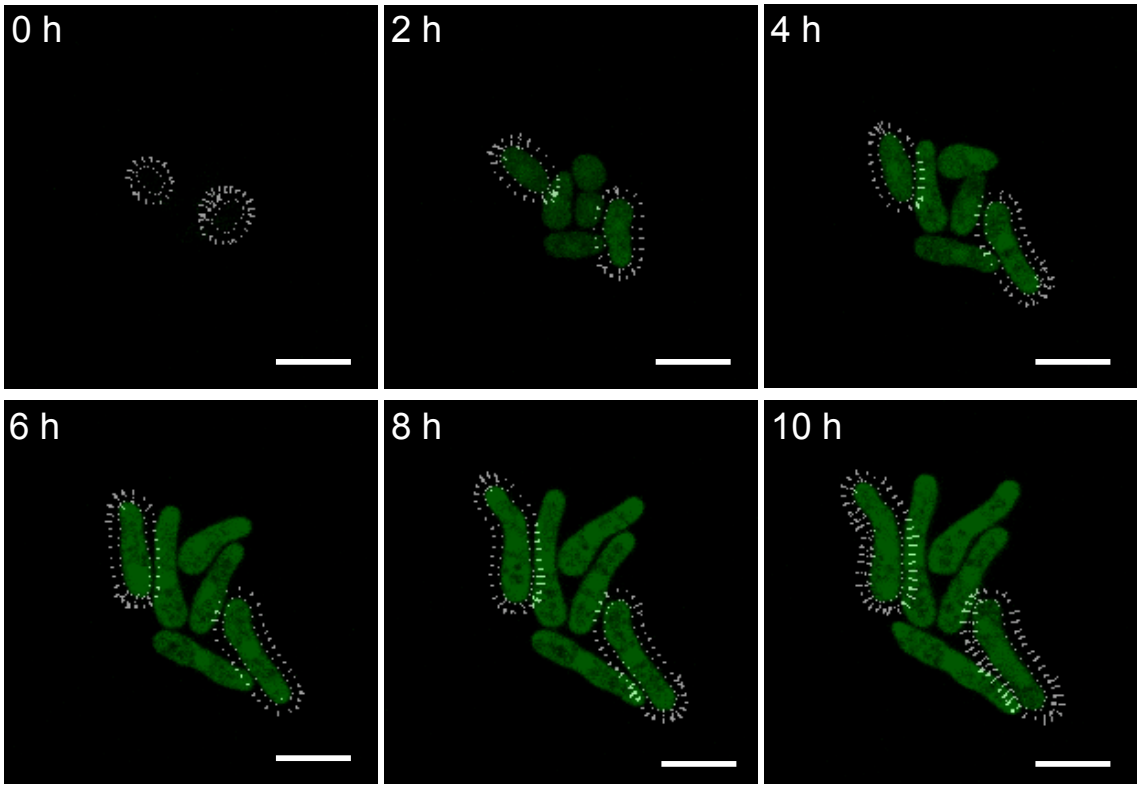


FIGURE 5.12: **Cell segmentation and tracking with QuimP.** Cells from the *wild-type* reporter strain; JY1325(*sxa2>GFP*) were cultured to a density of ~5x$10^6$ cells/ml before transferring onto a minimal media + agarose pad containing $10^{-5}$M P-factor on a microscope slide prepared for time-series live-cell imaging. Cells were imaged using a fluorescence microscope every 15 min for a period of 14 h. The resulting images were analysed using imageJ plugin software QuimP, which enables the accurate segmentation and tracking with time of multiple cells within the population. Presented is output from the software, tracing the outlines of two cells selected at the start of the analysis (time = 0 h). Images from 0-10 h are shown and intermediate time-points are omitted for clarity. Scale bar = 10 $\mu$m.

The segmentation and tracking process using QuimP is automated, with the only manual input required being the selection of which cells to track. During the tracking process, the selected cells within the image are quantified at each frame for a number of characteristics that we can use as measurements of the signalling response from single cells with time. Data output from the QuimP software includes values relating to both the transcriptional response (mean cell fluorescence, total cell fluorescence) and cell morphology (cell length, cell width, cell area, cell roundness).

In having the capability to image live reporter cells with time, combined with using the image analysis software QuimP, this now enables the quantification of single cell response to P-factor, which should provide much more detailed information on the temporal dynamics and cell-to-cell variability of the response, that is not possible from assays used previously.

### 5.6.2 End-point Ligand Induced Response

Initially, the use of image analysis with QuimP for quantifying signalling response was investigated in a manner that could be compared to end point dose-response data, such as those obtained from both the fluorescence plate-reader assays and through flow cytometry. This is to confirm quantification of signalling response through image analysis is able to produce similar dose-response profiles to those achieved in other assays, therefore validating it as a method to accurately quantify signalling response.

#### 5.6.2.1 Transcriptional Response

The transcriptional response of the *sxa2>GFP* reporter is measured by the induction of *sxa2>GFP*. In a plate-reader assay, this is quantified as the intensity of the fluorescence emitted from the whole cell population and in flow cytometry it is quantified as the intensity of fluorescence from single cells/particles. In using image analysis, transcriptional response can be quantified by the intensity of associated pixels that reside within the contours of the selected single cells on the image (the pixels contributing to the cell area). Single cell fluorescence measurements can be presented as the total cell fluorescence (sum of pixel intensities of all pixels within the contour of the cell) or the mean cell fluorescence (total cell fluorescence/number of pixels within the contour of the cell).

The *sxa2>GFP* reporter strain was grown in minimal media before transferring to an agarose pad containing 0M to $10^{-5}$M P-factor concentration. Live cells were imaged with time for 14 h, taking an image every 15 min using a Leica SP5 scanning confocal microscope. The duration of the imaging experiment was set to 14 h as previous experiments quantifying end-point induction of *sxa2>lacZ* have shown maximal signalling to be attained by $\sim$12 h (Smith, PhD Thesis 2010), therefore the majority of cells should have completed the signalling response by the 14 h time-point. On completion of the time-series imaging, multiple single cells (n$\geq$30) were selected at random from the 14 h time-point of each set of images and quantified for their mean and total fluorescence intensity using QuimP (Figure 5.13). Mean fluorescence is calculated as the average pixel intensity value of all pixels residing within the area of the cell.

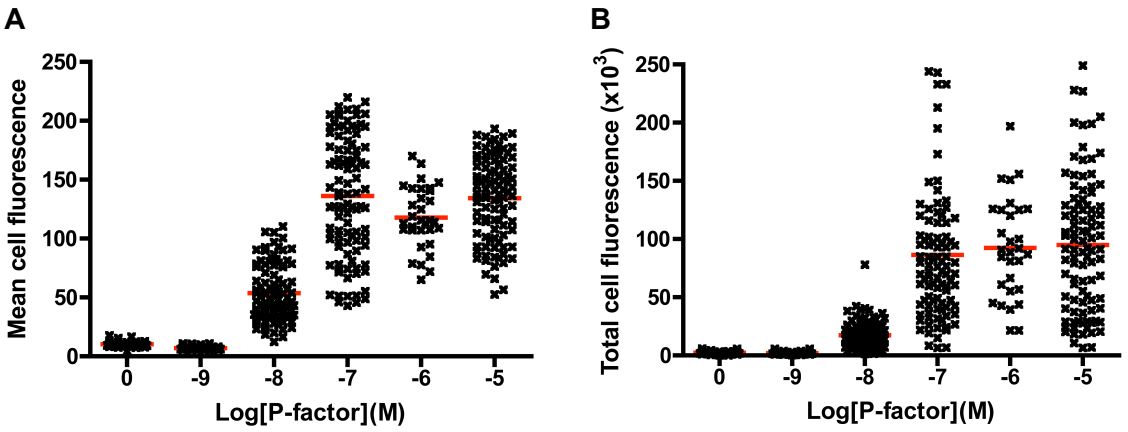


FIGURE 5.13: **Ligand-dependent transcriptional response using image analysis of single cells.** Reporter strain JY1325(*sxa2>GFP*) was grown in minimal media and incubated with 0M to $10^{-5}$M P-factor for a period of 14 h before imaging using a Leica SP5 scanning confocal microscope. Individual cells (n≥30) from the images were quantified for their fluorescence intensities using image analysis software QuimP. Cells from each image were selected at random and quantified for their mean fluorescence intensity (mean pixel intensity value) (A) and total fluorescence intensity (sum of intensities of all pixels within the area of the cell) (B). Each data point represents a single cell and the red bar indicates the mean of the analysed cell population.

Similar to flow cytometry data (Figure 5.4), the data from image analysis (Figure 5.13) gives insight into the distribution of response within the population in addition to a mean response from the single cells. The analysis indicates that induction of *sxa2>GFP* requires at least $10^{-8}$M P-factor. Cells treated with ≥$10^{-7}$M show similar mean levels of transcriptional response, indicating that the transcriptional response of the signalling pathway could be saturated at and above $10^{-7}$M ligand. There appears to be cell-to-cell variability in the cell population in terms of the level of fluorescence intensity of the cell, with some cells that respond at $10^{-8}$M achieving similar levels of mean fluorescence and total fluorescence as cells treated with $10^{-5}$M. This suggest cell-to-cell variability in sensitivity to ligand, indicating that some cells may be pre-disposed to respond to minimal P-factor concentration, whilst others will require a higher P-factor concentration to generate a similar level of transcriptional response.

Given that there are two possible methods of presenting the transcriptional response data from image analysis; mean cell fluorescence (mean pixel intensity of all pixels within the contour of a cell) and total cell fluorescence (sum of all pixel intensities within the contour of the cell), it could be possible to interpret data differently depending on which measure is used. To compare the two measures, dose-response profiles of each were calculated from the single cell fluorescence data (Figure 5.13). These profiles represent the mean population transcriptional response ± S.E.M. (Figure 5.14).

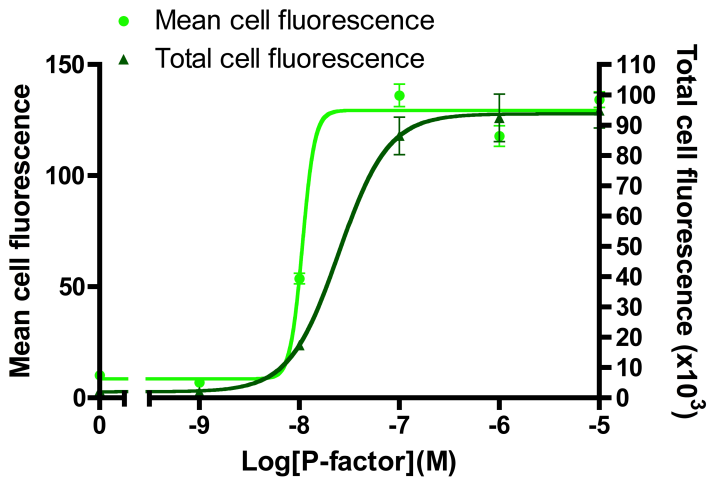


| | Basal | Maximal | $pEC_{50}$ |
|---|---|---|---|
| Mean cell fluorescence | 8.557 +/- 7.518 | 129.400 +/- 7.108 | 7.968 +/- 0.130 |
| Total cell fluorescence | 1.995 +/- 0.900 x10³ | 93.714 +/- 0.887 x10³ | 7.604 +/- 0.029 |

FIGURE 5.14: **Ligand-dependent mean cell fluorescence and total cell fluorescence response.** Reporter strain JY1325 *(sxa2>GFP)* was grown in minimal media and incubated with 0M to $10^{-5}$M P-factor for a period of 14 h before imaging using a Leica SP5 scanning confocal microscope. Individual cells from the images were quantified for their fluorescence intensities using image analysis software QuimP. Cells from each image were selected at random and quantified for their mean fluorescence intensity (mean pixel intensity value) and total fluorescence intensity (sum of intensities of all pixels within the area of the cell). The dose-response profiles of mean cell fluorescence and total cell fluorescence are compared. Results are the means ± S.E.M. from the analysed cell population (number of cells analysed ≥30). The table summarises the basal, maximal and $pEC_{50}$ values ± S.E.M. for each profile.

Comparing mean cell fluorescence to total cell fluorescence dose-response profiles indicates that both measures give similar ligand-dependent transcriptional response (Figure 5.14). There is however, a notable difference in the sensitivity, with the mean cell fluorescence measure indicating a more sensitive response to ligand compared to the total cell fluorescence measure ($pEC_{50}$; 7.968 ± 0.130 vs 7.604 ± 0.029). This is due to a comparably raised mean cell fluorescence value at $10^{-8}$M, possibly due to the fact that cells stimulated with P-factor at this concentration induce a transcriptional response but there is minimal morphology response, therefore increasing the calculated mean cell fluorescence value. As both mean and total fluorescence measures are calculated using the number of pixels covered by the cell area, these measures are influenced by the size of the cell. Measures of cell morphology can also be obtained using the image analysis software QuimP.

#### 5.6.2.2 Morphology Response

One of the major benefits of using image analysis to quantify signalling response is that morphology quantification can be achieved alongside the gathering of transcriptional data from the same cell. Cell elongation in response to P-factor stimulation (shmoo formation)

can cause the cell to elongate to 3x its original length (Davey, 1998). A measure of shmoo formation therefore represents a good additional characteristic to quantify the morphology signalling response. Cells elongate as they grow, therefore the length of an unstimulated cell can be variable, and is influenced by the stage the cell is at in the cell cycle. To quantify P-factor-dependent effect on morphology, a quantification of shmoo formation is sought. This is calculated as the 'elongation factor' of the cell, which is the ratio of cell length to cell width (length/width) (Figure 5.15). Unstimulated cells can be ~3-4 $\mu$m in width and ~7-11 $\mu$m in length, therefore the possible elongation factor range for unstimulated cells is ~1.75-3.5. Any cell with an elongation factor greater than the upper limit of this range is therefore likely to have undergone P-factor induced morphology response in the form of shmoo formation.

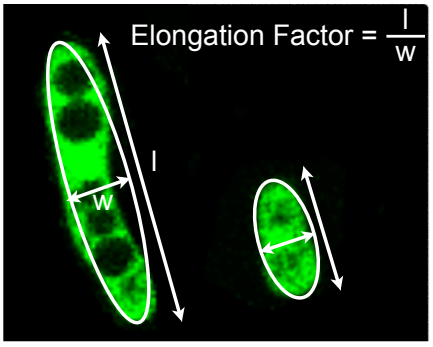


FIGURE 5.15: **Calculating elongation factor.** Elongation factor is calculated in QuimP using an algorithm fitting an elipse over the image of the cell. The elipse has the same centroid and area of the cell and the major and minor axis of the elipse are then calculated as approximations of the cell length and width respectively. Elongation factor is the ratio of length:width.

The same cells, quantified for their transcriptional response in Figure 5.14 were also quantified for their morphology response in terms of elongation factor using image analysis with QuimP (Figure 5.16).

The data showing ligand-dependent elongation factor of all cells analysed (Figure 5.16, A) and the analysed population average (Figure 5.16, B) shows an interesting relationship between the concentration of ligand stimulation and the morphology response. From 0M to $10^{-7}$M P-factor concentration there is no increase in elongation factor of the cells, whereas at concentrations $>10^{-7}$M, cells become much more elongated. This suggests a 'tipping-point' at $10^{-7}$M for the induction of shmoo formation.

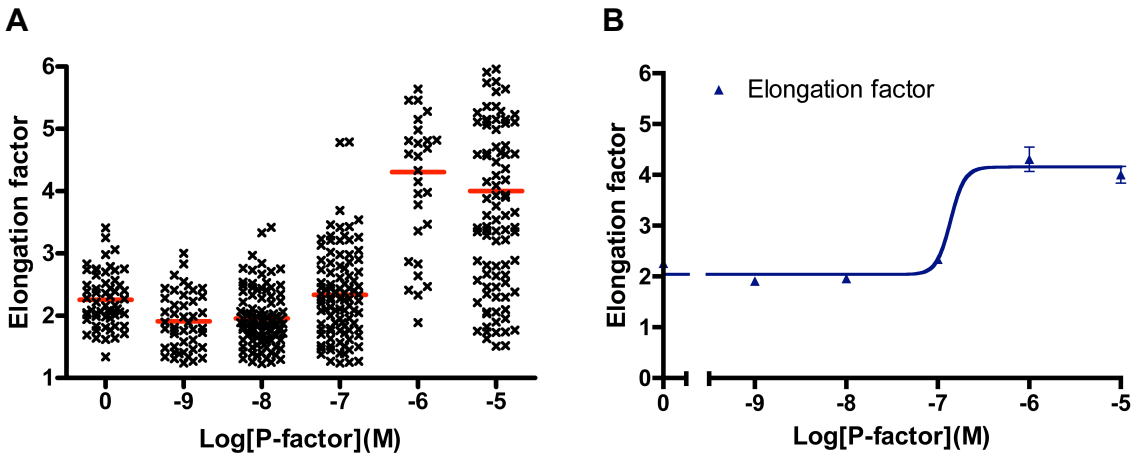


| | Basal | Maximal |
|---|---|---|
| Elongation factor | 2.256 +/- 0.060 | 4.308 +/- 0.239 |

FIGURE 5.16: **Ligand-dependent morphology response using image analysis of single cells.** Reporter strain JY1325(*sxa2>GFP*) was grown in minimal media and incubated with 0M to $10^{-5}$M P-factor for a period of 14 h before imaging using a Leica SP5 scanning confocal microscope. Individual cells from the images were quantified using image analysis software QuimP. Cells from each image (n≥30) were selected at random and quantified for their elongation factor (ratio of cell length:width) (A). Each data point represents a single cell and the red bar indicates the mean of the analysed cell population. The mean ± S.E.M. from the analysed cell population is plotted showing the mean response profile (B). The table summarises the basal and maximal response ± S.E.M. from all cells analysed.

#### 5.6.2.3 Transcriptional vs Morphology Response

Upon P-factor activation of the cell-surface receptors, the signal is transduced via activation of the G protein G$\alpha$ subunit Gpa1, before branching into the separate transcriptional and morphology response pathways. This branching occurs downstream of Gpa1 at another G protein, the small monomeric G protein Ras1. By comparing transcriptional response to morphology response, we can therefore gain further insight into the influence of ligand concentration on the branching of the signal into transcriptional and morphology responses. Both mean and total cell fluorescence response profiles (Figure 5.14) have been compared to the elongation factor response profile (Figure 5.16, B). The transcriptional and morphology data was gathered from the same segmented cells from time-series imaging (Figure 5.17).

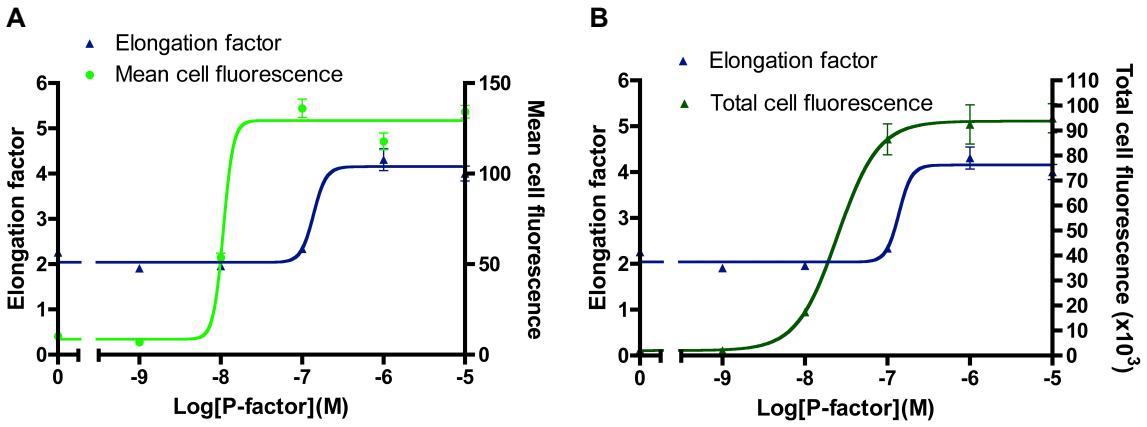


FIGURE 5.17: **Comparison of ligand-dependent morphology and transcriptional response from single cell data.** Reporter strain JY1325(*sxa2>GFP*) was grown in minimal media and incubated with 0M to $10^{-5}$M P-factor for a period of 14 h before imaging using a Leica SP5 scanning confocal microscope. Individual cells from the images were quantified for their morphology and transcriptional response using image analysis software QuimP. Cells from each image were selected at random and quantified for their mean fluorescence (mean pixel intensity), total fluorescence (sum of intensities of all pixels within the area of the cell) and elongation factor (ratio of cell length:width). The transcriptional and morphology response profiles are compared; mean fluorescence vs elongation factor (A) and total fluorescence vs elongation factor (B). Results are the means ± S.E.M. from all single cells included in the analysis.

Comparing transcriptional and morphology dose-responses (Figure 5.17) indicates that the transcriptional response is more sensitive to P-factor than the morphology response, given that mean cell fluorescence $pEC_{50}$ = 7.968 ± 0.130 , total cell fluorescence $pEC_{50}$ = 7.604 ± 0.029 compared to $pEC_{50}$ of 6.860 ± 0.110 for elongation factor data. This suggests that there may be a cellular mechanism to facilitate this increased sensitivity through ensuring a propensity for transferring signal amplitude into the transcriptional branch of the signalling response over the morphology response.

Endpoint fluorescence and morphology data from images of single fluorescent reporter cells gives dose-response profiles that are comparable to those obtained from population-based assays (compare Figure 5.17 to Figure 5.1). One of the advantages of quantification through image analysis is that the transcriptional and morphology data is obtained from the same cells, therefore this enables these two responses to be more closely compared. Time-dependent response such as those obtained from population-based assays and flow cytometry, can also be achieved using image analysis by quantifying cells from the live-cell time-series images at selected time-points.

### 5.6.3 Quantification of Population Response With Time

Given that we have obtained time-series images of live-cell fluorescent reporter cells stimulated with P-factor from 0M to $10^{-5}$M (Figure 5.11), we can use image analysis software

QuimP to investigate the time-dependent influence in addition to the dose-dependent influence on signalling response, similar to what was achieved using flow cytometry (Figure 5.6), but with the added benefit of also obtaining cell morphology data from the same individual cells analysed.

#### 5.6.3.1 Transcriptional Response With Time

To investigate transcriptional response with time using image analysis, the *sxa2>GFP* reporter strain was grown in minimal media, transferred to agarose pads containing 0M to $10^{-5}$M P-factor before imaging on a Leica SP5 scanning confocal microscope for 14 h, taking an image every 15 min. On completion of the time-series imaging, multiple (n≥30) single cells were selected at random from the images at 0 h and every subsequent 2 h, and quantified for their mean cell fluorescence and total cell fluorescence using QuimP. The mean transcriptional response of the population of analysed single cells was calculated from both the mean cell fluorescence measurements and the total cell fluorescence measurements of single cells to compare transcriptional response of the populations with time (raw data in Appendix B). Profiles of response with time could be calculated from these data and is presented as the mean ± S.E.M. for each concentration of P-factor (Figure 5.18).

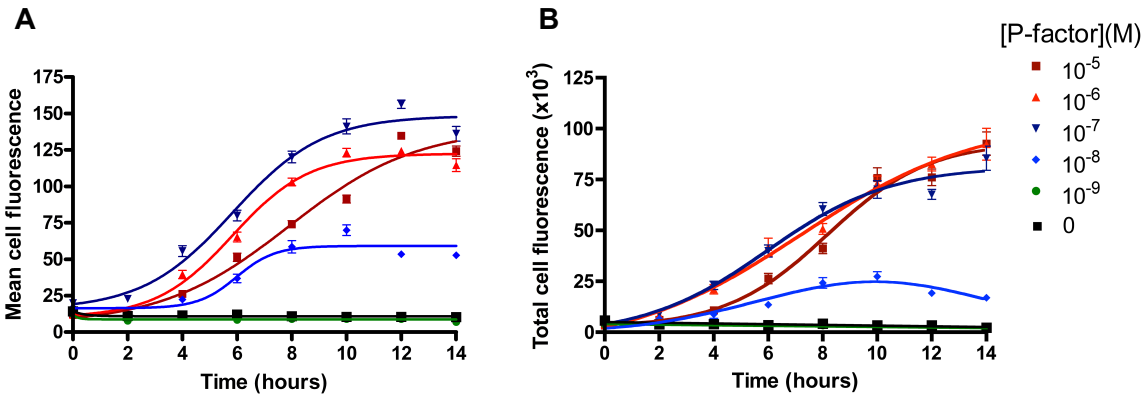


FIGURE 5.18: **Mean cell fluorescence and total cell fluorescence response with time.** Reporter strain JY1325(*sxa2>GFP*) was grown in minimal media and incubated with 0M to $10^{-5}$M P-factor for 14 h. Images of the cell culture were taken at 0 h and subsequently every 2 h using a Leica SP5 scanning confocal microscope. Individual cells from the images were quantified for their fluorescence intensities using image analysis software QuimP. Cells from each image taken at each time-point were selected at random and quantified for their mean (mean pixel intensity) and total (sum of intensities of all pixels within the area of the cell) fluorescence. Mean cell fluorescence (A) and total cell fluorescence (B) response profiles with time are shown. Results are means ± S.E.M. from ≥30 single cells included in the analysis.

The single cell transcriptional response with time for both mean cell fluorescence and total cell fluorescence display similar response profiles (compare Figure 5.18, A to B). At 2 h increase in cell fluorescence at P-factor concentration ≥$10^{-8}$M is observed. The raw single cell data (Appendix B.1 and B.2) indicates that not all of the cells show increase in

fluorescence at the same time, suggesting that cells within the population are not synchronised in their timing of initial response, with some cells inducing expression of *sxa2>GFP* more rapidly than others. This cell-to-cell variation in the initiation of the transcriptional response is likely to be due to the fact that cells are at different points in their cell cycle. Cells are required to arrest in $G_1$ phase for the mating-response to occur, therefore cells that are in $G_1$ phase when they are stimulated with P-factor will signal rapidly, whereas other cells at later stages of the cell cycle will continue through the cycle to reach $G_1$ phase before initiating a response. Cells treated with $10^{-7}$M to $10^{-5}$M P-factor display a similar pattern of increased fluorescence with time, beginning at ∼2 h before starting to plateau after ∼10 h. Populations treated with $10^{-8}$M P-factor display mean fluorescence increasing and plateauing, but reaching less than half the maximal response achieved at higher concentrations. There is no increase in fluorescence observed at $10^{-9}$M or 0M P-factor. These time-dependent profiles in transcriptional response are similar to those obtained using flow cytometry (compare Figure 5.18 to Figure 5.6).

#### 5.6.3.2 Morphology Response With Time

To investigate the temporal aspect of the morphology response, the same cells analysed for their transcriptional response (Figure 5.18) were also quantified for their elongation factor using image analysis software QuimP. The raw data for each single cell measurement (Appendix B.3) is used to calculate the population mean ± S.E.M. elongation factor with time for each P-factor concentration (Figure 5.19).

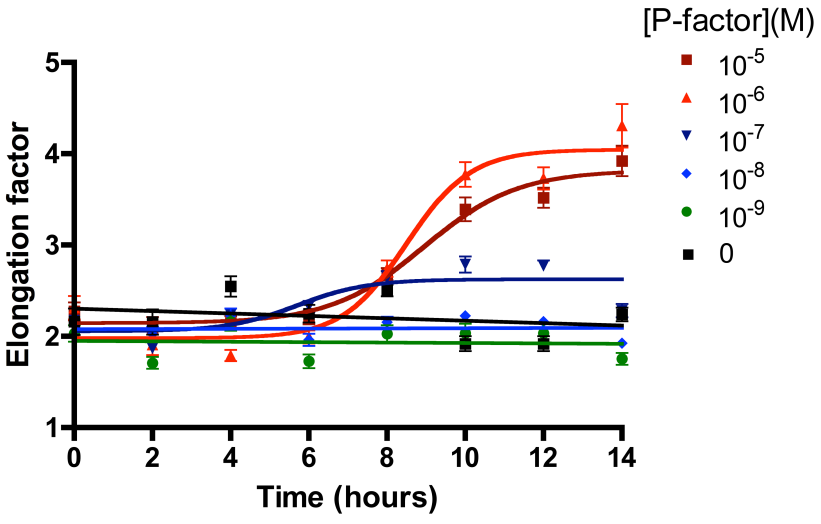


FIGURE 5.19: **Mean morphology response with time using image analysis of single cells.** Reporter strain JY1325(*sxa2>GFP*) was grown in minimal media and incubated with 0M to $10^{-5}$M P-factor for 14 h. Images of the cell culture were taken at 0 h and subsequently every 2 h using a Leica SP5 scanning confocal microscope. Individual cells from the images were quantified for their morphology using image analysis software QuimP. Cells from each image taken at each time-point were selected at random and quantified for their elongation factor (ratio of cell length:width). Results are means ± S.E.M. from all single cells included in the analysis.

The data presenting the elongation factor averaged over all of the analysed cells with time (Figure 5.19) again highlights that a morphology response to P-factor does not become apparent until 6 h, after which there is a rapid increase in mean elongation factor at $10^{-7}$M to $10^{-5}$M P-factor, before beginning to plateau after ∼10 h. There is a large difference in the maximum elongation factor reached at high P-factor concentration of $10^{-6}$M and $10^{-5}$M (4.045 ± 0.221 and 3.818 ± 0.145 respectively) compared to $10^{-7}$M (2.625 ± 0.140) and there is no apparent increase in mean elongation factor of the population with time for cells treated with $\leq 10^{-8}$M P-factor.

In comparing mean population transcriptional and morphology response with time we can deduce that the observable transcriptional response is not only more sensitive to P-factor (Figure 5.17), but it also precedes shmoo formation (compare Figure 5.18 to Figure 5.19). This is apparent from the data suggesting induction of *sxa2>GFP* is detected after 2 h, whilst increase in elongation factor is not observed until after 6 h of P-factor stimulation. This suggests that there could be mechanisms to allow a more sensitive transcriptional response that is activated prior to activation of the morphology response pathway, also pointing to the possibility that the transcription of genes in response to P-factor is an absolute requirement to achieve shmoo formation. We have also observed from single cell measurements that a clonal population of cells shows variability in both transcriptional and morphology signalling response. The population is not synchronous in the timing or amplitude of a signalling response.

### 5.6.4 Stochasticity in Cell-to-cell Signalling Response

To investigate the influence of ligand concentration on variability, measures for cell-to-cell variability within the population have been calculated for the transcriptional and morphology response of a population treated with P-factor from concentrations of 0M to $10^{-5}$M. Quantification of the population variability has been achieved using the cell segmentation software QuimP combined with analysis using bespoke Matlab code using images of the *sxa2>GFP* reporter cells. Having stimulated the *sxa2>GFP* reporter strain with P-factor for a period of 14 h, fluorescence images were then taken of cells at each P-factor concentration using a Leica SP5 scanning confocal microscope(Figure 5.20).

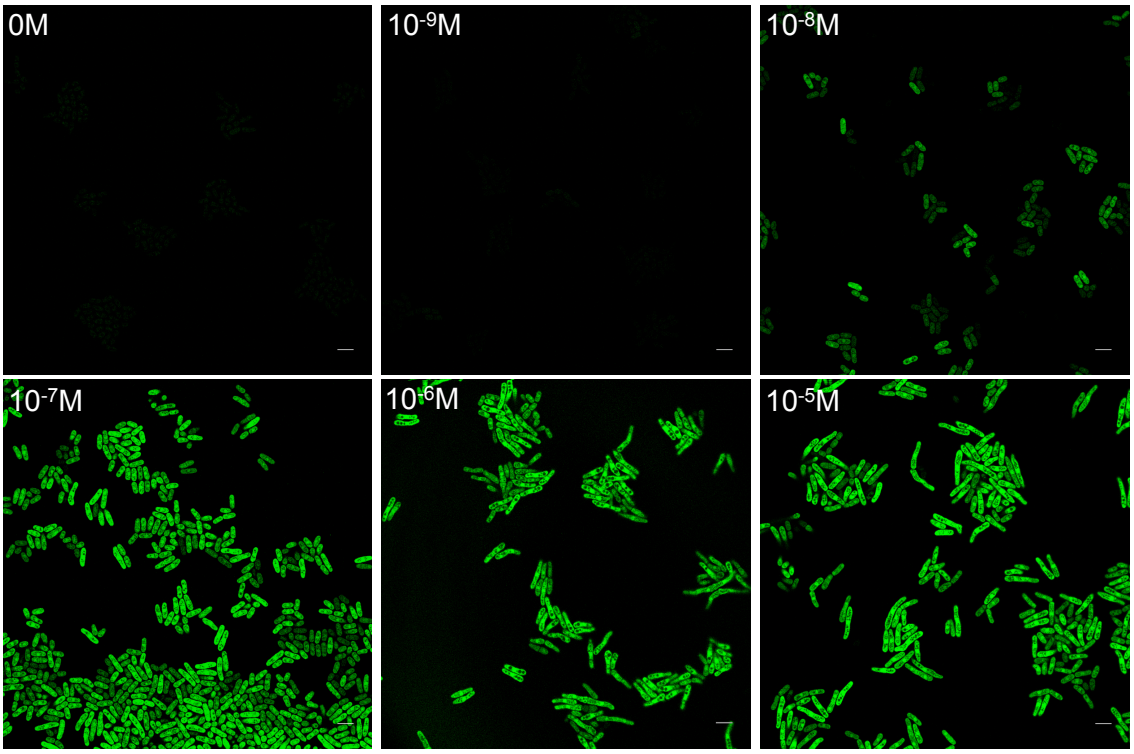


FIGURE 5.20: **Imaging of dose-dependent signalling response.** The *wild-type* reporter strain; JY1325(*sxa2>GFP*) was cultured in minimal media to a density of ~5x10$^6$ cells/ml and incubated with 0M to $10^{-5}$M P-factor for 14 h. Images of these cells were then obtained using a Leica SP5 scanning confocal microscope. Scale bar = 10 $\mu$m.

Through observations of the end-point images (Figure 5.20), it evident that there is cell-to-cell variability in the fluorescence intensity of cells as some cells have induced sxa2>GFP to a greater extent than others. At $10^{-8}$M P-factor concentration it is particularly evident that some cells within the population have had a large transcriptional response, whilst in others this is minimal. Quantification of the fluorescence intensity and morphology of a number of single cells (n≥30) from each of these images using QuimP allowed the subsequent calculation of the variation in signalling response within the populations. Variability was calculated as the coefficient of variation (CV), which is defined as the ratio of the standard deviation $\sigma$ to the mean $\mu$ and expressed as a percentage:

$$CV = 100(\frac{\sigma}{\mu}). \tag{5.1}$$

The CV was calculated using single cell measurements from images of *sxa2>GFP* reporter cells having been treated with 0M to $10^{-5}$M P-factor for a period of 14 h. From each image in Figure 5.20 ≥30 cells were selected randomly for inclusion in the analysis. This allowed investigation into the relationship between P-factor concentration and variability in both transcriptional response and morphology response (Figure 5.21).

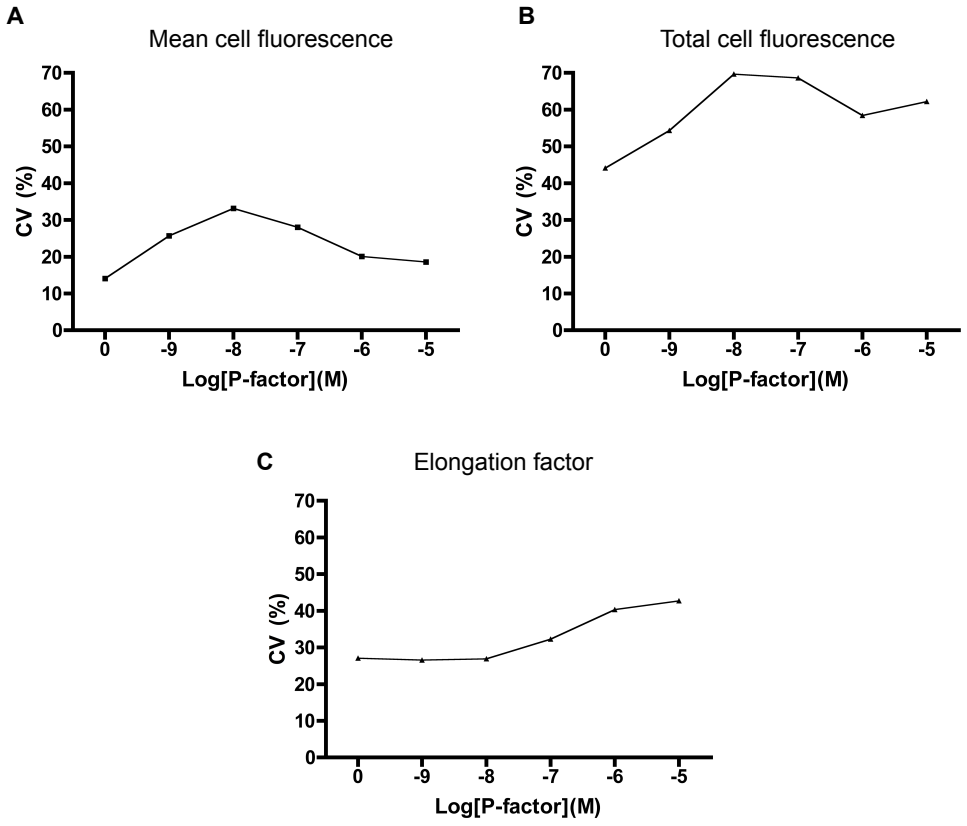


FIGURE 5.21: **Ligand-dependent cell-to-cell variation in signalling response.** Reporter strain JY1325(*sxa2>GFP*) was grown in minimal media and incubated with 0M to $10^{-5}$M P-factor for a period of 14 h before imaging using a Leica SP5 scanning confocal microscope. Individual cells (n≥30) from the images at each concentration were selected at random and quantified for their mean fluorescence (mean pixel intensity), total fluorescence (sum of all pixel intensities within the cell area) and elongation factor (ratio of cell length:width) using image analysis software QuimP. The cell-to-cell variability in mean fluorescence (A), total fluorescence (B) and elongation factor (C) within the analysed cell population was calculated as the coefficient of variation (CV).

P-factor induced variation within the population (Figure 5.21) follows a similar unimodal pattern for mean cell fluorescence and total cell fluorescence. Variation in the transcriptional response is reduced at low and high P-factor concentrations, and peaks at intermediate concentration of $10^{-8}$M. This is an intuitive result given that at very low or very high concentrations, the cell-fate 'decision' to commit (or not) to a signalling response is clear, whereas at intermediate concentrations this 'decision' is not so clear, therefore resulting in some cells inducing *sxa2>GFP* to a large extent and others not showing any induction. Another notable point is that variation in total fluorescence is generally greater than that of mean fluorescence, possibly as a result of different cells being at different points in their cell cycle or signalling response, hence giving more varied total fluorescence measurements. The variability in morphology does not follow the same pattern as transcriptional variability. In the case of elongation factor the variability remains relatively stable until $10^{-7}$M where it then increases gradually, peaking at $10^{-5}$M. Given previous data showing that significant

increased cell elongation factor is not apparent until $>10^{-8}$M P-factor stimulation, this is not surprising. Another factor contributing to the increased variability at high P-factor concentration is likely to be the fact that after 14 h some cells within the population will have undergone shmoo formation and be nearing the end of the signalling response, whilst other cells will have recently completed a response, recovered and divided, producing much less elongated daughter cells.

Using time-series live-cell images of the *sxa2>GFP* reporter strain, it was also possible to investigate how variability within the population alters in a time-dependent manner. JY1325 was grown in minimal media before transferring to agarose pads containing 0M to $10^{-5}$M P-factor on microscope slides prepared for time-series imaging. Images of the cell population were taken every 2 h for a period of 14 h. Subsequently, 30 cells from these images were randomly selected and quantified for mean cell fluorescence, total cell fluorescence and elongation factor using image analysis software QuimP. These data were then used to calculate CV within the population for transcriptional (Figure 5.22) and morphology (Figure 5.23) response, which could be plotted against time.

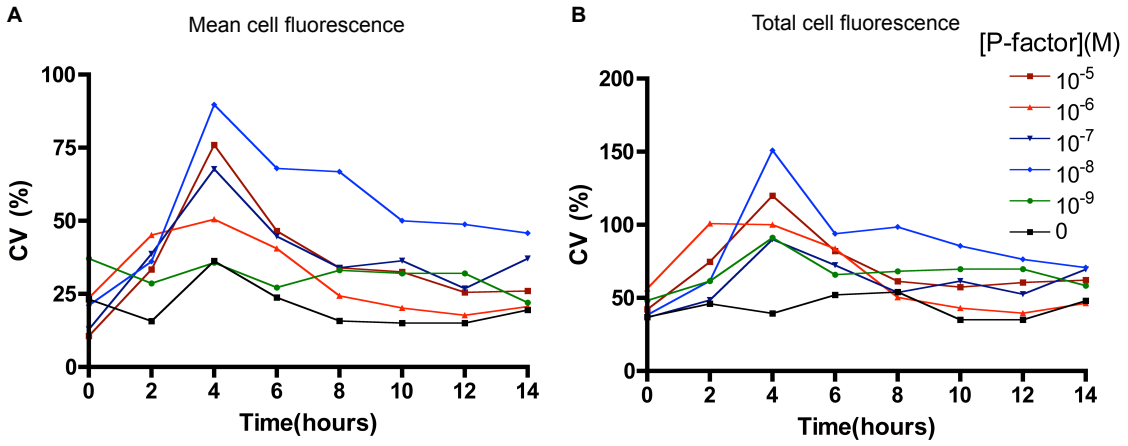


FIGURE 5.22: **Time and ligand-dependent cell-to-cell variability in transcriptional signalling response.** Reporter strain JY1325(*sxa2>GFP*) was grown in minimal media and incubated with 0M to $10^{-5}$M P-factor for 14 h. Images of the cell culture were taken at 0 h and subsequently every 2 h using a Leica SP5 scanning confocal microscope. Individual cells (n≥30) from the images were quantified for their transcriptional response using image analysis software QuimP. Cells from each image taken at each time-point were selected at random and quantified for their mean fluorescence (mean pixel intensity) and total fluorescence (sum of all pixel intensities within the cell area). For each image analysed at each time-point the cell-to-cell variability in mean fluorescence (A) and total fluorescence (B) was calculated as the coefficient of variation (CV).

There is minimal observed time-dependent change in variation in fluorescence of cells treated with 0M to $10^{-9}$M P-factor (Figure 5.22). At concentrations $>10^{-9}$M variation follows a similar trend for both mean cell fluorescence and total cell fluorescence, increasing initially from 0 h to ∼6 h then decreasing through to 14 h. This time-dependent variation

pattern highlights the lack of synchronisation between cells in the induction of a transcriptional response. The initial increase in variation is likely to be due to individual cells responding at different start times. The decrease following ∼6 h could be due to an effect of those cells having initiated a transcriptional response at a later time-point 'catching-up' in terms of cellular fluorescence, because of the high degree of GFP stability, resulting in similar fluorescence levels to those cells that had initiated response sooner. Again, it is at intermediate P-factor concentration ($10^{-8}$M) that the cell population shows the greatest cell-to-cell variability in transcriptional response (Figure 5.22).

Despite variability in transcription appearing to be dependent on time in addition to P-factor concentration, no such trend was observed for variation in cell morphology (Figure 5.23). This is possibly due to the variable nature of *S. pombe* cell size in an unstimulated population and lack of synchronicity of the timings of a morphology signalling response.

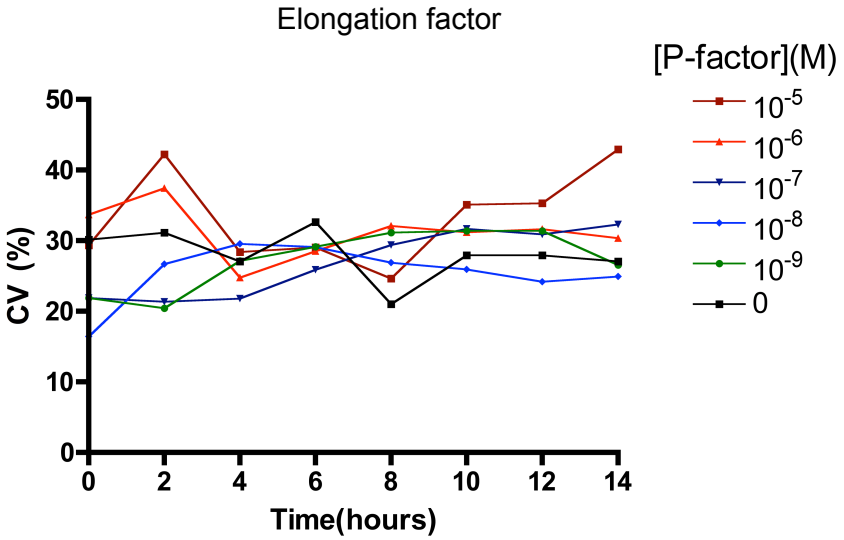


FIGURE 5.23: **Time and ligand-dependent cell-to-cell variability in morphology signalling response.** Reporter strain JY1325(*sxa2>GFP*) was grown in minimal media and incubated with 0M to $10^{-5}$M P-factor for 14 h. Images of the cell culture were taken at 0 h and subsequently every 2 h using a Leica SP5 scanning confocal microscope. Individual cells from the images were quantified for their morphology using image analysis software QuimP. Cells from each image taken at each time-point were selected at random and quantified for their elongation factor (ratio of cell length:width). For each image analysed at each time-point the cell-to-cell variability in elongation factor was calculated as the coefficient of variation (CV).

In using single cell analysis of time-series images of *sxa2>GFP* reporter cells, we are able to obtain quantitative data on signalling response for both transcription and morphology changes in response to P-factor that is comparable to data from other data collection methods such as population-based assays and flow cytometry. In obtaining single cell measurements using flow cytometry and image analysis we have observed from the distributions of single cell response in the population, that there is a large amount of cell-to-cell variability in the signalling response. In a given population of cells the addition of sufficient

P-factor to initiate a response does not result in every cell in the population committing to a signalling response, therefore in a population-based assay, the average response from the population is effected not only by the amplitude of the response, but also by the number of cells that responded to stimulation. Given the cell-to-cell variability in response of a clonal population, it would be beneficial when investigating cells response to ligand stimulation to only analyse those cells that commit to a signalling response.

## 5.7 Segmenting Signalling Cells Within the Population

To investigate the effect of P-factor concentration on the proportion of the population that is responding, the same populations of cells from previous image analysis of transcriptional and morphology response (Figure 5.18 and Figure 5.19) were segmented into 'responded' and 'non-responded' cells. To do this required classification criteria that would enable defining these types of cells within the population.

### 5.7.1 Setting Thresholds to Define a Signalling Cell

To be able to estimate the responded cell population, we had to define threshold values to identify cells that had sufficiently high fluorescence or elongation factor measurement to classify the cell as having undergone transcriptional or morphology response. Each single cell quantified could then be subjected to checks against threshold levels for transcriptional and morphology response before classification as a responded or non-responded cell. Thresholds were calculated for the time-series images obtained at each P-factor stimulation based on the mean single cell response from a control set, which was the single cell measurements obtained at the 0 h time-point. Thresholds were calculated to be the average value multiplied by a constant.

The threshold (T) for a transcriptional response of a single cell was calculated as

$$T = a(\frac{F}{n}), \tag{5.2}$$

where $F$ = sum of single cell mean cell fluorescence values, $n$ = number of cells and $a$ = 3 (function constant). The threshold (M) for a morphology response of a single cell was calculated as

$$M = b(\frac{E}{n}), \tag{5.3}$$

where $E$ = sum of elongation factor values, $n$ = number of cells and $b = 1.7$ (function constant). Both thresholds for a transcriptional response and morphology response are defined as the mean value from all cells analysed in the control set multiplied by constants. The values of the function constants $a$ and $b$ were determined by finding the smallest possible positive integer value ensuring that in the control set at time = 0 h, none of the cells could falsely be classified as having responded. By subjecting every cell to these classification criteria, the proportions of the population having committed to a P-factor induced response can be calculated.

### 5.7.2 Proportions of the Cell Population Displaying Response Characteristics

To investigate the time and ligand concentration effects on the proportion of the population committing to a signalling response, the cells analysed previously from live-cell time-series images for their transcriptional response (Figure 5.18) and morphology response (Figure 5.19) were subjected to classification as to whether they were responded or non-responded cells. Each individual cell, at each time-point, and for each P-factor concentration was checked against the threshold transcriptional response (T) and those cells classified as having responded (mean cell fluorescence >T) were counted and presented as the percentage of the analysed cell population that had undergone a transcriptional response (Figure 5.24, A). The same cells were also checked against the threshold morphology response (M) and those cells classified as having responded (elongation factor >M) were counted and presented as the percentage of the population having undergone a morphology response (Figure 5.24, B). Single cell fluorescence and morphology measures were calculated in QuimP and subsequently the data was subjected to classification procedures using bespoke Matlab code.

The percentage of the population responding with time (Figure 5.24) indicates that the concentration of P-factor stimulation influences the proportion of the population that is signalling in terms of a transcriptional and a morphology response. In terms of transcription, as we have seen previously, cells only signal if treated with $\geq 10^{-8}$M P-factor and the increase in percentage responding becomes apparent after ~2 h. By 6 h, only 7 % of the population has responded at $10^{-8}$M, 74 % at $10^{-7}$M, 84 % at $10^{-6}$M and 94 % at $10^{-5}$M. By 10 h at P-factor concentration $>10^{-8}$M, >95 % of the population has undergone a transcriptional response, whilst at $10^{-8}$M the proportion responding has peaked at 44 %. At the intermediate P-factor concentration of $10^{-8}$M the population shows signs of recovery from the response, as the percentage responded begins to decrease after 10 h (Figure 5.24, A).

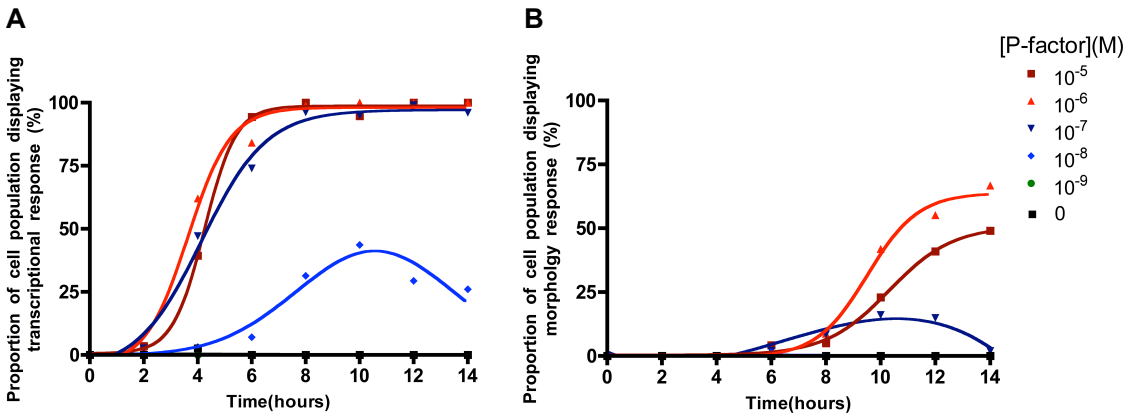


FIGURE 5.24: **Proportion of the cell population showing signalling response characteristics.** Reporter strain JY1325(*sxa2>GFP*) was grown in minimal media and incubated with 0M to $10^{-5}$M P-factor for 14 h. Images of the cell culture were taken at 0 h and subsequently every 2 h using a Leica SP5 scanning confocal microscope. Individual cells (n≥30) from the images were quantified for their fluorescence and morphology using image analysis software QuimP. Cells from each image taken at each time-point were selected at random and quantified for their mean fluorescence (mean pixel intensity) and elongation factor (ratio of cell length:width). For each image analysed, at each time-point, the percentage of cells analysed that had a fluorescence measure above the threshold fluorescence level for a non-responding cell was calculated (A). The percentage of cells displaying an elongation factor greater than the threshold level set for a non-responding cell was also calculated (B).

The responding population in terms of morphology indicates a different pattern of responding cells within the population. At concentrations ≤$10^{-8}$M, none of the cells within the population are showing a P-factor induced morphology response. At $10^{-7}$M, despite the transcriptional response being very high at this concentration, the percentage cells showing a morphology response peaks at just 16 % by 10 h. At higher concentrations (>$10^{-7}$M) the proportion is much higher, peaking at 66 % for $10^{-6}$M and 49 % for $10^{-5}$M at the 14 h time-point (Figure 5.24, B). In comparing the percentage responding population for transcriptional and morphology response it is clear that transcriptional response is observed prior to a morphology response and in much greater proportions of the population.

Defining responding cells within the population using fluorescence data alone from a *sxa2>GFP* reporter strain is problematic and results in misleadingly high proportions of the population that are apparently signalling. The problem is due to daughter cells of a mother cell that has undergone a transcriptional response being falsely counted as having responded themselves. This is due to the molecules of GFP expressed in response to P-factor in the mother cell being shared amongst the two daughter cells following recovery from the response and subsequent cell division, therefore resulting in daughter cells with high levels of fluorescence. The problem lies with the fact that GFP is extremely stable (Shaner et al., 2005) and therefore resides in the cell for much longer than the time taken for a cell to undergo the signalling response. To more accurately define cells that are in the process of signalling, we subjected cells to more stringent checks based on both

transcriptional and morphology data for classification as a responded cell. Cells were only classified as responded if they satisfied the criteria of having both mean cell fluorescence >T and elongation factor >M. Due to the fact that daughter cells of mother cells that have responded should have elongation factors <M, this should remove many of the false positives. This more stringent classification was used to obtain a more accurate representation of the subset of the population that is signalling (Figure 5.25, A). For comparison we also present percentage of the population that have mean cell fluorescence >T and elongation factor <M, to investigate the proportion of the population that shows transcriptional response, but do not commit to a morphology response (Figure 5.25, B).

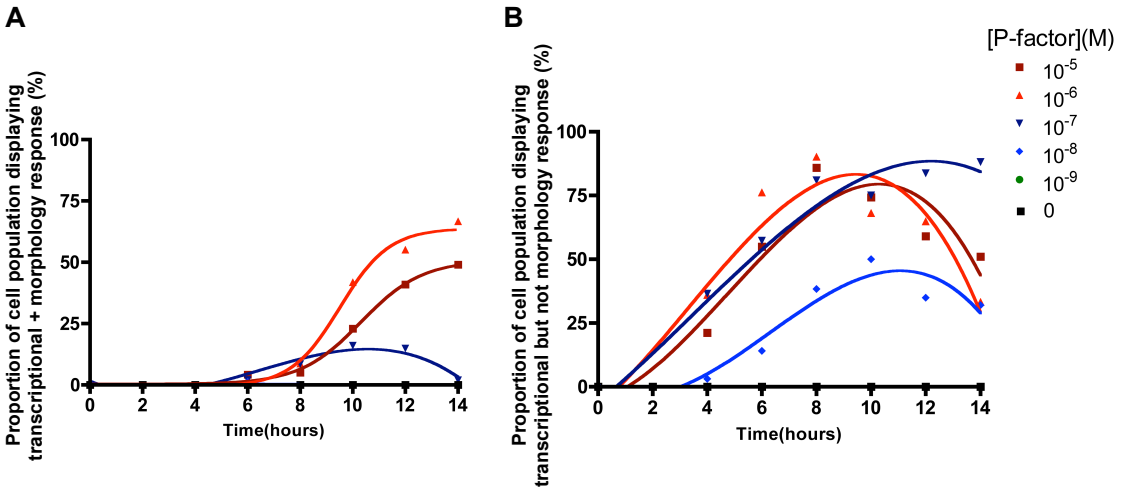


FIGURE 5.25: **Classification of the responding population-based on both transcriptional and morphology data.** Reporter strain JY1325(*sxa2>GFP*) was grown in minimal media and incubated with 0M to $10^{-5}$M P-factor for 14 h. Images of the cell culture were taken at 0 h and subsequently every 2 h using a Leica SP5 scanning confocal microscope. Individual cells (n≥30) from the images were quantified for their fluorescence and morphology using image analysis software QuimP. Cells from each image taken at each time-point were selected at random and quantified for their mean fluorescence (mean pixel intensity) and elongation factor (ratio of cell length:width). For each image analysed at each time-point, the percentage of cells analysed that had both a fluorescence measure above the threshold fluorescence level for a non-responding cell and an elongation factor greater than the threshold level set for a non-responding cell was calculated (A). For comparison the percentage of the analysed cells showing a fluorescence measure above the threshold fluorescence level for a non-responding cell but not having an elongation factor greater than the threshold level set for a non-responding cell was also calculated (B).

The data gives a more accurate representation of P-factor induced signalling in the population in terms of percentages of cells having responded to the P-factor (Figure 5.25, A). The percentages exactly match those when only the morphology was used as the classification criteria (compare Figure 5.25, A to Figure 5.24, B). This proves that in the case of every responding cell, induction of *sxa2>GFP* has to occur for that cell to undergo a morphology change. The data showing proportion of the population that displays transcriptional response but no morphology response (Figure 5.25, B) indicates that whilst cells treated with high P-factor concentration ($10^{-6}$M and $10^{-5}$M) will result in elongated

cells as indicated by the reduction in percentages after ∼8 h, cells treated with $10^{-7}$M do not display this reduction. This suggests that the majority of cells at $10^{-7}$M display a transcriptional response, but do not become very elongated (88 % of the population at 14 h). Again this implicates $10^{-7}$M as a 'tipping-point' for cell commitment to the morphology response.

Single cell quantification and subsequent classification to determine the proportions of the cell population that is signalling in response to ligand has proven to be useful in expanding on the quantitative information that can be obtained. Quantifying through time-series live-cell imaging and subsequent image analysis with QuimP has given greater insight into the signalling response of a clonal population of cells than could be gained from population-based assays. Data suggests that initially a single cell's commitment to a signalling response in terms of ligand induced activation of the signalling pathway and transcription of P-factor induced genes, is dependent on concentration of ligand. The probability of a cell response likely increasing with increased ligand concentration. An additional 'decision' then appears to be made subsequent to transcription whether to commit to the morphology response, again dependent on ligand concentration. To further investigate single cell signalling response and to probe the relationship between the two branches of the signalling response; transcriptional and morphology, we can track and quantify only the cells within the population that commit to a signalling response.

## 5.8 Quantification of Time-series Live-cell Signalling Response in Single Cells

Given that it is possible to segment the population with reasonable accuracy into signalling and non signalling cells in terms of both transcriptional and morphology response, it is possible to investigate signalling specifically in those cells that are committed to a signalling response. This will enable far more accurate characterisation of the signalling response to P-factor of *S. pombe* cells at the single cell level. By identification of the responding cells within the population from the time-series images of live cells, image analysis software QuimP can then be used to select and track the response of solely these responding cells. This type of analysis should eliminate much of the variability seen previously as a result of the lack of complete synchronicity of the signalling response within the population, because multiple single signalling cells can be quantified from the start to the end of their response (i.e. through one round of cell division). This should increase the accuracy of the quantification of signalling in terms of amplitude and the temporal dynamics of the signalling response.

### 5.8.1 Transcriptional Response From Signalling Cells

To investigate transcriptional response in the signalling cells with time, we first had to select which cells from the time-series live-cell images would be quantified. For P-factor concentrations where no P-factor induced transcriptional response was observed ($\leq 10^{-9}$), we simply used a random selection process to select 10 single cells for quantification. For cells treated with $10^{-8}$M, 10 cells were randomly selected from the proportion of the population that were classified as responding by having mean cell fluorescence >T (previously identified in Figure 5.24, A). Cells treated with $\geq 10^{-7}$M P-factor were randomly selected from the proportion of the population that was classified as responding by having both mean cell fluorescence >T and elongation factor >M (previously identified in Figure 5.25, A). These cells were identified by their co-ordinates on the images and then segmented and tracked, with time through one round of cell division. Each cell was tracked from the first available frame to the last frame prior to division into daughter cells. Cells were quantified for induction of *sxa2>GFP* through mean cell fluorescence (Figure 5.26) and total cell fluorescence (Figure 5.27) measurement using image analysis software QuimP.

Data displaying transcriptional response to P-factor with time of individual signalling cells in terms of mean cell fluorescence (Figure 5.26) indicates that even in genetically identical reporter cells, the duration and amplitude of the signalling response is variable from cell-to-cell. The data indicates that with increasing P-factor concentration, the time taken to complete a signalling response is increased. For all concentrations that result in a transcriptional response ($\geq 10^{-8}$M), the general pattern of response is similar, as a reasonably rapid increase in fluorescence is observed before plateauing for the remainder of the response. This is likely to be a result of increased P-factor concentration causing a longer $G_1$ arrest period, as previously observed from flow cytometry data (Figure 5.9). The plateau observed towards the end of the response indicates that transcription has ceased or slowed significantly. The reason a plateau, but not a decrease in mean cell fluorescence is observed is likely to be due to the slow maturation rate and high stability of the reporter protein, GFP. Despite this drawback of the reporter, it is still possible to use the time of the beginning of a plateau to estimate temporal aspects of the transcriptional signalling response in terms of terminating the response. Additionally, these same cells were also quantified for transcriptional response in terms of their total cell fluorescence (Figure 5.27).

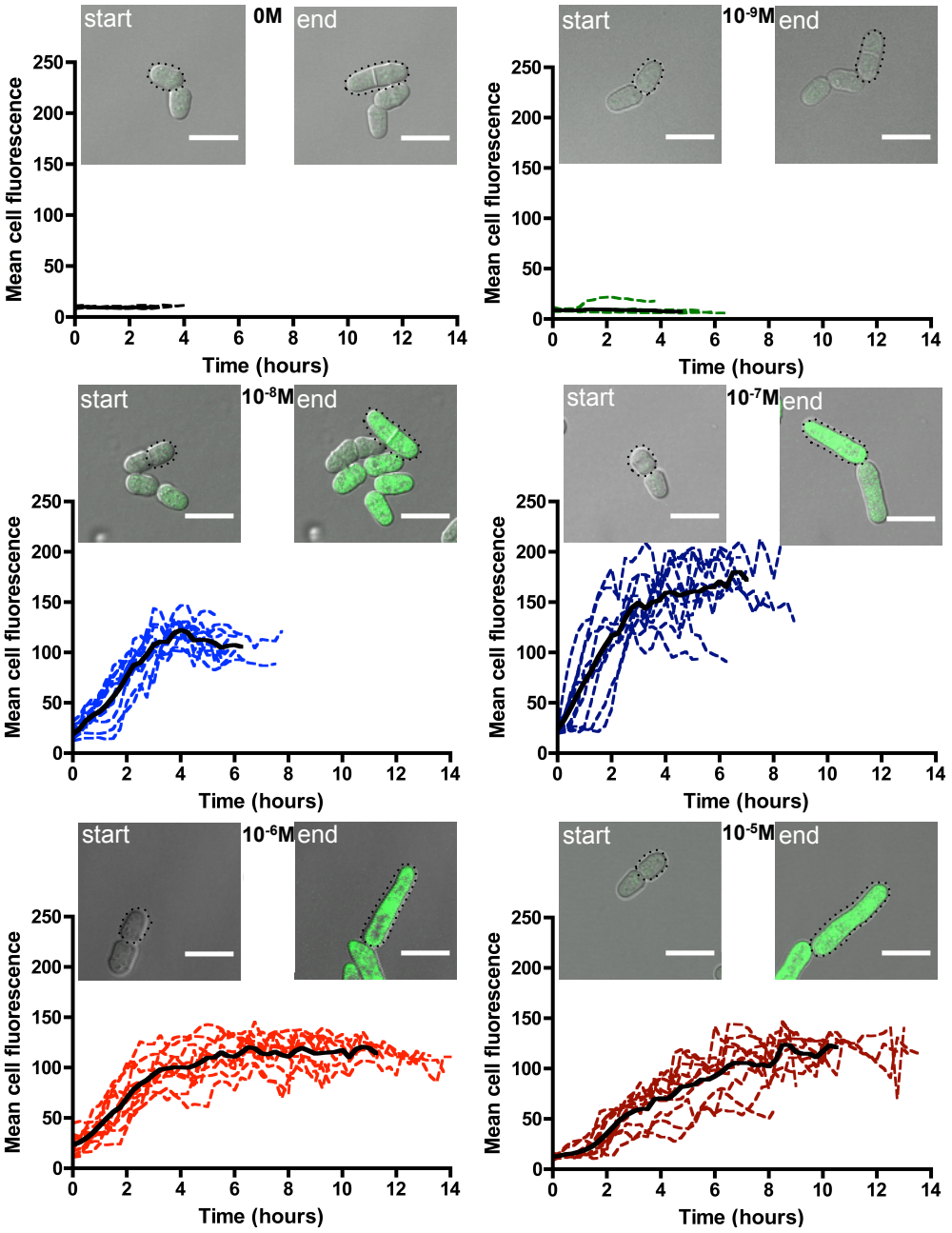


FIGURE 5.26: **Characterising live-cell time-series signalling response of single cells: mean cell fluorescence.** Cells from the *wild-type* reporter strain; JY1325(*sxa2>GFP*) were cultured to a density of ~5x10$^6$ cells/ml before transferring onto minimal media + agarose pads containing 0M to $10^{-5}$M P-factor. Pads were constructed on a microscope slide prepared for time-series live-cell imaging. Starting from a randomly selected field of view containing sufficient cells to monitor the response, images were taken every 15 min for a period of 14 h using a Leica SP5 scanning confocal microscope. At ligand concentrations resulting in a signalling response, from the cells classified as responding, 10 cells were selected at random, segmented and tracked with time from the first available frame to the final frame before the end of their signalling response (before cell division). For $\leq 10^{-9}$M P-factor treatments, cells to track were selected at random as there were no observable responding cells to select. Individual cells were quantified for their mean cell fluorescence (mean pixel intensity) at each frame. The **bold** line represents the average response from all cells quantified. Images are of one representative responding cell (light-field and fluorescence overlay) at each concentration, of the earliest frame post cell division (start) and the last frame pre cell division (end). Scale bar = 10 $\mu$m.

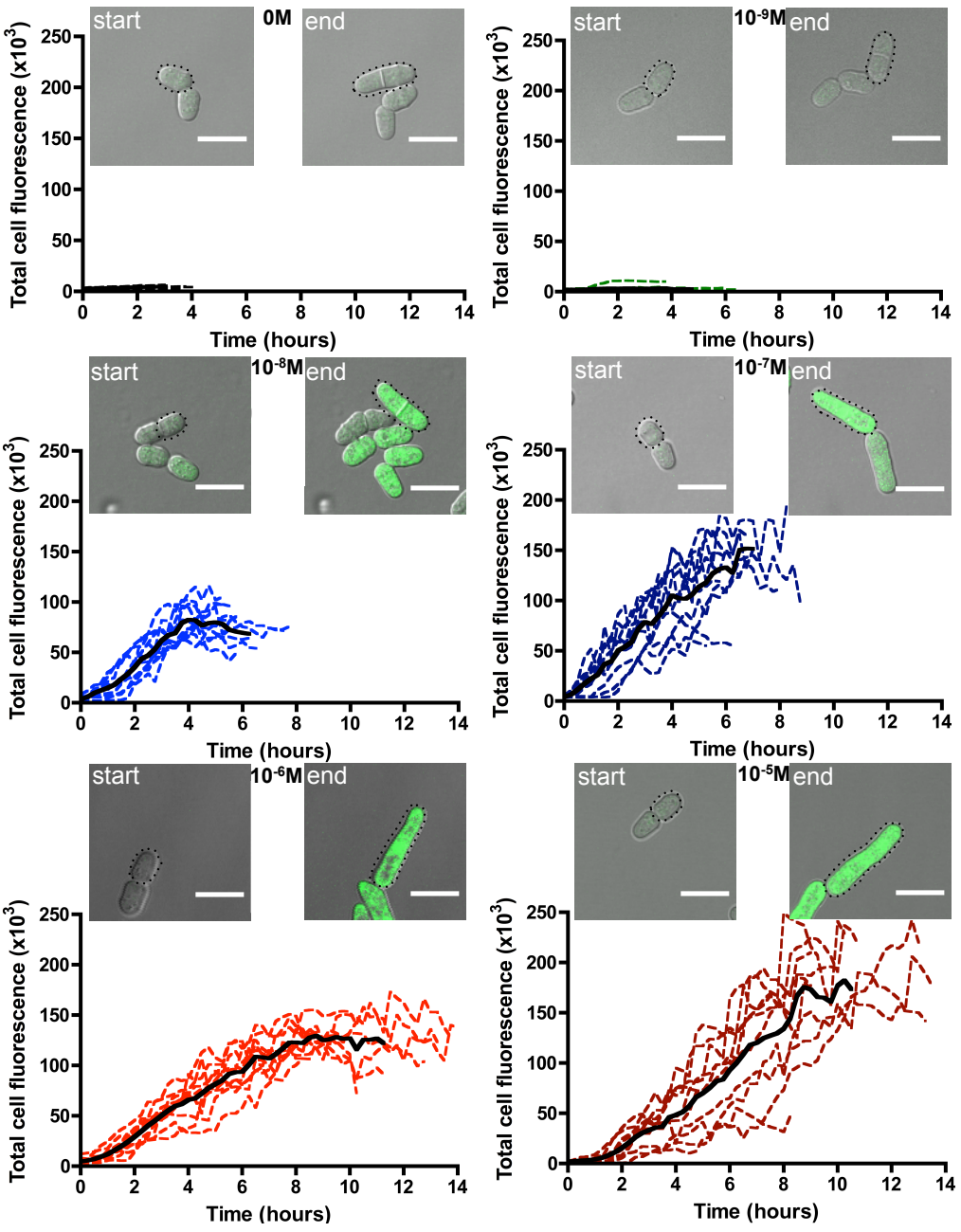


FIGURE 5.27: **Characterising live-cell time-series signalling response of single cells: total cell fluorescence.** Cells from the *wild-type* reporter strain; JY1325(*sxa2>GFP*) were cultured to a density of ~5x10$^6$ cells/ml before transferring onto minimal media + agarose pads containing 0M to $10^{-5}$M P-factor. Pads were constructed on a microscope slide prepared for time-series live-cell imaging. Starting from a randomly selected field of view containing sufficient cells to monitor the response, images were taken every 15 min for a period of 14 h using a Leica SP5 scanning confocal microscope. At ligand concentrations resulting in a signalling response, from the cells classified as responding, 10 cells were selected at random, segmented and tracked with time from the first available frame to the final frame before the end of their signalling response (before cell division). In the case of 0M and $10^{-9}$M P-factor treatments cells to track were selected at random as there were no observable responding cells to select. Individual cells were quantified for their total cell fluorescence (sum of all pixel intensities within the cell area) at each frame. The bold line represents the average response from all cells quantified. Images are of one representative responding cell (light-field and fluorescence overlay) at each concentration, of the earliest frame post cell division (start) and the last frame pre cell division (end). Scale bar = 10 $\mu$m.

Data presenting transcriptional response to P-factor with time of individual signalling cells in terms of total cell fluorescence (Figure 5.27) gives a very similar characterisation of single cell signalling response to that observed using mean cell fluorescence as the measurement (compare Figure 5.27 to Figure 5.26). This suggests that either of these single cell measurements might be suitable for use in this type of analysis.

#### 5.8.1.1 Comparing Ligand Concentration Effect on an Average Single Cell Transcriptional Response

To provide a comparison of the transcriptional response to varying ligand concentrations of single cells, the average signalling response (**bold** in Figures 5.26 and 5.27) were analysed. These average single cell responses were calculated from the mean cell fluorescence and total cell fluorescence data from each individual cell trace presented in Figure 5.26 and Figure 5.27. In addition to averaging the fluorescence intensity values, the time taken to complete the response (start to recovery/cell division) is also averaged for each P-factor concentration, giving average single cell response in terms of both transcription amplitude and time of response for each P-factor concentration. The dose-dependent effects of P-factor on the average single cell transcriptional response are compared (Figure 5.28).

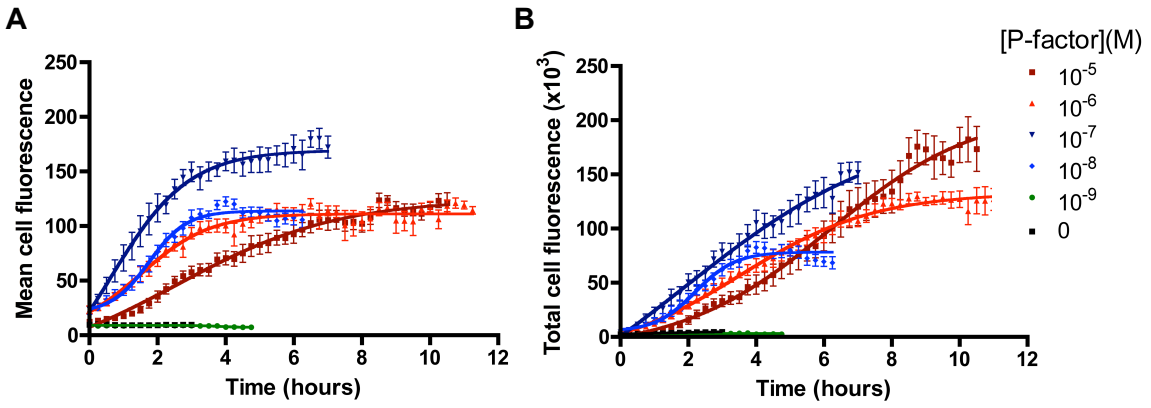


FIGURE 5.28: **The mean ligand-dependent time-series transcriptional response of a single cell.** Cells from the *wild-type* reporter strain; JY1325(*sxa2>GFP*) were cultured to a density of ~5x10$^6$ cells/ml before transferring onto minimal media + agarose pads containing 0M to $10^{-5}$M P-factor. Pads were constructed on a microscope slide prepared for time-series live-cell imaging. Starting from a randomly selected field of view containing sufficient cells to monitor the response, images were taken every 15 min for a period of 14 h using a Leica SP5 scanning confocal microscope. At ligand concentrations resulting in a signalling response, from the cells classified as responding, cells were selected at random, segmented and tracked with time from the first available frame to the final frame before the end of their signalling response (before cell division). For $\leq 10^{-9}$M P-factor treatments, cells to track were selected at random as there were no observable responding cells to select. Individual cells were quantified for their mean cell fluorescence (mean pixel intensity) and total cell fluorescence (sum of all pixel intensities within the cell area) at each frame as in Figure 5.26 and Figure 5.27. Results show the average mean fluorescence response (A) and the average total fluorescence response (B) ± S.E.M. from 10 single cells.

In analysing the data, it is possible to compare P-factor induced signalling response in closer detail and with more accuracy, as we are solely analysing the cells that have committed to a signalling response. The data shows a clear increase and plateau of fluorescence in signalling cells when using both mean cell fluorescence and total cell fluorescence as the measurement of transcription (Figure 5.28). Despite this similarity, it is useful to analyse data from both measurement types as we can learn subtly different information from the different data. The mean cell fluorescence data (Figure 5.28, A) suggests that cells committing to the signalling response at low P-factor concentration of $10^{-8}$M will induce *sxa2>GFP* to a similar extent as cells at $10^{-5}$M, with maximal mean cell fluorescence reaching 112.3 ± 1.662 at $10^{-8}$M and 122.8 ± 3.482 at $10^{-5}$M. This suggests an 'all or nothing' type transcriptional response. This is a slight misinterpretation, as we know from previous assays that cells treated at $10^{-8}$M do not elongate, therefore their maximal mean cell fluorescence value is increased as a result of a smaller cell area. This is also observed for mean cell fluorescence data at $10^{-7}$M, but in this instance a very rapid response is observed, increasing to a maximum mean fluorescence of 167.1 ± 3.903, which suggests that this could be a close to optimal concentration for the transcriptional response.

Given the influence of cell size on mean cell fluorescence data, it is possibly better to use total cell fluorescence as a measure of the amplitude of a transcriptional response (Figure 5.28, B). Here the differences in amplitudes are more distinguishable. However, this difference only becomes apparent after 4 h of the response, suggesting that in a cell that commits to a response (at $>10^{-9}$M P-factor), the level of initial transcription up until 4 h is independent of the P-factor concentration. The mean cell fluorescence measurements display a clearer initiation of transcription and plateau for each concentration, which aids in estimating the time when transcription starts and has stopped or slowed. At P-factor concentrations resulting in an increase in fluorescence, this increase becomes apparent after ∼30 min and transcription appears to stop/slow after ∼4 h. This stopping/slowing time appears to be longer, with plateau beginning at ∼7 h for $10^{-5}$M P-factor, possibly as a result of the initiation of mechanisms to protect against overstimulation when P-factor concentration is high. These more detailed temporal dynamics were not obtainable from previous plate-reader and flow cytometry based assays of fluorescent reporter strains.

In terms of the change in cellular fluorescence with time, there appears to be two phases; A rapid increase in fluorescence from ∼0-4 h followed by a more gradual increase or plateau when transcription has slowed or stopped. The rates of change in cellular fluorescence values in response to different P-factor concentrations could provide additional information about the effect of ligand concentration on the transcriptional response.

#### 5.8.1.2 Fluorescence Production Rates

We can discern additional information from the data for the average P-factor induced transcriptional response through investigating the change in fluorescence intensity in the duration of the signalling response. It is possible that altering the extent of P-factor stimulation of the signalling pathway might not only influence the quantity of fluorescent molecules through induction of *sxa2>GFP*, but also the rate at which they are being made. An estimate of the rates, which would incorporate transcription, translation, protein folding and formation of the fluorophore, can be obtained by calculating the rate of change in fluorescence intensity with time. Rates were calculated for the early response (0-4 h) using the general equation

$$Fl_{rate} = \frac{\Delta fluorescence}{\Delta t}, \tag{5.4}$$

where *fluorescence* = total cell fluorescence and $t$ = time (min).

For the early (0-4 h) response, the rates of change in fluorescence were calculated for each of the 10 cells at each P-factor concentration (Figure 5.29). In the case of the few cells that respond in less than 4 h (cells at 0M and $10^{-9}$M), the calculation was adjusted calculating the rate of change in fluorescence from 0 h to the final time-point of the response. Total cell fluorescence was used instead of mean cell fluorescence to calculate the rate, as this value was considered to more accurately represent the number of GFP molecules in the cell and is less influenced by cell size. Cell size should not greatly influence the rates calculated for each P-factor concentration regardless, as difference in cell size across all concentrations is minimal within 0-4 h.

Fluorescence production rate analysis (Figure 5.29) indicates that the rate of transcription initiation in the early stages of response to P-factor stimulation is dependent on the concentration of ligand. The rate increases from 0.013 ± 0.002 $\text{min}^{-1}$ at 0M to 0.333 ± 0.021 $\text{min}^{-1}$ at $10^{-8}$M. This rate is increased further to a peak of 0.421 ± 0.048 $\text{min}^{-1}$ at $10^{-7}$M. These intermediate P-factor concentrations appear to be the optimum to prompt a rapid, early response. When the concentration is increased above $10^{-7}$M, the fluorescence production rate is significantly decreased to 0.255 ± 0.024 $\text{min}^{-1}$ at $10^{-6}$M (unpaired $t$, $p<0.01$) and to 0.192 ± 0.036 $\text{min}^{-1}$ at $10^{-5}$M, suggesting that very high P-factor concentration is detrimental to the speed and amplitude of the early response. We have observed previously that $10^{-7}$M appears to be the 'tipping-point' concentration before large elongation factor can be achieved, therefore this decreased rate could be a result of a greater influence of the morphology response pathway competing with the transcriptional response, therefore causing a delay or reduction in transcription. There is also the possibility that

negative feedback mechanisms may exist that inhibit the transcriptional response upon activation of the morphology branch of the signalling pathway. An additional observation is that the fluorescence production rates display cell-to-cell variability, suggesting that there are differences in a cells capability to transcribe/express P-factor induced genes, possibly as a result of global variables such as the number of important molecules required for signal transduction and transcription / translation in the cell at the time they encounter the P-factor stimulation.

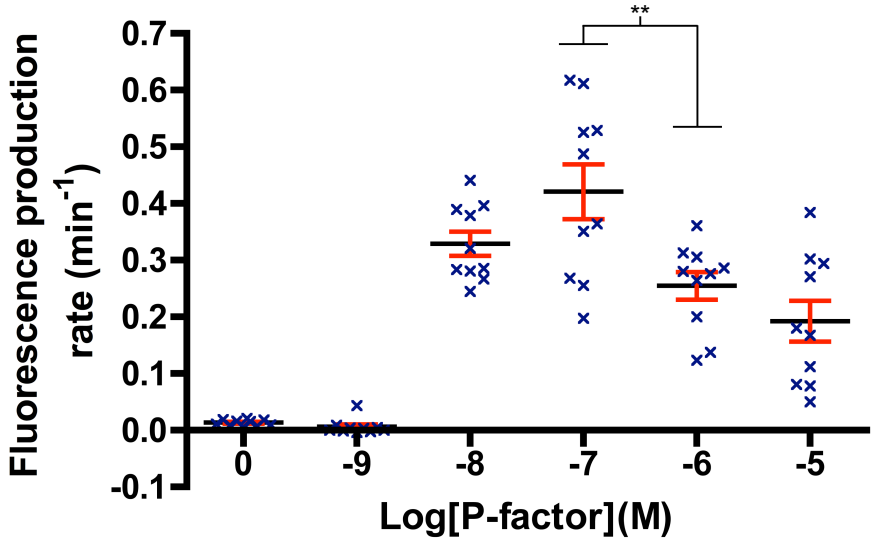


FIGURE 5.29: **Fluorescence production rate in single cell signalling response.** Cells from the *wild-type* reporter strain; JY1325(*sxa2>GFP*) were cultured to a density of ~5x10$^6$ cells/ml before transferring onto minimal media + agarose pads containing 0M to 10$^{-5}$M P-factor. Pads were constructed on a microscope slide prepared for time-series live-cell imaging. Starting from a randomly selected field of view containing sufficient cells to monitor the response, images were taken every 15 min for a period of 14 h using a Leica SP5 scanning confocal microscope. At ligand concentrations resulting in a signalling response, from the cells classified as responding, 10 cells were selected at random, segmented and tracked with time from the first available frame to the final frame before the end of their signalling response (before cell division). For ≤10$^{-9}$M P-factor treatments, cells to track were selected at random as there were no observable responding cells to select. Individual cells were quantified for their total cell fluorescence (sum of all pixel intensities within the cell area) at each frame as in Figure 5.27. Results show the fluorescence production rate for the early response to P-factor (0-4 h), with each data point representing the rate for a single cell and the black bar indicates the mean. Fluorescence production rate was calculated from 0-4 h using the formula $Fl_{rate} = \Delta$fluorescence/$\Delta$t. Statistically significant difference is indicated by ** ($p$<0.01) as determined by unpaired $t$ test.

### 5.8.2 Morphology Response From Signalling Cells

To investigate the morphology changes specifically in signalling cells, the same single cells as those selected and quantified for transcriptional response in Figure 5.26 and Figure 5.27 were also quantified for morphology response in terms of elongation factor using image analysis software QuimP (Figure 5.30).

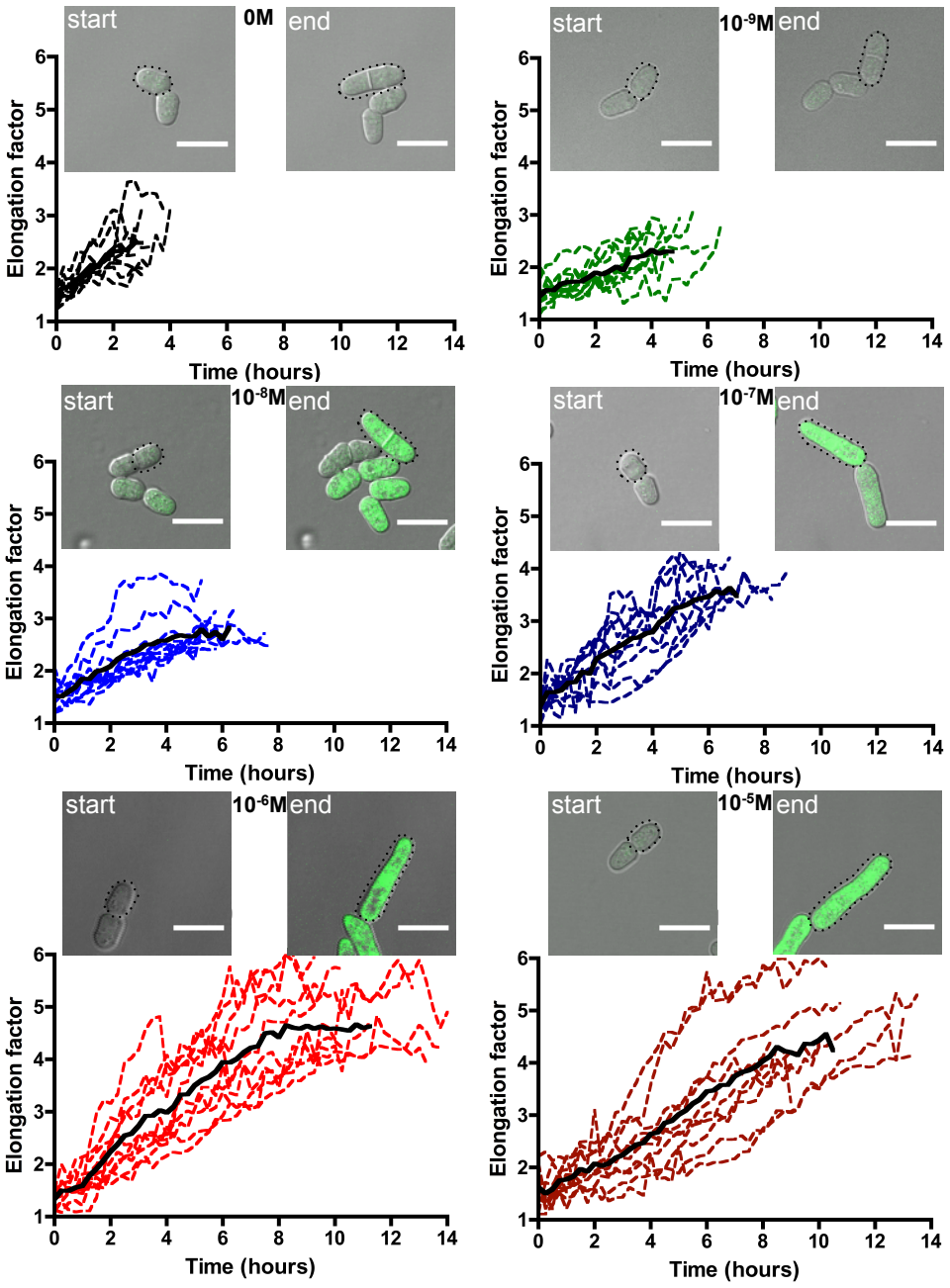


FIGURE 5.30: **Characterising live-cell time-series signalling response of single cells: morphology.** Cells from the *wild-type* reporter strain; JY1325(*sxa2>GFP*) were cultured to a density of ~5x10$^6$ cells/ml before transferring onto minimal media + agarose pads containing 0M to $10^{-5}$M P-factor. Pads were constructed on a microscope slide prepared for time-series live-cell imaging. Starting from a randomly selected field of view containing sufficient cells to monitor the response, images were taken every 15 min for a period of 14 h using a Leica SP5 scanning confocal microscope. At ligand concentrations resulting in a signalling response, from the cells classified as responding, 10 cells were selected at random, segmented and tracked with time from the first available frame to the final frame before the end of their signalling response (before cell division). For $\leq 10^{-9}$M P-factor treatments, cells to track were selected at random as there were no observable responding cells to select. Individual cells were quantified for their elongation factor (ratio of cell length:width) at each frame. The **bold** line represents the average response from all cells quantified. Images are of one representative responding cell (light-field and fluorescence overlay) at each concentration, of the earliest frame post cell division (start) and the last frame pre cell division (end). Scale bar = 10 $\mu$m.

Elongation factor traces from single cells (Figure 5.30) indicate that for all P-factor concentrations, elongation factor increases with time. This is apparent not only for cells that undergo a signalling response, but also for those showing normal vegetative cell growth at 0M. The effect of increasing P-factor concentration appears to be that the cells continue to elongate for an increasingly longer period of time until the cell division point. At concentrations $>10^{-7}$M, cells appear to become substantially more elongated and single cells are capable of continuing the signalling response for in excess of 12 h.

#### 5.8.2.1 Comparing Ligand Concentration Effect on an Average Single Cell Morphology Response

In order to investigate the effect of P-factor concentration on an average single cell morphology response, the mean elongation factor traces (**bold** in Figure 5.30) for each concentration of P-factor treatment were compared (Figure 5.31).

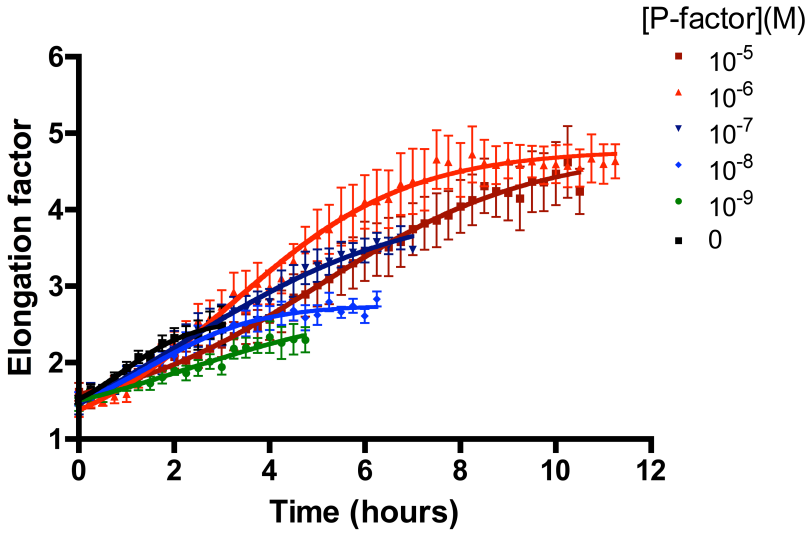


FIGURE 5.31: **The mean ligand-dependent time-series morphology response of a single cell.** Cells from the *wild-type* reporter strain; JY1325(*sxa2>GFP*) were cultured to a density of ~5x$10^6$ cells/ml before transferring onto minimal media + agarose pads containing 0M to $10^{-5}$M P-factor. Pads were constructed on a microscope slide prepared for time-series live-cell imaging. Starting from a randomly selected field of view containing sufficient cells to monitor the response, images were taken every 15 min for a period of 14 h using a Leica SP5 scanning confocal microscope. At ligand concentrations resulting in a signalling response, from the cells classified as responding, 10 cells were selected at random, segmented and tracked with time from the first available frame to the final frame before the end of their signalling response (before cell division). For 0M and $10^{-9}$M P-factor treatments cells to track were selected at random as there were no observable responding cells to select. Individual cells were quantified for their elongation factor (ratio of cell length:width) at each frame as in Figure 5.30. Results show the average elongation factor ± S.E.M. from 10 single cells.

The mean single cell morphology response data (Figure 5.31) indicates that an average cell undergoing normal vegetative cell growth will almost double its elongation factor from

1.5 ± 0.356 to 2.74 ± 0.362 within <4 h. The addition of P-factor at $10^{-9}$M and $10^{-8}$M does not result in more elongated cells, as they reach a similar elongation factor of 2.466 ± 0.189 and 2.721 ± 0.072 respectively, but take an increasingly longer period of time to reach this size. At intermediate P-factor stimulation of $10^{-7}$M, there is a further increase in the response time, but also cells become more elongated, reaching a maximum of 3.873 ± 0.236. Stimulation at $>10^{-7}$M results in cells that are more elongated and have longer response times, reaching a maximum elongation factor of 4.796 ± 0.170 for $10^{-5}$M P-factor stimulation. Similarly to fluorescence data, the elongation factor appears to plateau towards the later stages of the response, suggesting that cells slow down their elongation towards the end of the response, possibly in preparation for cell division.

#### 5.8.2.2 Elongation Rates

Additional information can be obtained from the average P-factor induced morphology response through investigating the change in elongation factor (elongation rate). It is possible that altering the extent of P-factor stimulation of the signalling pathway might not only influence the extent that the cell becomes elongated, but also the rate at which this elongation process occurs. As there are seemingly two phases to the response, an early response (0-4 h), whereby transcription initiation occurs, and a later phase (beyond 4 h) of the response, whereby at high P-factor concentrations, cells continue to elongate for a prolonged period of time, the rate of elongation is calculated within these two phases. The elongation rate is calculated in the early response to investigate whether P-factor causes any alteration in the rate of elongation compared to that of a vegetative growing cell. The later phase elongation rate is calculated within the 4-6 h time-frame, to investigate whether those cells that continue to elongate beyond 4 h, do so in a P-factor concentration-dependent manner, and again to determine whether this rate is different to vegetative cell elongation rates. An estimate of these rates can be obtained by calculating the rate of change in elongation factor from 0-4 h (early response) and 4-6 h (late response). For each of the 10 cells analysed, at each P-factor concentration, the elongation rate was calculated as

$$El_{rate} = \frac{\Delta elongation}{\Delta t}, \tag{5.5}$$

where $elongation$ = elongation factor and $t$ = time (min). The rates of change in elongation factor were calculated for each of the 10 cells at each P-factor concentration (Figure 5.32).

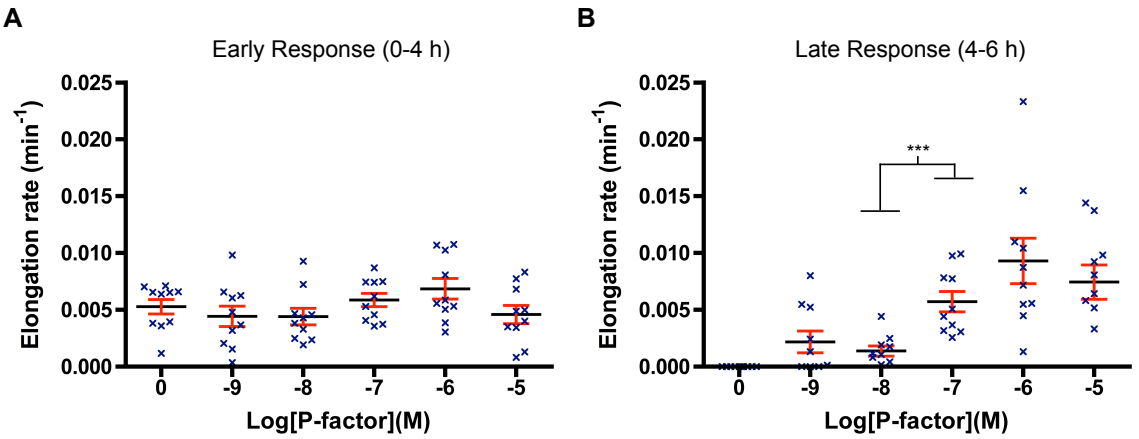


FIGURE 5.32: **Elongation rate in single cell signalling response.** Cells from the *wild-type* reporter strain; JY1325(*sxa2>GFP*) were cultured to a density of ~5x10$^6$ cells/ml before transferring onto minimal media + agarose pads containing 0M to 10$^{-5}$M P-factor. Pads were constructed on a microscope slide prepared for time-series live-cell imaging. Starting from a randomly selected field of view containing sufficient cells to monitor the response, images were taken every 15 min for a period of 14 h using a Leica SP5 scanning confocal microscope. At ligand concentrations resulting in a signalling response, from the cells classified as responding, 10 cells were selected at random, segmented and tracked with time from the first available frame to the final frame before the end of their signalling response (before cell division). For 0M and 10$^{-9}$M P-factor treatments, cells to track were selected at random as there were no observable responding cells to select. Individual cells were quantified for their elongation factor (ratio of cell length:width) at each frame as in Figure 5.30. Results show the elongation rate with each data point representing the rate for a single cell and the black bar indicates the mean. Elongation rates for the early response from 0-4 h (A) and late response from 4-6 h (B) are calculated as Elongation rate = El$_{rate}$=$\Delta$elongation/$\Delta$t. Significant difference is depicted by ***($p$<0.001) as determined by unpaired $t$ test.

The rates of change in elongation factor (Figure 5.32, A) indicate that in the early response (0-4 h), elongation rates do not significantly differ with increasing P-factor concentration (ANOVA, $F = 1.62$, $p = 0.17$). This suggests that within the time frame of a single normal vegetative cell division, P-factor is having no influence over the rate at which the cell grows. The elongation rate in the later response (4-6 h) (Figure 5.32, B) suggests a P-factor concentration effect on the elongation rate, with elongation rates being higher at 10$^{-7}$M to 10$^{-5}$M compared to those at 10$^{-9}$M to 10$^{-8}$M . The rate for 0M P-factor is 0 min$^{-1}$ and could be disregarded from comparisons here as these cells have already undergone cell division prior to the 4 h time-point.

### 5.8.3 Response Duration

We have observed from single cell traces that the time taken for completion of the response from start to end of a single round of cell division increases with increasing P-factor concentration. As the cells have to be in G$_1$ phase for a signalling response to occur, this should correlate well with the length of time spent in G$_1$-arrest. To investigate if P-factor concentration is increasing time spent in G$_1$-arrest in single cells, the mean cell division

times from the 10 signalling cells analysed at each P-factor concentration were calculated (Figure 5.33).

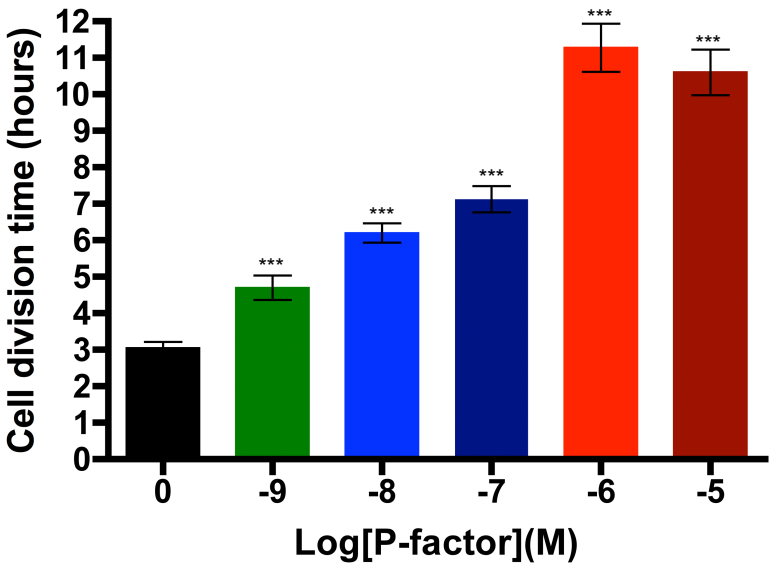


FIGURE 5.33: **Single cell duration of signalling response.** Cells from the *wild-type* reporter strain; JY1325(*sxa2>GFP*) were cultured to a density of ~5x10$^6$ cells/ml before transferring onto minimal media + agarose pads containing 0M to $10^{-5}$M P-factor. Pads were constructed on a microscope slide prepared for time-series live-cell imaging. Starting from a randomly selected field of view containing sufficient cells to monitor the response, images were taken every 15 min for a period of 14 h using a Leica SP5 scanning confocal microscope. At ligand concentrations resulting in a signalling response, from the cells classified as responding, 10 cells were selected at random, segmented and tracked with time from the first available frame to the final frame before the end of their signalling response (before cell division). For 0M and $10^{-9}$M P-factor treatments, cells to track were selected at random as there were no observable responding cells to select. Individual cells were quantified for the time taken for them to complete their response from the first frame at the start of a signalling response to the last possible frame before cell division. Results show the mean cell division time ± S.E.M. from 10 individual cells at each P-factor concentration. Cell division times that are significantly different to those at 0M P-factor are indicated with ***($p$<0.001), **($p$<0.01) or *($p$<0.05) as determined by unpaired $t$ test.

Investigations of cell-division time (Figure 5.33) confirm that time-taken for cell division increases in a P-factor concentration-dependent manner up to $10^{-6}$M (division time gradually increasing from 3.050 ± 0.162 h at 0M through to 11.280 ± 0.663 h at $10^{-6}$M P-factor concentration). This suggests that P-factor concentration has a graded effect on the time that a cell spends in $G_1$-arrest. The observation that there is no further increase in cell division time at $10^{-5}$M P-factor concentration, suggests that an upper limit on the possible response time may have been reached at this concentration.

### 5.8.4 Comparing Transcriptional and Morphology Response

We have previously observed from single cell population data that the transcriptional response is more sensitive to P-factor than the morphology response (Figure 5.17), and that a transcriptional response has to occur for there to be a morphology response. Given that we have both transcriptional and morphology data from the same individual signalling cells with time, it was possible to investigate in closer detail the relationship between the transcriptional and morphology P-factor induced response in single cells. Mean cell fluorescence data was compared to elongation factor data to investigate the temporal dynamics of the two responses in relation to each other. Average transcriptional and morphology response of single cells with time (Figure 5.28, A and Figure 5.31) was compared at P-factor concentrations of 0M to $10^{-5}$M (Figure 5.34).

Comparisons of transcriptional and morphology response (Figure 5.34) indicate that at low P-factor concentrations ($10^{-9}$M) there is no transcriptional response and gradual cell elongation to the point of cell division. The only impact of adding P-factor here is to arrest the cells for longer period of time compared to cells with 0M P-factor concentration. At the intermediate P-factor concentrations ($10^{-8}$M and $10^{-7}$M), there is a rapid induction of fluorescence, which halts or slows after ∼3 h. Up to this 3 h point the cells are elongating similarly to cells in the absence of P-factor, but after 3 h, when the initial 'burst' of transcription has ceased, the cells continue to elongate to beyond 6 h. The fluorescence change here over the course of the cell response is much larger than the elongation factor change, whereas at high P-factor concentrations ($10^{-6}$M and $10^{-5}$M), the extent of change in elongation factor is similar to the change in fluorescence. The transcriptional response in terms of maximal fluorescence at $10^{-6}$M and $10^{-5}$M P-factor concentrations does not appear to be greatly increased compared to that observed at intermediate concentrations, but the cell division time at these high concentrations is longer, resulting in cells becoming more elongated. At all concentrations, a P-factor concentration effect on elongation factor is not observed until after the initial transcriptional response. This highlights that the transcriptional response takes precedence over the morphology response in terms of both sensitivity and time.

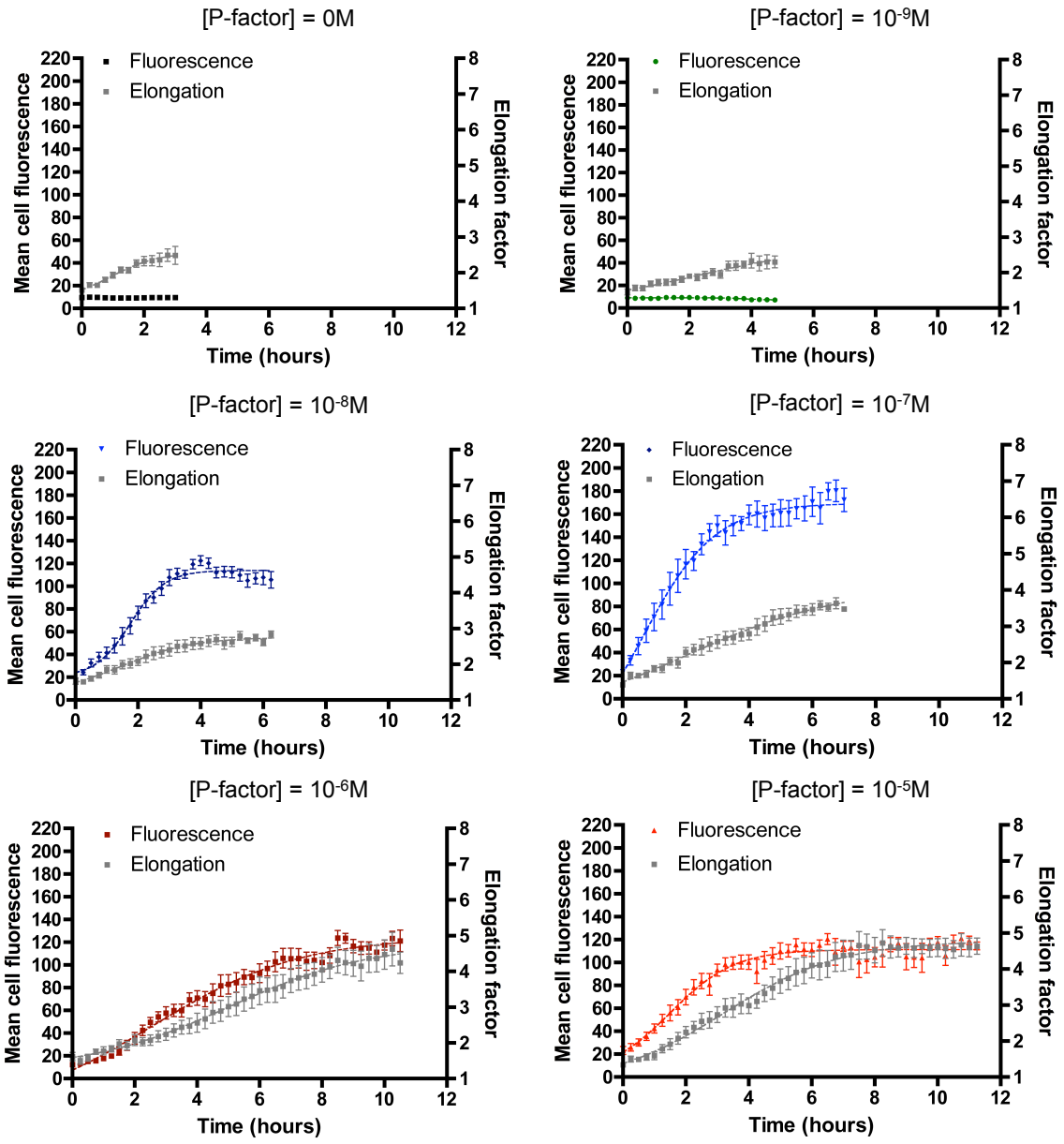


FIGURE 5.34: **Single cell time-series transcriptional vs morphology response.** Cells from the *wild-type* reporter strain; JY1325(*sxa2>GFP*) were cultured to a density of ~5x10$^6$ cells/ml before transferring onto minimal media + agarose pads containing 0M to $10^{-5}$M P-factor. Pads were constructed on a microscope slide prepared for time-series live-cell imaging. Starting from a randomly selected field of view containing sufficient cells to monitor the response, images were taken every 15 min for a period of 14 h using a Leica SP5 scanning confocal microscope. At ligand concentrations resulting in a signalling response, the responding cells were segmented and tracked with time from the first available frame to the final frame before the end of their signalling response (before cell division). For 0M and $10^{-9}$M P-factor treatments, cells to track were selected at random as there were no observable responding cells to select. Individual cells were quantified for their mean cell fluorescence (mean pixel intensity) and elongation factor (ratio of cell length:width) at each frame as in Figure 5.26 and Figure 5.30. Results are comparisons of the average single cell transcriptional response vs average single cell morphology response at each P-factor concentration. Results are means ± S.E.M. from 10 single cells.

We have extensively characterised *wild-type sxa2>GFP* reporter strains as quantitative reporters of signalling, using image analysis of time-series images to obtain quantitative insight into live single cell response to P-factor stimulation with time. Having established this quantification system, we can begin to investigate additional characteristics of the signalling response, such as whether signalling response is propagated through subsequent generations of cells. Additionally, now that an average *wild-type* single cells response has been characterised, we have a standard to compare to single cell responses of mutant strains and under perturbed environmental conditions.

### 5.8.5 Tracking Cell Lineages

To be able to investigate whether the signalling response is propagated through subsequent generations requires tracking cell lineages from mother cell through to subsequent daughter cells following cell division. Single cell lineages were to be tracked under conditions of prolonged P-factor stimulation to investigate whether cells become desensitised to continued stimulation. Additionally, to investigate recovery from a signalling response, single cell lineages were tracked following the removal of P-factor after initial stimulation for a period of time. Initially, as a control to provide a comparator to lineages under perturbed conditions, a single cell lineage was quantified using image analysis software QuimP on *sxa2>GFP* reporter cells undergoing vegetative cell growth in the absence of any P-factor (Figure 5.35).

A single cell in the process of vegetative cell growth maintains a low level of basal fluorescence with time through two generations of daughter cells. A cell will elongate between 2-3 times its original length before dividing, and one round of cell division takes ∼2 h 30 min - 3 h 30 min (Figure 5.35). These data provide a control lineage for comparison to investigations of cell lineages under perturbed conditions.

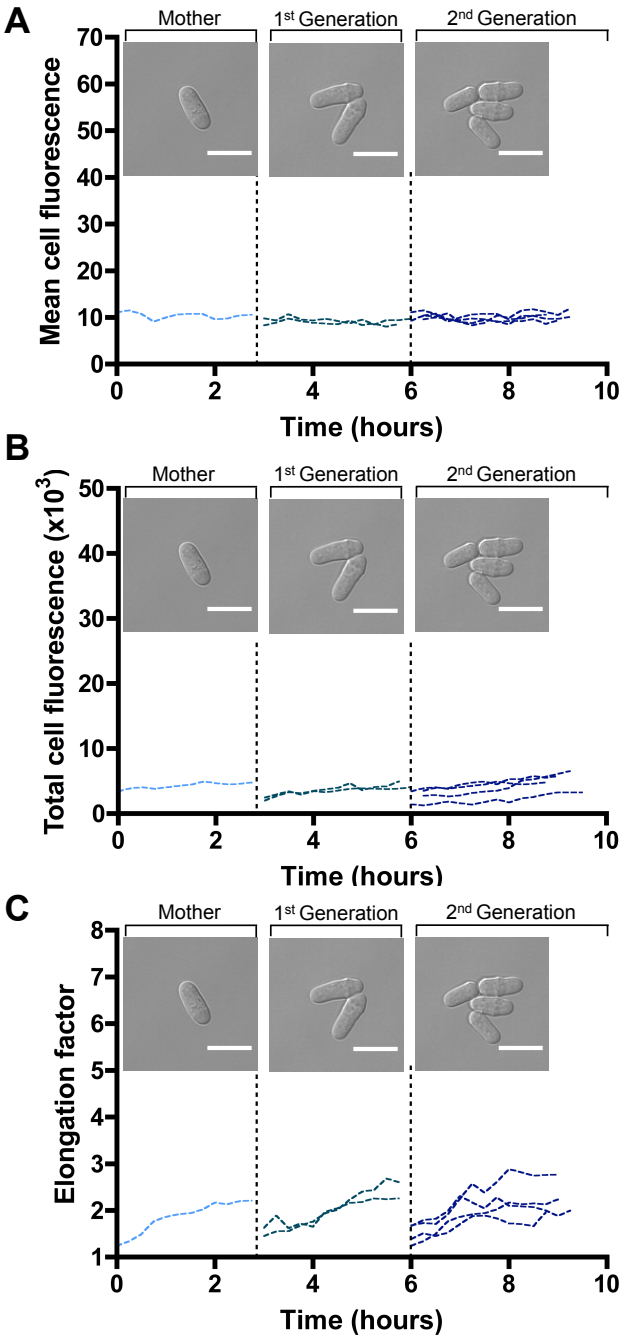


FIGURE 5.35: **Vegetative cell growth lineage.** Cells from the *wild-type* reporter strain; JY1325(*sxa2>GFP*) were cultured to a density of ~5x10$^6$ cells/ml before transferring onto a minimal media + agarose pad containing 0M P-factor. The pad was constructed on a microscope slide prepared for time-series live-cell imaging. The cells on the pads were imaged starting from a randomly selected field of view containing sufficient cells to monitor cell growth. Images were taken every 15 min for a period of 14 h using a Leica SP5 scanning confocal microscope. A single cell chosen to be representative of the population was segmented and its lineage tracked with time using image analysis software QuimP to quantify mean fluorescence (mean pixel intensity) (A), total fluorescence (sum of pixel intensities within the cell area) (B) and elongation factor (ratio of cell length:width) (C). Quantification of the mother cell and two subsequent generations of daughter cells are shown. The dashed lines indicate cell division and the light-field images are of the mother cell, $1^{st}$ generation and $2^{nd}$ generation cells selected for the quantification.

### 5.8.6 Prolonged Ligand Exposure

Cells have mechanisms to desensitise themselves to enable recovery from stimulation to ligand, for example through ligand induced internalisation of the cell surface receptor (Von Zastrow and Kobilka, 1992). Internalisation of the *S. pombe* P-factor receptor Mam2 in response to P-factor stimulation was observed in Chapter 4. To investigate if cells undergoing the P-factor induced mating-response would become desensitised and recover, cells were imaged through subsequent generations in conditions of prolonged P-factor stimulation. The *sxa2>GFP* reporter strain was grown in minimal media before transferring to an agarose pad containing $10^{-5}$M P-factor. Cells were incubated on the pad with P-factor for an initial 8 h, such that the majority of the cells will have had sufficient time, stimulated with P-factor to complete or almost complete an initial signalling response. Following this incubation period, live cells on the agarose pad were imaged for a further 14 h using a Leica SP5 scanning confocal microscope (Figure 5.36).

Observing cells under conditions of prolonged P-factor exposure (Figure 5.36) indicates that the cells do not become desensitised to the P-factor within the time-frame of the imaging experiment, which suggest a population of cells has the capability to continually respond to P-factor stimulation. To monitor the continuation of the signalling response through subsequent generations of a single cell lineage, two representative single cells that, at the 8 h point had almost completed transcriptional and morphology response to P-factor, were selected and tracked using image analysis software QuimP. The cells selected (Figure 5.36, B) were quantified for transcriptional and morphology response through 2 subsequent generations using QuimP (Figure 5.37).

Lineages of representative cells in conditions of prolonged P-factor stimulation (Figure 5.37) suggest that daughter cells in the same lineage of an initial cell that has completed a signalling response are capable of P-factor induced signalling response. Elongation factor gives a good indication of both a transcriptional and morphology response to P-factor having occurred, given that we know transcription occurs prior to cell elongation. The $2^{nd}$ generation cells of both representative cell lineages display an increased cell division time and increased elongation factor with time, indicative of P-factor induced response. Observations from the time-series live-cell imaging (Figure 5.36) and the quantification using image analysis (Figure 5.37) has also given insight into the behaviour of the $1^{st}$ generation cells (i.e. the daughters of cells that have completed a signalling response). These cells do not respond to P-factor, but instead complete their life cycle and divide within a short time-frame to produce the $2^{nd}$ generation cells, which can then initiate a signalling response (Figure 5.37).

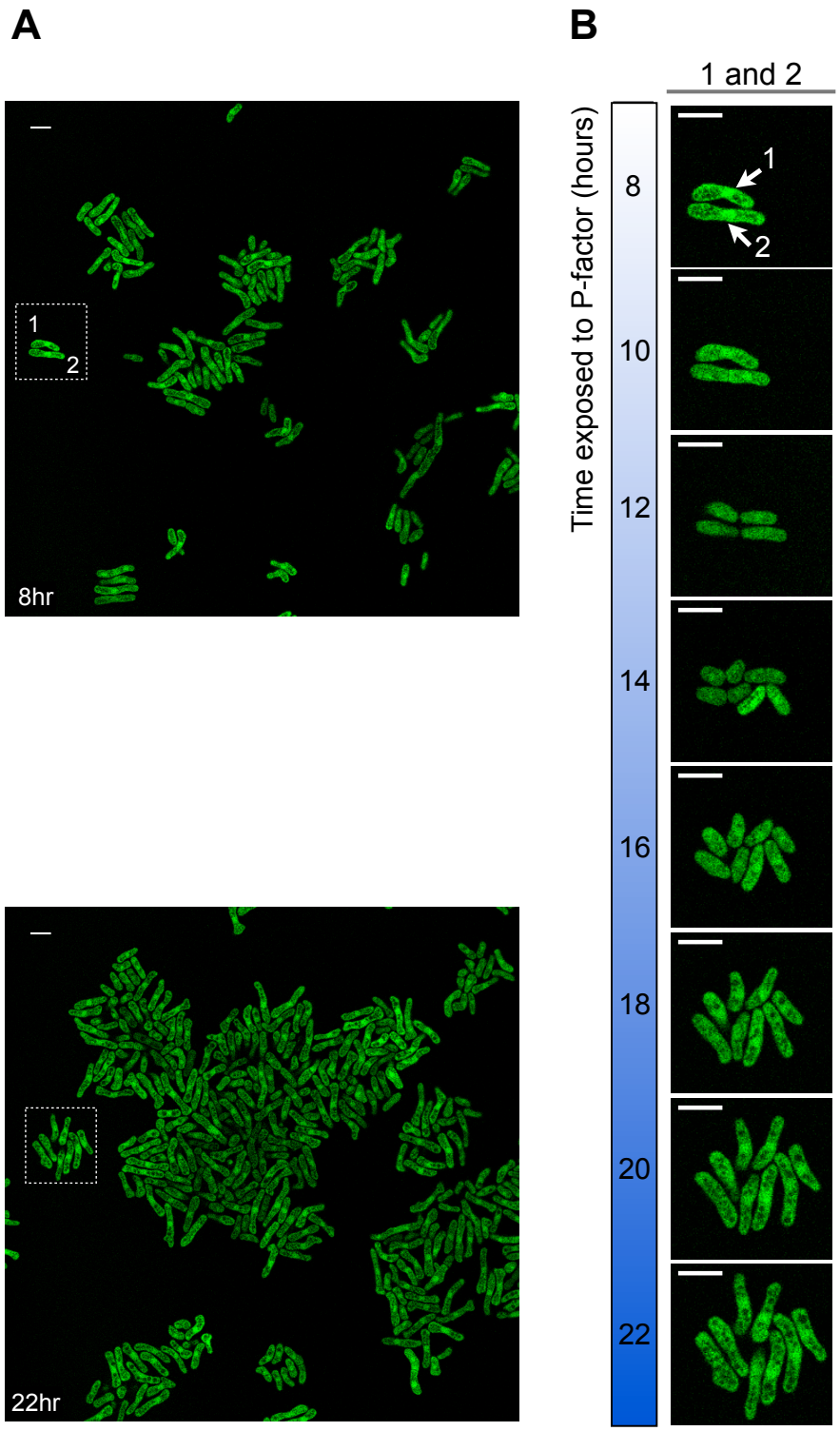


FIGURE 5.36: **Extended P-factor exposure.** Cells from the *wild-type* reporter strain; JY1325(*sxa2>GFP*) were cultured to a density of ~5x10$^6$ cells/ml before transferring onto a minimal media + agarose pad containing $10^{-5}$M P-factor. The pad was constructed on a microscope slide prepared for time-series live-cell imaging. The cells on the pad were incubated for 8 h before beginning the imaging. Starting from a randomly selected field of view containing sufficient cells to monitor the response, images were taken every 15 min for a period of 14 h using a Leica SP5 scanning confocal microscope. A: The population of cells at the start (0 h) and end (14 h) of the imaging experiment. B: Cells 1 and 2 were selected as representative examples of the cell population to track cell lineage under conditions of prolonged P-factor exposure. Scale bar = 10 $\mu$m

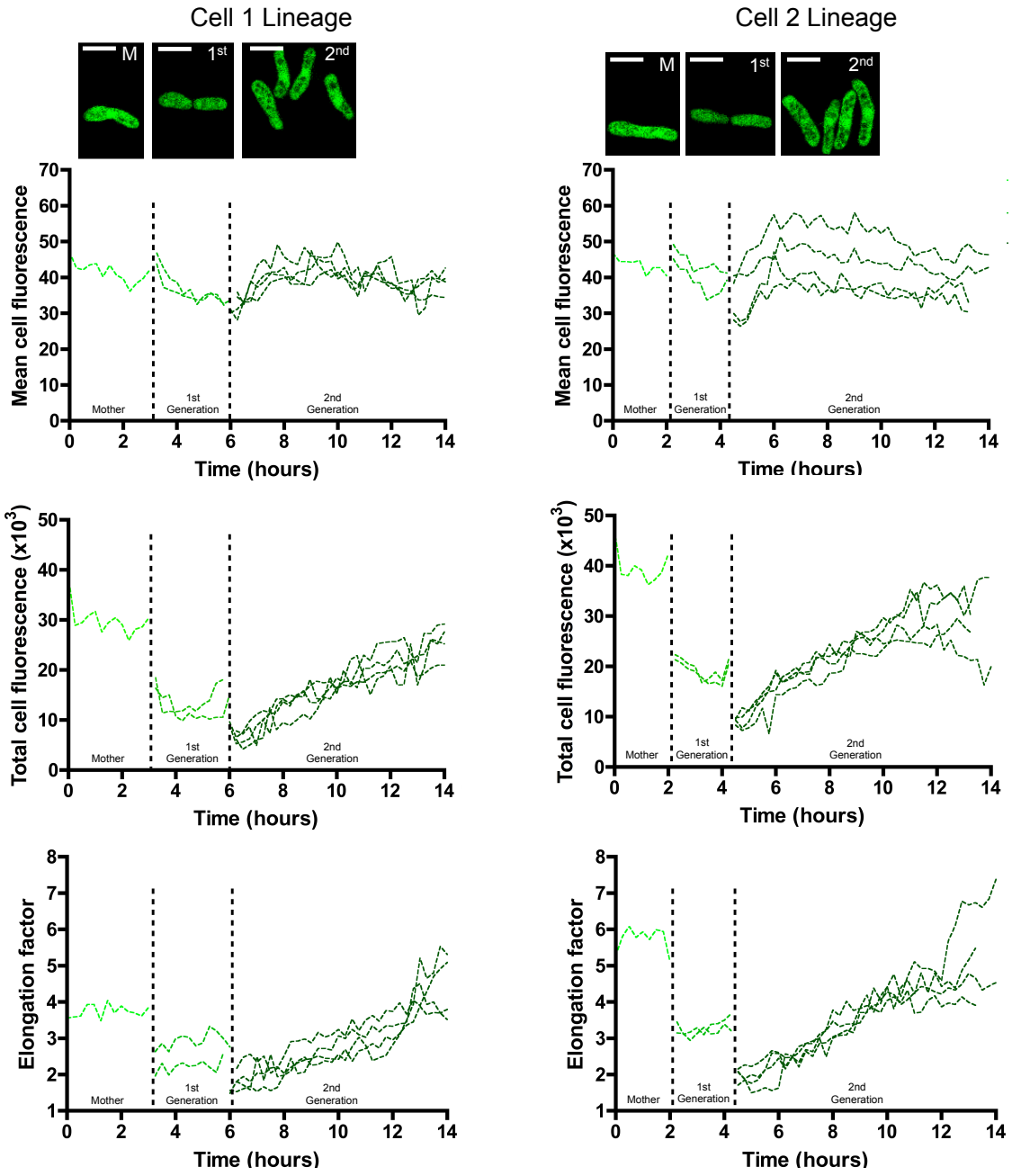


FIGURE 5.37: **Extended P-factor exposure: Single cell lineages.** Cells from reporter strain; JY1325(*sxa2>GFP*) were cultured to a density of ~5x10$^6$ cells/ml before transferring onto a minimal media + agarose pad containing $10^{-5}$M P-factor. The pad was constructed on a microscope slide prepared for time-series live-cell imaging. The cells on the pads were incubated for 8 h before beginning the imaging. Starting from a randomly selected field of view containing sufficient cells to monitor the response, images were taken every 15 min for a period of 14 h using a Leica SP5 scanning confocal microscope. Two single cells chosen to be representative of the population (Figure 5.36) were segmented and their lineages were tracked with time using image analysis software QuimP to quantify mean fluorescence (mean pixel intensity), total fluorescence (sum of pixel intensities within the cell area) and elongation factor (ratio of cell length:width). Quantification of the mother cell and two subsequent generations of daughter cells are shown. The images (inset) are of the mother cell (M), $1^{st}$ generation cells ($1^{st}$) and $2^{nd}$ generation cells ($2^{nd}$) used for the quantification. Scale bar = 10 $\mu$m and the dashed lines indicate the point of cell division.

### 5.8.7 Size Dependent Rapid Cell Division

The identification of subsequent $1^{st}$ generation cells emanating from cells that have completed P-factor induced response, having a rapid cell division time was a common occurrence within the cell population (from observation of the time-series imaging). In theory, any daughter cell in Figure 5.36 should be capable of initiating a response given that the cell will initially be in the correct phase of its cell cycle; $G_1$, and that P-factor is present at sufficient concentration to induce a response ($10^{-5}$M). The observation that some cells will seemingly not arrest in $G_1$ phase in response to P-factor, but instead initiate a rapid round of cell division, implies there is higher level control mechanism to determine commitment to a signalling response. One key difference of these 'rapid-dividers' is that they are daughters of cells that have completed a signalling response. Due to cell division by mitotic fission, the daughter cells will therefore be more elongated as a result of the elongation of the mother cells following P-factor induced response. Indeed, previous work has proposed molecular mechanisms linking cell size to the cell cycle (Moseley et al., 2009). To investigate the link between elongation factor and rapid cell division in the presence of P-factor, elongation factor at the start of a single round of cell division and time taken to complete cell division of randomly selected $1^{st}$ generation cells from Figure 5.36 was compared to that of cells undergoing normal vegetative growth (Figure 5.38).

Investigation of elongation factor vs cell division time (Figure 5.38) suggests that the majority of $1^{st}$ generation cells from mother cells that have completed a P-factor induced response at $10^{-5}$M P-factor stimulation have a reduced cell division time in comparison to untreated cells undergoing vegetative cell growth (Figure 5.38). Additionally, these cells are more elongated at the beginning of their cell division cycle, having over double the mean elongation factor compared to the untreated control. Significant (Pearson, $r$ = -0.64, $p$<0.001) negative correlation occurs within the data for elongation factor vs cell division time, indicating that if a cell is less elongated at the beginning of its cell division cycle then it should take longer to grow to the point of cell division. Taken together, these data indicate the length of the cell as a characteristic controlling cell cycle time. Furthermore, a cluster of 'rapid-dividers' representing the P-factor treated $1^{st}$ generation cells with cell division time <250 min can be identified (Figure 5.38, A). Comparing the cell division time of these rapid-dividers to that of vegetatively growing cells (Figure 5.38, B) indicates that rapid dividers have significantly reduced cell-division time (unpaired $t$, $p$<0.001).

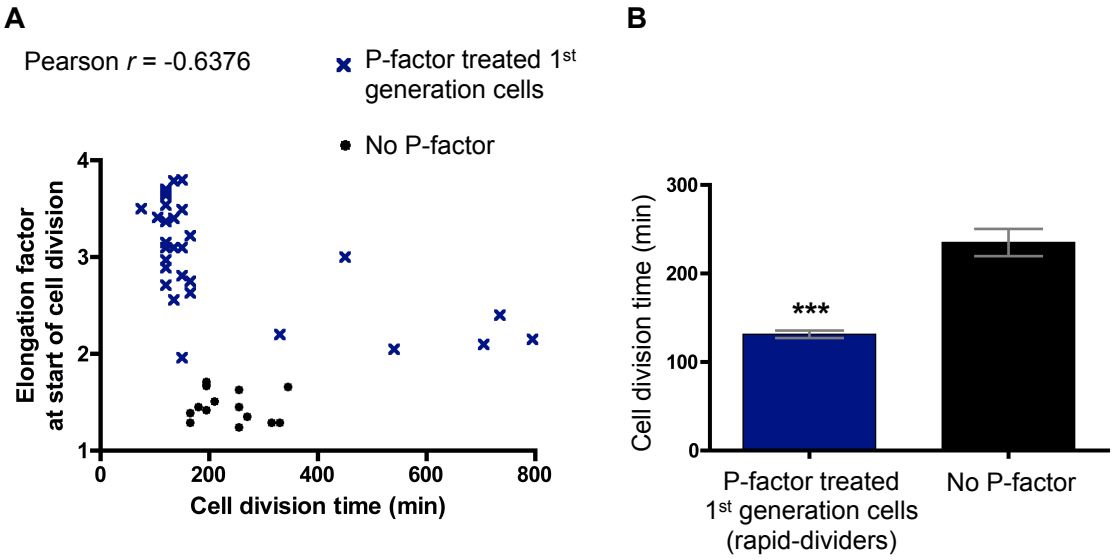


FIGURE 5.38: **Size dependent cell division time.** Cells from the reporter strain; JY1325(*sxa2>GFP*) were cultured to a density of ~5x10$^6$ cells/ml before transferring onto a minimal media + agarose pad containing $10^{-5}$M P-factor. The pad was constructed on a microscope slide prepared for time-series live-cell imaging. The cells on the pad were incubated for 8 h before beginning the imaging. Starting from a randomly selected field of view containing sufficient cells to monitor the response, images were taken every 15 min for a period of 14 h using a Leica SP5 scanning confocal microscope. First generation cells (n = 30), (daughters of a mother cell that has completed its signalling response), were segmented with image analysis software QuimP and quantified for their cell division time and elongation factor (ratio of cell length:width) at the first available frame following division of their mother cell. Relationship between cell division time and starting elongation factor of these first generation cells is analysed (A, P-factor treated $1^{st}$ generation cells). For comparison data from cells undergoing normal vegetative cell growth is included (n = 15) (A, No P-factor). The Pearson sample correlation coefficient $r$, is calculated from all data points. Cell division time of the 'rapid-dividers' from the P-factor treated $1^{st}$ generation cells (cell division time <250 min) is compared to cell division time of cells growing in the absence of P-factor (B). Results in B are the mean ± S.E.M. and significant difference is indicated by ***($p$<0.001) as determined by unpaired $t$ test.

Previous studies have coupled cell length to entry into mitosis through an intracellular gradient of the dual-specificity tyrosine-phosphorylation regulated kinase (DYRK) Pom1 (Martin and Berthelot-Grosjean, 2009; Moseley et al., 2009). As the cell grows Pom1 inhibits transition into mitosis, but when a critical cell size is reached, the spatial gradient of pom1 has sufficiently altered, which removes inhibition of mitosis, therefore triggering the cell to divide. Investigation of the relationship of cell length and cell division time in the presence of P-factor stimulation (Figure 5.38) indicates that this cell elongation sensing mechanism dominates over the mating-response pathway through promoting continuation through the cell cycle over P-factor induced $G_1$-arrest.

We have observed that at high P-factor stimulation, cells do not appear to become desensitised to P-factor. Subsequent daughter cells in a lineage of a mother cell that has itself undergone a signalling response are capable of themselves committing to a signalling response, seeming to follow a pattern of response→rapid cell division→response. Cells do

not therefore recover back to normal vegetative cell growth following continued stimulation. Another avenue to investigate the capability of cells to recover and resume vegetative growth was to remove P-factor from the cells environment after a period of time.

### 5.8.8 Recovery From Signalling Response

Physiologically, the P-factor induced signalling response is required for mating, but this process will not be 100 % efficient all of the time. Some cells will initiate a mating-response and elongate towards the source of P-factor but then not encounter a mating partner. Cells have evolved to be capable of adapting to changes in their environment in order to survive. This means that there is a requirement for cells to recover from stimulation and resume vegetative cell growth. To investigate this recovery process, we subjected *sxa2>GFP* reporter cells to an initial environment of minimal media containing $10^{-5}$M P-factor before washing and transferring cells to a new environment on a minimal media + agarose pad lacking P-factor. To monitor single cells having removed the P-factor stimulation, cells were then imaged for a period of 14 h using a Leica SP5 scanning confocal microscope (Figure 5.39).

Observation of the images indicate that cells are able to recover from the stimulation to resume normal vegetative cell growth (compare 16 h to 30 h in Figure 5.39, A). To investigate the recovery process quantitatively, 3 single cells were selected at the beginning of the imaging experiment (Figure 5.39, B) to follow their cell lineages and quantify the recovery in terms of cell morphology and transcriptional characteristics using QuimP (Figure 5.40).

Recovery from initial P-factor stimulation is observed from the cell lineages in terms of cell fluorescence (Figure 5.40). Both mean cell fluorescence and total cell fluorescence data indicates that induction of *sxa2>GFP* had ceased from the point at which P-factor was removed at 16 h. The subsequent decrease in cell fluorescence through the two generations of daughter cells indicates that GFP is being degraded within the cells with time. The $1^{st}$ generation cells again show rapid cell division behaviour, probably due to cell size effects as investigated previously (Figure 5.38). The $2^{nd}$ generation cells do not show any transcriptional response and also have elongation factor profiles and cell division times more reminiscent of cells in normal vegetative growth (compare Figure 5.40 to Figure 5.35).

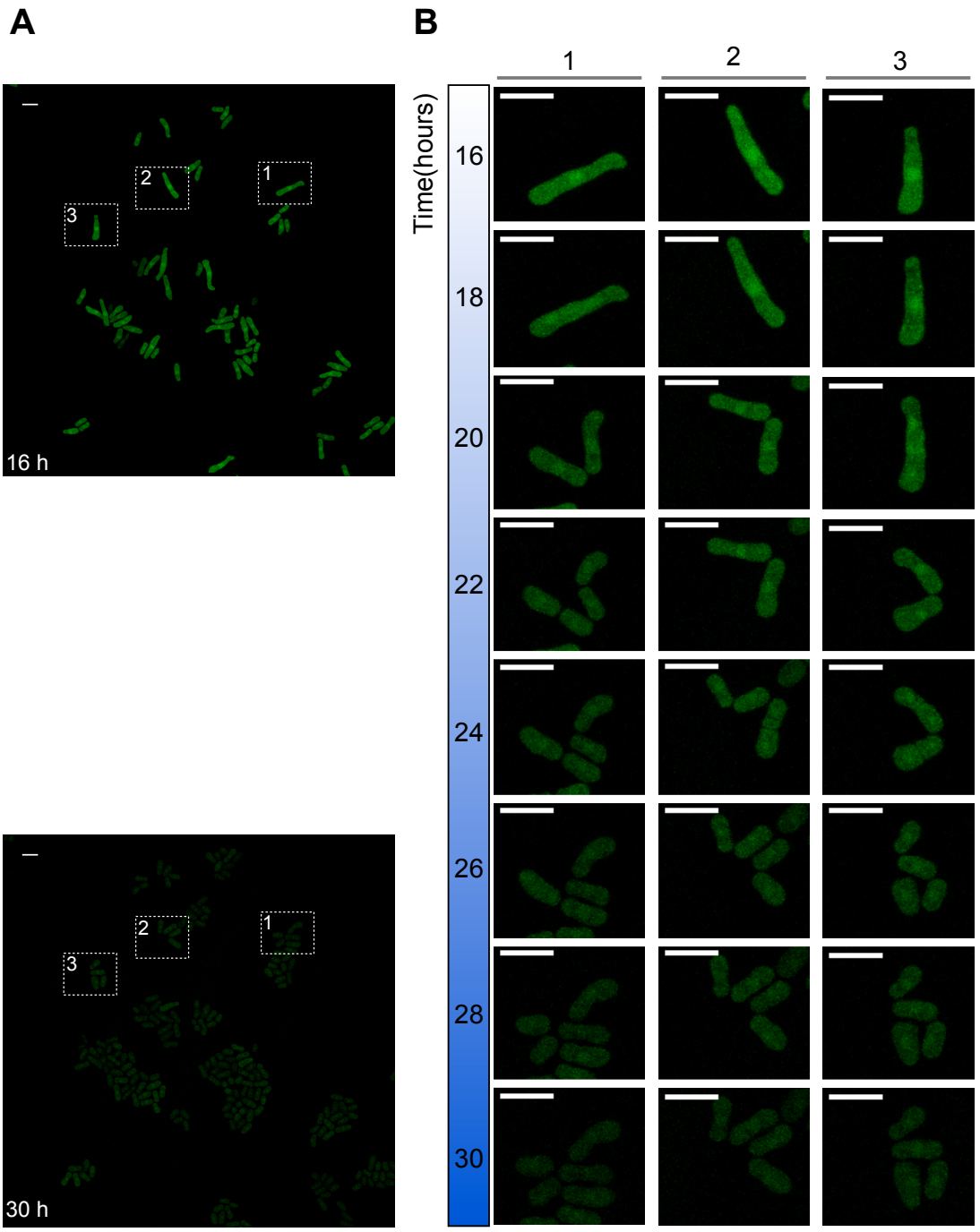


FIGURE 5.39: **Recovery following P-factor stimulation.** Cells from the reporter strain; JY1325(*sxa2>GFP*) were cultured to a density of ~5x10$^6$ cells/ml and incubated with $10^{-5}$M P-factor for 16 h before washing to remove P-factor and transferring onto a minimal media + agarose pad. The pads was constructed on a microscope slide prepared for time-series live-cell imaging. Starting from a randomly selected field of view containing sufficient cells to monitor the population, images were taken every 15 min for a period of 14 h using a Leica SP5 scanning confocal microscope. A: The population of cells at the start (16 h) and end (30 h) of the imaging experiment. B: Cells 1, 2 and 3 were selected as representative examples of the cell population to track cell lineage of cells recovering from a signalling response. Scale bar = 10 $\mu$m.

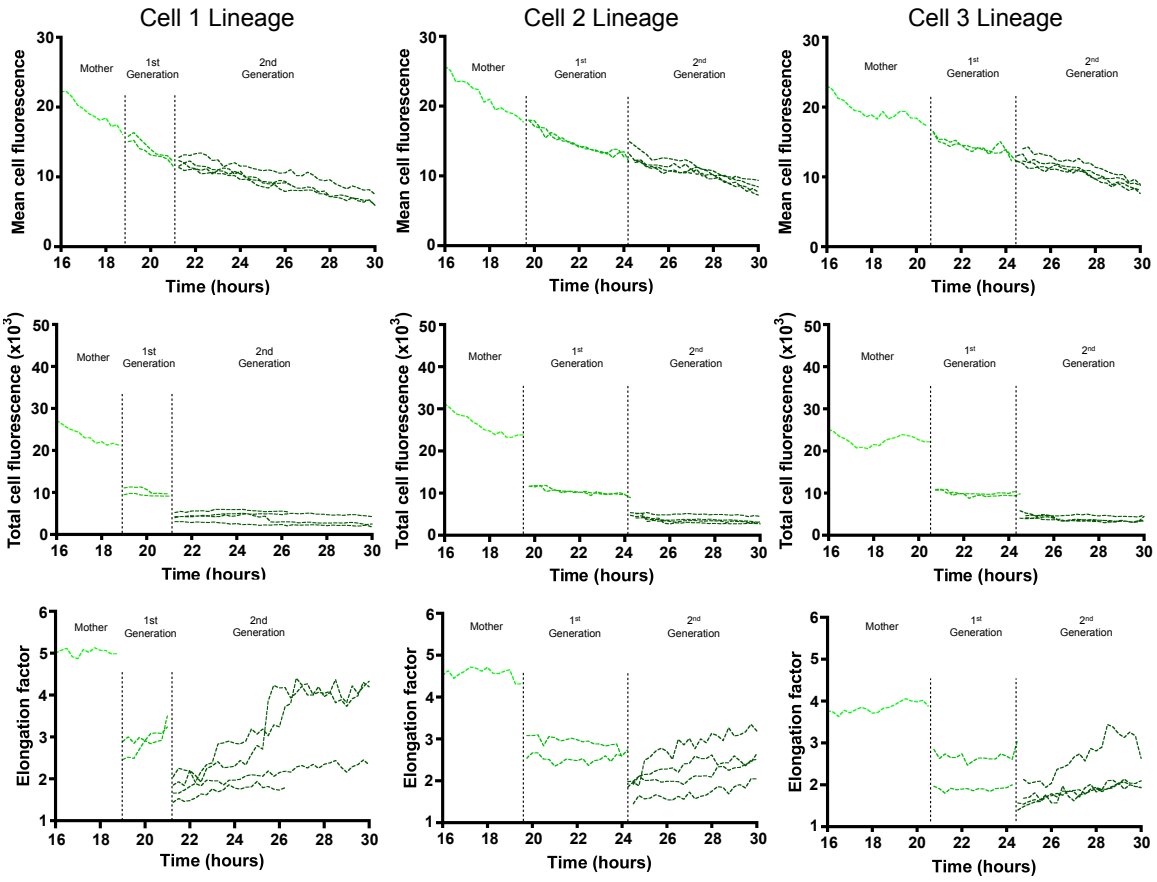


FIGURE 5.40: **Recovery following P-factor stimulation: Single cell lineages.** Cells from the *wild-type* GFP fluorescent reporter strain; JY1325(*sxa2>GFP*) were cultured to a density of ~5x10$^6$ cells/ml and incubated with 10$^{-5}$M P-factor for 16 h before washing to remove P-factor and transferring onto minimal media + agarose pads. Pads were constructed on a microscope slide prepared for time-series live-cell imaging. Starting from a randomly selected field of view containing sufficient cells to monitor the population, images were taken every 15 min for a period of 14 h using a Leica SP5 scanning confocal microscope. Three single cells chosen to be representative of the population (Figure 5.39) were segmented and their lineages were tracked with time using image analysis software QuimP to quantify mean fluorescence (mean pixel intensity), total fluorescence (sum of pixel intensities within the cell area) and elongation factor (ratio of cell length:width). Quantification of the mother cell and two subsequent generations of daughter cells are shown. Dashed lines indicate cell division points.

## 5.9 Single Cell Analysis of Signalling Mutants

A more detailed analysis of signalling response is achievable through analysis of time-series live-cell images of fluorescent reporter strains than was previously possible with population-based assays of either $\beta$-galactosidase or fluorescent reporter strains. Image analysis of single cell response with time allows quantitative data on transcription of the reporter and morphology of the same cell with time, giving greater insight into the temporal dynamics of P-factor induced signalling response. Given this more detailed method of quantifying signalling, image analysis was used to investigate some of the key data that has underpinned

much of the modelling work in Chapters 3 and 4 of this thesis; the dual role of the key regulatory protein Rgs1. It was hoped that through single cell analysis with time, a more detailed insight into the dynamics of the signalling response under these conditions may be obtained.

### 5.9.1 Rgs1

The role of Rgs1 in signalling was investigated through time-series live-cell imaging of the *sxa2>GFP* reporter strains either containing or lacking an endogenous copy of Rgs1. The *sxa2>GFP* reporter strains JY1325 and JY1333(ΔRgs1) were grown in minimal media before transferring to an agarose pad containing P-factor at a concentration of $10^{-5}$M. Cells were then imaged using a Leica SP5 scanning confocal microscope for a period of 14 h, taking an image every 15 min (Figure 5.41).

Time-series live-cell imaging of the *sxa2>GFP* reporter strains containing or lacking Rgs1 (Figure 5.41) displays the increased basal transcriptional activity of ΔRgs1 strains through increased cellular fluorescence at the beginning of the imaging experiment. There appears to be minimal further P-factor induction of *sxa2>GFP* with time in the strain lacking Rgs1, whereas in the presence of Rgs1 there is clear increased cellular fluorescence observable from ∼2 h onwards (Figure 5.41).

Cells (n = 15) from the time-series images were selected at random and tracked from the first frame of their cell division cycle to the final frame before cell division. At each frame, these single cells were quantified for their mean cell fluorescence, total cell fluorescence and elongation factor (Figure 5.42).

The transcriptional readouts from single *sxa2>GFP* reporter cells falsely implicate Rgs1 as behaving solely as a negative regulator of the transcriptional response (Figure 5.42, A and B). In the absence of Rgs1, cells show increased mean and total cell fluorescence at 0 h and throughout, compared to cells containing Rgs1. In the time taken to culture the cells, before adding them to the P-factor containing agarose pads, the strains lacking Rgs1 are therefore able to express GFP from the *sxa2* promotor in the absence of any external stimulation of the signalling pathway. With time there is little further induction of *sxa2>GFP* when these cells are stimulated by P-factor (Figure 5.42, A and B). In single cells containing Rgs1, there is clear induction of *sxa2>GFP* observable in the mean cell fluorescence of cells between 1-4 h following P-factor stimulation. This indicates the requirement of Rgs1 for rapid P-factor induced signal transduction.

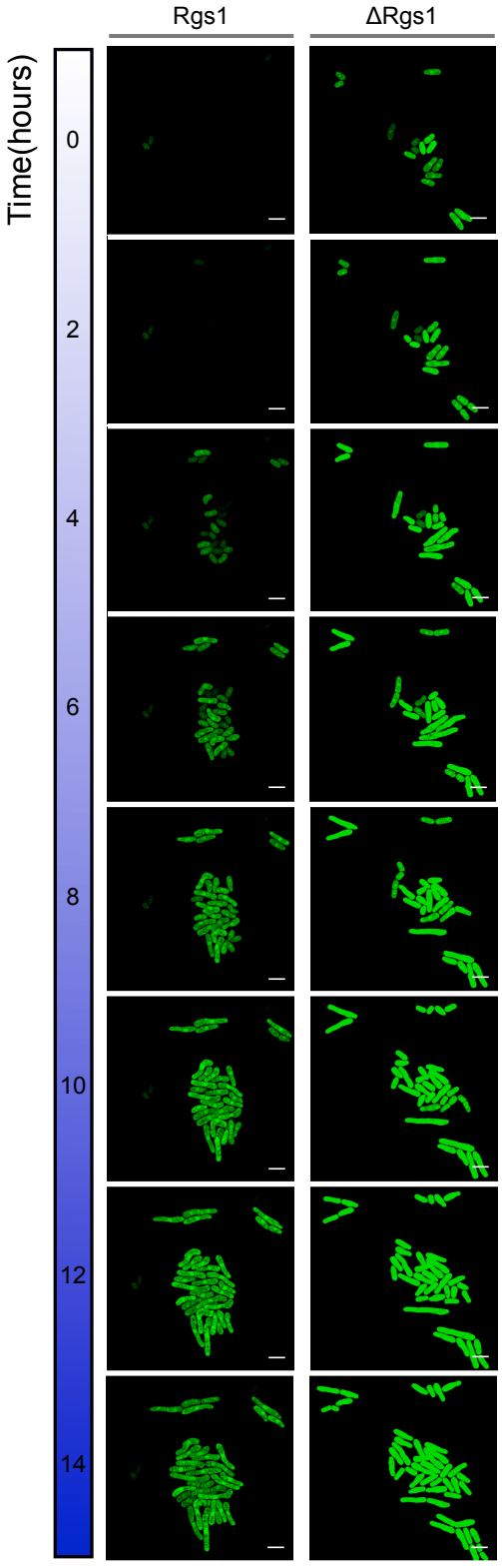


FIGURE 5.41: **Time-series live-cell imaging of a *sxa2>GFP* reporter: Rgs1 vs ΔRgs1.** Reporter strain; JY1325(*sxa2>GFP*) containing an endogenous copy of Rgs1 (Rgs1) and reporter strain; JY1333 deleted for its endogenous copy of Rgs1 (ΔRgs1) were cultured to a density of ~5x10$^6$ cells/ml before transferring onto minimal media + agarose pads containing $10^{-5}$M P-factor. Pads were constructed on a microscope slide prepared for time-series live-cell imaging. Starting from a randomly selected field of view containing sufficient cells to monitor the response, images were taken every 15 min for a period of 14 h using a Leica SP5 scanning confocal microscope. For clarity, images are shown at 0 h and every subsequent 2 h for the duration of the experiment. Scale bar = 10 $\mu$m.

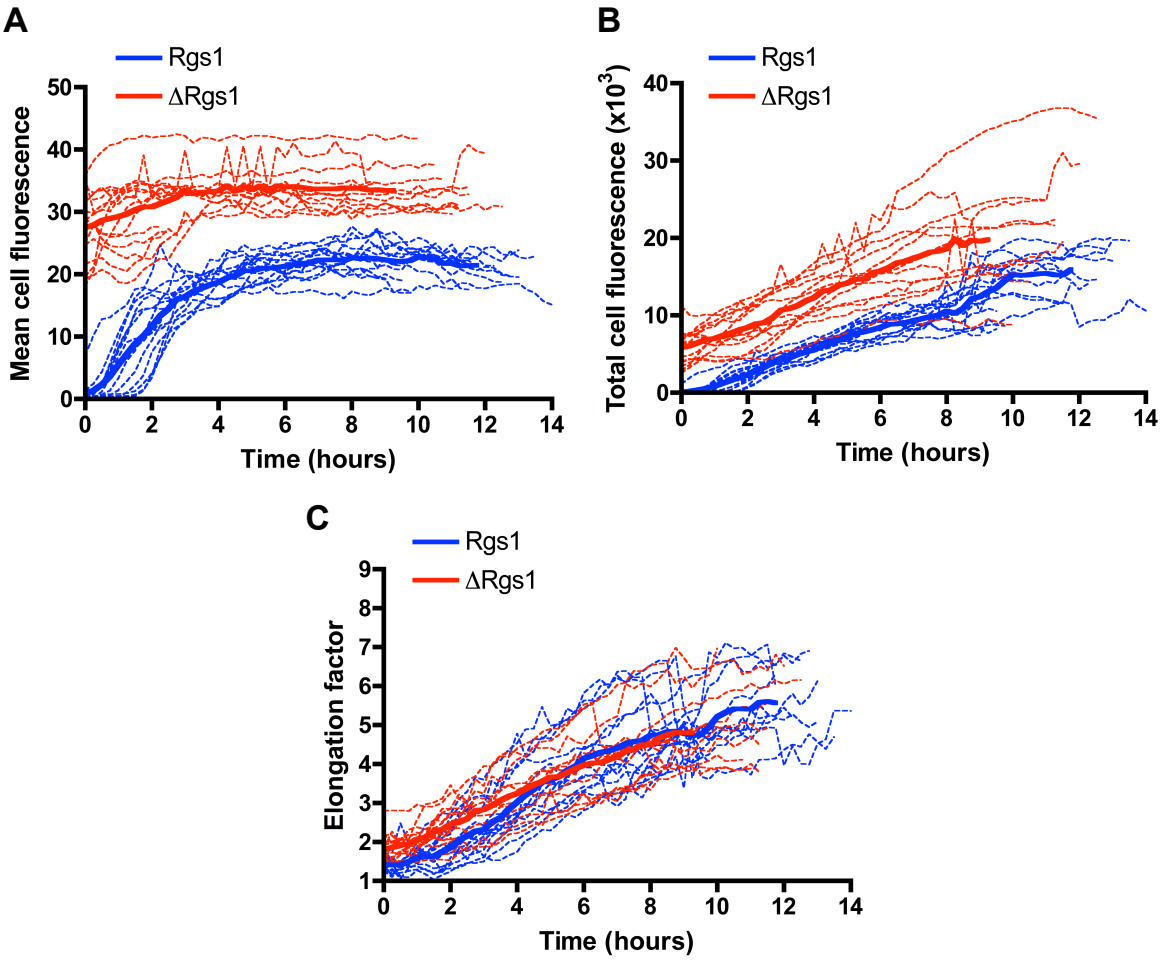


FIGURE 5.42: **Time-series single cell transcriptional signalling response: Rgs1 vs ΔRgs1.** Reporter strain; JY1325(*sxa2>GFP*) containing an endogenous copy of Rgs1 (Rgs1) and the reporter strain; JY1333 deleted for its endogenous copy of Rgs1 (ΔRgs1) were cultured to a density of ~5x10$^6$ cells/ml before transferring onto minimal media + agarose pads containing 10$^{-5}$M P-factor. Pads were constructed on a microscope slide prepared for time-series live-cell imaging. Starting from a randomly selected field of view containing sufficient cells to monitor the response, images were taken every 15 min for a period of 14 h using a Leica SP5 scanning confocal microscope. Single responding cells (n = 15) were segmented and tracked with time from the first available frame to the final frame before the end of the signalling response (before cell division) using image analysis software QuimP. Individual cells were quantified for their mean cell fluorescence (mean pixel intensity) (A), total cell fluorescence (sum of all pixel intensities within the cell area) (B) and elongation factor (ratio cell length:width)(C) at each frame. Average response profiles from all cells are indicated by the **bold** trace.

Time dependent change in elongation factor (Figure 5.42, C) indicates that cells have a very similar response to P-factor in terms of elongation in the presence and absence of Rgs1. The mean single cell response profiles show that cells will elongate to a similar extent in the presence and absence of Rgs1, but there is a difference in the response time, with mean time for cells containing Rgs1 being 11.717 ± 0.422 h and the mean time for ΔRgs1 cells being 9.1 ± 0.931 h (unpaired *t*, $p<0.01$). Cells therefore elongate to a similar extent, but in the presence of Rgs1, cells remain arrested for longer. The P-factor induced morphology

response appears to be only mildly effected by deletion of Rgs1, possibly because in the absence of Rgs1 there has already been sufficient transcriptional activity to 'prime' the cells ready for the subsequent cellular elongation.

#### 5.9.1.1 Using the *sxa2>Venus* Reporter to Investigate Rgs1 Activity

The interpretability of a transcriptional assay can be effected by the reporter protein used. One of the major problems of using GFP as a transcriptional reporter is its slow maturation time and high stability (Shaner et al., 2005), thus making it difficult to inform on responses that have rapid dynamics. Previously, we have demonstrated that the Venus fluorescent reporter can be used as an alternative in population-based assays of fluorescent reporter strains (Figure 5.2). Given that Venus was demonstrated to have reduced intensity of fluorescence compared to GFP, this might indicate it has decreased stability in the cells and therefore could provide a readout of the signalling response that is not masked by the accumulation of a highly fluorescent reporter protein, such as is the problem with GFP. Considering this, we also completed single cell time-series analysis of live *sxa2>Venus* reporter cells in the presence and absence of Rgs1.

The *sxa2>Venus* reporter strain containing Rgs1 JY1337, and the *sxa2>Venus* reporter lacking Rgs1 JY1483(ΔRgs1), were grown in minimal media before transferring to an agarose pad containing P-factor at a concentration of $10^{-5}$M. Cells were then imaged using a Leica SP5 scanning confocal microscope for a period of 14 h, taking an image every 15 min (Figure 5.43).

Through observation of the time-series imaging, the fluorescence of the *sxa2>Venus* reporter cells follows a similar pattern with time to the *sxa2>GFP* reporter cells, with increased fluorescence observed early in cells lacking Rgs1 (compare Figure 5.43 to Figure 5.41). With time, the increase in fluorescence is more apparent in the strain containing Rgs1, suggesting the requirement for Rgs1 to enable P-factor induced transcription with time (Figure 5.43).

Cells from the time-series images (Figure 5.43) were selected at random and tracked from the first frame of their division cycle to the final frame before cell division. At each frame, these single cells were quantified for their mean cell fluorescence, total cell fluorescence and elongation factor (Figure 5.44).

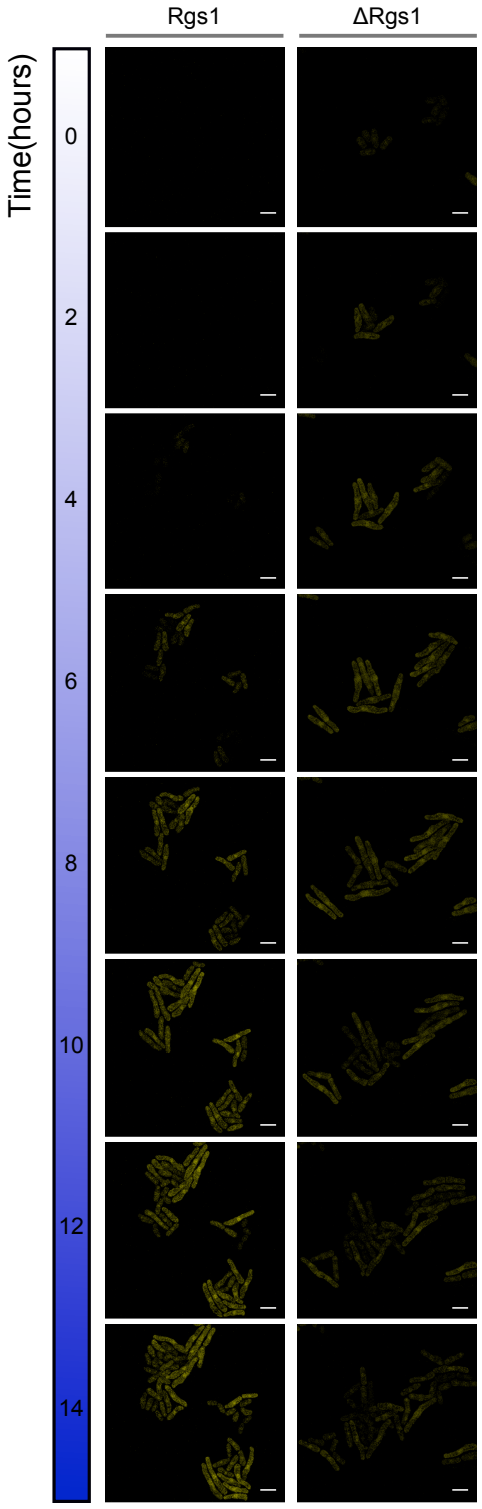


FIGURE 5.43: **Time-series live-cell imaging of a *sxa2>Venus* reporter: Rgs1 vs ΔRgs1.** The reporter strain; JY1337(*sxa2>Venus*) containing an endogenous copy of Rgs1 (Rgs1) and the reporter strain; JY1483 deleted for its endogenous copy of Rgs1 (ΔRgs1) were cultured to a density of ~5x$10^6$ cells/ml before transferring onto minimal media + agarose pads containing $10^{-5}$M P-factor. Pads were constructed on a microscope slide prepared for time-series live-cell imaging. Starting from a randomly selected field of view containing sufficient cells to monitor the response, images were taken every 15 min for a period of 14 h using a Leica SP5 scanning confocal microscope. For clarity, images are shown at 0 h and every subsequent 2 h for the duration of the experiment. Scale bar = 10 $\mu$m.

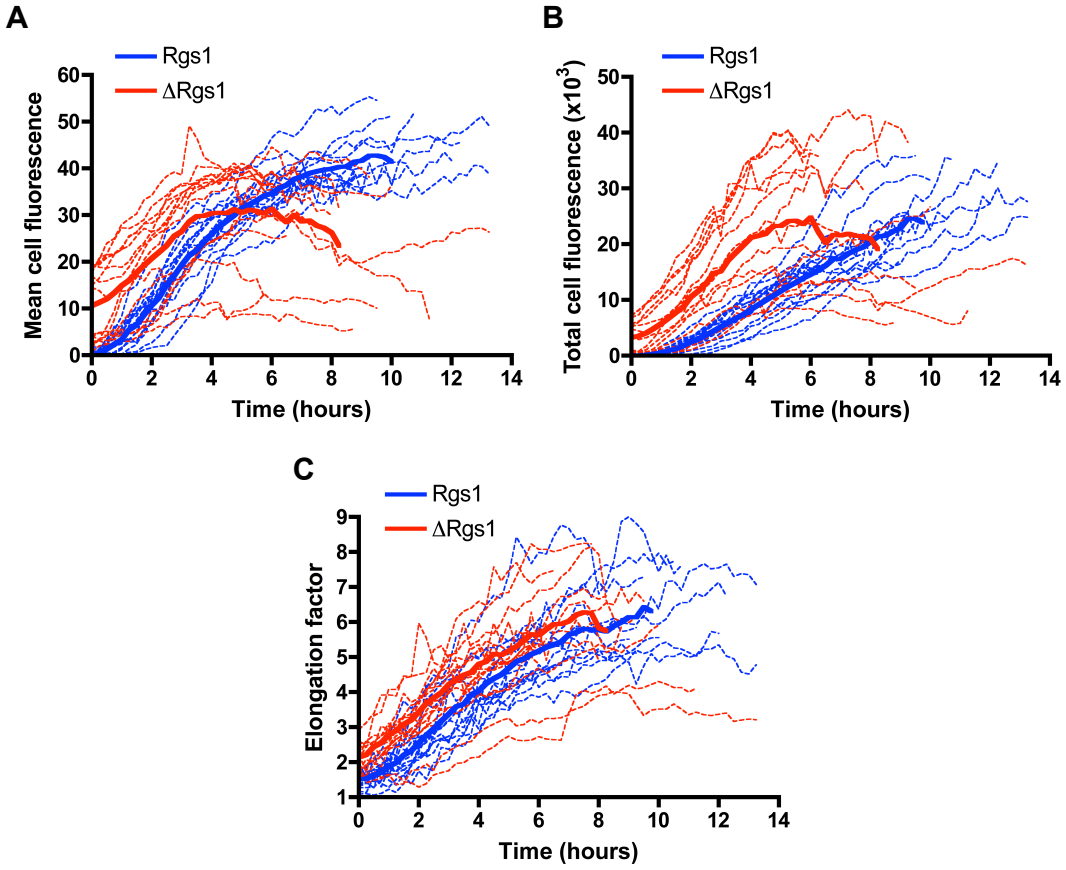


FIGURE 5.44: **Time-series single cell transcriptional signalling response: Rgs1 vs ΔRgs1.** The reporter strain; JY1337(*sxa2>Venus*) containing an endogenous copy of Rgs1 (Rgs1) and the reporter strain; JY1483 deleted for its endogenous copy of Rgs1 (ΔRgs1) were cultured to a density of ~5x10$^6$ cells/ml before transferring onto minimal media + agarose pads containing $10^{-5}$M P-factor. pads were constructed on a microscope slide prepared for time-series live-cell imaging. Starting from a randomly selected field of view containing sufficient cells to monitor the response, images were taken every 15 min for a period of 14 h using a Leica SP5 scanning confocal microscope. Single responding cells (n = 15) were segmented and tracked with time from the first available frame to the final frame before the end of the signalling response (before cell division) using image analysis software QuimP. Individual cells were quantified for their mean cell fluorescence (mean pixel intensity) (A), total cell fluorescence (sum of all pixel intensities within the cell area) (B) and elongation factor (ratio of cell length:width) (C) at each frame. Average response profiles from all cells are indicated in **bold**.

Transcriptional data for single cell response of the *sxa2>Venus* reporter strains (Figure 5.44, A and B) suggests that there is a P-factor induced transcriptional response with time in both cells containing and lacking Rgs1, but only in cells containing Rgs1 does this induction continue to achieve the highest maximal signalling levels in terms of cell fluorescence. This induction was not apparent in ΔRgs1 cells quantified from the *sxa2>GFP* reporter, suggesting that the stability of GFP was masking this information (compare Figure 5.44, A and B to Figure 5.42, A and B). The dual negative and positive influence of Rgs1 is observed with time in the *sxa2>Venus* reporter. The negative influence is highlighted by the increased fluorescence of ΔRgs1 at 0 h and the positive influence is observed

by the increased fluorescence towards the end of the response after ∼8 h induction with P-factor. Rgs1 therefore changes its role with time in single cells from blocking transcription to enhancing it, as P-factor stimulates the activation of the signalling pathway. Temporal dynamics of when P-factor induced transcription has ceased is much more detectable with the *sxa2>Venus* reporters, indicating the decreased stability of Venus compared to GFP. After ∼4 h, both the mean cell fluorescence and total cell fluorescence begins to plateau in the absence of Rgs1, whereas this plateau does not become apparent until after ∼8 h in the presence of Rgs1. This hints at a 'two-phase' transcriptional response, the first of which occurring without the requirement for Rgs1 up until ∼4 h and the second requiring Rgs1 to achieve further induction of transcription up until ∼8 h.

Elongation factor data from the *sxa2>Venus* reporters show similar results to those obtained with the *sxa2>GFP* reporter (compare Figure 5.44, C to Figure 5.42, C). Cells elongate to a similar extent in response to P-factor with or without Rgs1 present, but the time taken to reach the point of maximal elongation is prolonged when Rgs1 is present (mean cell cycle times; Rgs1 = 9.95 ± 0.534 h , ΔRgs1 = 8.15 ± 0.576 h). The presence of Rgs1 is therefore required to achieve maximal transcription and prolonged response times, but seemingly not to achieve maximal elongation factor. Much like ΔRgs1 cells having raised basal fluorescence, they also appear to have a raised basal elongation, possibly due to some initial activation of the morphology pathway before P-factor stimulation.

## 5.10 Summary

The use of fluorescent reporter strains is advantageous over using $\beta$-galactosidase reporters to quantify signalling response as cells do not have to be lysed to obtain a quantifiable readout of signalling and are therefore amenable to quantification of live-cell signalling response with time. *S. pombe* containing GFP and Venus under the control of the P-factor inducible *sxa2* promotor were characterised and compared by population-based assay and fluorescence microscopy. Dose-response profiles obtained from the *sxa2>GFP* and *sxa2>Venus* reporters showed similarity to profiles obtained from $\beta$-galactosidase reporter strains. The *sxa2>GFP* reporters give a higher intensity fluorescence signal compared to *sxa2>Venus* indicating GFP as a bright and stable reporter protein in *S. pombe*.

The *sxa2>GFP* reporter strain was utilised to investigate signalling at the single cell level rather than through population-based assay. Flow cytometry analysis has given insight into the distribution of a P-factor induced transcriptional signalling response within a population and highlights the cell-to-cell variability in the response. The percentage of cells that commit to a signalling response is a function of P-factor concentration, with increasing P-factor concentration resulting in increasing percentage of cells responding. This implies that population-based assay data, which is essentially a population average response must

not only be a function of the amplitude of an individual cells signalling response, but also the number of cells responding to stimulation.

Flow cytometry was also used to be able to combine single cell transcriptional measures with another quantifiable measure of P-factor induced signalling response; the distribution of cells arrested in $G_1$ phase of their cell cycle. Time-series $G_1$-arrest assays of P-factor induced signalling response indicated that low P-factor concentration ($10^{-9}$M) is sufficient to promote $G_1$-arrest, but not a transcriptional response. This implies cells have mechanisms to allow a greater sensitivity to P-factor for promoting $G_1$-arrest than for promoting P-factor induced transcription. Assays of $G_1$-arrest with time implied that recovery to vegetative cell growth is possible at low-intermediate P-factor concentrations, but high concentrations ($10^{-6}$M and $10^{-5}$M) can maintain the majority of the cell population in $G_1$-arrest phase.

An alternative quantification method to using flow cytometry was sought that would allow quantification of both morphology and transcriptional signalling response from single cells with time. A method was optimised to perform real-time monitoring of live cells through fluorescence microscopy. The *sxa2>GFP* reporter cells were imaged for 14 h on growth media + agarose pads that contained P-factor at a variety of concentrations. The time-series images generated were subjected to cell segmentation and analysis with quantitative image analysis software QuimP to enable quantification of single cell fluorescence intensity and morphology measures with time.

Quantitative image analysis of single cell transcriptional and morphology signalling response was utilised to extensively characterise single cell signalling characteristics. This method proved capable of reproducing dose-response and time-series data similar to that obtained through population assays and flow cytometry, therefore validating it as a method to assay signalling response. In using this analysis method, accurate cell morphology data was obtained as a measure of P-factor induced cell elongation. In comparing transcriptional and morphology data from the same cell, transcriptional response is proved to be more sensitive to P-factor concentration and to occur prior to P-factor induced cell elongation, therefore implying that cells have mechanisms to transmit P-factor concentration information into distinguishable transcriptional and morphology response. Close to maximal transcriptional response can be achieved at intermediate P-factor concentration of $10^{-7}$M, yet maximal elongation is only achieved at concentrations $>10^{-7}$M, therefore suggesting a 'tipping-point' at this concentration in a cells 'decision' to commit to a large morphology response.

Single cell measurements highlighted that stochasticity in a clonal population of cells in terms of both timing and amplitude of signalling response is apparent. P-factor concentration effects on this cell-to-cell variability showed that variability in terms of transcriptional response within the cell population is greatest at intermediate P-factor concentration. Cells

are not synchronous in the timing of response, resulting in gradual increase in variability from ∼2-6 h as cells initiate response different times.

At P-factor concentrations high enough to induce transcriptional response ($>10^{-9}$M), not all cells commit to a transcriptional or morphology response. This results in increased variability when analysing a population of cells. To remove this source of variability, response was quantified solely from cells within the population that had responded. Single cells were subjected to threshold checks to determine if the cell is signalling and from this subset, individual cells were tracked and quantified with time using QuimP. This allowed characterisation, previously unobtainable of an average single cell signalling response in terms of both transcription and morphology over the course of the cells lifetime. Characteristic response of a single cell includes initial induction of transcription between 1-4 h followed by subsequent cell elongation for a period of up to ∼12 h, the amplitude and length of time of which is dependent on P-factor concentration. Additional information was obtained regarding fluorescence production and cell elongation rates, which indicated a P-factor concentration effect on both of these rates.

Quantification by time-series imaging and subsequent image analysis was applied to cells under perturbed conditions. Under prolonged P-factor simulation at high concentration ($10^{-5}$M) cells were tracked through subsequent rounds of cell division, which indicated that the signalling response can be continued through generations. Additionally, ability to recover from signalling response was demonstrated by cell lineages of cells having P-factor treatment removed.

A higher level of control on P-factor induced signalling response has been demonstrated through the apparent sensing of cell elongation. Negative correlation was observed between cell elongation factor and cell division time, which suggested that even in the presence of P-factor if a single cell is too elongated at the beginning of its cell division cycle, then progression through the cell cycle to mitosis will dominate over a $G_1$-arrest and the mating-response.

Through single cell analysis of the *sxa2>Venus* transcriptional reporter strain, Rgs1 has been shown to change its role from negative regulator to positive regulator within the time frame of a single cell, P-factor induced signalling response. At the beginning of the response, Rgs1 is required to maintain a reduced level of signalling through the pathway but following P-factor induction of a response, Rgs1 becomes required to achieve a prolonged response time and maximal signalling levels in terms of transcription. A two-phase response is proposed, early response from ∼0-4 h, whereby initial induction of transcription is independent of Rgs1 and a later response after 4 h whereby Rgs1 activity can induce further signalling through the pathway, resulting in prolonged response time and increased transcription.

# Chapter 6

# Discussion and Conclusions

## 6.1 Overview

This thesis details studies which have expanded our understanding of key regulatory events in a classic G protein-mediated signalling pathway; the pheromone-response in *S. pombe*. Through a combination of quantitative experimental data from reporter strains, mathematical modelling and simulated signalling response, understanding of the impact of nucleotide exchange events on the G$\alpha$ subunit Gpa1 has been enhanced. A number of previously uncharacterised Gpa1 mutants have now been extensively characterised. Additionally, the Smith *et al.* ODE model of the G protein cycle has been manipulated to asses the sensitivity of the simulated signalling response to perturbation in nucleotide exchange reaction rate parameters. The model has also been extended to enable simulation of additional experiments assessing dominant activity of Gpa1 mutants. The model(s) have been validated against all of the newly characterised Gpa1 mutants, thus providing further model validation. Simulations have helped to predict the cause of the observed mutant effects on signalling response in terms of the how mutations may have influenced the kinetics of Gpa1 nucleotide exchange reactions, or Gpa1 interactions with other signalling components. Furthermore, such quantitative experimental assays and qualitative modelling of Gpa1 mutants in the presence and absence of the key RGS protein Rgs1, has implicated Rgs1 to be capable of negative regulation of signalling, independent of its primary function as a GAP for Gpa1.

An additional regulatory event is explored that has impact on the nucleotide cycling of the G$\alpha$ subunit. This regulation concerns the role of interaction between the C-terminal tail of the GPCR Mam2 and the RGS Rgs1. Interaction between these two proteins is shown to have influence over the sensitivity and amplitude of signalling response to pheromone. Removal of the C-terminal tail, hence removal of the GPCR-RGS interaction, results in cells with a phenotype reminiscent of cells lacking Rgs1. Additionally, the presence of the GPCR tail is suggested to have functional consequences on the efficiency of mating,

with cells lacking the tail displaying reduced mating efficiency to a similar extent to cells lacking Rgs1. Through fluorescence imaging of both Rgs1 and Mam2/Mam2Δtail, we have confirmed that the presence of the tail influences cellular localisation of Rgs1, the tail being required to direct Rgs1 PM localisation. Through an iterative cycle of mathematical model development and quantitative assay, a PM trafficking of RGS model has been developed that can explain the biological data and proposes that PM localisation, primarily directed by the Mam2 tail is required for efficient Rgs1-catalysed GTP hydrolysis on Gpa1.

Furthermore, investigations into a Mam2-Rgs1 fusion implied that Mam2 and Rgs1 are able to function with similar to *wild-type* activity when in a complex. An ODE model was built to enable simulation of this fusion data and subsequently the PM trafficking of RGS model was refined to include additional reactions involving Mam2-Rgs1 complexes. The final model was validated against a large set of experimental data, including data gathered on Gpa1 nucleotide exchange mutants. The key prediction made by the model was that PM localisation of Rgs1 alone was sufficient to compensate for a lack of GPCR-RGS interaction and enable efficient RGS function. This prediction was confirmed experimentally, therefore suggesting an additional layer of regulation of signal transduction via the control of subcellular localisation of Rgs1. Finally, an additional role for the C-terminal tail of Mam2 has been suggested. The Mam2 tail is demonstrated to be required for P-factor-induced internalisation of the receptor, implicating it in another level of regulation in terms of desensitising the cells to ligand stimulation.

In the final results chapter, work is detailed on developing better and more informative quantification of signalling response. Population-based assays of $\beta$-galactosidase reporter strains have been used extensively both in this thesis and previously to quantify signalling response from cells. Some of the drawbacks of such assays are highlighted and the use of fluorescent reporters of signalling as an alternative is detailed. Fluorescent reporters are extensively characterised, analysing dose-responses and time-series response from live-cells stimulated with P-factor. Fluorescent reporters are also characterised using flow cytometry to quantify end-point signalling responses in single cells. This additional single cell data demonstrates the distribution of response within the population and also the variability that is rife within a clonal population of cells. Relationship between the subset of the population that will commit to a signalling response and P-factor concentration is investigated. This suggested that an average response quantified from a population-based assay is a function not only of the amplitude of response, but also the percentage of the population responding.

One of the aims of the thesis was to develop, and characterise signalling response at the single cell level to obtain better understanding of the temporal dynamics of the signalling response. To achieve this, methods were optimised to perform live-cell imaging of *S. pombe sxa2>GFP* reporter cells. Subsequently, quantitative image analysis software QuimP was

utilised to quantify single cell characteristics, including measures of cell fluorescence intensity (transcriptional response) and cell elongation (morphology response). Dose-responses calculated from data obtained through image analysis were confirmed to be comparable to those obtained by population-based assays, therefore validating image analysis as a method for quantifying signalling response. Additionally, segmentation of the population into those cells that were responding enabled the average time and P-factor concentration-dependent single cell signalling response to be characterised.

Single cell data highlights cellular 'decision' mechanisms controlling commitment to transcriptional response and subsequent commitment to morphology response. Furthermore the transcriptional response appears to reach a maximal level at only $10^{-7}$M P-factor. This concentration appears to represent a 'tipping-point' for cells, above this, only the extent of cellular elongation is sensitive to further increase in P-factor concentration. Tracking and quantifying single *sxa2>GFP* reporter cell lineages has demonstrated that cells can recover and resume mitotic cell growth when stimulation is removed and that they will continually respond in conditions of prolonged stimulation. Additionally, data suggests that there is a higher level cellular decision making system controlling whether to commit to a mating-response or alternatively progress through the cell cycle that is dependent on cell size. This control mechanism appears to take precedence over a P-factor-induced mating-response.

## 6.2 Obtaining a Functional Labelled G$\alpha$ Protein

Labelling of the S. pombe G$\alpha$ subunit Gpa1, to enable visualisation and purification of the functional protein has proved problematic. The in-frame fusion of GFP to the C-terminus, or insertion of GFP in strategically chosen positions within the Gpa1 protein rendered the protein non-functional (Figures 3.3 and 3.6). Gpa1 has to interact Mam2, its downstream effector, Rgs1 and possibly other unidentified proteins. The attachment of a relatively large protein in GFP (26.9 kDa) is possibly obstructing such interactions, therefore influencing Gpa1 ability to transmit a signal. G$\alpha$ subunit activation requires intricate changes in conformation of switch I and II regions, and high affinity binding to GTP, enhanced by the presence of $Mg^{2+}$ ions to facilitate its activation (Birnbaumer and Zurita, 2010). Another feasible explanation is that the modification disrupts the ability of the protein to undergo these changes. Other G$\alpha$ subunits have been successfully tagged giving a functional protein (Hughes et al., 2001; Bunemann et al., 2003), but this remains a goal for Gpa1.

## 6.3 The Impact of Perturbed Nucleotide Exchange

Chapter 3 investigates the impact of perturbing nucleotide exchange on a G$\alpha$ subunit both through modelling and quantitative assays of Gpa1 mutants. Mutations within G proteins

effecting the activation and de-activation kinetics are the cause of an expanding number of human diseases (Farfel et al., 1999).

### 6.3.1 Nucleotide Exchange Mutant Behaviour

Two activating mutations in Gpa1 ($Gpa1^{Q244L}$ and $Gpa1^{R218C}$) were characterised as having increased basal signalling activity and decreased maximal signalling compared to Gpa1, which is consistent with these mutations compromising GTPase capability (Figures 3.11 and 3.22). The counter-intuitive, decreased maximal signalling of a G protein predominantly trapped in a GTP-bound state being as a result of the proposed requirement for recycling the G protein by GTP hydrolysis to achieve maximal signalling (Smith et al., 2009). G proteins with excessive signalling are a cause of a number of diseases, including adenomas of the thyroid, pituitary, adrenal and ovary (Lyons et al., 1990). Many of these diseases are a result of disturbing a key arginine residue, which usually accelerates GTP hydrolysis by holding an oxygen atom of the $\gamma$ phosphate in the correct position. In the case of Cholera, this key arginine residue is disrupted by the bacterium's (*Vibrio cholerae*) pathogenic exotoxin causing $G\alpha_s$ to be locked in the GTP-bound form (Chang and Bourne, 1989). $Gpa1^{R218C}$ was uncharacterised prior to this study. Initial characterisation suggests that this mutation has similar effects on signalling activity, therefore providing an ideal situation in a model system to more closely and quantitatively investigate the seemingly key role of the arginine finger in signal transduction.

Attempts using the Smith *et al.* ODE model to qualitatively reproduce the patterns observed in the data for mutations; $Gpa1^{Q244L}$ and $Gpa1^{R218C}$ predicted effects of these mutations on Gpa1 activity, additional to compromising GTP hydrolysis (Figure 3.35). In order to reproduce the increased basal levels of signalling observed for $Gpa1^{Q244L}$ and $Gpa1^{R218C}$, the spontaneous activation rates had to be increased (10x to simulate $Gpa1^{Q244L}$ and 5x to simulate $Gpa1^{R218C}$). The model therefore predicts that these mutations not only effect GTP hydrolysis, but also increase the proteins capacity to exchange GDP for GTP, independently of any stimulation by a GEF. This increased spontaneous activation may also be of significance in contributing to phenotypes observed in diseases resulting from similar mutations.

Mutations in both the glutamine and arginine residues of $G\alpha$ subunits are well-known to effect nucleotide exchange. An additional, far less characterised mutation of the glycine residue at position 83 in Gpa1 was extensively investigated for its effects on nucleotide exchange. In the small monomeric G protein family of Ras proteins, the equivalent mutation is responsible for rendering the protein insensitive to GAP activity and is frequently found in human cancers (Barbacid, 1987; Bos, 1989). Assays and modelling indicated that this mutation also effects signalling via a heterotrimeric $G\alpha$ subunit, and that the differential effects are dependent on what the glycine residue is replaced with (Figures 3.12 and 3.37).

Generally, mutation of glycine impaired signalling activity, although it is difficult to confirm whether this is a result of an inability to bind Rgs1. To reproduce experimental data for $Gpa1^{G83V}$ using the model(s) required perturbation of the RGS binding reaction rate, therefore suggesting this mutation to be influencing this event. Furthermore, the dose-response profile of $Gpa1^{G83A}$ resembles that of $Gpa1^{G223S}$, a mutant previously characterised as being unable to bind to Rgs1 (Ladds et al., 2007). An inability to bind to regulatory proteins such as proteins of the RGS family causes the dysregulation of signalling and is most likely to effect signal transduction pathways requiring the rapid attenuation of signal, such as required in retinal detection of photons ($G_t$), and contraction of vascular smooth muscle ($G_q$) (Farfel et al., 1999).

### 6.3.2 Nucleotide Exchange Parameter Perturbation

To investigate which parameters governing nucleotide exchange events were having the most impact on signal transduction, the Smith *et al.* model of the G protein cycle (Smith et al., 2009) was analysed under conditions of perturbed nucleotide exchange reaction rates. From analysis of nucleotide exchange parameter sensitivity, a more detailed understanding of the models behaviour was obtained. It was observed that only relatively small increases in response could be obtained through increased rates of G$\alpha$ activation (exchange of GDP for GTP). The most substantial increases in response were obtained through increased GTP hydrolysis of the proposed inert$G\alpha_{GTP}$ state. This suggests that the model assumes G protein signalling is (at least in the mating-response in *S. pombe*) already operating at optimum activation rates for signal transduction to occur, and highlights the importance of hydrolysis events in controlling the amplitude of response. Hydrolysis of GTP on G$\alpha$ is often considered a limiting factor in signal transduction, as intrinsic hydrolysis occurs extremely slowly and requires the aid of RGS proteins, which can increase this rate up to $10^3$-fold (Ross, 2008). The Smith *et al.* model predicts that maximal response can be increased further, even in the presence of RGS, suggesting RGS proteins as being of importance in controlling the level of response. The predicted effect of increased GTP hydrolysis, increasing response is counter intuitive and this behaviour might only hold in such systems where $G\alpha_{GTP}$ is sequestered in an inactive state, as is proposed to occur for the mating-response in *S. pombe*. Investigating increased hydrolysis rates on Gpa1 by quantitative assay using a mutant with such behaviour could confirm these model predictions.

## 6.4 An Extended Model to Simulate Dominant Activity

The Smith *et al.* model has been extended to enable simulations, whereby additional G$\alpha$ species with modified behaviours are added into a system already containing a *wild-type* G$\alpha$ species. This enabled further comparisons to be made between experimental

data and simulations that were previously not possible. This extended model was useful for investigating how modified G$\alpha$ species influenced signalling through competing with the *wild-type* G$\alpha$ for interaction with components of the signalling pathway. Through investigations with the model, we were able to predict that the inactive mutant Gpa1$^{G243A}$ and the GTPase deficient mutants Gpa1$^{Q244L}$ and Gpa1$^{R218C}$ were able to compete with endogenous signalling components, thus reducing response through binding and blocking activity through the GPCR and by sequestering of RGS respectively.

The outcompeting of endogenous GPCR signalling components through the expression of viral signalling components is a common mechanism viruses use to aid their pathogenicity (reviewed by Sodhi et al., 2004). This viral control of GPCR signalling pathways can contribute to a number of human diseases, including Acquired Immune Deficiency syndrome (AIDs) (Berger et al., 1999) and Kaposi Sarcoma (Chang et al., 1994). The problem is often in the form of virally expressed GPCRs or ligands that result in dominant activity over the normal cell signalling mechanisms, but can also involve viral expression of other downstream components such as G proteins. Mathematical models simulating the effects of addition of exogenous proteins could help to predict phenotypic response and also aid in identifying therapeutic targets to negate the effects of viral proteins in viral diseases.

## 6.5 New Insights Into Regulation by Rgs1

Much of the work presented in this thesis is focussed on investigating the mechanisms of signalling regulation by Rgs1. Regulation by Rgs1 is demonstrated to be more complex than was first assumed, with an additional layer of regulation imposed through controlling the subcellular localisation of Rgs1 and also negative regulatory effects being demonstrated that are independent of the proteins GAP activity. Additionally, single cell data investigating time-series response in cells containing/lacking endogenous Rgs1 demonstrates that Rgs1 influence on signal transduction changes over the time-frame of a cells response to high ($10^{-5}$M) P-factor stimulation. Rgs1 has little influence on the early response (0-4 h) other than as a negative regulator reducing basal activity prior to the induction of a response. In the late response (>4 h) Rgs1 becomes a positive regulator, being required to achieve maximal transcriptional response (Figure 5.44).

### 6.5.1 Subcellular Localisation of Rgs1

In 'resting' cells, the localisation of Rgs1 has been observed to be primarily nuclear and cytoplasmic, also with indication of attachment to microtubules (Figure 4.5). Given that the substrate for Rgs1 is Gpa1, which localises at the PM (Figure 3.2), this appears counter intuitive. Translocation to the PM is observed when overexpressing Mam2, but not Mam2$\Delta$tail in the same cell (Figure 4.6). This result suggests a number of things, firstly that Rgs1

interacts either directly or indirectly with the tail of the receptor and secondly, that a trigger is required in terms of increased receptor expression to direct PM localisation of Rgs1. Localisation of RGS proteins is known to be one mechanism in which to be able to regulate their specificity and function (Hollinger and Hepler, 2002).

#### 6.5.1.1 Plasma Membrane Localisation

Interaction of RGS proteins with receptors to direct PM localisation of RGS has been previously demonstrated for a number of other RGS proteins (Hollinger and Hepler, 2002). RGS proteins are capable of exerting GAP activity on many different G$\alpha$ subtypes (Hepler, 2003), therefore, it is possible that the interaction between GPCRs and RGS proteins aids in directing the specificity of RGS regulation of specific G protein signalling cascades. For example, RGS2 has been demonstrated to interact specifically with $\alpha_1$-adrenergic receptors, which play an essential role in regulation of vascular tone and blood pressure and are an important target for the treatment of hypertension (Hague et al., 2005). For Rgs1, it is specifically the C-terminal tail of the receptor that has been observed to be required to direct PM localisation, thus placing importance on the receptor tail in regulating the signalling response. The C-terminal receptor tail of the *S. cerevisiae* GPCR STE2 has also been shown to promote the PM localisation of the RGS protein SST2, via DEP domains in SST2 (Ballon et al., 2006). This docking only occurs when the receptor tail is in an unphosphorylated state. Rgs1 has two N-terminal DEP domains, but whether Rgs1 PM localisation is dependent on phosphorylation state of the Mam2 tail is yet to be determined. Due to the apparent functional significance of PM localisation of Rgs1 on the regulation of signalling, if PM recruitment is phosphorylation-state-dependent then GPCR kinases may also have an important role in controlling Rgs1 localisation. There are two candidates in *S. pombe*; Cki1 and Cki2, homologues of the *S. cerevisiae* casein kinases YCK1/2 (Robinson et al., 1993), which could potentially have an impact on the regulation of signalling through the regulation of Rgs1 localisation.

The trigger for PM localisation of Rgs1 appears to be increased expression of Mam2. The only known role for Rgs1 in *S. pombe* is in regulating the mating-response pathway (Pereira and Jones, 2001), therefore it is only required at the PM when the mating-response is stimulated by pheromone. Mam2 expression has been shown to be increased as a result of both nitrogen starvation and the activation of the signalling pathway following pheromone stimulation (Mata and Bähler, 2006; Xue-Franzén et al., 2006), therefore this is consistent with the observation that increased Mam2 expression is the trigger for Rgs1 to translocate to the PM and regulate Gpa1 activity. It is possible that only transient PM localisation of Rgs1 occurs in unstimulated cells and this could be stabilised by an increased concentration of Mam2. Purely the expression of some receptors, regardless of their activation state has been shown to be sufficient to localise RGS proteins to the PM, as has been demonstrated

for the mammalian RGS2 and RGS4 proteins (Roy et al., 2003). In other cases, for example RGS4 and other B/R4 family members, the activated form of the G protein can be sufficient to trigger translocation to the PM (Srinivasa et al., 1998; Druey et al., 1998). In preliminary experiments expressing the GTP-bound form of Gpa1 in *S. pombe*, PM localisation of Rgs1 was not observed, suggesting that activation of Gpa1 does not efficiently recruit Rgs1 to the membrane or perhaps that interaction of Rgs1 with $Gpa1_{GTP}$ is only transient.

Localisation of Rgs1 at the PM has functional consequences on signalling, as demonstrated by the fact that preventing PM localisation through removal of the C-terminal tail gives a ΔRgs1-like phenotype in terms of signalling activity and mating efficiency (Figures 4.3 and 4.4). Furthermore, signalling activity could be recovered in strains lacking the C-terminal tail by enhancing the Rgs1 PM localisation through addition of a small membrane targeting region of Gpa1 (Figure 4.26). The relevance of this is that it highlights the spatial regulation of Rgs1 localisation as being a key event in the overall regulation of the signalling pathway. Targeting the spatial regulation of RGS proteins, possibly through small molecules that could block interaction with the GPCR is therefore a possible avenue to explore for therapeutic intervention of GPCR/G/RGS protein related diseases.

#### 6.5.1.2 Nuclear Localisation

An intriguing observation when imaging Rgs1 was its apparent localisation in the nucleus, in association with microtubules of dividing cells prior to cytokinesis (Figure 4.5). The reason for Rgs1 localisation here is unclear, it might be that nuclear localisation is required to sequester Rgs1 away from Gpa1, thus allowing initial sensitivity to P-factor stimulation. If Rgs1 was constantly in close proximity to Gpa1, reverting it to its GDP-bound form, this would result in a requirement for a large stimulation by P-factor to overcome this negative regulation and trigger the mating-response, which may not be possible under physiological conditions. Many other RGS proteins have been identified as localising to the nucleus (reviewed by Sethakorn et al., 2010). Some nuclear functions of RGS proteins have been identified. For example nuclear RGS12 was shown to inhibit DNA synthesis and cell cycle progression, possibly through direct interaction with gene transcription machinery in COS-7 cells (Chatterjee and Fisher, 2002). Another example is RGS6, which is recruited to the nucleus through interaction with nuclear proteins to release transcriptional inhibition, thus promoting gene transcription (Liu and Fisher, 2004). The nuclear functions of RGS proteins are often independent of the RGS-domain, therefore implicating different domains as having different functional roles.

Even more puzzling is the possible association of Rgs1 with microtubules. As a result of the observed association, it is reasonable to assume additional roles of Rgs1 in the nucleus. One possibility is that Rgs1 is involved in regulating microtubule dynamics. Another RGS family member RGS14, was shown to segregate to centrosomes and astral microtubules,

regulating microtubule dynamics and thus control chromosome segregation during mitosis of HeLa cells. Reducing expression of RGS14 causes increased numbers of multi-nucleated cells and a decrease in cell proliferation (Martin-McCaffrey et al., 2004). The ΔRgs1 mutation in *S. pombe* is non-lethal, therefore if it has a functional role in the nucleus then it is non-essential. Further investigation is required to identify the possibilities.

### 6.5.2 A New Mathematical Model - Plasma Membrane Trafficking of RGS

An ODE model of the PM trafficking of RGS has been developed that describes the proposed mechanisms for RGS translocation to the PM and captures the experimentally determined importance of interaction with the GPCR in controlling RGS function (Table 4.7). The model includes three proposed mechanisms of PM translocation; via direct interaction with the PM, via direct interaction with $G\alpha_{GTP}$ and via interaction with the GPCR. Only one of these mechanisms, the interaction with the receptor has been experimentally determined through fluorescence imaging to direct PM localisation of Rgs1. The other two mechanisms have not been specifically verified, but are inferred on the basis that PM localisation is a requirement for Rgs1 function and that Rgs1 was shown to be capable of negatively regulating signalling in the absence of Mam2. If the core hypothesis that Rgs1 has to be localised at the PM to function is true then such alternative mechanisms to allow PM localisation must be possible. Indeed alternative mechanisms of PM localisation for RGS proteins are known. Although most RGS proteins do not contain specific motifs for membrane targeting, some contain exposed cysteine residues, which can rapidly and reversibly incorporate palmitate at the cell membrane in the absence of recognised motifs. The addition of thioester-linked palmitate can contribute to membrane localisation in addition to affecting protein interactions (Mumby, 1997).

Many mathematical models have been generated to describe GPCR signalling pathways including equilibrium models common in pharmacology (Kenakin, 2004), and thermodynamic equilibrium models (Sayar et al., 2008; Onaran et al., 1993). A kinetic model of the a receptor-G protein-RGS signalling unit based on the mating-response in *S. cerevisiae* was developed by Hao et al., 2003. They demonstrated that transcriptional induction of SST2, the RGS protein, caused by free (active) $G\beta\gamma$ produces a negative feedback loop leading to desensitisation of the pathway. The eventual re-sensitisation was shown to occur through ubiquitination and subsequent breakdown of SST2. Induction and subsequent degradation of RGS is something that is lacking from our current model. A more complete model of the *S. cerevisiae* pheromone-response pathway was developed by Kofahl and Klipp, 2004, in which they included many of the known complexes and interactions in the pathway. In addition to the receptor-G protein-RGS unit, they have association of a large complex of scaffold proteins, the $G\beta\gamma$-subunit and members of the MAPK cascade, which allows FUS3,

the MAPK, to activate transcription, cell cycle arrest and projectile growth. One of the main differences of these models compared to our PM trafficking of RGS model is that they do not include any element of spatial regulation being important for the regulation of the signalling response. Additionally RGS behaves solely as a negative regulator and there is a lack of inclusion of GPCR-RGS interactions.

The PM trafficking of RGS function model defined in this thesis is essentially a compartmentalised model with RGS being initially sequestered away from the compartment (PM) whereby the activation/deactivation of the G protein occurs. This compartmentalisation of RGS is achieved through initiating the model with a concentration of the sequestered RGS ($RGS_c$). Reactions are defined to allow for RGS to enter into the PM compartment (becoming $RGS_m$) and engage in GAP activity on GTP-bound forms of the G$\alpha$ subunit (Figure 6.1).

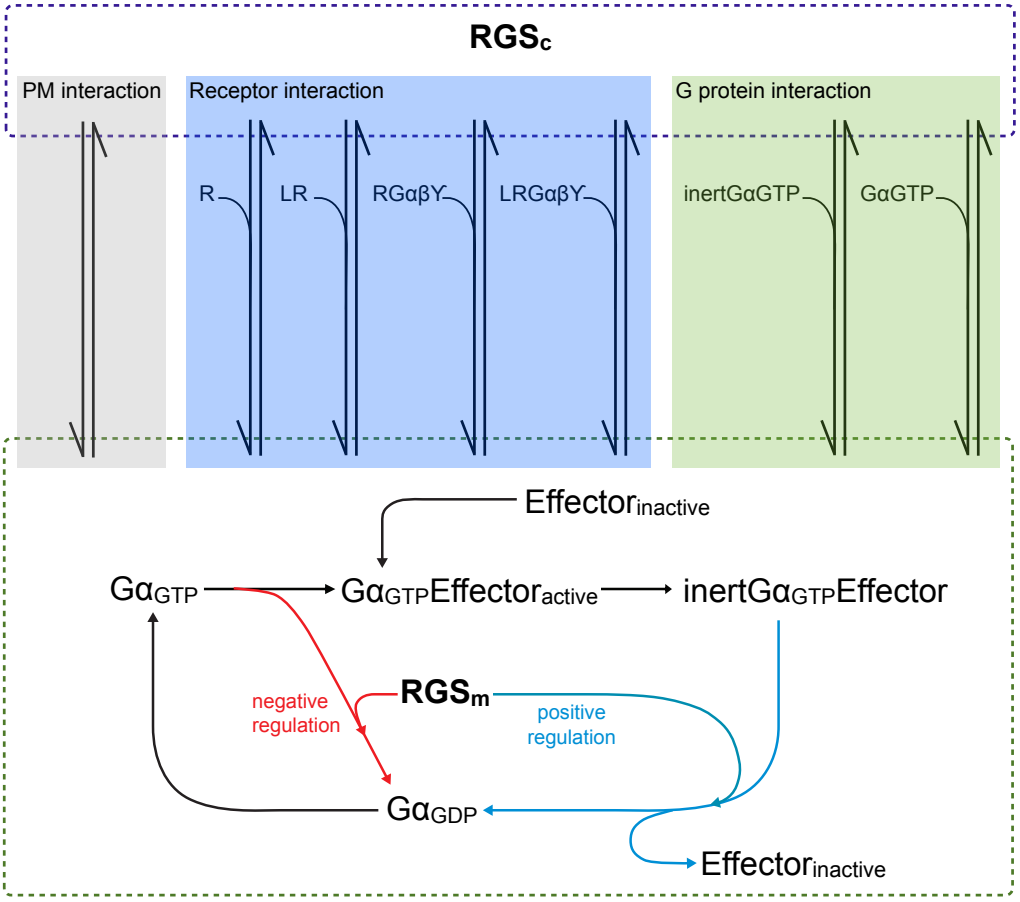


FIGURE 6.1: **Plasma membrane trafficking of RGS schematic.** A schematic representation of the PM trafficking model of RGS function. $RGS_c$ is sequestered outside of the compartment where the core G protein cycling occurs at the PM. Trafficking events including PM binding, receptor complex binding and $G\alpha_{GTP}$ binding translocate $RGS_c$ into this PM compartment, converting it into $RGS_m$ and allowing its involvement in hydrolysis reactions on $G\alpha_{GTP}$ and inert$G\alpha_{GTP}$.

## 6.6 Multi-protein Signalling Complexes

In many G protein signalling pathways, it is not understood whether the signalling components function as multi-protein complexes or whether proteins freely dissociate from each other to perform their individual roles. GPCR-RGS fusion data presented in chapter 4 suggests that the fused complex can function similarly to *wild-type* (Figure 4.14), therefore suggesting that functional multi-protein signalling complexes can exist in the mating-response signalling pathway. It is possible that Mam2, behaves as a molecular scaffold to organise the formation of the multiprotein signalling complex at the PM. It is apparent from the fusion data indicating *wild-type* signal transduction, that a complex consisting of ligand-GPCR-G-RGS is capable of transducing the signal. This complex could perhaps also include the downstream proteins including the effector for Gpa1, Ras1, and components of the MAPK cascade Byr2 and Byr1 all in close proximity docked at the PM. Receptors as scaffolds could selectively recruit functionally related proteins, which would be especially advantageous for mammalian GPCR signalling in a crowded environment with multiple different GPCRs G proteins and RGS proteins present (Neitzel and Hepler, 2006). The concept of a multiprotein or microdomain signalling complexes would enable close localisation and even continual contact of the proteins engaged in specific signal transduction cascades, helping to achieve rapidity as well as specificity. Evidence has emerged for such multiprotein signalling complexes that contain molecules involved in GPCR signalling pathways (Hur and Kim, 2002).

## 6.7 Cellular Decision Making

The mating-response in *S. pombe* is an example of a cell-fate decision system. Quantitative single cell transcriptional data from flow cytometry and image analysis, investigating the percentage of cells responding in a population has highlighted that cellular mechanisms must exist to determine whether to commit to a signalling response or not. This decision is closely linked to the capability to sense P-factor concentrations, with the percentage of a population committing to a signalling response increasing in a P-factor concentration-dependent manner (Figures 5.7 and 5.24). Additional decisions appear to be made on the level of commitment to a mating-response. There appears to be three possible response states; short $G_1$-arrest then recovery to vegetative growth, $G_1$-arrest and induction of transcription then recovery or finally, $G_1$-arrest, induction of transcription and subsequent commitment to shmoo formation prior to recovery. These three cellular decisions are demonstrated to be based on a cells ability to sense different P-factor concentrations. We know many of the components of the signalling cascade, but the biochemical mechanisms for the cell to convert data gathered at the PM in terms of ligand-binding to GPCRs into particular response types is not fully understood.

Through the tracking of subsequent generations of cells in the presence of P-factor, some interesting data was obtained suggesting cell size as an important variable in a cells commitment to mating. Data suggested that in the presence of P-factor stimulation, mechanisms sensing cell size namely the intracellular gradient of Pom1 (Martin and Berthelot-Grosjean, 2009) may take precedence over a commitment to a mating-response. Generally, cells that were large (in terms of cell length) at the beginning of their cell division cycle would continue with vegetative cell growth and only cells small enough would respond to P-factor and arrest in $G_1$ phase (Figure 5.38). This suggests a possible link between components of the cell size sensing mechanism and components of the mating-response signalling machinery. An alternative is simply that cell size sense-and-respond system has more rapid dynamics compared to P-factor sensing and response, therefore if a cell is larger then the cell is triggered to continue through the cell cycle before the cell has the opportunity to respond to P-factor.

Cellular responses are not completely deterministic, therefore if a particular input is received by a cell for example a particular concentration of P-factor then the cell will 'select' a certain response in a probabilistic manner. The internal strategies of cellular decision making are likely to be highly probabilistic (as discussed by Perkins and Swain, 2009). Based on observation and data from image analysis of single *S. pombe sxa2>GFP* reporter cells time-dependent response to varied P-factor concentrations, insight is gained into the decision-making processes that likely occurs to determine cell fate Figure 6.2. At each checkpoint in time, whereby a decision on future cell fate has to be made, the fate is most likely 'selected' in a probabilistic manner, with particular fates having a higher probability of being selected than others, most likely dependent on the level of P-factor concentration detected by the cell.

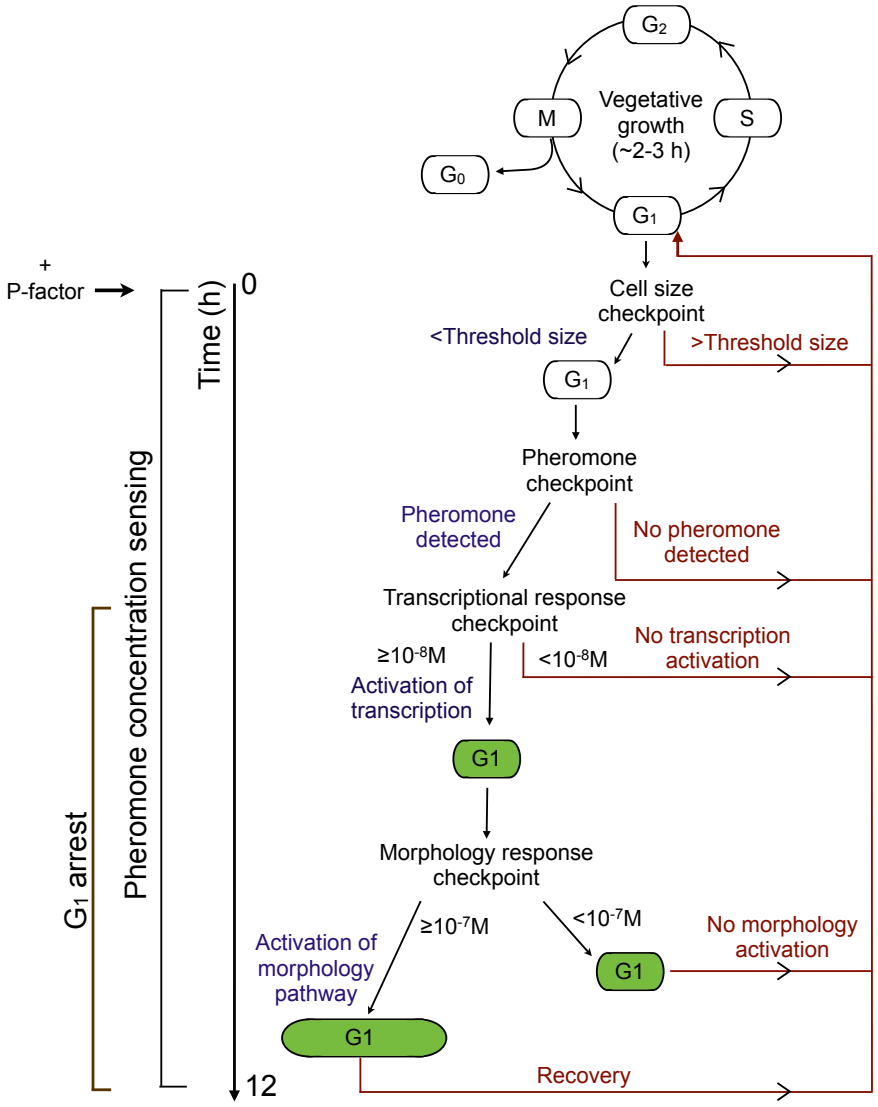


FIGURE 6.2: **Schematic timeline of single cell decision making when exposed to pheromone.** When subjected to P-factor stimulation, *S. pombe* cells appear to undergo a series of decisions. Under non-stimulatory conditions cells undergo vegetative cell growth. The addition of P-factor at time = 0 h results in a series of sense and respond mechanisms that can be separated in time. A cell size sensing mechanism precedes induction of pheromone induced response, therefore if cells are too big when in $G_1$ phase of their cell cycle they will not enter into a mating-response, despite the presence of pheromone. If passing the cell size checkpoint, cells then respond to the presence of P-factor. If P-factor is present then a cell will commit to $G_1$-arrest and can determine approximate concentration to induce appropriate response. Inducing transcription of genes required for mating occurs if the sensed concentration is $\geq 10^{-8}$M. Having surpassed this checkpoint a cell then determines whether to trigger a morphology response, again based on sensing pheromone concentration. The general rule being that if concentration $\geq 10^{-7}$M this should trigger morphology response through cell elongation. At the end of the response or at any checkpoint in the timeline the cell may terminate the continuation of response. This schematic is speculated from observations of live single *sxa2>GFP* reporter cell characteristic signalling responses with time.

### 6.7.1 Variability of Signalling Response

A high degree of cell-to-cell variability in the signalling response is evident from flow cytometry and image analysis data presented in Chapter 5. In a clonal population of cells variability is evident in both the amplitude and timing of the signalling response. Quantification of variability in terms of the amplitude of transcriptional response from *sxa2>GFP* reporter cells in response to P-factor stimulation suggested that the amount of variability within a population is partly dependent on P-factor concentration (Figure 5.21). Variation in amplitude of the transcriptional response was relatively low at low ($\leq 10^{-9}$M) and high ($\geq 10^{-6}$M) P-factor concentrations and it peaks at intermediate ($10^{-8}$M to $10^{-7}$M) concentrations. At low or high concentrations Mam2 at the surface of each cell will likely be sparsely populated with ligand or fully saturated with ligand respectively, therefore the cell is likely to have little trouble in processing this into a low or high level of transcriptional response. At intermediate concentrations, not all receptors will be saturated with ligand and some cells will likely achieve higher numbers of ligand-bound receptor than others. Considering this and adding to the observation that transcriptional response resembles a switch like-response, some cells in the population will commit to a transcriptional response, whereas others will achieve only a minimal response or fail to respond.

Although variation is reduced at high P-factor concentrations, when quantifying single cell transcriptional response with time through image analysis (Figures 5.26 and 5.27), it is obvious that cell-to-cell variability is still rife. Previous studies have proposed that a major cause of such variability lies with a cells ability to transmit a signal ('pathway capacity') and express genes ('expression capacity') (Colman-Lerner et al., 2005). Even in a clonal population of cells, there will be differences from cell to cell in global variables such as the number of signalling component molecules or ribosomes present in the cell at any given time, and this can contribute to a cells ability to transmit the signal through the pathway resulting in the induced expression of genes. Further to this, it has been demonstrated using fluorescent reporter *S. cerevisiae* strains that active cellular mechanisms can regulate the level of cell-to-cell variability within a population (Colman-Lerner et al., 2005). Expression of components of the MAPK cascade FUS3 and KSS1 can suppress and enhance variation from the pathway capacity respectively. It is possible that similar regulation of the ability of a cell to transmit a signal through the mating-response pathway could be achieved by the activity of *S. pombe* MAPK components Byr2, Byr1 and Spk1.

## 6.8 Limitations and Future Work

In order to increase understanding of G protein-mediated signalling in general, the mating-response in *S. pombe* and quantitative methods for investigating cell signalling pathways, it is necessary to criticise the work presented in this thesis to identify the limitations that

will help to encourage better and more informative future studies. Currently technology provides only incomplete information on the physiological dynamics of the *S. pombe* mating-response pathway, which highlights a need to develop improved technologies to measure signalling pathway dynamics in more detail and with more accuracy.

### 6.8.1 ODE Models of the Signalling Network

An obvious limitation of the mathematical models presented in this thesis is the lack of experimentally determined parameters. Initial concentrations of many of the species defined within the models are estimated based on similarity to concentrations determined in a similar mating-response signalling network in *S. cerevisiae* (Yildirim et al., 2004). Additionally, unknown reaction rate parameters have had to be defined initially based on intuition and subsequently hand tuned to fit to quantitative experimental data from population-based assays of reporter strains. Although good qualitative agreement is observed between simulations and experimental dose-response data, quantitative agreement is lacking, most likely as a result of this lack of true parameter values. The models are also incomplete in terms of all signalling components, and as a result, the predictions that the model is capable of generating are limited to events involving the signalling components defined in the model. It is not necessarily advantageous though, to have a very large and complicated model of the mechanisms of G protein signalling built solely on the *S. pombe* mating-response, especially if a generalised model is sought that could be transferrable to other G protein signalling systems. The ODE models are essentially deterministic models of a single cell response to ligand stimulus but they have been built primarily based on data from population-based assays.

To develop a more accurate model of single cell G protein-mediated signalling, future models could be developed based on single cell signalling data and optimised to fit to time-series experimental data in addition to dose-response data. If investigations into variability in signalling response is to be pursued, then better insight might be gained from developing stochastic rather than deterministic models of the pathway to give a more probability driven model with behaviour more representative of the living cell.

### 6.8.2 Existence of the Inert G$\alpha$ state

The extended PM trafficking model of RGS function builds upon the Smith *et al* model of the GTPase cycle and as a result, the extended model makes the same assumptions and includes the same concepts as the Smith *et al* model. The key assumption/proposal being that G$\alpha$ enters into an inert state following effector activation. Perhaps the most pressing limitation of the Smith *et al* model and by association, the extended models presented in this thesis is the lack of biochemical evidence for the existence of the inert state. Providing

evidence would require not only the isolation of Gpa1, but isolation of Gpa1 in a GTP-bound conformation, showing it to be incapable of downstream activation. The Gpa1$^{Q244L}$ and Gpa1$^{R218C}$ mutants characterised in this thesis may be able to satisfy these requirements. There is evidence for post-GTP hydrolysis conformational states that are capable of regulating effectors, using G$\alpha$ mutants that trap intermediate states in the G protein cycle (Gilman, 1987). The possibility of alternative GTP-bound states has been further raised by the existence of a tetra-coordinated transition state in the hydrolytic mechanism (Ross, 2008). This intermediate state can be mimicked experimentally using aluminium fluoride ($AlF_4$) binding to G$\alpha_{GDP}$ (Gilman, 1987), although it has not been determined whether the inert state Gpa1 resembles such transition states.

### 6.8.3 Spatial Regulation of RGS Model

The final PM trafficking model of RGS function predicts that Rgs1 can be localised to the PM in both Mam2 tail-dependent and independent mechanisms. Experimental evidence in terms of fluorescence imaging of Rgs1 localisation has failed to confirm PM localisation in the absence of the receptor tail, although indirect evidence is inferred from the observations that Rgs1 could function as a GAP for Gpa1 in the absence of the Mam2 tail. Simulating the signalling activity of *S. pombe* strains expressing Mam2$\Delta$tail is achieved through blocking all reactions in the model whereby $RGS_c$ is interacting with R or complexes containing R. This simulation is not strictly representative of the Mam2$\Delta$tail strains as removing the Mam2 tail has been shown to have additional effects on signalling response, independent of blocking the Mam2-Rgs1 interaction. Removal of the tail also influences sensitivity to ligand as a result of reduced receptor internalisation of Mam2$\Delta$tail compared to Mam2.

Future modelling efforts could focus on including the observed receptor internalisation into the current model as an additional regulatory event in the signalling network. Inclusion of such reactions involving the recovery from P-factor stimulation is something that has not been included at any stage of the model development as the focus has been on the regulation of the G protein activation state through nucleotide exchange reactions. Including more de-activation reactions will possibly overcome the problem of achieving variable ligand sensitivity responses as seen in some of the mutant data. One such reaction that is omitted from our models is the ligand dissociating from the GPCR. As a result, once the ligand-GPCR complex is formed, both the ligand and GPCR are sequestered in this state. Allowing ligand to dissociate and re-associate freely could enable increased sensitivity of response to be simulated as a reduced concentration of ligand could activate multiple GPCRs.

Given the in-depth single cell quantitative data now available and improved understanding of the transcriptional and morphology branches of the signalling pathway, it would also be interesting to attempt to build on the existing model to achieve a quantitative model of a single cell response with time and to incorporate possible mechanisms for signal splitting

into these two branches of response. An additional module could also be built onto the current model at the level of ligand-receptor binding, for example by coupling our model to ternary complex models describing transitions between different receptor states (Kenakin, 2004). This may help give insight into the mechanisms linking ligand binding properties and different receptor states with the downstream signalling response.

### 6.8.4 Using Image Analysis of Fluorescent Reporters to Quantify Signalling

Although advantageous for imaging and quantification from live cells, there are some drawbacks with the use of fluorescent proteins as transcriptional reporters of the signalling response. Data interpretability is skewed by the long (∼2 h) maturation time of the fluorescent protein, therefore the rapid dynamics likely to occur for G protein activation can not be accurately quantified. In addition to this, it can be difficult to discern when signalling has ceased because of the high stability of the proteins masking this information. Analysing at the single cell level through image analysis helps to overcome this, but also has problems of its own. In image analysis, the data that you can obtain is dependent on the quality of the images obtained from the microscopy, therefore it is heavily dependent on a reliable image collection process. Data can suffer from variability because of technical issues with microscope settings, microscope drift and interference over the course of long time-series image acquisition.

In regards to analysing the images once obtained, software packages such as QuimP used in this thesis have greatly enhanced the image processing into meaningful quantitative data, but still are not without limitations. To segment and track every single cell within the confines of an image containing numerous cells is often an impossibility, or to do it would be too time consuming. The segmentation and tracking process is automated, but requires some manual input in terms of initial cell selection and often will fail to successfully track all cells through space and time because of issues such as overlapping cells and large frame-frame shifts in a cells location.

As technology for microscopy improves and software developers improve algorithms for cell segmentation, tracking and quantification, image analysis as a method for accumulating highly informative data on a variety of single cell characteristics should provide a powerful tool for investigating single cell signalling behaviour. To further enhance the detail of data obtained from *S. pombe* reporter strains, it would be beneficial to develop strains with multiple quantifiable reporters at different points in the pathway. For example by the engineering of strains with labelled proteins for association/dissociation studies through FRET analysis or by introducing multiple fluorescent reporter proteins under the control of multiple different P-factor inducible promoters. Indeed, work has recently begun

in our laboratory, analysing FRET signals from Ras1 interactions with Gap1, immediately downstream of Gpa1, providing better insight into the temporal dynamics of signal activation/de-activation (Weston *et al.*, in preparation).

## 6.9 Advances and Conclusions

Many challenges still remain in understanding the regulation of G protein-mediated signalling in general and also in the mating-response pathway in *Sz pombe* in particular. This project has advanced a number of pre-existing problems, expanded our knowledge of regulatory mechanisms and demonstrated improved and more in-depth quantitative understanding at the level of single cell signalling responses. Furthermore, it has demonstrated the range of understanding that may be obtained through a systems biology approach to cellular signalling.

Key nucleotide exchange events in the core G protein cycle have been investigated. *In silico* explorations of the Smith *et al.* model and *in vivo* characterisation of new and existing Gpa1 mutant variants has enhanced our understanding of the effects of the dynamics of nucleotide exchange on signal propagation. Model simulations have been compared to Gpa1 mutant data to predict Gpa1 mutant behaviour and has provided predictions of GDP/GTP nucleotide exchange rates that could be tested in future experiments.

An additional layer of regulation of the mating-response pathway has been explained and incorporated into a predictive mathematical model of the signalling pathway that is capable of qualitative agreement with biological data. This regulation involves the spatial regulation of the RGS protein. The localisation of Rgs1 at the PM has been demonstrated to be required to facilitate Rgs1 regulation of signalling. The tail of the GPCR Mam2 is shown to be required to direct this PM localisation. The mathematical model incorporates a requirement for PM localisation of RGS and proposes mechanisms of PM trafficking that control its localisation and hence influence signal transduction.

For the first time, image analysis has been used to quantify both transcriptional and morphology time-series signalling response from live-cell *S. pombe* fluorescent reporter strains *sxa2>GFP* and *sxa2>Venus*. Valuable insights have been obtained into single cell dose and time-dependent signalling characteristics, highlighting the cell-to-cell variability in signalling response of a clonal cell population.

# Appendix A

# Validation of Plasma Membrane Trafficking Model of RGS Function

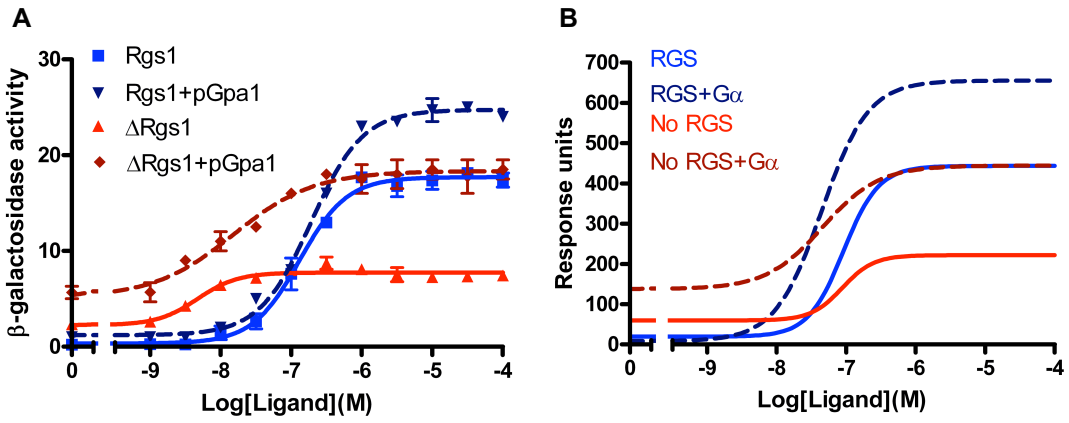


FIGURE A.1: **Model testing: Dependence on Gpa1 concentration.** The *wild-type* reporter strain; JY544, which contains an endogenous Rgs1 and Gpa1 (Rgs1) was transformed with vector pREP3x to express an additional copy of Gpa1 (Rgs1 + pGpa1). The reporter strain containing endogenous Gpa1 but lacking an endogenous Rgs1; JY630 (ΔRgs1) was also transformed with vector pREP3x expressing an additional copy of Gpa1 (ΔRgs1 + pGpa1). Cells were cultured in minimal media to a density of ∼5x10$^6$ cells/ml, incubated with 0 to $10^{-4}$M P-factor before assaying for $\beta$-galactosidase activity, measured as $OD_{420}/10^6$ cells. Results are the means ± S.E.M. of triplicate determinations from three independent isolates (A). Experimental data from Smith et al., 2009. Experimental data is compared to simulations of the equivalent model systems from Table 4.7 (B). Simulations are of an unmodified system (RGS), when G$\alpha$ concentration is doubled (RGS + G$\alpha$), when RGS is removed (No RGS) and from a system with no RGS and double the initial G$\alpha$ concentraion (No RGS + G$\alpha$). For the simulations the concentration of ligand was varied over the range 0-100 $\mu$M following 16 h simulated induction. Output from the model shows the accumulation of activated $G\alpha_{GTP}$Effector complexes over the duration of the simulated assay.

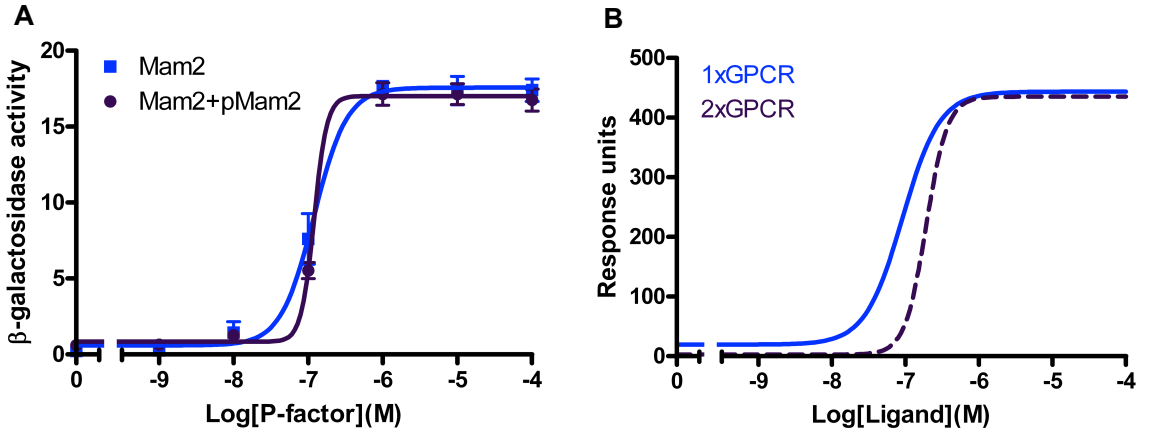


FIGURE A.2: **Model testing: Over-expression of Mam2.** Experimental data (A) from reporter strains; JY544, which contains endogenous Mam2 (Mam2) and JY544 expressing an additional copy of Mam2 from vector pREP3x (Mam2 + pMam2) is compared to simulated assays of the equivalent model system from Table 4.7 (B). Simulations are of an unmodified system (1 x GPCR) and a system initialised with double the concentration of receptor (2 x GPCR). For experimental data, cells were cultured in minimal media to a density of $\sim$5x10$^6$ cells/ml, incubated with 0 to $10^{-4}$M P-factor before assaying for $\beta$-galactosidase activity, measured as $OD_{420}/10^6$ cells. Results are the means $\pm$ S.E.M. of triplicate determinations from three independent isolates. For the simulations the concentration of ligand was varied over the range 0-100 $\mu$M following 16 h simulated induction. Output from the model shows the accumulation of activated $G\alpha_{GTP}$Effector complexes over the duration of the simulated assay.

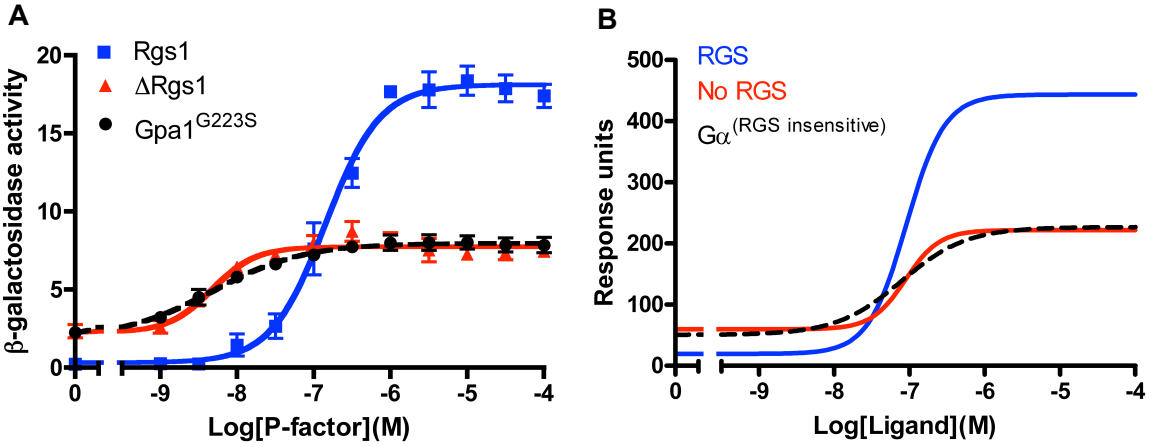


FIGURE A.3: **Model testing: Rgs1 insensitive Gpa1.** Experimental data (A) from reporter strains; JY544, which contains endogenous Rgs1 (Rgs1); JY630, which lacks endogenous Rgs1 ($\Delta$Rgs1) and a strain expressing an Rgs1 insensitive Gpa1 mutant in place of endogenous Gpa1 ($Gpa1^{G223S}$) is compared to simulated assays of the equivalent model system from Table 4.7 (B). Simulations are of an unmodified system (RGS), a system with concentration RGS = 0 nM (No RGS) and a system whereby G$\alpha$ interaction with RGS is blocked ($G\alpha^{(RGS\ insensitive)}$). For experimental data, cells were cultured in minimal media to a density of $\sim$5x10$^6$ cells/ml, incubated with 0 to $10^{-4}$M P-factor before assaying for $\beta$-galactosidase activity, measured as $OD_{420}/10^6$ cells. Results are the means $\pm$ S.E.M. of triplicate determinations from three independent isolates. Experimental data from Smith et al., 2009. For the simulations the concentration of ligand was varied over the range 0-100 $\mu$M following 16 h simulated induction. Output from the model shows the accumulation of activated $G\alpha_{GTP}$Effector complexes over the duration of the simulated assay.

# Appendix B

# Image Analysis: Single Cell Population Response

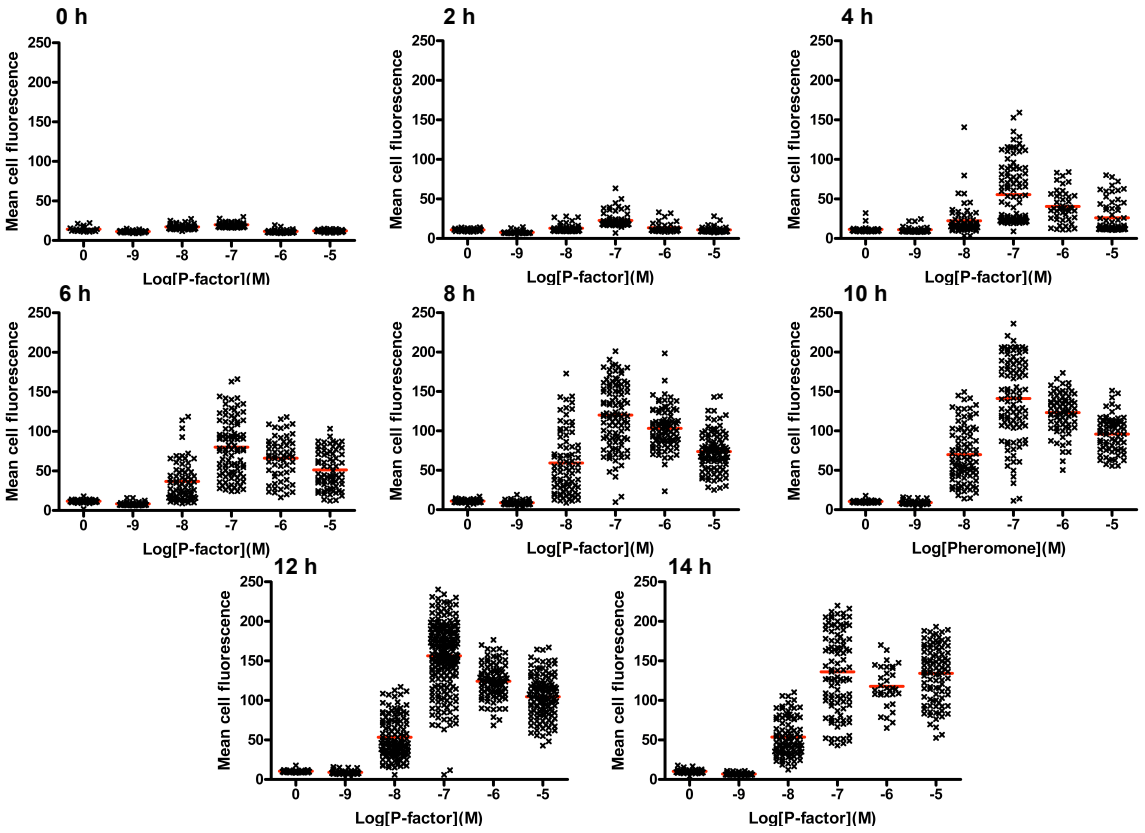


FIGURE B.1: **Mean cell fluorescence response with time using image analysis of single cells.** Reporter strain JY1325(*sxa2>GFP*) was grown in minimal media and incubated with 0M to $10^{-5}$M P-factor for 14 h. Images of the cell culture were taken at 0 h and subsequently every 2 h using a Leica SP5 scanning confocal microscope. Individual cells from the images were quantified for their fluorescence intensities using image analysis software QuimP. Cells from each image taken at each time-point were selected at random and quantified for their mean fluorescence intensity (mean pixel intensity). Each data point represents a single cell and the red bar indicates the mean of the analysed cell population.

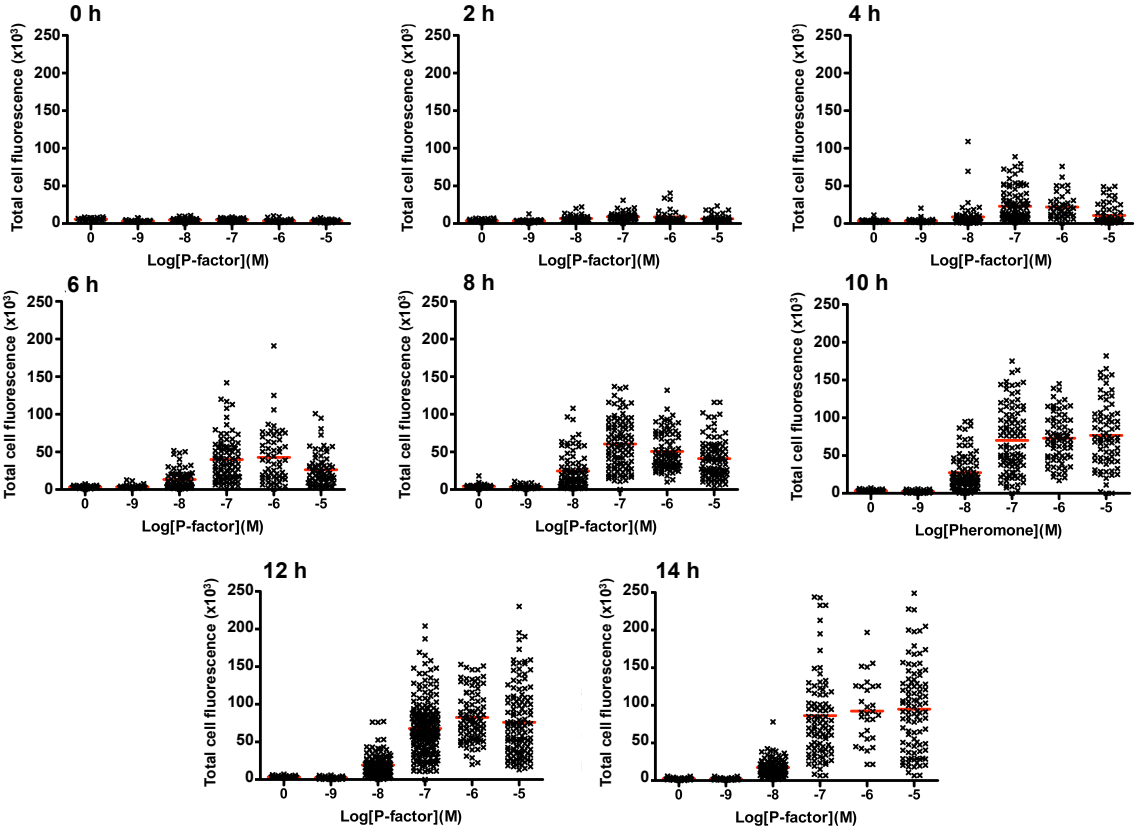


FIGURE B.2: **Total cell fluorescence response with time using image analysis of single cells.** Reporter strain JY1325(*sxa2>GFP*) was grown in minimal media and incubated with 0M to $10^{-5}$M P-factor for 14 h. Images of the cell culture were taken at 0 h and subsequently every 2 h using a Leica SP5 scanning confocal microscope. Individual cells from the images were quantified for their fluorescence intensities using image analysis software QuimP. Cells from each image taken at each time-point were selected at random and quantified for their total fluorescence intensity (sum of intensities of all pixels within the area of the cell). Each data point represents a single cell and the red bar indicates the mean of the analysed cell population.

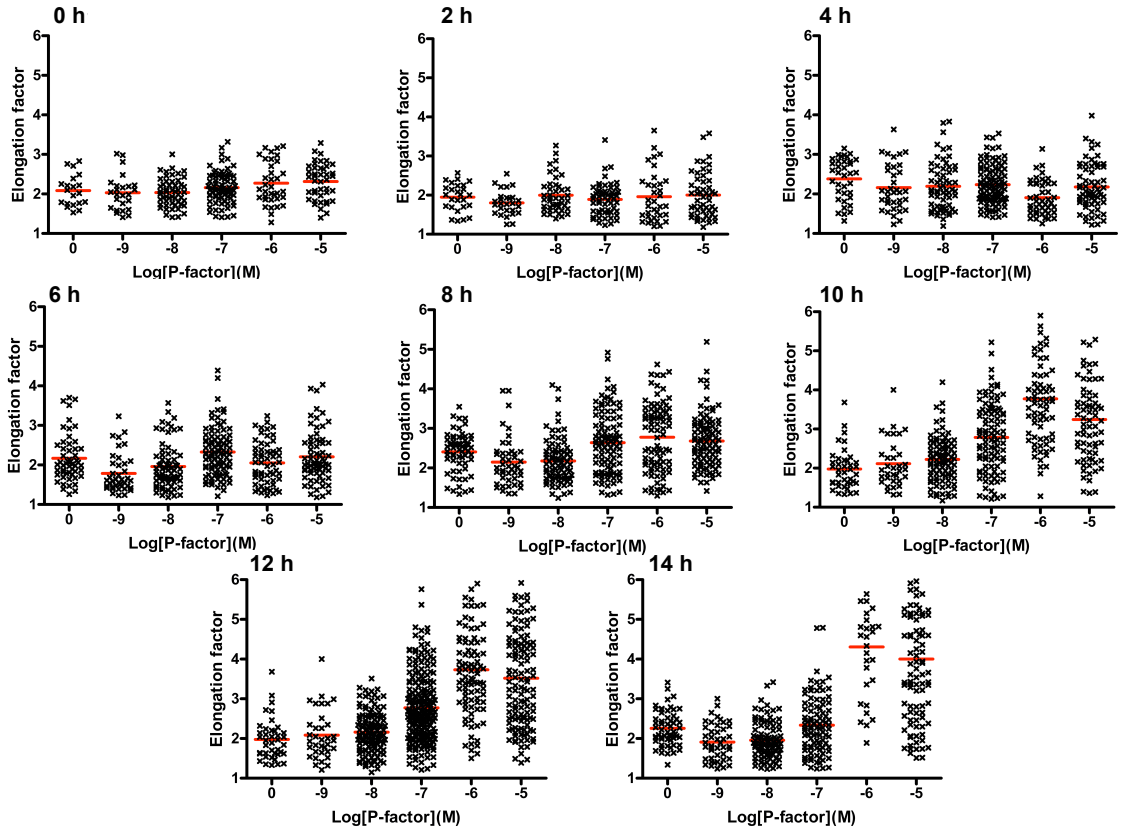


FIGURE B.3: **Morphology response with time using image analysis of single cells.** Reporter strain JY1325(*sxa2>GFP*) was grown in minimal media and incubated with 0M to $10^{-5}$M P-factor for 14 h. Images of the cell culture were taken at 0 h and subsequently every 2 h using a Leica SP5 scanning confocal microscope. Individual cells from the images were quantified for their morphology using image analysis software QuimP. Cells from each image taken at each time-point were selected at random and quantified for their elongation factor (ratio of cell length:width). Each data point represents a single cell and the red bar indicates the mean of the analysed cell population.

# Bibliography

**Abramow-Newerly, M., Roy, A., Nunn, C. and Chidiac, P.** (2006). RGS proteins have a signalling complex: interactions between RGS proteins and GPCRs, effectors, and auxiliary proteins. *Cell. Signal.* **18**, 579–591.

**Adams, S. R., Campbell, R. E., Gross, L. A., Martin, B. R., Walkup, G. K., Yao, Y., Llopis, J. and Tsien, R. Y.** (2002). New biarsenical ligands and tetracysteine motifs for protein labeling in vitro and in vivo: synthesis and biological applications. *J. AM. Chem. Soc.* **124**, 6063–76.

**Ajit, S. and Young, K.** (2005). Analysis of chimeric RGS proteins in yeast for the functional evaluation of protein domains and their potential use in drug target validation. *Cell. Signal.* **17**, 817–825.

**Andresen, M., Schmitz-Salue, R. and Jakobs, S.** (2004). Short tetracysteine tags to beta-tubulin demonstrate the significance of small labels for live cell imaging. *Mol. Biol. Cell* **15**, 5616–22.

**Avruch, J.** (1998). Insulin signal transduction through protein kinase cascades. *Mol. Cell. Biochem.* **182**, 31–48.

**Bach, M.** (1987). Cloning and expression of the OMP decarboxylase gene URA4 from *Schizosaccharomyces pombe*. *Curr. Genet.* **12**, 527–534.

**Ballesteros, J. A., Jensen, A. D., Liapakis, G., Rasmussen, S. G., Shi, L., Gether, U. and Javitch, J. A.** (2001). Activation of the beta 2-adrenergic receptor involves disruption of an ionic lock between the cytoplasmic ends of transmembrane segments 3 and 6. *J. Biol. Chem.* **276**, 29171–29177.

**Ballon, D. R., Flanary, P. L., Gladue, D. P., Konopka, J. B., Dohlman, H. G. and Thorner, J.** (2006). DEP-domain-mediated regulation of GPCR signaling responses. *Cell* **126**, 1079–93.

**Bansal, G., Druey, K. and Xie, Z.** (2007). R4 RGS proteins: regulation of G-protein signaling and beyond. *Pharmacol. Ther.* **116**, 473–495.

**Barbacid, M.** (1987). Ras genes. *Annu. Rev. Biochem.* **56**, 779–827.

**Barr, M., Tu, H., Van Aelst, L. and Wigler, M.** (1996). Identification of Ste4 as a potential regulator of Byr2 in the sexual response pathway of *Schizosaccharomyces pombe*. *Mol. Cell. Biol.* **16**, 5597.

**Bauman, P., Cheng, Q. and Albright, C.** (1998). The Byr2 kinase translocates to the plasma membrane in a Ras1-dependent manner. *Biochem. Biophys. Res. Commun.* **244**, 468–474.

**Berger, E., Murphy, P. and Farber, J.** (1999). Chemokine receptors as HIV-1 coreceptors: roles in viral entry, tropism, and disease. *Annu. Rev. Immunol.* **17**, 657–700.

**Berman, D. M., Kozasa, T. and Gilman, A. G.** (1996). The GTPase-activating protein RGS4 stabilizes the transition state for nucleotide hydrolysis. *J. Biol. Chem.* **271**, 27209–27212.

**Bernstein, L., Ramineni, S., Hague, C., Cladman, W., Chidiac, P., Levey, A. and Hepler, J.** (2004). RGS2 binds directly and selectively to the M1 muscarinic acetylcholine receptor third intracellular loop to modulate Gq/11$\alpha$ signaling. *J. Biol. Chem.* **279**, 21248.

**Berridge, M.** (1993). Inositol trisphosphate and calcium signalling. *Nature* **361**, 315–325.

**Birnbaumer, L., Abramowitz, J. and Brown, A.** (1990). Receptor-effector coupling by g proteins. *Biochim. Biophys. Acta* **1031**, 163–224.

**Birnbaumer, L. and Zurita, A.** (2010). On the roles of Mg in the activation of G proteins. *J. Recept. Signal Transduct.* **30**, 372–375.

**Blumer, J., Cismowski, M., Sato, M. and Lanier, S.** (2005). AGS proteins: receptor-independent activators of G-protein signaling. *Trends Pharmacol. Sci.* **26**, 470–476.

**Blumer, J., Smrcka, A. and Lanier, S.** (2007). Mechanistic pathways and biological roles for receptor-independent activators of G-protein signaling. *Pharmacol. Ther.* **113**, 488–506.

**Bockaert, J., Marin, P., Dumuis, A. and Fagni, L.** (2003). The 'magic tail' of G protein-coupled receptors: an anchorage for functional protein networks. *FEBS Lett.* **546**, 65–72.

**Bockaert, J. and Pin, J.** (1999). Molecular tinkering of G protein-coupled receptors: an evolutionary success. *EMBO J.* **18**, 1723–1729.

**Bornheimer, S. J., Maurya, M. R., Farquhar, M. G. and Subramaniam, S.** (2004). Computational modeling reveals how interplay between components of a GTPase-cycle module regulates signal transduction. *Proc. Natl. Acad. Sci. U.S.A.* **101**, 15899–904.

**Bos, J.** (1989). Ras oncogenes in human cancer: a review. *Cancer Res.* **49**, 4682–4689.

**Bosgraaf, L. and Van Haastert, P.** (2010). Quimp3, an automated pseudopod-tracking algorithm. *Cell Adh. Migr.* **4**, 46.

**Bosgraaf, L., van Haastert, P. and Bretschneider, T.** (2009). Analysis of cell movement by simultaneous quantification of local membrane displacement and fluorescent intensities using Quimp2. *Cell Motil. Cytoskeleton* **66**, 156–165.

**Bourne, H.** (1987). Discovery of a new oncogene in pituitary tumours? *Nature* **330**, 517–518.

**Bunemann, M., Frank, M. and Lohse, M.** (2003). Gi protein activation in intact cells involves subunit rearrangement rather than dissociation. *Proc. Natl. Acad. Sci.* **100**, 16077–16082.

**Carman, C., Parent, J., Day, P., Pronin, A., Sternweis, P., Wedegaertner, P., Gilman, A., Benovic, J. and Kozasa, T.** (1999). Selective regulation of G$\alpha$q/11 by an RGS domain in the G protein-coupled receptor kinase, GRK2. *J. Biol. Chem.* **274**, 34483–34492.

**Chan, R. and Otte, C.** (1982a). Isolation and genetic analysis of *Saccharomyces cerevisiae* mutants supersensitive to G1 arrest by a factor and alpha factor pheromones. *Mol. Cell. Biol.* **2**, 11.

**Chan, R. and Otte, C.** (1982b). Physiological characterization of *Saccharomyces cerevisiae* mutants supersensitive to G1 arrest by a factor and alpha factor pheromones. *Mol. Cell. Biol.* **2**, 21.

**Chang, F. and Bourne, H.** (1989). Cholera toxin induces cAMP-independent degradation of Gs. *J. Biol. Chem.* **264**, 5352.

**Chang, Y., Cesarman, E., Pessin, M., Lee, F., Culpepper, J., Knowles, D. and Moore, P.** (1994). Identification of herpesvirus-like DNA sequences in AIDS-associated Kaposi's sarcoma. *Science* **266**, 1865.

**Chatterjee, T. and Fisher, R.** (2000). Cytoplasmic, nuclear, and golgi localization of RGS proteins. *J. Biol. Chem.* **275**, 24013.

**Chatterjee, T. and Fisher, R.** (2002). RGS12TS-S localizes at nuclear matrix-associated subnuclear structures and represses transcription: structural requirements for subnuclear targeting and transcriptional repression. *Molecular and cellular biology* **22**, 4334.

**Chen, I. and Ting, A. Y.** (2005). Site-specific labeling of proteins with small molecules in live cells. *Curr. Opin. Biotechnol.* **16**, 35–40.

**Chen, S. and Hamm, H. E.** (2006). DEP domains: More than just membrane anchors. *Dev. Cell* **11**, 436–8.

**Cho, H., Harrison, K. and Kehrl, J.** (2004). Regulators of G protein signaling: potential drug targets for controlling cardiovascular and immune function. *Curr. Drug Targets Immune Endocr. Metabol. Disord.* **4**, 107–118.

**Cismowski, M., Takesono, A., Ma, C., Lizano, J., Xie, X., Fuernkranz, H., Lanier, S. and Duzic, E.** (1999). Genetic screens in yeast to identify mammalian non-receptor modulators of G-protein signaling. *Nat. Biotechnol.* **17**, 878–883.

**Clapham, D. and Neer, E.** (1997). G protein $\beta\gamma$ subunits. *Annu. Rev. Pharmacol. Toxicol.* **37**, 167–203.

**Clarke, M. and Sperandio, V.** (2005). Events at the host-microbial interface of the gastrointestinal tract III. Cell-to-cell signaling among microbial flora, host, and pathogens: there is a whole lot of talking going on. *Am. J. Physiol. Gastrointest. Liver Physiol.* **288**, G1105.

**Colman-Lerner, A., Gordon, A., Serra, E., Chin, T., Resnekov, O., Endy, D., Pesce, C. G. and Brent, R.** (2005). Regulated cell-to-cell variation in a cell-fate decision system. *Nature* **437**, 699–706.

**Craven, S. and Bredt, D.** (1998). PDZ proteins organize synaptic signaling pathways. *Cell* **93**, 495–498.

**Dajas-Bailador, F. and Wonnacott, S.** (2004). Nicotinic acetylcholine receptors and the regulation of neuronal signalling. *Trends Pharmacol. Sci.* **25**, 317–324.

**Dalous, J., Burghardt, E., Müller-Taubenberger, A., Bruckert, F., Gerisch, G. and Bretschneider, T.** (2008). Reversal of cell polarity and actin-myosin cytoskeleton reorganization under mechanical and chemical stimulation. *Biophys. J.* **94**, 1063–1074.

**Davey, J.** (1991). Isolation and quantitation of M-factor, a diffusible mating factor from the fission yeast *Schizosaccharomyces pombe*. *Yeast* **7**, 357–366.

**Davey, J.** (1998). Fusion of a fission yeast. *Yeast* **14**, 1529–1566.

**Davey, J., Egel, R. and Nielsen, O.** (1995). Pheromone procedures in fission yeast. *Methods in Molecular Genetics* **6**, 247–263.

**Davey, J. and Nielsen, O.** (1994). Mutations in cyr1 and pat1 reveal pheromone-induced G1 arrest in the fission yeast *Schizosaccharomyces pombe*. *Curr. Genet.* **26**, 105–112.

**De Vries, L., Elenko, E., Hubler, L., Jones, T. and Farquhar, M.** (1996). GAIP is membrane-anchored by palmitoylation and interacts with the activated (GTP-bound) form of g$\alpha$i subunits. *Proceedings of the National Academy of Sciences* **93**, 15203.

**De Vries, L., Zheng, B., Fischer, T., Elenko, E. and Farquhar, M.** (2000). The regulator of G protein signaling family. *Annu. Rev. Pharmacol. Toxicol.* **40**, 235–271.

**Denker, S., McCaffery, J., Palade, G., Insel, P. and Farquhar, M.** (1996). Differential distribution of alpha subunits and beta gamma subunits of heterotrimeric G proteins on golgi membranes of the exocrine pancreas. *J. Cell Biol.* **133**, 1027–1040.

**Der, C., Finkel, T. and Cooper, G.** (1986). Biological and biochemical properties of human rasH genes mutated at codon 61. *Cell* **44**, 167–176.

**DeWire, S., Ahn, S., Lefkowitz, R. and Shenoy, S.** (2007). $\beta$-arrestins and cell signaling. *Annu. Rev. Physiol.* **69**, 483–510.

**Didmon, M., Davis, K., Watson, P., Ladds, G., Broad, P. and Davey, J.** (2002). Identifying regulators of pheromone signalling in the fission yeast *Schizosaccharomyces pombe*. *Curr. Genet.* **41**, 241–253.

**Dohlman, H.** (2002). G proteins and pheromone signaling. *Annual review of physiology* **64**, 129–152.

**Dohlman, H., Apaniesk, D., Chen, Y., Song, J. and Nusskern, D.** (1995). Inhibition of G-protein signaling by dominant gain-of-function mutations in Sst2p, a pheromone desensitization factor in *Saccharomyces cerevisiae*. *Mol. Cell. Biol.* **15**, 3635.

**Dohlman, H. and Thorner, J.** (1997). RGS proteins and signaling by heterotrimeric G proteins. *J. Biol. Chem.* **272**, 3871.

**Donaldson, J.** (2008). Arfs and membrane lipids: sensing, generating and responding to membrane curvature. *Biochem. J.* **414**, e1–e2.

**Dormann, D., Libotte, T., Weijer, C. and Bretschneider, T.** (2002). Simultaneous quantification of cell motility and protein-membrane-association using active contours. *Cell Motil. Cytoskeleton* **52**, 221–230.

**Doupnik, C., Davidson, N., Lester, H. and Kofuji, P.** (1997). RGS proteins reconstitute the rapid gating kinetics of G$\beta\gamma$-activated inwardly rectifying K+ channels. *Proc. Natl. Acad. Sci.* **94**, 10461.

**Dowell, S., Brown, A. et al.** (2002). Yeast assays for G-protein-coupled receptors. *Receptors and Channels* **8**, 343–352.

**Druey, K., Sullivan, B., Brown, D., Fischer, E., Watson, N., Blumer, K., Gerfen, C., Scheschonka, A. and Kehrl, J.** (1998). Expression of GTPase-deficient Gi$\alpha$2 results in translocation of cytoplasmic RGS4 to the plasma membrane. *J. Biol. Chem.* **273**, 18405.

**Dulin, N., Sorokin, A., Reed, E., Elliott, S., Kehrl, J. and Dunn, M.** (1999). RGS3 Inhibits G Protein-Mediated Signaling via Translocation to the Membrane and Binding to Galpha 11. *Mol. Cell. Biol.* **19**, 714.

**Elenko, E., Fischer, T., Niesman, I., Harding, T., McQuistan, T., Von Zastrow, M. and Farquhar, M.** (2003). Spatial regulation of G$\alpha$i protein signaling in clathrin-coated membrane microdomains containing GAIP. *Mol. Pharmacol.* **64**, 11.

**Elowitz, M. B.** (2002). Stochastic gene expression in a single cell. *Science* **297**, 1183–1186.

**Evanko, D., Thiyagarajan, M. and Wedegaertner, P.** (2000). Interaction with G$\beta\gamma$ is required for membrane targeting and palmitoylation of G$\alpha$s and G$\alpha$q. *J. Biol. Chem.* **275**, 1327.

**Evans, R.** (1988). The steroid and thyroid hormone receptor superfamily. *Science* **240**, 889.

**Fall, C., Marland, E., Wagner, J. and Tyson, J.** (2002). *Computational cell biology*. Springer Verlag.

**Farfel, Z., Bourne, H. and Iiri, T.** (1999). The expanding spectrum of G protein diseases. *N. Engl. J. Med.* **340**, 1012.

**Faurobert, E. and Hurley, J.** (1997). The core domain of a new retina specific RGS protein stimulates the GTPase activity of transducin in vitro. *Proc. Natl. Acad. Sci.* **94**, 2945.

**Feinerman, O., Veiga, J., Dorfman, J., Germain, R. and Altan-Bonnet, G.** (2008). Variability and robustness in T cell activation from regulated heterogeneity in protein levels. *Science* **321**, 1081.

**Ferguson, S.** (2001). Evolving concepts in G protein-coupled receptor endocytosis: the role in receptor desensitization and signaling. *Pharmacol. Rev.* **53**, 1–24.

**Fields, S. and Song, O.** (1989). A novel genetic system to detect protein-protein interactions. *Nature* **340**, 245.

**Flower, D.** (1999). Modelling G-protein-coupled receptors for drug design. *Biochim. Biophys. Acta* **1422**, 207–234.

**Forsburg, S.** (1993). Comparison of *Schizosaccharomyces pombe* expression systems. *Nucleic Acids Res.* **21**, 2955.

**Fredriksson, R., Lagerstrom, M., Lundin, L. and Schioth, H.** (2003). The G-protein-coupled receptors in the human genome form five main families. Phylogenetic analysis, paralogon groups, and fingerprints. *Mol. Pharmacol.* **63**, 1256–1272.

**Garzón, J., Rodríguez-Muñoz, M. and Sánchez-Blázquez, P.** (2005). Morphine alters the selective association between mu-opioid receptors and specific RGS proteins in mouse periaqueductal gray matter. *Neuropharmacology* **48**, 853–868.

**Gibbs, J. and Marshall, M.** (1989). The ras oncogene–an important regulatory element in lower eucaryotic organisms. *Microbiol. Mol. Biol. Rev.* **53**, 171.

**Gilman, A.** (1987). G proteins: transducers of receptor-generated signals. *Annu. Rev. Biochem.* **56**, 615–649.

**Goddard, A., Ladds, G. and Davey, J.** (2005). Development of a semi-quantitative plate-based $\alpha$-galactosidase gene reporter for *Schizosaccharomyces pombe* and its use to isolate a constitutively active Mam2. *Yeast* **22**, 31–41.

**Goryachev, A. and Pokhilko, A.** (2006). Computational model explains high activity and rapid cycling of Rho GTPases within protein complexes. *PLoS Comput. Biol.* **2**, e172.

**Grimm, C., Kohli, J., Murray, J. and Maundrell, K.** (1988). Genetic engineering of *Schizosaccharomyces pombe*: a system for gene disruption and replacement using the ura4 gene as a selectable marker. *Mol. Gen. Genet.* **215**, 81–86.

**Hague, C., Bernstein, L., Ramineni, S., Chen, Z., Minneman, K. and Hepler, J.** (2005). Selective inhibition of $\alpha$1A-adrenergic receptor signaling by RGS2 association with the receptor third intracellular loop. *J. Biol. Chem.* **280**, 27289.

**Hall, R. and Lefkowitz, R.** (2002). Regulation of G protein-coupled receptor signaling by scaffold proteins. *Circ. Res.* **91**, 672.

**Hao, N., Yildirim, N., Wang, Y., Elston, T. and Dohlman, H.** (2003). Regulators of G Protein Signaling and Transient Activation of Signaling. *J. Biol. Chem.* **278**, 46506–46515.

**He, C., Yan, X., Zhang, H., Mirshahi, T., Jin, T., Huang, A. and Logothetis, D.** (2002). Identification of critical residues controlling G protein-gated inwardly rectifying K+ channel activity through interactions with the $\beta\gamma$ subunits of G proteins. *J. Biol. Chem.* **277**, 6088–6096.

**He, L., Bradrick, T., Karpova, T., Wu, X., Fox, M., Fischer, R., McNally, J., Knutson, J., Grammer, A. and Lipsky, P.** (2003). Flow cytometric measurement of fluorescence (förster) resonance energy transfer from cyan fluorescent protein to yellow fluorescent protein using single-laser excitation at 458 nm. *Cytometry Part A* **53**, 39–54.

**Heldin, C., Miyazono, K. and Ten Dijke, P.** (1997). TGF- signalling from cell membrane to nucleus through SMAD proteins. *Nature* **390**, 465–471.

**Hepler, J.** (2003). RGS protein and G protein interactions: a little help from their friends. *Mol. Pharmacol.* **64**, 547.

**Hepler, J. R.** (1999). Emerging roles for RGS proteins in cell signalling. *Trends Pharmacol. Sci.* **20**, 376–382.

**Hill, C., Goddard, A., Davey, J. and Ladds, G.** (2006). Investigating RGS proteins in yeast. In *Semin. Cell Dev. Biol.*, volume 17.

**Hoffman, C. and Winston, F.** (1987). A ten-minute DNA preparation from yeast efficiently releases autonomous plasmids for transformaion of *Escherichia coli*. *Gene* **57**, 267–272.

**Hoffman, C. et al.** (2005). Glucose sensing via the protein kinase A pathway in *Schizosaccharomyces pombe*. *Biochem. Soc. Trans.* **33**, 257–260.

**Hollinger, S. and Hepler, J.** (2002). Cellular regulation of RGS proteins: modulators and integrators of G protein signaling. *Pharmacol. Rev.* **54**, 527–559.

**Hughes, D., Fukui, Y. and Yamamoto, M.** (1990). Homologous activators of ras in fission and budding yeast. *Nature* **344**, 355–357.

**Hughes, T., Zhang, H., Logothetis, D. and Berlot, C.** (2001). Visualization of a functional G$\alpha$q-green fluorescent protein fusion in living cells. *J. Biol. Chem.* **276**, 4227.

**Hur, E. and Kim, K.** (2002). G protein-coupled receptor signalling and cross-talk: Achieving rapidity and specificity. *Cell. Signal.* **14**, 397–405.

**Hurst, J. H. and Hooks, S. B.** (2009). Regulator of G-protein signaling (RGS) proteins in cancer biology. *Biochem. Pharmacol.* **78**, 1289–97.

**Hutter, K. and Eipel, H.** (1978). Flow cytometric determinations of cellular substances in algae, bacteria, moulds and yeasts. *Antonie Van Leeuwenhoek* **44**, 269–282.

**Imai, Y., Miyake, S., Hughes, D. and Yamamoto, M.** (1991). Identification of a GTPase-activating protein homolog in *Schizosaccharomyces pombe*. *Mol. Cell. Biol.* **11**, 3088.

**Imai, Y. and Yamamoto, M.** (1992). *Schizosaccharomyces pombe* sxa1+ and sxa2+ encode putative proteases involved in the mating response. *Mol. Cell. Biol.* **12**, 1827.

**Ivey, F. and Hoffman, C.** (2005). Direct activation of fission yeast adenylate cyclase by the Gpa2 G$\alpha$ of the glucose signaling pathway. *Proc. Natl. Acad. Sci. U.S.A.* **102**, 6108.

**Jaroszeski, M. and Radcliff, G.** (1999). Fundamentals of flow cytometry. *Mol. Biotechnol.* **11**, 37–53.

**Jean-Alphonse, F. and Hanyaloglu, A.** (2010). Regulation of GPCR signal networks via membrane trafficking. *Mol. Cell. Endocrinol.* **331**, 205–214.

**Johnston, C. A. and Siderovski, D. P.** (2007). Receptor-mediated activation of heterotrimeric G-proteins: current structural insights. *Mol. Pharmacol.* **72**, 219–230.

**Jones, R. G. and Thompson, C. B.** (2009). Tumor suppressors and cell metabolism: a recipe for cancer growth. *Genes & Development* **23**, 537–548.

**Ju, W., Morishita, W., Tsui, J., Gaietta, G., Deerinck, T., Adams, S., Garner, C., Tsien, R., Ellisman, M. and Malenka, R.** (2004). Activity-dependent regulation of dendritic synthesis and trafficking of AMPA receptors. *Nat. Neurosci.* **7**, 244–253.

**Kaufman, M., Andris, F. and Leo, O.** (1999). A logical analysis of T cell activation and anergy. *Proc. Natl. Acad. Sci.* **96**, 3894.

**Kawamukai, M., Gerst, J., Field, J., Riggs, M., Rodgers, L., Wigler, M. and Young, D.** (1992). Genetic and biochemical analysis of the adenylyl cyclase-associated protein, cap, in *Schizosaccharomyces pombe*. *Mol. Biol. Cell* **3**, 167.

**Kenakin, T.** (2004). Principles: receptor theory in pharmacology. *Trends Pharmacol. Sci.* **25**, 186–192.

**Kikuchi, Y., Kitazawa, Y., Shimatake, H. and Yamamoto, M.** (1988). The primary structure of the leul+ gene of *Schizosaccharomyces pombe*. *Curr. Genet.* **14**, 375–379.

**Kimple, R., De Vries, L., Tronchère, H., Behe, C., Morris, R., Farquhar, M. and Siderovski, D.** (2001). RGS12 and RGS14 GoLoco motifs are G$\alpha$i interaction sites with guanine nucleotide dissociation inhibitor activity. *J. Biol. Chem.* **276**, 29275–29281.

**Kitamura, K. and Shimoda, C.** (1991). The *Schizosaccharomyces pombe mam2* gene encodes a putative pheromone receptor which has a significant homology with the *Saccharomyces cerevisiae* Ste2 protein. *EMBO J.* **10**, 3743.

**Kjaerulff, S., Lautrup-Larsen, I., Truelsen, S., Pedersen, M. and Nielsen, O.** (2005). Constitutive activation of the fission yeast pheromone-responsive pathway induces

ectopic meiosis and reveals Ste11 as a mitogen-activated protein kinase target. *Mol. Cell. Biol.* **25**, 2045–2059.

**Klar, A. and Miglio, L.** (1986). Initiation of meiotic recombination by double-strand dna breaks in s. pombe. *Cell* **46**, 725–731.

**Klipp, E. and Liebermeister, W.** (2006). Mathematical modeling of intracellular signaling pathways. *BMC Neurosci.* **7**, S10.

**Koelle, M. R. and Horvitz, H. R.** (1996). EGL-10 regulates G protein signaling in the *C. elegans* nervous system and shares a conserved domain with many mammalian proteins. *Cell* **84**, 115–125.

**Kofahl, B. and Klipp, E.** (2004). Modelling the dynamics of the yeast pheromone pathway. *Yeast* **21**, 831–850.

**Kovoor, A., Seyffarth, P., Ebert, J., Barghshoon, S., Chen, C., Schwarz, S., Axelrod, J., Cheyette, B., Simon, M., Lester, H. et al.** (2005). D2 dopamine receptors colocalize regulator of G-protein signaling 9-2 (RGS9-2) via the RGS9 DEP domain, and RGS9 knock-out mice develop dyskinesias associated with dopamine pathways. *J. Neurosci.* **25**, 2157.

**Laburthe, M., Couvineau, A., Gaudin, P., Maorett, J., Rouyer-Fessard, C. and Nicole** (1996). Receptors for VIP, PACAP, Secretin, GRF, Glucagon, GLP-1, and other members of their new family of G protein-linked receptors: structure-function relationship with special reference to the human VIP-1 receptors. *Ann. N. Y. Acad. Sci.* **805**, 94–109.

**Ladds, G. and Davey, J.** (2000). Sxa2 is a serine carboxypeptidase that degrades extracellular P-factor in the fission yeast *Schizosaccharomyces pombe*. *Mol. Microbiol.* **36**, 377–390.

**Ladds, G. and Davey, J.** (2004). Analysis of human GPCRs in fission yeast. *Curr. Opin. Drug Discov. Devel.* **7**, 683–691.

**Ladds, G., Davis, K., Das, A. and Davey, J.** (2005a). A constitutively active GPCR retains its G protein specificity and the ability to form dimers. *Mol. Microbiol.* **55**, 482–497.

**Ladds, G., Davis, K., Hillhouse, E. and Davey, J.** (2003). Modified yeast cells to investigate the coupling of G protein-coupled receptors to specific G proteins. *Mol. Microbiol.* **47**, 781–792.

**Ladds, G., Goddard, A. and Davey, J.** (2005b). Functional analysis of heterologous GPCR signalling pathways in yeast. *Trends Biotechnol.* **23**, 367–373.

**Ladds, G., Goddard, A., Hill, C., Thornton, S. and Davey, J.** (2007). Differential effects of RGS proteins on G alpha(q) and G alpha(11) activity. *Cell Signal.* **19**, 103–113.

**Ladds, G., Rasmussen, E., Young, T., Nielsen, O. and Davey, J.** (1996a). The sxa2-dependent inactivation of the P-factor mating pheromone in the fission yeast *Schizosaccharomyces pombe*. *Mol. Microbiol.* **20**, 35–42.

**Ladds, G., Rasmussen, E. M., Young, T., Nielsen, O. and Davey, J.** (1996b). The sxa2-dependent inactivation of the P-factor mating pheromone in the fission yeast schizosaccharomyces pombe. *Mol Microbiol* **20**, 35–42.

**Lambright, D., Noel, J., Hamm, H. and Sigler, P.** (1994). Structural determinants for activation of the $\alpha$-subunit of a heterotrimeric G protein. *Nature* **369**, 621–628.

**Lambright, D., Sondek, J., Bohm, A., Skiba, N., Hamm, H., Sigler, P. et al.** (1996). The 2.0 a crystal structure of a heterotrimeric G protein. *Nature* **379**, 311–320.

**Lämmermann, T., Bader, B., Monkley, S., Worbs, T., Wedlich-Söldner, R., Hirsch, K., Keller, M., Förster, R., Critchley, D., Fässler, R. et al.** (2008). Rapid leukocyte migration by integrin-independent flowing and squeezing. *Nature* **453**, 51–55.

**Landis, C., Masters, S., Spada, A., Pace, A., Bourne, H. and Vallar, L.** (1989). GTPase inhibiting mutations activate the $\alpha$ chain of Gs and stimulate adenylyl cyclase in human pituitary tumours. *Nature* **340**, 692–696.

**Lauffenburger, D. and Linderman, J.** (1996). *Receptors: Models for binding, trafficking, and signaling*. Oxford University Press, USA.

**Leonard, S. and Bertrand, D.** (2001). Neuronal nicotinic receptors: from structure to function. *Nicotine Tob. Res.* **3**, 203.

**Li, X., Yang, Z. and Greenwood, M.** (2004). G alpha protein dependent and independent effects of human RGS1 expression in yeast. *Cell. Signal.* **16**, 43–49.

**Liu, Z. and Fisher, R.** (2004). RGS6 interacts with DMAP1 and DNMT1 and inhibits DMAP1 transcriptional repressor activity. *J. Biol. Chem.* **279**, 14120–14128.

**Losick, R. and Desplan, C.** (2008). Stochasticity and cell fate. *Science* **320**, 65.

**Lui, K. and Huang, Y.** (2009). Ran GTPase: A key regulator of nucleocytoplasmic trafficking. *Mol. Cell. Pharmacol.* **1**, 148.

**Lyons, J., Landis, C., Harsh, G., Vallar, L., Grunewald, K., Feichtinger, H., Duh, Q., Clark, O., Kawasaki, E., Bourne, H. et al.** (1990). Two G protein oncogenes in human endocrine tumors. *Science* **249**, 655.

**Maeda, T., Mochizuki, N. and Yamamoto, M.** (1990). Adenylyl cyclase is dispensable for vegetative cell growth in the fission yeast *Schizosaccharomyces pombe*. *Proc. Natl. Acad. Sci.* **87**, 7814–7818.

**Majumdar, S., Ramachandran, S. and Cerione, R.** (2006). New insights into the role of conserved, essential residues in the GTP binding/GTP hydrolytic cycle of large G proteins. *J. Biol. Chem.* **281**, 9219.

**Marcus, S., Polverino, A., Chang, E., Robbins, D., Cobb, M. and Wigler, M.** (1995). Shk1, a homolog of the *Saccharomyces cerevisiae* Ste20 and mammalian p65PAK protein kinases, is a component of a Ras/Cdc42 signaling module in the fission yeast *Schizosaccharomyces pombe*. *Proc. Natl. Acad. Sci.* **92**, 6180.

**Marrari, Y., Crouthamel, M., Irannejad, R. and Wedegaertner, P.** (2007). Assembly and trafficking of heterotrimeric G proteins. *Biochem. J.* **46**, 7665–7677.

**Martin, S. and Berthelot-Grosjean, M.** (2009). Polar gradients of the DYRK-family kinase Pom1 couple cell length with the cell cycle. *Nature* **459**, 852–856.

**Martin-McCaffrey, L., Willard, F., Oliveira-dos Santos, A., Natale, D., Snow, B., Kimple, R., Pajak, A., Watson, A., Dagnino, L., Penninger, J. et al.** (2004). RGS14 is a mitotic spindle protein essential from the first division of the mammalian zygote. *Developmental Cell* **7**, 763–769.

**Massagué, J. and Wotton, D.** (2000). Transcriptional control by the TGF-$\beta$/Smad signaling system. *EMBO J.* **19**, 1745.

**Mata, J. and Bähler, J.** (2006). Global roles of Ste11p, cell type, and pheromone in the control of gene expression during early sexual differentiation in fission yeast. *Proc. Natl. Acad. Sci. U.S.A.* **103**, 15517–22.

**Matsuyama, A., Arai, R., Yashiroda, Y., Shirai, A., Kamata, A., Sekido, S., Kobayashi, Y., Hashimoto, A., Hamamoto, M., Hiraoka, Y., Horinouchi, S. and Yoshida, M.** (2006). ORFeome cloning and global analysis of protein localization in the fission yeast *Schizosaccharomyces pombe*. *Nat. Biotechnol.* **24**, 841–7.

**Maundrell, K.** (1990). *nmt1* of fission yeast. a highly transcribed gene completely repressed by thiamine. *J. Biol. Chem.* **265**, 10857.

**Maundrell, K.** (1993). Thiamine-repressible expression vectors pREP and pRIP for fission yeast. *Gene* **123**, 127–130.

**McEntaffer, R., Natochin, M. and Artemyev, N.** (1999). Modulation of transducin GTPase activity by chimeric RGS16 and RGS9 regulators of G protein signaling and the effector molecule. *Biochem. J.* **38**, 4931–4937.

**Milligan, G.** (1998). New aspects of G-protein-coupled receptor signalling and regulation. *Trends Endocrinol. Metab.* **9**, 13–19.

**Minic, J., Persuy, M., Godel, E., Aioun, J., Connerton, I., Salesse, R. and Pajot-Augy, E.** (2005). Functional expression of olfactory receptors in yeast and development of a bioassay for odorant screening. *FEBS J.* **272**, 524–537.

**Moore, C., Milano, S. and Benovic, J.** (2007). Regulation of receptor trafficking by GRKs and arrestins. *Annu. Rev. Physiol.* **69**, 451.

**Moseley, J., Mayeux, A., Paoletti, A. and Nurse, P.** (2009). A spatial gradient coordinates cell size and mitotic entry in fission yeast. *Nature* **459**, 857–860.

**Mumby, S.** (1997). Reversible palmitoylation of signaling proteins. *Curr. Opin. Cell Biol.* **9**, 148–154.

**Nagai, T.** (2002). A variant of yellow fluorescent protein with fast and efficient maturation for cell-biological applications. *Nat. Biotech.* **20**, 87–90.

**Neitzel, K. L. and Hepler, J. R.** (2006). Cellular mechanisms that determine selective RGS protein regulation of G protein-coupled receptor signaling. *Semin. Cell Dev. Biol.* **17**, 383–9.

**Neves, S., Ram, P. and Iyengar, R.** (2002). G protein pathways. *Science* **296**, 1636.

**Novick, A. and Weiner, M.** (1957). Enzyme induction as an all-or-none phenomenon. *Proc. Natl. Acad. Sci. U.S.A.* **43**, 553.

**Nowotschin, S. and Hadjantonakis, A.** (2009). Photomodulatable fluorescent proteins for imaging cell dynamics and cell fate. *Organogenesis* **5**, 217.

**Obara, T., Nakafuku, M., Yamamoto, M. and Kaziro, Y.** (1991). Isolation and characterization of a gene encoding a G-protein alpha subunit from *Schizosaccharomyces pombe*: involvement in mating and sporulation pathways. *Proc. Natl. Acad. Sci. U.S.A.* **88**, 5877.

**O'Hara, P., Sheppard, P., Thógersen, H., Venezia, D., Haldeman, B., McGrane, V., Houamed, K., Thomsen, C., Gilbert, T. and Mulvihill, E.** (1993). The ligand-binding domain in metabotropic glutamate receptors is related to bacterial periplasmic binding proteins. *Neuron* **11**, 41–52.

**Okazaki, K., Okazaki, N., Kume, K., Jinno, S., Tanaka, K. and Okayama, H.** (1990). High-frequency transformation method and library transducing vectors for cloning mammalian cDNAs by trans-complementation of *Schizosaccharomyces pombe*. *Nucleic Acids Res.* **18**, 6485.

**Oldham, W. and Hamm, H.** (2008). Heterotrimeric G protein activation by G-protein-coupled receptors. *Nat. Rev. Mol. Cell Biol.* **9**, 60–71.

**Onaran, H., Costa, T. and Rodbard, D.** (1993). Beta gamma subunits of guanine nucleotide-binding proteins and regulation of spontaneous receptor activity: thermodynamic model for the interaction between receptors and guanine nucleotide-binding protein subunits. *Mol. Pharmacol.* **43**, 245.

**Onken, B., Wiener, H., Philips, M. and Chang, E.** (2006). Compartmentalized signaling of Ras in fission yeast. *Proc. Natl. Acad. Sci.* **103**, 9045.

**O'Shea, J., Gadina, M. and Schreiber, R.** (2002). Cytokine signaling in 2002: New surprises in the Jak/Stat pathway. *Cell* **109**, S121–S131.

**Ozoe, F., Kurokawa, R., Kobayashi, Y., Jeong, H., Tanaka, K., Sen, K., Nakagawa, T., Matsuda, H. and Kawamukai, M.** (2002). The 14-3-3 proteins Rad24 and Rad25 negatively regulate Byr2 by affecting its localization in *Schizosaccharomyces pombe*. *Mol. Cell. Biol.* **22**, 7105.

**Padgett, R., Das, P. and Krishna, S.** (1998). TGF-$\beta$ signaling, Smads, and tumor suppressors. *Bioessays* **20**, 382–390.

**Peleg, S., Varon, D., Ivanina, T., Dessauer, C. and Dascal, N.** (2002). G (alpha)(i) controls the gating of the G protein-activated K (+) channel, GIRK. *Neuron* **33**, 87–99.

**Pereira, P. and Jones, N.** (2001). The RGS domain-containing fission yeast protein, Rgs1p, regulates pheromone signalling and is required for mating. *Genes Cells* **6**, 789–802.

**Perkins, T. J. and Swain, P. S.** (2009). Strategies for cellular decision-making. *Mol. Syst. Biol.* **5**, 326.

**Pierce, K., Premont, R. and Lefkowitz, R.** (2002). Seven-transmembrane receptors. *Nat. Rev. Mol. Cell Biol.* **3**, 639–650.

**Pitcher, J., Freedman, N. and Lefkowitz, R.** (1998). G protein-coupled receptor kinases. *Annu. Rev. Biochem.* **67**, 653–692.

**Pollok, B. and Heim, R.** (1999). Using GFP in FRET-based applications. *Trends Cell Biol.* **9**, 57–60.

**Ponting, C. and Bork, P.** (1996). Pleckstrin's repeat performance: a novel domain in G-protein signaling? *Trends Biochem. Sci.* **21**, 245–246.

**Ponting, C., Phillips, C., Davies, K. and Blake, D.** (1997). PDZ Domains: Targeting signalling molecules to sub-membranous sites. *Bioessays* **19**, 469–479.

**Raj, A. and van Oudenaarden, A.** (2008). Nature, nurture, or chance: stochastic gene expression and its consequences. *Cell* **135**, 216–26.

**Rajeswari, M. and Jain, A.** (2002). High-mobility-group chromosomal proteins, HMGA1 as potential tumour markers. *Curr. Sci. Bangalore* **82**, 838–844.

**Randazzo, P. and Kahn, R.** (1994). GTP hydrolysis by ADP-ribosylation factor is dependent on both an ADP-ribosylation factor GTPase-activating protein and acid phospholipids. *J. Biol. Chem.* **269**, 10758.

**Raser, J. and O'Shea, E.** (2004). Control of stochasticity in eukaryotic gene expression.

**Rens-Domiano, S. and Hamm, H.** (1995). Structural and functional relationships of heterotrimeric G-proteins. *FASEB J.* **9**, 1059–1066.

**Rincon, S., Coll, P. and Perez, P.** (2007). Spatial regulation of Cdc42 during cytokinesis. *Cell cycle* **6**, 1687–1691.

**Robinson, D. R., Wu, Y. M. and Lin, S. F.** (2000). The protein tyrosine kinase family of the human genome. *Oncogene* **19**, 5548–5557.

**Robinson, L., Menold, M., Garrett, S. and Culbertson, M.** (1993). Casein kinase I-like protein kinases encoded by YCK1 and YCK2 are required for yeast morphogenesis. *Mol. Cell. Biol.* **13**, 2870.

**Rodrigues, G. and Park, M.** (1994). Oncogenic activation of tyrosine kinases. *Curr. Opin. Genet. Dev.* **4**, 15–24.

**Ross, E.** (2008). Coordinating speed and amplitude in G-protein signaling. *Curr. Biol.* **18**, R777–R783.

**Ross, E. and Wilkie, T.** (2000). GTPase-activating proteins for heterotrimeric G proteins: regulators of G protein signaling (RGS) and RGS-like proteins. *Annu. Rev. Biochem.* **69**, 795–827.

**Roy, A., Lemberg, K. and Chidiac, P.** (2003). Recruitment of RGS2 and RGS4 to the plasma membrane by G proteins and receptors reflects functional interactions. *Mol. Pharmacol.* **64**, 587.

**Sacan, A., Ferhatosmanoglu, H. and Coskun, H.** (2008). Celltrack: an open-source software for cell tracking and motility analysis. *Bioinformatics* **24**, 1647.

**Sambrook, J., Fritsch, E. and Maniatis, T.** (1989). *Molecular cloning. 2*. Cold Spring Harbor Laboratory Press Cold Spring Harbor, New York.

**Sandiford, S. and Slepak, V.** (2009). The G$\beta$5- RGS7 complex selectively inhibits muscarinic M3 receptor signaling via the interaction between the third intracellular loop of the receptor and the DEP domain of RGS7. *Biochem. J.* **48**, 2282–2289.

**Sayar, K., Uğur, Ö., Liu, T., Hilser, V. and Onaran, O.** (2008). Exploring allosteric coupling in the $\alpha$-subunit of heterotrimeric G proteins using evolutionary and ensemble-based approaches. *BMC Struct. Biol.* **8**, 23.

**Scheffzek, K., Ahmadian, M., Kabsch, W., Wiesmüller, L., Lautwein, A., Schmitz, F. and Wittinghofer, A.** (1997). The Ras-RasGAP complex: structural basis for GTPase activation and its loss in oncogenic Ras mutants. *Science* **277**, 333.

**Scheschonka, A., Dessauer, C., Sinnarajah, S., Chidiac, P., Shi, C. and Kehrl, J.** (2000). RGS3 is a GTPase-activating protein for Gi$\alpha$ and Gq$\alpha$ and a potent inhibitor of signaling by GTPase-deficient forms of Gq$\alpha$ and G11$\alpha$. *Mol. Pharmacol.* **58**, 719.

**Schlessinger, J., Ullrich, A. et al.** (1992). Growth factor signaling by receptor tyrosine kinases. *Neuron* **9**, 383.

**Sethakorn, N., Yau, D. and Dulin, N.** (2010). Non-canonical functions of RGS proteins. *Cell. Signal.* **22**, 1274–1281.

**Shahrezaei, V. and Swain, P.** (2008). The stochastic nature of biochemical networks. *Curr. Opin. Biotechnol.* **19**, 369–374.

**Shaner, N., Steinbach, P. and Tsien, R.** (2005). A guide to choosing fluorescent proteins. *Nat. Methods* **2**, 905.

**Shav-Tal, Y., Singer, R. H. and Darzacq, X.** (2004). Imaging gene expression in single living cells. *Nat. Rev. Mol. Cell Biol.* **5**, 855–61.

**Shen, H., Nelson, G., Nelson, D., Kennedy, S., Spiller, D., Griffiths, T., Paton, N., Oliver, S., White, M. and Kell, D.** (2006). Automated tracking of gene expression in individual cells and cell compartments. *J R Soc Int* **3**, 787–794.

**Sigal, A., Milo, R., Cohen, A., Geva-Zatorsky, N., Klein, Y., Liron, Y., Rosenfeld, N., Danon, T., Perzov, N. and Alon, U.** (2006). Variability and memory of protein levels in human cells. *Nature* **444**, 643–646.

**Smith, B., Hill, C., Godfrey, E. L., Rand, D., van den Berg, H., Thornton, S., Hodgkin, M., Davey, J. and Ladds, G.** (2009). Dual positive and negative regulation of GPCR signaling by GTP hydrolysis. *Cell. Signal.* **21**, 1151–60.

**Snow, B., Krumins, A., Brothers, G., Lee, S., Wall, M., Chung, S., Mangion, J., Arya, S., Gilman, A. and Siderovski, D.** (1998). A G protein $\gamma$ subunit-like domain

shared between RGS11 and other RGS proteins specifies binding to G$\beta$5 subunits. *Proc. Natl. Acad. Sci.* **95**, 13307.

**Sodhi, A., Montaner, S. and Gutkind, J.** (2004). Viral hijacking of G-protein-coupled-receptor signalling networks. *Nat. Rev. Mol. Cell Biol.* **5**, 998–1012.

**Sprang, S. R.** (1997). G protein mechanisms: insights from structural analysis. *Annu. Rev. Biochem.* **66**, 639–678.

**Srinivasa, S., Bernstein, L., Blumer, K. and Linder, M.** (1998). Plasma membrane localization is required for RGS4 function in *Saccharomyces cerevisiae*. *Proc. Natl. Acad. Sci.* **95**, 5584.

**Stites, E., Trampont, P., Ma, Z. and Ravichandran, K.** (2007). Network analysis of oncogenic Ras activation in cancer. *Science* **318**, 463.

**Sugimoto, A., Iino, Y., Maeda, T., Watanabe, Y. and Yamamoto, M.** (1991). *Schizosaccharomyces pombe ste11+* encodes a transcription factor with an HMG motif that is a critical regulator of sexual development. *Genes Dev.* **5**, 1990–9.

**Sullivan, M. and Folk, W.** (1988). An improved procedure for measuring DNA replication with transient assays in eukaryotic cells. *Gene Anal. Tech.* **5**, 54–56.

**Sunahara, R., Dessauer, C. and Gilman, A.** (1996). Complexity and diversity of mammalian adenylyl cyclases. *Annu. Rev. Pharmacol. Toxicol.* **36**, 461–480.

**Takai-Igarashi, T.** (2005). Ontology based standardization of petri net modeling for signaling pathways. *In Silico Biol.* **5**, 529–536.

**Takegawa, K., Iwaki, T., Fujita, Y., Morita, T., Hosomi, A. and Tanaka, N.** (2003). Vesicle-mediated protein transport pathways to the vacuole in *Schizosaccharomyces pombe*. *Cell Struct. Funct.* **28**, 399–417.

**Tanaka, K., Davey, J., Imai, Y. and Yamamoto, M.** (1993). *Schizosaccharomyces pombe map3+* encodes the putative M-factor receptor. *Mol. Cell. Biol.* **13**, 80.

**Taussig, R. and Zimmermann, G.** (1998). Type-specific regulation of mammalian adenylyl cyclases by G protein pathways. *Adv. Second Messenger Phosphoprotein Res.* **32**, 81–98.

**Tesmer, J., Berman, D., Gilman, A. and Sprang, S.** (1997). Structure of RGS4 bound to AlF4–activated Gi [alpha] 1: Stabilization of the transition state for GTP hydrolysis. *Cell* **89**, 251–261.

**Toda, T., Shimanuki, M. and Yanagida, M.** (1991). Fission yeast genes that confer resistance to staurosporine encode an AP-1-like transcription factor and a protein kinase related to the mammalian ERK1/MAP2 and budding yeast FUS3 and KSS1 kinases. *Genes Devel.* **5**, 60.

**Tu, H., Barr, M., Dong, D. and Wigler, M.** (1997). Multiple regulatory domains on the Byr2 protein kinase. *Mol. Cell. Biol.* **17**, 5876.

**Tyson, R., Epstein, D., Anderson, K. and Bretschneider, T.** (2010). High resolution tracking of cell membrane dynamics in moving cells: an electrifying approach. *Math Model Nat Phenom* **5**, 34–55.

**van Rhee, A. and Jacobson, K.** (1996). Molecular architecture of G protein-coupled receptors. *Drug Dev. Res.* **37**, 1.

**Venter, J., Adams, M., Myers, E., Li, P., Mural, R., Sutton, G., Smith, H., Yandell, M., Evans, C., Holt, R. et al.** (2001). The sequence of the human genome. *Science* **291**, 1304–1351.

**Versele, M., Lemaire, K. and Thevelein, J.** (2001). Sex and sugar in yeast: two distinct GPCR systems. *EMBO Rep.* **2**, 574–579.

**Von Zastrow, M. and Kobilka, B.** (1992). Ligand-regulated internalization and recycling of human beta 2-adrenergic receptors between the plasma membrane and endosomes containing transferrin receptors. *J. Biol. Chem.* **267**, 3530.

**Vuong, T. M. and Chabre, M.** (1990). Subsecond deactivation of transducin by endogenous GTP hydrolysis. *Nature* **346**, 71–74.

**Wang, J., Golebiewska, U. and Scarlata, S.** (2009). A self-scaffolding model for G protein signaling. *J. Mol. Biol.* **387**, 92–103.

**Wang, X., Zeng, W., Kim, M., Allen, P., Greengard, P. and Muallem, S.** (2007). Spinophilin/neurabin reciprocally regulate signaling intensity by G protein-coupled receptors. *EMBO J.* **26**, 2768–2776.

**Watson, P., Davis, K., Didmon, M., Broad, P. and Davey, J.** (1999). An RGS protein regulates the pheromone response in the fission yeast *Schizosaccharomyces pombe*. *Mol. Microbiol.* **33**, 623–34.

**Weinstein, L. and Shenker, A.** (1993). G protein mutations in human disease. *Clin. Biochem.* **26**, 333–338.

**Weinstein, L., Shenker, A., Gejman, P., Merino, M., Friedman, E. and Spiegel, A.** (1991). Activating mutations of the stimulatory G protein in the McCune–Albright syndrome. *N. Engl. J. Med.* **325**, 1688–1695.

**Weiss, J., Morgan, P., Lutz, M. and Kenakin, T.** (1996). The cubic ternary complex receptor-occupancy model I. model description. *J. Theor. Biol.* **178**, 151–167.

**Welton, R. and Hoffman, C.** (2000). Glucose monitoring in fission yeast via the Gpa2 g$\alpha$, the Git5 Gß and the Git3 putative glucose receptor. *Genetics* **156**, 513.

**Wennerberg, K., Rossman, K. and Der, C.** (2005). The Ras superfamily at a glance. *J. Cell Sci.* **118**, 843.

**Wettschureck, N. and Offermanns, S.** (2005). Mammalian G proteins and their cell type specific functions. *Physiol. Rev.* **85**, 1159–1204.

**Whiteway, M., Hougan, L., Dignard, D., Thomas, D., Bell, L., Saari, G., Grant, F., O'Hara, P. and MacKay, V.** (1989). The STE4 and STE18 genes of yeast encode potential [beta] and [gamma] subunits of the mating factor receptor-coupled G protein. *Cell* **56**, 467–477.

**Willars, G. B.** (2006). Mammalian RGS proteins: multifunctional regulators of cellular signalling. *Semin. Cell Dev. Biol.* **17**, 363–76.

**Wong, H., Mao, J., Nguyen, J., Srinivas, S., Zhang, W., Liu, B., Li, L., Wu, D., Zheng, J. et al.** (2000). Structural basis of the recognition of the dishevelled DEP domain in the Wnt signaling pathway. *Nat. Struct. Biol.* **7**, 1178–1183.

**Wurthner, J., Mukhopadhyay, A. and Peimann, C.** (2000). A cellular automaton model of cellular signal transduction. *Comput. Biol. Med.* **30**, 1–21.

**Xu, X., Zeng, W., Popov, S., Berman, D., Davignon, I., Yu, K., Yowe, D., Offermanns, S., Muallem, S. and Wilkie, T.** (1999). RGS proteins determine signaling specificity of Gq-coupled receptors. *J. Biol. Chem.* **274**, 3549.

**Xue-Franzén, Y., Kjærulff, S., Holmberg, C., Wright, A. and Nielsen, O.** (2006). Genomewide identification of pheromone-targeted transcription in fission yeast. *BMC Genomics* **7**, 303.

**Yi, T., Kitano, H. and Simon, M.** (2003). A quantitative characterization of the yeast heterotrimeric G protein cycle. *Proc. Natl. Acad. Sci.* **100**, 10764–10769.

**Yildirim, N., Hao, N., Dohlman, H. and Elston, T.** (2004). Mathematical modeling of RGS and G-protein regulation in yeast. *Meth. Enzymol.* **389**, 383–398.

**Yu, R., Resnekov, O., Abola, A., Andrews, S., Benjamin, K., Bruck, J., Burbulis, I., Colman-Lerner, A., Endy, D., Gordon, A. et al.** (2008). The Alpha Project: a model system for systems biology research. *IET Syst. Biol.* **2**, 222.

**Zanchi, R., Howard, G., Bretscher, M. and Kay, R.** (2010). The exocytic gene secA is required for *Dictyostelium* cell motility and osmoregulation. *J. Cell Sci.* **123**, 3226–3234.

**Zhang, S., Watson, N., Zahner, J., Rottman, J., Blumer, K. and Muslin, A.** (1998). RGS3 and RGS4 are GTPase activating proteins in the heart. *J. Mol. Cell. Cardiol.* **30**, 269–276.

**Zhong, H., Wade, S., Woolf, P., Linderman, J., Traynor, J. and Neubig, R.** (2003). A spatial focusing model for G protein signals. *J. Biol. Chem.* **278**, 7278.

**Zimmermann, T., Rietdorf, J. and Pepperkok, R.** (2003). Spectral imaging and its applications in live cell microscopy. *FEBS Lett.* **546**, 87–92.